Upper-body Enhancive Robotic Exoskeleton for Load Handling at Full Reach

Thomas Magill

Submitted in accordance with the requirements for the degree of
Doctor of Philosophy

The University of Leeds
Mechanical Engineering
iDROS

May 2019

The candidate confirms that the work submitted is his own and that appropriate credit has been given where reference has been made to the work of others.

This copy has been supplied on the understanding that it is copyright material and that no quotation from the thesis may be published without proper acknowledgement.

The right of Thomas Magill to be identified as the author of this work has been asserted by him in accordance with the Copyright, Designs and Patents Act 1988.

© 2019 The University of Leeds and Thomas Magill

Unless stated in the text, the following copyright notices apply to usage of terms within

MATLAB®, Simulink®, Simmechanics™ and Simhydraulics™ are registered and unregistered trademarks of The MathWorks, Inc., 1994-2015. These are outlined further here:

http://uk.mathworks.com/company/aboutus/policies_statements/trademarks.html?s_tid=gf_trd

Automation Studio™ is an unregistered trademark of Famic Technologies Inc.

SOLIDWORKS is a trademark of Dassault Systèmes SolidWorks Corporation

SKF, CARD, ICOS, INSOCOAT, KMT, KMTA, NoWear, SensorMount, and Wave are registered trademarks of the SKF group

Acknowledgements

I would like to offer my thanks and gratitude to my two supervisors, Professor Abbas Dehghani and Dr Andrew Jackson for their support and guidance throughout my PhD research.

I would also like to thank Rob Bloomfield and Mechatech for their support but intellectual and financial throughout the project.

This research has been carried out by a team which has included Maciej Napora, Pourshid Fani and Konstantinos Drosos. My own contributions, fully and explicability indicated in the thesis, have been Chapters three to eight. The other member of the group and their contributions have been within the single joint design and test, as outlined in the appendices.

I would like to thank the three team members above, not just as my colleagues, but my friends throughout this research as well. I would also like to thank my friends Farzilnizam 'Farzil' Ahmad and Francisco Tapia Lara for supportive in the office.

I would also like to thank my family, Aidan and Carola Magill for believing in me, well as the new family that I have built up at Vineyard. I would like to thank David Flowers for putting up with my strange questions and personally. I would also like to thank Sue and David Richardson for making me feel at home. I would also like to thank Professor Tom Ward and Tania Barnett for listening to my stress and their cats for calming me down.

Abstract

Use of robotics within the industrial environment has allowed improved productivity, but only for aspects that are repetitive and thus programmable. Any deviation from a predefined situation causes the system to fail thus there is still the involvement of the human element. Bringing the strength of a robotic system, with the intelligence of a human controller allows increased adaptability. Industries where there is a variability of action but require additional strength benefit from this combination of man and machine.

Regarding this, there is a gap in regards to upper-body exoskeletons that enhance the user's strength at full reach. Current systems augment the user's carrying capacity, but do not state what their load manipulation at full reach.

The literature survey also shows that there is a gap in regards to optimisation of the exoskeleton systems with respect to both the geometry of the joints and the selection of the hydraulic circuit design. Current systems appear to have tried to get a prototype working as quickly as possible without simulation of the system first.

The first focus of this research is in the development of optimisation of joint geometry for revolute and gimbal joints. Several different designs are broken down into geometric equations that can then be fed into an optimisation routine to determine the ideal geometry for a given loading and motion range.

The second focus of this research is using the optimised joint geometry and design an upper-body exoskeleton that has load manipulation at full reach. This design consisted of an initial load manipulator, the elbow and the shoulder joint. This design was found to be heavy, but for similar load carrying methods of other exoskeletons and robotics, has a similar load to weight ratio.

The third focus of this research was a review of current hydraulic circuits in regards to an enhancive exoskeleton system. previous exoskeletons did not focus on this aspect of the design, meaning that efficiency and optimisation options have not been explored. Though servo valve systems can be used, additional benefits can be found with full pressure override regeneration circuits, so that return fluid can be used productively. Though pump based circuits were found not to be suitable for this design, they have shown promising energy recovery options for lower power systems.

The final focus of this research was to bring together the upper-body structural design and selected hydraulics and simulate them in a virtual environment. This saves money on component manufacture and has shown that there are issues to overcome in future development. The frequency response of the valves and system were found to be lower than required to follow the human motion which would be a limiting factor for zero loading on the user. The motion capture was also not optimised to match the motion limitations of the exoskeleton resulting in the actuators reaching the end stop limits.

The final conclusions of this research are that the optimisation design routines allows the easy selection of actuators and geometry to avoid singularity events in the motion and that hydraulic regeneration circuits will give a benefit to exoskeleton motion. The use of simulation over a prototype has meant that the costs have been reduced, and outlined areas of concern without wasted manufacturing.

Table of Contents

List of Figures

List of Tables

Abbreviations

AC	Alternating current
AI	Artificial Intelligence
BS	British Standard
BSI	British Standard Institute
BSSA	British Stainless Steel Association
BVH	Biovision Hierarchy, a motion capture file format
CAD	Computer-Aided Design
CE	Conformité Européene – European Conformity
CNC	Computer Numerical Control
CVT	Continuously Variable Transmission
DARPA	Defense Advanced Research Projects Agency
DC	Direct current
DIN	Deutsche Industrie-Norm - German Industrial Standard
DOF	Degrees of freedom
ECU	Electronic Control Unit
EHA	Electro-Hydraulic Actuator / Electro-Hydrostatic Actuators
EHPA	Exoskeletons for Human Performance Augmentation
FEA	Finite Element Analysis
FMECA	Failure Mode, Effects and Criticality Analysis
GUI	Graphical User Interface
HEPU	Hydraulic-electric power unit
HMRF	Hydromechanical resonant frequency
HSE	Health and Safety Executive
IHT	Innas Hydraulic Transformer
ISO	International Organization for Standardization
LEADUE	Leeds Enhancive Action at a Distance

LHS   Left-hand side

LPM   Litres per minute

MARC   modular adaptive robust control

MHA   Micro Hydraulic Actuator (

MHCC   Micro Hydraulic Compressor Converter

MPR   Main Pressure Rail

NFTSM   Non-singular Fast Terminal Sliding Mode

OEM   Original equipment manufacturer,

PEO Soldier   Program Executive Office Soldier

psi   Pounds per Square Inch.

PSO   particle swarm optimisation

RHS   Right-hand side

RMS   Root mean square

RMSE   Root mean square error

RPM   Revolutions per minute

SAE   Society of Automotive Engineers

SF   Safety factor

SPR   Secondary Pressure Rail

STL   Standard Tessellation Language

TDE   time delay estimation

THOR   tactical hazardous operations robot

TIER   Topographies with Integrated Energy Recovery

UID   Unique Identifier

VHT   variable hydraulic transformer

Chapter 1
Introduction

1.1 Background

The word exoskeleton has traditionally meant an external organ either bony, calcified or leathery on animals [1], typically in relation to insects or crustaceans whereas humans have an endoskeleton, a mineralised internal structure. The exoskeleton can be used for protection purposes, for example, crustaceans, which is mimicked by humans with artificial armour, typically thought of as suits of armour from the Middle Ages. These suits of armour, made from metal, leather and fabric had no motion support and relied only on the user for motion. Though normally custom made and fitted to the user, they could only be worn for a limited time due to the increased excursion required.

Since the middle of the 20th Century, research has been conducted on developing systems to assist human users, whether to bring the user up to normal human capabilities or to exceed them. America has been the forefront of developing systems for military use [2, 3] which enhance the user whilst Asian countries like Japan have been developing systems to assist people in undertaking normal activities [4, 5]. This focus is due to developments out of the Second World War and the Cold war. Where America has a thriving war machine, Japan has an ageing population.

There are several full-body enhancive exoskeletons being developed at the current time, but two of the main ones are SARCOS and PERCRO. SARCOS' XOS is a commercially developed exoskeleton, developed initially for military use, which uses hydraulics to enhance the strength of the user [3]. PERCRO is an academically developed system that uses electric motors to supply the motion [6]. Both claim to be able to lift significant weights, 90kg and 101.9 kg respectfully.

There are several half body exoskeletons like HAL [4] and BLEEX [2] that support the lower body. HAL started as an assistive system, but have started to expand into enhancive systems. BLEEX enhances the users load carrying capacity by placing the load on the back of the user.

Industry had taken on industrial robotics for large-scale mass production, where predefined, repeatable activities can be automated. Yet not all process can be automated due to some the activities tending to be for unique situations, or non-repeatable. There has been the development of humanoid robots with AI to assist with these events, but these are temperamental and require significant human support. From the DARPA challenge for humanoid robots in 2015, an average of 2.7 humans were required for setup, and 2.4 to supervise and control it [7]. Placing a user in direct control of a system brings into account advanced problem-solving capabilities and reduces the number of operators to one.

The use of simulations in engineering has developed over the years, with more companies using the techniques to assist with their design work. For example, Haldex states that the use of simulation software reduced development time by 50% and brought about a cost-saving for the company [8]. Also from the DARPA challenge, a virtual simulation may have assisted with the development of safe operation of the robot, prior to empirical interaction with the environment [7]. The ability to quickly develop virtual components that can be tested repeatedly with minimal cost and a large option of activities is ideal for the exoskeleton development process.

This research will look into developing an upper-body exoskeleton system. This will be done by examining different revolute design opportunities and look at how they can be optimised in regards to available actuators. This will then lead into the full design of the upper-body exoskeleton system that is matched to the motion of the user. In parallel to this, different hydraulic circuits will be examined for use in the exoskeleton finally culminating in the complete system being simulated following human motion capture data. This will then be finalised by bringing the hydraulic system and the exoskeleton virtual models together and have it follow motion capture data. Previous work has not focused on the optimisation and simulation side, which had meant that some of the initial prototypes have failed to match the requirements.

1.2 Motivation

Industrial requests for enhancing their workforce has led to the development of robotics within industry, though these are currently used for repetitive tasks with known motions and requirements. Intelligent robotics are in development,

though to reach human capabilities will take a long time and introduce new issues with human-robot interaction and relationship. Thus, the option of integrating a human within a robotic suit gives the best of both worlds: intelligent control and increased endurance and strength.

This project has a sponsor, Mechatech Ltd, who is looking to bring exoskeleton systems into the industrial environment to enhance the workforce whilst being economically viable. This does mean that there are certain limitations to options available due to cost, though does allow other options due to its limited environmental range.

The source of motion for the suit is critical as there are several options available for the system but with a user encased within the system, safety is critical. The motion system needs to be able to carry itself and not put weight on the user, whilst being as efficient as possible.

With these initial motivations, the benefits to society would be the main motivation. Helping people to work with reduced effort and the chance of injury is critical for the future. If a worker can work with less strain on their body, then they will spend less time off sick, or with detrimental injuries. A by-product of a healthy workforce is increased work output, as well as a reduction in litigation due to avoidable injuries.

If the system is mobile enough, there is also the possibility of its use in emergencies. The ability to augment the strength of a rescue worker would mean that trapped or injured humans and animals can be rescued quicker and receive treatment promptly. The use of cranes and heavy lifting equipment takes time to arrive at a disaster site, and risk causing more damage if the ground is not stable.

1.3 Team Project

The work covered within this thesis is part of a larger team project with the aim of developing a complete exoskeleton system. Within the enhancive exoskeleton team, one project focuses on structural elements of the system, one on the control and one on communications and power.

It was intended that these would all come together to form the complete exoskeleton system, but due to time constraints and change of focus for other students, this did not occur expect for an initial single joint design.

1.4 Aims and Objectives

1.4.1 Aims

The aim of this project is to design and simulate an upper-body exoskeleton system with a hydraulic circuit that is optimised for energy efficiency. This enhancive system will allow the user to lift heavier loads with a reduced metabolic cost.

1.4.2 Objectives

The objectives of the study will include:

- research into powered revolute joint design for optimisation;
- research into powered spherical joint design for optimisation;
- the use of joint optimisation to design an upper-body exoskeleton;
- research in the hydraulic circuit design to determine an optimal solution for the exoskeleton;
- development of a simulated exoskeleton that utilises available motion capture data, primarily aimed at computer game input, to examine the response of the hydraulic system;
- consideration of validation of the design and simulation with empirical results.

1.5 Contributions of this research

This research will contribute to the body of knowledge in exoskeletons based on the optimisation techniques and analysis of an example system

- The use of geometric optimisation of joints in upper-body exoskeleton design
- Focus on upper-body load manipulation at full-reach
- Critical analysis of hydraulic circuits in regards to an exoskeleton
- Multi-domain simulation of exoskeleton system

- Consideration of validation of the design and simulation with empirical results

1.6 Scope of this research

The scope of this research is on the design of an upper-body exoskeleton that has attempted to optimise the geometry of the structure to give the required torques. Examining the different design options with comparison to the requirements for the joint each will have optimisation routines run to determine the ideal geometry.

These idealised geometric values are then used to design the physical structure of the exoskeleton, making sure that strength and motion are supported. Working from the end effector at the hand, along to the back, each link adds to the previous one. This will mean that each joint is capable of fulfilling its assigned task.

Once this virtual exoskeleton has been constructed, it is then transferred to a virtual environment to test the hydraulic components. Different hydraulic circuits are compared to determine which are suitable for the exoskeleton and then using motion capture data, they are tested with possible demands.

Different hydraulic circuits are compared using the elbow joint as the basis. Ones that are suitable are then integrated into the full upper-body exoskeleton design in the virtual environment. This complete system is then tested with motion capture data to determine the response.

1.7 Outline of the thesis

Chapter 2 presents the literature review that covers the current enhancive exoskeleton systems, highlighting opportunities that have not been covered so far, particularly concerning optimisation of the joint geometry. This then proceeds on to the breakdown of the options for the joint actuator. The chapter ends with an examination of hydraulic circuit options.

Chapter 3 examines the requirement for the system as outlined by the sponsor through discussions with project team members. These are broken down and

examined to determine the impact that they will have on the design and hydraulics.

Chapter 4 presents the development of the equations for each joint type ready for optimisation. This initially focuses on the revolute joints, for example, those of the elbow, before expanding into 3D spherical joints. The optimisation focuses on developing the equations for the geometry for the joint, based upon available actuators and the torque required.

Chapter 5 covers the design of the upper body system, working systematically from the hand manipulator along the arm to the shoulder. As the hand is the end effector, it should be the initial design point for the system. As the design chain works along, each part needs to carry the previous part of the chain, and thus is likely to get larger.

Chapter 6 presents the examination of the hydraulic circuits which are compared with a simple simulation test. Benefits and limitations of the circuits are discussed to find the solution to proceed with.

Chapter 7 presents the combining of the design from Chapter 5 and the hydraulics in Chapter 6 into a single virtual environment. Motion capture data is supplied to the exoskeleton system to determine its response and limitations.

The final chapter is the conclusion of the thesis and outlines the results and future work that can be developed from this research.

The outline of the thesis is shown in a visual manner in Figure 1.1.
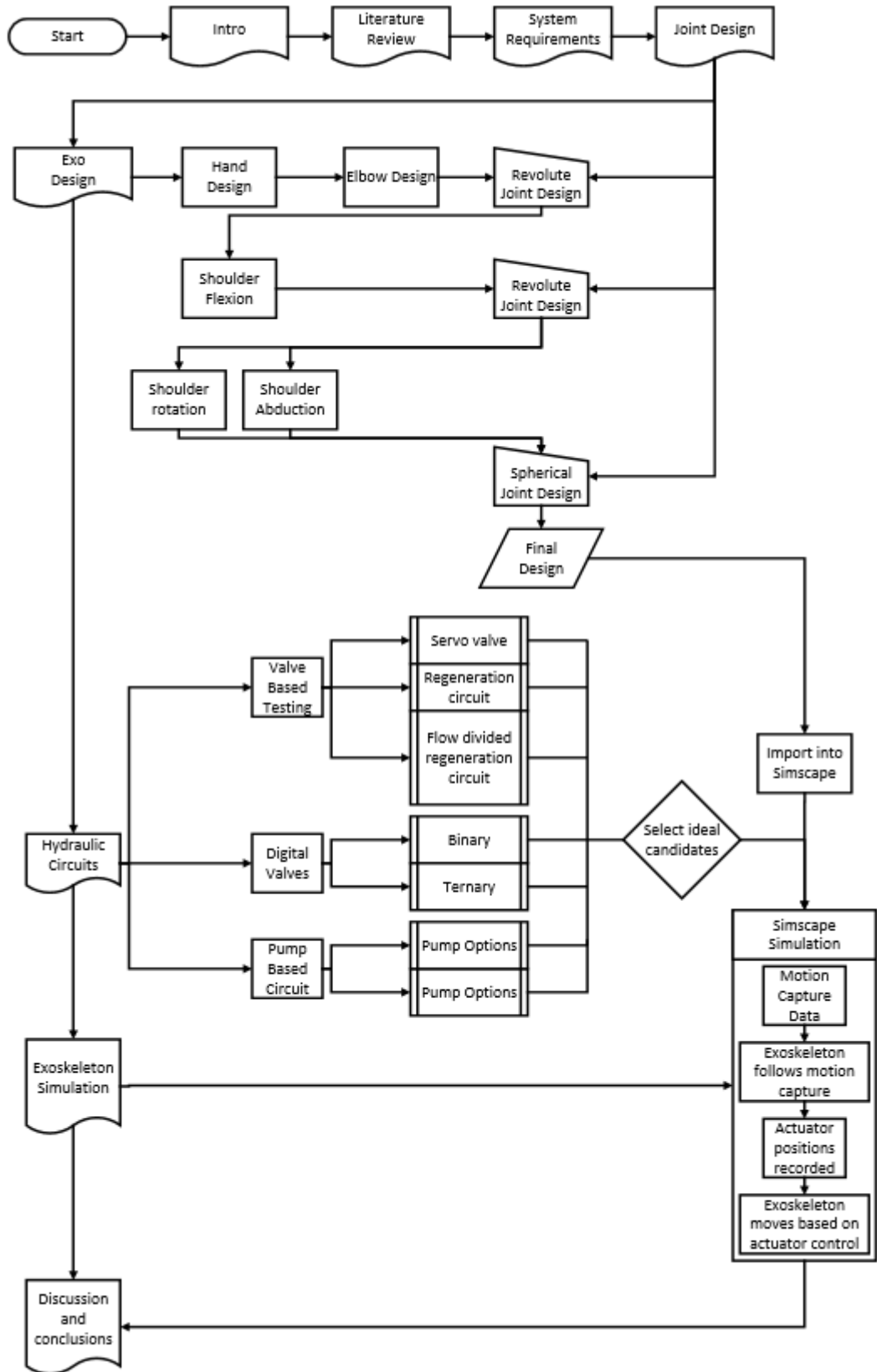
Figure 1.1: Flow diagram of chapters and processes within each chapter

Chapter 2
Literature Review

2.1 Introduction

A human exoskeleton is an external structure that supports the biological system; this can either bring the human up to normal motion, as for rehabilitation or to reduce the loading to enhance the user capabilities. In either case, the system would be expected to match normal human motion ranges and speeds to prevent strain and discomfort.

An initial example of augmentative exoskeletons is the "Hardiman" by the U.S. Office of Naval Research [9] which is a separate entity to the Defense Advanced Research Projects Agency (DARPA). The system has 30 degrees of freedom (DOF), including arms and wrists, utilising a hydraulic power source allowing a 25:1 increase in user strength. The system was very heavy, weighing 680kg, and has never powered up with a human user inside [10]. The system did highlight issues with human interface and power supply requirements.

In 2001, DARPA started the Exoskeletons for Human Performance Augmentation (EHPA) programme, which was to be transitioned to the Army Program Executive Office Soldier (PEO Soldier) in FY 2008 [11]. From this project, several systems have been put forward including the Berkeley Exoskeleton (BLEEX) and SARCOS.

This chapter covers a range of topics concerning the different background topics of the thesis. Examining the human motion range gives an initial idea of what is required for the exoskeleton, and how current projects have developed their systems to fit these requirements. This then follows on to the options that are available for upper-body exoskeleton design. This initially looks at the power source options: hydraulic and electrical to determine which is the basis of the exoskeleton.

With the power source determined, the method of supplying motion is compared from current products, as well as methods used in current exoskeleton designs. With an understanding of the actuator, the hydraulic opportunities are examined to determine what current research has been done on circuit optimisation and efficiencies.

2.2 Human Anatomy

Human anatomy has been studied significantly over the years, from da Vinci to Gray. As the exoskeleton is being directed by the human, and not the other way around, it should have a similar range of motion. This can either be via an anthropomorphic design and mimics the joints or a non-anthropomorphic design that follows designated endpoints of the human.

Though humans can be trained to have a large range of motions for certain joints, for example, gymnasts can perform side splits, for the majority of the general healthy population, the range of motion is reduced. There have been several studies on the range of motion for the human body [12-14], though not all give suitable motions for exoskeletons, for example, cross-legged sitting, or do not contain the motions sought to design against.

Though Roass' work is from 1982 [14] it does compare results from the American Academy of Orthopaedic Surgeons as well as Boone and Azen. He gives the range of motion for the lower body for around 100 subjects for hip, knee and ankle. Soucie's study of 700 subjects over a range of ages has generated a table of reference values [13], as shown in Table 2.2.1. For an enhancive system, it is likely to be used by the 20-44 age group, of both genders. There are differences between the genders in regards to flexibility, with women being more flexible than men are.

Table 2.2.1: Range of motion of human joints [13]

		Extension (°)	Flexion (°)	Pronation (°)	Supination (°)	Lateral Flexion (°)	Horizontal Extension (°)	Horizontal Flexion (°)	Abduction (°)	Adduction (°)	Lateral Rotation (°)	Medial Rotation (°)
Arm	Shoulder	50	172				140	40	45	180	90	110
	Elbow	4.7	150	82	90.6							
	Wrist	85	85						15	45	90	85

2.3 Current Exoskeleton developments

Current exoskeleton developments can be divided down into two main categories: enhancive and assistive.

Several systems have been developed, with the units examined being BLEEX (Figure 2.1.a), SARCOS (Figure 2.1.b), HAL (Figure 2.1.c), PERCRO (Figure 2.1.d), Nurse-assisting Exoskeleton (Figure 2.1.e).

2.3.1 Manipulator

The interaction between the system and the load is different for each system. For the lower body/full systems, BLEEX, SARCOS and PERCRO all direct the load through the system to the ground, whereas HAL does not and only augments the joint torques.

The load-carrying methods also differ in implementation. BLEEX is the only system that does not have arms as part of the system, and thus the load is on the back of the user. This does make self-access limited and relies on others to assist. The rest of the systems have arm support but have different ways of interacting with the loads. SARCOS has claws, HAL has no hands and PERCRO has grippers. Hardiman is an older exoskeleton that also used grippers, which had a target lift capability of 1500lbs [17] or 680kg.

A simple claw system, as used by the Sarcos, would be easy to implement into the exoskeleton. This would just involve an FEA analysis of the design though deciding what style would require further investigation. This would likely be a replaceable system so that different designs of the claw can be used. Whether this is a quick release system or not, is not directly linked to the hydraulic system, though the option of having a hydraulic quick-release jaw clamp could be an option.

The PERCRO BE hand unit has a moving jaw that closes on a ridged jaw, based on the sensing of the load applied by the user on an internal trigger. Rotation of the hand is done further up the exoskeleton near the elbow. This means that the user is inside the exoskeleton, and limits the free movement of the arms is required. The details of the hand are shown in Figure 2.2.

Figure 2.1: Current exoskeleton systems. a) BLEEX [15], b) SARCOS [3], c) HAL [4], d) PERCRO [6], e) Nurse assisting exoskeleton [5, 16].
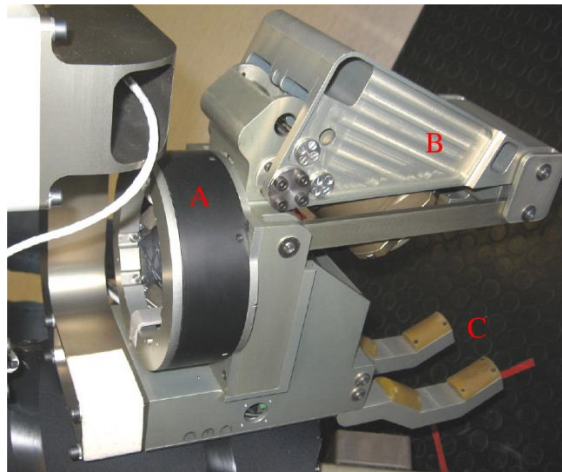
Figure 2.2: The gripper of the PERCRO's body extender: force sensor connected to the handle integrated into the gripper (A), moving jaw (B) and fixed jaws (C) [6]

The gripper of the Hardiman system has several axes [17] for the system, as shown in Figure 2.3. Axis 15 is the thumb tip flex, with axis 14 the thumb flex. This is a complex design, which is not repeated in industrial excavation systems on a large scale. Axis 13 is the wrist flex of the system with a swing of 70°, which could be done by the gross motion of the arm. Axis 12 is the forearm rotation, which has a swing of 160°, which would be difficult to replicate with gross arm motion. From this, Axis 14 and 12 would be easiest to replicate with a simple hydraulic system. Axis 15 and 13 would add additional complexity that would not add significant benefit-cost.
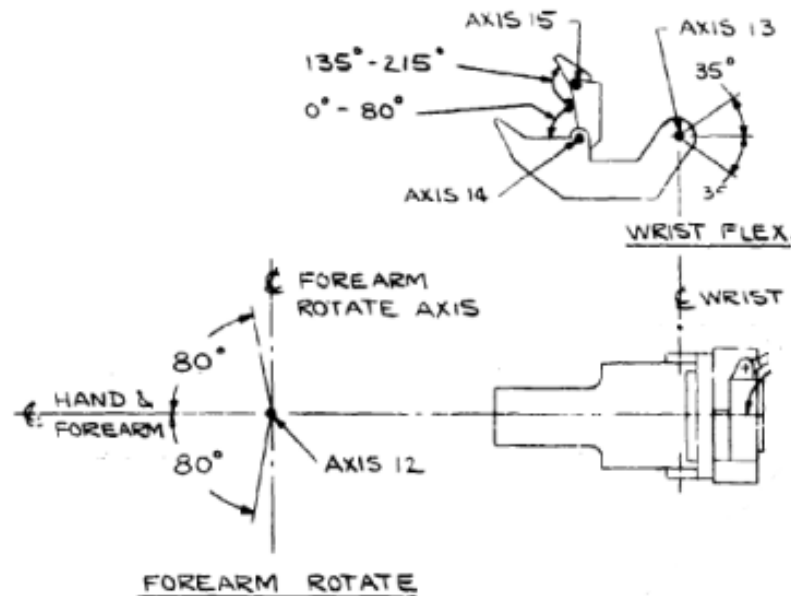
Figure 2.3: Subsection of Hardiman focusing on the end effector [17]

An initial thought would be to use the human hand and enhance its gripping force. The human hand is a complex mechanism and replicating the full range of motion with enhancement would result in a very large system. An example of a robotic system matching the range of motion of the human hand is ExoHand by Festo [18] and is shown in Figure 2.4. This uses eight pneumatic cylinders to power the hand, rather than hydraulics, so would give lower grip force, though in theory hydraulics could be used.
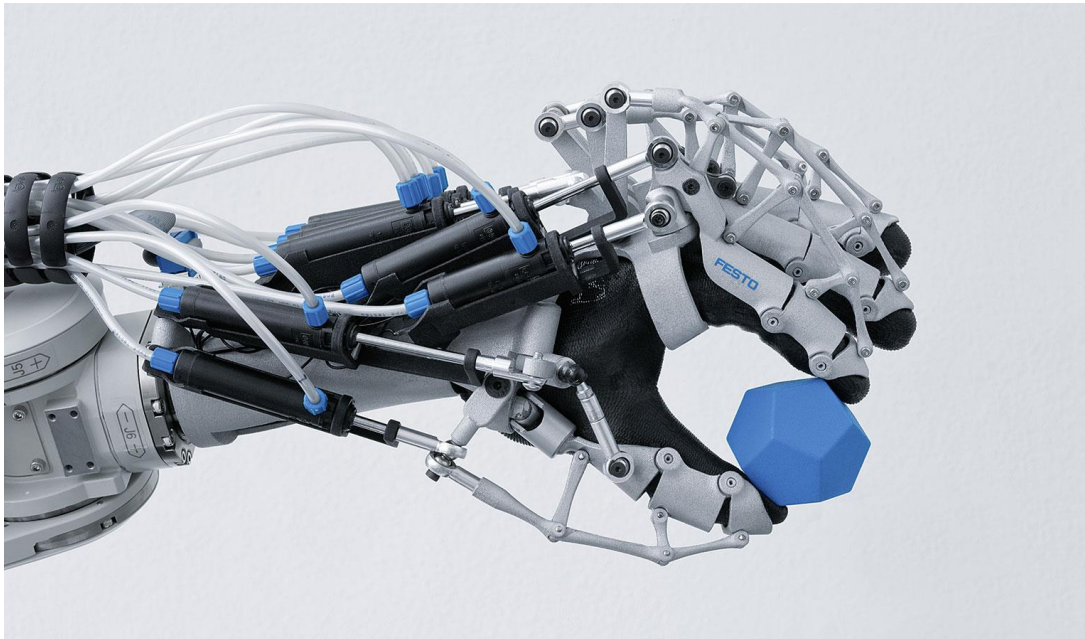
Figure 2.4: Festo ExoHand showing manipulation of all finger joints [19]

Depending on the force required for the gripping, there is the issue that with the ExoHand design, it is placing the human hand between the object being held and the actuators. This creates a pinch risk, which could damage the user. This would not be a viable design for a high-powered enhancive exoskeleton.

If the actuation system were inside of the hand, so that it was between the user and the load then there would no longer be a pinch risk. It would limit the range of the users closing action, as the volume of the gripper would reduce it.

Selecting a manipulator style depends on what the exoskeleton will be used for, and its objectives. Having no manipulator is unlikely to be an option for an exoskeleton for industrial use. BLEEX is designed as a load-carrying enhancer so that the user can carry heavier loads for longer. The use of claws does limit the interaction available for the user with the environment, and would only be suitable for load carrying and not manipulation. A gripper would be the ideal

choice but would add weight to the system. How the user controls the gripper is important to prevent the trapping of them. An indirect system, for example, a master-slave setup would prevent the user from injury but would mean that feedback would be limited.

2.3.2 Degrees of Freedom

For an upper-body system, the shoulder has three DOF, the elbow one and the wrist has three. The number of joints that need to be powered, or even exist, in the exoskeleton needs to be determined. Certainly having the shoulder and wrist powered will give the greatest flexibility in regards to motion and loading. As mentioned in Section 2.3.1, there is a question on what the end effector will be like, and thus could have zero to three degrees of freedom.

There are few upper-body exoskeletons to compare against, and thus comparison will be difficult. PERCRO reports that they have 22 independently actuated DOF [6], whilst SARCOS are commercial and do not release clear indications of the amount of powered and unpowered DOF. BONES has three DOF at the shoulder, one at the elbow and a distal module give forearm supination and wrist flexion [20]. HARDIMAN has six DOF with only radial/ulnar deviation (the motion of moving the wrist on the plane defined by the palm) not being supported [9].

With comparable systems supporting the full DOF for the shoulder and elbow, this would need to be matched for the exoskeleton design, though wrist motion support is variable.

2.3.3 Joint Design

In order to give the motion, the design of the actuation with the joint is critical.

BLEEX uses "bidirectional linear hydraulic cylinders in a triangular configuration with rotary joint" [10]. The location of the endpoints do not have a singular solution [2], and thus several equation-based models have been developed [2, 21]. The location of the cylinders in terms of anterior and posterior was also determined from the asymmetrical nature of a double-acting cylinder and the direction of joint motion that required the largest torque [2]. Rotary hydraulics were seen as too leaky or having high friction and were not chosen [21].

BLEEX currently uses three separate axes for multiple rotations around the hip [22]. Two of these appear to be intersecting with the user's hip, but the hip rotation is off the centre line. This is shown in Figure 2.5.
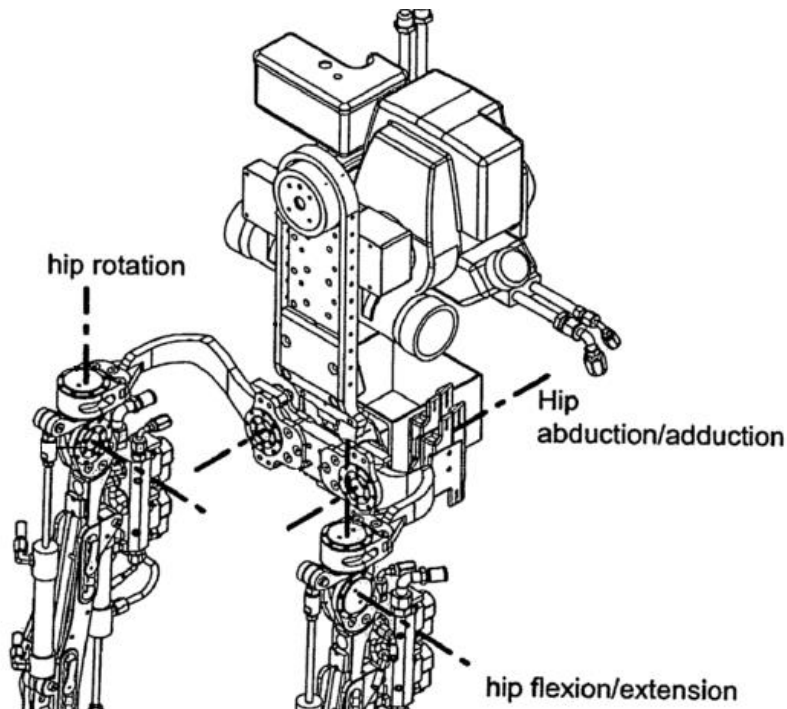
Figure 2.5: BLEEX lower extremity enhancer showing the axes of rotation for the hip [22]

With one of the axis not in line with the user, this would need to be compensated for with other components to prevent injury to the user. Similar systems appear in other exoskeletons due to its simplicity [23, 24], though alternatives that line up all three axes would be preferable.

SARCOS has several patents including ones for the joint mechanisms [23]. The patent covers a rotary drive that is driven by a variable radius pulley linked to flexible tendons being actuated by two or more linear hydraulic actuators.

HAL and PERCRO use electric drives, either harmonic or DC motor. It is unclear how HAL utilises the drive, but PERCRO uses them to drive ball screws to pull on cables to cause rotation directly on the pivot of the joint, similar to SARCOS.

PERCRO have patented a four-bar linkage for the shoulder and hip joints that keep the intersection of the two other axes at the same point. This is shown in Figure 2.6

Actuator two apparent axis

Centre of rotation

Actuator one axis

Actuator two input axis

Actuator three axis
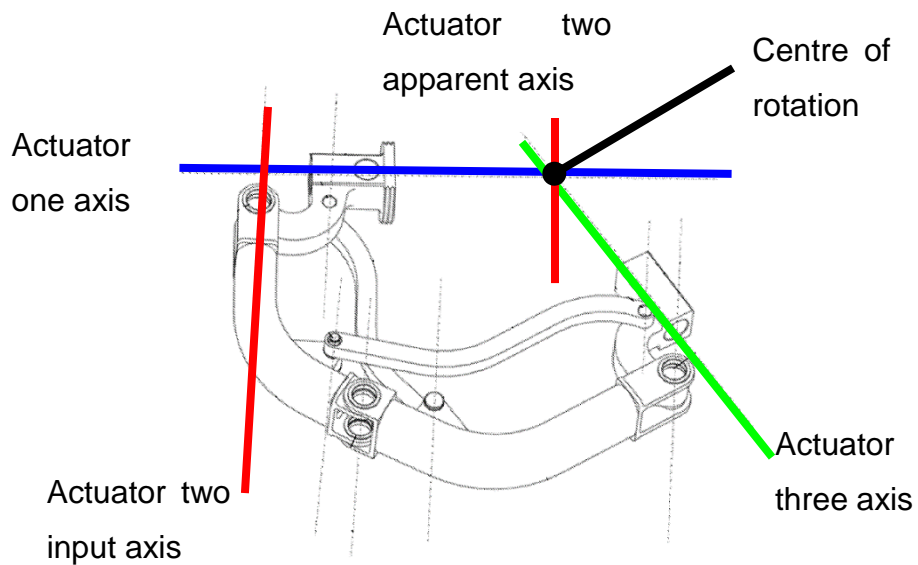
Figure 2.6: Outline of a for four-bar linkage joint for an exoskeleton shoulder or hip [25]

Actuator one and three axes are directly in line with the centre of rotation and are the pivot points for the abduction/adduction and flexion/extension respectively. To give the rotation around the centre of rotation, the axis of actuator two does not intersect the centre of rotation. Using the four-arm mechanism, this moves the rotational axis to intersect the centre of rotation. The four-bar mechanism keeps actuator three's axis intersecting the centre of rotation.

This is a simple design but is currently patented by Sant'Anna School of Advanced Studies for the use of an exoskeleton for the shoulder or hip joint. The first claim in the patent is for the physical setup as shown in Figure 2.6 and would require significant alteration to prevent the infringement of the patent.

Nurse-assisting Exoskeleton has the actuators to the rear of the unit so that there is no interference with the user. Ideally, this would be preferable for all units, though will limit certain motions.

There has been research into developing a high force, low mass exoskeleton using a parallel shoulder mechanism called BONES [20]. It uses two cylinders to position the rear of another actuator actuators. These second set of actuators are connected along one of the axes of the elbow joint. This is shown in Figure 2.7
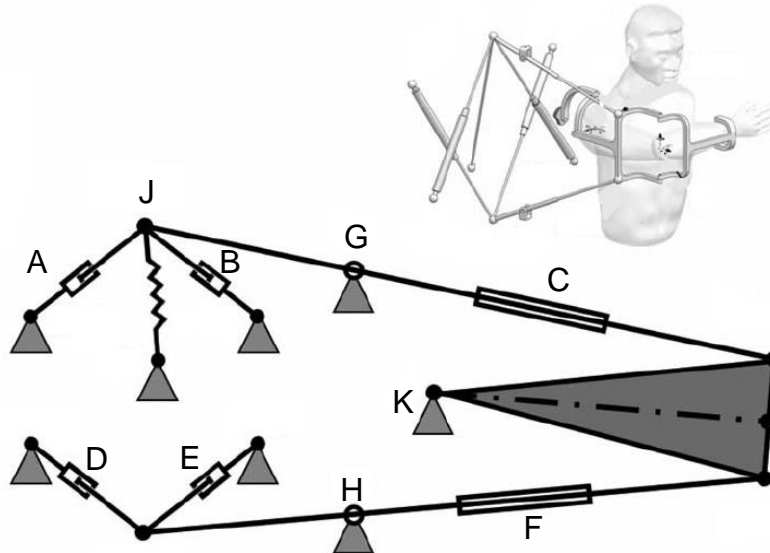
Figure 2.7: Shoulder-mechanism actuation diagram. Four cylinders configured in a "diamond structure" (A, B, D and E) drive two bars of changing length, i.e., C and F, respectively. Each bar is hinged by a yoke (G and H). A spring attached to J provides partial weight support for the arm. Point K is the centre of rotation for the shoulder. (Top right) Schematic solid model of the shoulder mechanism actuation is shown [20].

The amount of space required to the rear of the arm is large and would require significant mass to support the loads. The current loading is limited to 22Nm, but the system is capable of 42.2Nm [20].

There is an issue with the range of motion for the system. For the shoulder rotation, BONES has 105° of rotation compared to a human's 200°. For the shoulder flexion/extension, BONES has 80° of rotation compared to a human's 222°. For the shoulder abduction/adduction, BONES has 100° of rotation compared to a human's 225°. Analysis of the range of motion required for the exoskeleton has not been determined and thus raising the question of the viability of this design. Once a system has been completed, then a reduction in the motion range is possible, but to increase the range is likely to be more complicated.

This system is too large for a mobile exoskeleton system, and the suitability for other multiple degrees of motion joints is questionable.

The use of a spherical guide surfaces to allow three degrees of freedom within an exoskeleton joint has been patented by Boldt [26]. It is unclear what the

range of motion is available in rotation or abduction/adduction of the joint. An image from the patent is shown in Figure 2.8.
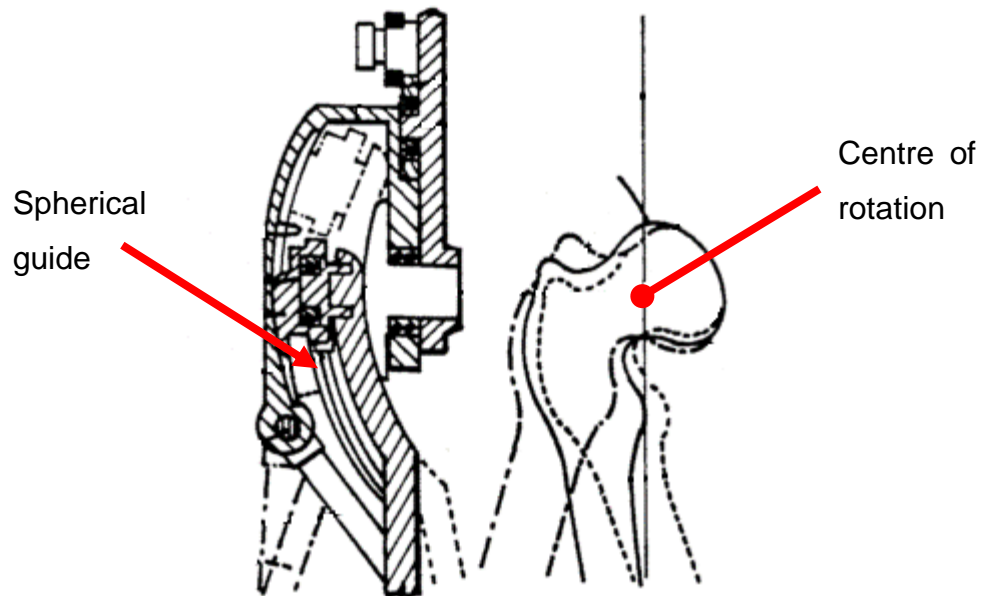
Figure 2.8: Three-axis mechanical joint for a power assist device, an alternative embodiment [26]

The claims in the patent are for a mechanical joint coupling two frame members around three mutually perpendicular axes. It does this with the use of multiple spherical guide surfaces that intersect the centre of the biological joint. Similar to a linear slide, actuators would then pull a second frame along the spherical guides.

2.3.4 Power source

BLEEX uses a hybrid hydraulic-electric portable power supply as it was deemed that hydraulics were "smallest actuation option available" with "high specific power" [10]. The hydraulic-electric power unit (HEPUs) on the BLEEX system is a 2.3kW internal combustion engine driving a hydraulic pump delivering 69bar of pressure and 220W of electrical power at 15V DC [27].

The BLEEX system uses a computer-controlled speed on the engine with it directly linked to the alternator and the gear pump. The pump is a gear pump with 3.2cm³ per revolution unit, running at 6300rpm at maximum requirements. If the engine is running with little requirement for hydraulic flow, the excess flow is returned to the tank via a solenoid valve. This would, therefore, introduce inefficiencies if the user spends time in a stationary or low motion state. It also

creates large variations of the engine load as the gear pump changes from delivering high pressure to dumping to the tank.

The high pressure is stored within an accumulator to allow for the dynamic response of the system. Once the hydraulic fluid has been utilised in the motion of the exoskeleton, 38% is used to cool the engine before being itself cooled in a heat exchange. Whether this causes increased degradation of the hydraulic fluid is unknown. The gear pump for the BLEEX system requires the oil temperature to be less than 65°C though cooling the engine increases the temperature of the oil higher than this. A heat exchanger brings the temperature down to below 60°C and resides in the tank at around 60°C. HSE recommends that water temperatures are kept at below 44°C to prevent scalding, with surfaces also below this temperature to prevent burns [28].

Similar to the BLEEX system, Sarcos uses hydraulics for actuation, though it is a tethered system and thus requires an external source. The size of the source is not clear, and thus whether it can be made portable is unknown.

For the electrical systems of HAL and PERCRO, the use of tethering is less of an issue that hydraulics as it would be a single power cable if the control systems can be attached to the frame. With the use of just electrical power, there is thus the question of what voltage and current are required.

The Nurse-assisting system uses pneumatics, and thus requires a compressor. Being a 'clean' source, with strict regulations over the usable pressures, the use within a building with a pneumatic infrastructure is simple and easy. Pneumatics in industry tend to have a centralised source and piping around the site, and as the exhaust can be vented to atmosphere, there is only the requirement for a single hose. The electrical requirements are lower than the pure electrical systems, as it only has to power the control system of computers and valves and thus could be run of local mains or battery power.

2.3.5 Safety

The noise of BLEEX's HEPU was determined to be 78 dBA at 1.5m from the unit at full power. The final results were 87 dBA whilst outside. In the UK, the limits for action to protect hearing are 80dBA for daily or weekly exposure [29]. For the BLEEX system, this is over the maximum exposure limit allowed. For a short duration, a daily exposure ready-reckoner gives 4 hours of daily exposure

[30]. This is based on the 80dBA allowing noise exposure points of 84, and cross-referencing with the 87 dBA that the BLEEX exposes the user to gives around 4 hours. The 87 dBA was also recorded at 1.5m from the system so would, therefore, be louder for the user, and this time duration reduced. Other systems have not reported noise levels at this current time.

2.3.6 Areas of limitations

BLEEX being a research project has outlined one initial design flaw in that the knee actuator was found not to be suitable for the torque requirements of a walking cycle, due to the difference in location of the joint to the human knee [2]. Thus the development of the system needs to take into account the full torque range required and make sure that the system can follow the human motion without encountering singularities.

SARCOS is currently tethered and thus does not have the mobility of the others. It is also unclear on the tethering type, whether it is hydraulic lines or just electrical power to a pump on the device. Thus an understanding of the power requirements is necessary to assist with the power source selection and to determine whether the system can be untethered or not.

PERCRO does not have enough power within the joint designs to allow normal walking speeds [6]. The maximum joint velocities are limited and resistance forces are higher than expected. With a system designed to have a lower load upon the user, the forcing of an unnatural gait is a limitation of the system. Thus making sure that the motion is capable of following the human without undue loading is required.

HAL is assistive, and thus the capability for the enhancive system in unknown. Though there are images of the system for augmentative applications, this is not expanded on. The images just show the load is lifted in the crook of the elbow. Thus for an enhancive system, the load interaction is critical to give the largest flexibility for the user.

2.4 Power source

There are several different technologies that can be utilised in an exoskeleton system for actuation, with hydraulics, pneumatics and electrical being primary

sources. There are several other technologies that could be utilised for part of the system [31].

Hollerbach et al. have conducted a review of actuator technologies for robotics [31], though there are also generalised reviews of the technologies available [32].

Comparing stress versus strain, shape memory alloys and hydraulics have the largest values for each, as shown in Figure 2.9. Some options give similar strains as hydraulics like muscles and pneumatics though they are several orders of magnitude smaller in stress. Similarly, there are options that give larger stress that hydraulics like magnetostrictor and thermal expansion though orders of magnitude smaller strains. Comparing the constant stroke work for these systems (diagonal lines from top left to the bottom right marked as J·m^{-3}) [32] gives hydraulics the highest energy density followed by shape memory alloys.
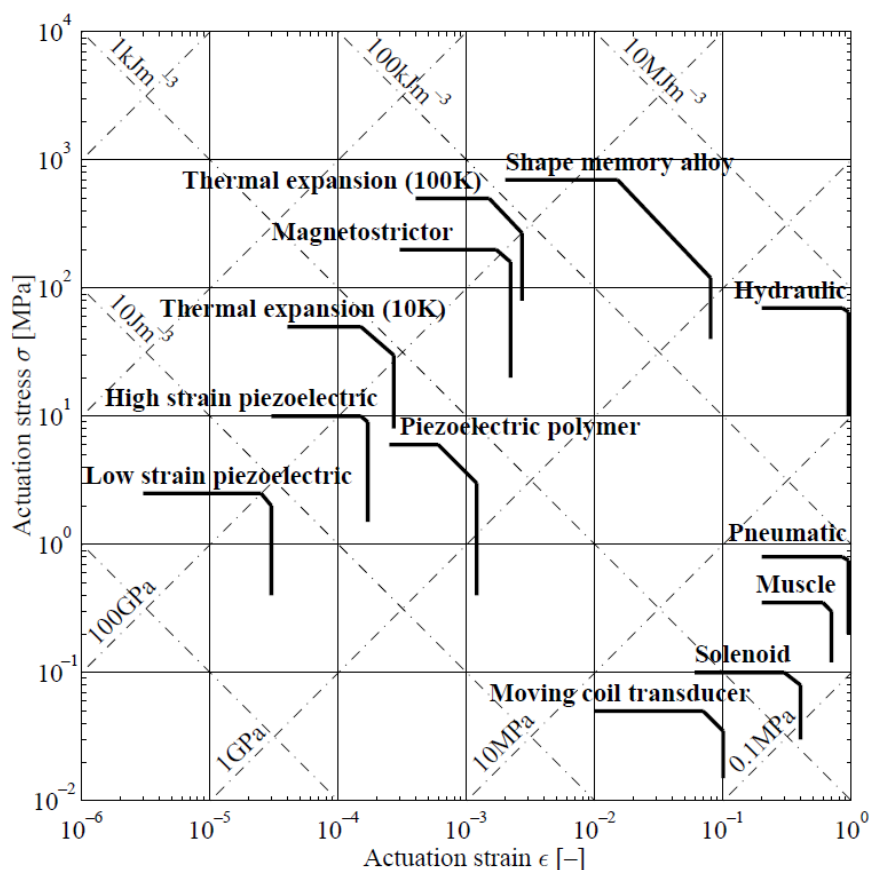
Figure 2.9: Actuation stress, σ, versus actuation strain, ε, for various actuators. Heavy lines bound the upper limits of performance [32].

Comparing the specific actuator stress versus strain, Figure 2.10, [32] shows that hydraulics is also the obvious choice with the highest energy per kg capability.
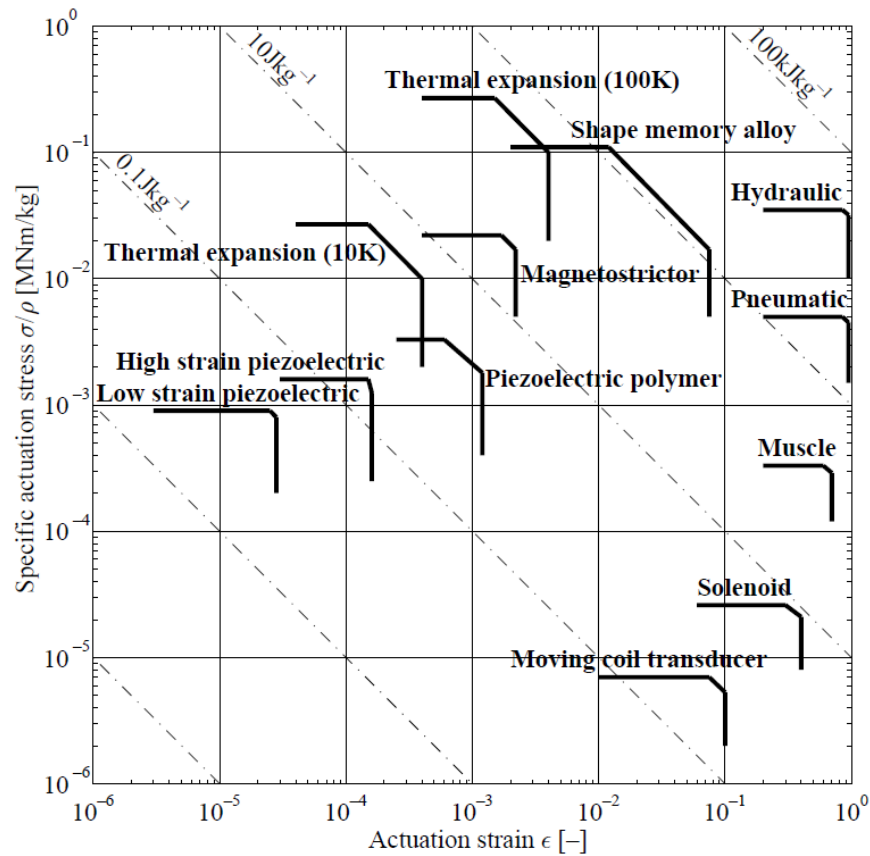
Figure 2.10: Specific actuation stress, σ/ρ, versus actuation strain, ϵ, for various actuators. Heavy lines bound the upper limits of performance [32].

When strain resolution is a factor, hydraulics is not the ideal choice for the system and is similar to pneumatics and shape memory alloys, see Figure 2.11. Hydraulics do have improved resolution compared to muscles, so this does mean that hydraulics should match the user position correctly.

A final positioner unit could be attached to the end of the hydraulic systems to give smaller movement control could be a possibility if it is required. One area that it could be vital would be fine finger control as picking up or holding small or fragile components. Piezoelectric actuators, particularly the polymer variety could be used, which have a similar resolution to strain ratio as hydraulics. The control for this would require non-anthropomorphic input, or anthropomorphic but with large scaling i.e. matching angle opening of the hand rather than the fingertip to thumb gap.
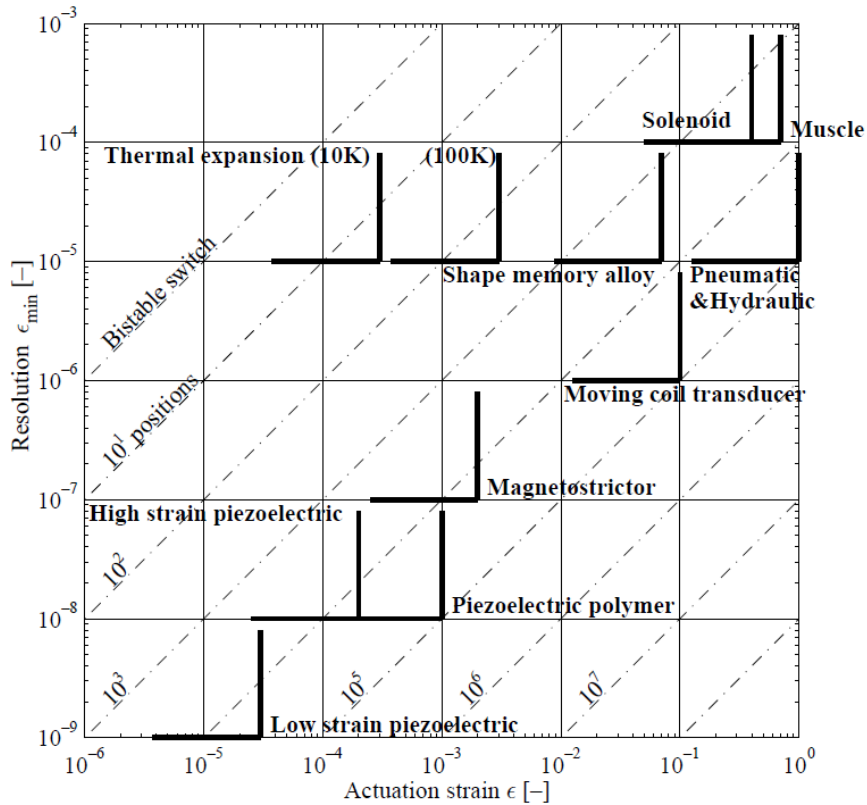
Figure 2.11: Strain resolution, ϵ_{min}, versus actuation strain, ϵ, for various actuators. Heavy lines bound the limits of performance [32].

The frequency of response can also be compared [32] with electrically controlled components like magnetostrictors and piezoelectric units having the highest available frequencies. Hydraulics have a reasonable maximum frequency response between $5x10^1$ and $3x10^2$ range, which is similar to the muscle frequency range at $5x10^1$ and $5x10^2$.

Huber shows that there are some options that have high efficiency with large power per unit volume, with hydraulics being one of the options. Pneumatics and solenoid units have lower efficiencies but factors smaller for power per unit volume. When comparing stress-strain versus frequency, hydraulics are of a similar frequency to muscles and pneumatics, though have higher stress-strain.

Hydraulics and pneumatics use a fluid medium to transfer power from source to motion. Hydraulics has been utilised in exoskeletons since very early designs like Hardiman right up to modern variants like BLEEX and SARCOS [10]. This is due to its high stress, strain and torque/mass and power/mass abilities. It is less efficient than electromagnetic and pneumatic systems, though research is currently in progress to determine what capabilities can be improved [33].

There are several options for using pneumatics but they all are based on the flow of air into a closed environment, similar to hydraulics. A lot of the basic theory of hydraulics can be transferred to pneumatics, though there are several differences between their usage.

The compressibility of air is significantly higher than that of water or hydraulic fluids, so though it gives compliance in the motion, the difficulty of the control is increased for quick movements.

Air is also cleaner than water or hydraulic system in a system leak. Air can be vented to the atmosphere though there might be a small amount of oil within the air for lubrication of the internal control system. A water hydraulic system will contain glycerol and other additives to protect internal components from wear and thus leakage needs to be at a minimum to prevent environmental contamination.

2.5 Motion Units

Following on from the structural design of the joint, there is the selection process for the actuators.

2.5.1 Linear actuators

There are three major structural designs for linear actuators: screwed, tie rod and welded cylinders, with a larger range of connection methods. Each of the structural designs could be used, though the pressure limits and sizing would dictate which would be suitable. The connection methods would thus be a larger driving force for each option.

The strength and buckling of linear actuators are examined in Appendix A.

Linear actuators require a mechanism to convert the linear to rotary motion. The mechanism should give at least the required torque throughout the rotation, as well as the full range of motion. As seen in BLEEX [2], this can be difficult to achieve, and thus the design of the joint mechanism with the actuator is critical. The moment arm and singularities can cause issues if they are not calculated correctly during the design phase.

2.5.2 Rotary actuators

As the exoskeleton is based around linear section rotating around a single point. This means that rotary actuators could be utilised within the system. Most industrial excavators use linear actuators for moving the arm, with rotary actuators for smaller motion parts, for example, steering units, or any motion that requires a large swing, for example, conveyor swing.

2.5.2.1 Vane

Rotary units come in two main variants: motor and oscillating actuator. Motor units have varying overall efficiency with pressure [34], with 1000psi (68.9bar, similar to BLEEX) having 86% overall efficiency. As the pressure increases, the volumetric efficiency decreases due to the expansion of the unit, increasing the leakage. The torque efficiency increases to a stable level, though this with the volumetric efficiency gives a limited area of high efficiency. A hydraulic motor works by flowing the hydraulic fluid through to give a continuous rotation of the shaft. This is unlikely to be overly useful for a system that has a fixed range of angular motion.

Oscillating actuators rotate the shaft between fixed angles, with the range dependant on the design. A vane actuator uses a shaft within a cylinder with two chambers. One dividing wall of the chamber is attached to the cylinder body with the other to the shaft. As pressure is pumped into one chamber, it pushes against both diving walls, forcing the shaft to rotate. To increase the torque of the actuator, it can have additional vanes installed, creating multiple chambers, though this reduces the angle range that can be travelled. Figure 2.12 [35] shows a simple version of this.

(a)   (b)
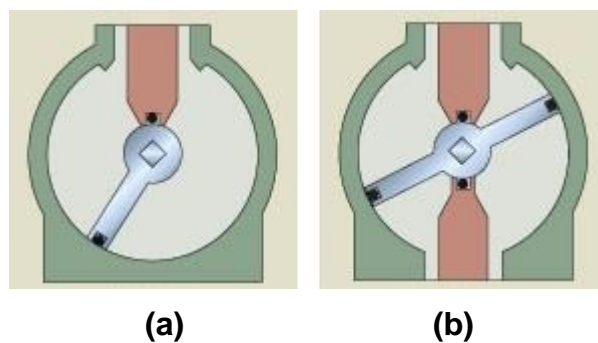
Figure 2.12: Vane actuator overview. a) single, b) double [35]

Leakage is an issue with the vane actuators, and this value will tend to be given with the specifications of the component. This would mean that the control system would need to compensate for the slow slippage of the system. The control of this would be dependent on the valve or pump controlling the system, with the larger the supply unit, the increased difficulty of giving a low compensatory flow. BLEEX looked at vane actuators, but due to the leakage did not decide to use them [2].

2.5.2.2 Helical

A helical shaft unit uses a linear piston with a helical thread on the inside. This piston either has another thread on the outside or guided by linear rods. The internal rod of the system has a matching thread to the piston such that as the piston travels up the cylinder, it causes the internal rod to rotate. This means that the dimensions are similar to a linear actuator, though the output is rotary rather than linear. The amount of rotation is dependent on the angle of the helical threads, as well as the travel of the piston.

Figure 2.13: Example helical actuator showing threads [36]

There are few manufacturers of this style of actuator due to the increased complexity, and thus the price tends to be higher than that of other designs. The use of them appears to be linked to industrial mobile equipment, either excavators or a more specialised system like refuse lorries. The higher axial bearing load that helical actuators can support is a benefit an exoskeleton system as joints rotate.

2.5.2.3 Scotch yoke and rack and pinion designs

A scotch yoke or rack and pinion actuator use a system similar to linear actuators, though with the rotating shaft between the two pressure faces. As the rod travels linearly, it is attached to the shaft with a yoke or rack and pinion causing rotation. To increase the amount of allowable rotation, cylinders have a corresponding increase in length. A scotch yoke system is limited to 90° to stop any binding of the joint, though a rack and pinion unit can have a larger rotation range. Figure 2.14 shows a simple version of a scotch yoke.

Figure 2.14: Scotch yoke actuator overview [35]

Due to the opposing piston action, these units can be long especially for high angles of rotation. Units tend to come in steps of 90°, though manufacturers do claim to be able to customise them for specific angle ranges. The larger the stroke the longer the actuator which could cause interference with other components.

For the rack and pinion design, there is a risk of backlash due to the interaction of the teeth. This would introduce positioning errors into the system.

The Scotch yoke system has a smaller range of motion than the rack and pinion design as it would have singularities.

Crank style

A variant of this would be two linear cylinders connected to yoke arms at 90 degrees to each other. This 90 degrees phase shift removes the singularity as is used in steam locomotives for powering the rotation of the drive wheels.

2.5.3 Conversion methods

As the joints on the exoskeleton are all rotary, the direct drive option is the simplest solution, though the conversion of the rotary into linear back into a rotary motion does give different packaging options. BLEEX has a linear to rotary conversion [2], SARCOS has linear to rotary [23], and PERCRO has rotary to linear to rotary [6].

2.5.3.1 Lead screw

The simplest method is the use of a lead screw that converts the rotary motion into a linear displacement where, the motor would be used to turn a screw rod, with an acme, ball or roller nut. Each type of system has its own advantages and disadvantages, which are compared against hydraulic and pneumatic cylinders in Table 2.2.

A simple nut system would generate significate wear and it is reported that up to 70% of the power is dissipated in heat compared to the 80% efficiency of the ball/roller systems [37]. Roller screws are recommended over ball screws for tasks that have higher requirements in precision or motion [38].

The Ultra Power roller screws by SKF [39] is designed to have an increased load-carrying capacity compared to the standard units. This means that a smaller unit can be used for a similar load, reducing the weight of the system. The smallest rod diameter is 60mm, which gives a load rating of 494kN, which is likely to be significantly higher than required.

Table 2.2: Comparison of linear screws against design as well as hydraulic and pneumatic cylinders [40]

	Exlar Roller Screws	Acme Screws	Ball Screws	Hydraulic cylinders	Pneumatic cylinders
Load ratings	Very High	High	High	Very High	High
Lifetime	Very long, many times greater than ball screw	Very low, due to high friction and wear	Moderate	Can be long with proper maintenance	Can be long with proper maintenance
Speed	Very high	Low	Moderate	Moderate	Very high
Acceleration	Very high	Low	Moderate	Very high	Very high
Electronic Positioning	Easy	Moderate	Easy	Difficult	Very Difficult
Stiffness	Very high	Very high	Moderate	Very high	Very low
Shock Loads	Very high	Very high	Moderate	Very high	High
Relative Space Requirements	Minimum	Moderate	Moderate	High	High
Friction	Low	High	Low	High	Moderate
Efficiency	>90%	approx 40%	>90%	<50%	<50%
Installation	Compatible with standard servo electronic controls	User may have to engineer a motion/actuator interface	Compatible with standard servo electronic controls	Complex, requires servo-valves, high pressure plumbing, filtering pumps, linear positioning and sensing	Very complex, requires servo-valves, plumbing, filtering, compressors, linear positioning and sensing
Maintenance	Very low	High due to poor wear char-acteristics	Moderate	Very high	High
Environmental	Minimal	Minimal	Minimal	Hydraulic fluid leaks & disposal	High noise levels

The inverted roller system, where the thread is on a rotating, but a linearly fixed unit, that moves a rod linearly, similar to a hydraulic actuator. This will have a similar issue of the minimum length of the system, whereas the standard system would have a rod the complete length, and move the nut along to the correct position.

The system would require a motor source for the motion. This could either be an electrical or hydraulic motor mounted to either be a direct drive or via a gearbox to shorten the length by increasing the width. There could also be the option to have the lead screw as part of the motor.

2.5.3.2 Wire cable

The SARCOS joint is covered under patent 8,516,918 B2 [23], Figure 2.15, which claims it is a variable torque device using a variable-radius pulley and antagonistic actuator pairs. This means that to prevent infringement, any pulley system should have either a fixed radius pulley or a not antagonistic pulling system. This could be done with a single actuator and a lower pulley to create a loop around the system, though other systems have looked into this. This is shown in Figure 2.16.
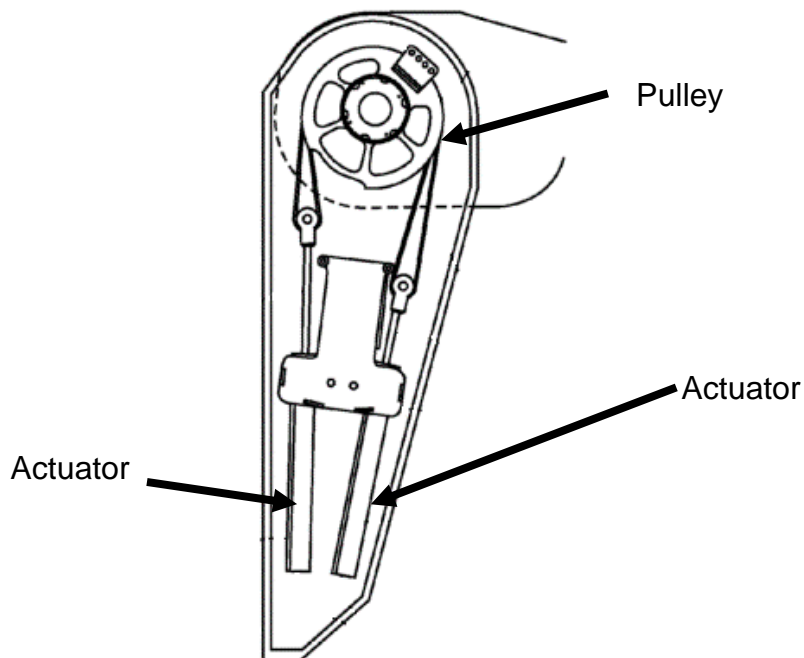
Figure 2.15: Details of the Raytheon actuator used in the SARCOS system [23]

PERCRO [41] uses a variant of Figure 2.16 using a pantograph to replace the idle pulley, as shown in Figure 2.17. They have reported that it is able to give

- 31 -

out 500Nm at 60°s⁻¹, to a maximum of 100°. They have also reported that it has more than 85% mechanical efficiency with a torque density of 80Nm·kg⁻¹. This compared to rotary hydraulics which has a range of 10,000 to 44,000 Nm•kg⁻¹ [32].
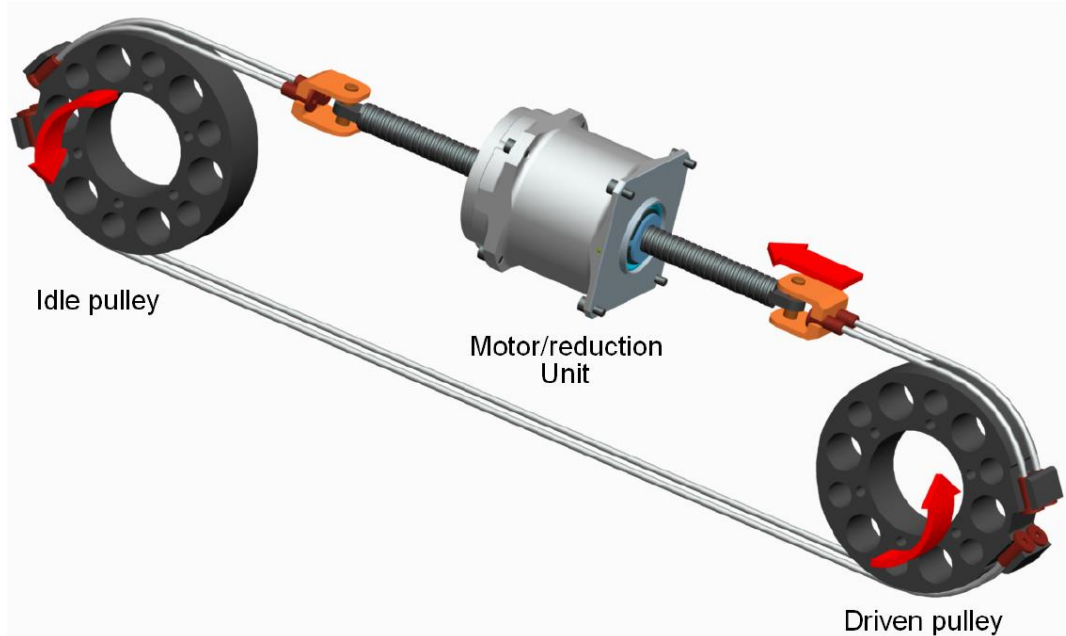
Figure 2.16: Example of a cable system. The actuator moves the cable in both directions causing one limb to rotate. The cable is looped around two pulleys to complete the circuit [41]
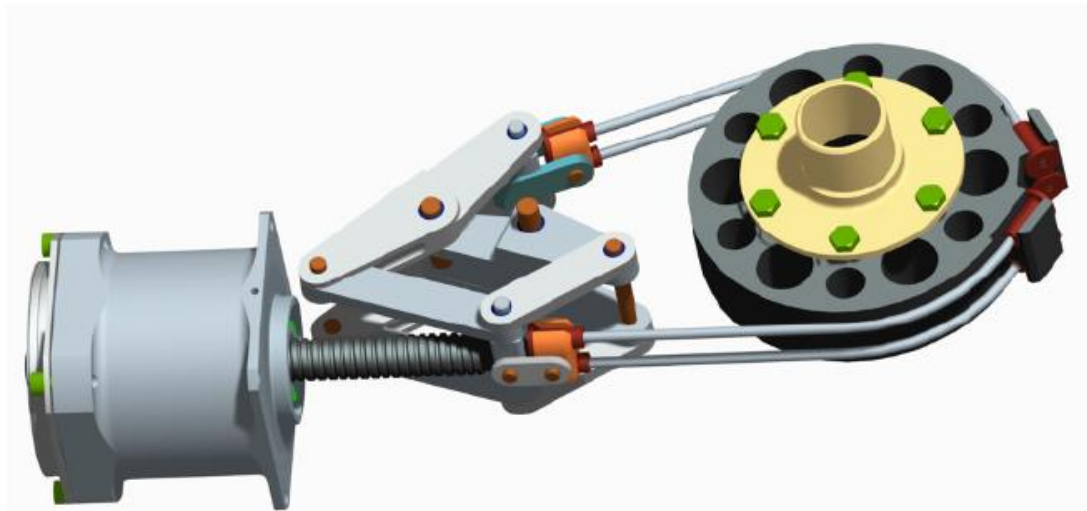
Figure 2.17: PERCRO actuator unit without the case to show the internal mechanism [6]

The main issue with the use of cables is the strength rating of the cables and the diameter of the pulleys. With cables, it is recommended that a safety factor of five is used to guarantee the life of the cable [42-44], which drops with a reduced design factor as shown in Figure 2.18.

This is also compounded if the wire rope has to bend around any pulleys. The smaller the ratio of pulley diameter (D) to rope diameter (d), the greater the reduction in strength as shown in Figure 2.19. For a tension rope with bending during movement, it is recommended that a ratio of D/d be 40 [44].
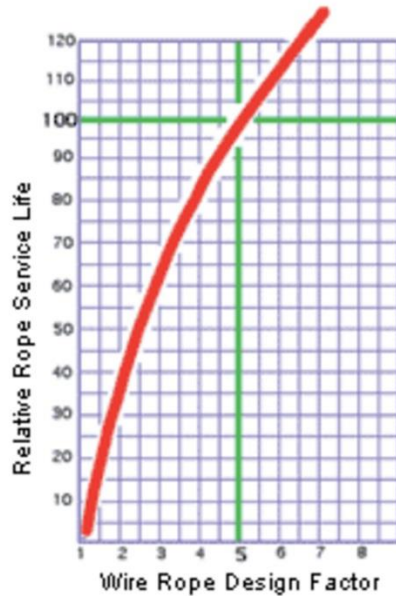
Figure 2.18: Wire rope design factor against relative rope service life [42]
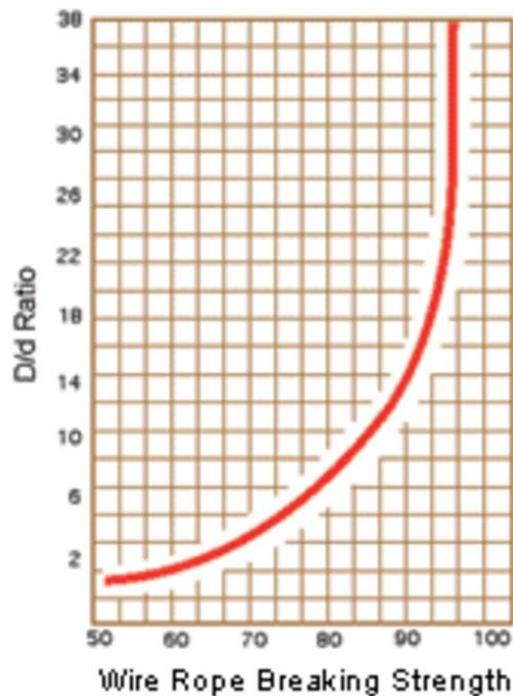
Figure 2.19: Wire rope breaking strength percentage against the D/d (pulley diameter/rope diameter) ratio [42]

For PERCRO, they report that its nominal torque is 500Nm from an 8000N continuous thrust force. This gives a radius of the pulley to be 62.5mm. Using

the data from BS EN 12385-4 [43] and Python, the cable size for 8000N is 4mm diameter for the strongest cables but with the increase to a design factor of five, it is 8mm.

The bend radius of the cable is also important, as any bend will reduce the strength of the cable, which would require a larger diameter cable. Using the D/d ratio of 40 from above, the diameter of the pulley should be 320mm, whilst PERCRO has it as 125mm. Using Figure 2.19, the ratio is only 15.6 and thus has a strength of around 91%.

This means that there are no cables that can comply with the design factor of five and the D/d ratio of 40. Only with ignoring these requirements can a cable be selected. This would lead to questions over strength and fatigue life, and what would happen if the system failed.

If the pulley diameter can vary, and only the loading and design factors are considered, then a cable can be selected. From the BSI and Python set, the pulley diameter varies between 240mm and 400mm as shown in Figure 2.20a. The red line shown is D/d = 40 showing that the results are only for combinations above this point. The 5mm results do not reach down to this line as the strength of the cables is not high enough for these combinations.

There are nine cables that have a pulley diameter of 240mm, with the lightest per meter being diameter 6mm class 6x7 with a steel core and to a rope grade of 1960.

When compared to the human, the size of the pulley is unfeasible. The length of the 50th percentile shoulder-elbow length is 363mm and the 50th for elbow-wrist is 287mm [45].

To have a small cable and a small pulley, the strength of the cable needs to increase. If the cable is 8mm in diameter, and the pulley is the PERCRO 125mm, then the stress in the cable is 159 kNm^{-2}. For the 6mm cable, it is 147.3 kNm^{-2} and for the 5mm cable, it is 143.9 kNm^{-2}.
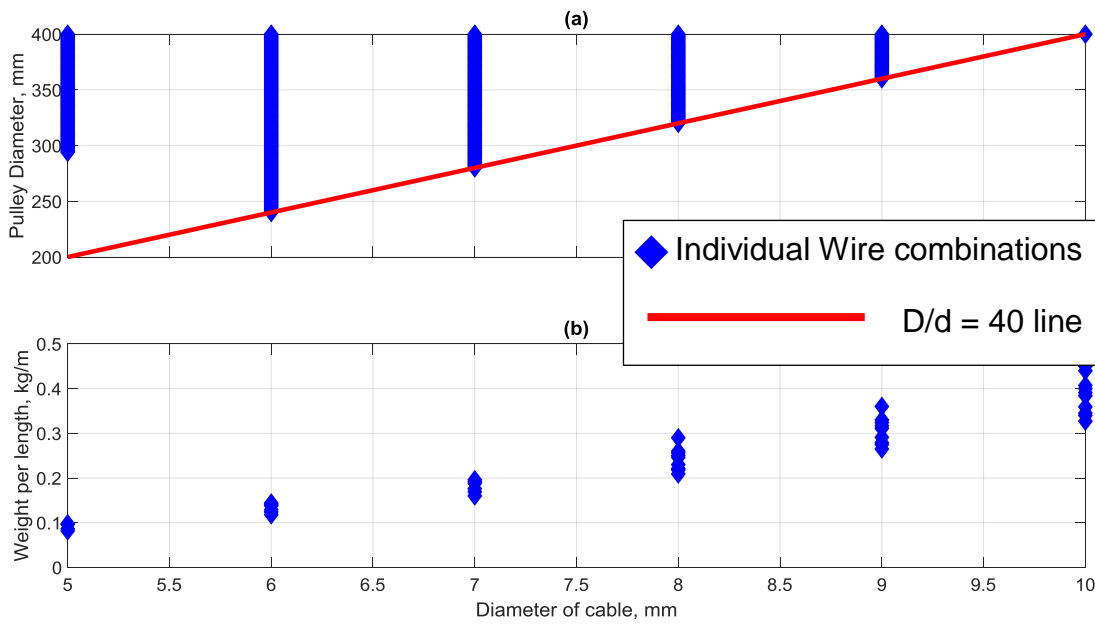
Figure 2.20: Cable diameter versus a) pulley diameter and b) weight per unit length with ♦ showing the individual combinations and the line being D/d = 40

The use of cable is questionable as for a smaller pulley, you need a smaller wire to stay above the D/d threshold, but a smaller diameter increases the force required for the cable with a larger cable being able to support a larger load.

The question of using stronger materials, like titanium, have been studied before for example in 1973 by Milburn [46]. His results concluded that though the titanium was stronger, the fatigue life was shorter compared to the cheaper steel solutions.

Rigid chain

A rigid chain or linear chain is a variation of a rack and pinion where the rack can bend in one direction. The chain is designed so that in one direction the links lock together and prevent bending, as shown in Figure 2.21. Another variation is similar to a zip where two chains are interlocked together to form a rigid beam.
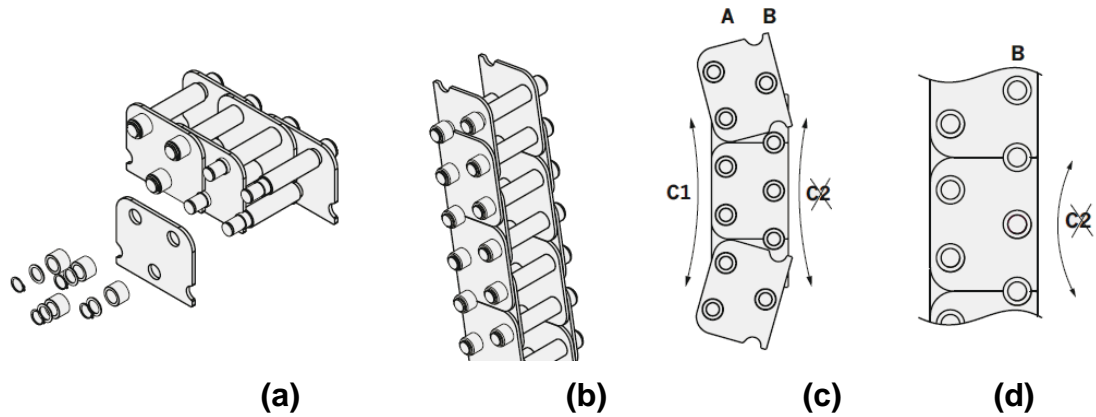
Figure 2.21: Technical information on Serapid's Linklift chain. a) shows the components of the chain, b) shows the completed chain, c) shows the allowed curvature, C1 and d) shows the prevented curvature [47]

Rigid chains are primarily used for lifting of weight, either for building components like windows or for larger system utilised in theatres.

The force output of rigid chains can be in the kN range as they are designed for lifting heavy loads. Serapid is an example company that supplies units for a variety of projects and their standard model range for the LiftLink system ranges from 20kN to 200kN.

As the chain can push as well as pull, there is no need for a pantograph system as used in the PERCRO system, though guidance would be required to stop the chain buckling. This is normally done by having a secondary chain that will bend in the opposite direction such that as one tries to collapse the other restricts it. This can fail if both are pushed inwards but this requires an outside force to occur.

A chain is significantly heavier than cable and will only bend in one direction. Cable motion source can, in theory, be placed to the rear of the unit and routed to the joint, but the linear chain cannot.

2.6 Hydraulics

2.6.1 Valve system

There are several valve designs that can be utilised each with their own characteristics. Spool valves transfer flow between several chambers and can have a large range of flow path options. Depending on the design and area of

the valve, there can be large pressure imbalances in the design that can give restoring or opening forces that are opposite to the direction of demanded movement. Due to the large sealing areas to prevent flow between chambers, friction forces can also prevent the motion to start, and thus usage of pilot valves is required. Transfer flow can be an issue if the travel of the valve is small and flow is directed into two chambers.

Poppet or cartridge valves seal the flow with an edge, either a cone-shaped orifice using a ball to create the seal or an edge contact where a sharp ring contacts a flat plate. They can come in multiple port options and have greater efficiency than spool valves, though have nonlinear flow characteristics and larger time lags for motion.

Servo valves do generate power losses, from pressure loss through the orifices as well as leakage [48]. Servo valves control by energy loss and will generate inefficiencies within the system.

2.6.2 Pump System

A pump-controlled system can be either opened or closed. An open system is very similar to a valve-based system, though rather than relying on a constant flow source with overflow through a pressure control valve, it has flow on demand. A closed system does not have a tank to pull and return oil to and thus there is an increase of efficiency of the system with no valves to lose power to. A double rod system with symmetrical areas of the piston is simple to implement into a closed-loop system with issues of cylinder preload being the limiting factor for dynamic performance.

A pump control differential system has the issue of asymmetric areas of a single rod cylinder resulting in issues of oil transfer. Several groups have researched this issue, with patents raised on solutions [33]. These systems rely on a tank to store the differential flow of the system, with some utilising additional pumps to draw this extra fluid into the system. A compensating system with check valves could be a useful design setup if the pump and motor unit is small enough to be located close to the actuating mechanism. This would only require one pipe to return to a central tank, without requiring a second pump or accumulator [33]. Recent research into pump controlled differential systems has been

focused on to asymmetrical pumps [33, 49, 50] which does not require a tank source but has an accumulator to store excess fluid.

It is an area of study, with several projects working on creating efficient hydraulic systems [51]. Due to this, the design and development of the required hydraulic power pack would be a necessity due to the lack of available components sold.

For a hydraulic circuit, the flow through the circuit is controlled by the pump and the flow to and from the tank is equal assuming zero to minimal leakage. The pressure for the system reduces for each element within the system, with the peak pressure originating at the pump. The pump is a flow source and requires an enclosed volume to build pressure. The hydraulic equations as defined by Kirchhoff's laws [52] are generalised in Appendix B.

2.6.3 Hydraulic circuit design

Comparable hydraulic usage to the exoskeleton would be excavators and other large industrial machinery. These tend to be valve-based systems, but the recent focus has been on alternative circuit design [51, 53]. These are based on the idea that pump based systems will give increased efficiency. Huang [53] notes that

> *"to the best knowledge of the authors, there are not many studies on the performance of the hydraulic system, especially on the swing system of hydraulic shovel"*

Though the focus of Huang is on the hydraulic swing, it is unclear whether they are just focusing on a small area of research. Companies would do internal studies of their hydraulic performance based upon what their requirements would be. For example, a fuel injection system would be classed as a hydraulic system containing pumps and valves but due to the specific sizing and requirements would not be published into the public domain. Commercial advantage and intellectual property would be a major reason for any studies on hydraulic performance not being published.

Increased efficiency needs to balance against whether there is increased weight. There is also an issue of increased control complexity that would make the determination of motion and debugging of the system to make sure that it moves in a known way due to the human interaction within the system. With several different options available, each needs to be examined and analysed to determine whether it would be suitable for the exoskeleton system.

2.6.3.1 Valve systems

Valve circuits are typically used as they allow a single flow source and manual control of the motion. With increased automation, proportional solenoid valves are used, though whether this is still a viable design route or not is being researched at the current time. One main benefit of valve-based systems is the instant high-pressure availability and high response rate of the valves, with estimates of up to between 150 to 200 Hz for the bandwidth.

The valve-based system is also simple to set up and design as each actuator is linked to a single servo valve. This is shown in Figure 2.22. This will be the baseline against which all other circuit designs will be compared.
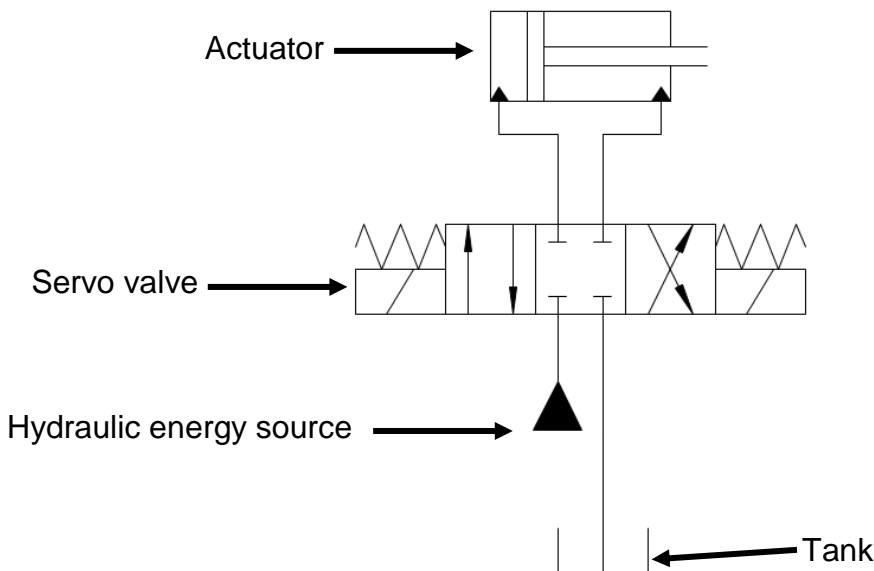
Figure 2.22: Basic servo circuit

Regeneration circuit

In a standard hydraulic valve based setup, there are a few options for energy recovery [54]. One method is with a regeneration circuit where the flow from the rod side is fed into the open side to supplement the flow, Figure 2.23.
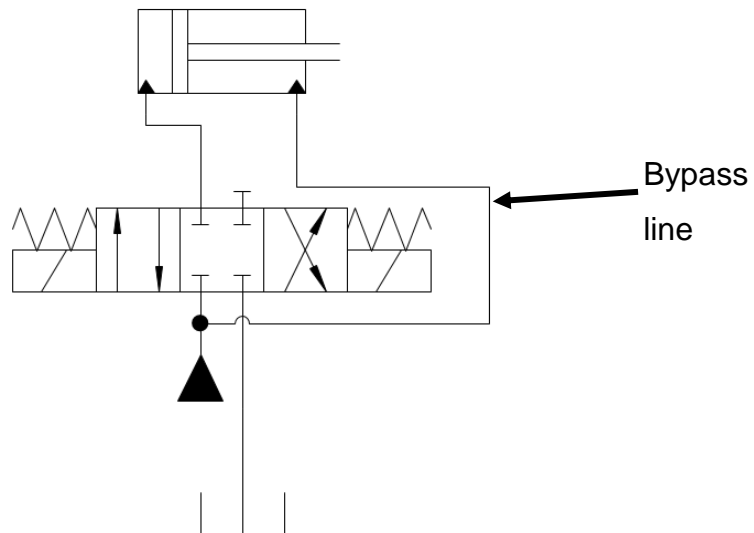
Figure 2.23: Basic Regeneration Circuit

This circuit works by the area differential of the piston causing the actuator to extend even though the pressure on both sides being equal. This causes flow from the rod side to be pushed into the extension side, supplementing the flow. This means that the supply flow can be reduced for the same extension speed, reducing the power of the supply source.

There are several issues with this circuit design. With the extension side seeing full pressure, the force output is reduced compared to the basic servo system. Retraction is also supplied only by the supply flow, which has been reduced. The controller would need to take this into account, and would also depend on the orientation of the actuator.

Regeneration circuit with full pressure override

To give the full pressure output, the circuit can be altered to include a check valve and pressure relief valve that will allow the system to give full force. This is shown in Figure 2.24.
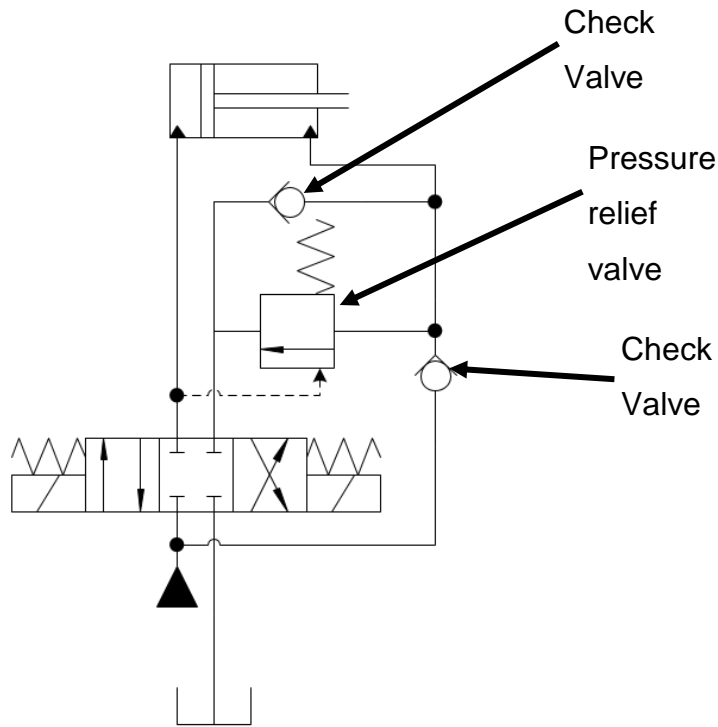
Figure 2.24: Regen Circuit with pressure-activated to full thrust

This does give full force, though at the lower speed of the supply system. This does not alleviate the slower retraction speed. Thus though this has some benefits over the basic circuit, there is the possibility that this still has control issues.

Alternative regeneration circuits

There are several alternative circuit designs, though these start to introduce additional valves, which would have their own associated pressure drops across them. Due to the system requiring to be as light as possible, these could end up adding additional weight for a small increase in efficiency. Most of the alternative designs have similar motion as the above units, though with additional components.

Flow divider design

One alternative design is the use of a motor style flow divider, Figure 2.25. This system uses the flow divider to split the flow between returning to the extension side and the valve. This means that when the unit is extending, then flow from the rod side is sent to both the extension side and the tank. When the unit is retracting, then the flow from the pump draws fluid from the extension side to support the retraction motion.
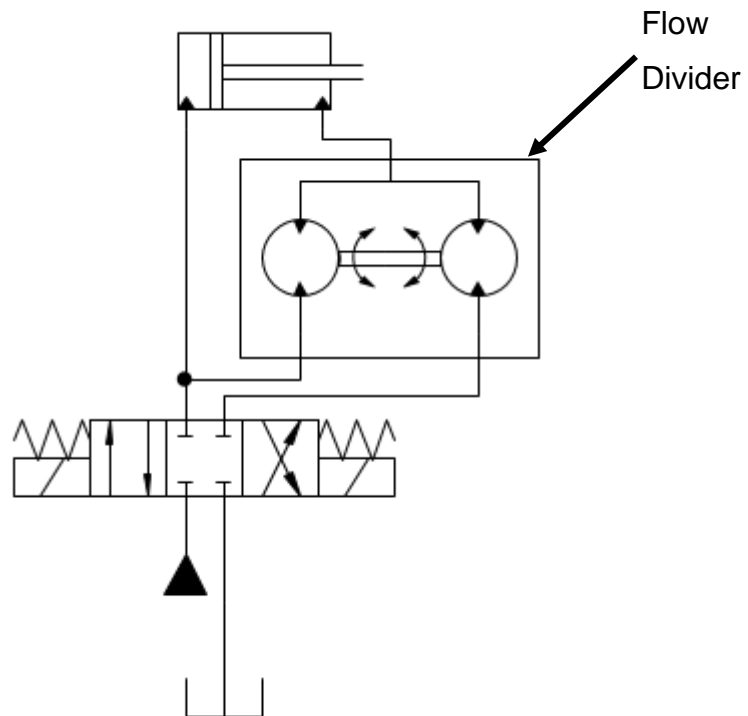
Figure 2.25: Regeneration circuit using motor-type flow divider

There are issues with motor-type flow dividers that could make this system inefficient. Motor type flow dividers tend to be inefficient at low flow rates, due to leakage across the component, and can even fail to work at these flow rates. Concentric is an example of a manufacturer and shows the performance of the units is dependent on the rotation speed of the system with 1500 RPM being the slowest that the unit will work. This is shown in Figure 2.26.

This circuit design also has the option for full pressure override, either with internal pressure controls (Figure 2.27) or servo valves.

Dual Servo Valve

The options to use solenoids for full thrust would allow improved control compared to hydraulically controlled units. Further development would lead to having two servo valves, Figure 2.28, each valve controlling each end of the actuator, allowing flow to transfer between the ends of the actuator. This would work similarly to the normal regeneration circuit, with full pressure option.

The cost of the additional servo valve would be a detrimental issue for this circuit design and a cost to benefit evaluation would be required to utilise it.
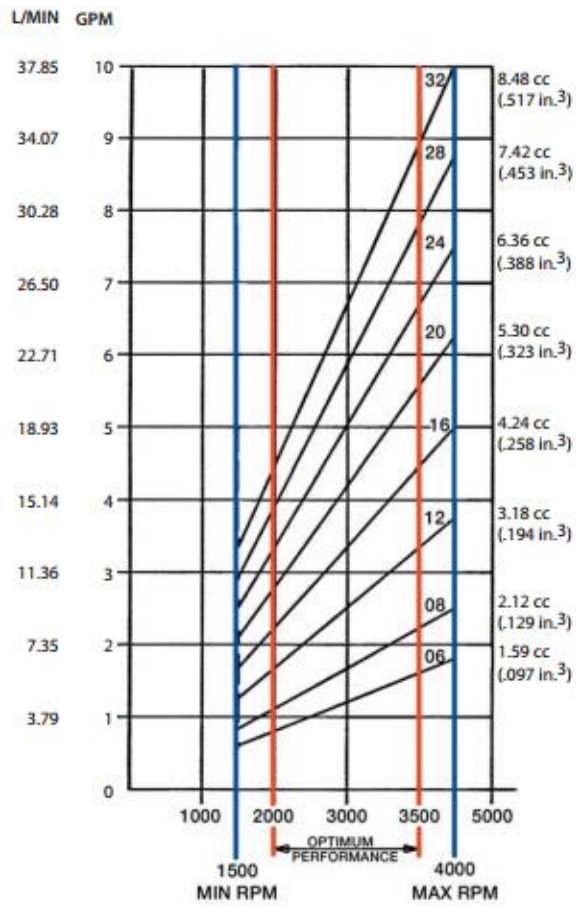
Figure 2.26: Performance characteristics of Concentric motor-type flow divider [55]
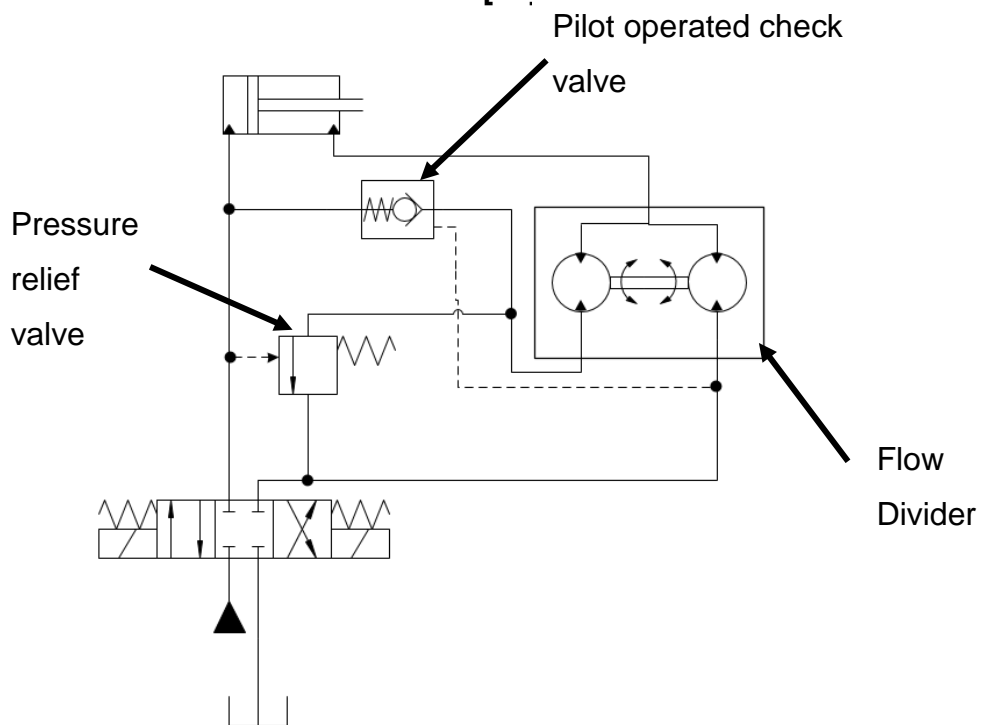
Figure 2.27: Regeneration circuit using motor-type flow divider with full thrust circuit
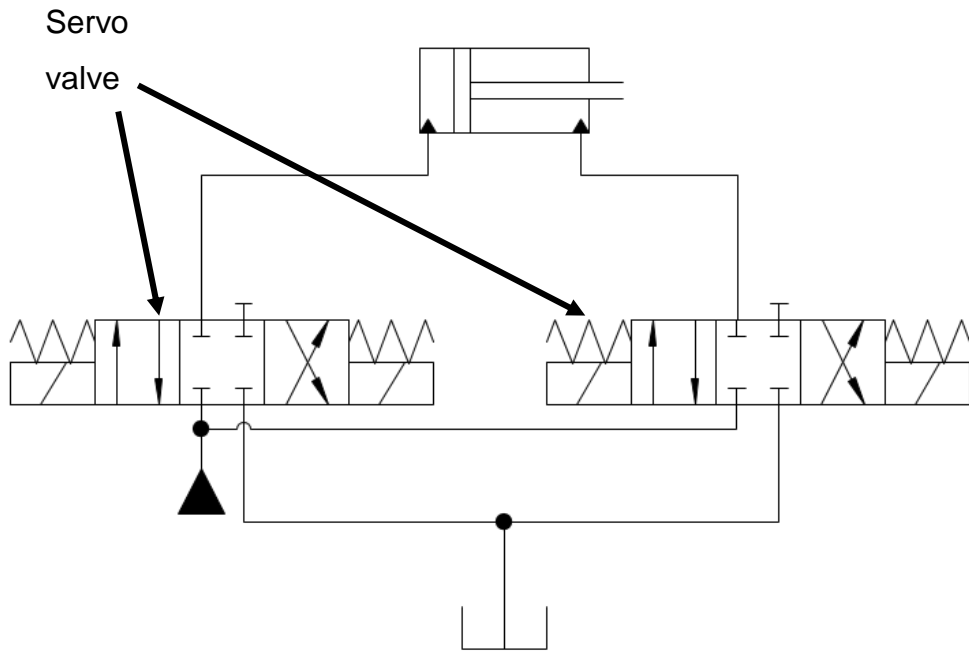
Servo
valve

Figure 2.28: Dual Servo regeneration Circuit

Examining the options, the majority of the regeneration circuits direct flow from the rod side to the extension side. This means that they will only work in one direction, which for a dynamic system is unlikely to be useful. The motor-type flow divider is able to support regeneration in both directions as it works similarly for the extension but then uses the flow into the rod side to draw fluid from the extension side. This would not work for a normal spool-type flow divider, as it would not create the vacuum required to draw the flow from the extension side. The option to allow full thrust would be required to allow the full force to be delivered for the system. Whether this is pressure-controlled or servo controlled would need to be determined.

TIER design philosophy

TIER (Topographies with Integrated Energy Recovery) system developed by Purdue University [56, 57] claims to allow energy recovery and storage with diagnostic and limp home options, with claimed cycle efficiencies increased by 33%. This system has two pressure lines compared to a standard hydraulic circuit, called the Main Pressure Rail (MPR) and Secondary Pressure Rail (SPR) respectively. These rails are supplied with pressure from their own pumps, but these can be linked to a single drive shaft. Actuators are connected at each end to all three lines with proportional 2/2 valves.
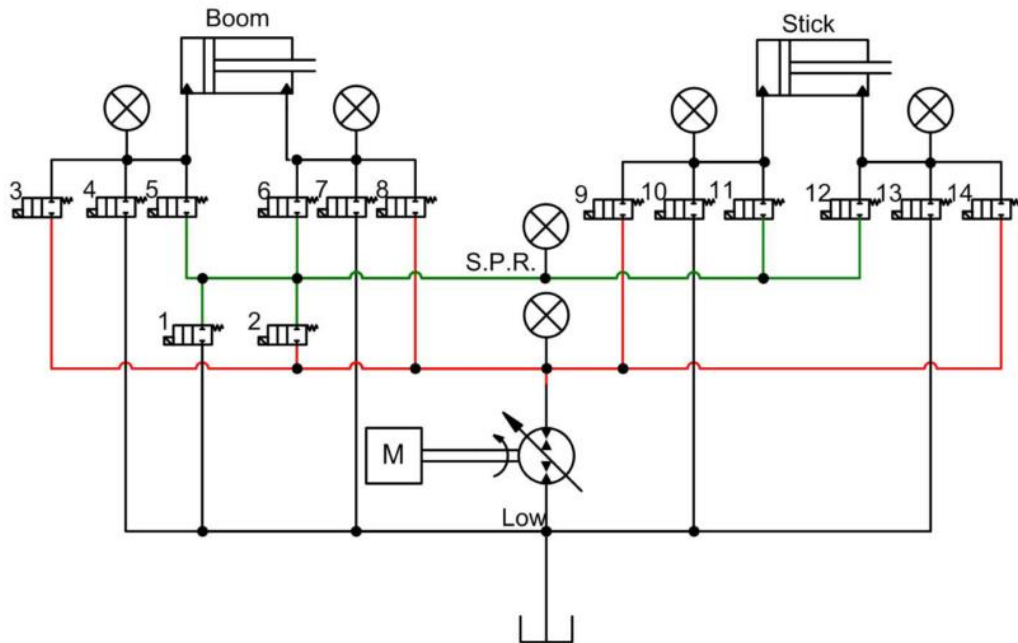
Figure 2.29: Original TIER system with Secondary Pressure Rail [57]

The actual layout of the system has been developed into four main designs: TIER[1], TIER[1+], TIER[2] and TIER[2+]. The simplest to implement would be TIER[1] but requires a valve to dissipate pressure and therefore energy to transfer fluid from MPR to SPR. TIER[2], Figure 2.30, would also be simple, though where the pumps are driven by separate motors could be an option to allow fixed displacement pumps, removing the requirement for a clutch and give additional redundancy. This would mean that one could not directly drive the other as a form of power regeneration and would instead convert it to an electrical storage system adding in inefficiencies. Having multiple pumps as per TIER[2+] would likely add additional weight and complexity for an exoskeleton system. TIER[1+] could be an option but mentioned by Andruch III et al. [57], the reality of efficient hydraulic transformers are still in progress.

Andruch outlines the advantages of the TIER system compared to other actuation methods [56], where only the displacement control system not having the energy recovery limitation compared to TIER. Displacement control is described as a dedicated pump/motor for each actuator.
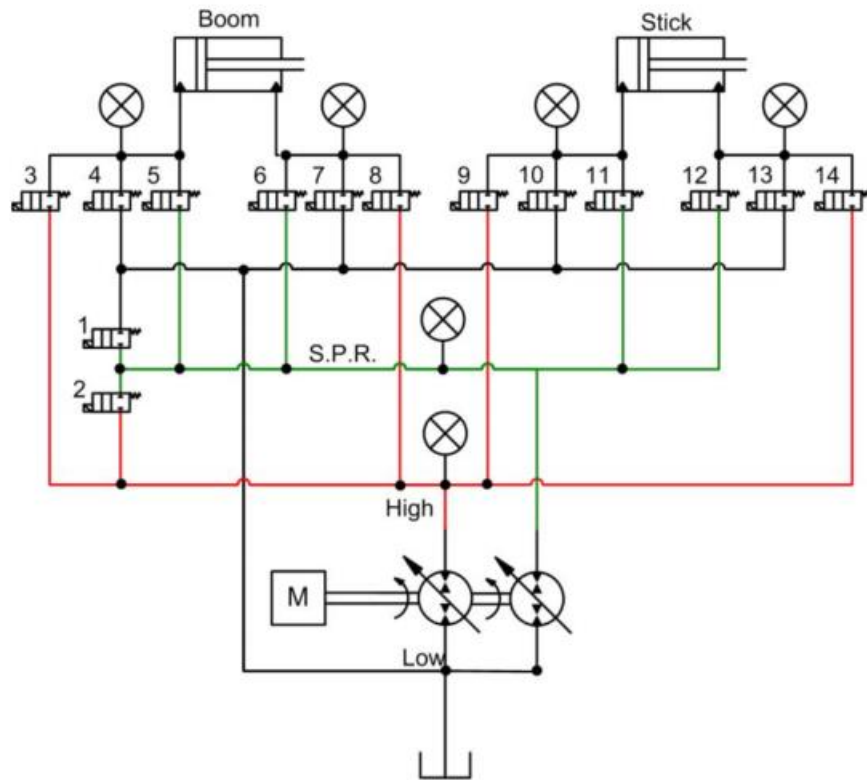
Figure 2.30: The TIER² system with extra pump/motor connected to the SPR for energy recovery [57]
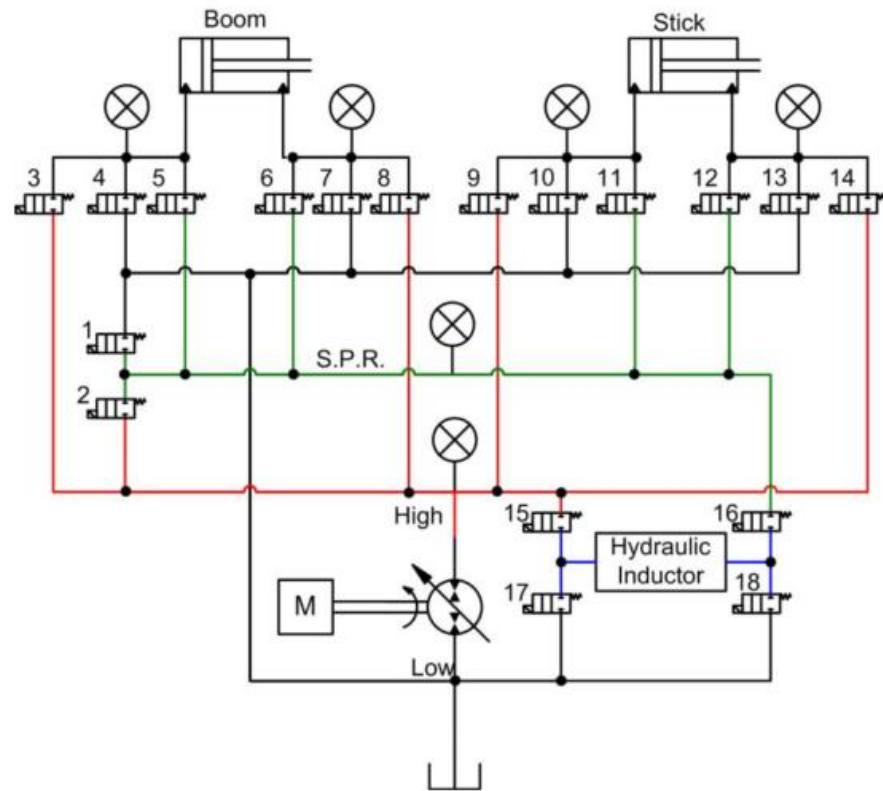
Figure 2.31: The TIER^{1+} system is very similar to the TIER^1 system except that valves 15-18 along with the Hydraulic Inductor form a hydraulic transformer between the MPR and SPR [57]

The control of the TIER designs would increase the complexity overall. With six valves per actuator, three per side, that gives 36 viable combinations of valves open and closed, singularly and multiple actuated. Whether all of these actuation options are suitable or not would require individual analysis, for example, though all valves closed would be used, would all valves open be used? Though opening the primary and secondary rail line valves on both sides would move the actuator the fastest, would opening up the tank line at the same time be suitable? The TIER system mentions that the control would be similar to a neural network, and would likely require this level of control setup to function smoothly.

For a simple valve based circuit, each actuator would need to be controlled by a single proportional servo valve.

There are the additional cost and weight of the valves as well. A regenerative circuit needs larger valves than what the pump would deliver, as the flow is being redirected from the other end of the cylinder. Taking the value of 20LPM required for the valve, this is about 4.4 gpm. Sun hydraulics make a 2-way, direct-acting solenoid-operated direction poppet valve that will flow four gpm for $105.90 each and weighs 1.16lbs (the valve code is DTDASCN212). This works out to be £79.60[1] and 526g. This comes to £477.60 and 3.16kg per actuator and this does not include any housing for the system. Using the QuickDesign™ tool by the manufacturer[2], they determine that a manifold for three valves would weigh 2.754lbs or 1.25kg. This makes a total weight of 5.7kg for the actuator and valves. If there were 20 degrees of freedom, then the total weight would be 113.2kg just for the actuator and housing.

2.6.3.2 Digital circuits

The use of digital valves in hydraulic research has been a focus over the recent years, with circuits similar to TIER with one pump and several valves Figure 2.32a [58] to closed-circuit systems with multiple pumps Figure 2.32b [59]

The single pump system is a variation of the servo valve design where multiple high-speed cheap valves are used to replace the expensive single one.

---

[1] Value determined on 9th September 2016. Values on website are either in Dollars or Euros

[2] QuickDesign™ tool can be access from http://www.sunhydraulics.com/design-your-own-custom-manifold-assembly though requires sign up before use

The use of multiple pumps is useful for multiple actuators as flow from one actuator can be used to assist the motor in another. Heitzig designates this a motor mode [59] and states that it

> *reduces the total efficiency at these flow rates, since pumps in motor mode generate losses without contributing to the output flow.*

Which could be a factor, but if one actuator is descending with 1LPM of flow, and another is rising at 1LPM, the work done by the pump should, in theory, be reduced. Certainly, digital valve usage does appear to be a viable design route with simulation results showing energy requirements being reduced by 38% [59]

(a)   (b)
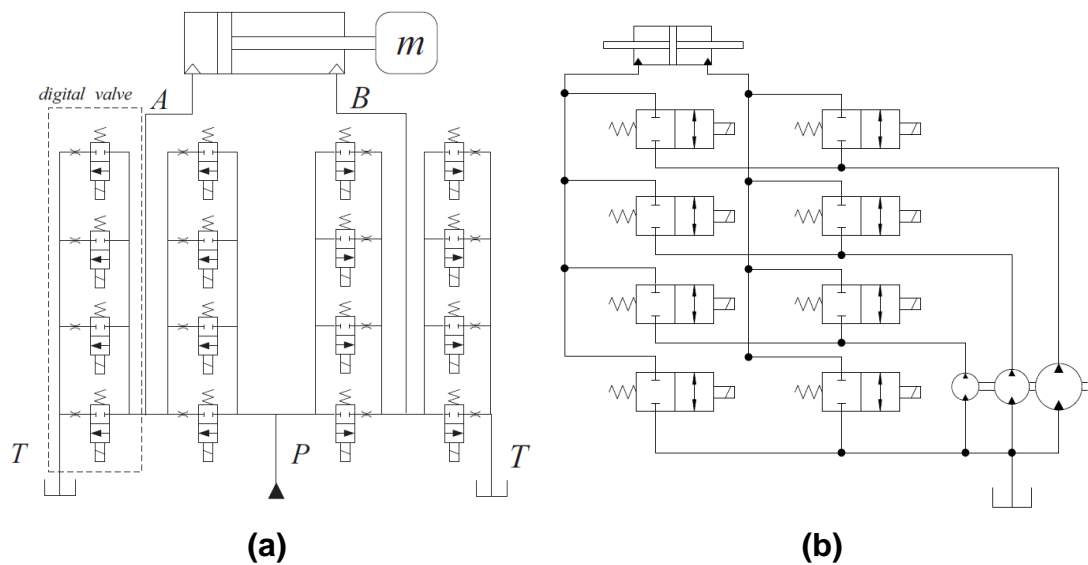
Figure 2.32: Hydraulic circuits with digital valves. a) with a single pressure source [58] and b) multiple pressure sources [59]

Part of the current research is on miniaturising the digital valves [60-62], though one must question how much interaction is going on between industry and academia. For example, [62] has a target of 0.7L/min @ 0.5 MPa and fitting within a Ø12 by 36mm volume, and [60] is a pilot valve based design for 30L/min @ 0.5MPa. Delphi Technologies latest diesel injectors operate at 300Mpa. Certainly, the fundamental design has not significantly changed from 2011 [63] as shown in Figure 2.33.

Certainly, in fuel injection systems, the design tolerances and expertise are high, for example, valve travel is around 25µm for academic available units [64] which could be smaller in commercial development. The flow rates are also comparable with example injectors giving a flow rate of 5L/min [65].

One issue with Figure 2.32b is that the actuator is symmetrical which means that a storage method is required for asymmetrical actuators. This could be similar to the pump based systems, though open-loop options would also support asymmetrical actuators [66] as shown in Figure 2.34. This does use a flow divider, that from 0 if has been noted that at low speeds this does not work at high efficiency. With the one-way valve $1V_{BS}$, this is similar to the closed-loop design.
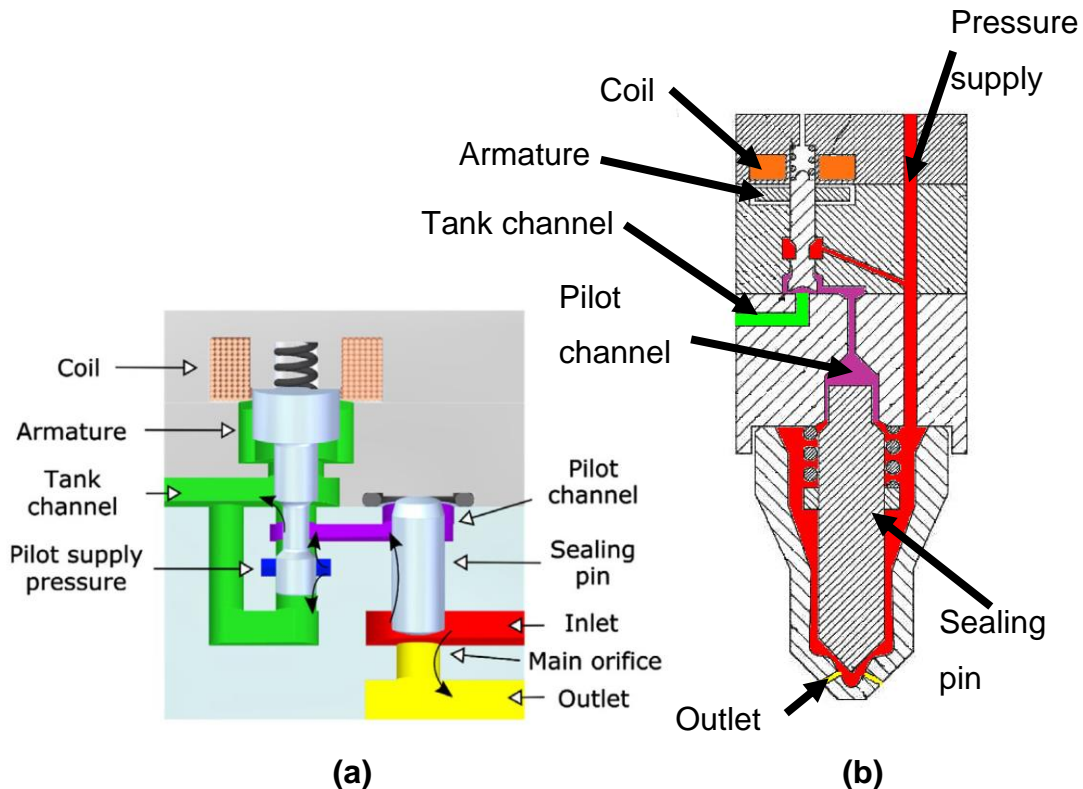
Figure 2.33: Digital valve controlling as a pilot for the outlet. a) Recent research design from 2017 [60], b) Diesel patent information from 2011 [63]

The system can also use an energy management device [67] to store energy for future events. A second simple loop circuit is attached to the motor/pump shaft driving a variable displacement motor/pump. When the pumps are running in motor mode, the secondary circuit is used to build pressure into an accumulator. When the system needs energy, the stored pressure can be used to continue turning of the motor/pump and therefore the main circuit.

2.6.3.3 Hydraulic transformers

Though the TIER system envisages using a hydraulic transformer to transfer pressure between the two pressure rails, there has been recent research into hydraulic transformers as a method to replace valves altogether.

Whereas a valve would reduce the pressure with constant flow, a transformer reduces the pressure with a proportional increase of flow rate along a constant power curve. This requires a third pressure connection to balance the flow rate.

Innas is a company that is developing hydraulic transformers and claims to have peak efficiencies of 97% [68], though they appear to be in the final stages of development with initial OEM integration happening at the current time. A recent design called variable hydraulic transformer (VHT) [69] states that it can improve efficiency, and mentions Innas as an example unit. Yang references Innas' paper, which has swash plate control as the focus but Yang states that the swashplate is fixed in Innas' design. It is likely that Yang is referencing the earlier report by Innas [70], where the indication is that the orifice plate is the unit that is moving rather than the swashplate. Innas' later design [68] has the swashplate rotating as shown in Figure 2.35.

Innas outlines the basic circuit layout in [70], Figure 2.36, with three poppet valves, and two servo valves. Innas states that the control would be based on the speed of the actuator requirements; controlled by a local Innas Hydraulic Transformer (IHT) controller feed information from both the actuator and the main Electronic Control Unit (ECU), though this is for the earlier design. Yang states that the VHT has benefits over the original IHT due to its load flow control, which would mean that the latest IHT design would likely have this benefit.

As the Innas design requires two servo valves, the cost and weight are likely to be higher than the standard servo valve system. This would, therefore, be unsuitable for smaller motion actuators, though for larger ones, could be a possibility.

As hydraulic transformers are a recent research area, there is limited simulation support available. Simulink does have orifice plates and swash plates within its environment, but these are focused on two-port and single degree of freedom units.
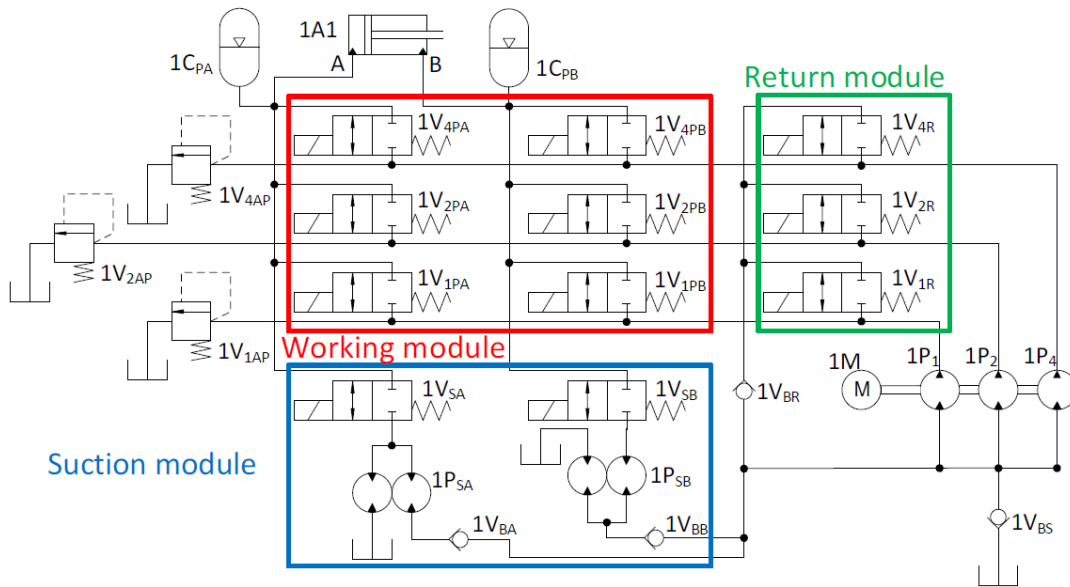
(a)
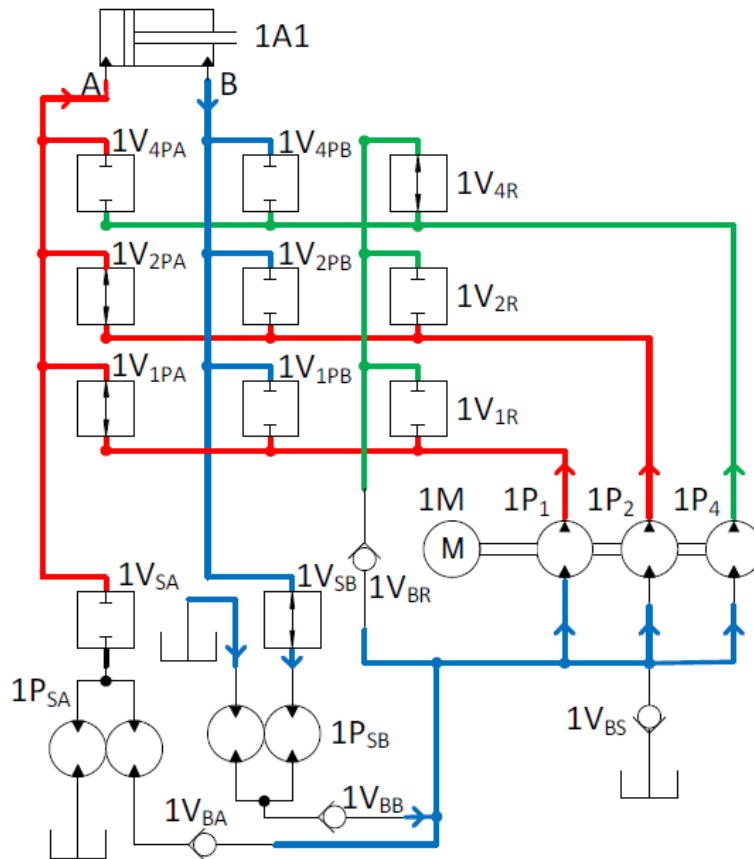
(b)

Figure 2.34: Digital hydraulic system layout using an asymmetric actuator [66]. a) Basic layout b) flow routes for when extending the actuator

a. Initial position of the swash block

b. Rotation β around the x-axis

c. Rotation φ around the z-axis

d. Rotation δ around the z'-axis
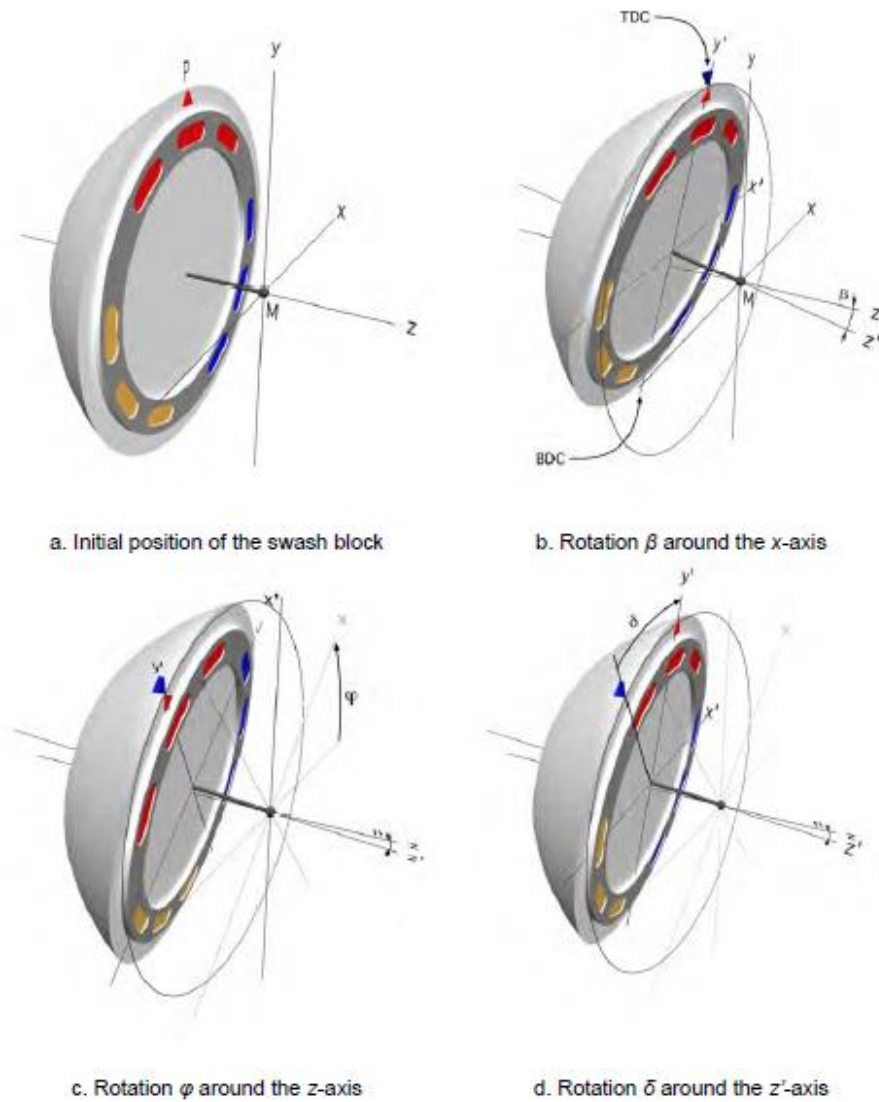
Figure 2.35: Rotation of the swash block around three axes from Innas' hydraulic transformer [68]

2.6.3.4 Dual pump/motor units

A similar system using two variable displacement pump/motor units mechanically coupled together and using high pressure and tank line has shown to achieve errors of less than 1mm [71]. The research shows that the control strategy assumes the motion being sufficiency low that overrunning and cavitation will not occur. What defines a sufficiency slow speed is not explicitly defined, though the results from the frequency response tests, 0.2Hz and 0.3Hz, gives a speed of 0.05 ms^{-1} and 0.03ms^{-1} respectively. The frequency of the system would be higher than this with an initial frequency bandwidth of 10Hz.
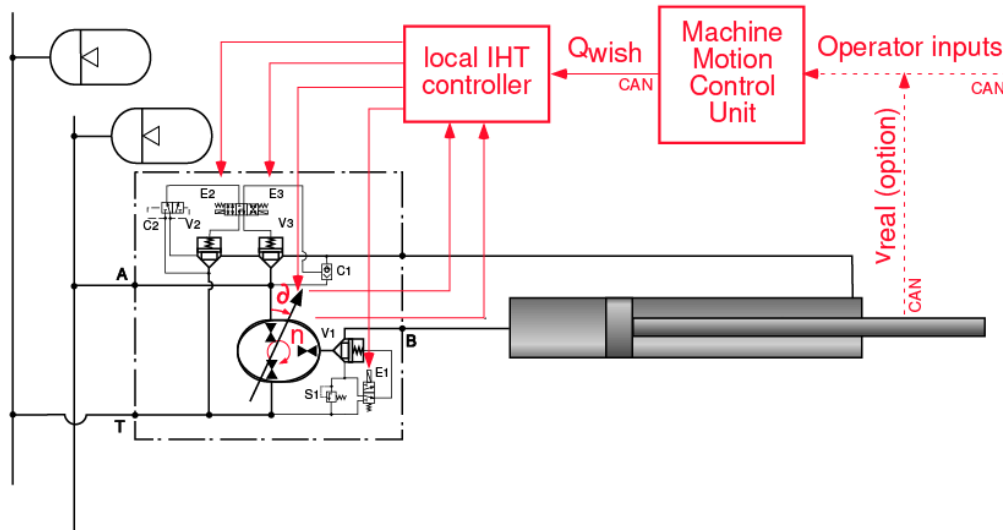
Figure 2.36: Local IHT circuit and the control concept by Innas [70]

One issue with the schematics shown by Lee [71], is that in all of the schemes the rod side is directly connected to the tank pressure line meaning that there cannot be any retraction force. These would not be viable for the exoskeleton due to the requirement for powered motion in both directions. Separating the two circuits would mean that extension and retraction would both be able to have pressurised motion, though the asymmetrical volume would need to be taken into account. A simplified circuit is shown in Figure 2.37.

Pump/motor 'A' is a variable pump so that the swash of the unit would control the flow rate through it, and thus the velocity of the shaft. The pressure would be dropped across the unit, giving the shaft a torque to transfer to pump/motor 'B'. As torque is linked to velocity and pressure within the pump system, pump/motor 'B' can control the pressure into the actuator system. This is complicated as the swash control increases or decreases the delivered volume with restriction creating pressure. This thus requires a control system to determine the pressure delivered.
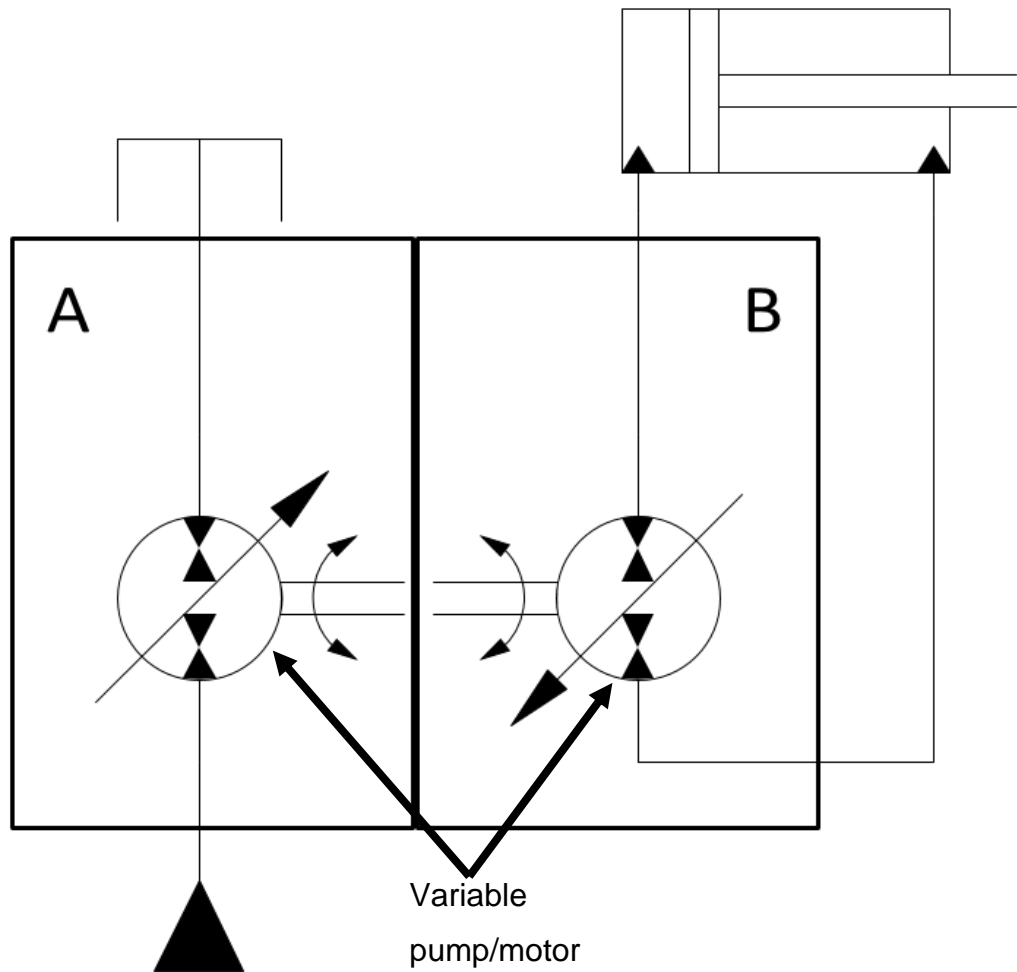
Figure 2.37: Dual pump/motor unit circuit system with isolated actuator side

If the supply is constant pressure, P_a, and flow rate Q_a, with limitations of 3000rpm for the shaft, and P_b to be less than or equal to 200bar, then certain other limitations can be determined.

If we let Q_a be 10LPM, and Pa be 200bar and inputting the values above, then the displacement ranges from 3.3 cm3/rev at 3000rpm to infinity cm3/rev for 0 rpm. This is not realistic, so setting a peak value of 10cm^3/rev gives a speed of 1000rpm. This would mean that the system would spin constantly, and thus be inefficient.

An alternative to this would be to have a fixed displacement pump for A and have a flow control valve for the flow rate through the unit. This is shown in Figure 2.38
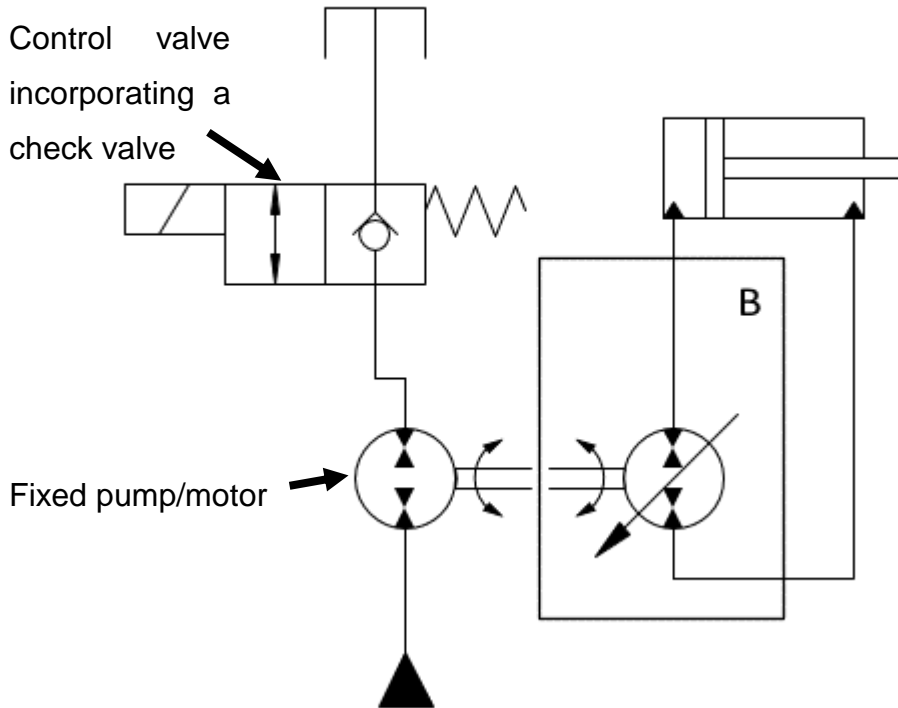
Figure 2.38: Dual pump system using a fixed pump/motor, a variable pump/motor and a 2/2 valve

With the actuator system separated from the primary system, the question of whether the main flow rate has to match that for the actuator. If the power supplied from the primary line is slightly higher than the peak power requirement of the actuator, then the system requires less energy. For the servo valve system, the flow rate and the pressure must both be equal to the maximum for each. These might not occur at the same point, and thus the true power of the system would be lower.

Using a servo valve would mean that the power into the joint is controlled by the speed of the shaft of the fixed pump/motor. This also means that the max torque, as well as the max rpm of the shaft, need to be taken into account to determine the source pressure and flow. If the fixed displacement pump is set to $6cm^3$/rev, and the max shaft speed is set to 3000rpm, then the peak flow rate is 18LPM. If the power is 400watts, then the supply pressure is thus 13bar. This would give the torque on the shaft of 1.3Nm, regardless of the speed.

The 2/2 valve used for controlling the speed of the actuator would require a check valve in the reverse direction, either as part of the valve as shown in Figure 2.38 or as a separate unit. This is so that when the system is recovering power, fluid is drawn from the tank and into the high-pressure circuit.

With the velocity and torque of the shaft controlled, the pressure and flow from the pump/motor B can be set. Altering the flow rate of A, with a fixed displacement, the flow rate of B changes, though the pressure is constant. For an altering displacement, and a fixed flow rate of A, the flow rate and the pressure of B changes. This is shown in Figure 2.39.
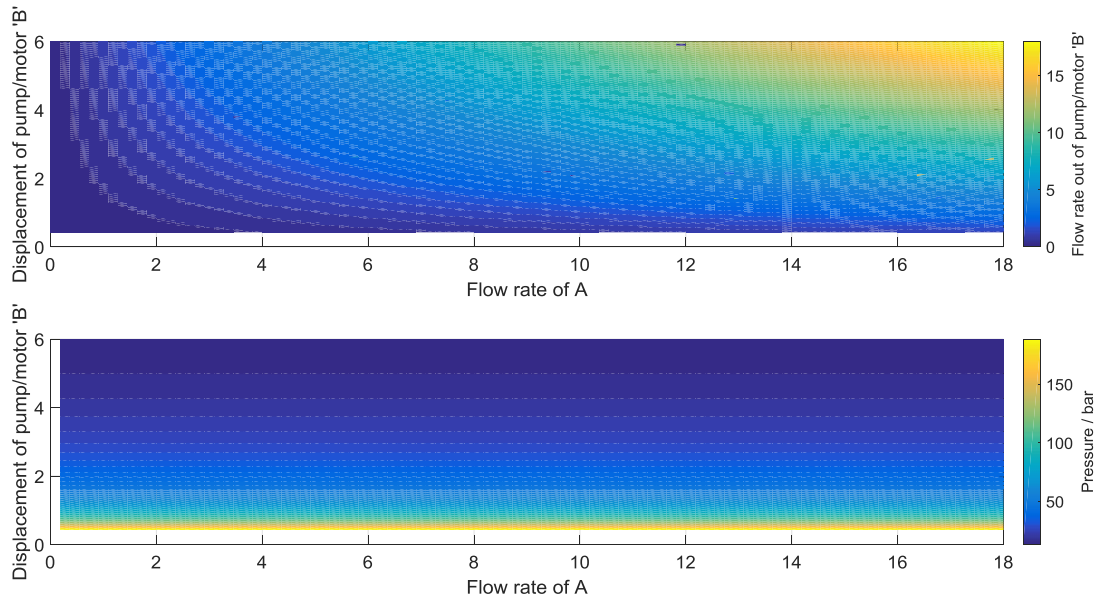
Figure 2.39: Control points of fixed displacement pump/motor, variable displacement pump/motor with valve flow control

The efficiency of this system would depend on the control system, though as the system is being powered by a continuous flow source when there is no motion required, there is an energy loss due to this continuous flow.

2.6.3.5 Pump circuit design

If the fixed pump/motor in Figure 2.38 were changed to an electrical motor, then each actuator would have a complete subassembly for the hydraulics. This is similar to the fly by wire systems used on planes, which use electrohydraulic actuators (EHA). This would locate all of the components for the motion into one system, which could increase the localised weight of the actuators. Each joint would have its own hydraulics specified for its requirements, independent of the rest of the exoskeleton.

There are several designs of the circuits available, though the options that include multiple pumps would unlikely be viable. Quan review of energy efficient direct pump controlled hydraulics [33] highlights the range of options for a pump based circuit.

A basic circuit shown in Figure 2.40 would be the starting point for the system. The pump supplies retraction and extension lines rather than pressure and tank lines. The pressure relief valves redirect the flow to the alternative line to protect the system. In an open system, these would normally be directed back to the tank. To give the makeup flow for the asymmetrical actuator, the pilot operated check valves link the closed-loop circuit to an accumulator which is also linked to the leakage of the pump.
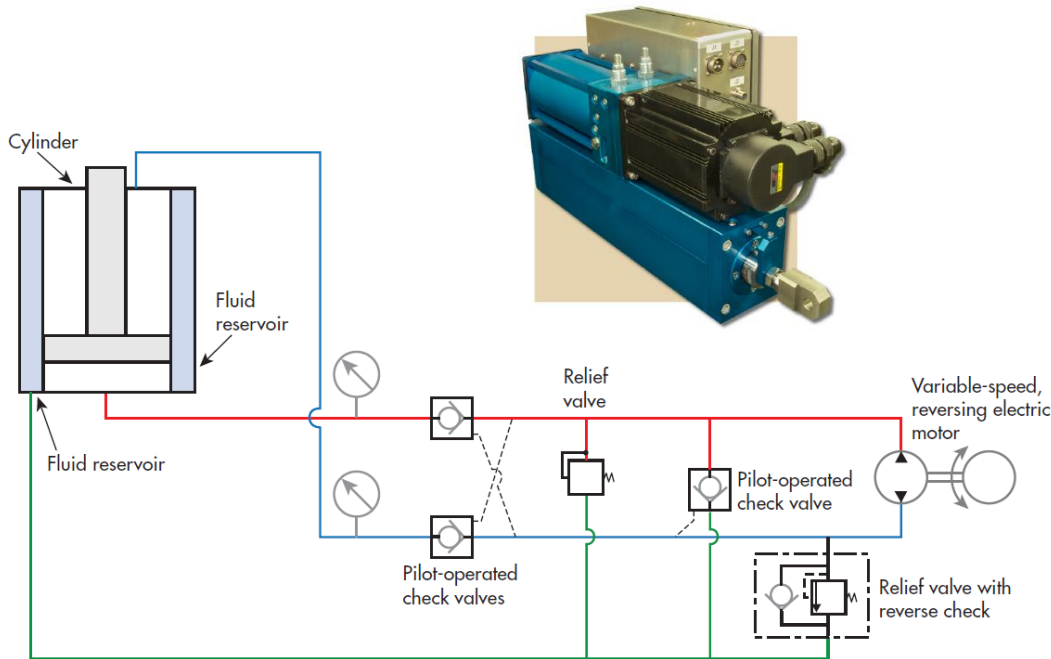
Figure 2.40: Schematic of an electrohydraulic actuator by Kyntronics showing the circuit including a tank around the cylinder, with the complete product shown [72]

The main issue with this design is that the bandwidth of the system is lower than that of the valve based circuit. Current valve system can reach 150 to 200 Hz, whilst current pump response is 20 to 30 Hz [73]. This is a 5 to 10 times reduction in bandwidth, though as the system is expected to be working at 10 Hz, this could be a viable system

Electro-Hydraulic Actuation (EHA)

EHA development is a possible design route to follow. This brings the pump and actuation into one single unit with Figure 2.40 [72] and Figure 2.41 [74] showing examples that are available at the current time. There are several developments going into this, with research still ongoing, especially into microsystems. A lightweight system that could be used has been developed by Yong-Kwun et al. [75, 76] which is lightweight and powerful and has been used

in an assistive wearable device [75, 76]. The development of the Micro Hydraulic Actuator (MHA) is covered in detail in [77]. The system uses an axial pump to power the hydraulics, which weighs 131g including the electrical motor. The hydraulic layout appears to be a double rod cylinder [76], though images within the reports are of single rod cylinders for the final products with only the concept system having a double rod cylinder.

Energy recovery for pump design

Whereas the servo valve system would use either a regeneration circuit or secondary high-pressure lines, a pump-based circuit would turn the electric motor/hydraulic pump into a hydraulic motor/electrical generator to convert the excess energy into a storable form.

This depends on the orientation of the force in regards to the motion required. When the force is opposing the motion, then energy into the system is required, but when the force is supporting the motion, then energy can be extracted. The regeneration circuits tend to only support the motion in one direction, and the secondary line circuits determine which lines are required to give the motion. The secondary line circuits do not extract energy; they just store it within a different circuit.
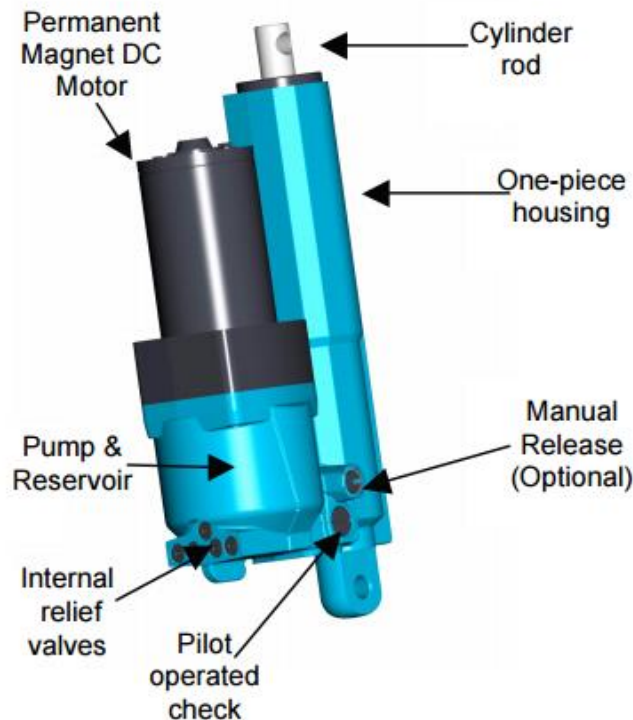
Figure 2.41: EHA system by Parker [74]

2.6.3.6 Novel open circuit displacement control architecture

Roman Ivantysyn [78] investigated the opportunities for energy recovered for a hydraulic digger by comparing open and closed circuits for displacement control. From his analysis, he developed a new style of an open circuit that could be used to expand on the open circuit system of the excavator. This is shown in Figure 2.42.

The system can be run as the normal servo valve system, though with each actuator having their own pump. It can also use the pressure from the actuators to drive the pump in a motor configuration to generate electricity, similar to the pump circuit. The links between the actuators mean that the actuators can be fed or feed adjacent units to allow faster motion, without affecting other actuators.

(1) Variable Pump   (3) Float Valve   (5) Pressure Spike Prevention
(2) Direction Valve   (4) Pump-Sharing Valve   (6) Discharge Valve
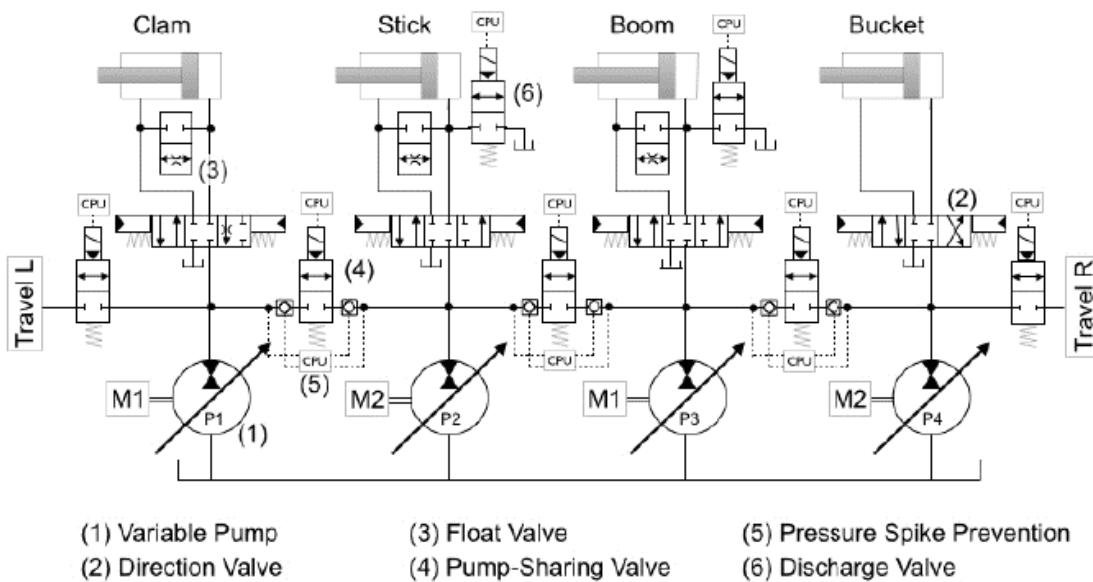
Figure 2.42: Roman Ivantysyn's novel displacement control in open circuit with pump sharing and float function [78]

The use of two pumps to move an actuator does allow a distributed system, though determining which actuators are beside each other in the sequence would require significant analysis. An option could be to have a linked node for pump sharing rather than a serial system. This could also be broken down into subsystems of actuators, for example, upper and lower systems.

With an excavator, there is a logically prescribed or likely order of actuation, which means that the activation of the pump sharing valves is a predictable

event. With an exoskeleton, there is the possibility that there is a random requirement that means that the control system becomes more complicated.

There is also the fact that the number of controlled valves is significant. For a two actuator servo valve system, there are only two valves, but with this system, there is at least three, possibly more for the floating option.

The simulation results of the system have shown that the energy saving of the system is close to 35% though this is only the initial results with additional savings envisioned for the system with circuit simplification. The design is still being investigated and empirical results are awaiting [78].

2.7 Gaps in the body of knowledge

Current enhancive exoskeleton research has primarily focused on lower body or full body, with a focus on the load being carried rather than manipulated. BLEEX does not have an upper body and carries the load on the back, requiring a second person to access it. SARCOS and PERCRO have upper bodies, but information about their load manipulation is limited. SARCOS only has claws, which limits its manipulation opportunities. PERCRO does have a gripper unit, but it is unclear the full capabilities of it.

The use of the actuators for current exoskeletons also leaves areas of improvement, ranging from structural design to actuation. BLEEX, for example, has issues with singularities in its motion, as well as having the hip rotation axis not coincidental to the human hip joint. PERCRO does have a four-bar mechanism to bring the axis together but is patented, limiting its opportunities in this work.

The actuation methods of the systems range in styles, from electrical to hydraulics, and the method of giving rotation. With hydraulics giving the ideal power source, this is the route selected for this thesis and has been used in BLEEX and SARCOS. Several systems use wire cable to transmit motion, but there is the question of suitability. The life and strength of cables mean that to comply with recommendations, the wire needs to be large in diameter, but this then requires a larger radius for pulleys. A rigid chain would give improved strength, but at a cost of weight.

Focusing on hydraulics, there does not to be any indication of performance analysis. the systems typically just state servo valve circuit, which might not be the ideal solution. If the system is untethered, then optimal use of the available power is critical. If power can be recovered from some motions, then this would increase the duration of use. With hydraulics being primarily used in excavators, current research can be modified for use in the exoskeleton system.

The main gaps are:

- Load manipulation overload carrying
- Exoskeleton and human joint coincidental
- Optimisation of joint design to prevent singularities and give required torque over the full range
- Hydraulic performance of the actuator system

2.8 Summary

As the exoskeleton is based around the human user, understanding human anatomy is necessary before starting the design. Human anatomy limits the range that exoskeleton needs to work at; both in displacement and velocity, but can give ideas on actuator placements and utilisation. Biomimetics is the study of biological systems and implementing them into engineering design, so is similar to the focus of this project.

For the two styles of major joints within the exoskeleton system, there are varieties of solutions for each.

For the revolute joint, the determination of the torque and angle range gives the quick initial selection of which rotary actuator is viable for the solution. For the linear actuator selection, the optimisation of the joint geometry is required which can then be compared to find the system with the most linear response. The ideal linear and rotary design weights can then be compared for a starting point in selecting the final solution.

For the spherical joint, several of the possible solutions were eliminated before any numerical analysis was done due to fundamental issues with the design that could risk injury to the user. Of the two chosen design routes, the two and five bar systems, both have benefits and drawbacks. The two bar system only has a component on one side of the horizontal plane, whilst the five bar has components on both side. The five-bar system places the majority of the weight

on the rear of the system whilst the two bar requires weight in the middle of the structure.

Based upon current exoskeleton development, systems that are going to market at the current time appear to be electrical motor or pneumatic based, though these are for assistive purposes rather than enhancive. Enhancive exoskeletons tend to use hydraulic systems though there is the question of how efficient and flexible they are.

SARCOS has not revealed their efficiency or circuit setup due to the commercial nature of their business though they are tethered. BLEEX has revealed its circuit and efficiencies and there are areas of improvement that can be developed.

Hydraulic research is starting to focus on closed-loop pump circuits with money being put into research in several countries. Determining which circuit basis would be suitable and ideal for the exoskeleton system is a major area that could be studied. There appears to be only one system that is starting to merge the two technologies, which are being developed by the Korean Institute of technology though they are currently focusing only on upper limb design. Developing this idea into a full enhancive system would mean that modularity is at the forefront of the system.

Chapter 3
System requirements

3.1 Introduction

This project has a sponsor that supplied a list of customer needs for the exoskeleton to meet. These are covered in Appendix D. This was then used to generate a list of product requirements for the exoskeleton, which are covered in Appendix E.

This chapter covers the requirements for the exoskeleton generated from discussions with the sponsor. The requirements are broken down into six sections covering design considerations and functional requirements, to environmental impact and safety. In Appendix E, each requirement has a Unique Identifier (UID). The discussion of the requirements will be linked to these and expanded upon.

As part of the requirements is to follow the human motion, analysis of motion capture data[3] is performed to clarify what these are.

3.2 Product requirements

3.2.1 Augmentation requirements

As an enhancive exoskeleton, the mechanical strength requirement is to be able to lift a weight of 45kg, with an ideal weight of 90kg (UID M-1). The loading onto the exoskeleton is not explicitly defined in the requirements; it is only described as a load-carrying capacity. Other systems either have this as a backload [80] or as an armload [3, 6]. In order for the system to be as flexible as possible, this load would ideally be at full reach of the exoskeleton. If this unit is to be used in industry, then being able to reach a distance and manipulate a mass is highly desirable. For example, for a worker loading a milling machine, they need to be able to reach in and manipulate the component. Thus, this will be the definition of the loading requirements: action at a distance.

---

[3] Motion capture data acquired from Carnegie University, which is originally intended to be used in game development [79]

3.2.2 Design requirements

The system is also to be suitable for a range of users, and though the initial design solution size range would be for the 50th percentile, the system should be adjustable (UID M-5). This is important for the limbs and trunk length, though the method of modification should be simple and intuitive. This could also affect the motions methods so a system tolerant to changes in limb length would be preferable.

Whether the system is tethered or untethered, (UID M-8) depends on the final design of the power source. Though the design will initially assume that there will be a mass on the back of the system for a power source, the size and weight of this are unknown at the current time.

From the original system requirements, the weight of the exoskeleton should not exceed 68kg, preferably 21kg (UID M-13). An initial comparison starting point is to compare this weight to current exoskeletons, as summarised in Table 3.1.

SARCOS and PERCRO are both full exoskeleton systems, and thus would be the first comparison points for the system. SARCOS does not give the weight for the exoskeleton. The PERCRO load to weight ratio is half of that for the max target weight for the exoskeleton. This could mean that the system weight could rise to 141.3kg to match the performance of PERCRO.

HAL and BLEEX are both lower-body systems, so a direct comparison is difficult. HAL is also an assistive system, not designed to augment the user to carry heavier loads.

Table 3.1: Weight comparison of different robots and exoskeleton systems

Model	Load kg	System Weight kg	Load to Weight Ratio
BLEEX	23.1	51.8	0.446
HAL (Lower limb system)[4]	40-100	~14	2.85-7.14
PERCRO	101.9	160	0.637
SARCOS[5]	90	*	*
Exo Max Weight	90	68	1.324
Exo Ideal Weight	90	21	4.296

Another source of load to weight ratios that can be used to compare the exoskeleton are industrial robots. The CR-35iA [81] is a human collaborative robot designed to work alongside a human safely whereas the R-1000 100F is an industrial robot [82]. Their respective information is shown in Table 3.2.

Table 3.2: Commercial collaborative and industrial robots examples

Model	Load kg	System Weight kg	Load to Weight Ratio
CR-35iA	35	990	0.035
R-1000 100F	100	665	0.150

These have a significantly lower load to weight ratios but are designed to move the load at distance. The CR-35iA has a reach of 1813mm, whilst the R-1000 100F has a reach of 2230mm. Both these reaches are longer than would be expected for the exoskeleton, but if the design was for 'action at reach' then a lower load to weight ratio than the competitors could be expected. If the system is used in a more sedentary environment, like a factory, then this could be

---

[4] HAL lower limb type (non-medical), double limb version, which is for mobility support (standing, sitting and walking) rather than augmentation
[5] SARCOS does not give the weight of the system in their literature

reasonable. The exoskeletons in Table 3.1 tend to be for walking motion support.

The power requirements cannot be defined until the actuation system has been determined, though this should be the lowest possible within the requirements (UID M-14). This thus leads backs to the untethered/tethered question. With the untethered option, the minimum requirement would be for one hour of usage, though with the preference of two hours and 40 minutes (UID M-15). The reasoning behind this time duration is that it is one-third of an 8-hour shift. Another option would be to run a system similar to Eva units from Neon Genesis Evangelion, a Japanese anime from the mid-1990s, where they have an umbilical cord and can switch between them with five minutes of battery supply [83].

Reliability will be based on at least 95% rating, which determines some of the calculations for strength and sizing of the components (UID M-27).

There is a requirement that the size of the longest dimension i.e. the shoulder width, the increase is no larger than 100% of the original human dimension, preferably only 25%. This would thus give a maximum volume for the system, for example with a shoulder width of 50cm, then the width of the exoskeleton should not exceed 100cm, preferably less than 62.5cm (UID M-38). This is due to the system working in un-adapted environments and the standard size of building furniture like doors. According to the building regulations for England [84], the smallest size of effective door clear width is 750mm for existing buildings but is larger for new buildings at 800mm.

3.2.3 Human requirements

Analysis of common human manoeuvres has been used in other exoskeleton development programs, and will also be used here (UID M-2). The range of motion and the speed of a human is the basis of the respective attributes for the exoskeleton (UID M-28). The system will be designed so that the capability of the hydraulics is that for moving the exoskeleton at the human speeds without hindering the human (UID M-20 and M-24). The human will be in control of the exoskeleton movements and not vice-versa (UID M-20 and M-24). If the human moves slower, then the control system should pick this up and reduce the speed

of the exoskeleton. The human should neither push or be pulled by the exoskeleton by not moving at the required speed (UID M-26).

The entering and wearing of the system should be simple and should not require outside assistance (UID M-33). This is critical for exiting to prevent injury to the user. Several systems attach to multiple points on the human, in an anthropomorphic design, though the method of entering or exiting the system is then in question. One example of donning an exoskeleton without assistance can be seen in the fictional power loader from Aliens [85]. Here Ripley, the lead character, places her feet into contact sockets and lowers a harness that locks her in as well as gives protection to the user. Her arms are not constrained and just uses a control stick to give arm control. This allows the quick exit required for the final scene of the film. With a system that straps along the user, donning the system would require additional time, and possibly support, and certainly exiting the system in an emergency would be difficult unless a quick release system was included like small explosive bolts. BS EN ISO 13482:2014 in section 5.9.2.2, the inherently safe design to reduce physical stress and posture hazards as section (c) states:

> *"…command devices that are detachable or hand-held instead of being permanently attached to the personal care robot in an inappropriate position."*

The control system should be simple enough to allow wear and play, with minimum training time (UID M-19, 26 and 37). This is hard to determine in the design stage until initial prototypes are constructed and tested. Certainly, the system should be intuitive, whereby it is obvious what any control devices do and not impede the gait of the user. Altering the gait of the user would create issues of fatigue.

One of the aims for the system is to increase the endurance of the user and reduce the metabolic consumption of the user whilst in use. This can be done by making sure that the loading on the user is minimised regardless of the loading on the exoskeleton (UID M-20 and 24).

3.2.4 Environmental requirements

Cleanliness requires that the system does not produce any by-products, which would push the system to not be powered by a chemical reaction engine similar to BLEEX (UID M-7). The use of hydrogen power cells could be an option if the

by-product is water (UID M-30). This is also referenced in BS EN ISO 13482:2014 5.7.1 [86].

The use of hydraulics can cause an environmental hazard if they leak into the environment (UID M-7). Though BS EN ISO 13482:2014 [86] covers this in 5.7.3, other standards have a higher requirement, for example, the mining industry with the MDG 15 by the New South Wales Government [87, 88].

3.2.5 Commercial requirements

With a commercial sponsor seeking to develop and market the system, there are some requirements outlined for this.

The ideal price for the system requested is $10k, with the marginally acceptable value being $30k (UID M-16). Once the system has been developed, cost reduction exercises can be implemented to bring the cost down, especially with bulk purchase benefits. As the exoskeleton could be replacing current options, like a forklift, then the price range of these should also be compared. If the exoskeleton is significantly higher, then there is no motivation for industry to purchase.

The appearance of the system should be considered, though the final design should not be compromised for aesthetics (UID M-17). Lights both spotlights for work and warning orange lights would be simple requirements for working. The use of a consistence colour scheme over the range would be a simple aesthetic option, like the Caterpillar yellow.

Maintainability and maintenance will be required for the exoskeleton ideally once a year, though once per week is acceptable (UID M-21). All work would need to be done by a competent person (UID M-31). Access is thus a critical requirement. For accessing parts for the hydraulics, like drains and filters, would need to be simple, and not require the disassembly of a significant amount of the exoskeleton.

3.2.6 Safety considerations

The personal care robot types, as specified in section 6.1.2 of BS EN ISO 13482:2014 [21, 31, 86] has restraint type robots, with high powered physical assistance as a type 2.2 variant. This states the safety functions should include

protective stops, limits to the workspace, safety-related speed and force control (UID M-25 and 30).

The protective stops, speed and force control would be based upon the control programming of the system. The use of sensors to feedback conditions would be required for this.

The use of limits to the workspace is different for the exoskeleton system compared to other robots classed in BS EN ISO 13482:2014. The workspace is theoretically infinite due to the mobility of the suit. Protective and safeguarded space, where the exoskeleton will stop motion automatically based on an environmental obstacle, would depend if this were an addition to the motion sensor system. For a manually controlled suit, based upon the intelligence of the user, this would not be used (Annex B.3 of BS EN ISO 13482:2014)

3.3 Exoskeleton motion

3.3.1 Introduction

From 3.2.3, the exoskeleton needs to match the human motion for acceleration, velocity and range of movement.

To determine the torques required for the exoskeleton, the acceleration of each of the joints needs to be determined. The velocity will give the flow requirements of the actuators and the range of movement will be used in the design process. This can be extracted from motion capture data.

Motion capture data is expensive to generate, as it requires time within a dedicated room set up with several cameras. The enhancive exoskeleton team was able to generate some motion capture data, though the time required for extraction and processing is significant. This has meant that it was unable to be utilised in this thesis. Carnegie Mellon Graphics Lab has pre-processed motion capture data for several motions, including walking and item handling. The motion capture does not include ground reaction forces, as the data appears to be for computer game development as it includes combat motions, but this is not required for the upper body exoskeleton. This motion capture data has been used to generate analysed data.

The motion capture data is stored in a format called BVH (acronym of Biovision hierarchical data), which is a format developed by Bio Vision, a computer games company. The formats tend to be open-source allowing the extraction of the data into a variety of programs, including MATLAB. The code for MATLAB was developed by A Wetzler [89].

Previous studies have superimposed the human joint motion onto the exoskeleton frame [2], but have found that due to kinematic and inertial differences, the system does not perform as expected. If the motion capture is used to define endpoint locations then by using inverse kinematics the exoskeleton can determine its own motion. This turns the exoskeleton from a joint matching, anthropomorphic design to an endpoint one. This allows any deviations in dimensions between the user and the exoskeleton to be flexible and increases the user safety as there are fewer restraints on them.

3.3.2 Motion capture analysis

The joints can either be thought of as revolute or ball joints with the analysis of them is slightly different. For a revolute joint, it is defined as three points on a plane with an angle between them. For the ball joints, a plane is also needed to be defined, which is based upon the shoulder and spine data points. The angle that the upper arm has to the plane gives flexion, whilst abduction is measure in relation to the plane. The two layouts are shown in Figure 3.1.

For the ball joint, the 20° angle is the abduction/adduction range, and the 45° is the flexion/extension. The internal/external rotation is not included, as it requires additional information for it to be determined. This would be the lower arm for the exoskeleton.

Once the angle has been calculated, this is then differentiated to give the angular velocity and again to give the acceleration [79], as shown in Figure 3.2.

This is only for a single motion, picking a box up off the floor, thought the list of actions recorded is larger.
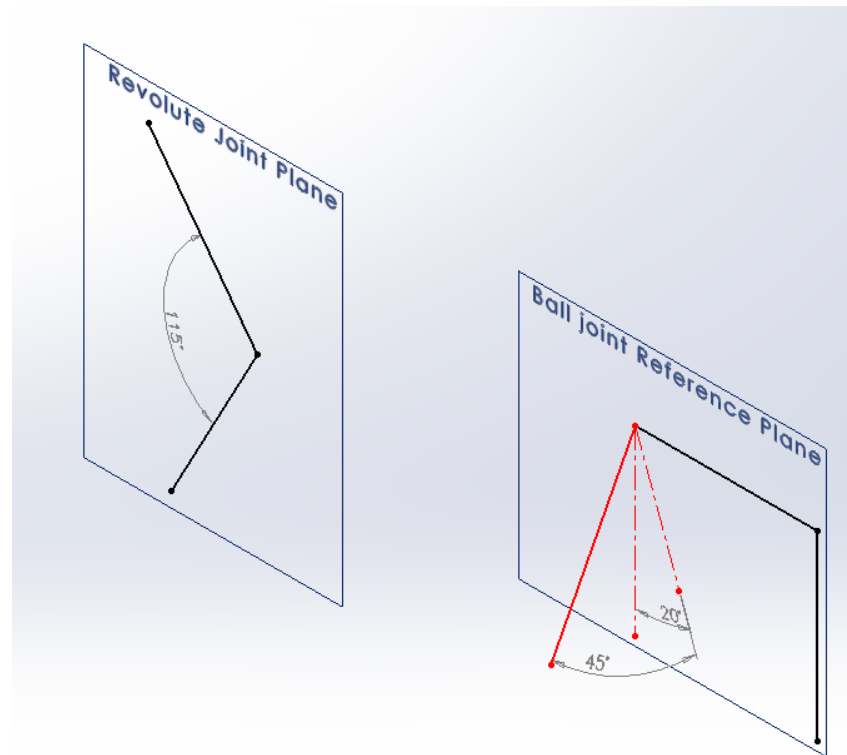
Figure 3.1: Joint Angle determination from motion capture data

The range of motion is large, nearly 60°, though the quick position change at around 1.5 seconds causes a spike in the velocity and thus the acceleration. This is an issue with human motion, there is a risk of short, high speed, high acceleration events that will impact the motion of the exoskeleton

Once all of the motions have been calculated, a distribution of them can be created. This is important for the acceleration as this is used to determine the torque of the joint and thus the size of the actuators.

As shown in Figure 3.3, the acceleration data for elbow can be given as a probability density, showing that the majority of the acceleration for the motions is low. It appears to be a normal distribution, implying that acceleration and deceleration are equal in magnitude.

The probability density function does not include repeats of each motion, for example, the walking motion is only a few seconds long, though in reality would be significantly longer. The ratio of each action to an average days activities is not recorded in this data, and if this was included, then a more precise probability density function could be generated. For example, if the user were just standing still all day, then there would likely be a reduction in the standard

deviation of the probability density function, as the action does not have a very large range of accelerations.
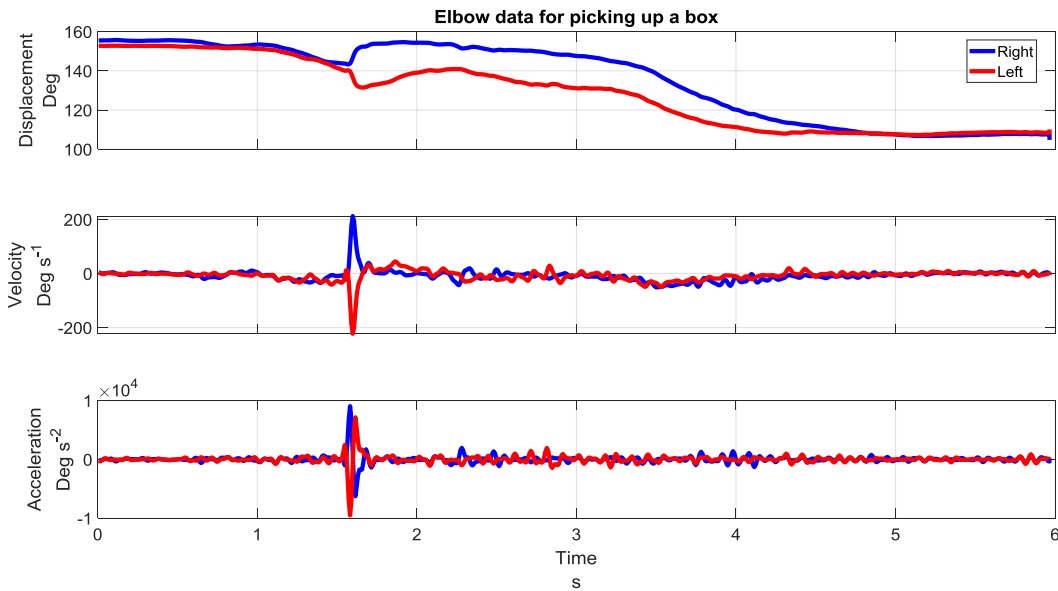
Figure 3.2: Displacement, velocity and acceleration of the elbow joint when picking a box up off the floor.

Perry and Rosen have conducted similar work [90], though their work was conducted on a seven DoF computational model, and generated histograms of the torque of the human. This is only the torques of the human, rather than of the exoskeleton, which is likely to be different. Though the position, velocities and the accelerations should be the same, the torques will be different due to the increased mass of the load and exoskeleton. They noted that some of the histograms are not all normal distributions, but bi- or trimodal relating to "key anthropomorphic configurations" [90], particularly in relation to gravity.
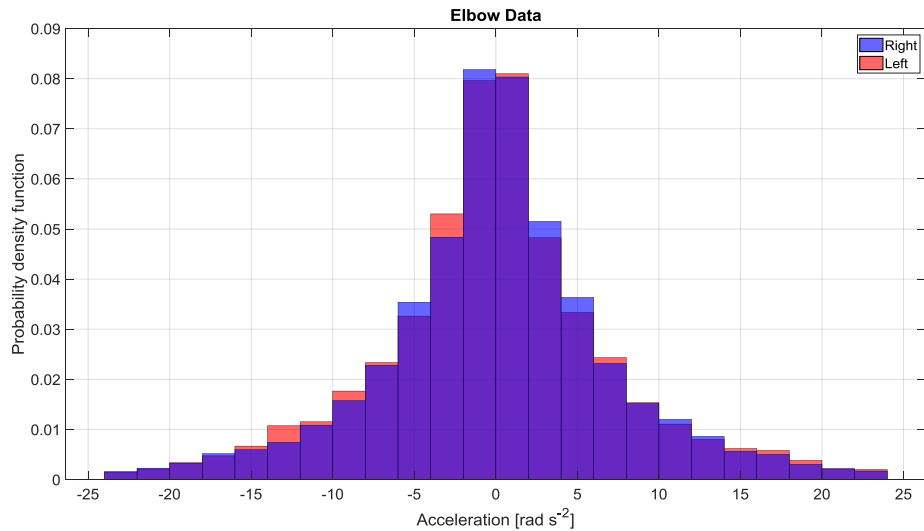
Figure 3.3: Probability density function of the acceleration for the elbow joint for a range of motions

From Figure 3.3, a 95th confidence interval can be determined and used to eliminate some of the extreme values. As the motion is for right and left joints, this generates four values. The other joint results are in Appendix F.

All of the ranges can then be calculated, and these are shown in Figure 3.4.
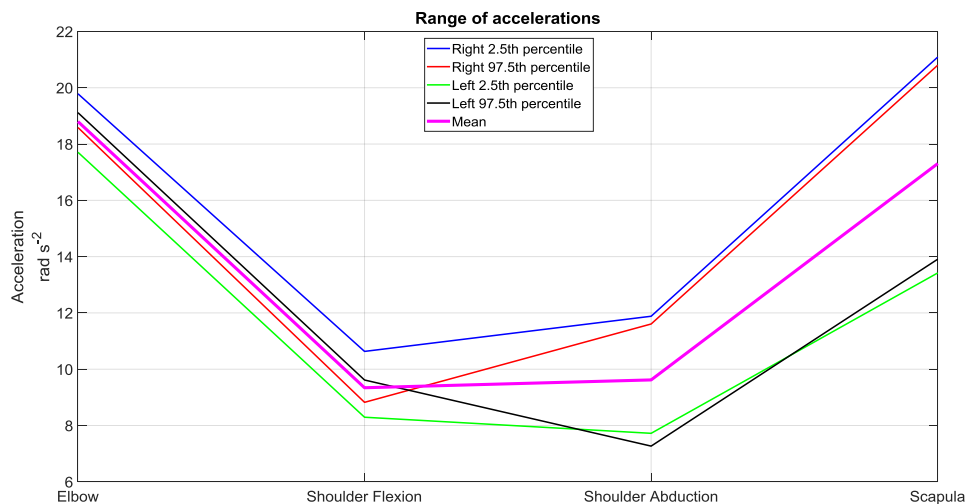
Figure 3.4: Acceleration ranges for the different joints

The accelerations per joint are similar, though the scapula does have some range in its results. The reason for this is unclear. The joints also tend to be between 10 and 20 rad s^{-2}. The mean values are shown in Table 3.3.

Table 3.3: Mean Acceleration for joints in human motion

Joint	Mean Acceleration rad·s^{-2}
Elbow	18.80
Shoulder Flexion	9.34
Shoulder Abduction	9.62
Scapula	17.31

The elbow has the largest mean acceleration, as it has a large range, though this would not explain the scapula having the second largest. The elbow does a lot of the gross motion of the arm, with the should requiring smaller accelerations due to the increased distance from the hand to the shoulder magnifying its output. The scapula also has a short arm from the pivot to the end, which would explain the higher accelerations.

3.4 Discussion

With a range of design requirements, the development of the exoskeleton needs to balance a range of demands.

As the acceleration is required for the torque calculation, determining the range is critical for the exoskeleton design. Humans can have very quick small motions, normally associated with reflex actions that are likely to be required to be followed by the exoskeleton. There could be an event that requires the user to jerk away from danger, for example, a fire or something falling that needs to be followed by the exoskeleton to remove them from the situation.

With a high acceleration, there is a likelihood that a high torque will be required. Depending on the value of the torque, it would be possible to determine what accelerations the designers of the systems were expecting.

3.5 Summary

The original requirements give some flexibility in their interpretation, and thus for the loading, it was decided that 'action at a distance' would give the system the greatest flexibility. This is likely to decrease the load to weight ratio when

compared to other exoskeleton systems and could make it more comparable to industrial robots. This is a novel aspect though, as previous systems only carry the load or manipulate it at close range limiting their usefulness in an industrial setting.

The human interaction with the exoskeleton is important and understanding the range of motion and speeds that the human might move at is required to assist with the design. The majority of the joints have similar acceleration.

This leads to the joint design, which needs to be optimised to give the required loading and motion.

Chapter 4
Joint geometry

4.1 Introduction

Current work on exoskeletons focuses on getting an initial system up and running as quickly as possible with little regards to the optimisation of the design and components. Either they use a simple joint with an internally or externally located actuator, for example, BLEEX, or pulley based systems using cables, for example, PERCRO. The optimisation of the joint range and torques to give the required output does not appear to have been undertaken with rigour. This means that the joint either is not able to support the full range of motion, i.e. BLEEX with squatting, or there is a question on the safety factors used, as shown for the cabled systems in Chapter 2

There are two main types of joints on the human body, and thus also on the exoskeleton: revolute joints that have one degree of rotation and a spherical joint giving three degrees of rotational freedom. The elbow can be approximated to a revolute joint. The shoulder is more complicated than a pure spherical joint due to the clavicle motion causing the joint centre to move.

In order to assist with the design process, the joints of the exoskeleton need to be broken down into simple geometric equations so that they can be examined for optimisation. The simplest joint is that of the revolute joint, where there are several mechanisms that can be used to transfer linear into rotary motion.

The spherical joint moves the equations into three-dimensional space, which to fit around the human, has been selected to be a gimbal joint. The dimensions of this joint, both radially and the circumference, is broken down into simple equations for optimisation.

If the hydraulics are to be optimised for the system, then the structural design of the hardware should also be optimised to give the greatest possibility of high efficiency. Using the generated equations, these can then be put through an optimisation routine to determine the ideal geometry.

Equations in this chapter are grouped together and numbered. This due to several of the individual equations being linked by defining one geometric design.

Currently, there does not appear to have been any work done for this, certainly within exoskeleton research, and thus these equations have been generated for this thesis.

4.2 Analysis of planar displacements

The revolute joint lies on a single plane and can be described as rotation around the z-axis, and translation on the XY plane.

The determination of the motion system can be built using matrix transformations [91]. This allows the construction of each of the joints as relationships to each other within a unified space.

The rotation matrix around the z-axis is given by equation (4.1).

$$\begin{Bmatrix} X \\ Y \\ 1 \end{Bmatrix} = \begin{bmatrix} \cos\theta & -\sin\theta & 0 \\ \sin\theta & \cos\theta & 0 \\ 0 & 0 & 1 \end{bmatrix} \begin{Bmatrix} x \\ y \\ 1 \end{Bmatrix} \tag{4.1}$$

The translation matrix along the x-axis is given by equation (4.2)

$$\begin{Bmatrix} X \\ Y \\ 1 \end{Bmatrix} = \begin{bmatrix} 1 & 0 & s \\ 0 & 1 & 0 \\ 0 & 0 & 1 \end{bmatrix} \begin{Bmatrix} x \\ y \\ 1 \end{Bmatrix} \tag{4.2}$$

Which can be written as $R_z(\theta)$ and $T(s,0,0)$ respectively.

The translation matrix is moving the endpoint along the x-axis, and there is a translation matrix for the y-axis as well. The Y-axis motion can be replicated with $R_z(\pi/2) \cdot T(s,0,0)$.

4.3 Revolute joint

From Table 2.1, the elbow has a significant range of 154.7°, which can be rounded up to 150°.

For a joint to rotate to an obtuse angle, or even towards 180°, the pivot needs to allow the limbs either to overlap or sit beside each other. For the limbs to overlap, the two limbs will be offset horizontally, though the joint will be in the

centre line of the limbs. For the limbs to sit beside each other once folded, the joint needs to be offset from the limb.

Several different design routes can be followed in order to give the range of motion. Current design involves either having the actuator on the inside or the outside of the limb, as per BLEEX or an excavator respectively. Other options include four-bar linkage designs or patella designs. The benefits and drawbacks for each joint option need to be examined to determine the ideal solution.

4.3.1 Internal actuator

The internal actuator design has the actuation system on the inside of the joint, whereby as the actuator contracts, the joint closes. This partially exists in nature as muscles can only give a force in contraction, but is used in a variety of systems. There are some limitations on the use of this design due to the interference of the actuator to the limbs as the system tends towards the closed position. The minimum length of the actuator also dictates the dimensions of the system.

An outline of the design is shown in Figure 4.1.
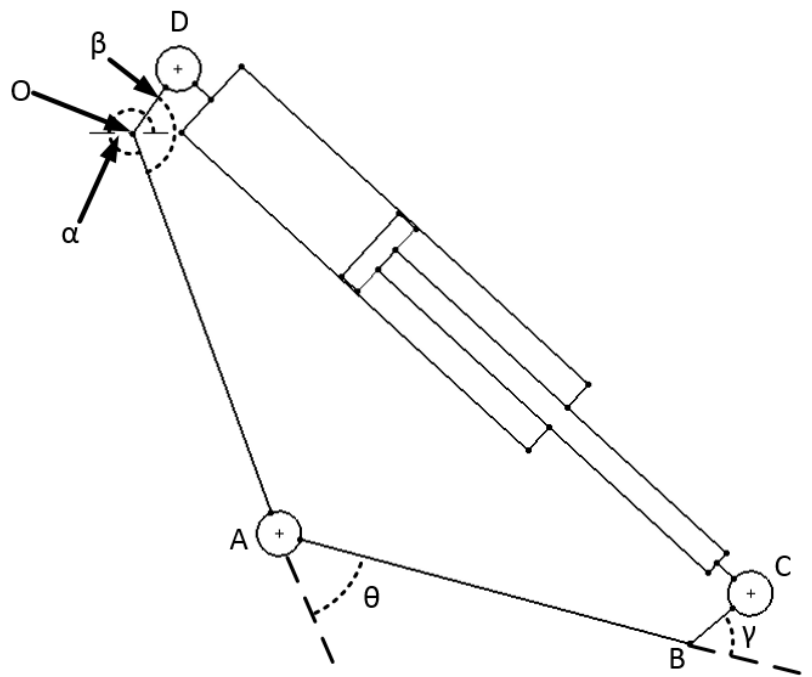
Figure 4.1: Internal Actuator diagram showing endpoints and angle

$\overrightarrow{OA}$ is the primary limb and is fixed in space. $\overrightarrow{AB}$ is the secondary limb and $\overrightarrow{OA}$ rotates. $\overrightarrow{OD}$ and $\overrightarrow{BC}$ are the actuator mounting points to the limbs.

The equations for the system are given in equation (4.3).

$$\left[\vec{A}\right] = \mathbf{R_Z}(\alpha) \cdot \mathbf{T(OA, 0, 0)} \cdot \mathbf{k}$$

$$\left[\vec{B}\right] = \mathbf{R_Z}(\alpha) \cdot \mathbf{T(OA, 0, 0)} \cdot \mathbf{R_Z}(\theta) \cdot \mathbf{T(AB, 0, 0)} \cdot \mathbf{k}$$

$$\left[\vec{C}\right] = \mathbf{R_Z}(\alpha) \cdot \mathbf{T(OA, 0, 0)} \cdot \mathbf{R_Z}(\theta) \cdot \mathbf{T(AB, 0, 0)} \cdot \mathbf{R_Z}(\gamma)$$
$$\cdot \mathbf{T(BC, 0, 0)} \cdot \mathbf{k}$$

$$\left[\vec{D}\right] = \mathbf{R_Z}(\alpha + \beta) \cdot \mathbf{T(OD, 0, 0)} \cdot \mathbf{k}$$

(4.3)

Where α is the angle between the x-axis and $\overrightarrow{OA}$, β is the angle between the $\overrightarrow{OA}$ and $\overrightarrow{AD}$, and γ is the angle between the $\overrightarrow{AB}$ and $\overrightarrow{BC}$. These angles are static. θ is the angle of the revolute joint and is dynamic.

To reduce the number of variables for the optimisation α will be set to 0° and β and γ set to be 90°. This gives the motion range shown in Figure 4.2.
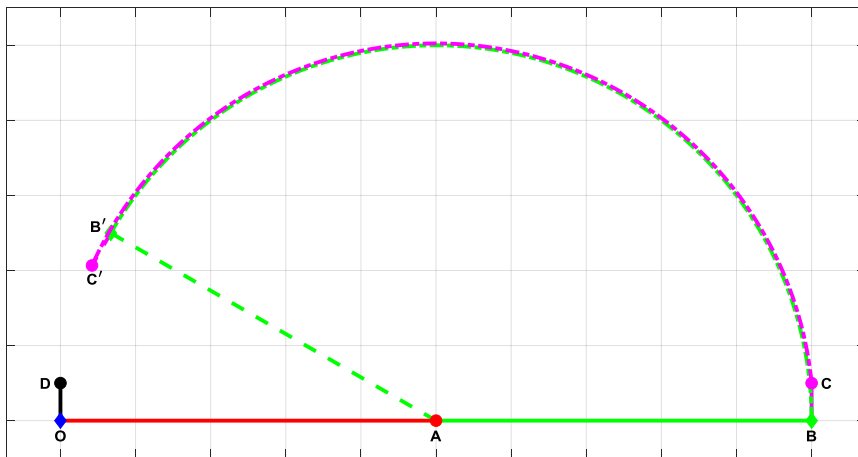
Figure 4.2: Motion range of the internal actuator. Labelling is the same as Figure 4.1, with B′ and C′ being the final motion endpoints.

As θ increases, points B and C rotate round A, ending at B' and C'. The dashed line indicates the final locations of $\overrightarrow{AB}$ and $\overrightarrow{BC}$. The dash-dot lines indicate the path that the points follow to the final location. This visually shows how much the actuator between C and D needs to travel to give the full range of motion.

There is the possibility of the internal actuator design of having singularities. As the actuator retracts, there is the possibility of the actuator becoming in line with the actual joint axis giving a zero moment arm. This is what appears to happen to the BLEEX system, and would mean that the system would require an external motion to break away from the singularity, which could cause injuries to the user. Geometric dimensions that result in this will be removed from the solutions, as a zero moment arm would require infinite force to move the joint, and thus would fail on the actuator safety factor.

4.3.2 External actuator

The external actuator design is similar to the internal actuator with the number of components, though there are some significant differences in its operation. Similar to the internal design, it encounters singularities during its motion, typically around full extension or retraction. It also has the benefit of the inside of the joint does not have any components that would restrict closing. Getting the system to give the full range of motions is difficult though, as it requires an extension of the lower limb past the joint.

This joint is typically found on excavator arms which have a large motion range but is also used on the BONES system [92] for the elbow motion.

The main difference between the internal and external joint when using hydraulics is the area imbalance of the piston, and the direction of the highest force required. In the excavator example, the highest force is when the actuator is extending and closing the joint as this is when the machine is under the highest load when digging. For BLEEX, they determined that standing from the squat, and thus the extension of the leg would require the highest load and have an internal actuator. The increase of pressure to give the increased force is dependent on the area differential of the rod and piston.

The external actuator system is shown in Figure 4.3.
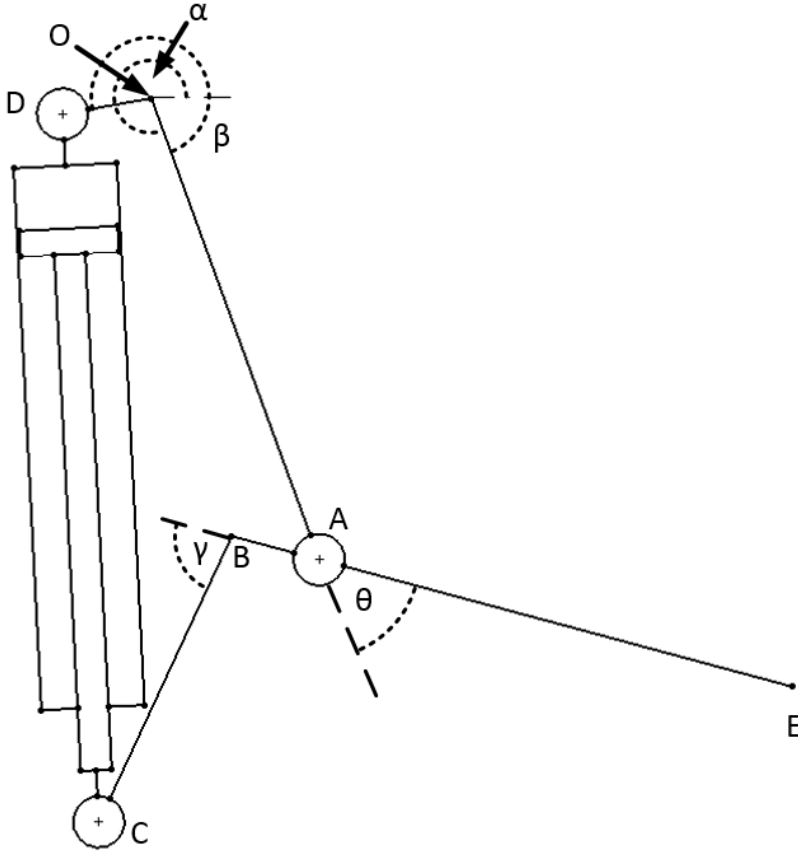
Figure 4.3: External Actuator diagram showing endpoints and angle

$\overrightarrow{OA}$ is the primary limb and is fixed in space. $\overrightarrow{AE}$ is the second limb and rotates. $\overrightarrow{AB}$ is the rear extension from A and $\overrightarrow{BC}$ and $\overrightarrow{OD}$ are the mounting points for the actuator.

The equations for the system are given in equations (4.4)

$$[\vec{A}] = \mathbf{R_Z(\alpha) \cdot T(OA, 0, 0) \cdot k}$$

$$[\vec{B}] = \mathbf{R_Z(\alpha) \cdot T(OA, 0, 0) \cdot R_Z(\theta - \pi) \cdot T(AB, 0, 0) \cdot k}$$

$$[\vec{C}] = \mathbf{R_Z(\alpha) \cdot T(OA, 0, 0) \cdot R_Z(\theta - \pi) \cdot T(AB, 0, 0) \cdot R_Z(\gamma)}$$
$$\mathbf{\cdot T(BC, 0, 0) \cdot k} \qquad (4.4)$$

$$[\vec{D}] = \mathbf{R_Z(\alpha + \beta) \cdot T(OD, 0, 0) \cdot k}$$

$$[\vec{E}] = \mathbf{R_Z(\alpha) \cdot T(OA, 0, 0) \cdot R_Z(\theta) \cdot T(AE, 0, 0) \cdot k}$$

Where α is the angle between the x-axis and $\overrightarrow{OA}$, β is the angle between $\overrightarrow{OA}$ and $\overrightarrow{AD}$, and γ is the angle between $\overrightarrow{AB}$ and $\overrightarrow{BC}$. These angles are static. θ is the angle of the revolute joint and is dynamic.

To reduce the number of variables for the optimisation α will be set to 0° and β and γ set to be 90°. This gives the motion as shown in Figure 4.4
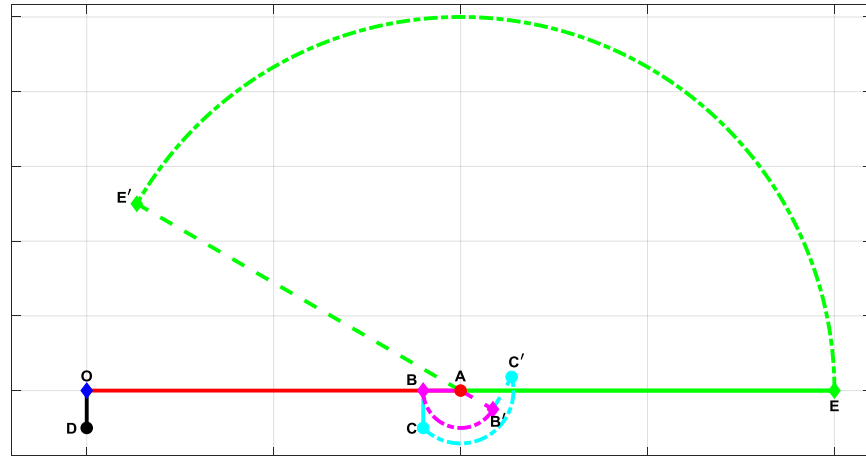
Figure 4.4: Motion range of the external actuator. Labelling is the same as Figure 4.3, with B′, C′ and E′ being the final motion endpoints.

The path of E to E' is the same as B to B' for the internal actuator. The stroke from D to C/C' is small that the internal actuator design. A smaller stroke is beneficial as it means that the basic length of the actuator can be smaller.

C' is above $\overrightarrow{AO}$ which would give a singularity as $\overrightarrow{DC}$ cross point A. The dimensions to avoid this would require significant optimisation, and for a large motion range, could be impossible.

4.3.3 Patella design

The patella is used within biological systems to extend the moment arm of the muscles to reduce the force required to move the limb. Muscle systems only work in retraction, and thus design for a dual motion system is different.

Though this design is based upon the knee joint, it can be used for any revolute joint within the system. To the author's knowledge, this is a novel design in using two actuators in the configuration.

The setup is shown in Figure 4.5.
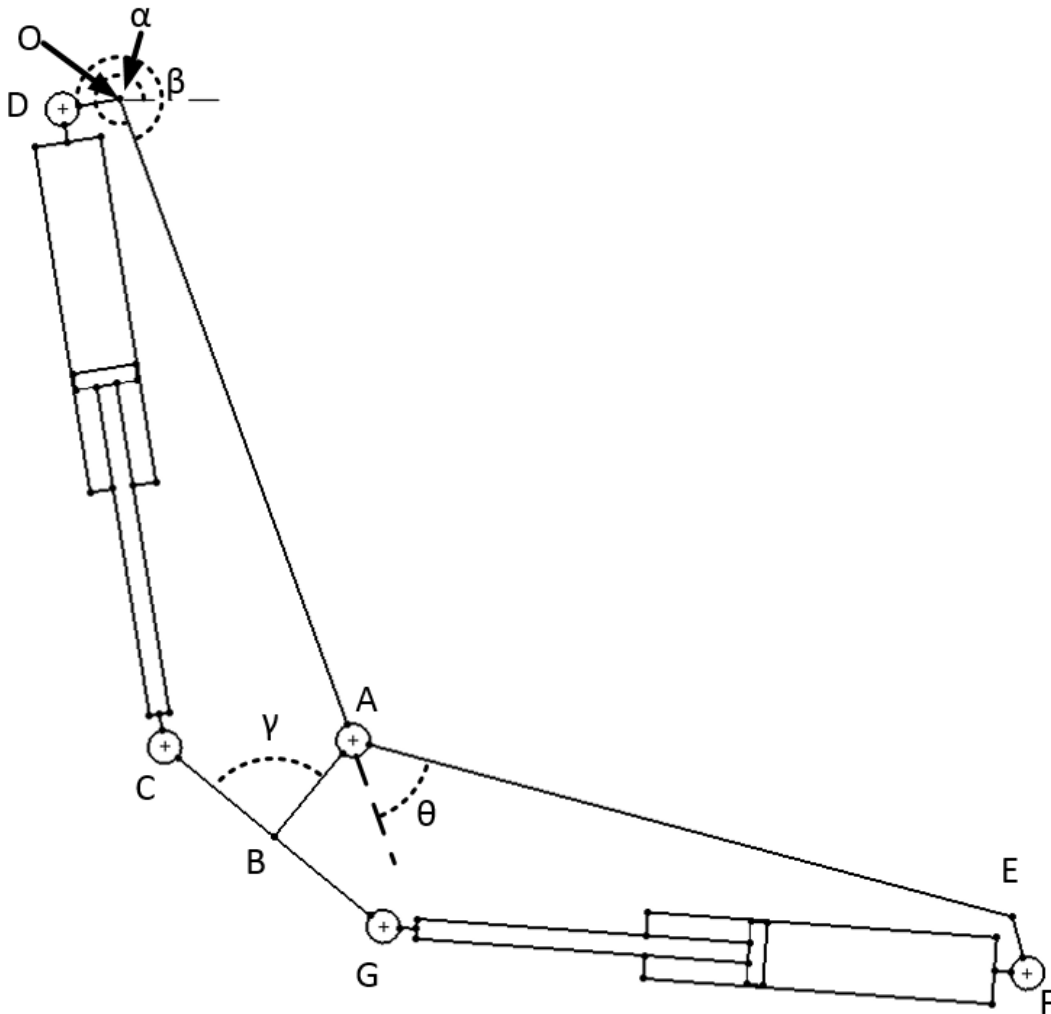
Figure 4.5: Patella Design diagram showing endpoints and angle

$\overrightarrow{OA}$ is the primary limb and is fixed in space. $\overrightarrow{AE}$ is the secondary limb and rotates. $\overrightarrow{OD}$ and $\overrightarrow{EF}$ are the actuator mounting points to the limbs. $\overrightarrow{AB}$ is the offset of the patella with $\overrightarrow{BC}$ and $\overrightarrow{BG}$ being the offset from the centre of the patella to the actuators.

The system appears to be similar to that of the external unit, though with each actuator only pushing the connection half of the required angle.

Though the design does not have to be symmetric, to simplify the equations it is assumed to be symmetrical around the $\overrightarrow{AB}$ axis, thus $\overrightarrow{OA}$ is equal in length to $\overrightarrow{AE}$ and $\overrightarrow{OD}$ is equal in length to $\overrightarrow{EF}$. To also aid in simplification, $\overrightarrow{CD}$ is assumed to be the same length as $\overrightarrow{FG}$, and thus $\overrightarrow{AB}$ bisects θ.

The equations are given in equations (4.5).

$$[\vec{A}] = R_Z(\alpha) \cdot T(OA, 0, 0) \cdot k$$

$$[\vec{B}] = R_Z(\alpha) \cdot T(OA, 0, 0) \cdot R_Z\left(\frac{\theta - \pi}{2}\right) \cdot T(AB, 0, 0) \cdot k$$

$$[\vec{C}] = R_Z(\alpha) \cdot T(OA, 0, 0) \cdot R_Z\left(\frac{\theta - \pi}{2}\right) \cdot T(AB, 0, 0) \cdot R_Z(\pi + \gamma) \qquad \textbf{(4.5)}$$
$$\cdot T(BC, 0, 0) \cdot k$$

$$[\vec{D}] = R_Z(\alpha + \beta) \cdot T(OD, 0, 0) \cdot k$$

Where α is the angle between the x-axis and $\overrightarrow{OA}$, β is the angle between the $\overrightarrow{OA}$ and $\overrightarrow{OD}$, and γ is the angle between the $\overrightarrow{AB}$ and $\overrightarrow{BC}$. These angles are static. θ is the angle of the revolute joint and is dynamic.

To reduce the number of variables for the optimisation α will be set to 0°, and β and γ set to be 90°. This is shown in Figure 4.6.
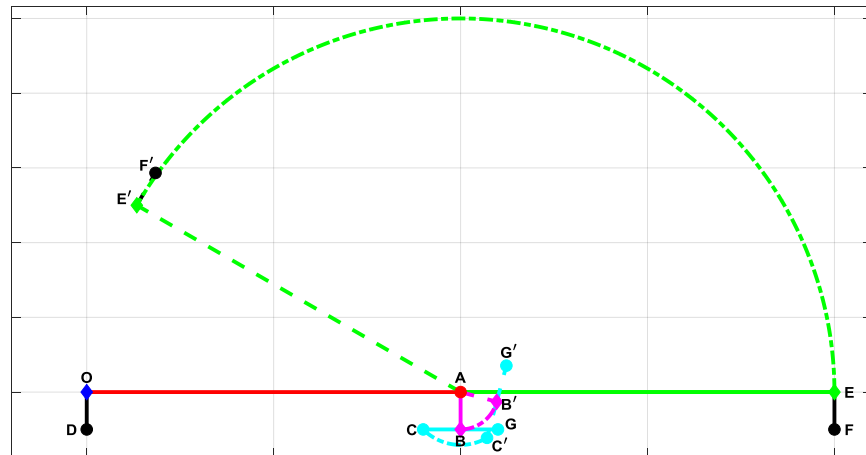
Figure 4.6: Motion range of patella design. Labelling is the same as Figure 4.5, with B′, C′ and E′ being the final motion endpoints.

The motion range appears similar to that of the external actuator, but the actuator endpoint C' do not cross the line $\overrightarrow{OA}$. This means that a singularity will be less likely to occur. The moment arm around A from C is also more consistent.

This system is similar to the external actuator system, though with a floating mid connector it requires two actuators and additional control requirements. This does make this solution more expensive than the single actuator solution

though the possibility of increased moment arm would be a benefit. For certain motions, only one actuator could be activated though the calculations are based on both actuators moving at the same rate.

The additional control aspects originate from attempting to keep the extensions of the actuators coordinated. This could be via the control software, or via hydraulic circuits. The recommended way is to have two servo valves, and use the control to keep them in sync [93]. It is an expensive solution, but with a safety-critical system, this should not be simplified. The use of the control solution gives a synchronization range of 0.025-0.051mm, compared to 0.254-1.524mm for the circuit based solutions [93]

4.3.4 Linkage designs

Four bar linkages have been used in a variety of components and designs, and thus there are numerous examples, though whether they are of a suitable mechanism to allow a limb to fold to nearly 180° is dependent on the setup.

A simple design is shown in Figure 4.7.
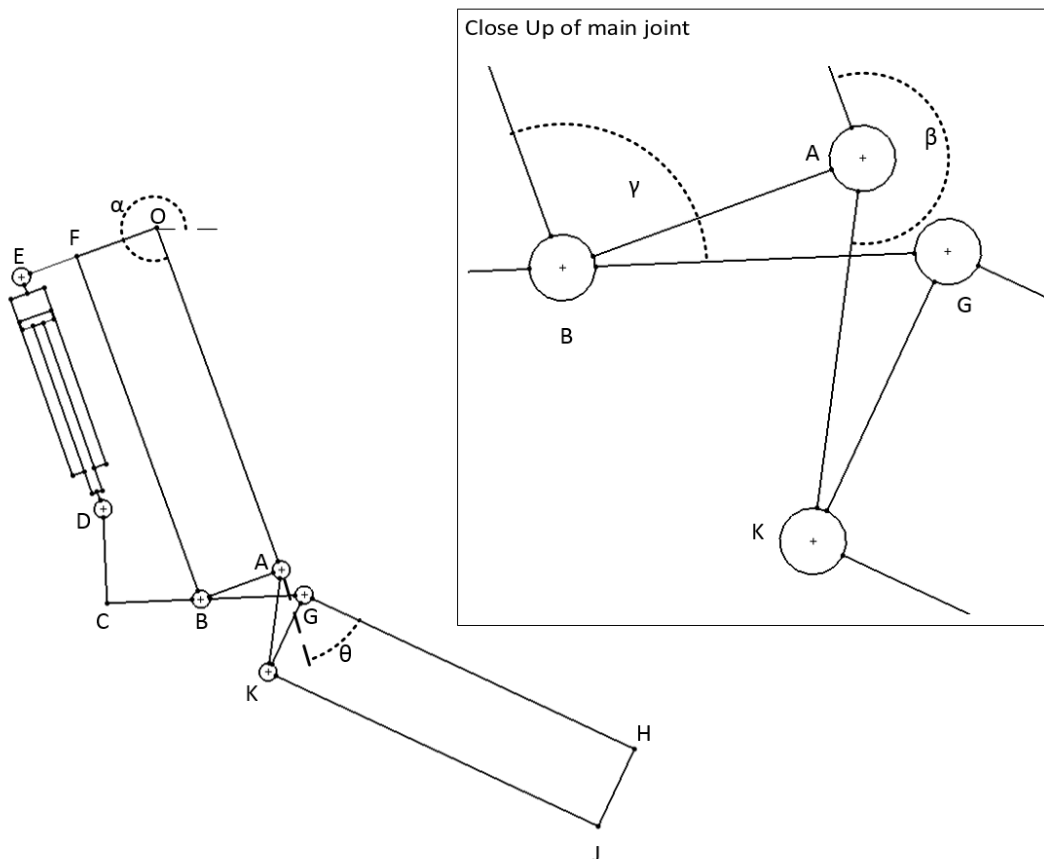
Figure 4.7: Four-Bar system diagram showing endpoints and angle

It is assumed that $\overrightarrow{OA}$, $\overrightarrow{BF}$, $\overrightarrow{GH}$ and $\overrightarrow{(JK)}$ are all the same length, as well as $\overrightarrow{OF}$, $\overrightarrow{AB}$, $\overrightarrow{GK}$ and $\overrightarrow{HJ}$. These all form rectangles with right angles and are rigid. $\overrightarrow{AK}$ and $\overrightarrow{BG}$ are the cross-links and are the same length. $\overrightarrow{BC}$ and $\overrightarrow{BG}$ are collinear. $\overrightarrow{CD}$ is perpendicular to $\overrightarrow{BC}$. $\overrightarrow{EF}$ is collinear with $\overrightarrow{OF}$.

This gives the following equations as shown in equation (4.6)

$$[\vec{A}] = R_Z(\alpha) \cdot T(OA, 0, 0) \cdot k$$

$$[\vec{B}] = R_Z\left(\alpha - \frac{\pi}{2}\right) \cdot T(OF, 0, 0) \cdot R_Z\left(\frac{\pi}{2}\right) \cdot T(FB, 0, 0) \cdot k$$

$$[\vec{C}] = R_Z\left(\alpha - \frac{\pi}{2}\right) \cdot T(OF, 0, 0) \cdot R_Z\left(\frac{\pi}{2}\right) \cdot T(FB, 0, 0)$$
$$\cdot R_Z(\gamma - \pi) \cdot T(BC, 0, 0) \cdot k$$

$$[\vec{D}] = R_Z\left(\alpha - \frac{\pi}{2}\right) \cdot T(OF, 0, 0) \cdot R_Z\left(\frac{\pi}{2}\right) \cdot T(FB, 0, 0)$$
$$\cdot R_Z(\gamma - \pi) \cdot T(BC, 0, 0) \cdot R_Z\left(\frac{\pi}{2}\right) \cdot T(CD, 0, 0) \cdot k$$

$$[\vec{E}] = R_Z\left(\alpha - \frac{\pi}{2}\right) \cdot T(OE, 0, 0) \cdot k$$

$$[\vec{F}] = R_Z\left(\alpha - \frac{\pi}{2}\right) \cdot T(OF, 0, 0) \cdot k$$

$$[\vec{G}] = R_Z\left(\alpha - \frac{\pi}{2}\right) \cdot T(OF, 0, 0) \cdot R_Z\left(\frac{\pi}{2}\right) \cdot T(FB, 0, 0)$$
$$\cdot R_Z(\gamma) \cdot T(BG, 0, 0) \cdot k$$

$$[\vec{H}] = R_Z(\alpha) \cdot T(OA, 0, 0) \cdot R_Z(\beta) \cdot T(AK, 0, 0)$$
$$\cdot R_Z\left(\gamma + \frac{\pi}{2}\right) \cdot T(GK, 0, 0) \cdot R_Z\left(-\frac{\pi}{2}\right)$$
$$\cdot T(GH, 0, 0) \cdot k$$

$$[\vec{J}] = R_Z(\alpha) \cdot T(OA, 0, 0) \cdot R_Z(\beta) \cdot T(AK, 0, 0)$$
$$\cdot R_Z\left(\gamma + \frac{\pi}{2}\right) \cdot T(GK, 0, 0) \cdot R_Z\left(-\frac{\pi}{2}\right)$$
$$\cdot T(GH, 0, 0) \cdot R_Z\left(-\frac{\pi}{2}\right) \cdot T(HJ, 0, 0) \cdot k$$

$$[\vec{K}] = R_Z(\alpha) \cdot T(OA, 0, 0) \cdot R_Z(\beta) \cdot T(AK, 0, 0) \cdot k$$

(4.6)

Where γ is defined by an anti-parallelogram.

An anti-parallelogram can be described as two ellipses that are tangential with the foci of the ellipses defined by A, B, G and K, as shown in Figure 4.8. These ellipses are equal in size such that the equations (4.7), (4.8) and (4.9) are true.

$$2\varepsilon := \left\| \overrightarrow{AK} \right\| = \left\| \overrightarrow{BG} \right\| \tag{4.7}$$

$$2\zeta := \left\| \overrightarrow{AB} \right\| = \left\| \overrightarrow{GK} \right\| \tag{4.8}$$

$$2\varepsilon > 2\zeta \tag{4.9}$$
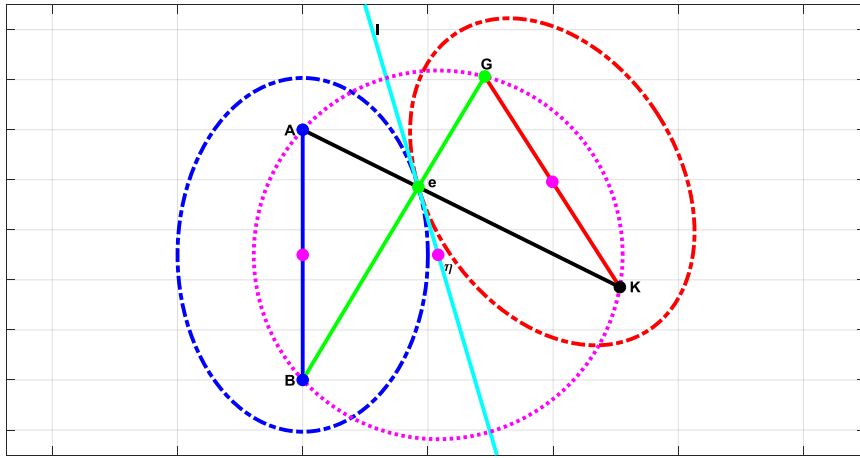
Figure 4.8: Details of the anti-parallelogram mechanism showing the four bars, the ellipse definitions and the mirror line (l)

Line l in Figure 1.8 is the tangential line of the two ellipses and is the plane of reflection between $\overrightarrow{AB}$ and $\overrightarrow{GK}$. The point, e in Figure 4.8, that the line touching the ellipses is defined in (4.10), and is the instantaneous pole.

$$\left(\varepsilon \cdot \sin \varphi, \sqrt{\varepsilon^2 - \zeta^2} \cos \varphi \right) \tag{4.10}$$

If a perpendicular line is drawn from the midpoint of AB and GK, they intersect at point η. For the simplest case, if AB is vertical, then η has the location of

$$\eta = \left[\frac{\sqrt{\varepsilon^2 - \zeta^2}}{\cos \varphi}, \mathbf{midpoint}(\overrightarrow{AB}) \right] \tag{4.11}$$

These two points can then be used to define line l which is the line of reflection from A and B to G and K.

This means that points G and K can be defined as

$$\overrightarrow{[BG]}$$
$$= \left[\frac{BG\sqrt{-AB^2 + BG^2}\cos(\varphi)}{AB \cdot \sin(\varphi) + BG}, -\frac{(AB^2 - BG^2)\sin(\varphi)}{AB \cdot \sin(\varphi) + BG} \right] \quad \textbf{(4.12)}$$

$$\overrightarrow{[AK]}$$
$$= \left[-\frac{BG\sqrt{-AB^2 + BG^2}\cos(\varphi)}{AB \cdot \sin(\varphi) - BG}, \frac{BG(-BG \cdot \sin(\varphi) + AB)}{AB \cdot \sin(\varphi) - BG} \right] \quad \textbf{(4.13)}$$

These can be converted to angles as shown in equations

$$\beta = \tan^{-1}\left(\frac{\dfrac{BG(-BG \cdot \sin(\varphi) + AB)}{AB \cdot \sin(\varphi) - BG}}{-\dfrac{BG\sqrt{-AB^2 + BG^2}\cos(\varphi)}{AB \cdot \sin(\varphi) - BG}} \right) \quad \textbf{(4.14)}$$
$$= \tan^{-1}\left(-\frac{-BG \cdot \sin(\varphi) + AB}{\sqrt{-AB^2 + BG^2}\cos(\varphi)} \right)$$

$$\gamma = \tan^{-1}\left(\frac{-\dfrac{(AB^2 - BG^2)\sin(\varphi)}{AB \cdot \sin(\varphi) + BG} + AB}{\dfrac{BG\sqrt{-AB^2 + BG^2}\cos(\varphi)}{AB \cdot \sin(\varphi) + BG}} \right) \quad \textbf{(4.15)}$$
$$= \tan^{-1}\left(\frac{BG \cdot \sin(\varphi) + AB}{\sqrt{-AB^2 + BG^2}\cos(\varphi)} \right)$$

To further simplify the equations, α being the angle between the x-axis and OA will be set to 0°. This is shown in Figure 4.9.

There are a larger number of moving components, both independent and linked. The internal and external designs had two moving sections, and the patella three. The four-bar also has three moving sections: the lower arm of GHJK, the crosslink AK and the crosslink DCBG. The number of joints though is higher. The internal and external only require three joints, the patella five and the four-bar six.
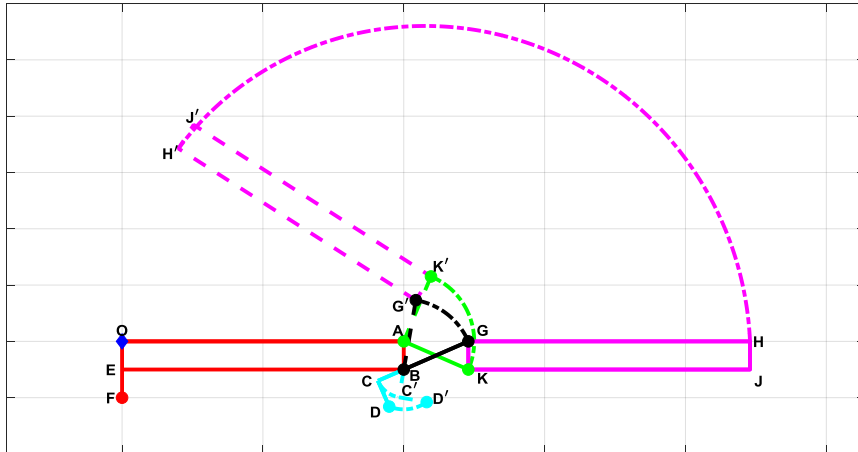
Figure 4.9: Motion range of the four-bar. Labelling is the same as Figure 4.7, with B′, C′ and E′ being the final motion endpoints.

The motion of point H to H', appears to be a constant curve, but as the design does not have a defined point of revolution, as shown in Figure 4.10.
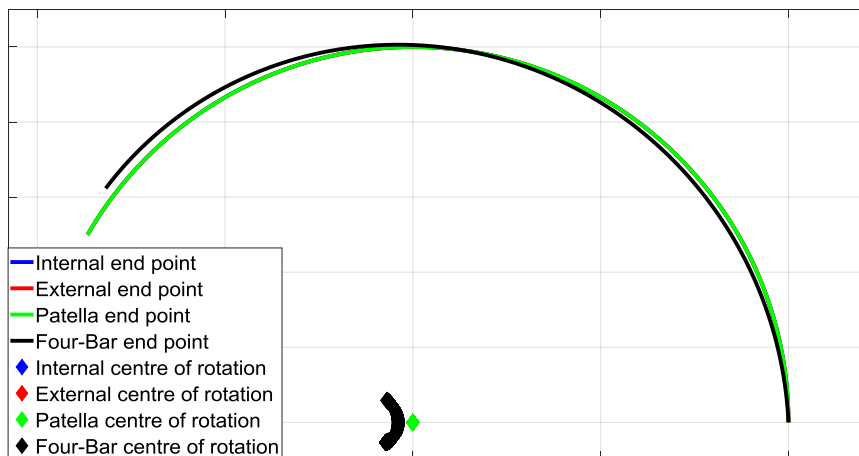
Figure 4.10: Location of endpoint at θ increases, with the centre of rotation for internal, external, patella and four-bar designs

For the internal, external and patella designs, the centre of rotation does not change, and all follow the same path for the endpoint. The four-bar design does not have the same centre of rotation and varies with θ. This change of centre could cause difficulties for any controller that is used.

There is an option to make the system symmetrical so that there is an actuator on each limb so that the force output from one is halved. As they would be

rigidly connected, this will reduce the error between the actuator extension difference, but could cause one to start to cavitate or lose pressure.

One major issue with this design is that as the joint approaches 180° of rotation, the cross members start to become collinear. This could cause singularity issues and weaken the perpendicular support for the joint.

4.3.4.1 Hoeken's Linkage

One variant of the four-bar design is the Hoeken linkage. This variant has been used in a variety of solutions from container ship cover hatches [94] to humanoid robots [95]

The Tactical Hazardous Operations Robot (THOR) [95-97] is a humanoid robot that uses Hoeken's[6] linkage as the joint design for the knee and hip. This is due to its ability to give a constant torque profile, 115Nm, with a large degree of motion, 150° [96]. This is shown in Figure 4.11 and Figure 4.12.

There have been several studies on the Hoeken linkage, with tables of range of motion available [98] giving the optimized results for straightness and constant velocity. These were used in the THOR system though there is the possibility that these are different from the optimised torque output for the inverted system. THOR is based on the constant velocity system [96]. Other studies have tried additional methods of optimising the system [99], using differential evolution optimisation.

The system has been converted to matrix transforms as per the previous examples and the setup is shown in Figure 4.13.

---

[6] There is some confusion on whether the system is Hoeken's linkage, Hoecken's linkage or Chebyshev's Lambda mechanism. Hoeken is Dutch for corners, whilst Hoecken and Chebshev are both named after inventers. Hoeken could be a misspelling of Hoecken. The mechanism was first demonstrated in the Plantigrade machine in Paris 1878 by Chebshev, whereas Hoecken was born in 1874.
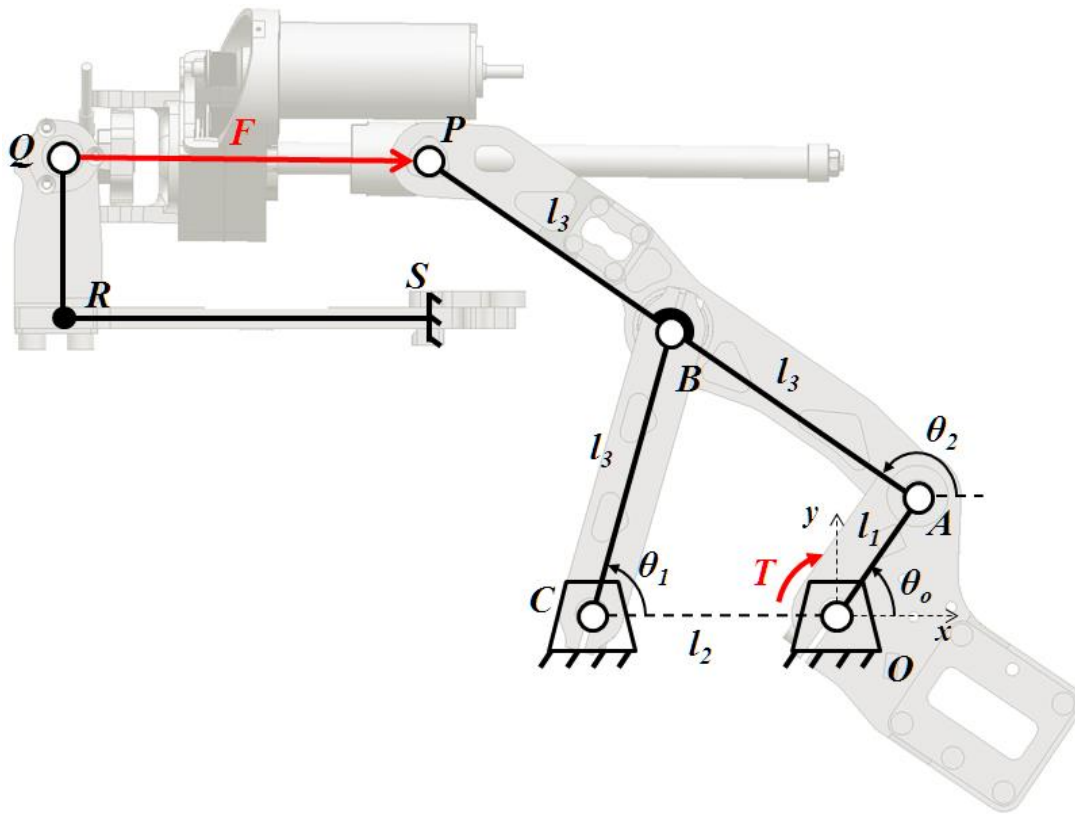
Figure 4.11: Hoeken's linkage schematic overlain on CAD render of the knee joint on THOR [95]
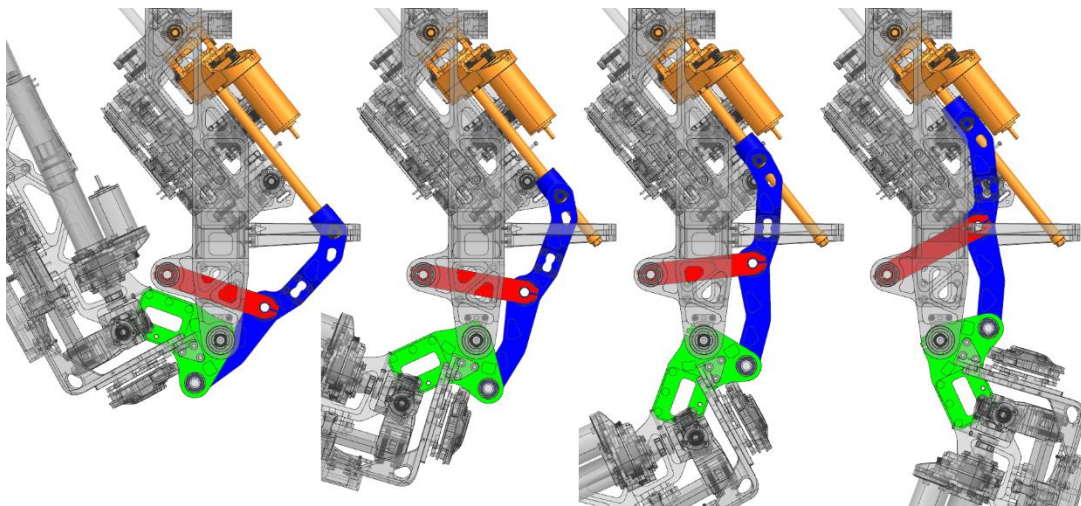
Figure 4.12: Render demonstrating motion profile of Hoeken's linkage in the knee joint of THOR (-5 to +135 degrees) [95]
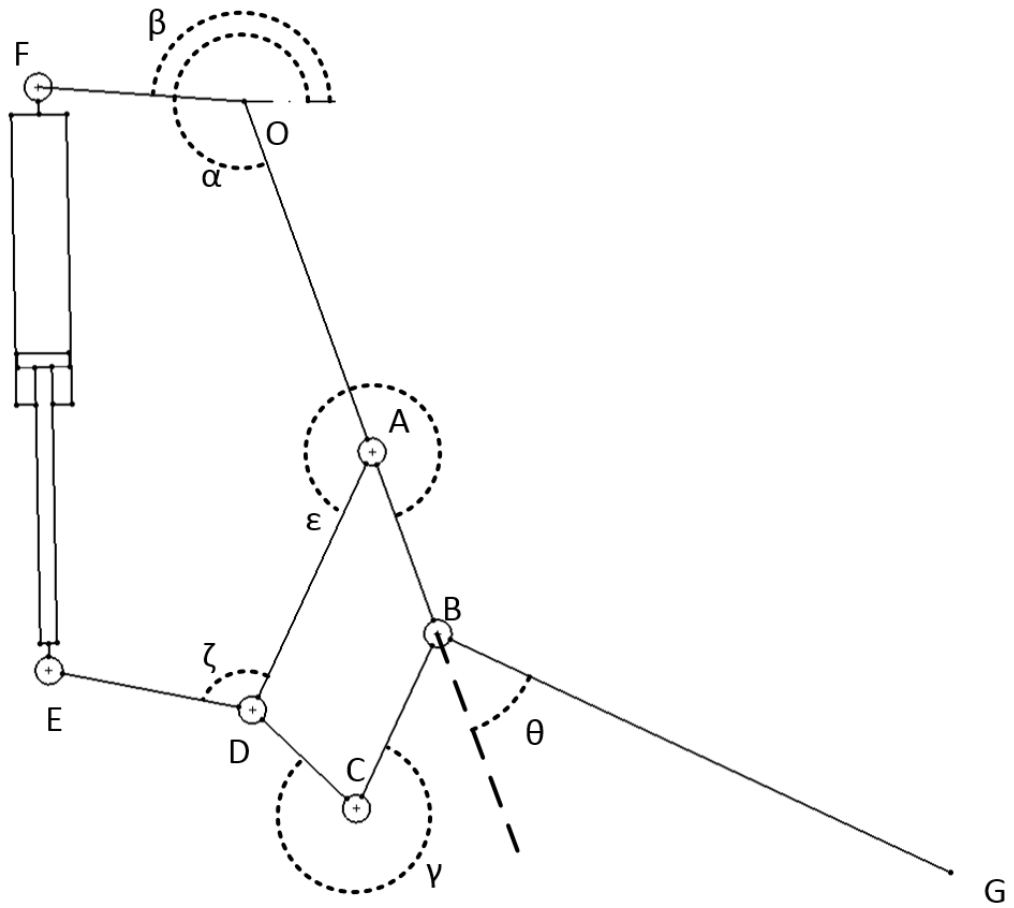
Figure 4.13: Hoeken's linkage diagram showing endpoints and angle

$\overrightarrow{OA}$ and $\overrightarrow{AB}$ are assumed to be collinear. $\overrightarrow{BC}$ and $\overrightarrow{BG}$ are assumed to be perpendicular. α and β and are all fixed angles, whilst θ, γ, ε and ζ vary with time. $\overrightarrow{CD}$ and $\overrightarrow{DE}$ are rigidly connected, and thus angle ∠CDE is fixed.

With the equations defining the motion are given in (4.16).

$$[\vec{A}] = R_Z(\alpha) \cdot T(OA, 0, 0) \cdot k$$

$$[\vec{B}] = R_Z(\alpha) \cdot T(OB, 0, 0) \cdot k$$

$$[\vec{C}] = R_Z(\alpha) \cdot T(OB, 0, 0) \cdot R_Z\left(\theta - \frac{\pi}{2}\right) \cdot T(BC, 0, 0) \cdot k$$

$$[\vec{D}] = R_Z(\alpha) \cdot T(OB, 0, 0) \cdot R_Z\left(\theta + \frac{\pi}{2}\right) \cdot T(BC, 0, 0)$$
$$\cdot R_Z(\gamma) \cdot T(CD, 0, 0) \cdot k$$
$$= R_Z(\alpha) \cdot T(OA, 0, 0) \cdot R_Z(\varepsilon) \cdot T(AD, 0, 0) \qquad \textbf{(4.16)}$$
$$\cdot k$$

$$[\vec{E}] = R_Z(\alpha) \cdot T(OA, 0, 0) \cdot R_Z(\varepsilon) \cdot T(AD, 0, 0) \cdot R_Z(\zeta)$$
$$\cdot T(DE, 0, 0) \cdot k$$

$$[\vec{F}] = R_Z(\alpha + \beta) \cdot T(OF, 0, 0) \cdot k$$

$$[\vec{G}] = R_Z(\alpha) \cdot T(OB, 0, 0) \cdot R_Z(\theta) \cdot T(BG, 0, 0)$$

Where $\overrightarrow{OA}$ and $\overrightarrow{BG}$ are the limbs of the system. $\overrightarrow{AD}$, $\overrightarrow{BC}$ and $\overrightarrow{CD}$ are the components of the Hoeken linkage mechanism.

To determine point D, the use of intersecting circles can be used. Where a circle of radius $\|\overrightarrow{AD}\|$ with centre A, intersects with a circle of radius $\|\overrightarrow{CD}\|$ with centre C. This gives two points, but the correct result is for the one which puts point D to behind the joint at B.

To simplify the model for optimisation, α is set to 0°, β is set to 90° and $\overrightarrow{CD}$ and $\overrightarrow{DE}$ are collinear. The motion range is shown in Figure 4.14
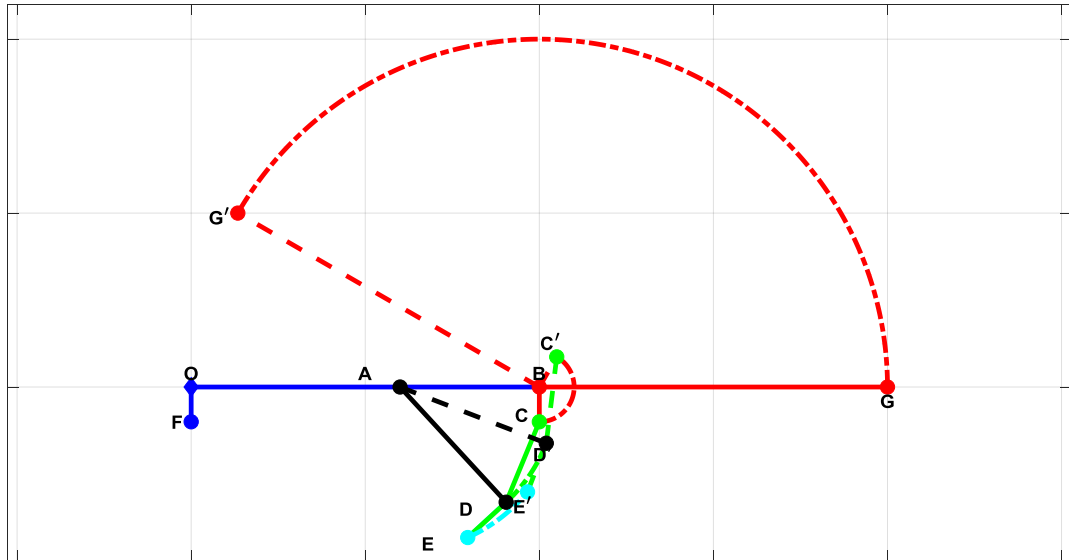
Figure 4.14: Motion range of Hoeken's linkage. Labelling is the same as Figure 4.13, with B′, C′ and E′ being the final motion endpoints.

With additional parts, the motion of the Hoeken's linkage has a higher complexity than the other joints, bar the four-bar system. As the joint rotates, the Hoeken's linkage amplifies the motion of E on to C. This means that though E might move by a small rotation, C has a larger range.

There is a risk of a singularity, in that if line CD crosses point B. This would be easy to determine if the perpendicular distance between the line and point become zero, then the singularity occurs, and the solution is not valid.

Similar to the four-bar linkage, there are issues of the increased number of bearings. Whether these overlap with each other or not would depend on the loading through each bearing and could be set with minimum lengths into the optimisation routine.

The THOR design uses an electric motor turning a lead screw with a nut attached to give the range of motion. This means that the basic length can be small compared to a hydraulic unit. In this case, the strain of the system is greater than that of hydraulics, though the output force is likely to be less.

4.4 Spherical or Gimbal joint

There are several options for multiple degrees of freedom joints for robotic systems, but for an exoskeleton system, several are not suitable. With the user giving the centre of rotations, the system would need to work around this or compensate for the difference. There is also the requirement that the exoskeleton does not interfere with the user as this could cause injury.

The gimbal joint uses multiple curved sections to give three axes of revolution between two different objects. This means that the centre of rotation of the joint can be within the human body, for example, the shoulder joint, and allows rotation around it. The issue of gimbal lock, when one or more of the joint axes become parallel, is an issue that needs to be accounted for. This can be as simple as having limits within the system to prevent it from reaching this point, as it does not need full rotation.

The motion source for the shoulder would have flexion/extension at one end and abduction/adduction at the other. The rotation would be between the gimbal arms and could be either a linear actuator or a rotary unit. The sizing of the rotation actuator would be critical to allow correct motion range and prevent trapping of the user.

The gimbal joints allow an open exoskeleton system that could increase the safety of the user. To facilitate this, the optimisation has included an STL human model that has been used to determine the interaction between the arms of the gimbal and the human. The m-function, *inpolyhedron* by Sven Holcombe [100], was used to calculate the interaction of the arm lines and the STL model. For any result that included any part of the gimbal line construct was eliminated, reducing the input range of motion, or forcing the increase of the radius of for the gimbal.

4.4.1 Two bar joint

The simplest method is to have two lengths for the joint, with actuation at each pivot. The rear and the middle joint would give abduction/adduction and rotation, with the end giving flexion/extension in the case for the shoulder and hip. A simple version is shown in Figure 4.15.
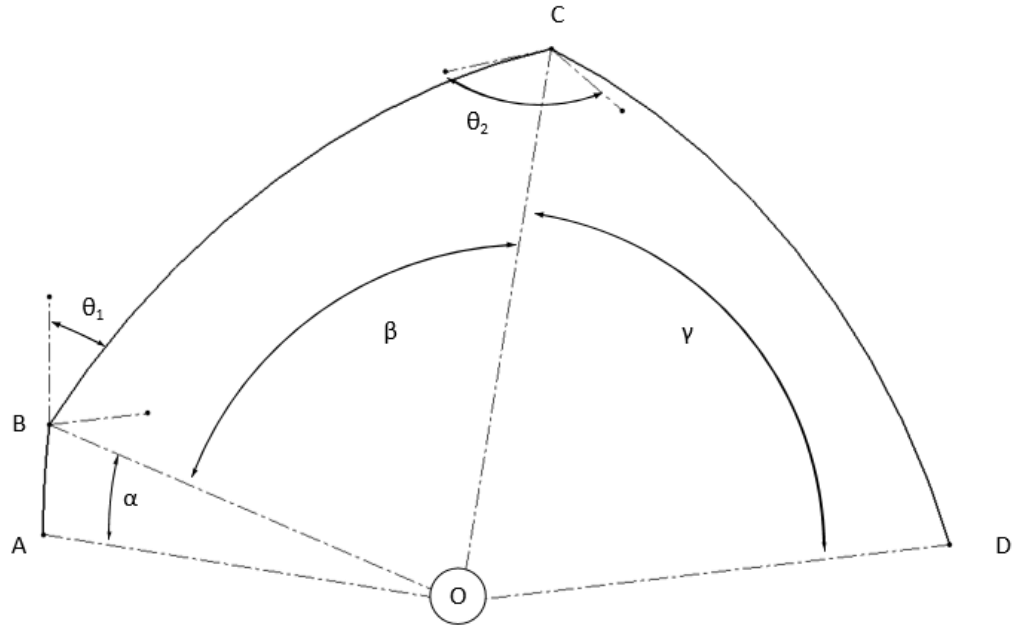
Figure 4.15: Two bar joint.

This is simple to construct, and with revolute actuators, should not require additional bearings. With the use of linear actuators, there is likely to be a limit in motion due to the requirement for the actuator to be in line with the joints. This would also likely extend the envelope of the exoskeleton.

The issue is that the mass is spread along the joint, and would require significant strength in the joint beams

The equations for setting up the two bar joint are similar to the revolute joint but are within a 3D environment rather than 2D. The basic equations of motion are given in (4.17).

$$R_x(\theta) = \begin{pmatrix} 1 & 0 & 0 \\ 0 & \cos(\theta) & -\sin(\theta) \\ 0 & \sin(\theta) & \cos(\theta) \end{pmatrix}$$

$$R_y(\theta) = \begin{pmatrix} \cos(\theta) & 0 & \sin(\theta) \\ 0 & 1 & 0 \\ -\sin(\theta) & 0 & \cos(\theta) \end{pmatrix}$$

$$R_z(\theta) = \begin{pmatrix} \cos(\theta) & -\sin(\theta) & 0 \\ \sin(\theta) & \cos(\theta) & 0 \\ 0 & 0 & 1 \end{pmatrix}$$

$$k = \begin{pmatrix} 0 \\ 0 \\ \text{Radius} \end{pmatrix}$$

(4.17)

These then can give the locations for the endpoints for the limbs, as shown in Figure 4.15, and are given in (4.18).

$$\left[\vec{A}\right] = \mathbf{R_z}(\alpha) \cdot \mathbf{R_y}(\beta) \cdot \mathbf{R_x}(\gamma) \cdot \mathbf{k(OA)}$$

$$\left[\vec{B}\right] = \mathbf{R_z}(\alpha) \cdot \mathbf{R_y}(\beta) \cdot \mathbf{R_x}(\gamma) \cdot \mathbf{R_z}(\theta_1) \cdot \mathbf{R_y}(\psi) \cdot \mathbf{k(OB)}$$

$$\left[\vec{C}\right] = \mathbf{R_z}(\alpha) \cdot \mathbf{R_y}(\beta) \cdot \mathbf{R_x}(\gamma) \cdot \mathbf{R_z}(\theta_1) \cdot \mathbf{R_y}(\psi) \cdot \mathbf{R_z}(\theta_2)$$
$$\cdot \mathbf{R_y}(\phi) \cdot \mathbf{k(OC)}$$

(4.18)

O is the centre of the gimbal joint. α, β and γ are used to line up point A in regards to the human and are fixed in time. This allows the initial point to be anywhere on a sphere rather than along one of the principal axis. This helps prevent contact between the gimbal joint and the human. $\|\overrightarrow{OA}\|$, $\|\overrightarrow{OB}\|$ and $\|\overrightarrow{OC}\|$ are of equal lengths and are the distance from the points to the origin. ψ and ϕ are the fixed angle sweep between A to B and B to C respectively. θ_1 and θ_2 are the motion inputs for the joint.

As the inputs directly give the output of the system, then determining the angle of the output to the centre of rotation is simply converting $\vec{C}$ to spherical coordinates.

As the limbs are curves and not straight a three-dimensional curve needs to be computed. This is done by taking the two ends of the arc and the radius of the arc and putting them through the equations given in (4.19).

$$\vec{U} = \left(\overrightarrow{P_1} \times \overrightarrow{P_2}\right) \times \overrightarrow{P_1}$$

$$\vec{V} = \mathbf{radius}\frac{\vec{U}}{\|\vec{U}\|}$$

(4.19)

The endpoints are defined as 0 and the 2-argument arctangent of the norm cross product of $\overrightarrow{P_1}$ and $\overrightarrow{P_2}$ and the dot product of $\overrightarrow{P_1}$ and $\overrightarrow{P_2}$. A vector of values can be generated between these two points, as given in (4.20)

$$\mathbf{t} = \left(\mathbf{0} \cdots \mathbf{atan2}\left(\|\overrightarrow{P_1} \times \overrightarrow{P_2}\|, \overrightarrow{P_1} \cdot \overrightarrow{P_2}\right)\right)$$

(4.20)

This array of values can be converted to the curve with the equation given in (4.21)

$$\vec{T} = \vec{P_1}\cos(t) + \vec{V}\sin(t) \qquad\qquad (4.21)$$

Figure 4.16 shows this mechanism motion range.
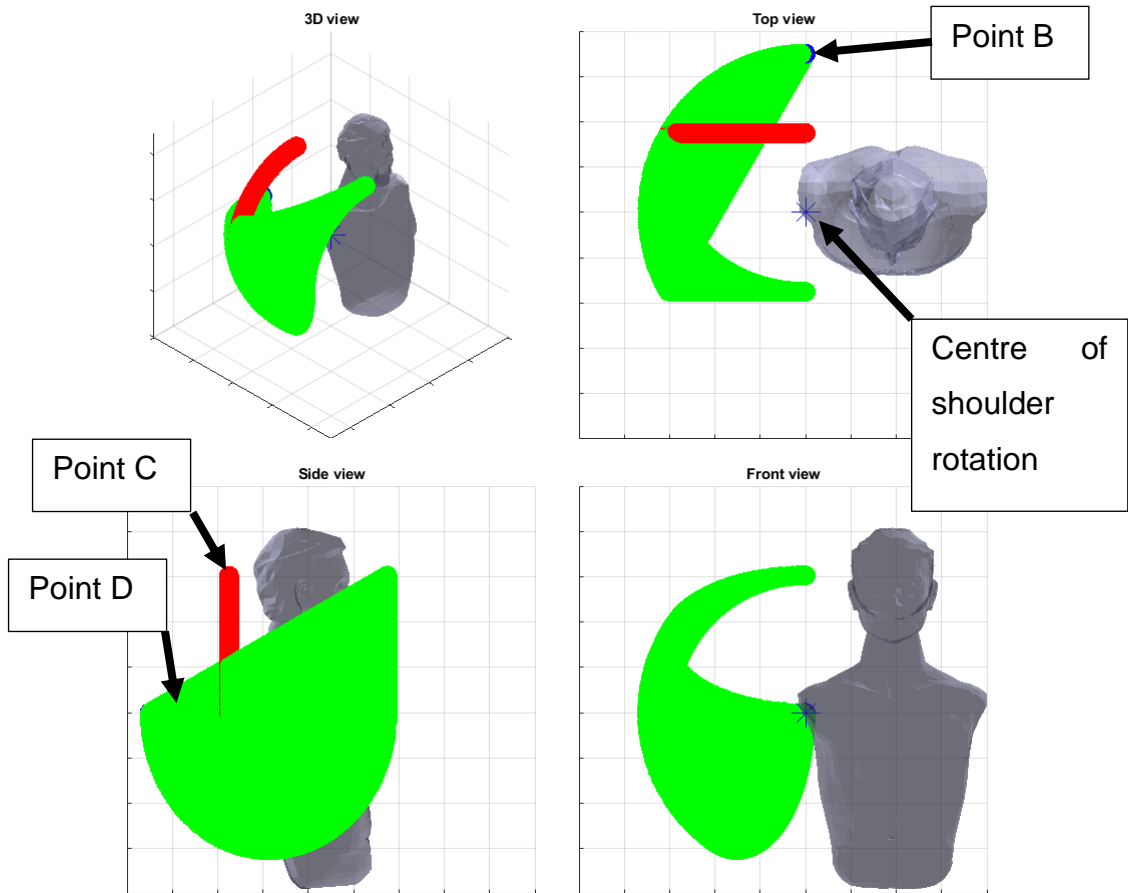
Figure 4.16: Complete workspace environment of the two-bar joint for initial starting values. The asterisk indicates the shoulder centre of rotation, the rear blue dot is the location of point B, the red curve is the location of point C as θ1 changes, and the green surface is the location of point D as θ1 and θ2 change. The human model is included.

The two bar joint has a large range of motion for the endpoint, where θ_1 ranges between 0-90°, and θ2 ranges between 0-180°. When θ_1 is at 90°, i.e. horizontal to the floor, then the endpoint D follows the bottom arc of the range of motion as the plane that D follows is perpendicular to the floor. As θ_1 approaches 0°, the plane that D follows starts to become parallel to the floor, giving altering the angle of the arc.

4.4.2 Five bar joint

A variant of the gimbal joint is a five bar joint, which has been examined by several groups [101-104], though there does not appear to have been any focus on using the joint for an exoskeleton system at the current time.

Similar to Figure 4.15, Figure 4.17 shows the five-bar system.

The 5R spherical parallel manipulator has the benefit that the actuation system can be on the rear of the system, leaving the majority of the weight on the back of the user.

The five-bar system uses two actuators for two degrees of freedom, so an extra mechanism is required for the final degree of motion.

The main issue is the increased size, as well as the requirement for additional bearings. There are also the issues that at the end of the actuator there require three links off the one joint that needs a base a follower with powered motion, and one with a floating action.
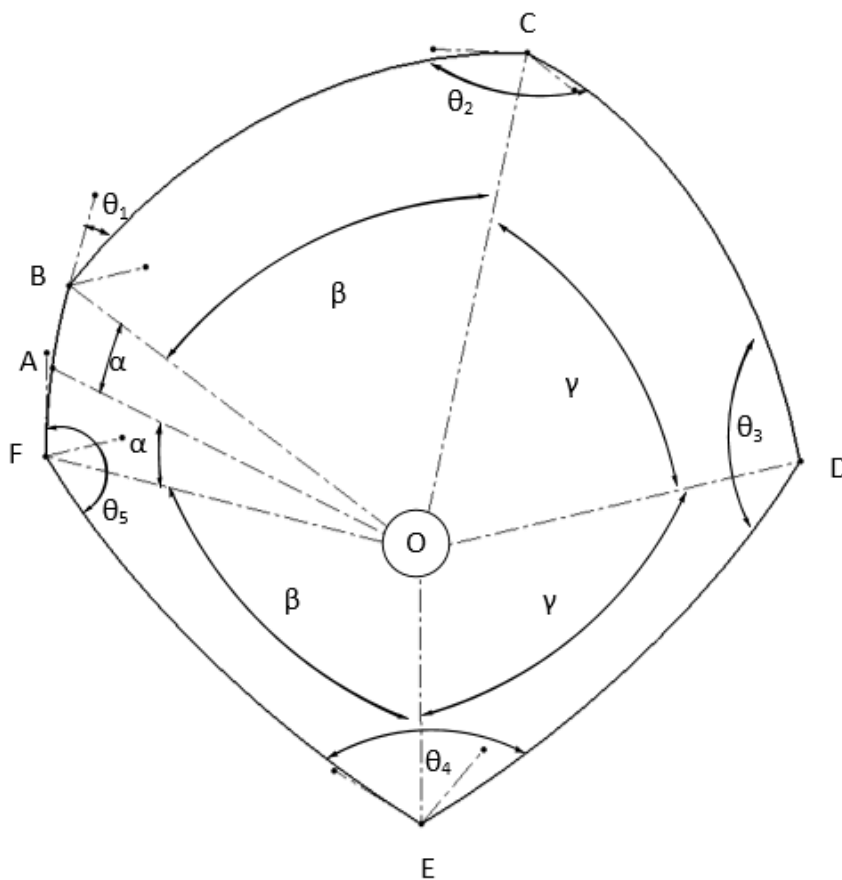
Figure 4.17: Five bar joint

Similar to the two bar joint, the five-bar joint can be expressed in several equations given in (4.22)

$$\left[\vec{A}\right] = \mathbf{R_z}(\alpha) \cdot \mathbf{R_y}(\beta) \cdot \mathbf{R_x}(\gamma) \cdot \mathbf{R_y}(\psi) \cdot \mathbf{k(OA)}$$

$$\left[\vec{B}\right] = \mathbf{R_z}(\alpha) \cdot \mathbf{R_y}(\beta) \cdot \mathbf{R_x}(\gamma) \cdot \mathbf{R_y}(\psi) \cdot \mathbf{R_z}(\theta_1) \cdot \mathbf{R_y}(\phi)$$
$$\cdot \mathbf{k(OA)}$$

$$\left[\vec{B}\right] = \mathbf{R_z}(\alpha) \cdot \mathbf{R_y}(\beta) \cdot \mathbf{R_x}(\gamma) \cdot \mathbf{R_y}(-\psi) \cdot \mathbf{R_z}(\theta_5) \cdot \mathbf{R_y}(\phi)$$
$$\cdot \mathbf{k(OA)}$$

$$\left[\vec{E}\right] = \mathbf{R_z}(\alpha) \cdot \mathbf{R_y}(\beta) \cdot \mathbf{R_x}(\gamma) \cdot \mathbf{R_y}(-\psi) \cdot \mathbf{k(OA)}$$

(4.22)

O is the centre of the gimbal joint. α, β and γ are used to line up point A in regards to the human and are fixed in time. This allows the initial point to be anywhere on a sphere rather than along one of the principal axis. This helps prevent contact between the gimbal joint and the human. $\|\overrightarrow{OA}\|$, $\|\overrightarrow{OB}\|$ and $\|\overrightarrow{OC}\|$ are of equal lengths and are the distance from the points to the origin. ψ and ϕ are the fixed angle sweep between A to B and B to C respectively. θ_1 and θ_2 are the motion inputs for the joint. θ_2 and θ_4 move but do not have direct input into their positions, relying on the solution to point D.

To determine point D, the equations by Jesús Cervantes-Sánchez [104] can be used with the selected nomenclature, as given in (4.23).

$$\mathbf{D_z} = \frac{-\mathbf{b} \pm \sqrt{\mathbf{b^2 - 4ac}}}{2\mathbf{a}}$$

$$\mathbf{D_y} = \mathbf{S} \cdot \mathbf{D_z} + \mathbf{T}$$

$$\mathbf{D_x} = \mathbf{M} \cdot \mathbf{D_z} + \mathbf{N}$$

(4.23)

Given the parameters in (4.24)

$$a = M^2 + S^2 + 1$$

$$b = 2(M \cdot N + S \cdot T)$$

$$c = N^2 + T^2 - r^2$$

$$M = \left(\frac{C_z \cdot E_y - C_y \cdot E_z}{C_y \cdot E_x - C_x \cdot E_y} \right)$$

$$N = \frac{1}{2} \left(\frac{(2r^2 - L^2)(C_y - E_y)}{C_y \cdot E_x - C_x \cdot E_y} \right) \qquad \textbf{(4.24)}$$

$$S = \left(\frac{C_z \cdot E_x - C_x \cdot E_z}{C_x \cdot E_y - C_y \cdot E_x} \right)$$

$$T = \frac{1}{2} \left(\frac{(2r^2 - L^2)(C_x - E_x)}{C_x \cdot E_y - C_{.y} E_x} \right)$$

$$L = 2r \sin \frac{\beta}{2}$$

Where r is the radius of the sphere given by OB.

There are two solutions for D from (4.24) of which the result that gives an obtuse angle to the plane OBC is selected.

The curved beams can then be calculated similarly to the two bar joint.

The workspace of the five bar joint can also be determined from the equations to show the complete endpoint locations. This is shown in Figure 4.18. The endpoints of the system are shown as the yellow area, with the centre of the joint being the dark diamond in the middle of the sphere. The back is the pale line at the right of the sphere.
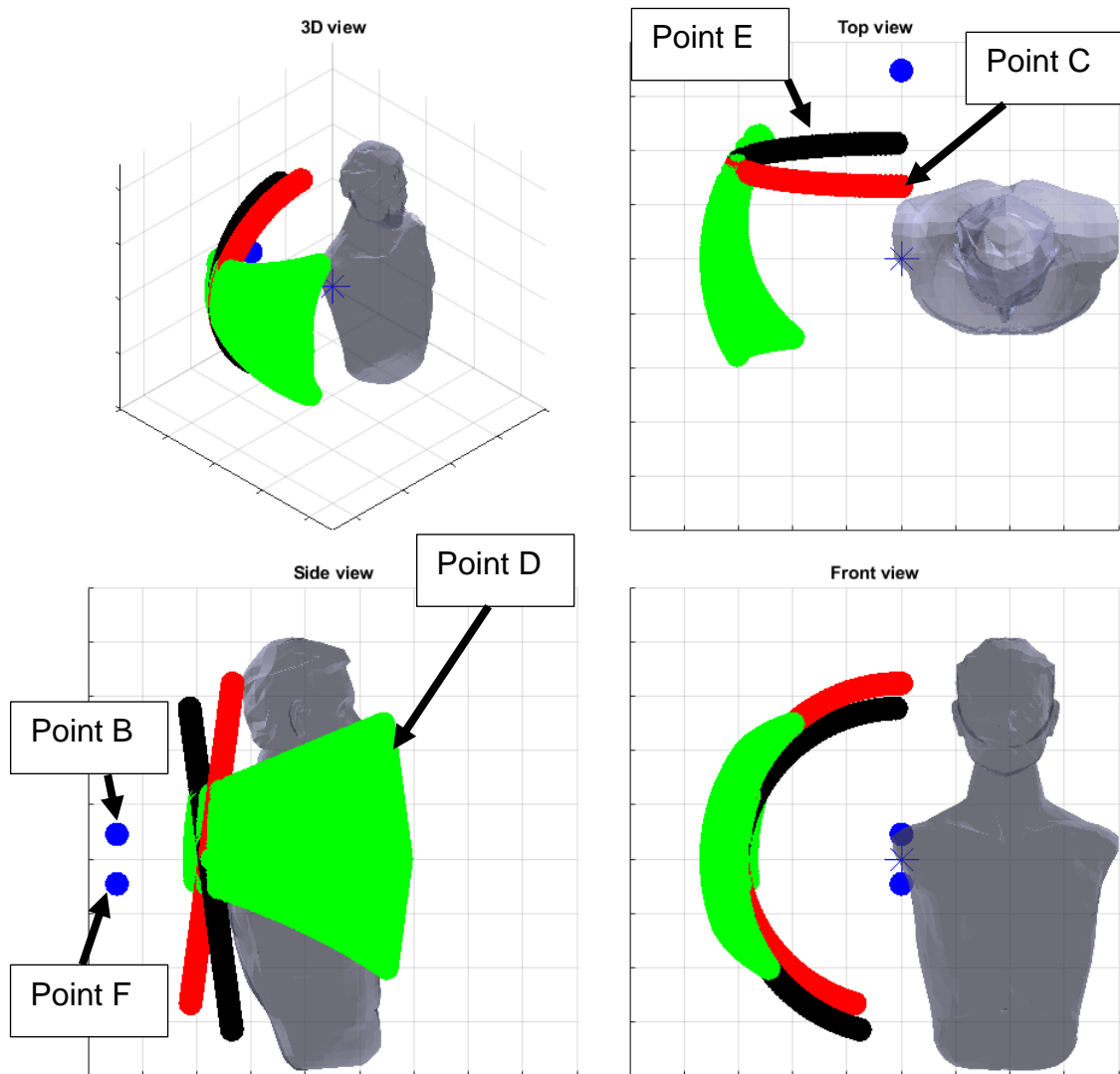
Figure 4.18: **Complete workspace environment of the five bar system for initial starting values. The asterisk indicates the shoulder centre of rotation, the rear blue dots are the locations of point B and F, the red curve is the location of point C as θ_1 changes, the black curve is the location of point E as θ_5 changes, and the green surface is the location of point D as θ_1 and θ_5 change.. The human model is included.**

The five-bar model has a symmetrical solution around the horizontal plane the intersects the shoulder centre of rotation. The motion range of the shoulder is not symmetrical, so this could mean that some of the actuator outputs are not used.

4.4.3 Four bar extension to two bar and five bar joint

One method of reducing the angle range of the flexion-extension would be the use of a parallelogram to create a parallel bar at the end of the gimbal. In a two dimensional linkage, this is a simple four-bar joint but becomes more

complicated with a spherical joint. A layout for this is shown in Figure 4.19 and shows the additional variables.

To the author's knowledge, extending the two bar and five bar with the parallel additions does not appear to have been developed, and is thus a novel solution.
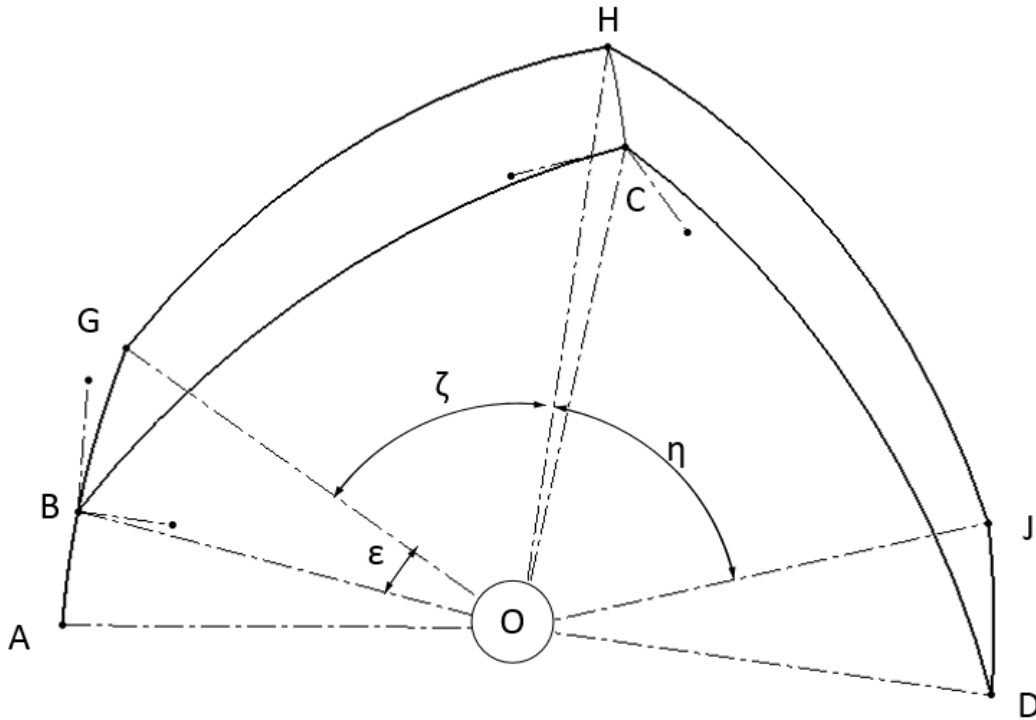
Figure 4.19: Four bar extension for the two bar system

The extension to the two-bar extension has the additional equations given in (4.25)

$$[\vec{G}] = R_z(\alpha) \cdot R_y(\beta) \cdot R_x(\gamma) \cdot R_y(\varepsilon) \cdot k(OA)$$

$$[\vec{H}] = R_z(\alpha) \cdot R_y(\beta) \cdot R_x(\gamma) \cdot R_z(\theta_1) \cdot R_y(\psi) \cdot R_z(\zeta) \cdot R_y(B)$$
$$\cdot k(OB) \qquad\qquad \textbf{(4.25)}$$

$$[\vec{K}] = R_z(\alpha) \cdot R_y(\beta) \cdot R_x(\gamma) \cdot R_z(\theta_1) \cdot R_y(\psi) \cdot R_z(\theta_2)$$
$$\cdot R_y(\phi) \cdot k(OC)$$

ε is the offset angle of the four-bar system from the original two-bar system and is the same for BE, CF, and DG. ζ and η are the four-bar links equivalent lengths for ψ and ϕ respectively.
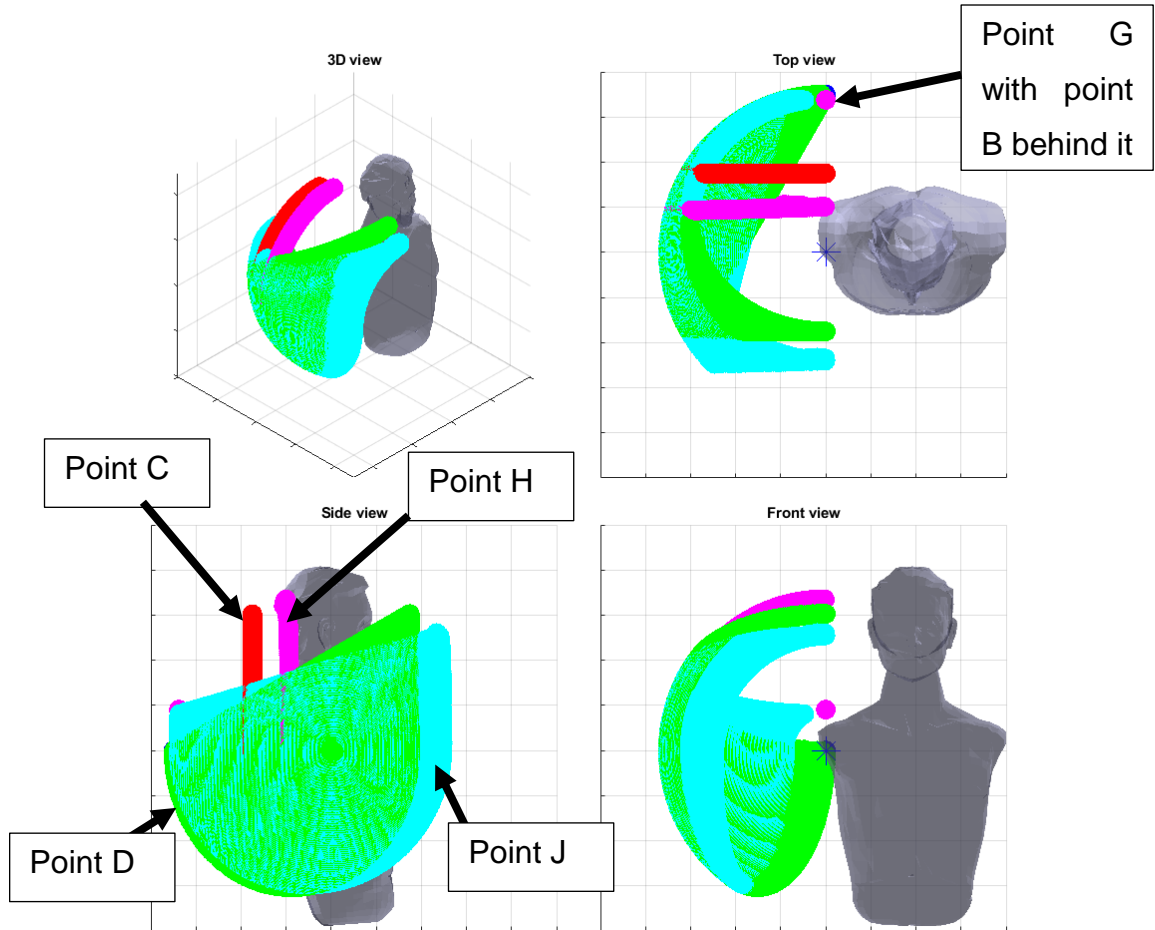
Figure 4.20: Complete workspace environment of the two-bar system with four-bar extension for initial starting values. The asterisk indicates the shoulder centre of rotation, the red curve is the location of point C as θ₁ changes, and the green surface is the location of point D as θ₁ and θ₂ change. Point B is behind point G on the top view. Point H is a curve, similar to point C, whilst the surface of point J is also shown. The human model is included.

With the four-bar extension to the two bar system, it can be seen that point J follows a similar curve to that of point D, with an offset caused but the angle ε.

As the mechanism moves, there is a chance of singularities forming if line HJ crosses D. This is due to the bi-stable point that J can occupy in regards to point D: either above or below line CD. This cross over will occur in the system when line HJ has a zero perpendicular distance to point D, and thus angles that this can occur at will be removed from the solution.

The five-bar system uses the same above equations to determine the four-bar location.
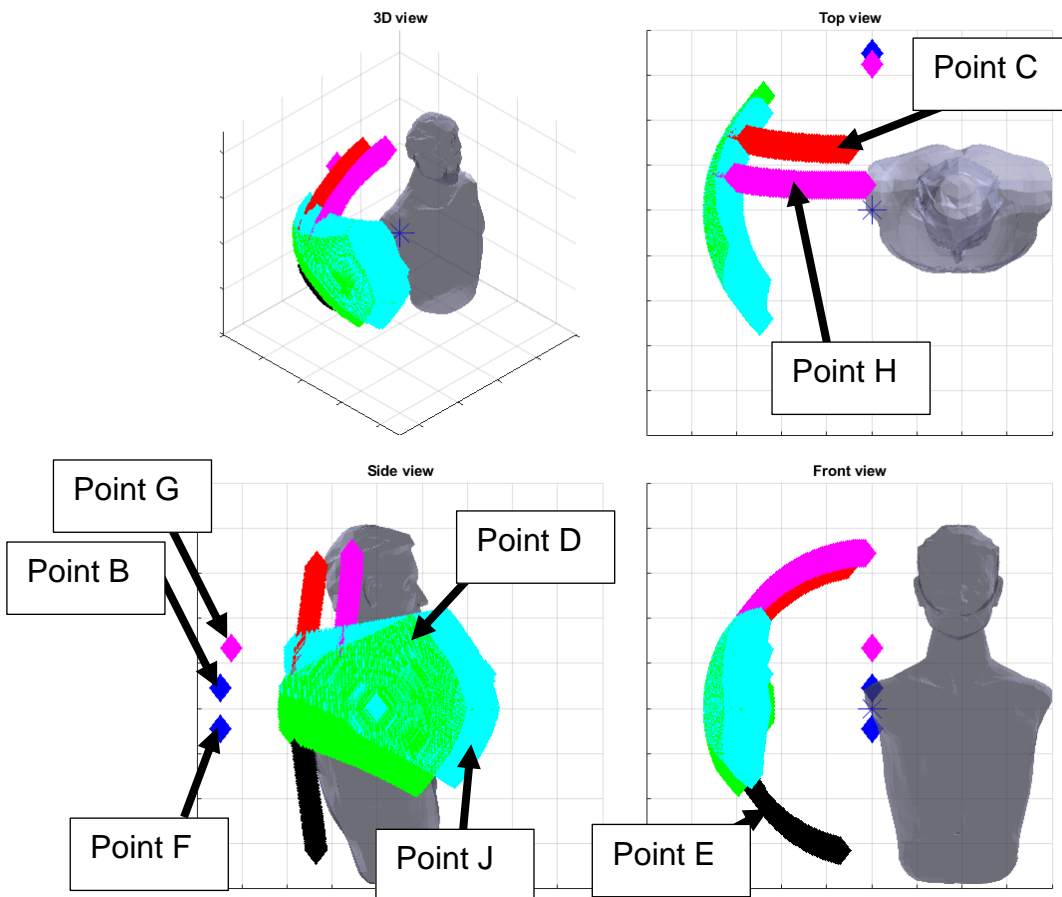
Figure 4.21: Complete workspace environment of the five bar system for initial starting values. The asterisk indicates the shoulder centre of rotation, the rear blue dots are the locations of point B and F, the red curve is the location of point C as θ_1 changes, the black curve is the location of point E as θ_5 changes, and the green surface is the location of point D as θ_1 and θ_5 change. Point H is a curve, similar to point C, whilst the surface of point J is also shown. The human model is included The human model is included

The workspace sample for the five-bar with four-bar extension is similar to the five-bar example, but with the additional singularity issues as the two-bar with four-bar extension system, in that, a singularity occurs when the perpendicular distance between line HJ and point D become zero.

4.4.4 Bevel gear extension to two bar and five bar joint

As the shoulder requires flexion/extension motion, an additional actuator is needed, as the five bar system will only give two degrees of motion. Where the actuator is connected is important as the angle between the final gimbal arm and the next limb will change as the five bar joint rotates. For example, when the gimbal arms are moving from vertical coincident to horizontally forwards, i.e. BC and CD on moving from being vertically collinear to on to a horizontal plane

as seen from Figure 4.17, the flexion actuator has to move in tandem to keep the arm at the same angle relative to the ground.

This can be compensated for by the converting of the endpoint from a single pivot into a mated gear set. This would keep a base plate that has a centre line plane that intercepts the centre of rotation and the backplate. This would simplify the control system, as it would not have to compensate and determine the location of one of the limbs to give the correct flexion of the shoulder. A sample gear configuration is shown in Figure 4.22.
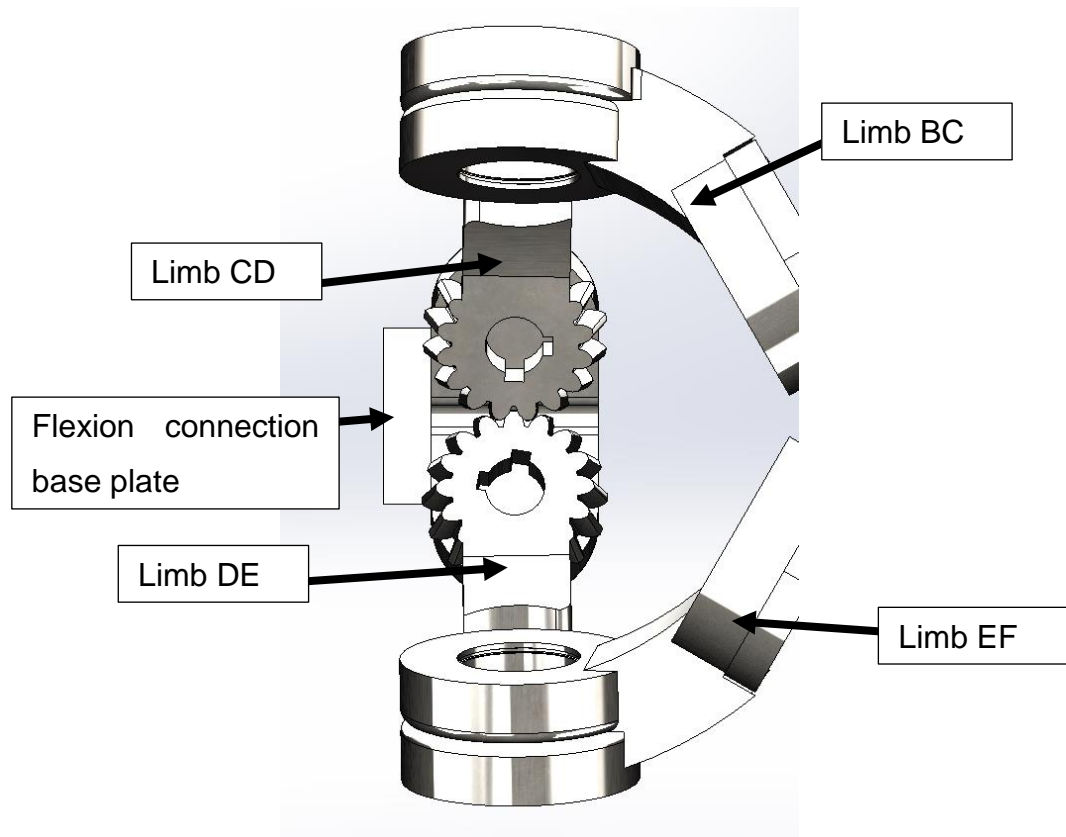
Figure 4.22: Simple gear set up to keep a fixed reference for the end effector

In the setup described in Section 4.4.2, limb DE is free to rotate around point D with no interaction with limb CD. With the design shown in Figure 4.22, if limb DE rotates, and limb CD does not, then this will cause the flexion connection based plate to rotate. If the limbs move in sequence, then the flexion connection base plate will remain vertical, simplifying the flexion range.

4.5 Optimisation

4.5.1 Revolute joint

The revolute equations can be used to generate the endpoint locations for each of the links of the system, each building along the chain. All of the points have a fixed related distance apart, except for the linear actuator endpoint relationship, which can vary its length dynamically causing the other points to rotate. The equation that defines the actuator length given by equation (4.26) which is shown in Figure 4.23.

$$\|\vec{A} - \vec{B}\| = L_{base} + L_{ext}(t), \quad (4.26)$$

where A and B are the endpoints of the actuator on the XY plane, L_{base} is the length of the actuator at zero extension and $L_{ext}(t)$ is the actual extension at the current point in time. $L_{ext}(t)$ can vary between 0 and 80% of the maximum stroke, L_{max}, as recommended to give enough support against bucking [105].
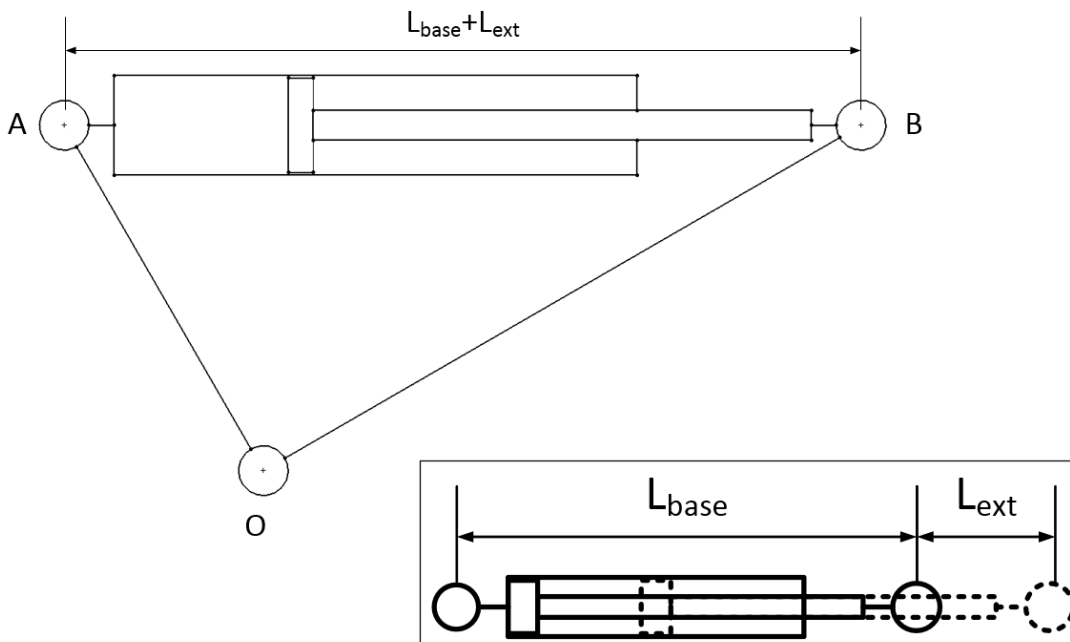
Figure 4.23: Relationship of A to B based on a linear actuator

The limit conditions are when θ is 0 and θ_{closed}, and when $L_{ext}(t)$ is either 0 or $0.8 \cdot L_{max}$. The relationship between the limits conditions for θ and $L_{ext}(t)$ is determined by the setup of the joint.

The first constraint for each system is that for all θ within the joint angle range, then $\left\|\vec{B} - \vec{A}\right\| \geq L_{base}$ to prevent the actuator from being shorter than its physical minimum length during the motion. This is given by equation (4.27).

$$\forall \boldsymbol{\theta} \in \boldsymbol{\theta_{range}}: (\left\|\vec{B} - \vec{A}\right\| \geq L_{base}) \qquad \textbf{(4.27)}$$

The second constraint is determined from the moment arm of the system between the actuator and the joint pivot. This is the minimum distance between the actuator and the joint of rotation. This is given in equation (4.28) [106]:

$$\textbf{momentArm} = \frac{\left\|(\vec{B}-\vec{A})\times(\vec{A}-\mathbf{O})\right\|}{\left\|\vec{B}-\vec{A}\right\|}, \qquad \textbf{(4.28)}$$

where O is the centre of rotation for the torque.

Torque output from the actuator is required to be greater than that of the demanded torque and less than the buckling limit of the actuator. This gives a safe and usable solution.

$$\textbf{momentArm} \geq T_{Required} \wedge \textbf{momentArm} < F_{buckling}, \qquad \textbf{(4.29)}$$

The cost function for optimisation is to determine the maximum moment arm for the actuator, where the actuator details are selected from the list given in Appendix N. This means that all of the actuators are individually put through the optimisation routines. If 100 actuators are used, then for the four joint options there will be 400 optimisation runs. If all the variables within the system were design variables, then the optimisation would only need to run once but would require custom parts for the whole system.

There is the possibility that there will be multiple solutions due to the number of actuators and designs, then units that generate results that have a linear extension to angle output and the smallest volume of fluid required would be selected.

There is a possibility that for a selected actuator, there could be several local minimums that depend on the initial starting conditions. Thus, a global optimisation is required. Arora [107] recommends stochastic methods over deterministic methods for global optimisation problems. These methods include

- Multistart method

- Clustering method

- Controlled random search: Nelder-Mead Method

- Acceptance-Rejection Methods

- Stochastic Integration

One issue with the optimisation is that though the variables are continuous within their allowable ranges, not all combinations will generate a valid solution. For example, if the moment arm becomes negative for part of the motion, then this is not a valid solution and is this a non-smooth optimization problem [107]. For example, Figure 4.24 shows an example graphical solution to a problem including feasibility area and the cost function contours. The cost function contours have areas removed to represent the areas where the solution fails.
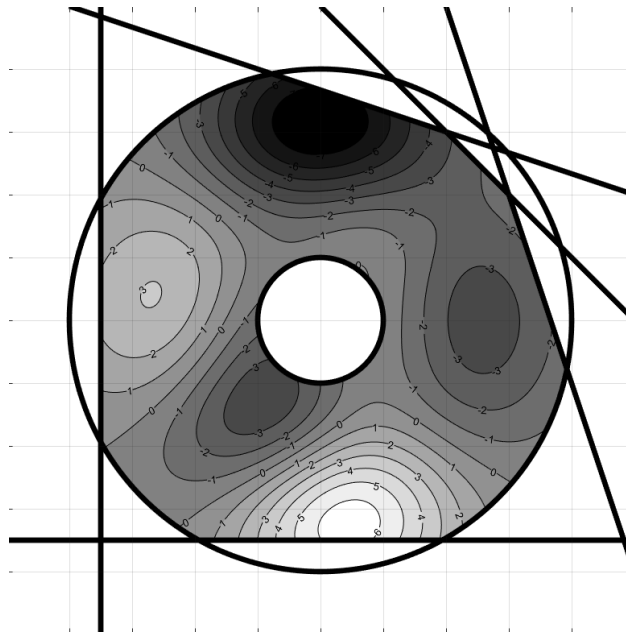
Figure 4.24: Example Graphic solution for an optimisation problem including feasibility area and cost function contours

This can be overlaid with the starting points for the optimisation, Figure 4.25, though as the areas of non-solution are unknown, these will be tested and eliminated on the first pass.
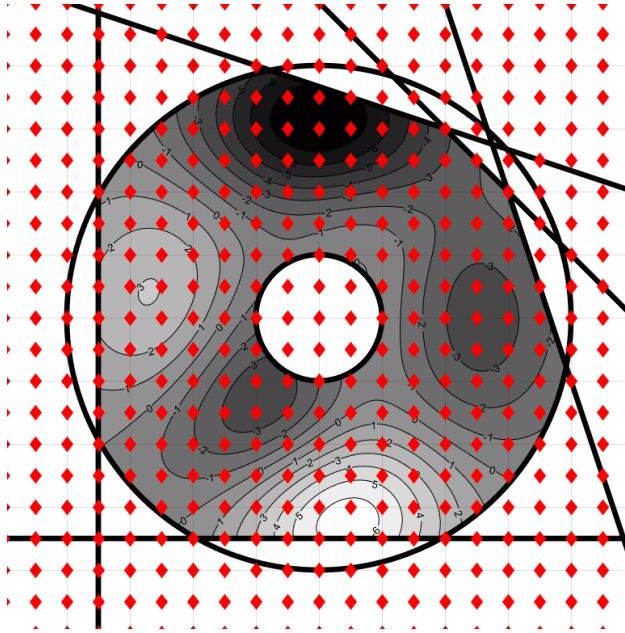
Figure 4.25: Starting points for the example optimisation

A quiver plot of the gradient of the cost function surface can be plotted as shown in Figure 4.26.
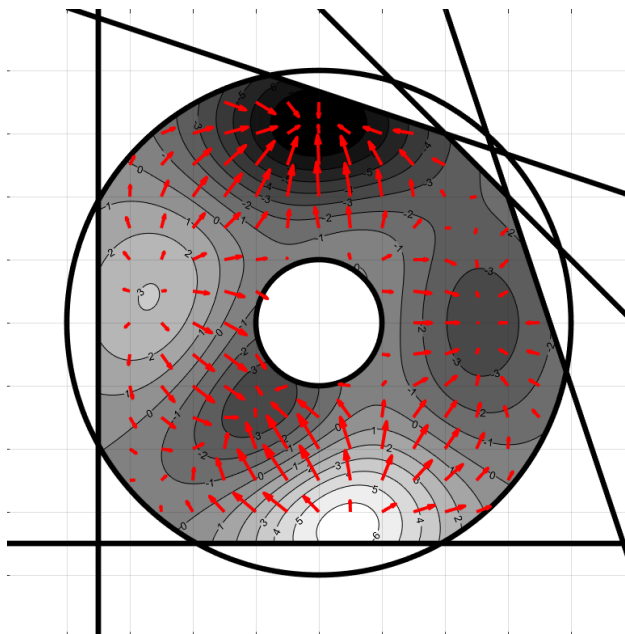
Figure 4.26: Gradient plot of the direction the local optimiser will follow to the solution

It can be seen that there are three areas where the solution will tend towards, two local minima and one global at the top. It can also be seen that some of the arrows points towards areas of non-solution, for example, the peak at the nine o'clock position has solutions that either tends to the outside or centre. This can be more easily seen in Figure 4.27.
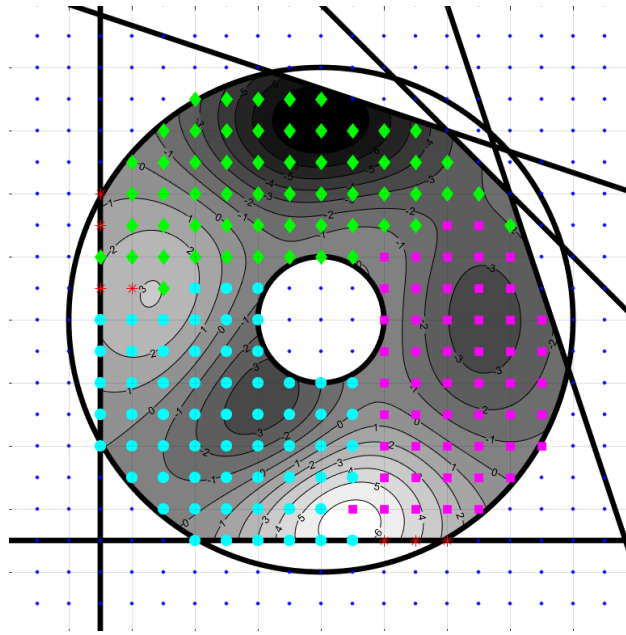
Figure 4.27: Solution river basins

The small dots are those results that are outside the solution to start with and thus are unable to compute a valid solution. The asterisks are points that end with an invalid solution, for example then end on the edge of the ring. The diamonds are those solutions that end in the top minima, the squares are those that end in the right-hand minima, and the large dots are those that end in the left-hand minima.

These are similar to river basins in that the solution will run to the local minima, but as the algorithm does not follow a continuous line down the slope to the minima, there are some points that appear to jump across them. For example, at the bottom, there is a square point in the large dot area where it would be expected to be a large dot.

The solution endpoints for the asterisks will be higher than those of the minima and thus would be eliminated from the global solution. It also highlights the issue of selecting a starting point and possible clustering selection

4.5.2 Spherical joints

The spherical joint optimisation is simpler than the revolute joint's, as there are no actuators to give multiple results. The cost function is looking for the maximum range for abduction and rotation for each design, eliminating any points that will contact the user.

4.6 Summary

For the two styles of major joints within the exoskeleton system, there are varieties of solutions for each.

For the revolute joint, the determination of the torque and angle range gives the quick initial selection of which rotary actuator is viable for the solution. For the linear actuator selection, the optimisation of the joint geometry is required which can then be compared to find the system with the most linear response. The ideal linear and rotary design weights can then be compared for a starting point in selecting the final solution.

For the spherical joint, several of the possible solutions were eliminated before any numerical analysis was done due to fundamental issues with the design that could risk injury to the user. Of the two chosen design routes, the two and five bar systems, both have benefits and drawbacks. The two bar system only has a component on one side of the horizontal plane, whilst the five bar has components on both sides. The five-bar system places the majority of the weight on the rear of the system whilst the two bar requires weight in the middle of the structure.

- 114 -

Chapter 5
Exoskeleton Design

5.1 Introduction

The exoskeleton system is a multiple degrees of freedom system with the majority of the motions driven. The motion and loading for each joint needs to be determined and a solution selected for each. Whether a joint is powered or not depends on the requirement for that joint.

The design of the exoskeleton will begin from the end-effector (hand) actuator working along the arm to the shoulder. This is due to determining the loading of each in sequence and making sure that they can support each other along the chain.

An initial single joint design was developed before the upper body exoskeleton optimisation development to assist with the team members' work. This was an initial starting point for the exoskeleton project, conducted before the upper body design work started. See Appendices G through K.

With an understanding of the requirements for the design (Chapter 3), as well as optimisation techniques for developing the geometry (Chapter 4), these will to be brought together for the upper body exoskeleton.

Working from the end effector hand, along the arm to the back means that each joint should be capable of the calculated motions and torque requirements. An initial actuator hand has been developed as the starting point, which leads into the elbow. This is the first revolute joint of the system and goes through the optimisation routines as described in Chapter 4. The shoulder is next and goes through an optimisation routine for the gimbal joint design.

Once the design has been completed, it is compared to current exoskeleton systems and robotic systems to see what affect the action at a distance design philosophy does to the design process.

5.2 Safety factor

A major factor in the sizing of the actuators is the safety factor. It is the assumption that the actual loading and geometry of the system are not truly

known and thus to reduce the risk of failure the components are made a factor stronger than required. This can either be calculated by the 'classical rule-of-thumb factor of safety' or a more in-depth statistical method [108]. A full FMECA (Failure Mode, Effects and Criticality Analysis) [109] would be suitable towards the final product, but after the alpha prototype has been completed to allow an understanding of what issues would arise.

5.2.1 Rule of Thumb

The simple values to determine are the material, geometry and reliability. The contribution of the material is based on data sheets rather than from test samples, and thus the material factor of safety is 1.1. The geometry factor of safety is based on the tolerances of the parts, though will be required to be tight or average, giving a value of 1.0. As discussed in Chapter 3 about the requirements, one was for the reliability of the system to be 98%, which gives a value of 1.3.

The factors that are more difficult to determine are the load stress factor and failure factor. The load stress safety factor is 1.4 due to the loading being not well known due to the limited ability to determine the actions of the user. With shock loading, the true value of the loading is difficult to determine. The failure analysis has a factor of 1.2 as the units will be designed to have stresses lower than the fatigue limit of the materials

By multiplying the five sub safety factor values, the final safety factor is calculated to be 2.4 [108].

5.2.2 Statistical method

Using a statistical factor of safety [108], a different safety factor can be determined. The basic equation is given in equation (5.1).

$$FS = 1 + t_{z=0} \frac{\sqrt{\left(\frac{\rho_{a1}}{\bar{S}_{a1}}\right)^2 + \left(\frac{\rho_{ap}}{\bar{\sigma}_{ap}}\right)^2 - t_{z=0}^2 \left(\frac{\rho_{ap}}{\bar{\sigma}_{ap}}\right)^2 \left(\frac{\rho_{a1}}{\bar{S}_{a1}}\right)^2}}{1 - t_{z=0}^2 \left(\frac{\rho_{a1}}{\bar{S}_{a1}}\right)^2} \quad \textbf{(5.1)}$$

Where $t_{z=0}$ is the reliability factor, a normal distribution with a mean of 0 and a standard deviation of 1, $\bar{S}_{a1}$ is the mean of the allowable strength, ρ_{a1} is the

standard deviation of the allowable strength, $\bar{\sigma}_{ap}$ is the mean of the applied stress and ρ_{ap} is the standard deviation of the applied load.

Selecting a reliability factor 98% gives a value of 2.05 for $t_{z=0}$ which is read from the normal distribution plot.

It is not required to determine the mean stress and standard deviation as the ratio of standard deviation over mean stress is called the coefficient of variation, which is determined from the analysis.

The allowable strength coefficient, $\left(\frac{\rho_{a1}}{\bar{S}_{a1}}\right)$, is based on a rule of thumb. If the material properties are well known is 0.05, but can range from 0.01 to 0.15 depending on the knowledge of the material. The selection of the materials will be limited to standard materials or aerospace grade. This means that the properties will be well known and would be specified by ISO standards.

Looking up a range of yield values of DIN 1.4401 stainless steel, one of the most commonly used stainless steels [110], gives a mean yield of 271Mpa and a standard deviation of 35Mpa. This gives an allowable strength coefficient of 0.13.

For the applied load, $\left(\frac{\rho_{ap}}{\bar{\sigma}_{ap}}\right)$, this is broken down into the following equation (equation (5.2))

$$\frac{\rho_{ap}}{\bar{\sigma}_{ap}} = \sqrt{4\left(\frac{\rho_r}{\bar{r}}\right)^2 + \left(\frac{\rho_F}{\bar{F}}\right)^2 + \left(\frac{\rho_{sa}}{\bar{N}_{ss}}\right)^2 + \left(\frac{\rho_{fa}}{\bar{N}_{fa}}\right)^2} \qquad \textbf{(5.2)}$$

Where $\left(\frac{\rho_r}{\bar{r}}\right)$ is the geometry tolerance and tends towards zero, $\left(\frac{\rho_F}{\bar{F}}\right)$ is dependent on the range of the loading, $\left(\frac{\rho_{sa}}{\bar{N}_{ss}}\right)$ is the coefficient of stress, and tends to be very small and tends towards zero, and $\left(\frac{\rho_{fa}}{\bar{N}_{fa}}\right)$ is based on the loading, and for a nonzero mean multiaxial fatigue failure theory is 0.25.

This gives a final factor of safety of 2.16, which is lower than that of the rule of thumb, which tends to be conservative in its value [108].

Following this, the selection of the materials used is covered in Appendix L.

5.3 Exoskeleton 'hand' and lower arm

The exoskeleton will need to interact with the environment via a manipulator, the 'hand' of the system. BLEEX does not have an upper arm system, but Sarcos, PERCRO BE and HAL all do. Sarcos uses attachable claws for lifting and interacting with the environment, and is a simple solution, though requires a range of attachments. PERCRO BE has a gripper that has a grasping force of 1700N, though the load capacity of the arm is only 500N [6]. HAL does have a whole-body system, though the image associated with it shows the user lifting using their forearms [4].

5.3.1 Manipulator options

There are several options for the manipulator ranging from a simple claw-like Sarcos to a more complicated system similar to the fictional Caterpillar P-5000 work loader from the film Aliens [85]. Current systems are reviewed in Chapter 2.

The option to have an actuated system that allows the user to grip and rotate an object is an opportunity. This does add weight to the end of the arm, and this has to be balanced against the increased flexibility.

There are gripper systems on the market to be used with robotics that tend to run off pneumatics rather than hydraulics. This would require an additional pump source and safety system that would increase the weight significantly. The strength of these systems would also be a limitation for the exoskeleton.

There are products that could be attached to the system that could provide a gripping action, for example, Hurst's StrongArm [111] as shown in Figure 5.1. This is a development from the company that developed the Jaws of Life® system. The StrongArm system is designed to be used by a single user and is a hydro-electronic system. It is unclear, due to commercial propriety, whether this is a valve or pump based circuit. Other products use an external power source and have control via a valve on the tool.

Figure 5.1: Hurst StrongArm unit for firefighters [111]

The StrongArm is more than capable of fulfilling the requirements, though the weight would be an issue. The StrongArm has the lowest spreading force 24kN, with the highest at 30kN. The StrongArm system weighs a maximum of 12.9 kg with the door opener tip and battery. This does not include any mounting options for the system.

If there were a requirement to develop a system, there would be a need for at least one actuator, with the possibility of two. Rotary-lift combination actuators would bring this into a single unit, which would give the open/closing actuation similar to that of the StrongArm with rotary options.

HSK is a company that makes rotary-lift combination units, with DHK-H-ZH 40 with a rotation of 180° would be an example that could be used [36]. This unit gives a torque of 65Nm and a retraction force of 4380N. For a 45kg load, this could be up to 147mm offset from the centre line of the actuator to prevent rotation. The grip force would be dependent on the lever configuration of the system. There are several patents concerning the design of this system, with Porter's, Herwig's, and Wettlaufer's [112-114] being examples, though these do not give absolute dimensions within the patent. The 5000psi MOC Combi by Hurst [115] does have max pulling and cutting force which can be used to determine what gripping force HSK's unit would give with the same geometry.

For the Hurst unit, it has a pulling force of 85kN at 5000psi, 344bar, whilst the HSK only uses 100bar. Reducing the pressure down would give 24.7kN of pulling force compared to the HSK of 9.7kN. This gives a ratio of 5.6 for the area difference. Working similarly for the cutting force, which is 535kN at 344 bar, this would be 155.2kN of cutting force at 100bar. Reducing this by the area ratio would give a gripping force of 27.6kN, which is significant.

The maximum weight of the HSK unit is 9.8kg, which does not include any of the mounting, jaws or power supply and control. This could mean that the system could be up to 15kg in total. This weight, including the target lifting weight of 45kg, would be transferred to the elbow, and thus would need to resist this weight.

5.3.1.1 Control

Controlling the system would be from a flight stick style system that the user would grip on to. As the user moved their arm, they would pull or push on the stick. Normally this would be detected as an angular change, but if the flight stick were connected to a six-degree force sensor, then this would be three forces and three torques that would be sensed. This does mean that there would be a limited motion of the flight stick in regards to the exoskeleton, but the control will detect the force input and move the exoskeleton to minimise it. This idea comes from the work loader from Aliens [85]. This would also mean that the user is not enclosed in the system like PERCRO [6] or Hardiman [9], increasing safety as described in Chapter 3.

As the exoskeleton 'hand' replaces the pronation/supplication of the forearm, a top-hat switch on the flight stick would control it. This is likely to be non-intuitive, to begin with, and a new user is likely to attempt pronation/supination until they get used to the setup.

5.3.2 Lower Arm Design

There are several options for the end effector for the exoskeleton with each having benefits and limitations. Simple claw designs are the lightest and easiest to implement into the design, though they are limited on what interactions they can have on the environment. A more complicated system with opening and closing jaws, with the option with rotation, are heavier and require control systems.

The end effector is slightly beyond the exoskeleton design at the current time and will be assumed a fixed mass for subsequent components.

The initial design dimension is the distance between the elbow joint and the control stick. Based on U.S. Army personnel [45] the 50th percentile distance between the forearm and the centre of the grip is 348mm for males and thus will be the basic distance.

The main section of the lower arm structure should lie along the same plane as the user's forearm, and thus the controller is moved off the exoskeleton arm centre line.

The actuator has the majority of the mass in its' housing, and thus moving it as close as possible to the joint reduces the inertia of the arm. Of the four basic locations of the actuator; above, below, inside and outside, several are not suitable. With the actuator on the top of the arm, there is a likelihood that the actuator will contact the upper arm on bending the elbow, and would need to be considered for this. On the inside or outside, it increases the width of the design, with the outside expanding the grip position to further away from the normal user range, and with the inside actuator pushing the exoskeleton structure wider. Certainly, for inside or outside, the actuator axis can be perpendicular to the elbow axis and reduce the inertia further. Under the arm is the simplest solution, which should not interfere with the exoskeleton without making it wider.

Connecting the joints together when using rotary units normally requires keys, though Robert Parmley in section 4 of his book [116] outlines 15 ways to connect a gear to a shaft. Connecting a gear to a shaft is a typical design challenge, but the theory can be used here as well. Using the Pugh's method for decision methods from [108] on the table by Parmley, Table 5.1 can be generated showing that Loctite followed by tapered bushings are the ideal choice.

With a safety-critical system, there is a risk in using adhesives to join the components together as there is a large possibility of a large value in the torque holding strength standard deviation. Thus tapered bushings, which will have manufacturer supported torque limits would be the ideal solution, followed by the tapered shaft and tapered rings.

Table 5.1: Pugh's method table based on details from Robert Parmely [116]

Issue: Connecting shaft to component	Pinning	Clamping	Press fits	Loctite	Setscrews	Splining	Integral Shaft	Knurling	Keying	Staking	Spring Washer	Tapered shaft	Tapered rings	Tapered bushing	Die-cast assembly
Torque capacity	E	G	F	G	F	E	E	G	E	P	P	E	G	E	G
Ease of Replacing gear	P	E	F	G	E	E	P	P	E	F	E	E	E	E	P
Reliability under operation	E	F	G	G	P	E	E	G	E	P	G	E	G	E	G
Versatility in applications	E	F	F	E	G	F	G	P	P	P	F	G	E	G	E
Ability to meet environmental specs	E	G	G	E	F	E	E	G	E	G	G	E	G	G	G
Machining requirements	H	M	M	L	M	H	H	M	H	M	M	H	M	M	L
Ability to use prehardened parts	P	E	E	E	G	E	E	P	E	P	E	E	E	E	F
Relative cost	H	M	M	L	L	H	H	M	H	L	M	H	M	H	L

Excellent	High
Good	Medium
Fair	Low
Poor	

Tapered bushings and shafts need controlled machining and thus add to the cost of manufacturing. Tapered rings have the tapers on the internals of the components and thus just need straight bores. SKF is an example manufacturer of tapered rings, though they call them keyless bushings [117].

SKF provides calculations to give the minimum hub diameter required to transmit the torque of the bushings. This is due to, as the bushings expand, the pressure could cause the outer material to fail due to hoop stresses. This is based on the bushing design, shade factor of the interface and the material yield strength.

Several of the designs have additional benefits, for example, self-centring to no axial hub movement.

The cross-section of the arm is a simple square, as this is easy to manufacture, and means that the machining process can be done from one face if it has a two-dimensional profile. The size of the square is based off the width of the connector. This could be further optimised, though, for an initial prototype design, this will be left for the current time.

5.3.3 Final design

With a rough original design outlined, an initial lower arm setup can be designed. This is shown in Figure 5.2.
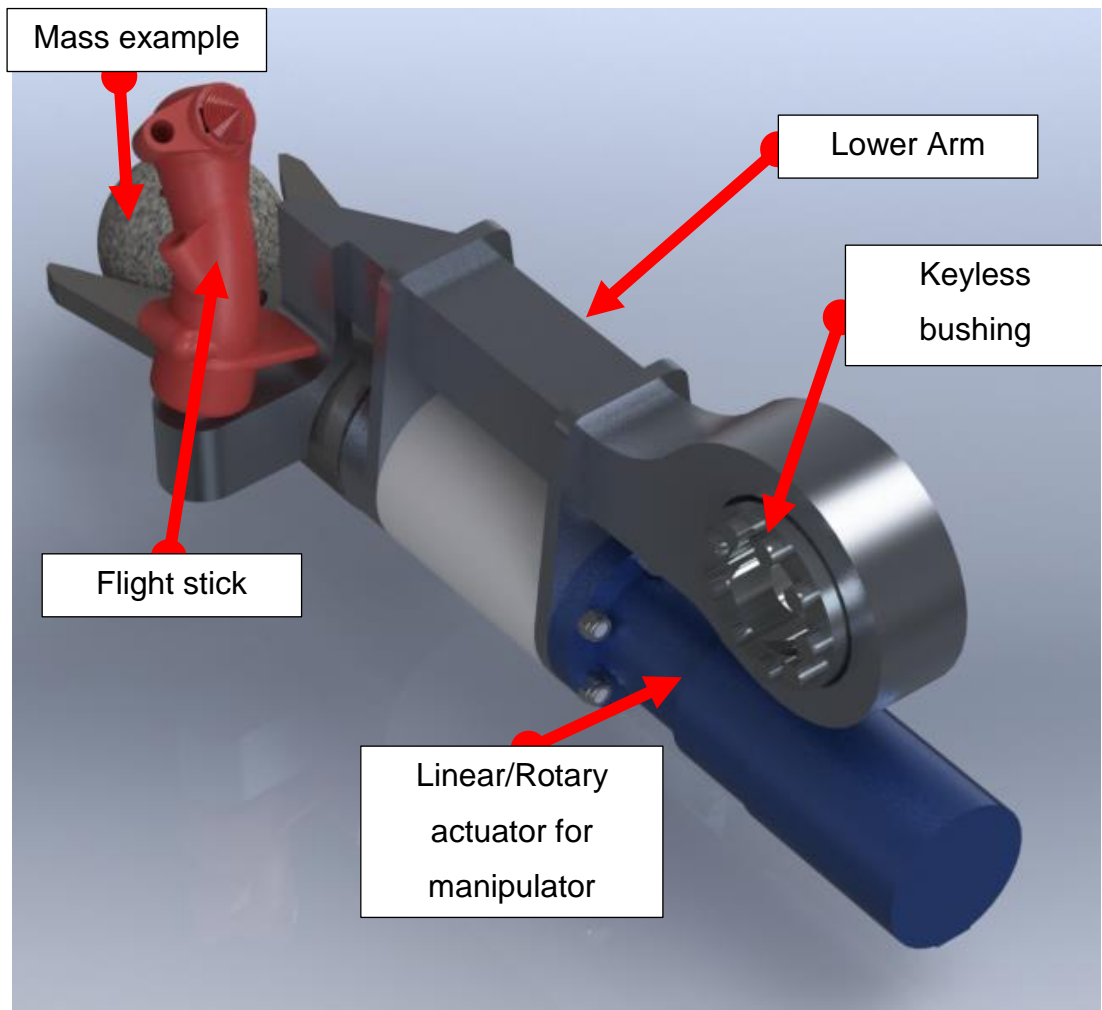
Figure 5.2: Initial design for lower arm

The image includes a 45kg 'marble' block for an initial determination of the loads for the design. It also includes a flight stick control[7] for the user to move the arm as well as the manipulator.

The weight of the hand is 16kg, with the arm section including control stick and bushing is 4.95kg.

---

[7] Model for flight stick is from https://www.thingiverse.com/thing:776116 by schrodingers_cat and is used under the Creative Commons – Attribution – share Alike license (CC BY-SA 3.0), https://creativecommons.org/licenses/by-sa/3.0/. The model has been mirrored for use on both sides. It is not intended to be used for commercial application but as a visual placeholder for this thesis.

This design is an original one for this thesis, using ideas from the Aliens Power loader (gripping/rotating manipulator and control stick) and current technology used in search and rescue.

5.4 Exoskeleton elbow

With the lower arm mass partially determined, the elbow joint requirements can be investigated. Whereas the end manipulator does not need to mimic the user, the elbow joint would need to follow them. With an anthropomorphic design, the range of the motion will be determined by anatomic limits.

The human range of motion for the elbow is 0° and 140-146° [90] extension-flexion, with pronation of 80° and supination of 85° [90]. The forearm bones rotating around each other do the pronation and supination. As these rotations are within the limb itself, rather than within the elbow joint, this would not be suitable to directly mimic on the exoskeleton. As these muscles rotate the wrist, the rotating hand manipulator would directly follow this motion, but controlled by the hat switch rather than gross user motions.

Current elbow designs, as reviewed in Chapter 2, either uses rotary or linear actuators: PERCRO uses their rotary actuator and BONES uses linear actuators. Other revolute designs, like BLEEX's knee joint, have issues that optimisation of the joint geometry will help to overcome.

5.4.1 Lifting requirements

The equations from Appendix M are used to give an initial value for the torque required. Using the lower arm mass and moment of inertia, the torque can be calculated. For the load torque, the total mass of the lower arm is 65.95 kg, including 45kg load, with a centre of the mass location at 390mm. This gives a load torque of 252.32Nm.

The friction torque of the system would depend on the bearings being used. The use of double row tapered bearings gives the range of support likely to be required by the exoskeleton. With the support of radial, axial and moment, loading the system should have stability within the joints. The torque of the units is dependent on the loading of the unit as shown in equation (5.3) [118].

$$M = \mu F \frac{d}{2} \qquad (5.3)$$

Where M is the bearing torque, μ is the coefficient of friction which is 0.0018~0.0025, F is the bearing load and d is the shaft diameter. For the smallest unit by Nachi, 25KDE13, the basic dynamic loading is 71kN, which is significantly higher than any force that is likely to be experienced by the exoskeleton. Using these values, the friction is only 2.2Nm that can be safely ignored, as it is one-hundredth of the size of the load torque.

The lower arm, as designed in 5.3.2, does not have a bearing, instead of having a bushing to connect to a rotary actuator. If a linear system is the selected solution, then the lower arm needs to be modified to accept a bearing.

To give motion to the joint, the maximum acceleration of the joint needs to be known, as well as the mass moment of inertia. As calculated in Chapter 3, the acceleration for the elbow is 18.80 rad s^{-2}. From the model, the moment of inertia is 12.74kgm². This gives an acceleration torque of 239.51Nm.

The demand torque is thus 491.83Nm, with the cushioning torque being 731.34Nm. The cushioning torque is the demand torque plus the acceleration torque minus any friction torque, as outlined in Appendix M. This is then multiplied by the safety factor to give the torque required for the system. This gives a target torque of 1578.82Nm, which is rounded up to 1580Nm.

This either will be the full amount for the internal, external, Hoeken or rotary actuators or halved for the patella design.

5.4.2 Actuation system

With the initial torque value decided, as well as rough dimensional limits, the joint can be optimised using the geometries created in Chapter 4.

5.4.2.1 Linear actuators

The torque and limits were run an optimisation with the joint options from Chapter 4 with a limb range of 50 to 288mm, and the space between components of 72 to 150mm. These dimensions are based on the minimum size of bearings components and the 50th percentile of the male forearm-centre of grip length [45]. A list of the actuators in the study is in Appendix N. There

were no solutions for the internal, external or patella design, but 27 valid ones for the Hoeken design, for which the moment arm is shown in Figure 5.3.

The reason that the internal, external and patella designs were unable to supply any results was due to the high torque required. For example, for an internal actuator design with a moment arm of 100mm needs an actuator to give a force of 15.8kN to give the 1580Nm torque. If the pressure is assumed 100bar, the diameter of the cylinder to give this force is 45mm. A larger pressure will give a smaller actuator, but due to the equation for a circular area, this is not linearly proportional. A pressure of 250 bar requires a cylinder of diameter 28.4mm, rather than the 18mm for a 1:2.5 reduction.

Figure 5.3 shows how the moment arm varies according to the joint angle for the 27 valid geometric solutions. A single solution needs to be selected, and in regards to the moment arm, the larger is preferred.
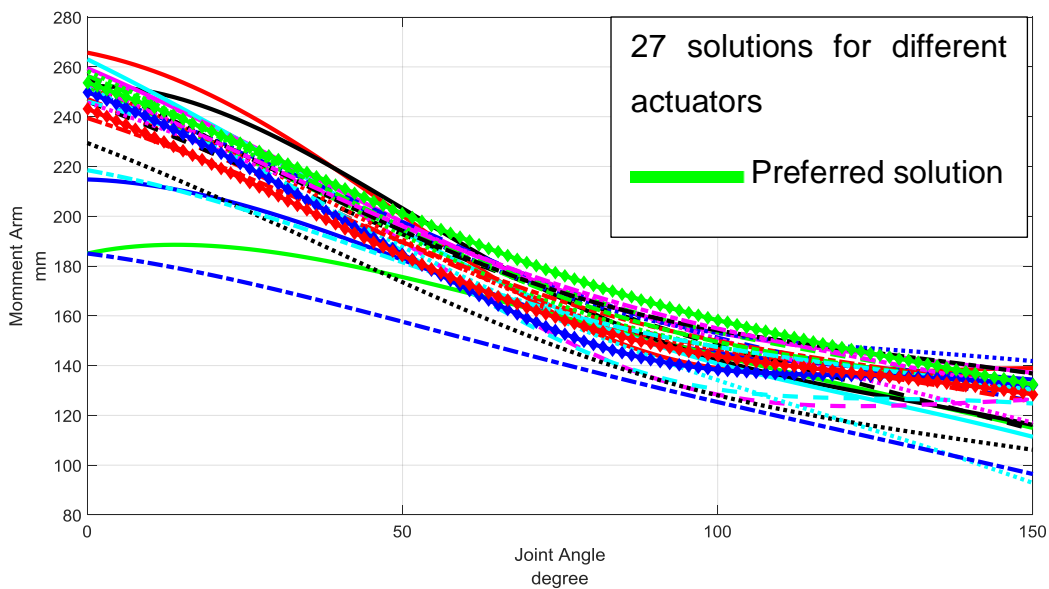
Figure 5.3: Hoeken moment arm solutions for the elbow

There is also the control to consider, and a solution that has little change of moment arm to angle would be preferable as it would reduce the requirement of linking the elbow angle to torque compensation. This would mean that the expected torque out would be similar, regardless of the current angle, if the angle measure was wrong. This can be seen as a linear percentage increase of the actuator in regards to angle, as shown in Figure 5.4.
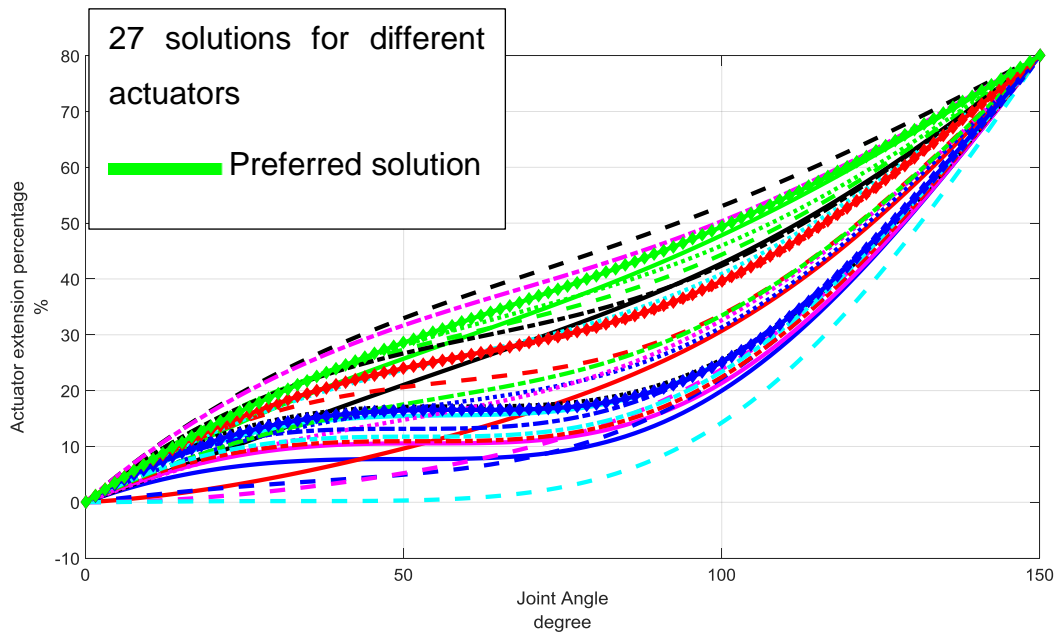
Figure 5.4: Elbow angle versus actuator extension percentage for all solutions

There are several solutions that appear to nearly linear, but there are also units that appear to be close to stationary points, points where the derivative of the line is zero. These solutions are not suitable for the design as there would be very little angular control for a set extension. This would mean that the arm would have a significant play in these areas, and make the exoskeleton dangerous to use.

The derivative of these curves can be calculated, as shown in Figure 5.5.

The units with stationary points are easier to determine from these results and can be eliminated, those that are close to zero. This still leaves several viable units, but if the control requirement for minimal moment arm change in regards to joint angle is applied, then the units with close to having a derivative of zero would be the solutions.

This can also be defined as having a linear fit that is close to zero, whilst also having the fit have a root mean square results also close to zero. This can be defined as the line having an m valve close to zero for the one-degree polynomial equation, $y=mx+c$. These are shown in Figure 5.6 with the units with the top five units in regards to RMSE shown in Table 5.2.
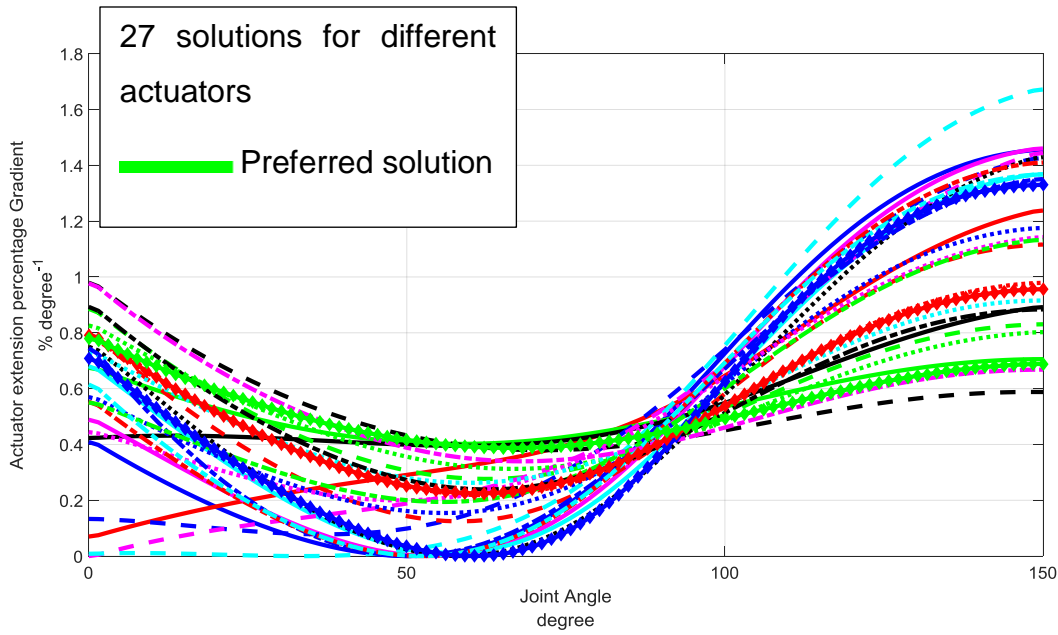
Figure 5.5: Elbow angle versus actuator extension percentage gradient for all solutions
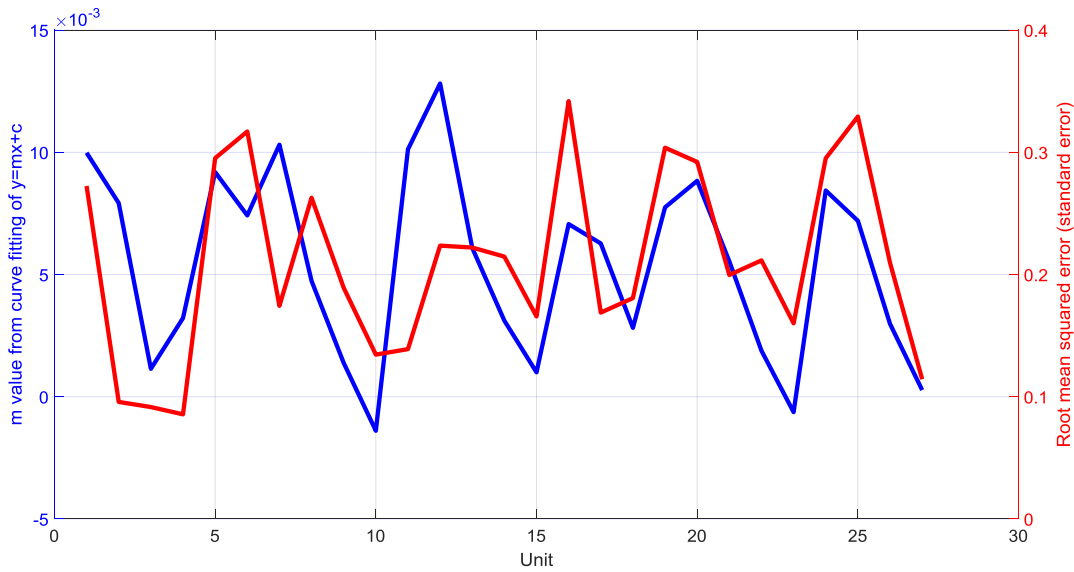
Figure 5.6: linear curve fitting of units based on the actuator extension percentage gradient and the root mean squared error of the fit

Table 5.2: Top five units from elbow optimisation

	Model	Mounting	Cylinder Bore	Rod	Stroke	SF	m	RMSE	Line Style in plots
4	CDL2	MT4	40	22	150	12.1	0.0032	0.0856	
3	CDL2	MT4	40	22	125	12.1	0.0011	0.0916	
2	CDL2	MT4	40	22	100	12.1	0.0079	0.0958	
27	CDM1	MT4	40	25	150	12.1	0.0003	0.1144	
10	CDH1	MT4	40	28	150	17.2	-0.0014	0.1345	

These units are all from the same manufacturer, though with a range of model designs. The top three units are the same design, including bore size and just differ in the stroke length. This would mean that this design of cylinder would be the ideal candidate, and thus unit 3, the middle stroke length of the three, has been selected.

5.4.2.2 Rotary actuator

Selecting a rotary actuator requires the simple lookup of available products that will give at least the required motion and torque. A list of 390 units was used to give a range of manufacturers and design styles (see Appendix O).

The lightest unit for the torque and rotation is a vane design, weighing 14kg. It has a specific torque of 164.3Nm·kg^{-1} and has a maximum torque of 2300Nm.

The issue with this unit is the maximum allowable loading of the shaft, which radially is 30kN, but axially only 50N. This means that if the shoulder were abducted, the unit would fail.

The first unit that has a reasonable axial load is a helical design that rotates 180° and weighs 29.2kg. The unit has a torque capacity of 2500Nm, but more significantly, can support up to 11.25kN radially, and 24.9kN axially.

5.4.3 Design

With two valid solutions, one for the linear design and one for the rotary design, the comparison between them needs to be done. Rough initial mock-up designs are shown in Figure 5.7.

The weight of the arm is the first consideration between the designs. The Rotary design weighs 38.94kg whilst the linear is 19.48kg. This does not include the gripper and control at 17.53kg. The weight of the linear actuator is 4.78kg compared to the 29.2kg for the rotary unit. The linear actuator design has an increased number of components that increases the weight and could also increase the price. The weights are higher than other exoskeletons, but for a system to give the action at a distance, this is a likely consequence due to the higher torque requirements.

Moment arm to the centre of mass is similar for both at 604mm and 641mm for the rotary and linear respectively. This gives a mass loading of 601.2Nm and 515.7Nm.

Moment of inertia of the rotary unit is 44.02kgm² compared to 40.17 kgm² for the linear system.
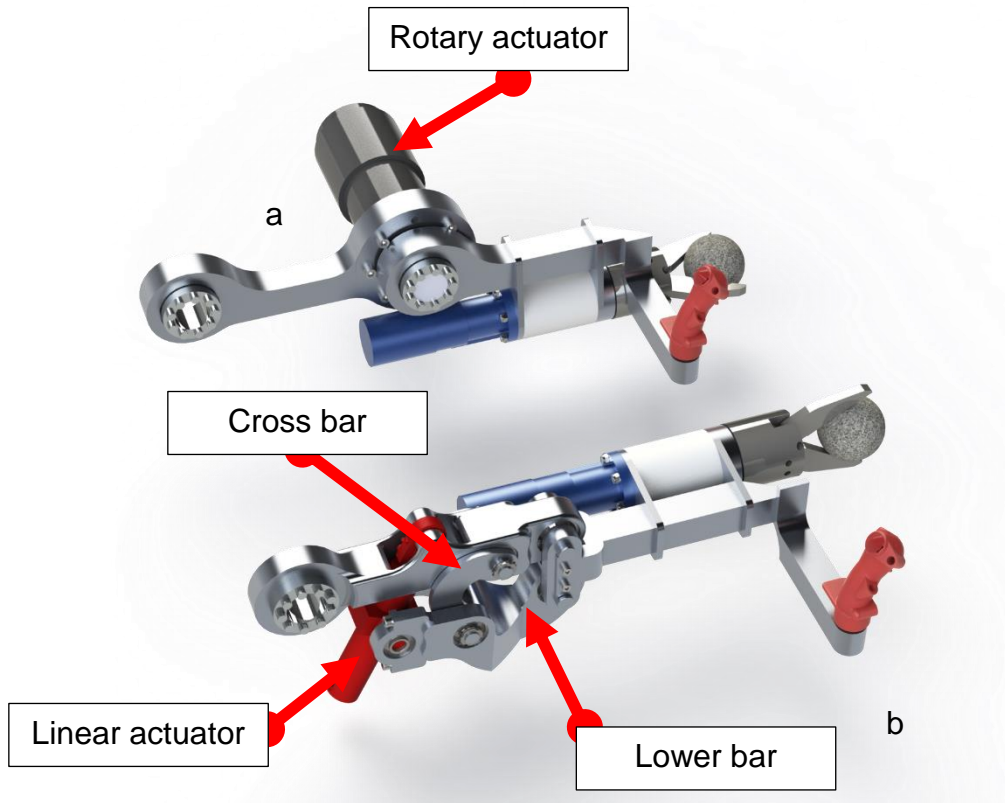
Figure 5.7: Arm comparison of the elbow joint. a) rotary actuator design and b) Hoeken Linkage design

The volume of the actuators is a critical value as it gives the required flow for the hydraulics. From the datasheet for the HKS unit, it is 0.509dm³. For the extension side of the linear actuator, the volume is 0.126dm³ giving over a four-times reduction in the required flow rate.

As mentioned in Section 5.3.2, the location of the manipulator actuator is dependent on the upper arm so that they do not collide. With the rotary actuator, this is simple, as it does not need to change, though with the linear solution, the structure is lower and thus the manipulator has been moved to the side as seen in Figure 5.7.

5.4.4 Final design arm design

The final design is shown in Figure 5.8.
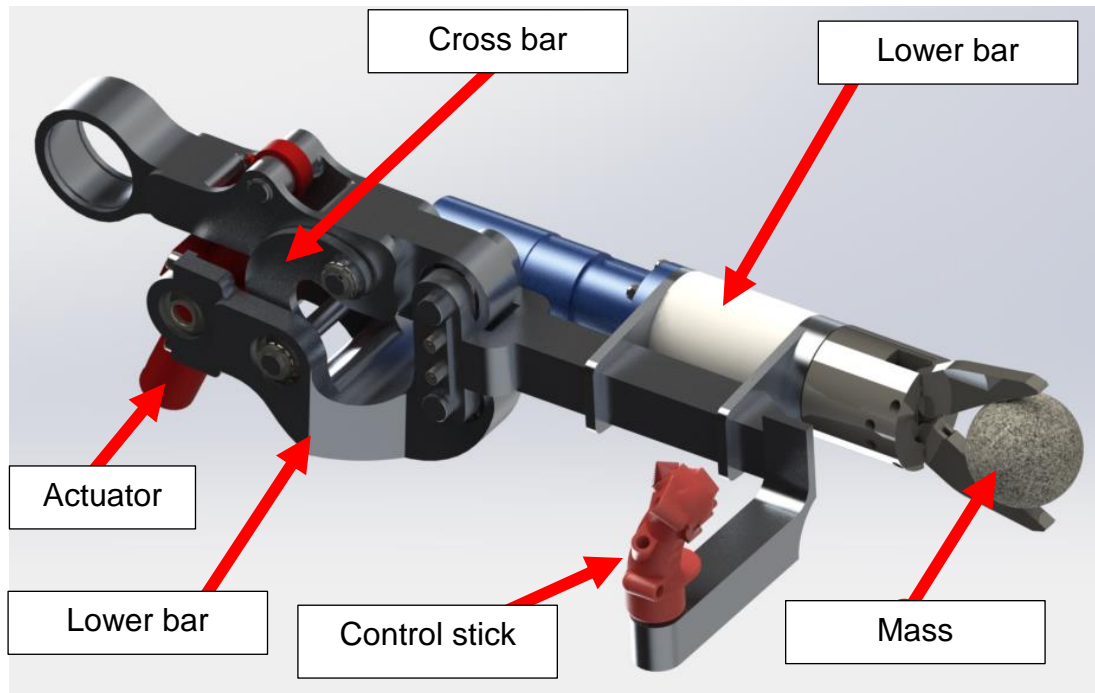
Figure 5.8: Final arm design

The lower arm has been designed to requirements as outlined in Chapter 3.

By using the 45kg target weight in all of the calculations, as well as the human motion, the elbow joint has been developed to give the action at a distance with the maximum load, whilst also being able to move at the required speeds.

The prototype design is not adjustable at the current time and would require further development to give flexibility. It is currently designed for a 50th percentile male dimensions as the starting point.

The target acceptable weight of 68kg has not been reached with this design due to both arms being a total of 38.96kg without shoulders. This is nearly 60% of the acceptable weight being used in the arms. Figure 5.9 shows the distribution of specific torques for the units used in the design process, which highlights the majority of the units have a specific torque of between 50 and 60Nm kg^{-1}. For a system to support 45kg at 0.5m requires 220.7Nm, increased to 463.47 with the 2.1 safety factor, then the weight of the actuator would 9.3kg. This is 27.4% of the acceptable weight for both arms for just the actuators and no structural components or motion requirements. This gives an indication that the design for action at a distance will not meet the weight requirements.
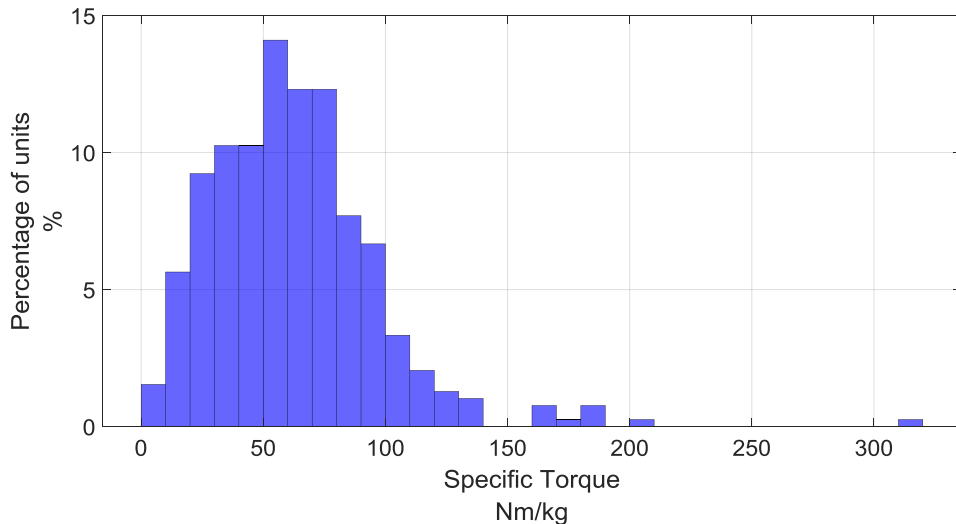
Figure 5.9: Distribution of rotary units used in the design process based on the percentage of units, which lie in the same bin for specific torque

The duration and reliability were taken into account with the safety factor calculation, so should not be a concern at the current time for this design, though additional empirical testing is required.

The access into the system is simple as there is only the control as an attachment point, and this does not enclose the hand. This increases the safety as the user can retract their arm if required with no restrictions.

5.5 Exoskeleton Shoulder

With the arm design completed, the shoulder with its multiple degrees of freedom needs to be designed. This will involve at least three actuators to give the three basic degrees of freedom: flexion, rotation and abduction. As mentioned in Chapter 2, spherical joints making sure that the three-axis intersect is critical.

5.5.1 Motion requirements

The human range of motion for the shoulder flexion is between 130 and 180° and extension of between 30 and 80°[90], with the abduction of 180° and adduction of 50° [90]. Rotation is measured along the upper arm segment with internal rotation of between 60 and 90° and external of 90°[90].

These range of motions are based on a ball joint, but with a gimbal joint, these become interlinked and thus make the solution complicated especially for the flexion motion. The flexion motion is shown in Figure 5.10.
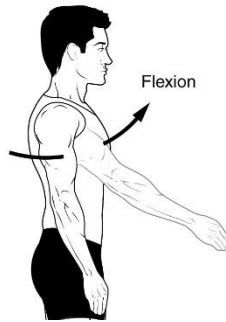
Figure 5.10: Flexion of the shoulder [119]

Whereas the vertical axis for the arm is typically defined as 0° for the flexion motion, the gimbal is defined from the angles from the rear of the device.

Using Figure 5.11, and assuming that α and θ_1 are zero and θ_2 is 90° with β being equal to γ, then OA and OD are perpendicular to each other on the same horizontal plane. This would make CD coincidental with the arm at 0° and the range of motion for flexion the same as the human, 180° flexion and 80° extension.
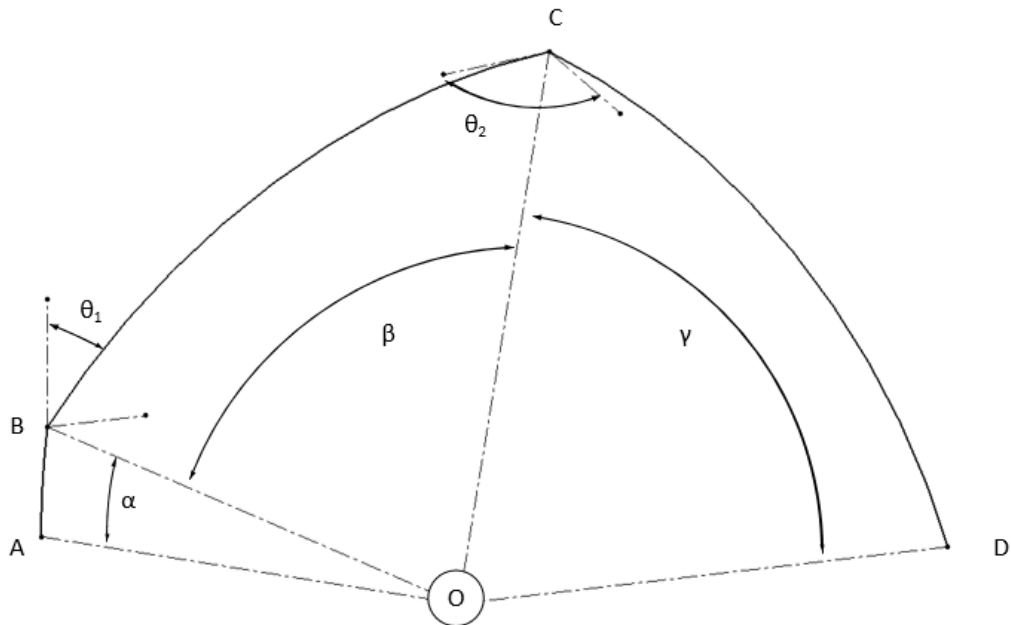
Figure 5.11: Two bar joint.

As the gimbal moved, the line CD will no longer be vertical, and as the 0° the flexion motion is based on this line, it will change. For example, if the gimbal

had moved so that θ_1 is 90° and θ_2 is 180°, the whole of the gimbal is on the horizontal plane. A vertical line is now 90° to line CD and the flexion range is 90°. In turn, the extension is now 170°. The flexion/extension range is the same, 260°, but the ratio of flexion to extension has changed.

To make sure that regards of the motion range for the gimbal, that the shoulder has the full flexion range, then the actuator needs to be able to give 180° flexion for when the CD line is vertical, and 170° of 'extension' when horizontal (90° offset plus 80° extension from vertical). This means an actuator that has nearly 360° of motion.

This is a large motion range, likely to result in a heavy actuator, so a range of 270° has been selected. This will reduce the flexion/extension range, but it is unlikely that the user will reach the full limits of motion.

5.5.2 Flexion

5.5.2.1 Torque requirements

Following the outline for torque determination from Appendix M, the loading toque will be 541.6Nm from the weight of the arm. The acceleration from Chapter 3 and the moment of inertia of the joint gives an acceleration torque of 410.0Nm and thus a demand for 951.6Nm. The cushioning torque is 1361.6Nm and thus with the safety factor included, the required torque is 2939.5Nm. These values are based on the 'action at a distance' requirement.

5.5.2.2 Actuation system

Linear

As the flexion/extension is a simple revolute joint, this can be put through the revolute joint optimisation routine. However, the large-angle range is an issue as it is nearly a full revolution. This large angle range and high torque resulted in zero solutions for the initial batch of actuators, and thus a selection of 1006 additional larger units were added to the optimisation (list in Appendix P), but these also failed to give any valid solutions.

With no results suitable due to the large motion range, the use of the crank style set up, as shown in Chapter 2, gives an unlimited range of motion. To give the full rotation, the stroke of the actuators is equal to double the offset and divided by 80% to give support as discussed in Chapter 2.

From this offset, the diameter can also be determined based on a variety of pressures for the required torque, which is shown in Figure 5.12.
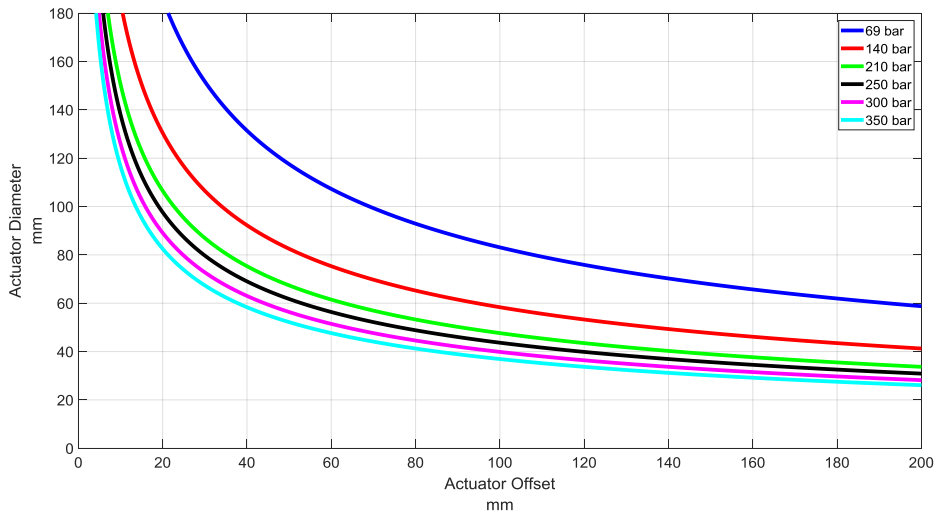
Figure 5.12: Offset versus required actuator diameter not including rod size

The larger the diameter, the smaller the required stroke and offset, and thus a balance is required to determine a suitable size

Using the actuators from before, the offset and smallest actuator diameter can be determined, as shown in Figure 5.13.
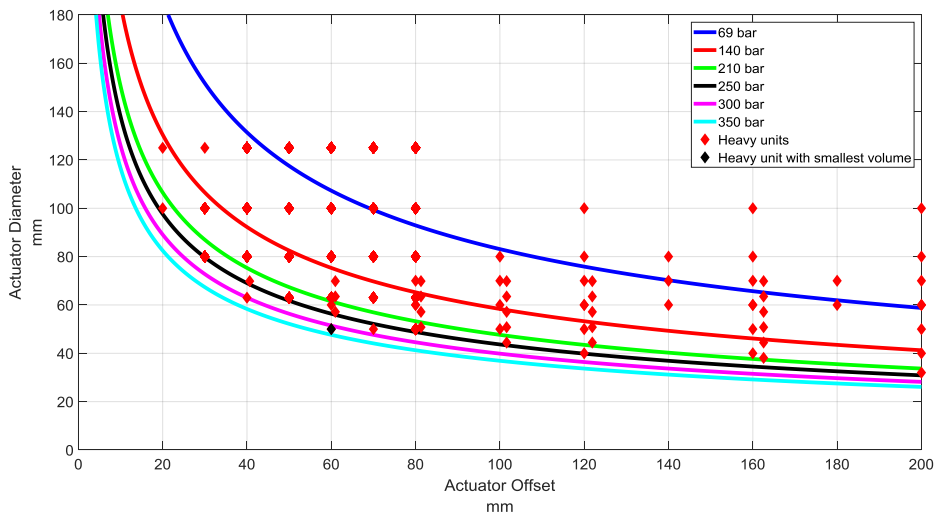
Figure 5.13: Smallest diameter actuator for offset length based on stroke

The light linear actuators for the elbow design did not have any that would give the required torque, so only the heavy actuators that can are shown. The actuator with the smallest volume is also shown, as this would be an ideal one for the flow considerations, which has a 50mm diameter, and a 120mm stroke

for a volume of 0.24L. This is a BOSCH actuator: CDL2 MT4, which is also the family that the elbow actuator is from.

Rotary

With a high torque required the size of the actuators increases. The unit with the largest specific torque is a rack and pinion design with a length of 823mm, which gives 103.38Nm/kg. This is an unreasonable unit size, as it would start to overlap the elbow. More critically, the overlap to the rear could cause motion issues, as the user is unlikely to be able to see the cylinders and thus could collide with objects.

The first viable design is a helical design that has a specific torque of 80.4Nm/kg. This unit, DA-H 125, has the additional benefit of having a large radial and axial support, 17.5kN and 34.1kN respectfully. This means that additional bearings are not required.

Figure 5.14 shows a sectioned view of a helical design.
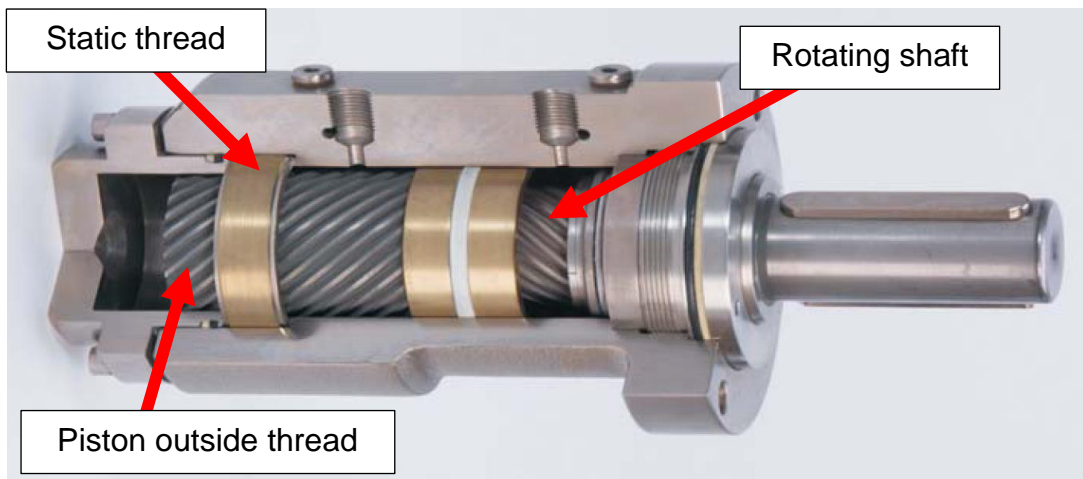
Figure 5.14: Example helical actuator showing threads [36]

As the piston moves from left to right, the outside threads interact with the static threads, that causes the piston to rotate clockwise as viewed from the output shaft end. As the piston rotates, a thread on the inside interacts with the threat on the rotating, output shaft. This causes the output shaft to rotate clockwise as well. The two thread meshes cause twice the rotation that could be achieved with just one, increasing the rotational to linear ratio.

5.5.2.3 Discussion

With a large range of motion, several of the options are unsuitable. The linear option does not have a viable solution apart from the crank design, and the increased complexity of this option would not make it a primary solution.

The rotary actuator is thus the solution selected.

5.5.2.4 Final Design

As shown in Figure 5.15, the rotary actuator has been selected and connected to the system with a keyless bushing.
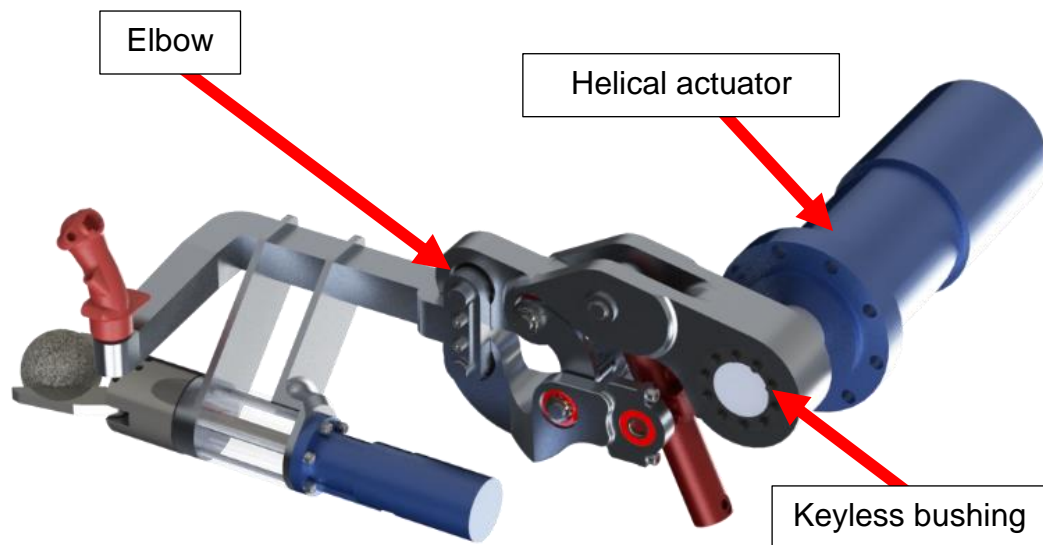
Figure 5.15: Shoulder flexion

As mentioned in 5.4.4, the human motion and the target weight is used in the design process and therefore this requirement is met.

The weight of the system has increased to 105kg, so one arm is in excess of the ideal weight by itself.

5.5.3 Rotation and abduction

Rotation and abduction of the shoulder are controlled by the gimbal joint of the shoulder. From Chapter 3, the two and five bar joints would be suitable for this joint. Interference between the arm and shoulder could limit the motion range, with any downward pointing joints being most susceptible to interfering with the arm. This does mean that a two-bar joint would be preferable to the five bar joint to prevent the exoskeleton colliding with itself.

5.5.3.1 Motion requirements

Similar to the elbow joint, the optimisation of the gimbal joint allows the optimum lengths to be used for the system. The equations do not include the actuator lengths and thus can be determined later. The only limitations are angle ranges, as discussed in Section 5.5.1, and protecting the user.

The outline of the designs are covered in Chapter 3 but are reshown in Figure 5.16, for ease of reference.

2 Bar linkage

Figure 5.17 shows the results from the two bar linkage optimisation. θ_1 is the input into the rear actuator with a motion range of 90° (270° to 360° due to orientation) and θ_5 is the input into the front actuator with a motion range of 180° (again 180° to ° to 360° due to orientation). Rotation and abduction ranges show that the system can give a large range, though some combinations cannot exist. The optimisation of the two bar linkage gives a rear bar angle of 40.6° and a forward bar angle of 78.0°, and the radius of the sphere to be 300mm. This gives a rotation range of -90° to 90° and an abduction range of -70.5° to 61.4°.

If the system includes the four-bar extension, as shown in Figure 5.18, then the motion range decreases though the results cover more of the θ range. The optimisation gives the same angle for the connecting bars to be 60° with the sphere increasing in size to 349mm. The angle range for rotation is -90° to 90°, the same as the simpler two-bar system, but the abduction range decreases to -60° to 60°.

The abduction range has decreased due to the singularity issue, as mentioned in Section 4.4.3. This reduction in abduction range, as well as the increase in sphere size makes the four-bar extension a worse choice compared to the simpler design.
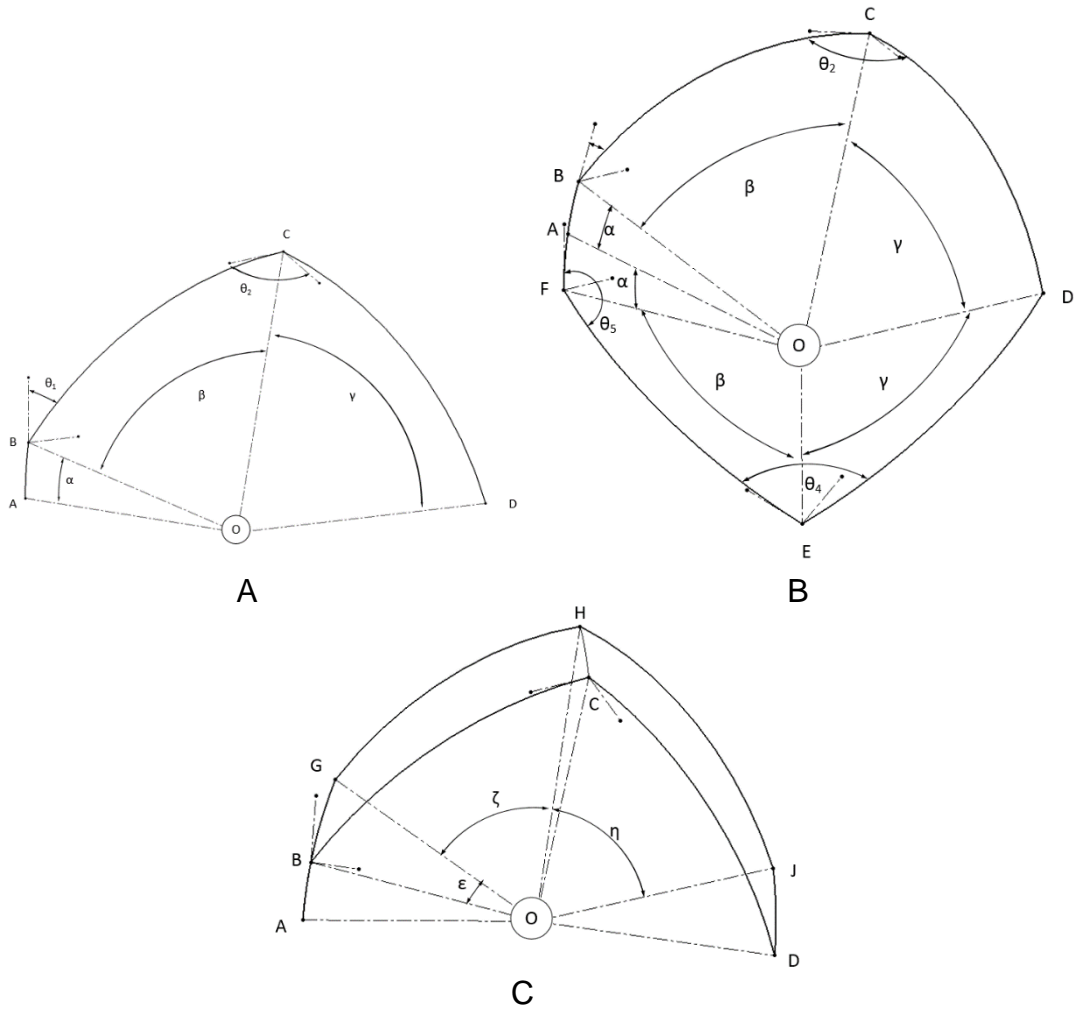
Figure 5.16: The three different gimbal configurations. A) two-bar gimbal, B) five bar gimbal, C) four-bar extension on the two bar gimbal, but can be attached to five bar as well.
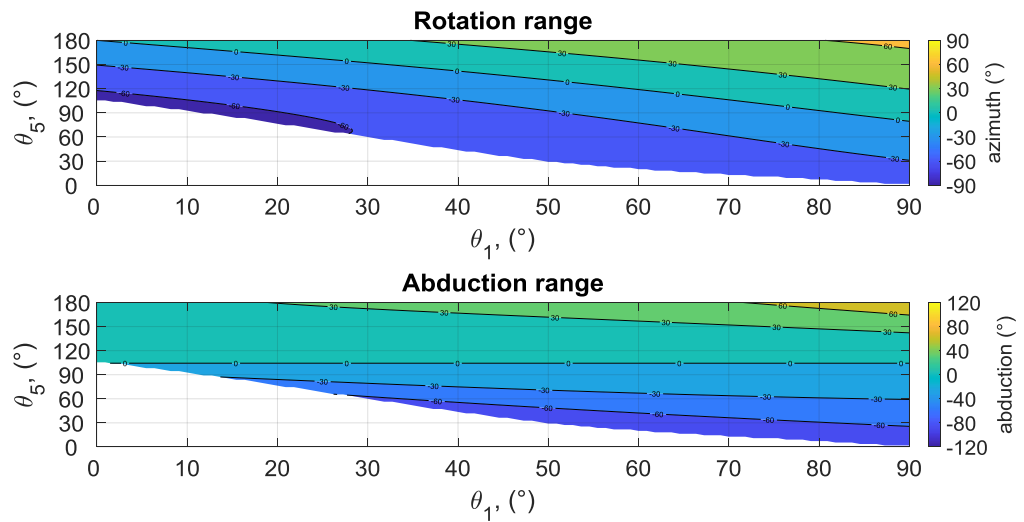
Figure 5.17: Motion range of two bar system
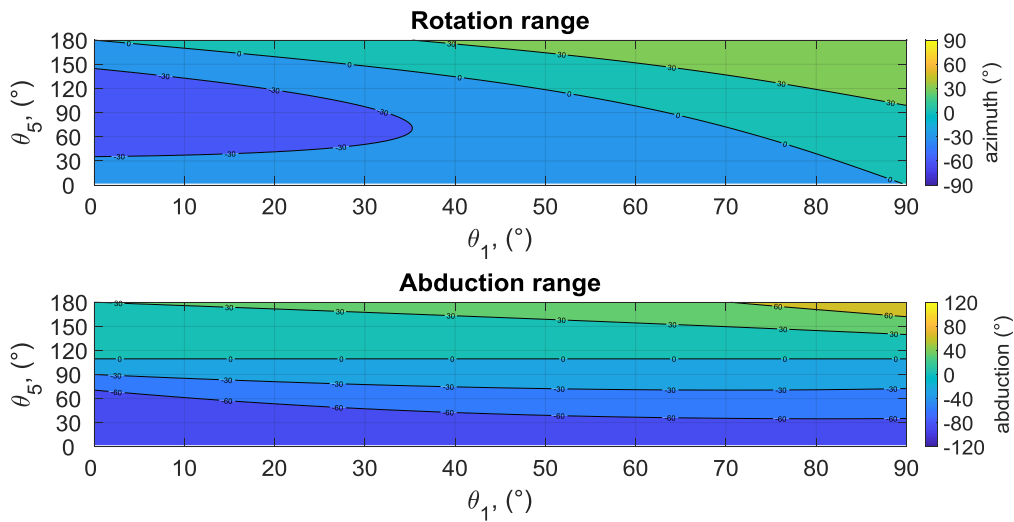
Figure 5.18: Motion range of two bar system with four-bar extension

If the values of the two-bar optimised system are put into the two-bar with four-bar extension, then the solution generated is shown in Figure 5.19. The solution has a reduced area of working due to contact with the user, as well as singularity issues.
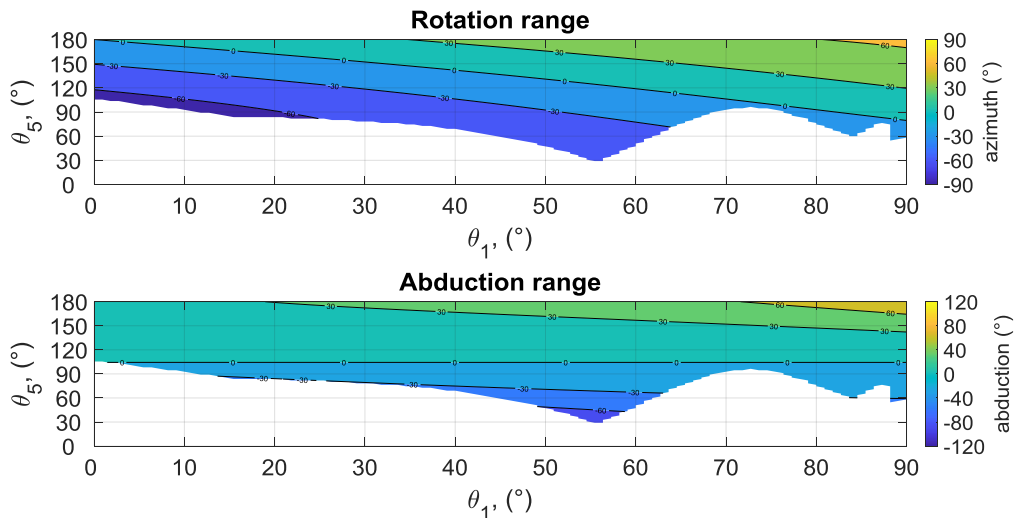
Figure 5.19: Motion range of two bar system with four-bar extension using the two bar optimised values

5 Bar linkage

Developing into the five bar system, as shown in Figure 5.20, it can be seen that the solution does not have the complete range, and does not have a realistic range for the exoskeleton. The rear bar is also longer at 85.3° and the front bar shorter at 39.2°. An inversion of the two-bar solution.
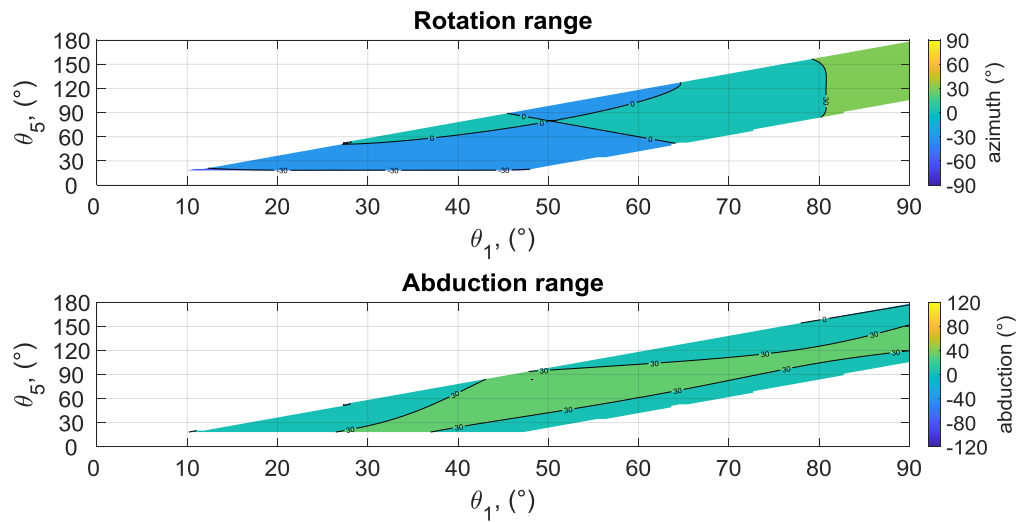
Figure 5.20: Motion range of five bar system

As there is now a lower section, the probability of contact with the user increases. This has resulted in a smaller workspace than the two-bar solution. The rotation range minimum has decreased towards zero to -34.3° but the maximum has increased to 111.2°. This is only a range of 145.5° compared to the 180° of the two-bar solution. Similarly, the abduction range has decreased to -70.3° to 52.4°.

Adding the four-bar extension to the five bar system, as shown in Figure 5.21, fails to generate a suitable solution, with the problems of the five bar and four-bar extension combined.

The four-bar solution of the five-bar mechanism also gives bar angles of 60° each but has a reduced range of motion for rotation of -37.2° to 28.9°. The angle of abduction decreases to -24.4° to 37.0°.

As the cost function is only looking at the differences at the maximum and minimum values, then there is no guarantee the solution will have a continuous surface. This has caused the fractured nature of the results seen in Figure 5.21.
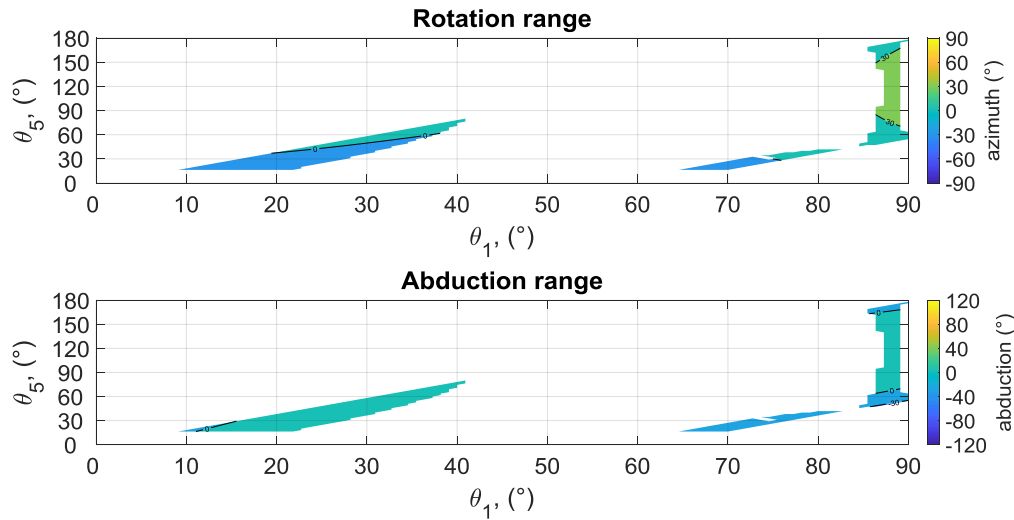
Figure 5.21: Motion range of five bar system with four-bar extension

5.5.3.2 Torque requirements

As the weight of the arm and shoulder flexion is now known, the torque for the shoulder can be determined.

Following the previous sections, the loads can be outlined in Table 5.3.

Table 5.3: Shoulder torque requirements

	Load Torque Nm	Acceleration Torque Nm	Demand Torque Nm	Cushion Torque Nm	Final Torque Nm
Shoulder Middle	605.75	281.69	887.45	1169.14	2523.94
Shoulder Rear	464.90	359.59	824.49	1184.08	2556.20

The loading for the two actuators is similar, and would likely be of the same model, if not the same range. As the rear shoulder unit is closer to perpendicular to the rest of the arm, the loading torque is smaller, as it has a smaller moment arm for the mass to load. The inertia increases with the additional arm and actuator between the middle and rear shoulder pivots, and thus the acceleration torque is higher for the rear actuator.

5.5.3.3 Actuation system

Linear

The use of linear actuators on a curved arm introduces an issue with the actuator having to be along the tangent of the curve, and thus taking up additional room. For a radius of 300mm and an actuator length of 300mm, the endpoint is 453 mm from the centre of the joint. This is shown in Figure 5.22.

This extra offset could collide or interfere with other components, and this is a risk.

The use of a five-bar system would allow the use of linear actuators on the rear of the system, which is a significant benefit. The weight is transferred to the back, rather than being distributed along the arm. The limited motion range of the five bar system does not make this feasible for this exoskeleton design, but others with reduced motion range, it would be a possible route.

The weight of the system does not just require the weight of the actuators, but the support structure as well. For the tangent version, the 300mm of structural support would be significant, especially with bearings.
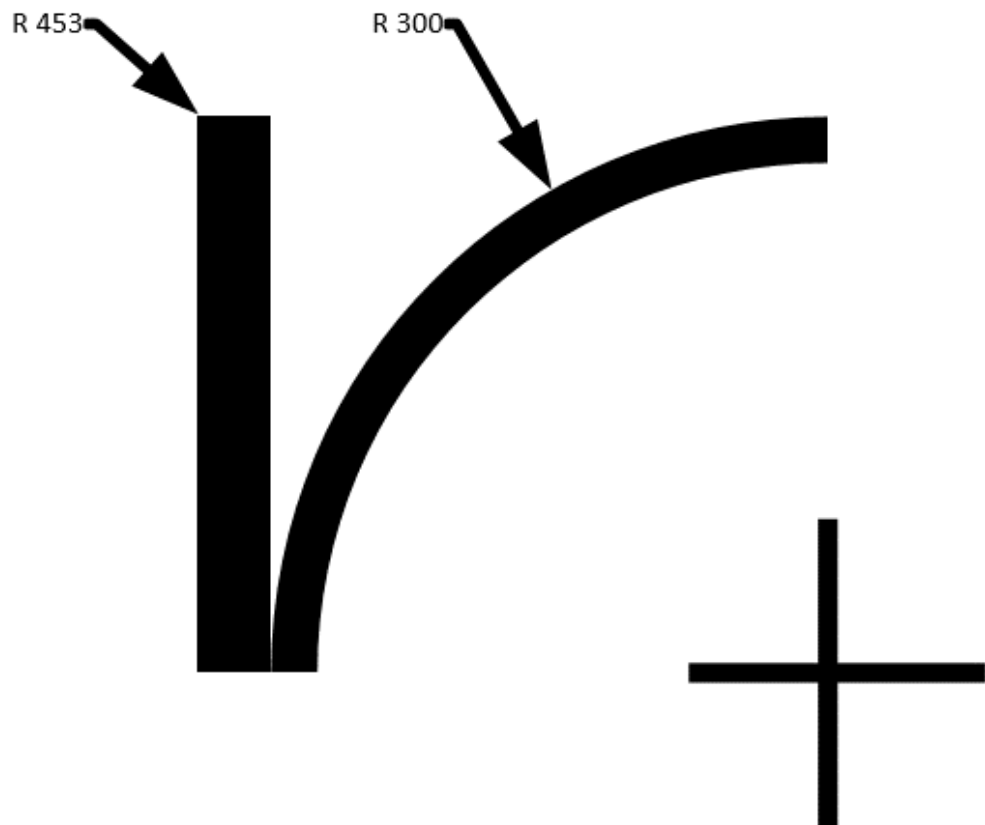
Figure 5.22: Additional radius encountered if a linear actuator used

There is also the angle range limitations, which would require optimisation and thus the increase in weight and complexity. Certainly, for the elbow, there were limited solutions, and the complexity for the flexion would have similar results for the other shoulder joints.

Rotary

The torques are similar to those of the shoulder flexion, and doing a component lookup from Appendix O gives similar results.

For the middle shoulder actuator, the lightest designs are the rack and pinion versions, followed by the helical designs. The lightest of these are foot-mounted actuators, which would require structural mounting to be placed away from the user. These weigh 48 and 52 kg, with specific torques of 58.8 and 56.5 Nm/kg. For slightly heavier actuators, there are helical designs that are front mounting and are the same model as those of the flexion shoulder joint.

For the rear unit, the lightest units are vane designs. These have very high specific torques, at 320 and 200nm/kg, but the axial loading is limited. The maximum axial loads are 50N, which means any forward loading would cause the actuator to fail. As 50N is only around 5kg, and motion that moves the axis of the actuator from parallel to the ground will likely overload the actuator. The next units are helical, similar to the one used on the flexion of the shoulder.

5.5.3.4 Discussion

The first decision is which gimbal design to use. The two bar gimbal design is the simplest though requires the actuator to be positioned along the limb. For the five bar system, there are the additional lower arms that risk coming into contact with either the exoskeleton or the user, giving limit motion range.

Using linear actuators increases the complexity and bulkiness of the design and thus rotary actuators would be a preferable solution.

5.5.3.5 Final design

Bringing all of the arm components together, the design is shown in Figure 5.23.
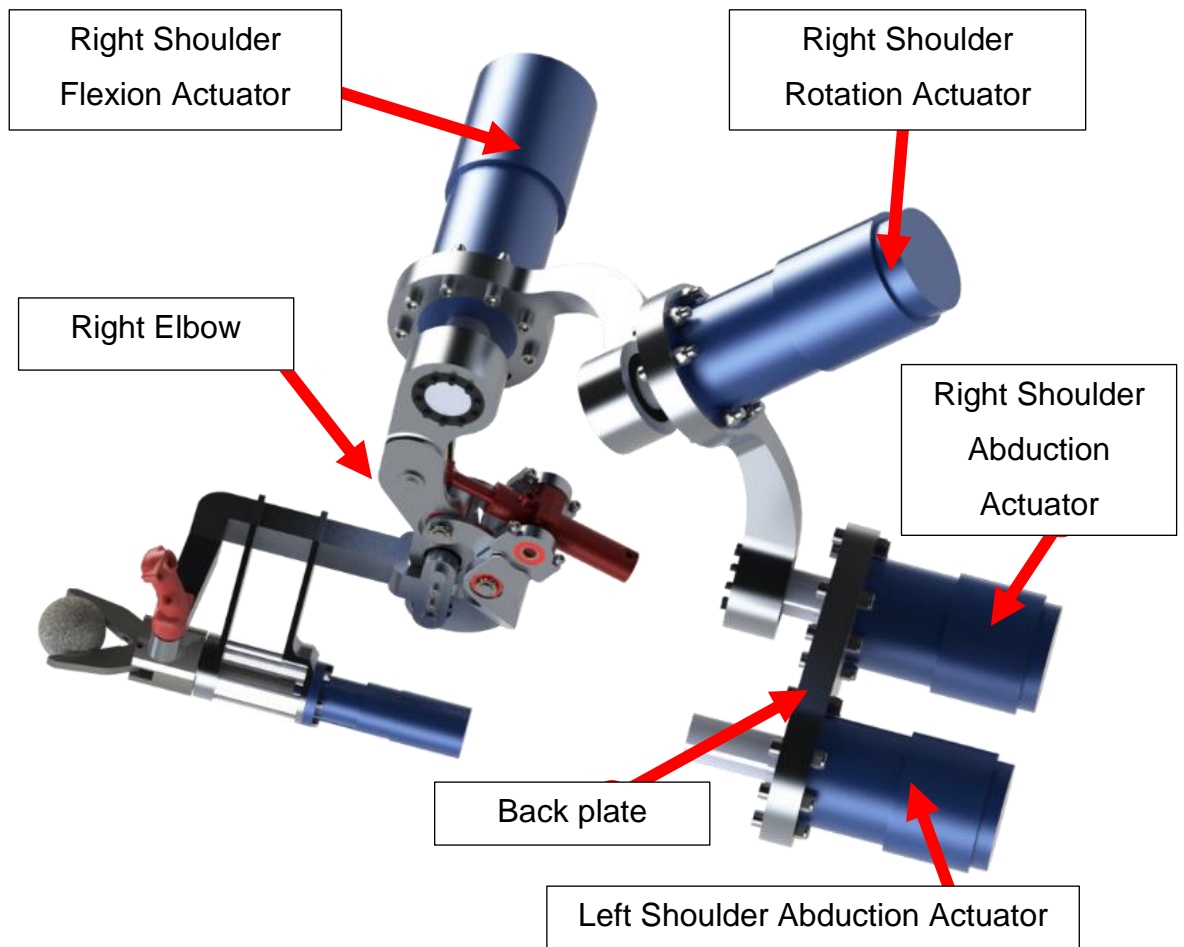
Figure 5.23: Completed arm

5.6 Final system

The final upper body system is shown in Figure 5.24, an extension of Figure 5.23, with both arms. It can be seen that this is not a directly anthropomorphic design, due to the concerns about safety, though does have three DOF at the shoulder, one at the elbow, and an additional two for the manipulator. This gives a total DOF of 12.

Drawings for the components are in Appendix Q.
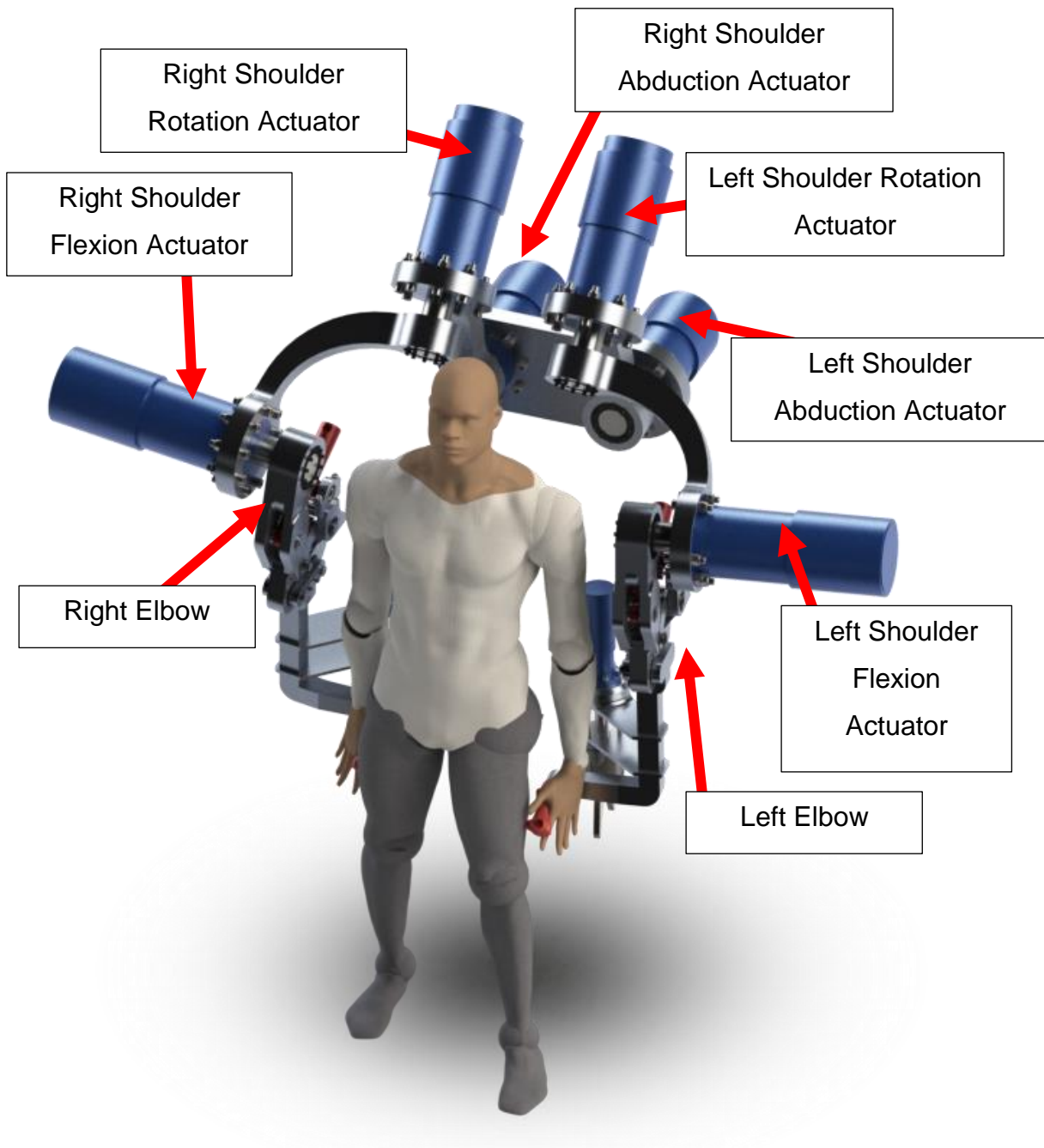
Figure 5.24: Final design of the upper-body exoskeleton

With the design completed, it can be compared to the requirements from Chapter 3.

5.7 Discussion

In order to differentiate this new exoskeleton from general exoskeleton design, the system should have a name. It has been decided that the system will be called Leeds Enhancive Action at a Distance Upper-body Exoskeleton (LEADUE)

As the design process used the target weight of 45kg per arm, it will have met the 90kg carry load requirement. This requirement has also been used in assuming that the load is at full reach so that the action at a distance is supported.

The tethering requirement has not been examined at the current time due to the hydraulics not being selected, though, with the size of the actuators, the system being tethered is a high probability.

The final weight is 463.16 kg, compared to the acceptable weight of 68kg. A breakdown of the weights for the exoskeleton are shown in Table 5.4.

Table 5.4: Weights of components in the exoskeleton

	Weight (kg)
Structural	65.03
Actuators	340.56
Couplings	18.00
Bearings	5.24
End Effector	32.30
Controls	0.50
Bolts	1.33
Circlips	0.02
Lock Nuts	0.18
	463.16

As the design focus was on action at a distance, this is the reason that the weight has exceeded the requirements.

As discussed in Section 3.2.2, the system will be compared to current exoskeletons. These have been reproduced in Table 5.5, including the final design for the upper body exoskeleton, but the methodology of load interaction is different between this design and other exoskeletons.

If the load was carried with the arms bent at 90°, as if carrying a box, then the system would carry 127kg per arm or 254kg in total[8]. This gives a load to weight ratio of 0.548 that is between BLEEX and PERCRO.

BLEEX carries the weight on its back, whilst SARCOS carries it with a farmers walk[9]. It the exoskeleton is used in this manner, then it can carry 382kg per

---

[8] The fullsterkeur ("full strength") lighting stone used in strong man competitions, which would be carried in a similar manor, is 155kg. The Husafell stone is 182kg [121].

[9] The farmer's walk is commonly used in strongman contests where the competitors carry a heavy weight in each hand with the arms being parallel to the body. The

arm or 764kg in total. This gives a load to weight ratio of 1.650. This takes the system above the load to weight range of the other exoskeleton systems. The structural integrity might not support this load, and thus would need to be verified.

Table 5.5: Weight comparison of different robots and exoskeleton systems

Model	Load	System Weight	Load to Weight Ratio
BLEEX	23.1	51.8	0.446
HAL - (Lower limb system)[10]	40-100	~14	2.85-7.14
PERCRO	101.9	160	0.637
SARCOS[11]	90	*	*
LEADUE	90	463.16	0.194
LEADUE - Close to body carrying	254	463.16	0.548
LEADUE - Farmers Walk	764	463.16	1.650

At the current time, this is only an upper-body system and thus the final weight will increase. If PERCRO is used as the load to weight ratio baseline, then the system can increase in weight by 736.2kg for the lower body.

As raised in Chapter 3, for action at a distance, the comparison is between the final system and industrial robots, as outlined in Table 5.6.

World's Strongest Man competition has the athletes carrying over 160kg in each hand over a set distance which is time limited [122]

[10] HAL lower limb type (non-medical), double limb version, which is for mobility support (standing, sitting and walking) rather than augmentation

[11] SARCOS does not give the weight of the system in their literature

Table 5.6: Commercial collaborative and industrial robots examples

Model	Load	System Weight	Load to Weight Ratio
CR-35iA	35	990	0.035
R-1000 100F	100	665	0.150
LEADUE	90	463.16	0.194
LEADUE with full lower body allowance	90	1199.37	0.075

With the exoskeleton being used in the action at a distance mode, the load to weight ratio comparison is comparable as neither of the two commercial systems can move. If the weight is increased with the lower body, as per the last entry in Table 5.6, then the load to weight ratio lies between the commercial systems, but with the added ability of mobility for the exoskeleton.

The human element has been incorporated for speeds and reduced impact based on the motion capture data during the design process. As the system has been designed to match the human motion, then there will be minimal to zero loading on the user.

Entering and exiting the system is also simplified, as the connection points will be a simple, multiple point harness for the torso, and the person holding the control sticks. This means that emergency egress is quick and easy, with only a quick-release catch located in the chest area to activate.

The pricing of the system is above that of the acceptable range, as a quote from the helix actuator company put the price at around €2401. For 8 units, this is €19208 or £17220.60[12], which leaves £12779.40 for the structural components and gripper

Another reason for the heavier weight is likely due to the high safety factor used. As reviewed in Chapter 2, other exoskeleton systems have a lower safety factor than the one chosen for this design, with some lowering them below recommended levels, for example, those using cables. For a system that encloses a human, and has the risk of injury, possibly fatally, then safety should

---

[12] Conversion on 23rd July 2019 at 15:06 UTC

be the number one priority, and designing to a reasonable safety factor is a necessity.

5.8 Summary

This chapter has covered the design process for the exoskeleton, looking into it following a systematic step through the process starting with the end effector and working down to the base.

Using the optimisation techniques for the joint design from Chapter 4, the design has attempted to make sure that component selection and geometry give the greatest chance for a full range of motion with the required strength.

This has led to the development of drawings and a model that can be simulated to verify the loading of the system.

Chapter 6

Exoskeleton Hydraulics

6.1 Introduction

Previous exoskeleton systems that use hydraulics have not focused on optimising the hydraulic circuits, but have used servo valve-based systems. There is, therefore, the question of whether recent hydraulic theory could be brought into the exoskeleton domain. If the efficiency can be improved, then less energy is required and if untethered, run for a longer period.

With several circuit options available, as discussed in Chapter 2, these need to be compared to determine which would be suitable for simulation for the complete exoskeleton. To simplify the simulation, only the elbow joint will be used in these tests and can be imported (geometry (STL format), joints and kinematic data) into the Simscape multidomain physical workspace to determine the hydraulic requirements for a variety of motions. Simscape is the physical modelling environment extension to Simulink by MathWorks. It allows the integration of Simulink control with multibody and hydraulic components.

As the hydraulics will be required to follow human motion, the difference between the input and response should be minimised. If a circuit is unable to match the motion, then it will be unsuitable for the exoskeleton.

The circuits are not novel, but the critical analysis of hydraulics in exoskeleton usage to improve efficiency and reduce power consumption is.

As hydraulics are nonlinear, an examination of current theory on different control strategies required first. Many are model-dependent, in that they require an understanding of the hydraulic circuit design to compare against. Model-independent control is another route, which can theoretically be used for any circuit design.

The setup and tuning of the hydraulic components in Simscape is covered in Appendix R.

6.2 Hydraulic control

With the hydraulic components setup, the control linking them together is required. There have been several studies concerning the control of hydraulics due to their nonlinear responses [123].

The state-space model as shown in [123] and shown for convenience in equations (6.1) to (6.4).

$$\dot{x}_1 = x_2 \tag{6.1}$$

$$\dot{x}_2 = \frac{1}{m_t(x_2)}\left[(x_3 - \alpha \cdot x_4)A_p - F_t(x_2) - u_2\right] \tag{6.2}$$

$$\dot{x}_3 = \frac{\beta_A(x_3)}{V_A(x_1)}\left[Q_A(x_3, u_1) - A_p \cdot x_2\right] \tag{6.3}$$

$$\dot{x}_4 = \frac{\beta_B(x_3)}{V_B(x_1)}\left[Q_B(x_4, u_1) - \alpha \cdot A_p \cdot x_2\right] \tag{6.4}$$

Where $x_1 \equiv x_p$ is the position of the piston, $x_2 \equiv \dot{x}_p$ is the velocity of the piston, $x_3 \equiv P_A$ is the pressure of chamber A, and $x_4 \equiv P_B$ is the pressure of chamber B. m_t is the total mass, V_x are the volumes of the cylinder chambers respectively, Q_x is the flow rates of the cylinders respectively and A_P is the piston area with α being the piston area ratio.

It can be seen that there are x terms as denominators in some of the equations, which makes constructing the standard state-space equations difficult. The normal State-Space equations are given in equations (6.5), (6.6) and (6.7).

$$x = Ax + Bu \tag{6.5}$$

$$y = Cx + Du \tag{6.6}$$

$$x|_{t=t_0} = x_0$$

(6.7)

Where x is the state vector, u is the input vector, y is the output vector, and x_0 is the initial condition of the state vector.

This has led to state estimations at certain positions by using neural networks [124], continuous tuning ([125], using modular adaptive robust control (MARC) [126] and particle swarm optimisation (PSO) [127]) or even the use of a dual system [128]. The range of methods shows that nonlinear control for hydraulics is still being developed, with different thoughts showing promising results

Recent control design work on nonlinear hydraulics has looked into the use of Non-singular Fast Terminal Sliding Mode (NFTSM) [129] which is not based on a model. This is due to the selection of an NFTSM-type sliding surface that gives a finite-time convergence of the system.

The control is based upon the equation (6.8)

$$\tau = M(\theta)\ddot{\theta} + V(\theta,\dot{\theta})\dot{\theta} + G(\theta) + F + D$$

(6.8)

Where $\theta, \dot{\theta}, \ddot{\theta} \in \mathbb{R}$ represent the angular position of the joint, velocity, and acceleration of a joint, respectively; $\tau \in \mathbb{R}^n$ is the actuator torque; $M(\theta) \in \mathbb{R}^{n \times n}$ is the inertia matrix of the joint structure; $V(\theta,\dot{\theta}) \in \mathbb{R}^n$ is the centrifugal/centripetal matrix; $G(\theta) \in \mathbb{R}^n$ is the gravitational vector; $F \in \mathbb{R}^n$ is the friction term; and $D \in \mathbb{R}^n$ denotes the disturbance torques [129].

Defining the dynamic equations as given in (6.9)

$$v = \bar{M}\ddot{\theta} + \bar{H}$$

(6.9)

Where $\bar{M}$ is a constant, which needs to be determined, and $\bar{H}$ is defined as given in (6.10)

$$\bar{H} = (M_K - \bar{M})\ddot{\theta} + H$$

(6.10)

Where $M_k = \text{diag}^{-1}(K_{u1}, ..., K_{un})M(\vec{\theta})$ for which K_{un} are the gains for $v(t)_i$, and $H = [h_1, ..., h_n]$, and $h_i = K_{ui}^{-1}(V(\theta,\dot{\theta})\dot{\theta} + G(\theta) + F + D - K_{xi}x_i - Q_{etci})$. These are estimated using time delay estimation (TDE).

For the sliding surface, the equation is given in (6.11).

$$s = e + a \cdot \text{sgn}^{\gamma_1} e + b \cdot \text{sgn}^{\gamma_2} \dot{e} \qquad \textbf{(6.11)}$$

Where **e** is the error between desired and actual position, i.e. **e** = θ_d - θ, with derivatives of **e** using derivatives of **θ**. *a, b, γ_1 and γ_2* being constants, where *a>0, b>0, 1<γ_2<2*, and *γ_1>γ_2*. $\sin^b a$ is a simplification in writing of $|a|^b \sin(a)$

To reduce the chattering of the system, yet keep a fast finite-time convergence, the dynamic attractor of the reaching phase is defined as given in (6.12)

$$\dot{s} = -|\dot{e}|^{\gamma_2 - 1}[k_1 s + k_2 \text{sgn}(s)] \qquad \textbf{(6.12)}$$

Where *k_1 and k_2* are greater than zero.

Thus, the control method is defined as given in (6.13) and (6.14).

$$v = \bar{M}\delta + \hat{H} \qquad \textbf{(6.13)}$$

$$\delta = \ddot{\theta}_d + b^{-1}\gamma_2^{-1}\text{sgn}^{2-\gamma_2}\dot{e}(1 + a\gamma_1|e|^{\gamma_1 - 1}) + k_1 s \\ + k_2 \text{sgn}(s) \qquad \textbf{(6.14)}$$

Where $\hat{H}$ denotes the estimates of the nonlinearities and other unknowns which cannot be defined. This is expressed as given in (6.15)

$$\hat{H} = \bar{H}(t - L) = u(t - L) - \bar{M}\ddot{\theta}(t - L) \qquad \textbf{(6.15)}$$

Where •(*t-L*) is the time-delayed value of •.

Thus giving the final equation as shown in (6.16).

$$v = \bar{M}\big[\ddot{\theta}_d + b^{-1}\gamma_2^{-1}\text{sgn}^{2-\gamma_2}\dot{e}(1 + a\gamma_1|e|^{\gamma_1 - 1}) + k_1 s \\ + k_2 \text{sgn}(s)\big] + u(t - L) - \bar{M}\ddot{\theta}(t - L) \qquad \textbf{(6.16)}$$

Graphically, this is shown in Figure 6.1.
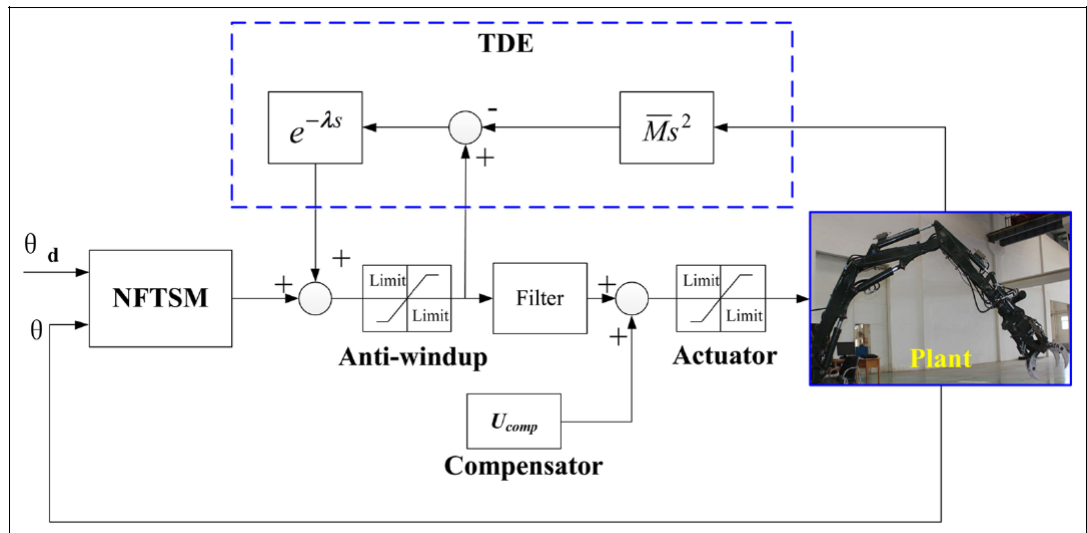
Figure 6.1: Overall scheme of the control method from Liang et al. [129]

This controller is used as originally defined by Liang [129] and has not been modified with novel ideas in this thesis.

6.2.1 Tuning

For each of the circuits, the values of the control variables will be different, thus each will need to be tuned. Of the seven variables, these have been simplified down to four where a = 0.3L, b = 0.02L, k_1 = 100L, and k_2 = 30L, where L is a tuneable constant varying between zero and infinity [129]. M, γ_1, and γ_2 are also defined as tuneable. The basis of the values for a, b, K_1 and K_2 come from [129] and could also be optimised, but there is an exponential increase in the time for the optimisation with each variable added.

To determine the values of the variables, the *Simulink Design Optimization* toolbox was used. This has a GUI tool that allows the user to define the:

- design requirements
- parameters to optimise
- optimisation method

Each circuit is given two requirements to comply against: the endpoint should follow the reference motion signal, and that the output from the controller is limited to a ± 10 range, equivalent to the voltage input for the servo valve. The reason for the second requirement is due to the anti-windup block, as shown in Figure 6.1.

The anti-windup block bounds the signal to ±10V, as this is the range of the servo valve input. This means ideally that the output from the NFTSM and TDE additional should be within this range. If the position of the actuator starts to become unstable, then there is a risk that the input into the anti-windup block becomes larger than the bounds. If the command then overcompensates in the other direction, then there is a risk of turning the servo command into a square wave rather than a smooth continuous signal.

For the digital circuits, the bounds are set to ±15LPM and ±40LPM respectively, and for the pump circuits are ±3000rpm.

6.3 Methodology for circuit testing

To compare the different hydraulic circuits, a virtual test environment will be developed based on the exoskeleton elbow, as shown in Figure 6.2.
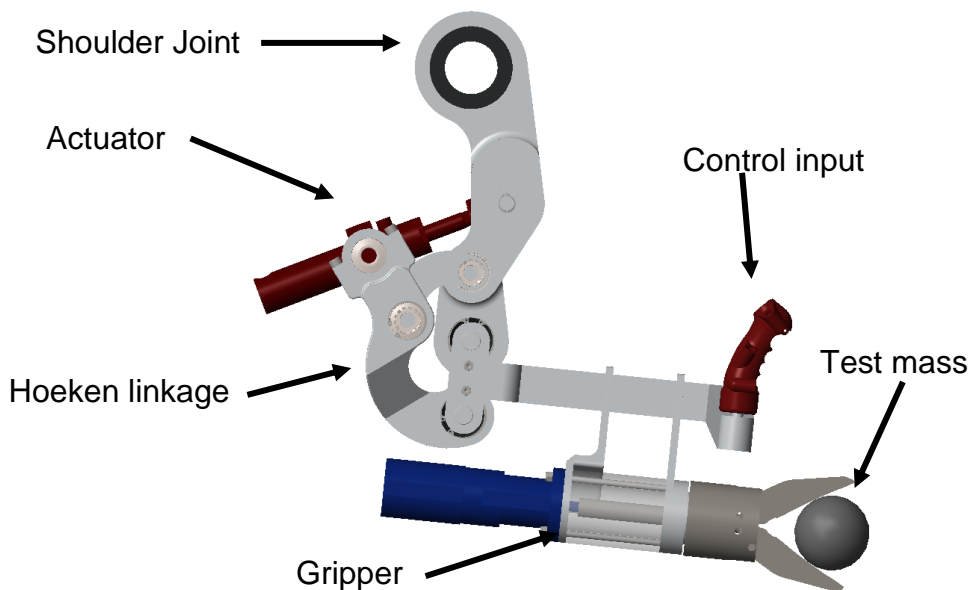
Figure 6.2: Elbow joint for circuit testing

To test the response of each circuit, there are two inputs: motion and mass. The motion consists of sending a position demand to a control algorithm for the hydraulic circuit whilst the mass will be set to either 1g or 45kg to give the minimum and maximum loading of the elbow. 1g is used rather than 0g due to the model requiring a minimum mass to determine inertia.

The motion command signal is an arbitrary one generated to test the range and speed of the circuit and joint. The command signal will vary between the limits

of motion for the actuator, but limited in speed to less than 400mm·s^{-1}. This speed limit was selected based on the motion results from Chapter 3.

The first part of the command signal is a stabilisation period of 3 seconds. This allows the hydraulics and joint to stabilise around 50mm, the middle stroke of the actuator.

The second part of the command signal is a stepping motion between several extensions of the actuator. The velocity between these points is between 100 and 150mm·s^{-1} which are based on the velocities of the human motion.

The third part of the signal is the same steps as the second part, but with higher velocities.

The final part is a chirp signal, a sinusoidal signal that varies in frequency with time. The chirp for the test starts at 10 Hz and finishes at 20 Hz. 10Hz was selected based upon the human motion having up to 10Hz bandwidth [130], and 20 Hz as the system should be able to respond faster than required. Bandwidth is defined as the maximum sinusoidal frequency that can be tracked.

The complete command signal is shown in Figure 6.3.
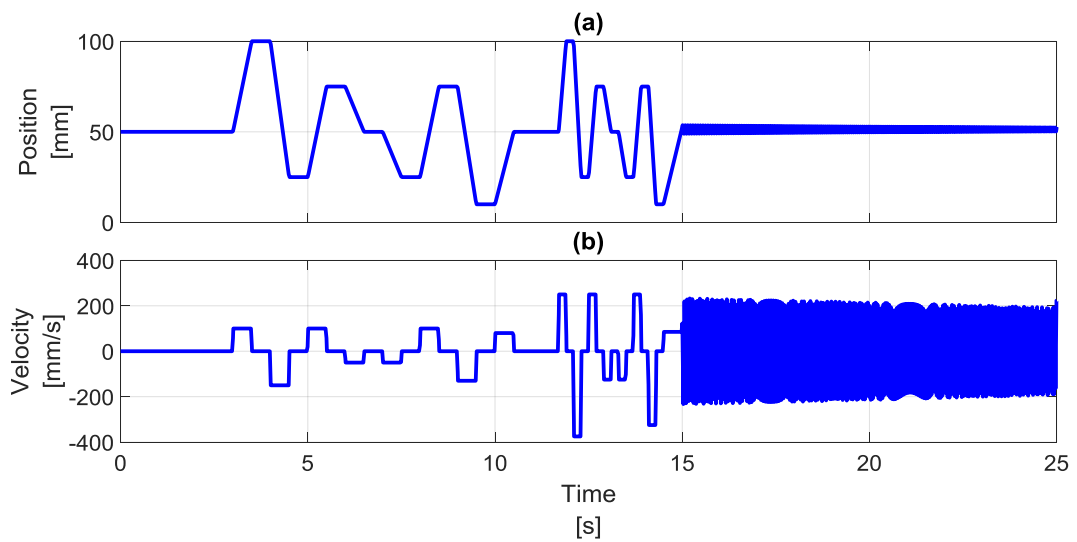
Figure 6.3: Input demands into test systems. a) the actuator extension demand, b) the velocity of the actuator extension.

Each circuit will be compared with the same input command signal to determine the error between the input and the response. This will be the first measure of the performance of each circuit, with units with lower RMSE being selected. As the exoskeleton is required to follow human motion, then any error between the demand and response needs to be minimised to prevent loading on the user.

The second measure of performance will be the power required for the circuit to follow the motion. To generate a baseline, the command signal is put directly into the actuator as position demand, and the force and velocity recorded. The force and velocity can be multiplied together to give the actuator power. For an untethered system, power requirements need to be minimised so that the power source can be reduced, or stored power can last longer.

This power requirement is in the time domain and can be simplified to two metrics so that different circuits can be compared based on the average power and the peak power. The average power is that of the complete cycle, and the peak is the highest value throughout the time domain. The first few sections of the command signal should give a low power requirement due to several points of zero motion, but the chirp phase should give higher power results.

These two metrics for the direct input model are shown in Figure 6.4 with increasing mass load.
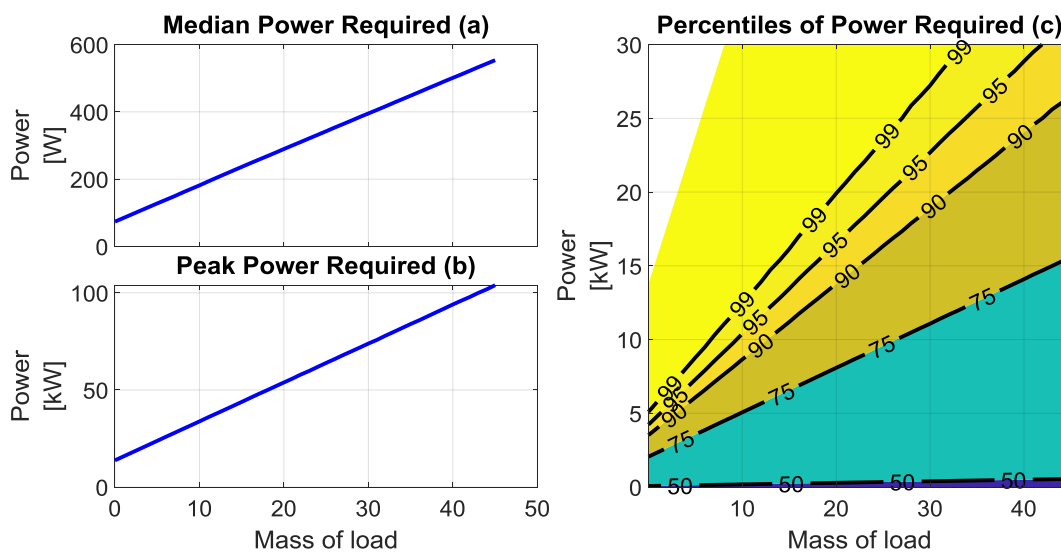
Figure 6.4: Average and peak power requirements for the joint with direct command. a) median power, b) peak power and c) percentiles of power required

The median power peaks at 553.3W at maximum load, whilst the peak power point apexes at 103.9kW, over 18700% increase. From the percentiles of power required, 90% of the power is 26.6kW or less for all loads, with 75% of the power being 16.6kW or less. If the total time is 25 seconds, then this means that the peak event duration is small, less than 1ms in duration.

6.4 Hydraulic circuit testing

6.4.1 Servo-based

6.4.1.1 Servo Valve

With the servo valve being the simplest system, this is the baseline that the rest of the systems will be compared to, and is shown in Figure 6.5. The circuit consists of a pressure source (simplified in the diagram), the proportional valve, route to the tank and the cylinder.
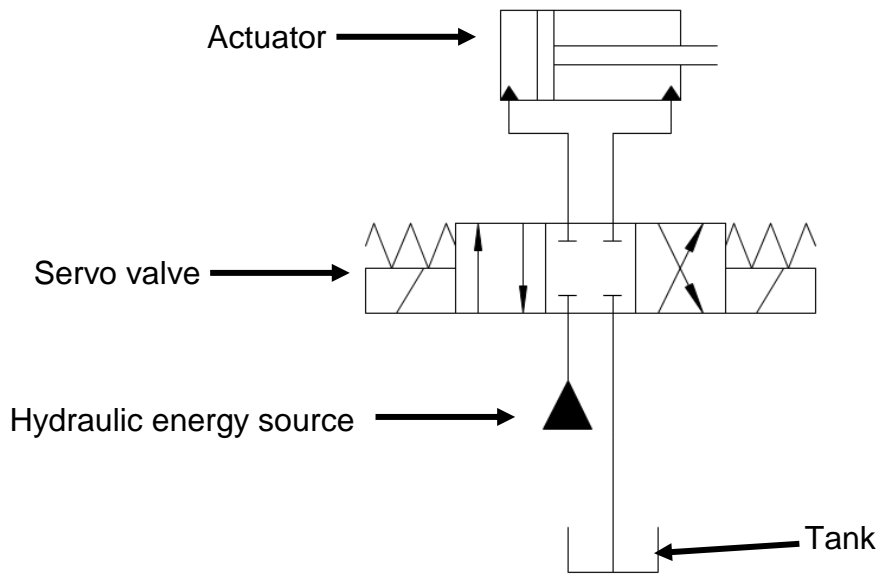
Figure 6.5: Basic Servo circuit

Using the input as described in Section 6.3, the response of the servo circuit is shown in Figure 6.6 for both the minimum and maximum load.

The servo valve shows that a small voltage is required to give motion to the system, even though the servo valve is set to be 10LPM. The 10LPM value is for when there is a pressure differential of 10 bar over the valve. With the flow returning to the tank, there should be a low resistance force on the actuator, and only friction of the piston and choking of the valve to resist the motion.

The position error is small for the low-speed steps but becomes the error and delays increase in the high-speed section. The maximum load position does have overshoot issues, though there are damping issues with both loads. Any underdamped events will be felt by the user and could lead to a feedback loop if they try to compensate.
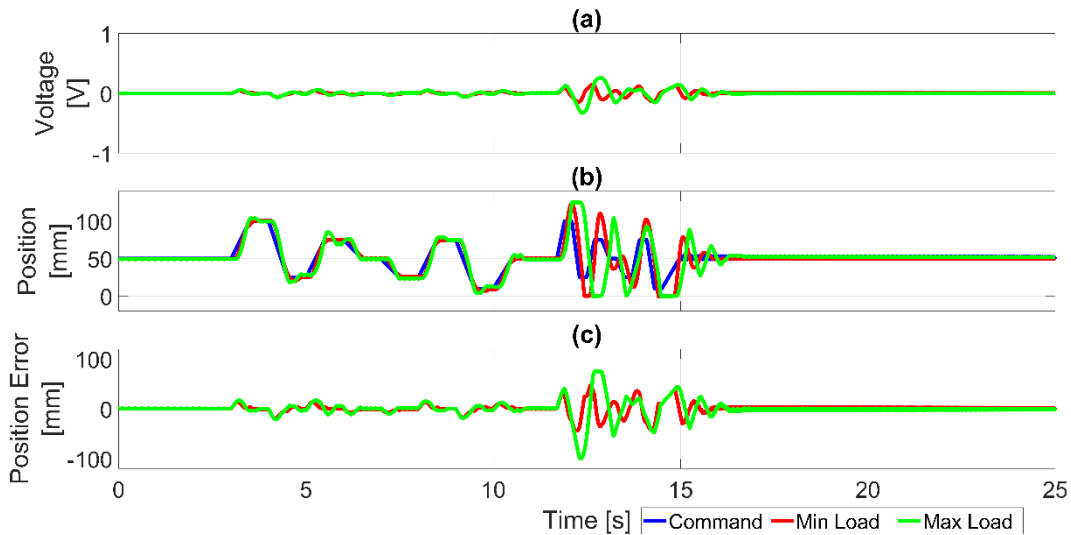
Figure 6.6: Servo valve circuit. a) voltage from the controller for valve opening, b) position, c) position error between command and circuit response.

There is a slight delay between the demand and hydraulic positions due to the servo valve and fluid inertia. This becomes worse with the maximum load with the higher pressures required to move the load. Delays will place loading onto the user such that it could feel that they are pulling the exoskeleton, rather than easily following them.

The chirp event is focused on in Figure 6.7 due to the change in position scale.
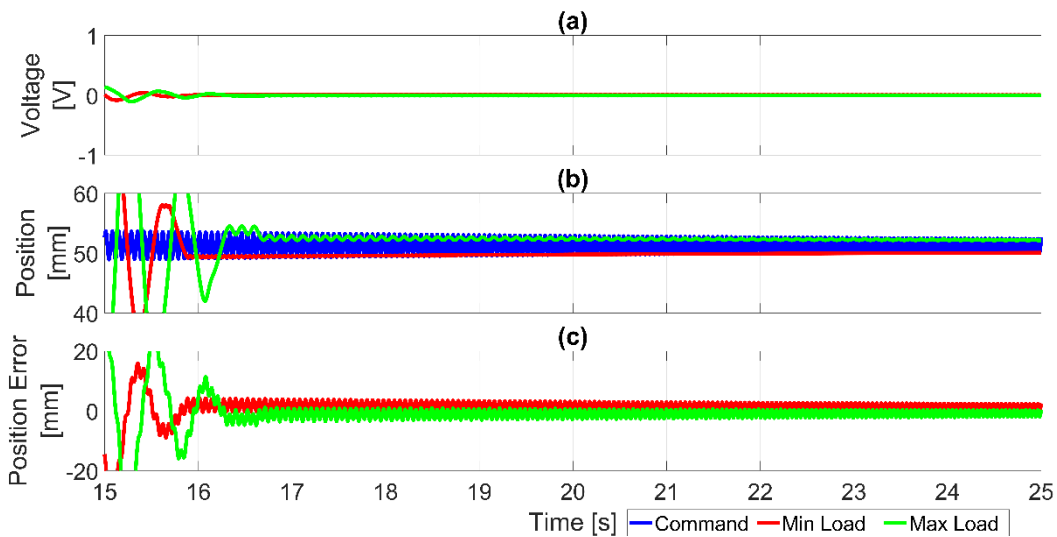
Figure 6.7: Servo Valve circuit focusing on the chirp event. a) voltage from the controller for valve opening, b) position, c) position error between command and circuit response.

The chirp response shows that there is a stabilisation time from the larger input oscillations that takes about 1 to 1.5 seconds to settle down. This could cause injuries to the user if this becomes uncontrolled.

The actuators are unable to follow the demand signal, with the minimum load position showing very little response, but with the maximum load showing some motion in the signal.

6.4.1.2 Regeneration circuit

The simple regeneration circuit is compared to the servo valve to show the difference in motion outputs. Using the sample actuator size, this will not give the double speed response as it is not a 2:1 bore to rod area system. This is shown in Figure 6.8. The components are the same as the basic servo circuit, but with a slightly different flow path.
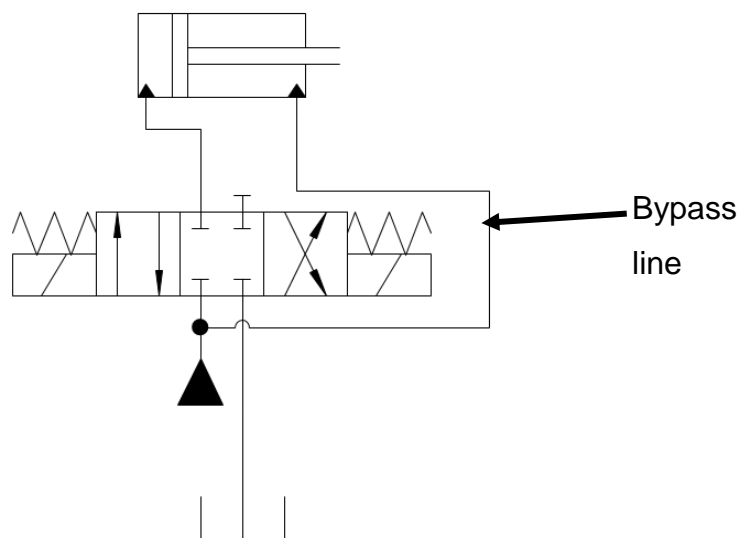
Figure 6.8: Basic Regeneration Circuit

Using the input as described in Section 6.3, the response of the regeneration circuit is shown in Figure 6.9 for both the minimum and maximum load.

The minimum load position is similar to the basic servo valve, though the system fails when the maximum load is applied. Unlike the servo valve version, the rod side during extension is not linked to the atmosphere but linked to the high-pressure side. This decreases the difference in pressure across the piston and thus the force is lower. This means that it is slower to extend, but will be at the same rate for retraction as the servo system.
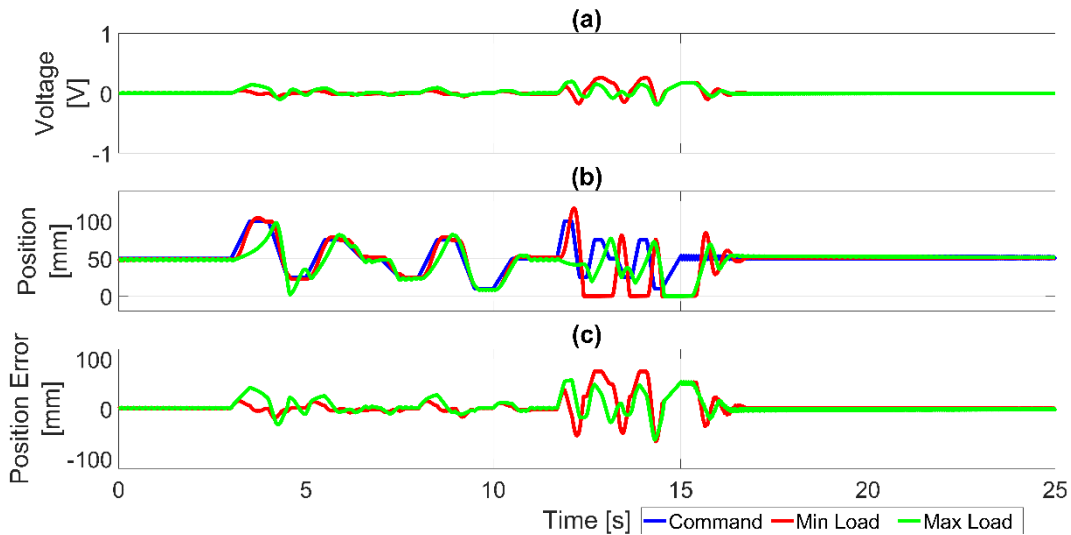
Figure 6.9: Regeneration circuit. a) voltage from the controller for valve opening, b) position, c) position error between command and circuit response.

The chirp event is focused on in Figure 6.10 due to the change in position scale.
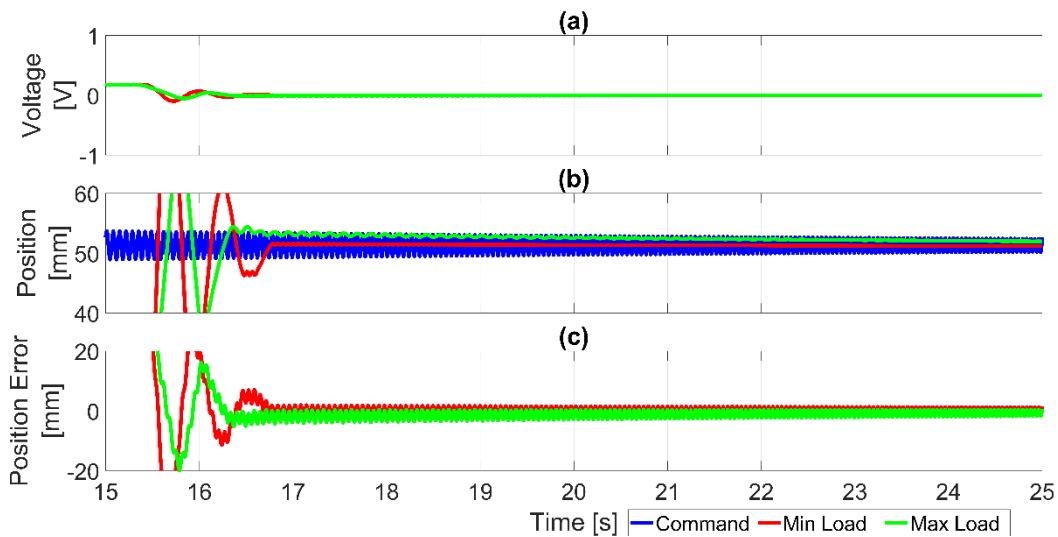
Figure 6.10: Regeneration circuit focusing on the chirp event. a) voltage from the controller for valve opening, b) position, c) position error between command and circuit response.

The chirp position responses are similar to those of the basic servo circuit, though there does appear to be a longer stabilisation time for the minimum load.

The errors in the maximum load positioning, when compared to the servo valve circuit, would mean that this solution is not ideal. As a positive position of the actuator is the flexion of the elbow, then this will affect any lifting motion. This could cause instability in the user and risk injury.

6.4.1.3 Regeneration circuit with pressure override

The regeneration circuit with pressure override allows the system to divert the flow from the rod side to the tank to increase the pressure difference, as shown in Figure 6.11. This circuit requires additional components compared to the previous two circuits, though they are ubiquitous parts.
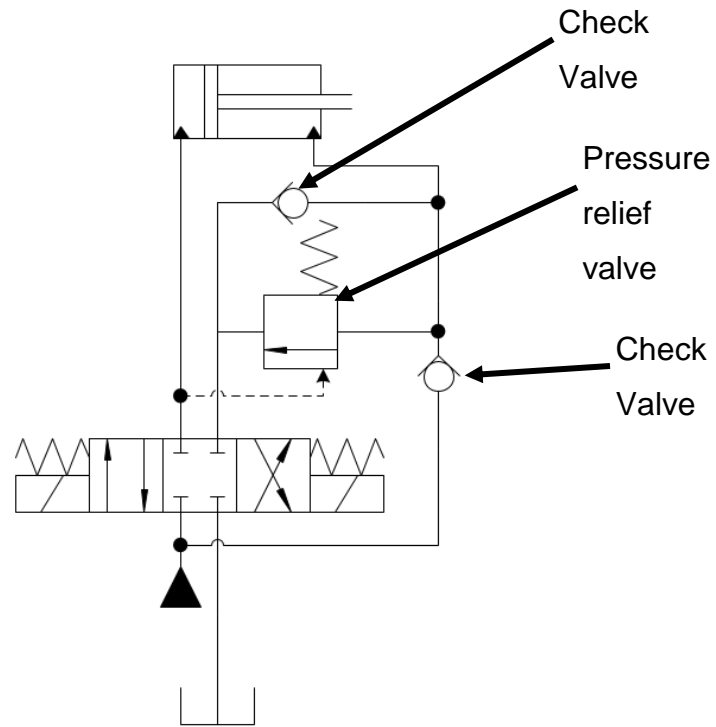
Figure 6.11: Regeneration Circuit with pressure-activated to full thrust

Using the input as described in Section 6.3, the response of the regeneration circuit with pressure-activated to full thrust is shown in Figure 6.12 for both the minimum and maximum load.

When the position response is compared to those of the simpler regeneration results, it can be seen that the maximum load position response has improved, and is closer to the servo circuit. This indicates that the override part of the circuit is working correctly, bypassing the regeneration aspect of the circuit to allow correct motion positioning.
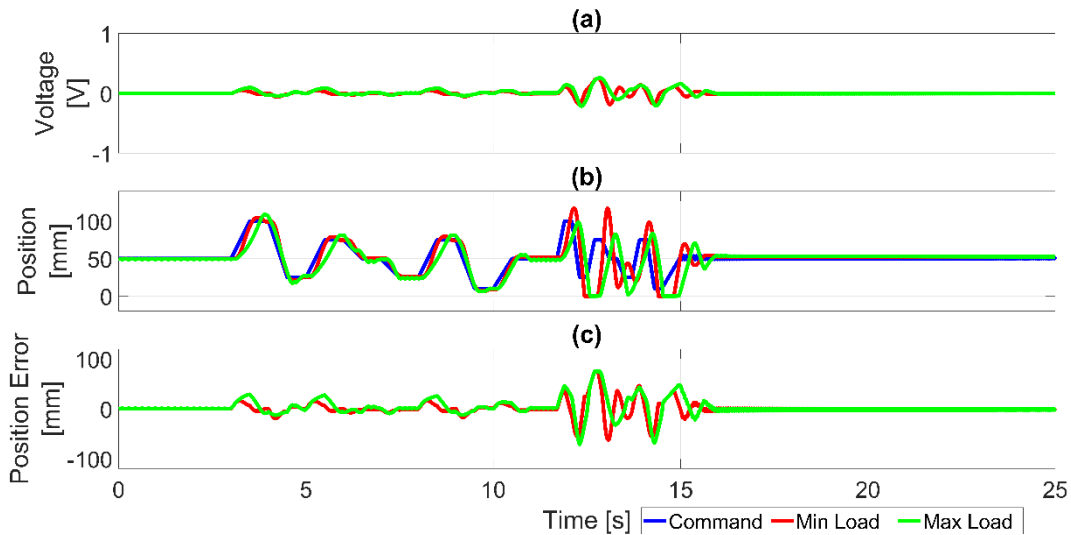
Figure 6.12: Regeneration circuit with pressure override. a) voltage from the controller for valve opening, b) position, c) position error between command and circuit response.

The chirp event is focused on in Figure 6.13 due to the change in position scale.
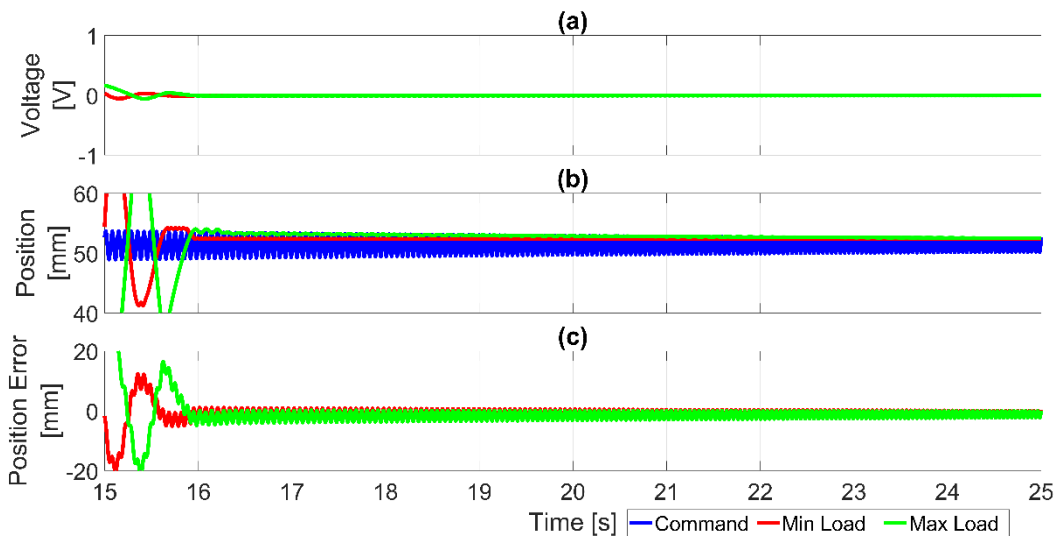
Figure 6.13: Regeneration circuit with pressure override, focusing on the chirp event. a) voltage from the controller for valve opening, b) position, c) position error between command and circuit response.

The chirp position results are similar to those of the servo response, but it appears that the stabilisation time is slightly quicker for the maximum load. The regeneration circuit with pressure override becomes stable at 15.95s compared to 16.30s for the servo valve. With the user bandwidth at 10Hz [130], then this increase of 0.35 seconds is significant.

This means that the regeneration circuit with pressure override could be an alternative to the servo valve circuit in regards to position response, but whether it reduces the power requirement will also be compared.

6.4.1.4 Flow Divider

Similar to the regeneration circuit, the use of the flow divider to draw fluid into or out of the piston chamber is another circuit of interest and is shown in Figure 6.14. This introduces another component that, as mentioned in 2.8.4.1.d, is questionable about its capacity to work with slow-motion events.
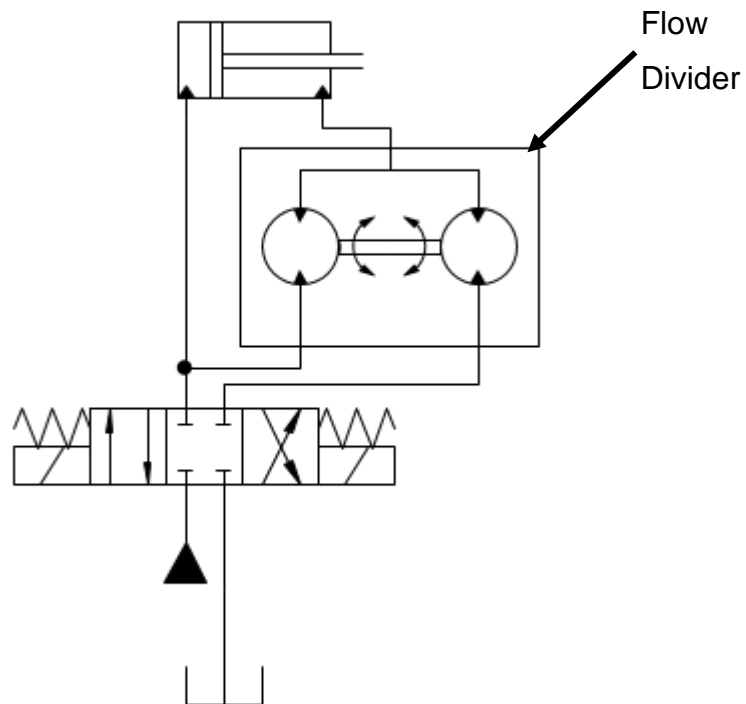
Figure 6.14: Regeneration circuit using motor-type flow divider

Using the input as described in Section 6.3, the response of the flow divider circuit is shown in Figure 6.15 for both the minimum and maximum load.

For the minimum load, the position becomes unstable in the fast response section of the demand. This is not a reasonable response for the exoskeleton and would cause harm to the user. The maximum load response has oscillations throughout the positioning and thus is not suitable as will cause fatigue in the user.
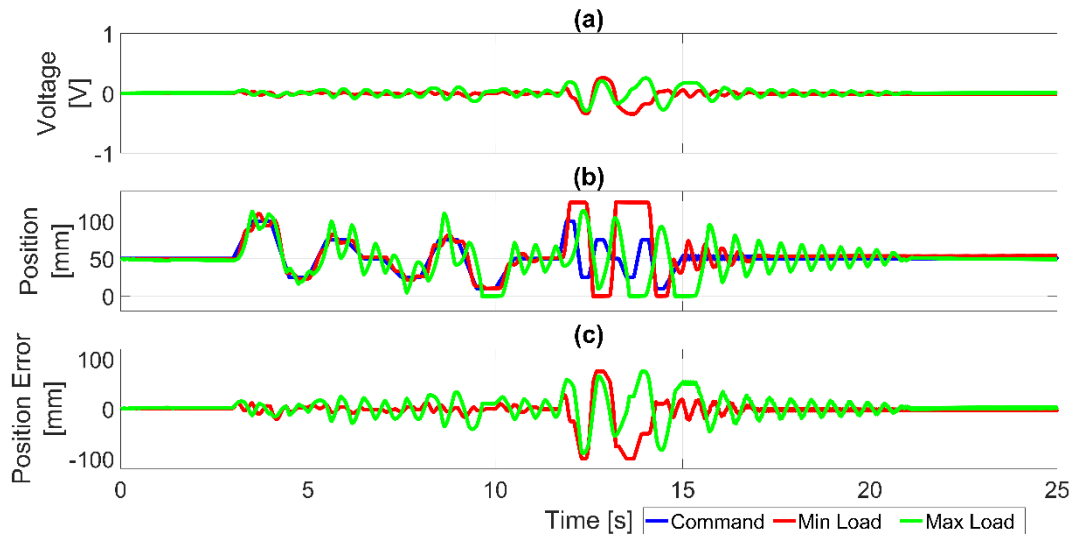
Figure 6.15: Flow divider circuit. a) voltage from the controller for valve opening, b) position, c) position error between command and circuit response.

Closer examination of the chirp phase is not required, as this circuit design would be rejected based on the errors in the initial demand sections.

With the flow divider, it has the highest efficiency when the flow is within a limited band, as shown in Figure 2.25, and when the system needs zero flow, there is power loss across the divider. As the divider is also a gear type, the spin up and down of the shaft will have inertia giving a delay in the response.

6.4.1.5 Comparison of servo-based systems

The systems can be compared using a couple of methods. The first is by examining the positional error, and the second is the power usage.

Examining the errors collated in Table 6.1 shows that the RMSE for all bar the flow divider circuit is less than 20mm. This is significant as the stroke is only 100mm. This is especially important with the maximum error as some extend into the extension support range of between 100 and 120mm.

Table 6.1: RMSE and Max results for different hydraulic methods

	1g results		45kg results	
	RMSE	Max error	RMSE	Max error
Servo	10.1	46.8	16.6	100.0
Regeneration	18.9	75.1	16.3	62.0
Regeneration circuit with pressure override	13.5	75.0	16.0	75.1
Flow Divider	21.8	100.2	22.6	88.8

To assist with which is the ideal result, then a simple decision matrix can be created where the results in each column are numbered one to four with one being the lowest error and summing each row. With this method, the Regeneration with override has a score of seven, the regeneration and servo have a score of nine each and the flow divider has a score of 15.

The servo has the best results for the low mass, but some of the worst for the high load.

For a power requirement aspect, the results given in Table 6.2, shows the average power of the pump into the system as well as the average power out through the relief valve. The difference will be the actuator power.

From the results, it can also have a decision matrix generated for the average power results with the regeneration basic circuit being the lowest power system followed by the regeneration with pressure override. The servo and flow divider results come in joint last.

The regeneration with override is slightly worse than without in terms of power due to the loss through the override valve.

Looking at the power requirements over a range of loads, as shown in Figure 6.16, it can be seen that for the pump power, the servo valve system has the lowest power in as per the initial results.

Table 6.2: Average power for the servo based circuits for the given motion

	Average pump power [kW]		Average Relief valve power [kW]		Average Actuator power [kW]	
	Min load	Max load	Min load	Max load	Min load	Max load
Basic Servo	3.20	3.24	2.32	2.27	0.88	0.97
Regeneration	3.32	3.33	2.77	2.90	0.55	0.43
Regeneration circuit with pressure override	3.32	3.33	2.73	2.76	0.59	0.57
Flow Divider	3.32	3.33	2.72	2.27	0.60	1.06
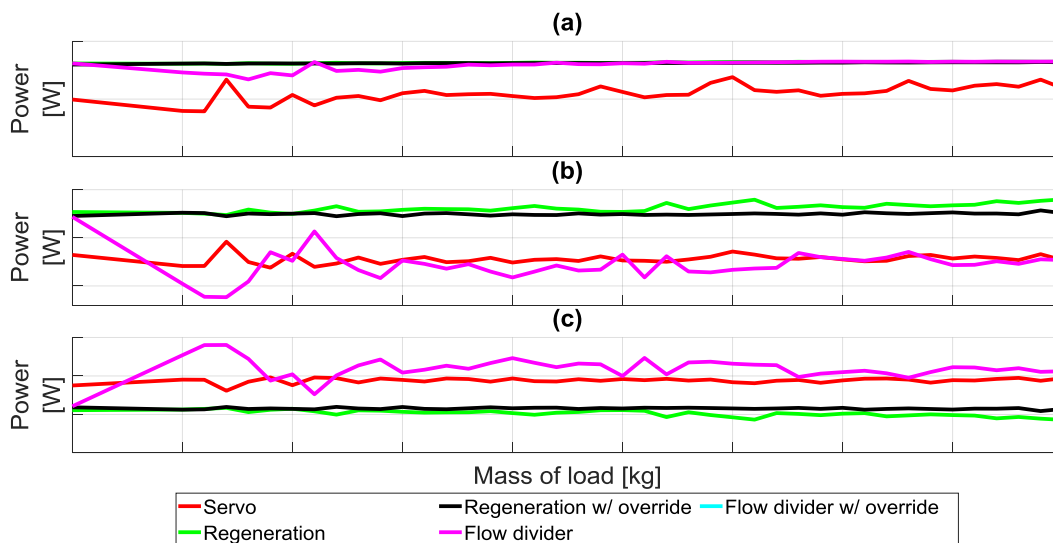
Figure 6.16: Power of the valve based circuits with increasing mass. a) the average input power as calculated from the pump, b) the average output power through the relief valve, c) the difference in power between a) and b) gives the average power supplied to the actuator.

For the actuator power, the results tell a similar story in that the regeneration circuits have the lowest power requirements. The flow divider results show variations possibly due to the spin-up and slow down of the divider.

6.4.1.6 Conclusions of servo-based circuits

The servo valve circuit can be seen as the baseline to compare against. The basic regeneration circuit and flow divider circuits have worse

The servo valve circuit, as it is used in current exoskeleton systems, can be seen as a baseline to compare the others. The regeneration circuit does not perform as well as the servo circuit for following the motion demand and has a higher power requirement, which eliminates it from its use in the exoskeleton system. The flow divider circuit has the worst error response in regards to positioning, which is linked to the efficiency of it when there is a low flow demand.

The regeneration circuit with pressure override has similar performance to the servo valve system in regards to errors, but with lower power requirements of between 32% and 40% depending on loading. This is a significant power saving and thus the regeneration circuit with pressure override will be put forward for the complete system testing.

6.4.2 Pump systems

For the pump setup, the control is linked to an electric motor that has two limits, rather than just one: the rotational velocity and the torque. Previously the controller was only giving either an opening value or a flow requirement. Thus determining which to control is important.

As the speed of the pump is linked to the flow rate, it was decided that this would be the signal to control, and allow the system to determine the torque required. As the controller is position based, this also makes more sense as the input of the position error is thus controlled by the velocity of the motion. If the controller were for a force-based system, then a torque output would be suitable.

The pump size required can be determined from the piston area and the maximum speed of the motion required. The piston area of the actuator is $0.0013m^2$, and the maximum speed for the demand is $0.4m \cdot s^{-1}$. These can be multiplied together to give a flow rate of $0.0052m^3 \cdot s^{-1}$ or 31.2 LPM. Using the TAKAKO pumps (see Appendix R) the largest size is the $6.29cm^3$ displacement pump giving 18.87LPM at no load. There are a limited number of pumps around

this size range, with many smaller ones only for lower pressures or significantly larger in output. The TAKAKO pump is also bidirectional, which is also difficult to find due to most manufacturers expecting the pump to be used in a servo circuit design where the pump only turns in one direction. The thus introduce one-way valve to help keep the pressure in the output line.

6.4.2.1 Variant One

The basic system, as shown in Figure 6.17, uses a pump-motor to move the oil around the circuit. The pilot operated check valves and the pressure relief valves are linked to an accumulator. This would normally be a tank in other systems, but to allow tilting of the system, this is not possible. If the system tilted too far, then the system could start to suck air rather than oil, causing uncontrolled motion.
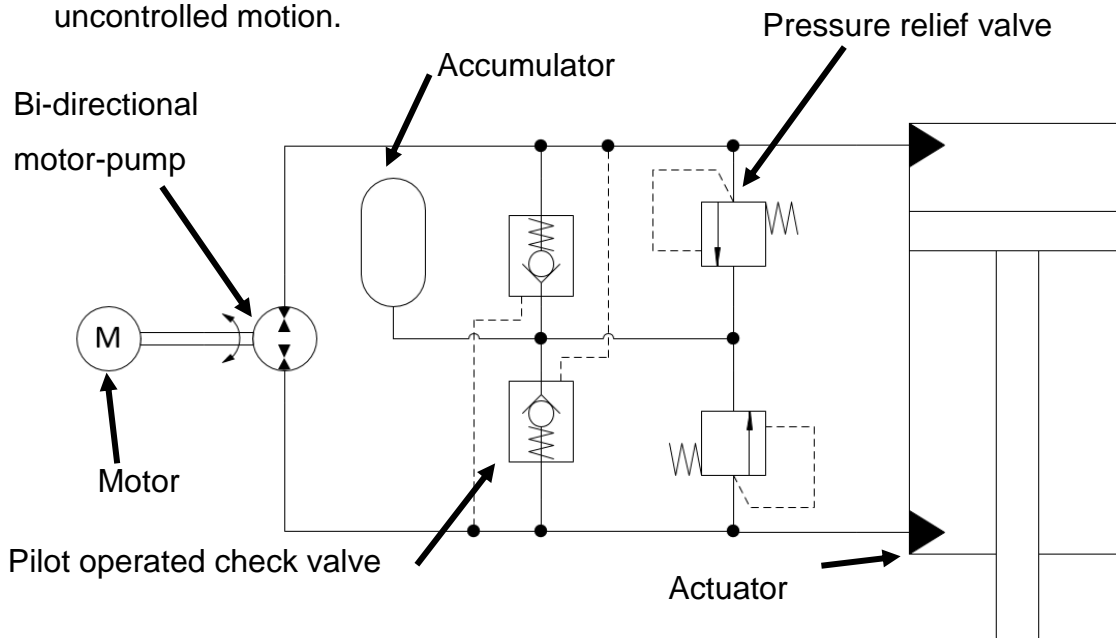
Figure 6.17: Basic pump circuit

Using the input as described in 6.3, the response of the base pump circuit is shown in Figure 6.18 for both the minimum and maximum load.

The initial impression of the pump circuit is the amplitude of oscillations in the RPM and position signals. As the controller is for the velocity of the pump, this is the origin for it. The torque signal for the pump appears to be oscillating, though only the maximum load results reach the maximum torque of 28.7Nm. This torque is 9kW motor at 3000rpm, which tend to be three-phase AC. Oscillations in the position will cause injury and fatigue in the user and are undesirable.
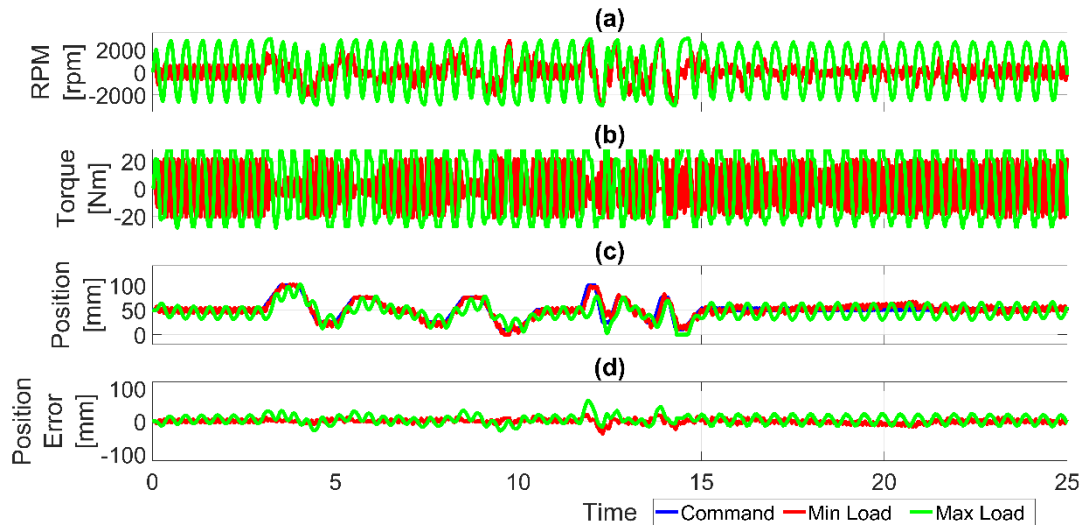
Figure 6.18: Variant one setup of the pump circuit. a) RPM demand from the controller for the motor, b) the torque response of the motor, c) position, d) position error between command and circuit response.

To have high-velocity motion typically requires a high gain in the controller. This has an adverse effect on the errors as the high gain magnifies all of the commands, including small offsets. As mentioned in Chapter 2, pumps have a smaller bandwidth response than servo valves, which could be an issue with this style of the circuit.

The chirp event is focused on in Figure 6.19 due to the change in position scale.
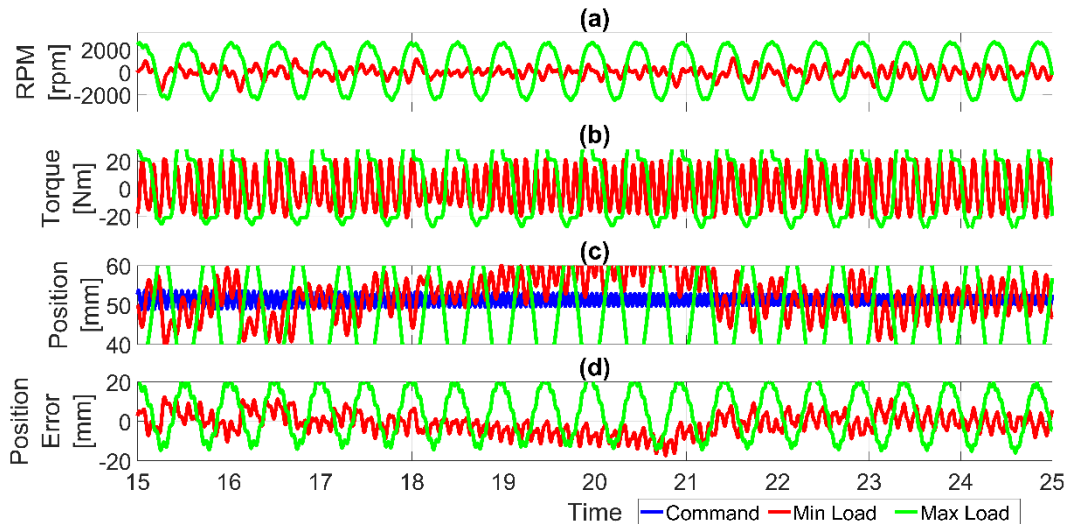
Figure 6.19: Variant one setup of the pump circuit Servo Valve circuit focusing on the chirp event. a) RPM demand from the controller for the motor, b) the torque response of the motor, c) position, d) position error between command and circuit response.

Examining the results at a smaller scale for the chirp phase, the minimum load response is not consistent and has a low-frequency oscillation around the

position demand, as well as high-frequency response. The maximum load appears to have one frequency of high amplitude in the position response, which gives a high position error of ±20mm, which is unacceptable for an exoskeleton system.

These issues are likely caused by the controller values, and thus could be re-tuned to give improved results. Currently, the tuning has used four tuneable variables, but there are four additional ones that could be optimised. The processing time for optimisation will exponentially increase and could become unfeasible.

Similar to the other systems, the pump circuit can be examined for the power, but also for the pump circuit, power regeneration can be reviewed. The power requirements are shown in Figure 6.20.
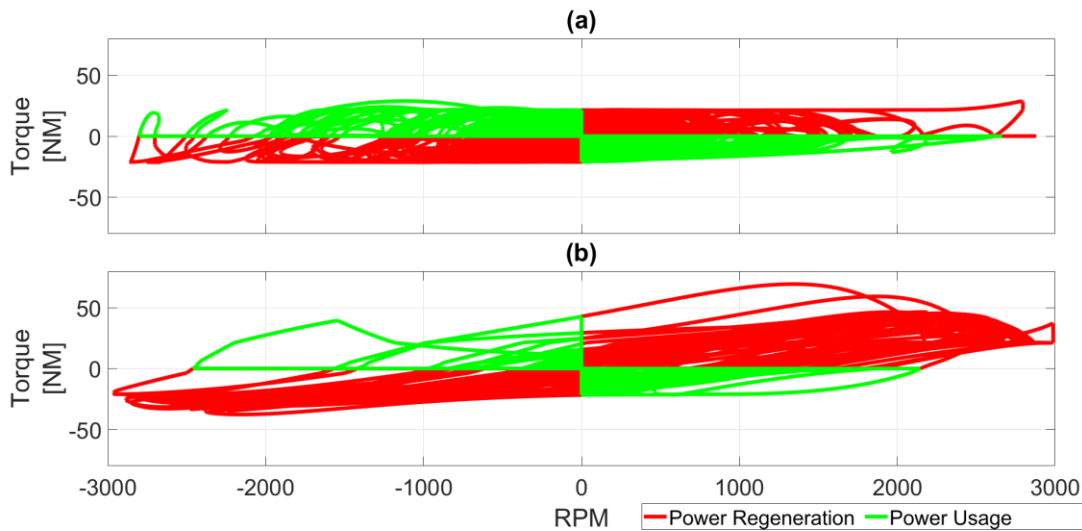
Figure 6.20: Power response from the a) minimum and b) maximum load.

When the torque is supporting the motion, for example, flexion of the elbow, then there is a power usage for the exoskeleton. Without power expenditure, there is no motion. Inversely, when the torque is hindering the motion, for example, the extension of the elbow, then this is a braking motion and power can be recovered.

For the minimum load power requirements (a), there is an average power requirement for 3.07kW but could recover 2.47kW of power. This is a recovery of 80.7% of the power usage. As there will be mechanical inefficiencies, and taking a value of 90% of the power recovery, this reduces the regeneration to 65.4% of the power usage. This is a significant value and for an 8-hour shift,

would have cost savings for electricity if the system were tethered. It would also mean that for an untethered device, it would only require the equivalent of a 2.8hr battery. This would give cost and weight savings for the exoskeleton.

For the maximum load power requirements, the average power is 39.3kW and can only recover 391W. This is only 0.9% or 0.8% with mechanical efficiencies. This is not as supportive of this circuit design, as it would give no cost or weight savings.

6.4.2.2 Variant Two

With the option to lock the actuator when there is a very small error, this should remove some the oscillations in the results. This is accomplished with a valve as shown in Figure 6.21.   The additional valve switches the circuit open and closed as required. The additional pressure relief valves are required to stop overpressure events from causing damage.   If these valves did open, the actuator would start to move, and the system would open the lock valve to try to compensate this motion.
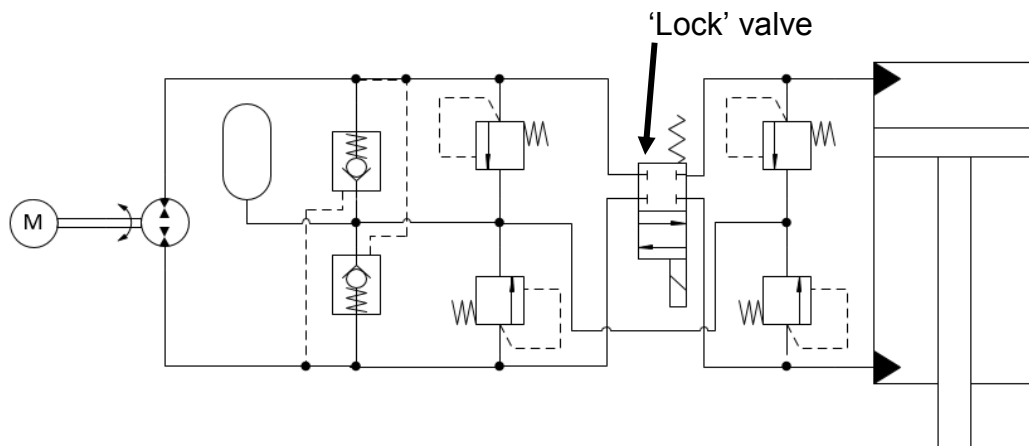
Figure 6.21: Pump circuit with a locking valve.

Using the input as described in 6.3, the response of the base pump circuit is shown in Figure 6.22 for both the minimum and maximum load.

It is difficult to determine any improvements that the locking valve has given to the simpler pump circuit. The additional cost of another valve, as well as two more pressure relief valves, is not economically supported.
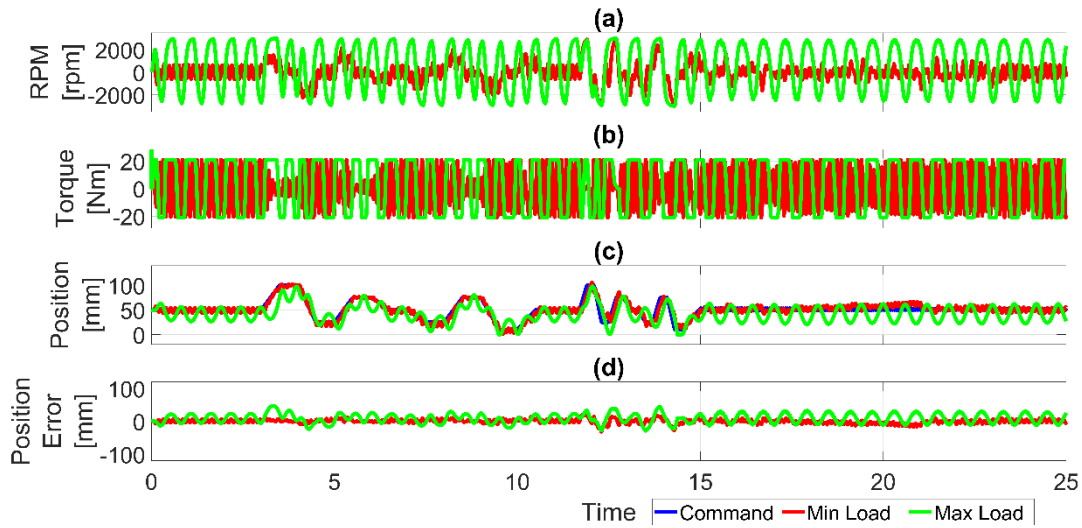
Figure 6.22: Variant two setup of the pump circuit. a) RPM demand from the controller for the motor, b) the torque response of the motor, c) position, d) position error between command and circuit response.

6.5 Comparison of results

Comparing the different options, some are obviously not suitable.

From the servo-based circuits, the regeneration with pressure override appears to give lower power consumption to the standard servo based circuit and does not add significant additional components.

The binary and ternary options did not perform as expected and would need significant work to develop the circuits to help eliminate the oscillations. Introducing accumulators to absorb high-pressure spikes from the opening of the valves could be considered, but the effect this would have on a fast response would need to be investigated. There is also the question of cross-talk issues when multiple actuators are connected, and how any shock loads would transfer to other motions. These issues are time-intensive and require significant study to determine the solutions, and as such have not been developed further at the current time for this project.

Though the pump based circuits show good possibilities for power regeneration, the control algorithm has issues with small errors and quick response times, thus making it unsuitable. Further design and simulation would overcome these issues, but like the binary and ternary systems, it would be time intensive for this thesis, and thus also left for future research.

Thus for the full system simulation, the regeneration with pressure override circuit will be used.

Tuning of each of the joints for the exoskeleton could be required, due to the different masses, but with the controller supposed to be robust, this might not be necessary. Each joint will have its own controller, rather than a single, full system one.

6.6 Summary

As hydraulics are nonlinear, an examination of current theory on different control strategies required. Many are model-dependent, in that they require an understanding of the hydraulic circuit used to create a baseline against. Model-independent control is another route, which alleviates the requirement to know the hydraulic circuit, and allows the transfer of the basic equation across different designs.

With the control method determined, the circuits from Chapter 2 are built in the Simscape environment with the elbow joint to start initial tuning and comparison of the circuits.

There has been research into several ways to control hydraulic circuits due to their nonlinear nature, with recent research into NFTSM being selected. NFTSM does not attempt to model the circuit itself, which allows it to be adapted to different circuits without significant work. Re-tuning of the control variables was done using optimisation based upon attempting to match the command signal.

How the fluid is transferred from the source to the actuator is also an area of current research, especially in an attempt to reduce the power requirements and costs whilst also increasing efficiency. From the initial testing results, two of the new research paths, digital and pump circuits, did not perform as well as the conventional servo based circuits but did show some promising opportunities that could be researched further.

With the design completed, and the hydraulic circuits selected, the amalgamation of both can be done for a full design test.

Chapter 7
Exoskeleton Simulation

7.1 Introduction

With the exoskeleton design complete, this can be imported into the Simscape workspace to determine the hydraulic requirements for a variety of human motions. The motions are sourced from motion capture data [79].

The motion capture drives points within the Simscape environment that can be linked to the exoskeleton structure. These links are constrained either with limits or with internal forces.

This chapter covers the simulation of the complete upper body exoskeleton system. In order to determine the power of the actuators, their motion has to be computed. This is done with the exoskeleton following motion capture data. This position data is then fed back into the model actuators. Three test input models will be used: direct, servo circuit and regeneration with full pressure override circuit. The direct control model inputs the positional data straight back into the actuators to generate a controlled baseline for the exoskeleton. The hydraulic circuits use the controller developed in Chapter 6 to convert the positional request into a signal for the valve.

Three motions will be analysed: standing still, level ground walking and picking up a box. The standing still motion will be used to give a baseline for the other simulations. The level ground walking will be used to determine whether the system can follow the human motion correctly. Previous lower-body exoskeletons have noted that they do cause deviation to gait and thus making sure that the upper body does not create motion instabilities. The picking up the box motion will be used to determine the response of the hydraulics to high loading.

The aim of this chapter is to test the exoskeleton system in a virtual environment to give an initial understanding of the response to determine whether there are any issues with the design, without the cost of building a physical system. Each helical actuator is around £2000, each servo is around £1000, and thus an initial prototype costing would be £20,000. This makes simulation a cost-effective interim step to determine likely issues.

7.2 Methodology

The exoskeleton is required to follow the input motions of the user, and this is replicated by the use of motion capture data. The setup of this is covered in Section 7.3 and outlines how the motion capture data is linked to the exoskeleton frame.

With the motion capture and exoskeleton linked, the initial simulation records the positions of the actuators as they follow the motions. This is covered in Section 7.4. Three motion captures will be used, each with their own time durations: standing still, level ground walking and picking up a box.

The motions all start with a two-second stabilisation phase to bring the exoskeleton from a neutral position to the start of the motion capture data. This is covered in Section 7.5.1, and are removed from the actual motion capture analysis.

With the positions of the actuators for following the motions recorded, they are used as the input into three exoskeleton systems. The first is a direct input of the positions straight into the actuators. This will be the baseline of comparison for any motion deviation of the exoskeleton. This will also generate a torque and power baseline for the system. The second and third systems are hydraulic circuits from the work conducted in Chapter 6. The servo valve circuit and the regeneration with pressure override have been connected to the exoskeleton actuators.

Analysis of the results starts with comparing the deviation of the matched points between the motion capture and the exoskeleton. This will give an idea of how the exoskeleton responds on a macro scale, before analysis of the actuator results. As this is the link between the user and the exoskeleton, positional errors for this will mean loading on the human. This error is measured with the Cartesian coordinate's based on the exoskeleton wrist point.

The actuator positions will be compared as a true scale to determine any end limit stops. This coordinate system is based on the exoskeleton with the x-axis along the forearm, the y-axis positive in the elbow joint flexion and the z-axis perpendicular to the shoulder-elbow-wrist plane of the arm.

Force and torque outputs will be compared to determine whether there are any failures. With a safety factor involved, it is expected that the majority of the torque or force will be lower than this limit. This limit is 47.6% of the full range, which is from the safety factor of 2.1 determined in Chapter 5.

The power of the different circuits will also be compared to determine which gives the smallest requirement. One measure of the power will be based on the actuators, calculated from the force/torque and velocity. For the hydraulics circuits, there is also the pump output that can be converted into power based upon the pressure and flow rate.

Of the current exoskeleton systems, only BLEEX has comparative hydraulic details of their system. Other systems are either electrical-based, like PERCRO, or the details have not been released like SARCOS. BLEEX is also a lower body system, so though it is not directly comparable for torques and power, it is a comparative baseline for magnitudes.

7.3 Simscape model

The Simscape model links the motion capture data points to the exoskeleton model. The motion capture data is from Carnegie Mellon Graphics Lab [79] and is data point-based, rather than a complete skeletal model. There are few sources of available motion capture data, mainly due to the cost and processing time available. The enhancive exoskeleton team did spend time generating motion capture data, but processed data was not available for this thesis. This means that the exoskeleton needs to be attached to these data points with different relationships to mimic the harness and handgrips. The initial simulation visuals are shown in Figure 7.1.

The red spheres are the joints of the human, whilst the green cubes are the ends of the limbs. The connecting rods are not of a fixed length due to measurement rounding in the motion capture data, and not represented in the simulations. They are shown in Figure 7.1 for clarity.

With the joint points following the motion capture data, then the exoskeleton has to be set up to follow these. The main connection points are the back and the hands.

Shoulder joint

Elbow joint

Wrist joint

End of limb

Middle of spine

(a)   (b)
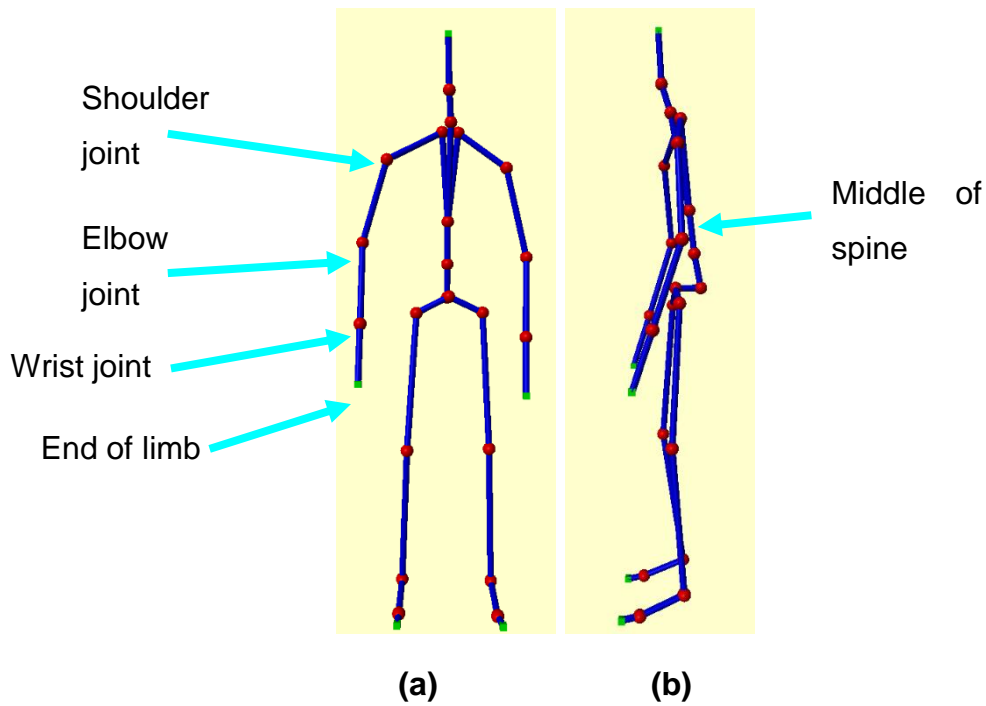
Figure 7.1: Model of the human motion capture. a) front view, b) side view.

The back connection is based on a plane made from the middle point of the spine, and the two shoulders. This can be constructed with a T piece connector that has telescoping joints, a joint with one translation and three rotational degrees of freedom, from the three points. This is shown in Figure 7.2. This replicates the harness orientation that would connect the user torso to the exoskeleton. The harness is the connection system that would constrain the torso of the user to the exoskeleton, with the other two connections being the wrist and feet. This harness system would detect upper body motion for bending and rotation.

The hand connections are based on the wrist location for the motion capture and its corresponding location on the exoskeleton. The wrist was chosen rather than the end of the fingers so that the exoskeleton arm follows the plane created by the human shoulder-elbow-wrist. The end of the fingers have additional degrees of freedom that is not replicated in the exoskeleton.

The wrist connection point was generated with two L shaped components. The vertical link of the L is connected to either the shoulder or the elbow points. The horizontal leg of the L is coincidental between the two L shapes, thus creating a stable, non-rotating reference axis perpendicular to the plane.
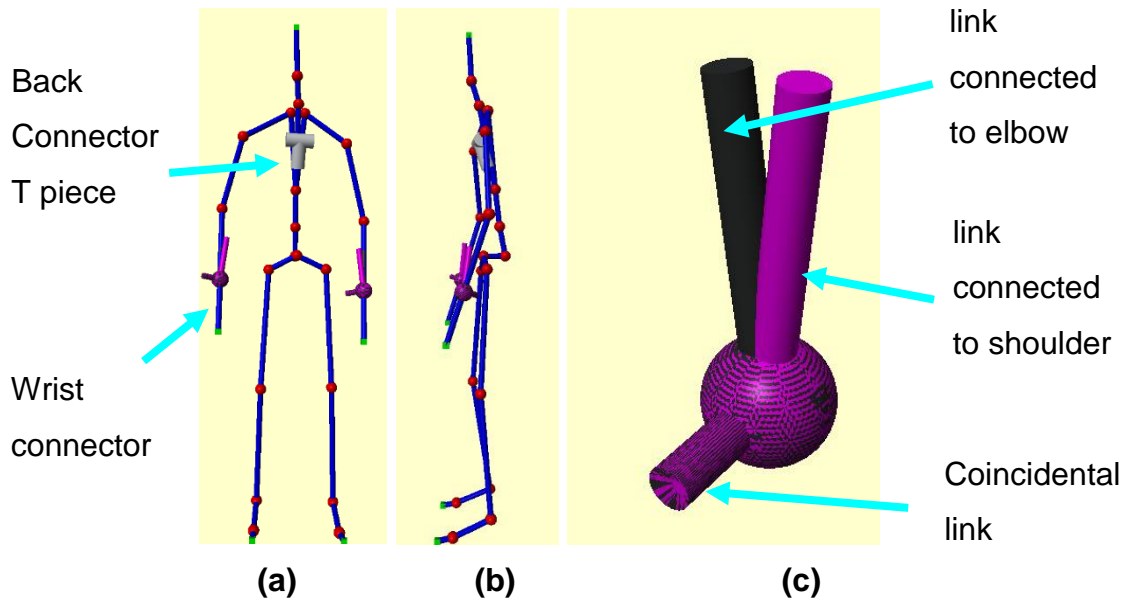
Figure 7.2: Model of the human motion capture with exoskeleton attachment guidance parts. a) front view, b) side view, c) wrist connector focus

With the human input setup, the upper-body exoskeleton can be placed on top of this, as shown in Figure 7.3.

The back is offset from the T connector so that the centre of rotation for the exoskeleton shoulders are the same as the humans. The wrist points of the human are matched to corresponding points on the exoskeleton forearm.

7.4 Initial motion setup

The initial motion setup records the displacement of the actuators based upon the exoskeleton attempting to match the locations of the human control point, the wrist, and the equivalent on the exoskeleton.

As shown in Figure 7.4, human motion data gives the positional data for the T connector and the hand guides. The T connector connects directly to the exoskeleton, but the guides go through a wrist matcher. The wrist matcher is a gimbal joint so that the hands are dynamically, rather than rigidly connected to prevent positional assembly errors in Simscape. The gimbal joint in Simscape has three axes of prismatic motion and three of rotational. The internal forces of the joint is a spring-damper system for the prismatic motion and on the X-axis, which is coincident with the lower arm.
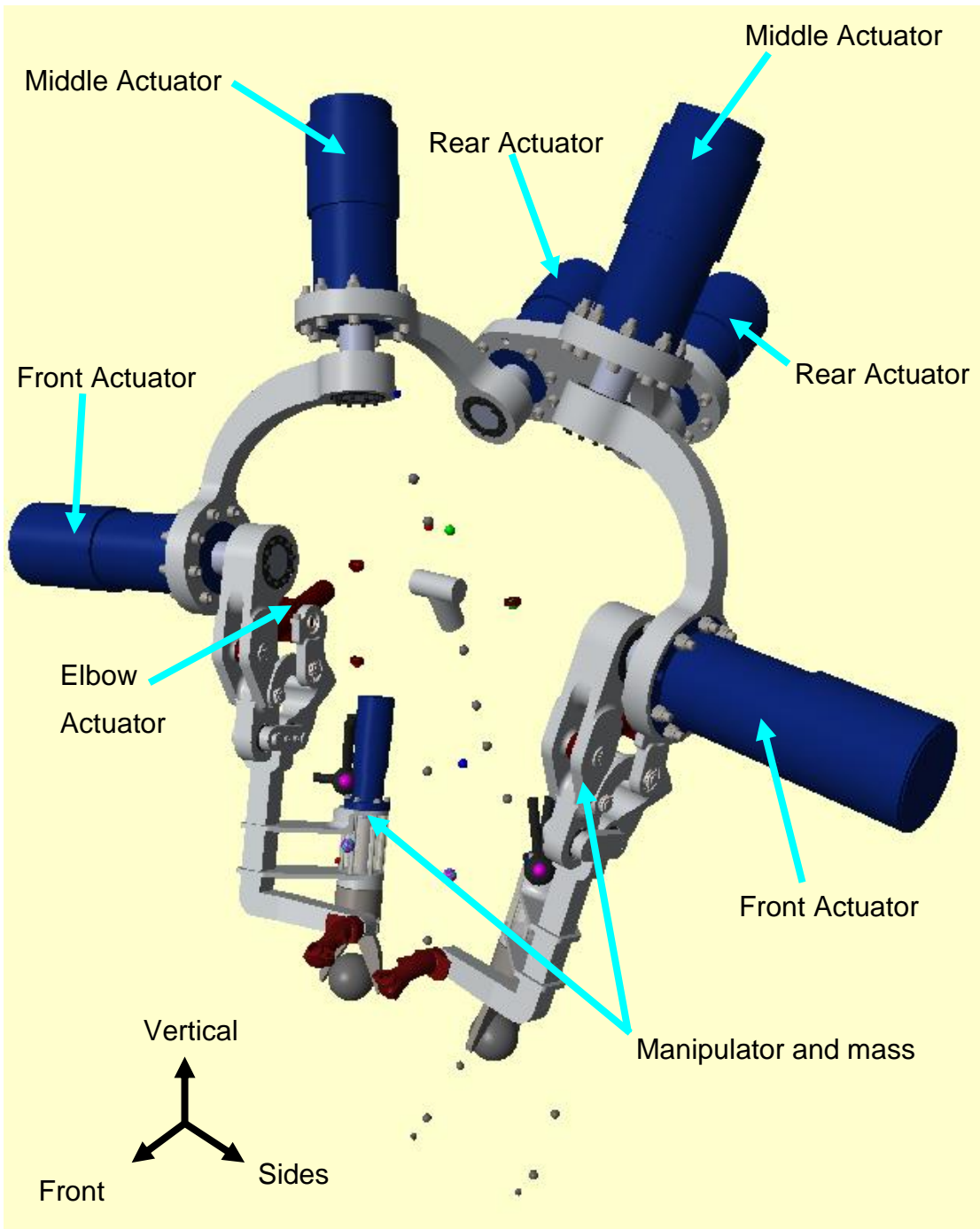
Figure 7.3: Simulink visual of exoskeleton system. Floating small spheres are control points for the human motion, with the large black sphere with 'tails' are the hand position controllers. The T piece in the middle is the orientation control for the back.
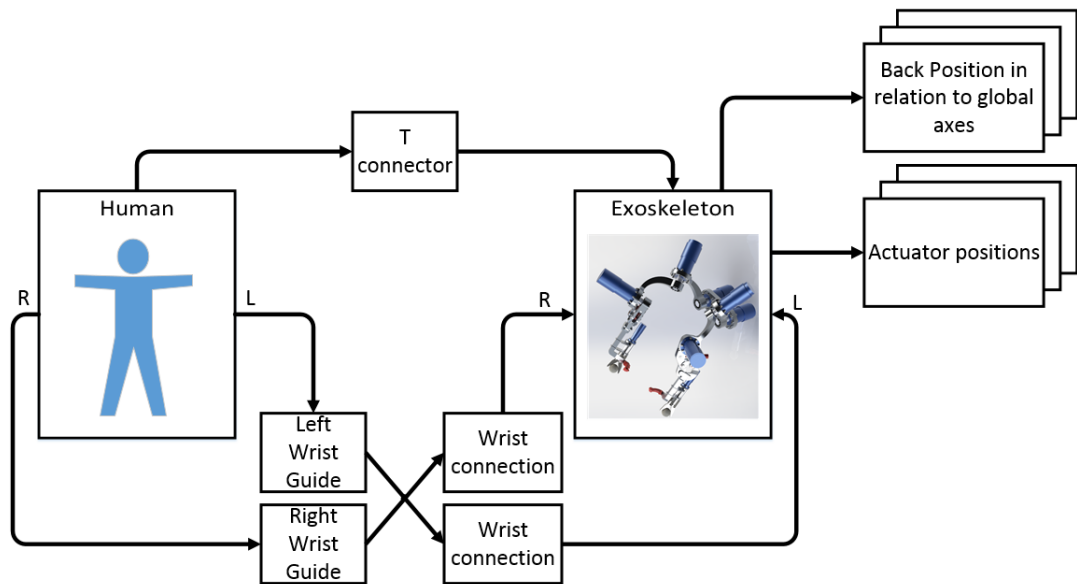
Figure 7.4: The input Simulink model for the initialisation motion.

The output signals are the position of the exoskeleton back in relation to the global axes and the actuator positions. The back position is recorded to simplify the next simulations by removing the T connector piece as it contains several telescopic spherical joints, which can be computationally intensive.

As the exoskeleton is not rigidly connected to the wrist points, there is an initial error at the start of each simulation before they are pulled together. Therefore, there is a two-second stabilisation window for the motion, which is not presented in the following results.

7.5 Test setup

The setup for generating motion test results is different for that from the initial motion model, in that there is no constraint between the wrist locations. The motion recorded from the initial setup is put into the joints, and it is expected that the exoskeleton should follow the same path. This is shown in Figure 7.5.

The back and actuator positions are fed into the exoskeleton, whilst the human still follows the motion capture data. The exoskeleton has three setups: the direct input version, the servo valve circuit and the regeneration circuit. The wrist guides and matchers are replaced with positional error measurements that are recorded for analysis. The actual actuator motion and torque/force are recorded. For the hydraulic circuits, the pump data is recorded.
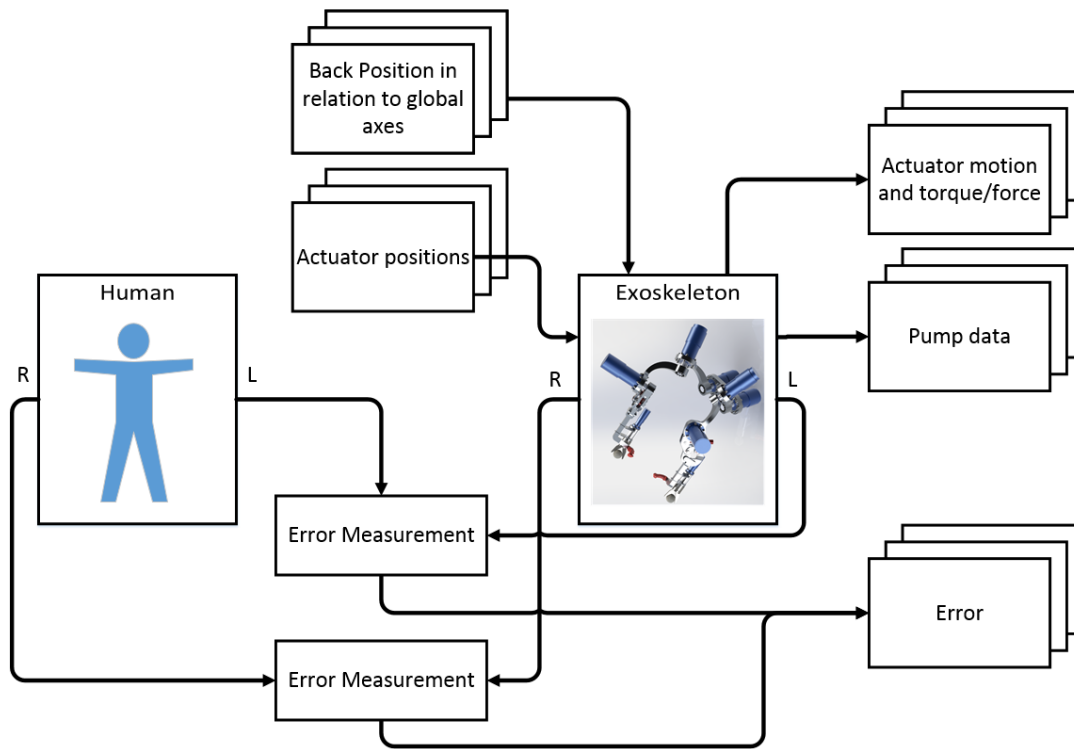
Figure 7.5: The test setup for exoskeleton driven motion showing inputs of back and actuator positions, and the measurement of the errors between the wrist locations.

This is not the method that would be used for the final system, which would be closer to an inverse kinematics solution, but for initial comparisons, reduces the complexity of the model. This is especially true as the Simulink inverse kinematics model assumes an open-loop model, but the elbow joint is a closed-loop. This would then require a method to convert the elbow angle to the linear actuator extension, which could be a simple lookup table.

7.5.1 Stabilisation phase

As mentioned in the methodology (Section 7.2), the exoskeleton starts from a neutral position before the motion capture and has a two-second stabilisation phase to move to the starting location. This stabilisation phase is included in the initial motion data to prevent large discontinuities in the controller.

The stabilisation phase motion capture points are fixed to their first data point for the two-second duration in the initial motion setup. As the Simscape model contains the centring force for the wrist points, this pulls the exoskeleton from the neutral position it starts in to the start of the motion capture data.

The direct input will follow the initial motion data for the actual testing and will show any small deviations between the human and exoskeleton. The hydraulics could have small positional errors due to the use of the controller, but it is expected that once they have stabilised, there is no additional motion. The stabilisation phase for the standing still is shown in Figure 7.6, with a smaller Y scale in Figure 7.7.
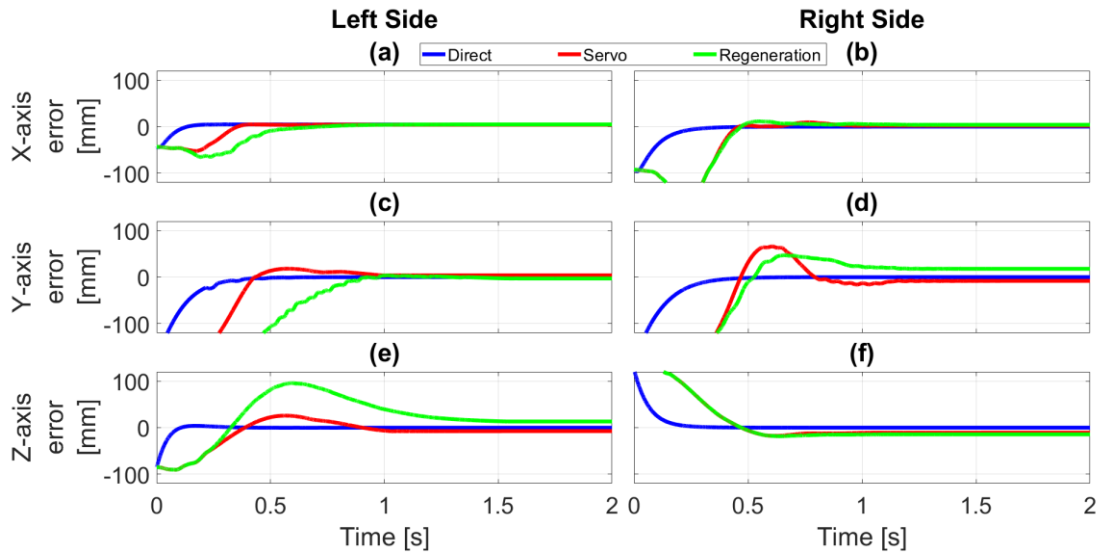
Figure 7.6: Deviation between the human wrist and the location of the wrist on the exoskeleton during stabilisation. a) LHS x-axis error, b) RHS x-axis error, c) LHS y-axis error, d) RHS y-axis error, e) LHS side z-axis error, f) RHS z-axis error. (RHS: Right-hand side, LHS: Left-hand side)

The direct input has sub-millimetre errors for all of the axes except the X-axis on the left side, (a), which has an error of 4.7mm. The exoskeleton is symmetrical for both sides, but the human is not. This small deviation is from the slight difference in the motion capture arm lengths. As humans are not perfectly symmetrical, this will occur in reality as well. Whether the person would compensate for this or not would need to be investigated in future research. The use of adjustable arm length will remove this error, but this was not included in the initial prototype design.

The hydraulics take longer to stabilise, with the direct input reaching stabilisation typically in less than 0.5 seconds with the hydraulics taking up to 1.5 seconds, but all of the results appear to reach a steady value by 2 seconds. As the motion to the starting point is large, there is a delay in reaching the starting point.
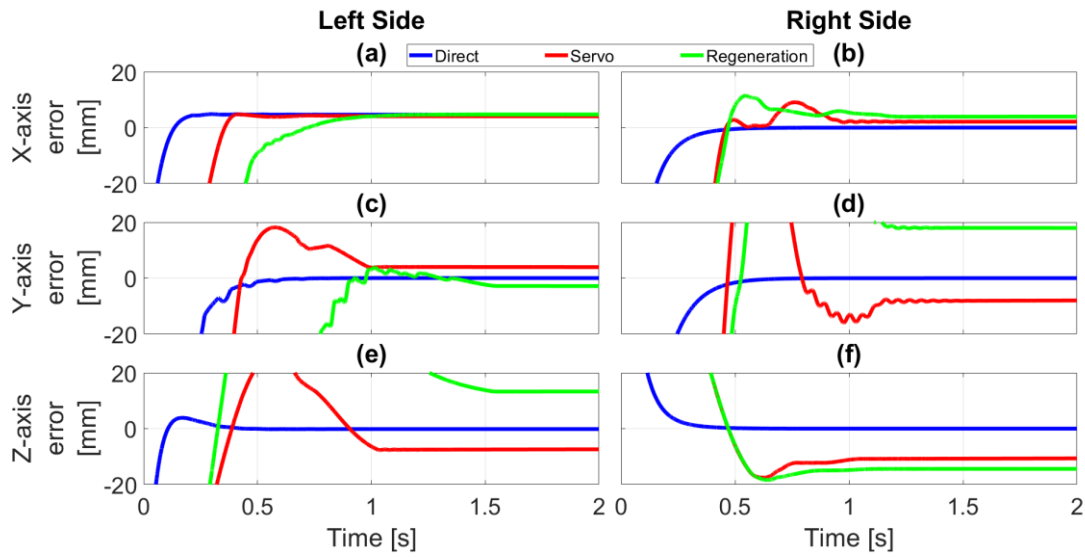
Figure 7.7: Deviation between the human wrist and the location of the wrist on the exoskeleton during stabilisation with a smaller scale. a) LHS x-axis error, b) RHS x-axis error, c) LHS y-axis error, d) RHS y-axis error, e) LHS side z-axis error, f) RHS z-axis error.

The hydraulics also have larger overshoots and do not stabilise at the same level as the direct input for several of the results. This initial error between the hydraulics and the direct input is due to this stabilisation period and the controller. The controller detects that there is an error between the demand and actual positions, and moves the control valves accordingly. As the error reduces, so does the control signal, to the point where the flow rate through the valves is not significant enough to move the actuators. The control signals can be seen in Figure 7.8.

The full range output for the control signal is 10V, and to move the actuators towards the starting positions only requires a small flow, and therefore voltage. As the motion is not fast, this does not require a large flow rate to move the actuators.
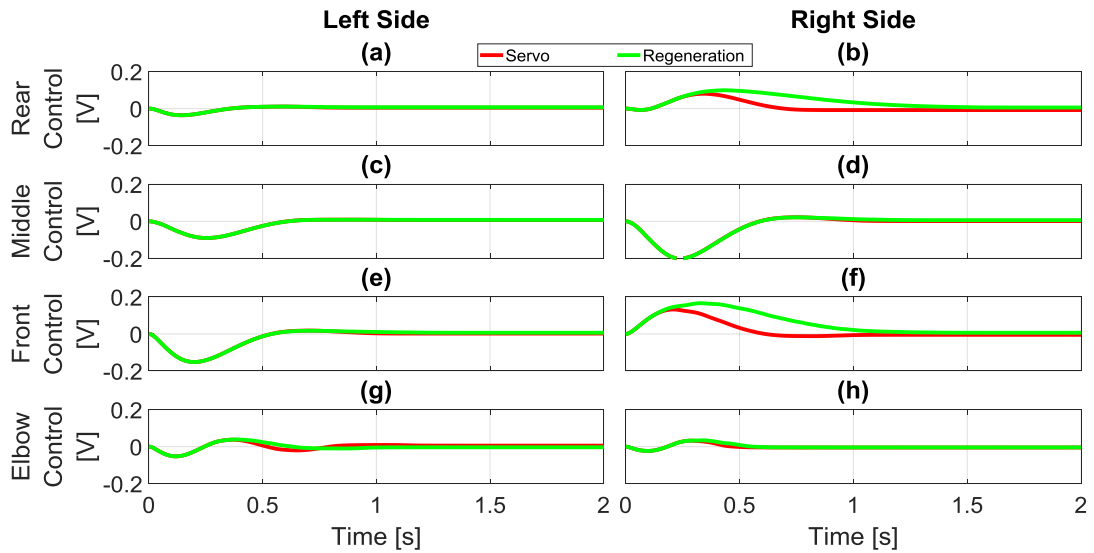
Figure 7.8: Control signals during the stabilisation phase. a) LHS shoulder rear actuator control signal, b) RHS shoulder rear actuator control signal, c) LHS shoulder middle actuator control signal, d) RHS shoulder middle actuator control signal, e) LHS shoulder front actuator control signal, f) RHS shoulder front actuator control signal, g) LHS elbow actuator control signal, h) RHS elbow actuator control signal.

7.6 Motion One: Standing still

The first motion is of the human standing still with their arms by their side and is the baseline motion.

The position error between the human and exoskeleton wrist locations, as mentioned in the methodology (section 7.2), is the first response to be analysed. This is shown in Figure 7.9. The standing still motion capture is 3.8 seconds in duration.

The direct input appears stable for all of the axes except for the left-hand side Y-axis (c). This has small spikes in the data and would indicate an end stop condition where the actuator is not able to move completely to the required position. The hydraulic errors appear to be continuing to approach zero error indicating that the controller is still working to remove the error in position. The LHS Y-axis shows a deviation for the servo valve results with the route cause to be investigated.

The positional error between the human and exoskeleton wrist locations is controlled by the positions of the actuators also need to be examined and can be seen in Figure 7.10.
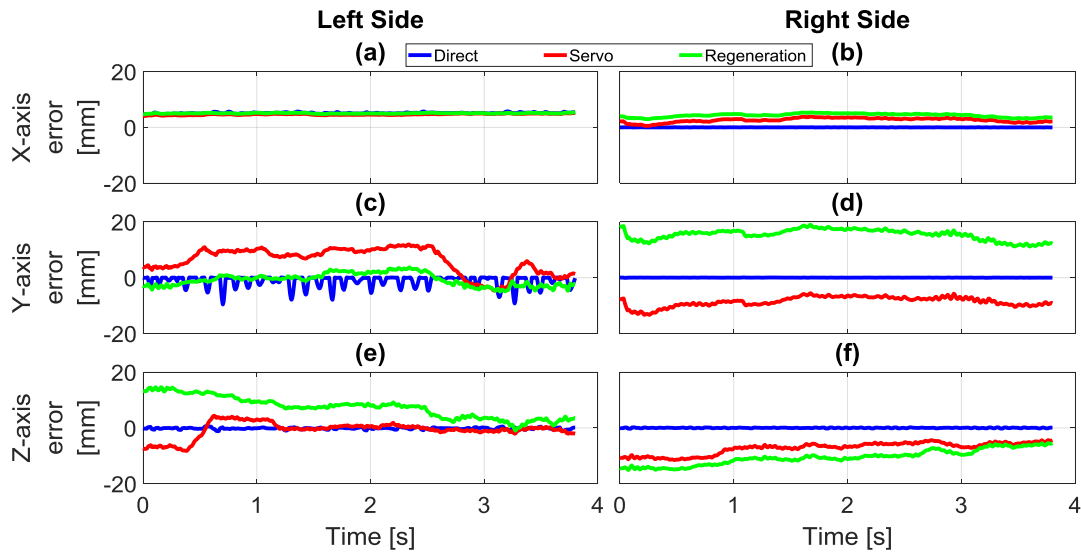
Figure 7.9: Error between the human wrist and the location of the wrist on the exoskeleton for standing still. a) LHS x-axis error, b) RHS x-axis error, c) LHS y-axis error, d) RHS y-axis error, e) LHS z-axis error, f) RHS z-axis error.
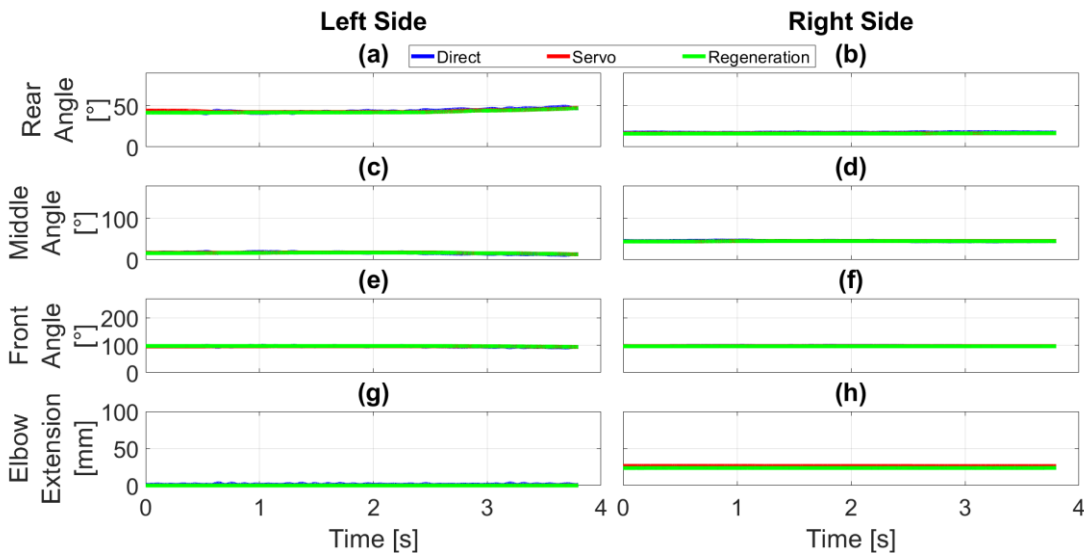
Figure 7.10: Actuator motion for standing still. a) LHS shoulder rear actuator angle, b) RHS shoulder rear actuator angle, c) LHS shoulder middle actuator angle, d) RHS shoulder middle actuator angle, e) LHS shoulder front actuator angle, f) RHS shoulder front actuator angle, g) LHS elbow actuator extension, h) RHS elbow actuator extension.

When standing still, none of the shoulder actuators (a-f) have reached their limits, but the left-hand side elbow actuator (g) has an extension of zero. With an extension of zero, if the input demand requires a value less than this, then there will be no motion. Once the input demand becomes positive, then the actuator can move, which gives the results seen in Figure 7.9 (c).

As the scale for Figure 7.10 is for the full range motion of the actuators, it is difficult to see the deviation between the direct input and the hydraulic circuits. Figure 7.11 shows these positions zeroed at the start of motion.
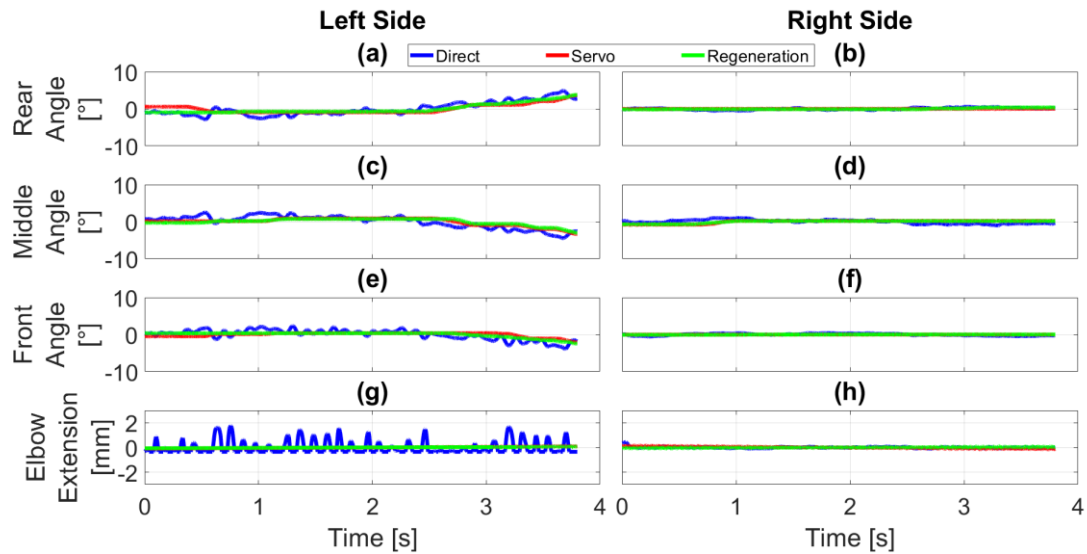
Figure 7.11: Actuator motion for standing still with the signals zeroed at the first point. a) LHS shoulder rear actuator angle, b) RHS shoulder rear actuator angle, c) LHS shoulder middle actuator angle, d) RHS shoulder middle actuator angle, e) LHS shoulder front actuator angle, f) RHS shoulder front actuator angle, g) LHS elbow actuator extension, h) RHS elbow actuator extension.

From Figure 7.11, it can be seen that the left side elbow actuator has reached an end condition, with the direct input results showing 'bounce' from the end stop, whilst the hydraulics do not. The direct results contain these fluctuations due to the initial motion setup, and how the two wrist points are connected. The connection points are linked with a spring-damper mechanism as mentioned in Section 7.4, which means that as the human wrist moves, it can cause the exoskeleton wrist point to oscillate slightly around that point. Though the spring-damper mechanism has been set to minimise this, it still will generate some oscillations, particularly if one of the actuators is reaching an end stop condition, as per the left-hand side for the standing still motion. As the elbow actuator is limiting the motion in one direction, this causes a shock up the arm that is pickup up by the shoulder actuators. This would apply to both sides, but the right-hand side has not reached its end stop so does not show this response. This why the right-hand side is stable, but the left-hand side is not. The hydraulics do not show the same response, indicating that they are damping out this issue.

The hydraulic circuits do have deviations between them, though at the start this is due to the stabilisation phase as discussed in Section 7.5.1. Towards the end on the left-hand side shoulder actuators (a, c, e) they have slightly different micro errors, but the macro trend is the same.

The source for the error from the LHS Y-axis wrist error cannot be easily determined from the results. There are no large step changes in the servo results, though there is a slight difference in the LHS rear actuator that would be magnified up due to the distance from the wrist.

There is also a small fluctuation throughout the wrist error signals shown in Figure 7.9 but is of a sub-micron level, which might not be noticeable by the user. As seen from Figure 7.11, the hydraulics do not have these micro motions and thus would be from the motion capture data, as shown in Figure 7.12. The results are based upon the global axes of the simulation, rather than the local axes of the exoskeleton control point, but do show that the human was not perfectly still.
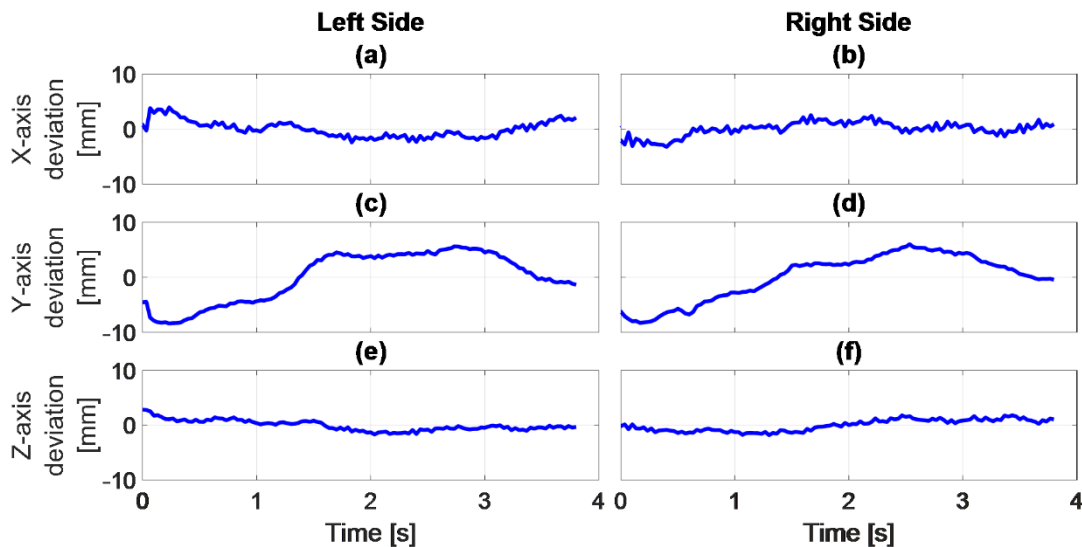
Figure 7.12: Deviation of the human wrist in relation to the global axes. a) LHS x-axis deviation, b) RHS x-axis deviation, c) LHS y-axis deviation, d) RHS y-axis deviation, e) LHS z-axis deviation, f) RHS z-axis deviation.

Whether these micro motions would be detectable to the human, or whether they would be absorbed by the control stick would require empirical testing.

As the position is based upon the control algorithm, the force and torque values need to be examined to verify that they do not overload the actuators and cause a failure. The force/torque curves can be seen in Figure 7.13.
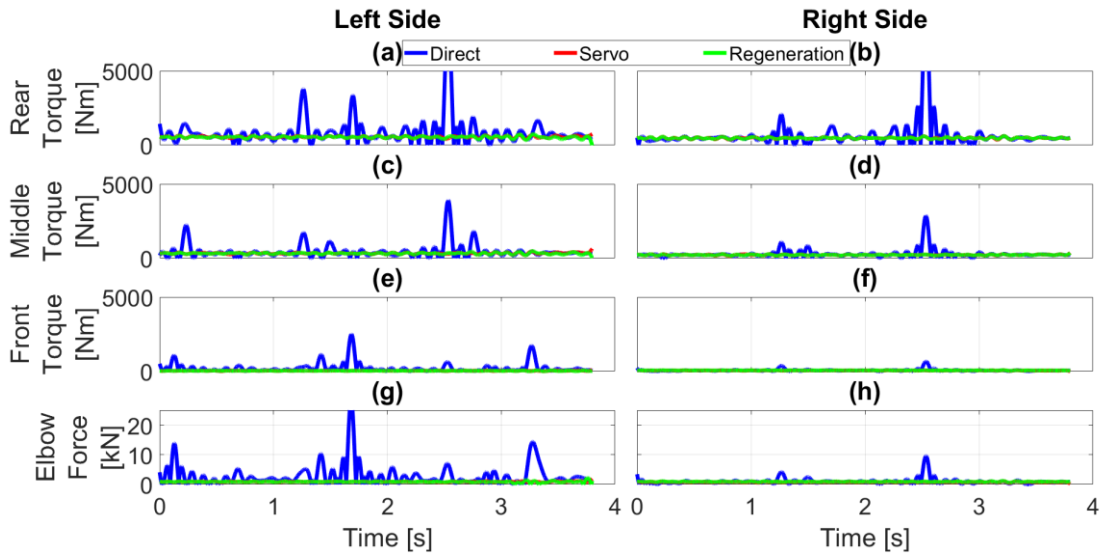
Figure 7.13: Force/torque curves for standing still, with y-axis limited to the full-range output of actuators. a) LHS shoulder rear actuator torque, b) RHS shoulder rear actuator torque, c) LHS shoulder middle actuator torque, d) RHS shoulder middle actuator torque, e) LHS shoulder front actuator torque, f) RHS shoulder front actuator torque, g) LHS elbow actuator force, h) RHS elbow actuator force.

The direct results show significant force events that are not replicated in the hydraulic circuit results, which are higher than the full-range output of the actuators. The position block that is feeding the direct input does not have a force limit in its attempt to bring the exoskeleton to the correct position, unlike the hydraulics. This means that small, high acceleration motions will be amplified for the direct motion results making a comparison between it and the hydraulics impossible. Thus, Figure 7.14 and all subsequent force and torque plots will have the direct results removed.

Figure 7.13 has the y-axis limits to the full range of the actuator outputs, and it can be seen that with the limits reduced to those of the safety factor limit, they are still low as shown in Figure 7.14. The safety factor limit is the full range divided by the safety factor, 2.1 (as from Chapter 5), as this is what the design methodology stated as the ideal working range, with forces above this being only for shock events. The mean torques and forces are given in Table 7.1.

The force and torque multiplied by their respective velocities give the power for each actuator, and added together will give the instantaneous power for the exoskeleton. This is shown in Figure 7.15.
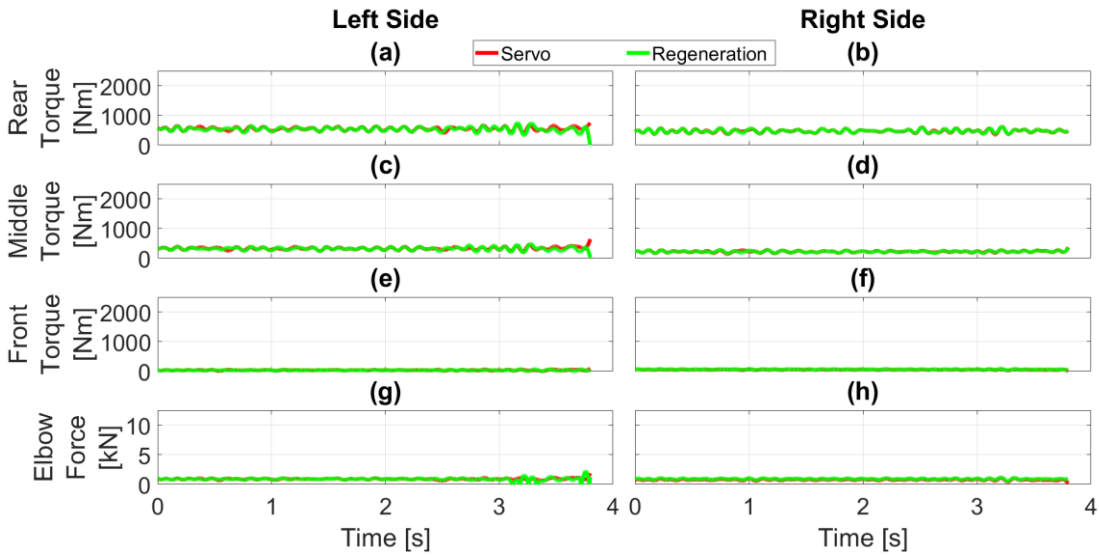
Figure 7.14: Force/torque curves for standing still. a) LHS shoulder rear actuator torque, b) RHS shoulder rear actuator torque, c) LHS shoulder middle actuator torque, d) RHS shoulder middle actuator torque, e) LHS shoulder front actuator torque, f) RHS shoulder front actuator torque, g) LHS elbow actuator force, h) RHS elbow actuator force.

Table 7.1: Mean torques and forces for the standing still motion

	Servo Circuit	Regeneration Circuit
RHS rear shoulder actuator	474 Nm	475 Nm
RHS middle shoulder actuator	223 Nm	223 Nm
RHS front shoulder actuator	56 Nm	62 Nm
RHS elbow actuator	792 N	916 N
LHS rear shoulder actuator	552 Nm	537 Nm
LHS middle shoulder actuator	331 Nm	323 Nm
LHS front shoulder actuator	40 Nm	37 Nm
LHS elbow actuator	911 N	895 N
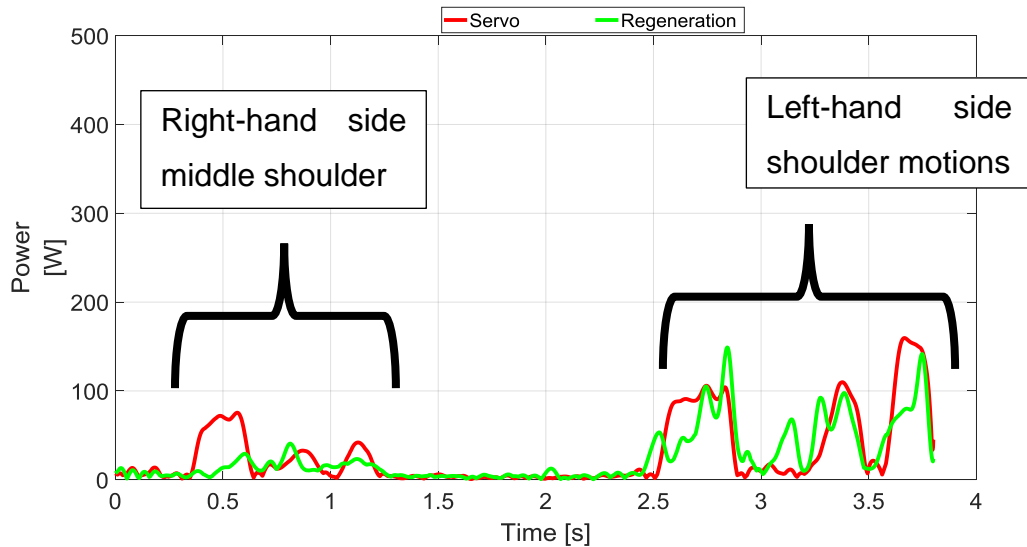
Figure 7.15: Exoskeleton power requirements for standing still.

The power levels for both at low, less than 200W, but there are some peaks in the results, due to the motion of the actuators. The first peak for the motion in the right-hand side middle shoulder actuator, whilst the ones after 2.5 seconds are due to the motion of the left-hand side shoulder motion with its stepping motion response, as seen in Figure 7.11.

There is a difference between the two hydraulic circuits, which is replicated in these results. The servo valve has wider power peaks, but the regeneration circuit is noisier. The mean power for the cycle is 29.6W for the servo valve, but 25.3W for the regeneration circuit.

For the hydraulic circuits, the pump flow and pressure is recorded, and these can be multiplied together to give the power usage of the pump which is shown in Figure 7.16.

The pump power usage is higher than the power for the actuators, indicating that there is significant power loss across the valves. This is one issue that servo valve-based circuits have, as mention in Chapter 2. The trends are the same as the actuator power, but significantly higher. The average power for the cycle is 628W for the servo valve, but 617W for the regeneration circuit.

As the system has a constant pressure source, then the high-pressure pipe will always be at 200bar, regardless if less pressure is required. As the standing still motion does not need the full pressure, as seen by the force and torque not being at maximum value, then this excess pressure is turned into heat. This is

an issue with servo valve circuits in that they always need to have maximum pressure available at all times.
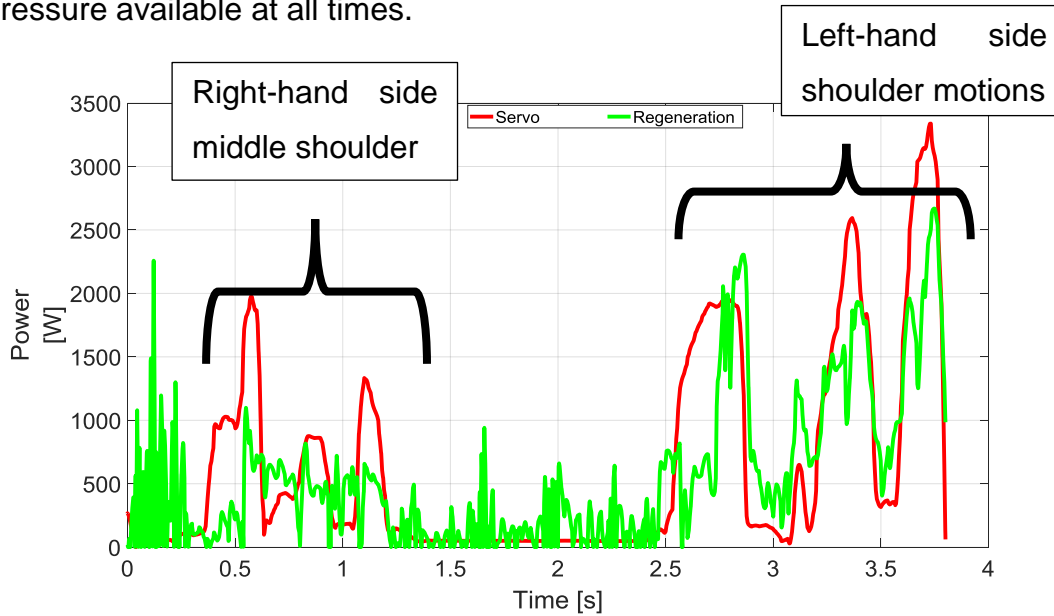
Figure 7.16: Power usage of the pump for standing still.

Comparing this power to BLEEX which has a 2.3 kW motor [2], then the pump power appears very high for a static motion. BLEEX is also only using 69bar, rather than the 200bar for this system. This is a 290% increase in pressure, which would mean that if BLEEX were using the higher pressure then the pump power would be 6.7 kW.

The equation for the pump power is the pressure times the flow rate, and as the pump source is at constant pressure, then the size is due to the flow rates, which are shown in Figure 7.17. This covers both the flow rate as recorded from the pump as well as calculated from the actuator motion.

The servo circuit results appear to be very similar, but the regeneration circuit has significantly more noise in the pump results. The regeneration circuit has one of the outflows connected to the pump directly and does not go through the valve. This appears to be generating shock waves that are travelling between the pipe and the valves and actuators. This could lead to a water hammer effect and damage some of the components.
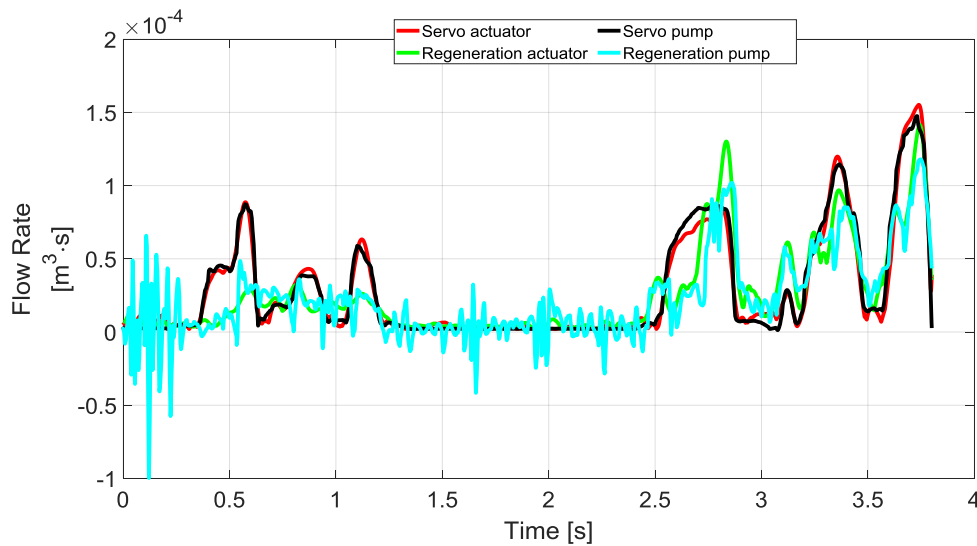
Figure 7.17: Flow rates for the hydraulic circuits calculated either from the actuator motion and torque/force or as measured from the pump.

The pump side can be modified to use accumulators and a smaller pump to even out the power requirements. As can be seen from Figure 7.16 and the average power, there is not the need for the power source to be the maximum value, but can be the average power. This is also true for Figure 7.17, in that full flow is not constantly required, but an accumulator can even out the delivery in time. Determining the pump and accumulator size would require the details of the daily usage of the exoskeleton. This is linked to the motion capture data daily distribution as mentioned in 3.3.2. Thus, the analysis of the pump power at the current time does not give a true indication of what the final power requirements will be, and will be omitted from the other motions.

7.7 Motion Two: Walking

Walking is typically thought of as a lower-body activity, but the upper body is used for balance. Other exoskeleton systems have commented that they have not been able to match the gait cycle [6], and thus additional motion interference from the upper body would cause additional strain on the user and could cause them to fall. Motion two is of the user walking in a straight line, with 0.1g of mass carried. 0.1g was used due to the requirement that each component in the simulation model having a mass for inertia calculations.

The position error between the human and exoskeleton wrist locations, as mentioned in the methodology (section 7.2), is the first response to be analysed.

This is shown in Figure 7.18. The walking motion capture is 3.6 seconds in duration.
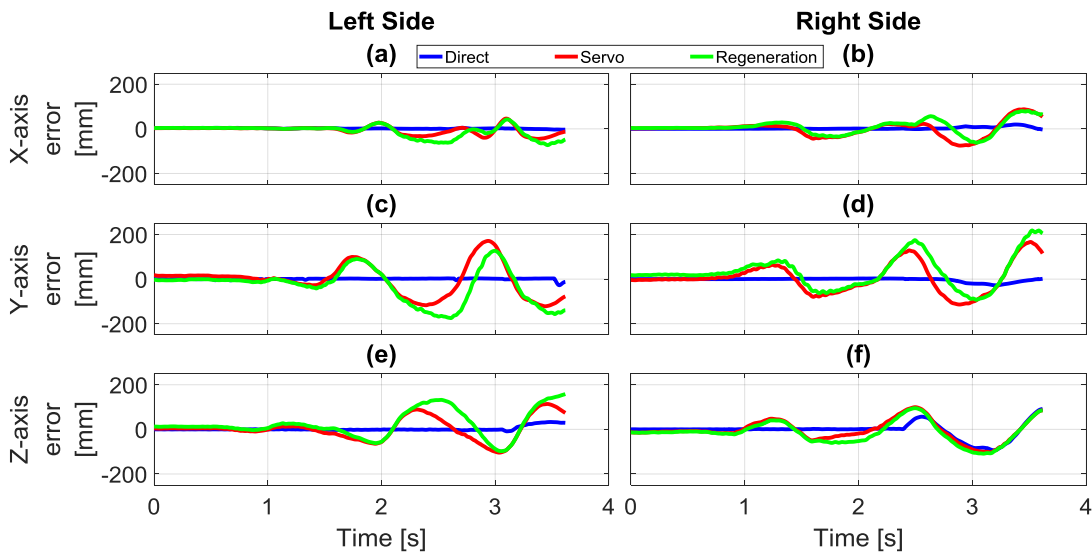
Figure 7.18: Deviation between the human wrist and the location of the wrist on the exoskeleton for walking. a) LHS x-axis error, b) RHS x-axis error, c) LHS y-axis error, d) RHS y-axis error, e) LHS z-axis error, f) RHS z-axis error.

The direct input error is stable but does start to deviate around 2.5 seconds. The hydraulics are unstable, and though they follow a similar trend, they are not close to having zero error. It appears that with the swinging of the arm motion whilst walking has not been followed correctly with the hydraulics, either due to a delay in the hydraulic flow, or the controller.

Determining the cause of the errors starts with examining the exoskeleton joint positions, which can be seen in Figure 7.19.

The direct input has three of the actuators reaching the zero motion endpoints, the right rear actuator (b), the left rear actuator (a) and the left elbow actuator (g). The right rear actuator reaching the end stop coincides with the deviation seen in the right-hand side wrist position errors in Figure 7.18. When the actuator has reached the full motion range, then it is unable to match the wrist position correctly. Similarly, on the left-hand side, the contact of the rear actuator has caused a deviation in the wrist matching. The elbow actuator at zero extension does not appear to have caused large errors in the wrist positioning, as the motion capture arm will have a straight arm.
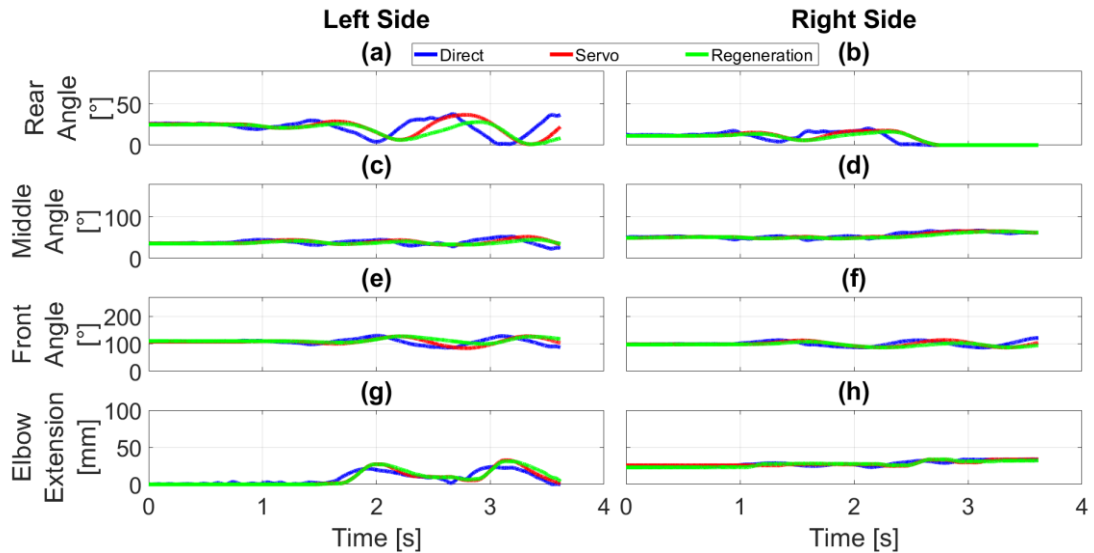
Figure 7.19: Actuator positions during walking. a) LHS shoulder rear actuator angle, b) RHS shoulder rear actuator angle, c) LHS shoulder middle actuator angle, d) RHS shoulder middle actuator angle, e) LHS shoulder front actuator angle, f) RHS shoulder front actuator angle, g) LHS elbow actuator extension, h) RHS elbow actuator extension.

The hydraulic actuator positions are more concerning; as there is the delay seen in Figure 7.18 seen here. The delay appears to be around 0.2 to 0.25 seconds but is inconsistent. The root cause is not directly obvious from these results.

Examining the position data zeroed at the start of motion removed will allow the analysis of the trends to be easier to determine, and are shown in Figure 7.20.

With the y-scale expanded, the delay is easier to determine. It appears that the hydraulics have a filtering effect on the demand, which can be seen the easiest in the left middle shoulder actuator (c). There is a filter in the controller, see Figure 6.1, set at 20 Hz, which is twice the value of the human motion bandwidth at 10 Hz [130]. This would only give a 0.05-second delay, rather than the 0.2-second delay that is seen here.

Examining the control voltage signal against the positions should assist in determining the cause of the delay, and is shown in Figure 7.21.

The servo valve does have a 'Proportional and Servo-Valve Actuator block' to convert the voltage input into the displacement for the valve. This has an internal loop that takes the error between the input and output and puts it through a saturation limit, then a gain, integration and first-order lag. This would cause a delay in the output from the controller to the valve, and though tuning

was conducted, based on datasheet values, empirical testing would improve the simulation of this block.
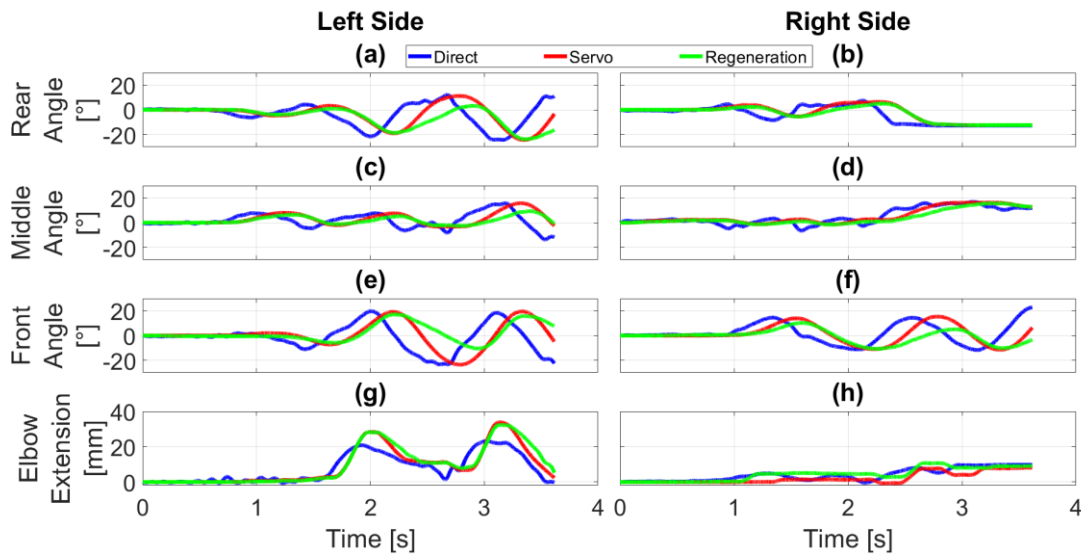
Figure 7.20: Actuator positions during walking with the signals zeroed at the first point. a) LHS shoulder rear actuator angle, b) RHS shoulder rear actuator angle, c) LHS shoulder middle actuator angle, d) RHS shoulder middle actuator angle, e) LHS shoulder front actuator angle, f) RHS shoulder front actuator angle, g) LHS elbow actuator extension, h) RHS elbow actuator extension.
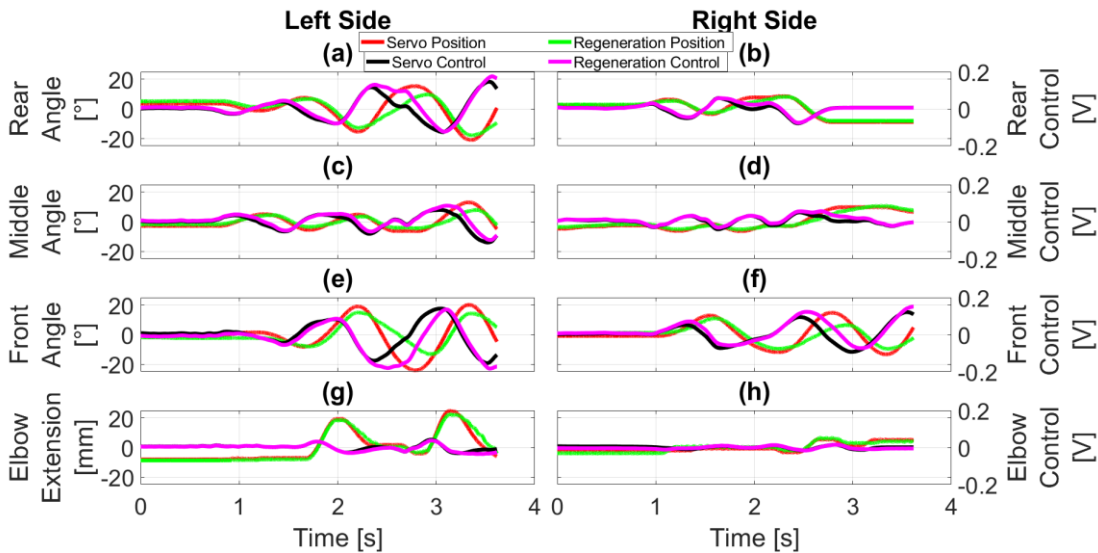
Figure 7.21: Actuator position and control signal during walking. a) LHS shoulder rear valve control voltage, b) RHS shoulder rear valve control voltage, c) LHS shoulder middle valve control voltage, d) RHS shoulder middle valve control voltage, e) LHS shoulder front valve control voltage, f) RHS shoulder front valve control voltage, g) LHS elbow valve control voltage, h) RHS elbow valve control voltage.

The maximum closed-loop bandwidth of the hydraulics is dependent on the frequency response and the damping ratio [131]. The frequency response is the lower of the valve resonant frequency or the Hydromechanical resonant frequency (HMRF). The valve resonant frequency can be determined from the datasheet, and for the valve used is 55Hz. The HMRF is based on the hydraulic and mechanical setup. The higher the fluid volume and load mass, the lower the HMRF. A low HMRF results in a system that has difficulty following the command signal in a responsive manner.

The damping ratio is a measure of internal leakages and friction of the hydraulic actuators and is typically very low as manufacturers aim to minimise these. The damping ratio can be as low as 0.03 to 0.05.

The maximum closed-loop bandwidth is given in Equation (7.1) [131].

$$f_{max} < 2 \cdot Z_n \cdot (The\ lesser\ of\ f_v\ or\ f_n) \qquad \textbf{(7.1)}$$

Where f_{max} is the maximum system closed bandwidth, Z_n is the damping ratio, f_v is the valve resonant frequency and f_n is the HMRF.

Using a value of 0.05 for the damping ratio, and the valve resonant frequency, then the maximum bandwidth is 5.5Hz. This is equivalent to 0.18 seconds, which is close to the 0.2 seconds delay that can be seen in the position results.

The HMRF can be calculated as described in equation (7.2) [132]

$$HMRF = \left(\frac{1}{\pi}\right) \cdot \sqrt{\left(\frac{A \cdot \beta}{M \cdot L_s}\right)} \qquad \textbf{(7.2)}$$

Where A is the average piston area, β is the bulk modulus, M is the effective mass on the cylinder, and L_s is the effective stroke length. For the elbow, this would be a value of $0.0011m^2$ for A, a mass of 65kg, and the effective stroke length of 0.1m. The bulk modulus is 1.5×10^9 Pa. This gives a value of 160Hz for the HMRF for the elbow joint.

The equivalent for a hydraulic motor is described in equation (7.3) [133]

$$HMRF = \frac{\sqrt{\dfrac{2 \cdot E}{J} \cdot \dfrac{\left(\dfrac{V_g}{2\pi}\right)^2}{\left(\dfrac{V_g}{2} + V_r\right)}}}{2\pi} \qquad (7.3)$$

Where V_G is the displacement of the actuator, J is the moment of inertia for the system, E is 1400 N·mm^{-2} and V_R is the volume of the line. This gives a value for the rear shoulder actuator of 5.9Hz. As the line volume increases, the frequency decreases.

However, the motion has delays in the results, the torque and force outputs are expected to remain with the safety factor range. The torques and forces can be seen in Figure 7.22.
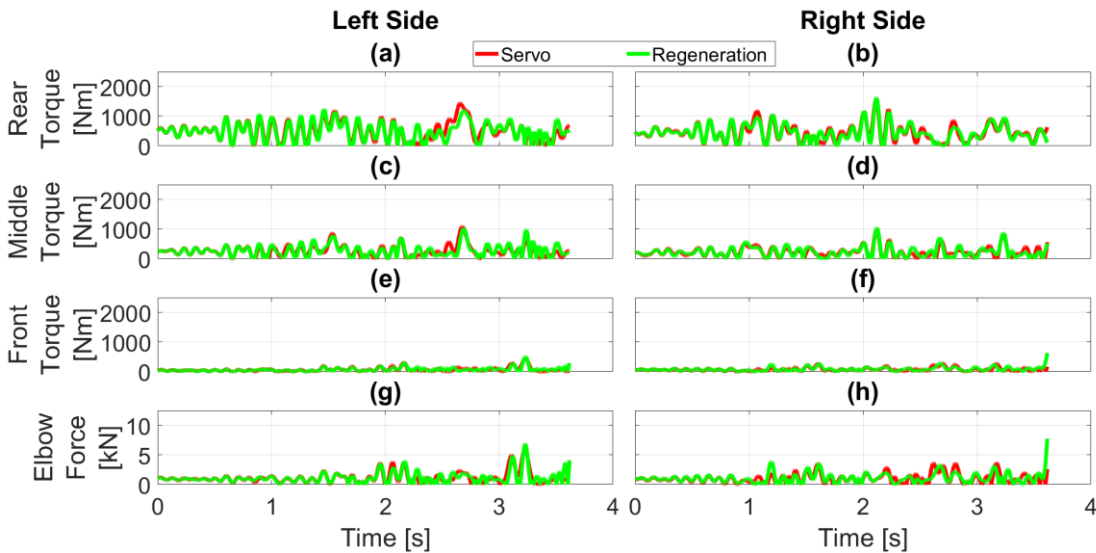
Figure 7.22: Force/torque curves for walking. a) LHS shoulder rear actuator torque, b) RHS shoulder rear actuator torque, c) LHS shoulder middle actuator torque, d) RHS shoulder middle actuator torque, e) LHS shoulder front actuator torque, f) RHS shoulder front actuator torque, g) LHS elbow actuator force, h) RHS elbow actuator force.

Examining the torque and forces, as the torque and force are based on the acceleration of the actuators, the delay response is not apparent. The trends of both the servo and regeneration circuits are the same, so though there are differences in the positional data, particularly the left rear and front shoulder actuators (a and e) and the right front shoulder actuator (f), these are not apparent in the torque data. The mean torques and forces are shown in Table 7.2.

The mean torques and forces are close to the standing still values, with the highest torque percentage difference of 192%, an increase from 37Nm to 71 Nm for the left front shoulder actuator for the regeneration circuit. The elbow actuator forces increase between 20 and 35% from the standing still results.

The power for the actuators can be calculated, and are shown in Figure 7.23.

The power requirements are higher than for standing still and the mean powers are 640.1W and 520.0W for the servo and regeneration circuits respectively. This is around a 2000% increase in mean power required.
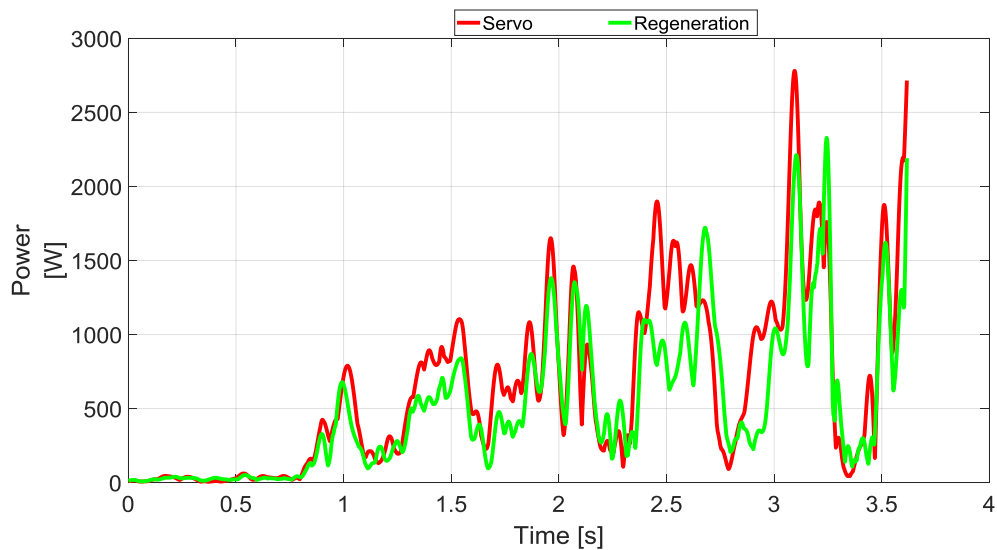
Figure 7.23: Exoskeleton power requirements for walking

The cause of the high power increase is due to the additional displacement of the actuators due to the frequency response, rather than increased torques and forces, as outlined from Table 7.2 results.

By improving the frequency response, then power requirements will reduce.

7.8 Motion Three: Picking up a box

Motion three is of the human reaching down and picking a box up off the floor. The mass component increases in weight from 1g to 45kg each at 2.90 seconds. The total duration of the motion capture is 6.0 seconds.

Table 7.2: Mean torques and forces for level-ground walking

	Servo Circuit	Regeneration Circuit
RHS rear shoulder actuator	453 Nm	449 Nm
RHS middle shoulder actuator	231 Nm	232 Nm
RHS front shoulder actuator	75 Nm	83 Nm
RHS elbow actuator	1067 N	1100 N
LHS rear shoulder actuator	503 Nm	503 Nm
LHS middle shoulder actuator	263 Nm	278 Nm
LHS front shoulder actuator	66 Nm	71 Nm
LHS elbow actuator	1139 N	1166 N

The servo valve model was not able to complete the full simulation due to a failure in the computations. The simulation starts to reduce the step size to compensate for a high-speed event, and thus takes exponentially longer than expected, causing the simulation to time out. The use of the daessc solver, a solver specifically for Simscape™ was used, though running the simulation through the other two recommended solvers of ode15s and ode23t did not solve the error.

The position error between the human and exoskeleton wrist locations, as mentioned in the methodology (Section 7.2), is the first response to be analysed. This is shown in Figure 7.24.

The wrist deviation curves are very large, but the hydraulic circuits follow the trend of the direct input, meaning that this was an issue with the original motion generation, rather than the hydraulic circuits. As the motion capture data was from an outside source, there was no control on the finer aspects of the motion. Recording motion capture specifically for the exoskeleton will alleviate this issue.

Examining the position of the actuators just for the direct drive, as shown in Figure 7.25, shows that several of the actuators reaching their full motion range with one, right side rear shoulder actuator, travelling between both limits.
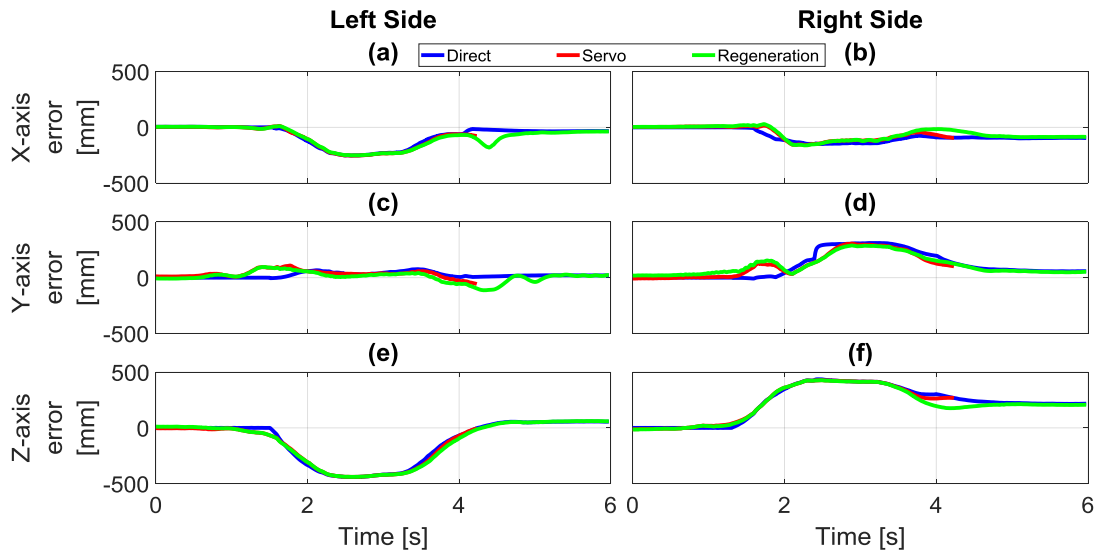
Figure 7.24: Deviation between the human wrist and the location of the wrist on the exoskeleton for picking a box up off the floor. a) LHS x-axis error, b) RHS x-axis error, c) LHS y-axis error, d) RHS y-axis error, e) LHS z-axis error, f) RHS z-axis error.

This result is unexpected, as the system was designed to give a large range of motion. This requires examination of the initial motion setup output, to determine the root cause of this error.
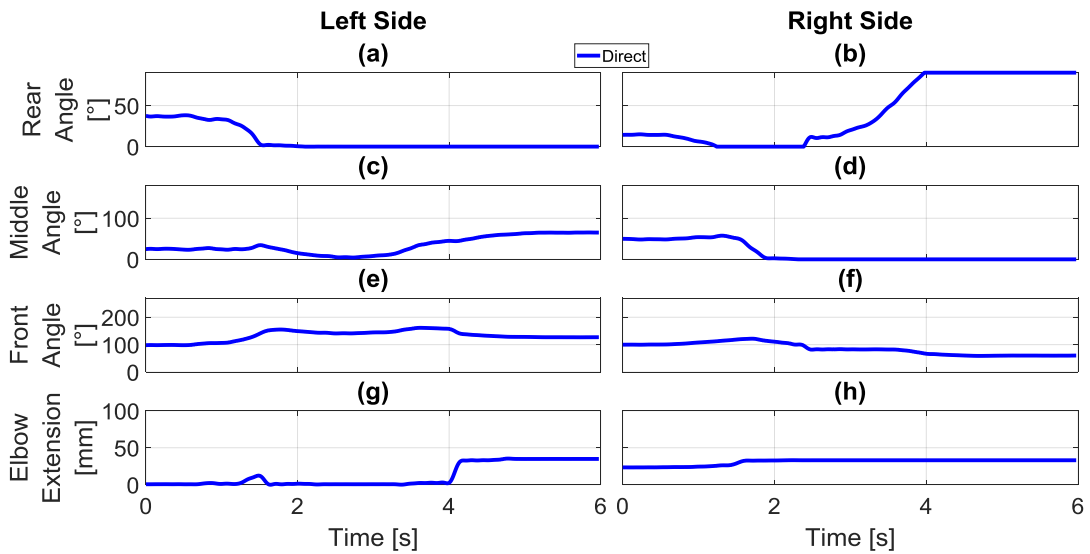
Figure 7.25: Actuator motion for picking a box up off the floor for just the direct input results. a) LHS shoulder rear actuator angle, b) RHS shoulder rear actuator angle, c) LHS shoulder middle actuator angle, d) RHS shoulder middle actuator angle, e) LHS shoulder front actuator angle, f) RHS shoulder front actuator angle, g) LHS elbow actuator extension, h) RHS elbow actuator extension.

The deviation starts at around 1.5 seconds, where the person is starting to lead over, which is also when the rear shoulder actuators on both sides reach their zero motion limits as shown in Figure 7.26.

Removing the exoskeleton, and showing just the motion capture data, it can be seen that the human is bending their elbows away from the body, shown in Figure 7.27.

Middle Actuator

Front Actuator

Rear Actuator

Motion range of rear shoulder actuators with 0° being vertical

(a)   (b)
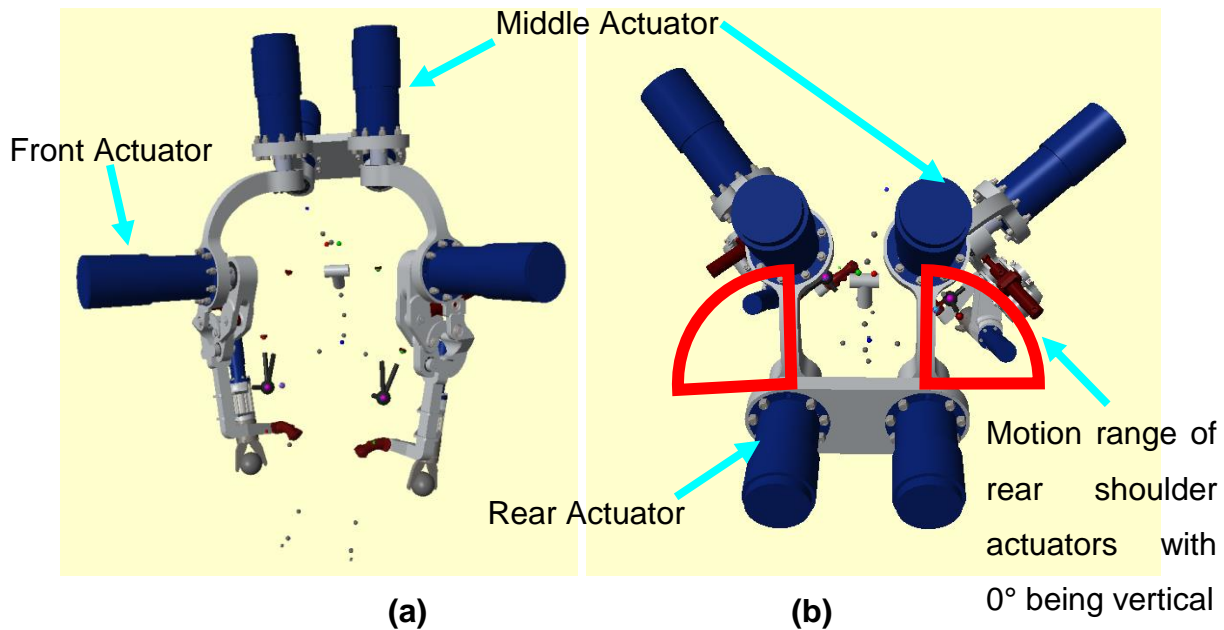
Figure 7.26: Position of the actuators at 1.5 seconds into simulation. a) view from the front of the exoskeleton, b) view from the rear of exoskeleton showing rear actuators at the 0° positions

This motion involves the abduction of the shoulder joint, the rear shoulder actuator, as well are supination of the forearm. The exoskeleton does not replicate supination of the forearm from the human movements but uses the control stick to direct the gripper rotation. This would mean that the shoulder-elbow-wrist plane would be closer to parallel to the median plane rather than the transverse plane as in Figure 7.27.

As the initial input data was not able to follow the motion correctly, then only the trends of the hydraulics to direct motion can be compared, rather than absolute values, which are shown in Figure 7.28 as the actuator positions zeroed at the first point.

(a)   **(b)**
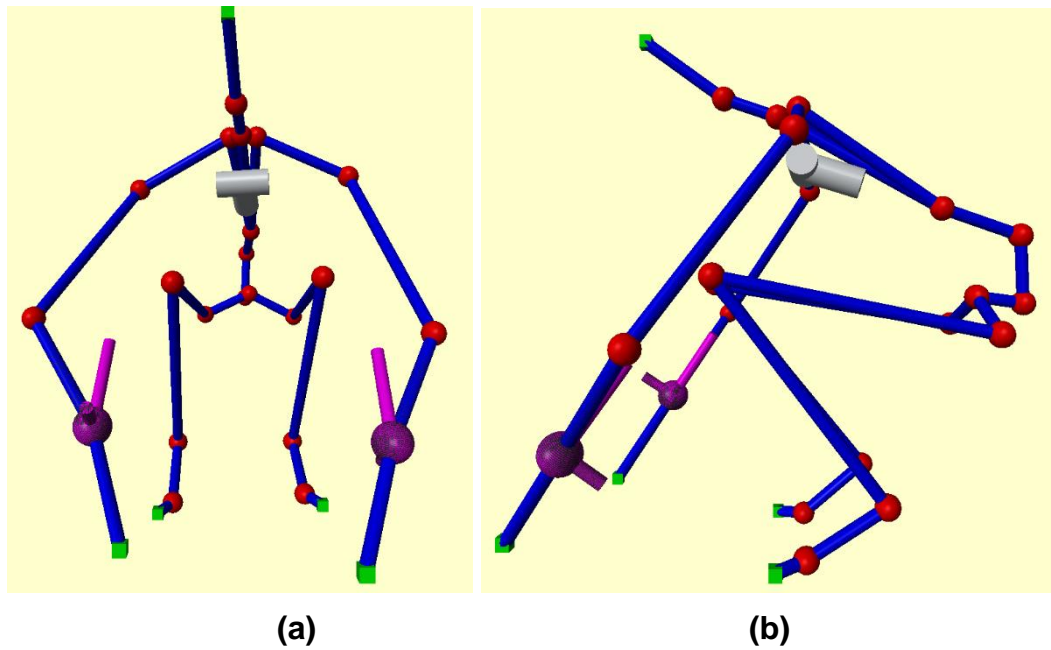
Figure 7.27: Motion capture position at 2.9 seconds, when the mass increases. a) front view, b) side view.
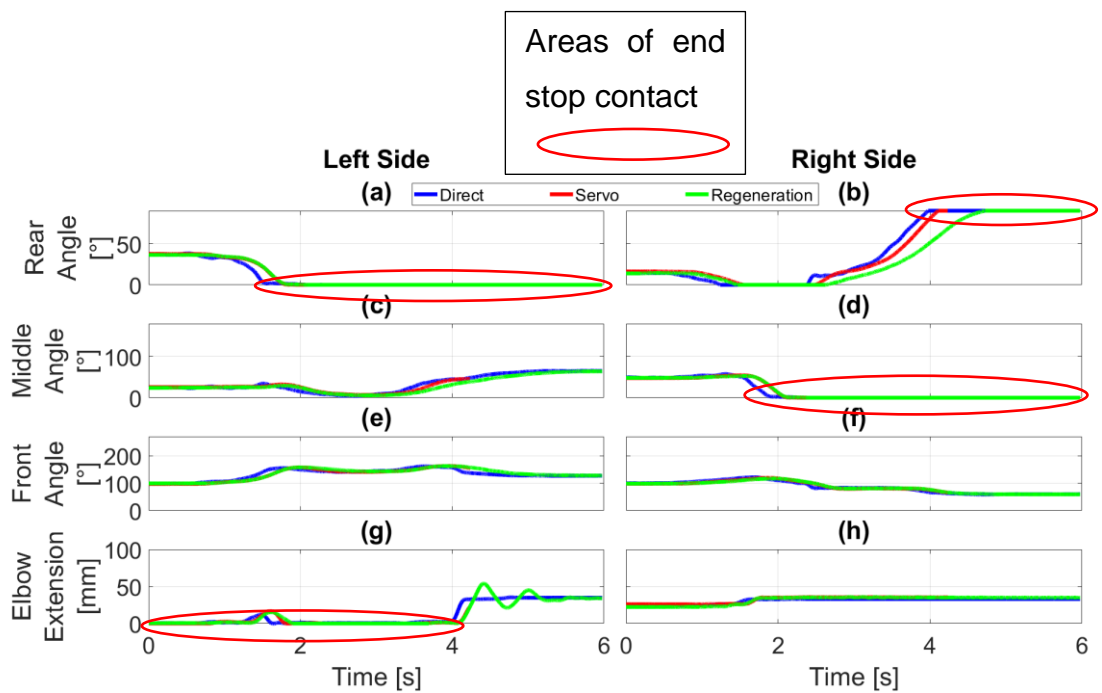
Figure 7.28: Actuator positions during picking up a box off the floor motion with the signals zeroed at the first point. a) LHS shoulder rear actuator angle, b) RHS shoulder rear actuator angle, c) LHS shoulder middle actuator angle, d) RHS shoulder middle actuator angle, e) LHS shoulder front actuator angle, f) RHS shoulder front actuator angle, g) LHS elbow actuator extension, h) RHS elbow actuator extension.

The hydraulic circuits are able to follow the direct command, with a couple of areas where they are showing delayed motion. The left-hand elbow actuator

extension does if the first result to show an obvious underdamped response during motion. This response appears similar to the oscillations in the hydraulic comparison chapter (Chapter 6), where there was an underdamped response moving from the high-speed section into the chirp phase, as seen in Figure 6.13. This is also the period when the servo circuit error occurs, indicating that this motion might be the root cause of its simulation failure.

The torques and forces should still be within the design limits, but examining the responses in Figure 7.29, the elbow actuators exceeds this several times. Figure 7.30 shows these values against the full output range for the actuators.
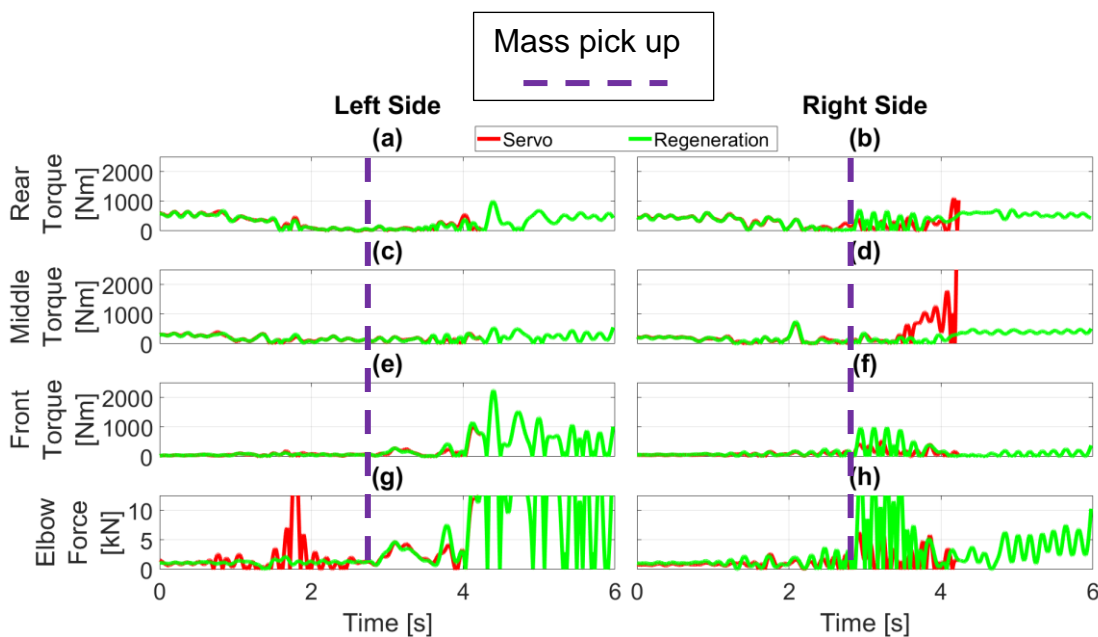
Figure 7.29: Force/torque curves for picking a box up off the floor with y-axis limited to SF limit. a) LHS shoulder rear actuator torque, b) RHS shoulder rear actuator torque, c) LHS shoulder middle actuator torque, d) RHS shoulder middle actuator torque, e) LHS shoulder front actuator torque, f) RHS shoulder front actuator torque, g) LHS elbow actuator force, h) RHS elbow actuator force.
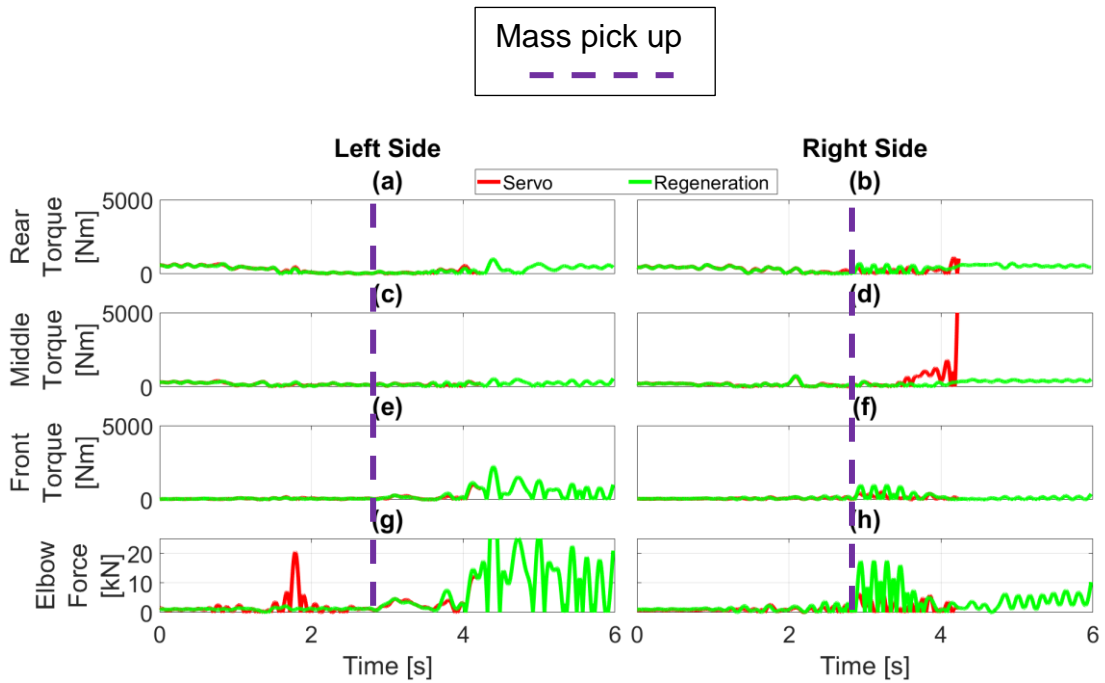
Figure 7.30: Force/torque curves for picking a box up off the floor with full torque and force output scales. a) LHS shoulder rear actuator torque, b) RHS shoulder rear actuator torque, c) LHS shoulder middle actuator torque, d) RHS shoulder middle actuator torque, e) LHS shoulder front actuator torque, f) RHS shoulder front actuator torque, g) LHS elbow actuator force, h) RHS elbow actuator force.

The high forces are occurring when the human is lifting the heavier mass of 45kg from 0.1g. As the person is straightening up, the force path of the load changes throughout the structure, especially as the lower arm starts to become horizontal to the floor. The weight is increased at 2.9 seconds, and it can be seen that several of the torque and force signals have a change in response at this time (b, f, g and h in particular). As the loading is instantaneous, due to there no floor contact for the mass, this will put in a shock load into the hydraulics. As the simulation progresses, these will be damped out, but any sudden movements, for example at four seconds for the left side elbow, introduces large forces to move the increased mass.

The elbow actuators for both hydraulic circuits do have points between the full actuator output and the safety factor limit, but this is still a viable working area. This range of forces is for shock loading events on the exoskeleton, and would not cause it to fail.

The duration, percentage of total motion capture time, and the maximum force values for the elbow actuators are tabulated in Table 7.3.

Table 7.3: Duration and percentage of motion time of the force above the safety factor limit of the elbow actuators and above the maximum force output for the regeneration circuit.

	Period above the safety factor [s]	Period above actuator maximum [s]	Percentage of motion above the safety factor [%]	Percentage of motion above actuator maximum [%]	Peak value
Right elbow actuator	0.21	0.00	3.4	0.0	17 kN
Left elbow actuator	1.08	0.14	18.0	2.4	47 kN

The duration of the peak above the actuator maximum is 0.14 seconds and is nearly twice what the actuator is expected to output at 25kN at 200bar. This could cause a failure in the cylinder or pressure line and would be equivalent to 358bar. Monitoring the pressure in the lines so that the valve could release this excess pressure is a possibility, as is the use of pressure relief valves.

The actual load increase is can be seen in the right-hand side of the exoskeleton at 2.9 seconds. This is the cause of the oscillations in the actuator forces and torque. The load change is an instantaneous event, rather than a smooth weight transfer as there is no floor to have a reactionary force against. The left-hand side load pickup is visible as a small rise in the elbow actuator, but there are no significant changes in the shoulder units.

From the velocity and force/torque of the joints, the power can be calculated, as shown in Figure 7.31. These powers are for the complete system, with each actuator added to the power requirements.
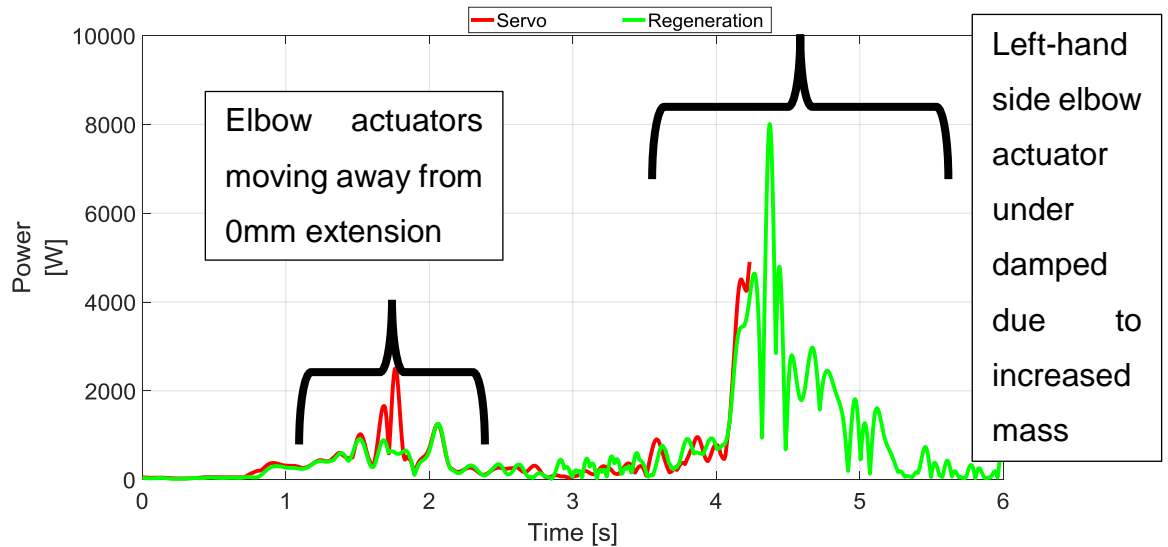
Figure 7.31: Exoskeleton power requirements for picking a box up off the floor.

The power does not show the box pick up event, so though the force and torques have large events, certainly for the servo valve, it is not represented here. The underdamped event is clear to see as a very high power requirement, but its short duration does not affect the average power requirements. The average power for the servo valve is 475W and 717W for the regeneration circuit. If the oscillations at the end of the regeneration circuit were removed, then the average power is only 320W.

7.9 Validation

To verify the results, an empirical setup would be required, but due to budget and timing constraints, this has not been possible. The team was able to test an early single joint design, Appendix K, but not a full system.

The empirical testing would be conducted by starting with a single joint, the elbow, and slowly adding additional actuators as the testing progresses. For each of these steps, the system would be tested first with direct position input rather than straight to human testing. This would be the safest method of initial testing to make sure that the gains of the controller are working correctly, and the exoskeleton is stable. A human would now be involved but at a distance, possibly with a master and slave setup. This means that if the system did become unstable due to the unknown range of inputs, then the risk to humans

is negated. Once the system is tuned and deemed stable, then a user can enter into the exoskeleton workspace.

7.10 Discussion

The exoskeleton matches the wrist control positions at the start of each of the simulations, but as the motion capture progresses, this is not always the case. For the walking motion, the frequency response of the exoskeleton caused a delay in following the swinging of the arms. With higher loads and fluid volumes, the frequency response of the system reduces, and even if higher frequency response valves were used, the HMRF would be the limiting factor. This would thus require the human to move at a slow rate. For the box pick up, the motion capture data involved motions that are not replicated in the exoskeleton directly, but mimicked in the manipulator. The exoskeleton attempted to follow the motion regardless but encountered the actuator limits that have been set to protect the user.

The hydraulics followed the trends of the direct actuator positions, with the only issue being the frequency response. If the motions are slow, for example, the standing still or the box pickup, then the hydraulics will follow the motion trend, though the high-speed arm swings it was not able to follow. PERCRO has an issue in matching gait, which is similar to the issue found here. With a slower walking motion, the hydraulics are more likely to be able to follow the user. This will put a load onto the user, which could cause additional fatigue, which is a negative outcome.

The direct input results have high peaks in the force and torque, which are attenuated with the hydraulics. The high forces and torques are due to the system having no limit on the force and attempts to match the wrist position without this consideration. The forces and torques in the hydraulics were below the safety factor limit for both the standing still and walking motions, but some peaks were encountered in the box pick up. Forces and torques between the safety fact limit and the maximum output are allowable as this is the shock load area, an area of force and torque that is not for continuous use, but there to protect the system. One of the actuators did have a small period where the force was above the actuator maximum output, which could cause failure, but was linked to an underdamped position response.

The power of the actuators did have high peaks, but the averages were below 500W if the underdamped section is removed, and below 1000W if included. Though the peak events are high, the use of accumulators will level out the power requirements allowing a smaller motor to be used.

7.11 Summary

It has been shown that the exoskeleton design has some issues with frequency response and following the motion capture data. The frequency response is due to the size and weight characteristics of the design, which is due to the requirements of the exoskeleton.

The torque and forces were typically below the safety factor limit, indicating that the design selection process was correct. Though the system was not tested to extreme loading at full reach, this is only due to having limited motion capture data. This is a compromise due to the lack of available motion capture data specifically focused on this exoskeleton design and limitations.

The average power requirements for the system are low, making the hydraulic solution viable if the frequency response could be improved.

Chapter 8
Summary, Conclusions and Future Work

8.1 Summary

As outlined in Chapter 1, specific objectives for this research were defined. Each objective will be compared to the work completed to show whether it was met or not. This comparison will link back to previous chapters, outlining the supporting evidence that this objective was completed, or an explanation of why it was not.

There are six objectives covered the development of the optimisation routines which were utilised in the design of an upper-body exoskeleton. Parallel to this, hydraulic circuits were examined to determine which could be utilised in the exoskeleton system. These were finally brought together into a full simulation utilising motion capture data.

8.1.1 The use of geometric optimisation of joints in upper-body exoskeleton design

In Chapter 4, several design options for revolute joints were examined, with endpoint equations generated for each. The designs varied from simple joints with an actuator on the inside to complex Hoeken linkage designs. The relationships between the endpoint equations, for example, the length of the actuator were also defined.

The second part of Chapter 4 focused on the spherical joint options for the shoulder. Two and five bar systems were examined for their possibilities in use for the exoskeleton. These were extended with 'parallel' four-bar joints, to determine if this would reduce the motion range required at the end of the shoulder joint. These four systems were defined as equations that could then be optimised for the range of motions required.

The equations that were developed were then utilised in the design for the elbow joint, Chapter 5, but it was found that due to the large torques required by the load, only one design had solutions, the Hoeken linkage design. These solutions were then compared to each other to determine the ideal geometry for the elbow. As the solutions were limited to using existing available actuators,

there is the possibility that allowing a bespoke actuator would give a larger range of design options.

The spherical equations that were developed were also utilised in the design of the shoulder in Chapter 5, and it was found that the two-bar system gave the largest range of motion. This does mean that the actuators are spread along the structure, rather than just at the rear of the exoskeleton.

8.1.2 Focus on action at a distance for the upper-body load manipulation

The design methodology started with the end effector and working back towards the rear of the exoskeleton. This was done to make sure that each additional joint would support the arm for the required load.

The final design was compared to current exoskeletons and was shown to be three times heavier than the heaviest current design, with a lower load to weight ratio. When the exoskeleton was compared to industrial robots, the exoskeleton was found to be of a similar weight and load to weight ratio. Due to the focus on 'action at a distance', this has increased the weight of the actuators to support the higher torques required. This does mean that the comparison to industrial robots is closer to the intended reach range than current exoskeletons.

8.1.3 Critical analysis of hydraulic circuits in regards to an exoskeleton

Chapter 6 started to compare the different hydraulic circuit designs originally outlined in Chapter 2. The work focused on three main routes: servo based digital valves and pump based.

The servo-based results showed that simple changes to the flow paths could reduce the power requirements for the system. Though these changes do add weight and complexity, these could reduce the weight of any power system attached to the exoskeleton.

The digital valve results did not perform as well as the servo valve-based systems. The idea that having multiple, but cheap digital valves compared to singular proportional ones did not appear to work for the simple test exercise.

This is an area of ongoing research and future development could bring this back to the fore for exoskeletons.

The pump based systems showed disappointment but also the promise of future opportunities. The pump based circuit is currently also being developed and is being developed as standalone systems. There is an issue with the bandwidth of a pump based circuit being less than a servo valve circuit. With a lower bandwidth, high-frequency events could not be followed correctly, though the improved controlled design could improve this. The main benefit would be the ability to regenerate power from the actuators.

Whereas a servo valve circuit can use accumulators to even out the flow demand, the motor of a pump-based circuit has to be able to give the maximum torque required and the maximum speed. As power is torque times the angular velocity, a high torque, low-speed event might require the same power as a low torque, high-speed one. This is an inverse decay curve, but electric motors typically only utilise a small section of this viable area. The use of continuously variable transmission would allow output into this range but would add weight and inefficiency.

8.1.4 Multi-domain simulation of exoskeleton system

With the design completed and hydraulic circuits selected, these were transferred to a Simscape model to simulate the complete system. Using motion capture data, the position of the exoskeleton was set to attempt to match the location of attachment points. This would not give the forces, but the motion data to be put into a hydraulically powered model.

The results showed that there were issues with the frequency response as well as matching the motion capture data. With the large loads and fluid volumes, the frequency response of hydraulics reduces, which has caused a delay in the exoskeleton in following the motion capture. Selecting higher frequency valves is unlikely to solve the issue for all of the joints due to the bandwidth limit being the lesser of the valve or hydraulic resonant frequencies.

The motion capture data did not have any limitations on the motion that the exoskeleton does. The main limitation is that the pronation/supination of the forearm is replicated in the manipulator design rather than following the human.

This changes how the human will interact with the world, and thus motion capture taking this into account will improve the simulation.

The average power was also found to be of a magnitude similar to that of BLEEX. Though the system is significantly heavier, the power requirements are low, meaning that a small pump/motor setup could be used, and tethering limited to an electrical power supply.

8.1.5 Consideration of validation of the design and simulation with empirical results

Due to cost and time constraints, a full empirical system was not built and thus the simulation results could not be directly compared.

The simulation results have shown where empirical testing will need to begin focus on, determining the frequency response of the physical system. This would need to be done sequentially up the arm. This would need to be systematic in that testing is conducted remotely before a human test subject can control the device.

8.2 Conclusions

The conclusions from this research have shown that a systematic design methodology can be used to develop an upper-body exoskeleton. The use of optimisation techniques for the different joint geometry has been researched and shown that this can be used to give initial starting designs. The use of geometric optimisation has not been shown in other exoskeleton designs, though has been mentioned as a possible route.

There are a limited number of enhancive upper-body exoskeletons, due to the focus on the improvement of mobility, and thus this research attempts to give a starting point for future research for this. The design methodology is not limited to the upper body exoskeleton and could be used for the lower limbs, as well as other industrial sectors like robotics or heavy machinery.

The weight of the design has caused concern due to its significant increase to comparable exoskeleton designs, but the focus on 'action at a distance' is the cause of this. Previous research has focused on a carrying capacity close to the body, but this is not always possible, for example, reaching into the

workspace of a CNC milling machine to place and remove parts. The ability to manipulate a load at range is novel for this design.

With the possibility of rapid motion from the human user, the hydraulics have to match the speed whilst giving the required force. Attempting to balance these requirements with efficiency has shown that there is still work required to find the ideal solution. There are several new hydraulic designs that have shown some promising results, but require additional work to move forward. These typically involve the development of the control system, but will also require empirical testing to tune the simulation. The response of the pump based circuits, for example, were not suitable for the exoskeleton for the designs tested, but research into this circuit design is continuing in other areas. Products are available to purchase of this design, but the response requirements are high for the exoskeleton.

The simulation of the exoskeleton following motion capture data has shown how the human input motion can cause failure in the model. Forearm rotation in the human is not mimicked directly by the exoskeleton, and thus motion capture data that considers this would benefit the simulation results. This would need to be done specifically for this task.

The simulation of the exoskeleton rather than prototype testing has resulted in a smaller capital requirement. The use of the virtual environment is becoming a critical step in the engineering design process, determining issues and limitations before physical components are demanded. This also reduces the environmental impact, as parts are not scrapped.

The overall aim of the project was to design and simulate an upper-body exoskeleton system with a hydraulic circuit that is optimised for energy efficiency. The design of the upper-body has been developed using optimisation, but the selection of the hydraulic circuits has shown that additional work is required. The high loading and speeds that could be required have created issues with the control of the hydraulics, and thus performance has not been idealised. It has shown that the exoskeleton is capable of lifting the required load, though, with limited motion capture data, this has not been able to be fully shown at reach.

8.3 Future work

There are several options for future work.

1. With an initial prototype design completed, a mock-up to determine complete motion ranges would assist and confirm the design. This could be rapidly prototyped on a 3D printer, though it would have limited powered capabilities. It would allow the examination of possible collision areas, as well as possible gimbal lock events. The visibility of the user could also be investigated due to the larger shoulder actuators.

    a. This would be done incrementally, starting with the elbow up to shoulder to allow individual joint testing

2. Additional motion capture data focused on the limitations of the exoskeleton would improve the simulation results. This could require a simple mock-up, as per (1), but if this is 3D printed, this should be light and recyclable. The full motion range, and focus on 'action at a distance' could be investigated with this.

3. Daily motion capture statistics would improve the understanding of motion range probability. The current design is based upon individual short events, but this is unrealistic. The percentage of the working day doing certain tasks would improve the design, as it could reduce the standard deviation of the motion range probability. This would, in turn, reduce the peak torques required.

4. With the high loading requirements, the number of actuators and geometric solutions was small. This could be improved with either designing for a lower load, or a bespoke actuator solution. This would increase the optimisation solve duration and would require determining the function to minimise.

5. Integration of the actuators directly into the structure of the exoskeleton could reduce the size and weight of the system. This would require a significant redesign of the system due to the integration of hydraulic seals and flow paths. It could make the system 'cleaner' as pipes could be integrated into the structure itself, reducing the risk of damage to them.

6. Additional research into digital valves and the pump circuits could improve results from these, which could lead to new opportunities regarding efficiency and power recovery. There were some indications

of possible opportunities from these circuit designs but were not able to be capitalised on in this project.

7. The use of full contact simulation software would indicate contact risks and dangerous motions. Simscape does not have a full environmental contact library, which means that currently if the exoskeleton enters into the human, then this is not detected. This would also mean that environmental aspects like confined spaces could also be investigated. As there are several areas of the design that would be blind spots to the user, an understanding of how the user might need to change their movement to compensate could be shown.

8. As the weight of the upper-body system is significantly higher than what other exoskeletons can lift, a lower-body system would be designed specifically for the system.

References

1. Oxford English Dictionary. *"exo-, prefix".* Oxford University Press.
2. Chu, A. *Design of the Berkeley Lower Extremity Exoskeleton (BLEEX).* Doctor of Philosophy thesis, University of California, Berkeley, 2005.
3. Sarcos. *XOS.* [Online]. 2015. [Accessed 18th June 2015]. Available from: http://www.sarcos.com/?page_id=15
4. Cyberdyne. *Other HAL Series.* [Online]. 2015. [Accessed 4th November 2015].
5. Yamamoto, K. et al. Development of power assisting suit for assisting nurse labor. *JSME International Journal Series C-Mechanical Systems Machine Elements and Manufacturing.* 2002, **45**(3), pp.703-711.
6. Marcheschi, S. et al. Body Extender: whole body exoskeleton for human power augmentation. In: *2011 IEEE International Conference on Robotics and Automation.* New York: IEEE, 2011.
7. Murphy, R.R. Meta-analysis of Autonomy at the DARPA Robotics Challenge Trials. 2015, **32**(2), pp.189-191.
8. MathWorks. *Haldex Reduces Braking and Stability System Development Time by 50% with MathWorks Consulting Services.* [Online]. 2019. [Accessed 3rd April 2019]. Available from: https://uk.mathworks.com/company/user_stories/haldex-reduces-braking-and-stability-system-development-time-by-50-with-mathworks-consulting-services.html
9. Specialty Materials Handling Products Operation, G.E.C. *Machine augmentation of human strength and endurance.* http://www.dtic.mil/dtic/tr/fulltext/u2/692178.pdf, 1969.
10. Dollar, A.M. and Herr, H. Lower extremity exoskeletons and active orthoses: Challenges and state-of-the-art. *IEEE Transactions on Robotics.* 2008, **24**(1), pp.144-158.
11. *Statement by Dr. Tony Tether.* Subcommittee on Terrorism, Unconventional Threats and Capabilities, House Armed Services Committee, U.S. House of Representatives DARPA, 2006. p.36. 03/29/2006 Available from: https://www.darpa.mil/attachments/TestimonyArchived(March%2029%202006).pdf
12. Hemmerich, A. et al. Hip, knee, and ankle kinematics of high range of motion activities of daily living. *Journal of Orthopaedic Research.* 2006, **24**(4), pp.770-781.
13. Soucie, J.M. et al. Range of motion measurements: reference values and a database for comparison studies. *Haemophilia.* 2011, **17**(3), pp.500-507.
14. Roaas, A. and Andersson, G.B.J. Normal Range of Motion of the Hip, Knee and Ankle Joints in Male Subjects, 30–40 Years of Age. *Acta Orthopaedica Scandinavica.* 1982, **53**(2), pp.205-208.
15. Zoss, A.B. et al. Biomechanical design of the Berkeley lower extremity exoskeleton (BLEEX). *IEEE-ASME Transactions on Mechatronics.* 2006, **11**(2), pp.128-138.
16. Yamamoto, K. et al. Development of power assisting suit - (Miniaturization of supply system to realize wearable suit). *JSME International Journal Series C-Mechanical Systems Machine Elements and Manufacturing.* 2003, **46**(3), pp.923-930.

17. Specialty Materials Handling Products Operation, G.E.C. *Reseach and development prototype for machine augmentation of human strength and endurance.* 1971.
18. Festo. *ExoHand.* [Leaflet]. 2012.
19. Festo. *ExoHand.* https://www.festo.com/group/en/cms/10233.htm: Festo.
20. Klein, J. et al. Optimization of a Parallel Shoulder Mechanism to Achieve a High-Force, Low-Mass, Robotic-Arm Exoskeleton. *IEEE Transactions on Robotics.* 2010, **26**(4), pp.710-715.
21. Zoss, A.B. *Actuation Design and Implementation for Lower Extremity Human Exoskeletons.* Doctor of Philosophy thesis, University of California, Berkeley, 2006.
22. Kazerooni, H. et al. *Lower extremity enhancer* 2009.
23. Jacobsen, S.C. et al. *Biomimetic mechanical joint.* US 8,516,918 B2. 2013.
24. Jacobsen, S.C. and Olivier, M. *Contact displacement actuator system.* 2009.
25. Bergamasco, M. et al. *An exoskeleton structure for physical interaction with a human being.* WO 2013/186705 A2. 2013.
26. Kenneth Boldt, A., Pa. *Three axis mechanical joint for a power assist device.* 5,282,460. 1994.
27. Amundson, K. et al. Development of hybrid hydraulic-electric power units for field and service robots. *Advanced Robotics.* 2006, **20**(9), pp.1015-1034.
28. Health and Safety Executive. *Managing the risk from hot water and surfaces in health and social care.* (6). http://www.hse.gov.uk/pubns/hsis6.htm: HSE, 2012.
29. *The Control of Noise at Work Regulations 2005 2005.* http://www.legislation.gov.uk/: The Stationery Office Limited.
30. Health and Safety Executive. *Noise exposure ready-reckoner (Daily exposure).* http://www.hse.gov.uk/noise/dailyexposure.pdf: Crown, 2007.
31. Hollerbach, J.M. et al. A comparative analysis of actuator technologies for robotics. In: Oussama, K. et al. eds. *The robotics review 2.* MIT Press, 1992, pp.299-342.
32. Huber, J.E. et al. The selection of mechanical actuators based on performance indices. *Proceedings of the Royal Society a-Mathematical Physical and Engineering Sciences.* 1997, **453**(1965), pp.2185-2205.
33. Quan, Z.Y. et al. Review of energy efficient direct pump controlled cylinder electro-hydraulic technology. *Renewable & Sustainable Energy Reviews.* 2014, **35**, pp.336-346.
34. Rotary Actuators. In: *Fluid Power Circuits and Controls.* CRC Press, 2001, pp.153-191.
35. Rotomation Inc. *Pneumatic actuators take a spin.* [Online]. 2016. [Accessed 23rd March 2016]. Available from: http://hydraulicspneumatics.com/other-technologies/pneumatic-actuators-take-spin
36. HKS Dreh-Antriebe GmbH®. *DHK-H-ZH.* [Online]. 2019. [Accessed 5th April 2019]. Available from: https://www.hks-partner.com/en/products/rotary-lift-combinations/dhk-h-zh/

37. SKF. *Ball and roller screws* [Online]. 2017. [Accessed 10th Jan 2017]. Available from: http://www.skf.com/uk/products/linear-motion/ball-and-roller-screws/index.html

38. SKF. *Roller screws.* [Online]. 2017. [Accessed 10th Jan 2017]. Available from: http://www.skf.com/uk/products/linear-motion/ball-and-roller-screws/roller-screws/index.html

39. SKF. *Roller screws, SKF, April 2014.* PUB MT/P1 14489 EN ed. [Exhibition catalogue]. SKF, 2014.

40. Exlar Actuation Solutions. *Roller Screw Basics.* [Leaflet]. http://exlar.com/content/uploads/2014/09/Roller-Screw-Basics.pdf: Exlar Actuation Solutions, 2014.

41. Bergamasco, M. et al. A novel compact and lightweight actuator for wearable robots. In: *2010 IEEE International Conference on Robotics and Automation*, *3-7 May 2010*, 2010, pp.4197-4203.

42. Python. *Cable technical information.* [Online]. 2017. [Accessed 7th July 2017]. Available from: http://pythonrope.com/inspmanual/inspman_25.shtml

43. British Standards Institute. BS EN 12385-4:2002+A1:2008. *BS EN 12385-4:2002+A1:2008 Steel wire ropes. Safety. Stranded ropes for general lifting applications.* https://0-bsol.bsigroup.com.wam.leeds.ac.uk/Bibliographic/BibliographicInfoData/000000000030170955: BSI, 2002.

44. British Standards Institute. *Safety requirements for cableway installations designed to carry persons — Ropes —.* 2004.

45. Gordon, C.C. *2012 Anthropometric survey of u.S. Army personnel: Methods and summary statistics* 2012 ed. Defense Technical Information Center: Defense Technical Information Center, 2012.

46. Milburn, D.A. *Study of a titanium wire rope developed for marine applications.* Department of the Navy, 1973.

47. SERAPID France. *LINKLIFT - technical guide,* [Exhibition catalogue]. SERAPID France, 2017.

48. Fenjan, R. Study the Hydraulic Performance of an Electrohydraulic Servo Valve with Mechanical Feedback. 2019.

49. Huang, J.H. et al. Development of a dual-acting axial piston pump for displacement-controlled system. *Proceedings of the Institution of Mechanical Engineers Part B-Journal of Engineering Manufacture.* 2014, **228**(4), pp.606-616.

50. Huang, J.H. et al. Development of an asymmetric axial piston pump for displacement-controlled system. *Proceedings of the Institution of Mechanical Engineers Part C-Journal of Mechanical Engineering Science.* 2014, **228**(8), pp.1418-1430.

51. Center for Compact and Efficient Fluid Power (CCEFP). *High Efficiency Excavator - Test Bed 1: Heavy Mobile Equipment.* [Leaflet]. http://www.ccefp.org/research/testbeds/high-efficiency-excavator: CCEFP, 2015.

52. Martin, H. *The design of hydraulic components and systems.* London: Ellis Horwood, 1995.

53. Huang, J.H. et al. Development of a dual displacement controlled circuit for hydraulic shovel swing motion. *Automation in Construction.* 2015, **57**, pp.166-174.

54. Trinkel, B. *Fluid Power eBook — Fluid Power Circuits Explained.* [Online]. http://hydraulicspneumatics.com/ebooks/fluid-power-ebook-

fluid-power-circuits-explained: Hydraulics & Pneumatics, 2007.
[Accessed 8th September 2016]. Available from:
http://hydraulicspneumatics.com/ebooks/fluid-power-ebook-fluid-power-circuits-explained

55. Concentric. *Rotary gear flow dividers, Concentric, 06-2012.* [Exhibition catalogue].
http://www.concentricab.com/_downloads/Catalogs/Flow_div_0612.pdf: Concentric, 2012.

56. Andruch, J.P. *Design, Simulation and Control of Hydraulic System Topographies with Integrated Energy Recovery.*
http://www.nfpa.com/nfpafoundation/pdf/purdueuniversity-design-simulation-and-control-of-hydraulic-system-topographies-with-integrated-energy-recovery.pdf: National Fluid Power Association, 2011.

57. Andruch, J. and Lumkes, J.H. Regenerative Hydraulic Topographies using High Speed Valves. In.: SAE International, 2009.

58. Wu, J. et al. A compound control strategy for the digital valve based hydraulic position tracking system. In: *Proceedings of the 33rd Chinese Control Conference*, *28-30 July 2014*, 2014, pp.7869-7873.

59. Heitzig, S. et al. Energy Efficiency of Hydraulic Systems with Shared Digital Pumps. *International Journal of Fluid Power.* 2012, **13**(3), pp.49-57.

60. Lantela, T. and Pietola, M. High-flow rate miniature digital valve system. *International Journal of Fluid Power.* 2017, **18**(3), pp.188-195.

61. Linjama, M. et al. Mechatronic Design of Digital Hydraulic Micro Valve Package. *Procedia Engineering.* 2015, **106**, pp.97-107.

62. Zhang, J. et al. Design and experimental research of a miniature digital hydraulic valve. *Micromachines.* 2018, **9**(6).

63. Male, A. et al. *Fuel Injector* 2011.

64. Lillington, R. et al. A dynamic model for the drive and electro-mechanics of a solenoid based electronic fuel injector. *Proceedings of the Institution of Mechanical Engineers, Part D: Journal of Automobile Engineering.* **0**(0), p.0954407017739333.

65. Bingqi, T. et al. Study of the fluctuation in the cycle fuel injection quantity in a common-rail system for a heavy-duty vehicle diesel engine. *Proceedings of the Institution of Mechanical Engineers, Part D: Journal of Automobile Engineering.* 2015, **229**(7), pp.819-834.

66. Locateli, C.C. et al. Digital hydraulic system using pumps and on/off valves controlling the actuator. In: *8th FPNI Ph.D Symposium on Fluid Power, FPNI 2014*: Web Portal ASME (American Society of Mechanical Engineers), 2014.

67. Locateli, C.C. et al. Actuator speed control using digital hydraulics. In: *ASME/BATH 2014 Symposium on Fluid Power and Motion Control, FPMC 2014*: Web Portal ASME (American Society of Mechanical Engineers), 2014.

68. Achten, P. and van den Brink, T. *A hydraulic transformer with a swash block control around three axis of rotation.*
http://www.innas.com/download.html: Innas.

69. Yang, G.Z. and Jiang, J.H. Power characteristics of a variable hydraulic transformer. *Chinese Journal of Aeronautics.* 2015, **28**(3), pp.914-931.

70. Vael, G.E.M. et al. *Toward Maximum Flexibility in Working Machinery, IHT Control in a Mecalac Excavator.* http://www.innas.com/download.html: Innas.

71. Lee, S. et al. *Passivity based backstepping control for trajectory tracking using a hydraulic transformer.* New York: Amer Soc Mechanical Engineers, 2016.

72. Richter, C. *All-in-One Actuator is Showcase of Simplicity*. [Press release]. 2017. Available from: https://www.hydraulicspneumatics.com/hydraulic-pumps-motors/all-one-actuator-showcase-simplicity

73. Johnson, J. *Pump control vs valve control: Efficiency or performance?* [Online]. 2007. [Accessed 10th October 2016]. Available from: http://hydraulicspneumatics.com/200/TechZone/HydraulicPumpsM/Article/False/46094/TechZone-HydraulicPumpsM

74. Parker. *Compact EHA: Electro-Hydraulic Actuators for high power density applications,* [Exhibition catalogue]. http://www.parker.com/Literature/Oildyne/Oildyne%20-%20PDF%20Files/Compact-EHA-Catalog-HY22-3101E-7-13.pdf: Parker, 2013.

75. Yong-Kwun, L. and Soo-Jun, L. A bio-mimetic robot arm actuated by micro EHA. In: *Ubiquitous Robots and Ambient Intelligence (URAI), 2013 10th International Conference on*, *Oct. 30 2013-Nov. 2 2013*, 2013, pp.39-44.

76. Yong-Kwun, L. Design of exoskeleton robotic hand/arm system for upper limbs rehabilitation considering mobility and portability. In: *Ubiquitous Robots and Ambient Intelligence (URAI), 2014 11th International Conference on*, *12-15 Nov. 2014*, 2014, pp.540-544.

77. Soojun, L. et al. Development of Micro Hydraulic Actuator for force assistive wearable robot. In: *Robotics (ISR), 2013 44th International Symposium on*, *24-26 Oct. 2013*, 2013, pp.1-6.

78. Ivantysyn, R. and Weber, J. Novel Open Circuit Displacement Control Architecture in Heavy Machinery. In: ASME, ed. *8th FPNI Ph.D Symposium on Fluid Power*, *June 11-13, 2014*, *Lappeenranta, Finland*. Fluid Power Net International (FPNI), Lappeenranta University of Technology, Finland, 2014, p.8.

79. *CMU Graphics Lab Motion Capture Database.* [Online database]. http://mocap.cs.cmu.edu/: Carnegie Mellon Graphics Lab,.

80. Kazerooni, H. et al. Hybrid control of the Berkeley Lower Extremity Exoskeleton (BLEEX). *International Journal of Robotics Research.* 2006, **25**(5-6), pp.561-573.

81. FANUC UK Limited. *CR-35iA,* [Exhibition catalogue]. http://www.fanuc.eu/uk/en,

82. FANUC UK Limited. *Robotics Product overview,* [Exhibition catalogue]. http://www.fanuc.eu/uk/en,

83. *Neon Genesis Evangelion.* [Various]. Anno, H. dir. Gainax, Tatsunoko Production, 1995-1996.

84. HM Government. *Access to and use of buildings.* https://assets.publishing.service.gov.uk/government/uploads/system/uploads/attachment_data/file/441786/BR_PDF_AD_M2_2015.pdf: HM Government,, 2015.

85. *Aliens.* [Various]. Cameron, J. dir. USA: 20th Century Fox, 1986.

86. Insitute, B.S. *Robots and robotic devices — Safety requirements for personal care robots.* BSI Standards Publication, 2014.

87. Chief Inspector of Mining. *MDG 15: Mobile and transportable plant for use on mines and petroleum sites.* https://www.resourcesandenergy.nsw.gov.au/miners-and-explorers/safety-and-health/publications/mdg/1-999: NSW Department of Planning and Environment, NSW Resources Regulator, 1992.

88. Chief Inspector of Mining. *Guideline for fluid power system safety at mines.* https://www.resourcesandenergy.nsw.gov.au/miners-and-explorers/safety-and-health/publications/mdg/1-999: NSW Department of Planning and Environment, NSW Resources Regulator, 2010.

89. *Linear Blend Skinning.* [m code]. https://uk.mathworks.com/matlabcentral/fileexchange/43039-linear-blend-skinning: Aaron Wetzler, 2013.

90. Pons, J.L. *Wearable robots: biomechatronic exoskeletons.* Chichester: John Wiley, 2008.

91. McCarthy, J.M. *Geometric design of linkages.* New York: Springer, 2000.

92. Klein, J. et al. Biomimetic Orthosis for the Neurorehabilitation of the Elbow and Shoulder (BONES). In: *2008 2nd IEEE RAS & EMBS International Conference on Biomedical Robotics and Biomechatronics, New York.* IEEE, 2008, pp.535-541.

93. Trinkel, B. *Synchronizing cylinder movement.* [Online]. 2010. [Accessed 22nd April 2019]. Available from: https://www.hydraulicspneumatics.com/other-technologies/book-2-chapter-22-synchronizing-cylinder-movement

94. Hamilton, W. *Hatch cover actuating mechanism.* 1965.

95. Knabe, C. *Hoeken's linkage Robotic Joint.* [Online]. 2015. [Accessed 30/11/2016]. Available from: https://seelio.com/w/1lsy/hoekens-linkage-robotic-joint

96. Knabe, C. et al. An inverted straight line mechanism for augmenting joint range of motion in a humanoid robot. In: *ASME 2014 International Design Engineering Technical Conferences and Computers and Information in Engineering Conference, IDETC/CIE 2014*: American Society of Mechanical Engineers (ASME), 2014.

97. Lee, B. et al. Design of a human-like range of motion hip joint for humanoid robots. In: *Proceedings of the Asme International Design Engineering Technical Conferences and Computers and Information in Engineering Conference, 2014, Vol 5b, New York.* Amer Soc Mechanical Engineers, 2014.

98. Norton, R.L. *Design of machinery: an introduction to the synthesis and analysis of mechanisms and machines.* Dubuque, IA: McGraw-Hill, 2008.

99. Bulatović, R.R. and Dordević, S.R. On the optimum synthesis of a four-bar linkage using differential evolution and method of variable controlled deviations. *Mechanism and Machine Theory.* 2009, **44**(1), pp.235-246.

100. *inpolyhedron.* [m code]. https://uk.mathworks.com/matlabcentral/fileexchange/37856-inpolyhedron-are-points-inside-a-triangulated-volume: MathWorks, 2016.

101. Kong, X. Forward Displacement Analysis and Singularity Analysis of a Special 2-DOF 5R Spherical Parallel Manipulator. *Journal of Mechanisms and Robotics.* 2011, **3**(2), pp.024501-024501-6.

102. Kiper, G. and Bilgincan, T. Function generation synthesis of spherical 5R mechanism with regional spacing and Chebyshev approximation. *Mechanism and Machine Theory.* 2015, **90**, pp.37-46.

103. Ouerfelli, M. and Kumar, V. Optimization of a Spherical Five-Bar Parallel Drive Linkage. *Journal of Mechanical Design.* 1994, **116**(1), pp.166-173.

104. Cervantes-Sánchez, J.J. et al. On the 5R spherical, symmetric manipulator: workspace and singularity characterization. *Mechanism and Machine Theory.* 2004, **39**(4), pp.409-429.

105. Enerpac. *Safety seminar handbook.* [Leaflet]. http://www.enerpac.com/sites/default/files/safetyhandbook_eng_3.pdf: Enerpac, 2016.

106. Weisstein, E.W. *"Point-Line Distance--3-Dimensional." From MathWorld--A Wolfram Web Resource. .* [Online]. [Accessed 09/11/2016]. Available from: http://mathworld.wolfram.com/Point-LineDistance3-Dimensional.html

107. Arora, J.S. *Introduction to optimum design.* 3rd ed. London;Amsterdam;: Elsevier/Academic Press, 2012.

108. Ullman, D.G. *The mechanical design process.* 4th, international ed. Boston, MA;London;: McGraw-Hill, 2010.

109. O'Connor, P.D.T. *Practical reliability engineering.* 3rd ed. Chichester: Wiley, 1991.

110. British Stainless Steeel Association. *50 Grades of Stainless Steel.* [Online]. 2016. [Accessed 18th Janurary 2016]. Available from: http://www.bssa.org.uk/50-grades-of-stainless-steel.php

111. Hurst. *StrongArm®.* [Online]. 2016. [Accessed 10th August 2016]. Available from: http://www.jawsoflife.com/en/product-type/strongarm

112. Porter, T.M. *Spreader tool.* 1982.

113. Herwig, P. et al. *Spreader tip for a rescue tool.* US2016144205 (A1) 2016.

114. Wettlaufer, E. et al. *Portable rescue tool and method of use.* US2011214471 (A1). 2011.

115. Hurst. *MOC Combi.* [Online]. 2016. [Accessed 10th August 2016]. Available from: http://www.jawsoflife.com/en/product/5000-psi-moc-combi

116. 15 Ways to Fasten Gears to Shafts. In: *Illustrated sourcebook of mechanical components.* McGraw-Hill, 2000, pp.4-29 to 4-33.

117. SKF. *SKF FX Keyless Bushings, September 2010.* 2 ed. [Exhibition catalogue]. 2010.

118. NACHI-FUJIKOSHI Corp. *NACHI Ball & Roller Bearings, CORP, N.-F., 04/2014.* [Exhibition catalogue]. Japan, 2014.

119. OpenStax. *Anatomy and Physiology.* https://cnx.org/contents/qCnsYyus@6/Types-of-Body-Movements: OpenStax, 2019.

120. Satran, P.R. and Rosenkrantz, L. *The Baby Name Bible: The Ultimate Guide By America's Baby-Naming Experts.* St. Martin's Press, 2007.

121. IMG. *Husafeel Stone.* [Online]. 2018. [Accessed 19th September 2018]. Available from: http://theworldsstrongestman.com/events/husaffel-stone/

122. IMG. *Farmer's Walk.* [Online]. 2018. [Accessed 19th September 2018]. Available from: http://theworldsstrongestman.com/events/farmers-walk/

123. Banfield, I. et al. Hybrid position-force control of climbing parallel robot using electrohydraulic servo actuators. In: *ASME 2011 International Design Engineering Technical Conferences and Computers and Information in Engineering Conference, IDETC/CIE 2011, August 28, 2011 - August 31, 2011*, *Washington, DC, United states*. American Society of Mechanical Engineers, 2011, pp.1203-1210.

124. Shouling, H. Neural predictive force control for a hydraulic actuator: simulation and experiment. *Applied Artificial Intelligence.* 2009, **23**(2), pp.151-67.

125. Liu, G.P. and Daley, S. Optimal-tuning nonlinear PID control of hydraulic systems. *Control Engineering Practice.* 2000, **8**(9), pp.1045-1053.

126. Chantranuwathana, S. and Huei, P. Adaptive robust force control for vehicle active suspensions. *International Journal of Adaptive Control and Signal Processing.* 2004, **18**(2), pp.83-102.

127. Ye, Y. et al. Position control of nonlinear hydraulic system using an improved PSO based PID controller. *Mechanical Systems and Signal Processing.* 2017, **83**(Supplement C), pp.241-259.

128. Seong-Ryeol, L. and Yeh-Sun, H. A dual EHA system for the improvement of position control performance via active load compensation. *International Journal of Precision Engineering and Manufacturing.* 2017, **18**(7), pp.937-44.

129. Liang, X. et al. Robust position control of hydraulic manipulators using time delay estimation and nonsingular fast terminal sliding mode. *Proceedings of the Institution of Mechanical Engineers, Part I: Journal of Systems and Control Engineering.* 2018, **232**(1), pp.50-61.

130. Napora, M.G. *Control Aspects of a Full-body Enhancive Robotic Exoskeleton.* PhD thesis, University of Leeds, 2018.

131. Johnson, J. *The importance of frequency response.* [Online]. 1996. [Accessed 10th October 2016]. Available from: http://hydraulicspneumatics.com/200/TechZone/HydraulicValves/Article/False/6495/TechZone-HydraulicValves?page=3

132. Johnson, J. *Hydromechanical resonant frequency and cylinder speed.* [Online]. 2012. [Accessed 17th May 2019]. Available from: https://www.hydraulicspneumatics.com/cylinders-amp-actuators/hydromechanical-resonant-frequency-and-cylinder-speed

133. Hatami, H. Hydraulic Formulary. *Sales Industry Sector Metallurgy.* [Online]. 2013, p.43. [Accessed 13th July 2015].

Appendix A
Linear actuator strength

The strength of an actuator is not just determined by the pressure and the area of the cylinder, but the influence of off-axis loading, mounting and buckling. These are critical due to the safety requirements due to protecting the user, but having a very high safety factor would make the system unusable due to the weight.

The force applied will not always be applied in the axis of the actuator, especially if the actuator is not vertical. This places a moment on both the end seals and the internal seals of the piston. This is mitigated partially by the use of rotating mountings for example hinge or universal eye rods, though this cannot always remove all of the stress.

Limiting the maximum extension of 80% [A.1] of the available extension is a starting limit. This can be a hard stop within the cylinder with the use of stop sleeves. This does add mass to the system but prevents overextension. If the design already incorporates this in the design equations, this should not be an issue.

A.1 Buckling

Buckling of the cylinder is a safety factor that needs to be addressed as with a small overload could cause serious injury or death to the user. Several manufacturers already automate the calculation or simplify it into simple tables to ease the choice selection of the design. Though these can be ignored, Frank Yeaple puts it simply [A.2]:

"Ignore them at your own risk"

Assuming a max force of 15 kN as a worst-case scenario for the force required, and using Bosch Rexroth's selection program [A.3], with a pressure of 210 bar, trunnions and 100 mm of travel give a cylinder size of a bore diameter of 40 mm and a rod diameter of 25. It also gives the safety factors for the cylinder as shown in Table A.1. The load pressure is 119 bar at full extension and 196 bar at full retraction.

Table A.1: Cylinder safety factors for example cylinder by Bosch Rexroth based upon load and system pressure

Buckling calculation safety factor at load pressure	7.1
Bending calculation safety factor at load pressure	10.0
Safety factor for buckling calculation at system pressure	4.0
Safety factor for bending calculation at system pressure	9.4

Yeaple's basic equation [A.2] of allowing the compressive strength of 10,000 to 20,000 psi for a system where the effective rod length-to-diameter ratio does not exceed 6:1. Converting these to metric units gives 689.5 to 1379.0 bar.

For a load of 15kN, this means that the cylinder lies between 11.8 mm and 16.6 mm. This also would limit the effect rod length to 70.6mm to 99.6mm.

A.2 Euler's critical load

A simple theory to determine the buckling load is Euler's critical load is expressed in equation (7.1).

$$P = \frac{\pi^2 EI}{(Kl)^2} \qquad\qquad \textbf{(A.1)}$$

Where P is the critical load, E is Young's modulus, I is the inertial momentum, K is the column effective length factor and l is the unsupported length of the column. With both ends pinned, K is equal to 1.

With the BLEEX unit, the critical load is 1.6kN, while for the Bosch unit, it is 252kN. For the BLEEX unit, this appears quite low, where Baragetti states [A.4]:

"[Euler's critical Load] represents the lower, over conservative extreme"

For the Bosch unit, if this is lower extreme, then the safety factor for 15kN is 16.8, which is over double that of the Bosch result. This means that Bosch assumes that their unit is weaker than Euler's calculation would predict.

A.3 ISO equation

There is a standard by ISO that gives the buckling strength of hydraulic actuators [A.5]. This has a FORTRAN program that was converted to MATLAB and is in Appendix C. Assuming that the BLEEX unit has an external diameter of 1", then the ISO buckling load is 12.8kN. For the one recommended by Bosch Rexroth, the outside diameter is 50mm, and thus the buckling load is 170kN. To get a buckling load of 15kN with the ISO standard, the safety factor would be 11.4 for the calculation to give a load of 15kN. This would indicate that the ISO standard overestimates the safety factor compared to the Bosch Rexroth units.

A.4 Research simulations

There is still research in predicting the buckling load via simulation rather than empirical results. The ISO standard is still current, though is under review to improve the calculations. Baragetti et al. [A.4] propose a new method for determining buckling which includes support friction and wear rings.

Timoshenko's model [A.6] contains no K_f factor, which is the bending stiffness of the system. The 2-wear ring model can be solved, though the 4-wear ring system requires FEA modelling to determine K_1 and K_2. The value for K_f for the system described in the paper in table 3 [A.4], reproduced in Table A.2 does not match with results that are generated from equation 33, reproduced in equation (A.2), from the values of table 1 and table 2, reproduced in Table A.3 and Table A.4 respectively.

Table A.2: The limit load and bending stiffness results according to different models. Adapted from table 3 in [A.4]

Model	Limit load [N]	Kf [N mm/rad]
Timoshenko's, no Kf	3855	-
2 wear rings, rod only	3111	8071 · 103
4 wear rings, rod and piston	3629	29777 · 103

$$K_f = \frac{\delta E_a \pi t d_s}{8s}\left(\delta + \frac{t}{3}\right) \qquad\qquad \text{(A.2)}$$

Table A.3: The dimensions and properties of the experimental actuator. Adapted from table 1 in [A.4].

Parameter	Value	Parameter	Value	Parameter	Value
d_s [mm]	20	f_0 [mm]	1.5	$J_s \approx J_p$ [mm⁴]	7854
D_{ci} [mm]	25	δ_1 [mm]	27.1	J_c [mm⁴]	16286
D_{ce} [mm]	30	δ_2 [mm]	18.4	E_s, E_c [MPa]	206000
a [mm]	1163	x_p [mm]	63.6	E_a [MPa]	600
b [mm]	1276	f	0.07	K_f [N mm/rad]	26111000

Table A.4: Parametrization for the sensitivity analysis, including default values and variation range. Adapted from table 2 in [A.4].

Parameter	Base value	Range
Wear ring width t [mm]	6	$5.5 \div 6$
Wear ring thickness s [mm]	3	$2.5 \div 3$
Wear ring Young's modulus [MPa]	600	$260 \div 3000$
Friction coefficient f [—]	0.07	$0 \div 0.3$
Distance xp between the wear rings [mm]	63.6	$20 \div 150$
Rectilinear imperfection $f0$ [mm]	1.5	$0 \div 3$

If the dimensions used in the paper are put into Euler's and the ISO equations, the critical loads are 7.6 kN and 4.4 kN respectively, with the load limits given from the paper being 3.9 kN and 3.1 kN

For the Timoshenko model, the BLEEX dimensions give a critical load is 17.2kN, whilst for the Bosch, dimensions give a load of 2580kN. This gives a safety factor of 1.2 and 172 respectively for a target load of 15kN. This gives a higher load rating than Euler or ISO, and would not be ideal to use.

For the 2-wear ring model, the BLEEX dimensions give a critical load of 14.2kN and Bosch gives 196.8kN. This gives safety factors of 0.9 and 13.1 respectively.

From these results, as outlined in Table A.5, there is not a consistent equation that gives the lowest or highest value. Euler gives the lowest loading for BLEEX whilst the highest for the paper values. Timoshenko gives the highest loading for both BLEEX and Bosch, and within [A.4] is also the highest value. From this, the ISO standard and the two wear ring model would be closest to the ideal results.

Table A.5: Buckling loads equation result comparison

	Euler	ISO	Timoshenko	Baragetti
BLEEX	1587	12792	17254	14154
Paper	7628	4447	3855	3111
Bosch	252330	170299	2580188	196836

References

A.1.   Enerpac. Safety seminar handbook. [Leaflet]. http://www.enerpac.com/sites/default/files/safetyhandbook_eng_3.pdf: Enerpac, 2016.

A.2.   Yeaple, F. Fluid power design handbook. In: 1990, 2nd, revis and expand New York. Dekker.

A.3.   AG, B.R. Mill type cylinder. [Online]. 2016. [Accessed 16th June 2016]. Available from: http://www.boschrexroth.com/ics/Vornavigation/Vornavi.cfm?CFID=246 15829&CFTOKEN=12218725&Language=en&Region=none&VHist=St art,p537326&PageID=p537327

A.4.   Baragetti, S. and Villa, F. Effects of Geometrical Clearances, Supports Friction, and Wear Rings on Hydraulic Actuators Bending Behavior. Mathematical Problems in Engineering. 2016, 2016, p.17.

A.5.   BSI standards. BS ISO/TS 13725:2001. Hydraulic fluid power. Cylinders. Method for determining the buckling load. https://0-bsol.bsigroup.com.wam.leeds.ac.uk/Bibliographic/BibliographicInfoData /000000000030057375: BSI, 2001.

A.6.   Timoshenko, S.P. and Gere, J.M. Theory of Elastic Stability (2nd Edition). Dover Publications. Available from: https://app.knovel.com/hotlink/toc/id:kpTESE0003/theory-elastic-stability/theory-elastic-stability

Appendix B
Hydraulic equations

For a hydraulic circuit, the flow through the circuit is controlled by the pump and the flow to and from the tank is equal assuming zero to minimal leakage. The pressure for the system reduces for each element within the system, with the peak pressure originating at the pump. The pump is a flow source and requires an enclosed volume to build pressure. These are defined in Kirchhoff's laws [B.1] and are generalised below

$$P_S - P_{atm} = (P_s - P_1) + (P_n - P_{atm}) + \sum_{i=2}^{n}(P_i - P_{i-1}) \qquad \textbf{(B.3)}$$

$$Q_{in} = Q_{out} \qquad \textbf{(B.4)}$$

Where P_S is the pressure of the source, P_{atm} is atmospheric pressure, P_i is the pressure after a restriction causing a pressure drop where there are n+1 restrictions.

The basic equation for a pump is the following [B.2]:

$$Q = D\omega \qquad \textbf{(B.5)}$$

Where Q is the flow rate, m^3s^{-1}, D is volumetric displacement, m^3rad^{-1}, and ω is the rotational speed rad·s^{-1}. Normally, the pump is driven at a constant speed, but for a pump-based system, this is incorrect.

This will include volumetric efficiency in actual components, and thus equation (B.5) becomes

$$Q = \eta_v D\omega \qquad \textbf{(B.6)}$$

Where η_v is the volumetric efficiency, typically within the 90% range.

The supply to this pump is supplied via a motor, where the power is related to the hydraulics with the following equation:

$$Power = T\omega = PQ \qquad \textbf{(B.7)}$$

Where T is the torque, Nm, and P is the differential pressure, Nm^{-2}. Which can be transposed to:

$$T = \frac{PQ}{\omega} \tag{B.8}$$

And including equation (B.6) gives:

$$T = \eta_v PD \tag{B.9}$$

The input torque will include inefficiency's, and thus equation (B.9) becomes:

$$T = \frac{\eta_v PD}{\eta_m} \tag{B.10}$$

Where η_m is the mechanical efficiency of the supply source which is also typically in the 90% range. The power required from the power supply is thus:

$$H = \frac{PQ}{\eta_v \eta_m} \tag{B.11}$$

The requirements of the system will be defined by the actuator system and thus Q and P can be viewed as vectors. These become $\vec{Q}$ and $\vec{P}$ respectively. This is due to the variation in flow requirements for the system.

B.1 Valve based system

For a valve-based system, the flow rate of all the systems is totalled for each actuator and the maximum calculated, and the peak pressure determined:

$$Q_{Tmax} = \max \sum_{i=1}^{n} \vec{Q_i} \tag{B.12}$$

$$P_{max} = \max_{1 \leq i \leq N} \vec{P_i} \tag{B.13}$$

Where Q_{Tmax} is the maximum of the sum of the flow rates, and P_{max} is the maximum pressure that the system reaches. This can be put into equation (B.11).

$$H = \frac{P_{max} Q_{Tmax}}{\eta_v \eta_m} \tag{B.14}$$

For a known cycle, for example within a factory manufacturing environment, the mean of the flow rate, $\overline{\vec{Q}}$, would be used along with an accumulator. For a cycle that varies, for example, an excavator or an exoskeleton, the use of an

accumulator is difficult to specify and might not be used. For the exoskeleton system, there are some motions that are repetitive can be defined, for example, gait motion, though for a fully flexible system, this would not be used as a defining motion.

To supply the max flow and pressure at all times, the power requirements are likely to be large. This means that the power supply will move towards either a 3 phase AC system or in the case of BLEEX, a petrol engine. Both have health and safety issues with the 3 phase AC giving an electrocution risk and the petrol engine with noise and vibration.

B.1.1 Pressure loss in control valves

Control valves have an associated pressure drop across the valve in order to control the flow. To give a designated flow rate, either the area or the pressure drop can be altered to give the targeted value.

B.2 Pump-based system

The power requirements of each of the actuators will be different, and looking at them as separate units means that the pumps can be sized to each individually. It also means that though each will require their own motor, these will be lower power and more likely to be DC supplied.

Using the equations from above, the power can be calculated from equation (B.11).

$$\vec{H} = \frac{\vec{P}\vec{Q}}{\eta_v \eta_m} \tag{B.15}$$

Where $\vec{H}$ is the power vector of the system. Though this power is likely to be lower compared to the pump based system, the torque of the electric motor is the critical value of the system. Using equation (B.15), inserting the vector of pressure,

$$\vec{T} = \frac{\eta_v \vec{P} D}{\eta_m} \tag{B.16}$$

Where $\vec{T}$ is the torque vector required.

Using equation (B.7) and equation (B.16), the rotational speed of the system can be determined.

$$\text{Power} = \vec{T}\vec{\omega} = \frac{\vec{PQ}}{\eta_v \eta_m} \qquad \text{(B.17)}$$

$$\vec{\omega} = \frac{\vec{PQ}}{\eta_v \eta_m} \times \frac{\eta_m}{\eta_v \vec{P} D} = \frac{\vec{Q}}{\eta_v^2 D} \qquad \text{(B.18)}$$

References

B.1.   Martin, H. The design of hydraulic components and systems. London: Ellis Horwood, 1995.

B.2.   Chapple, P. Principles of hydraulic system design. Chipping Norton: Coxmoor, 2003.

Appendix C

ISO buckling code

C.1 isoBuckling_f2m_SI

```matlab
function force_result = isoBuckling_f2m_SI(D1e,D1i,D2,L1,L2,L3)
%%
% % switch version
% %     case 'BLEEX'
% %         D1e = 1*25.4e-3;    % m % outside of cylinder
% %         D1i = 19.05e-3;     % m % inside of cylinder
% %         D2  = 7.04e-3;       % m % rod diameter
% %         L1  = 100e-3; % m % end of cylinder to cylinder pivot
% %         L2  = 80e-3;  % m % end of cylinder to rod pivot
% %         L3  = 20e-3;
% %     case 'bosch'
% %         D1e = 50e-3;%1*25.4e-3;    % m % outside of cylinder
% %         D1i = 40e-3;%19.05e-3;     % m % inside of cylinder
% %         D2  = 22e-3;%7.04e-3;       % m % rod diameter
% %         L1  = 100e-3; % m % end of cylinder to cylinder pivot
% %         L2  = 80e-3;  % m % end of cylinder to rod pivot
% %         L3  = 20e-3;
% %     case 'paper'
% %         D1e = 30e-3;    % [m] % outside of cylinder
% %         D1i = 25e-3;    % [m] % inside of cylinder
% %         D2  = 20e-3;     % [m] % rod diameter
% %         L1  = 1163e-3; % m % end of cylinder to cylinder pivot
% %         L2  = 1276e-3;  % m % end of cylinder to rod pivot
% %         L3  = 70e-3;
% % end
e_off_axis = 0;

E1  = 240e9; % N/m^2 % modulus of elasticity of tube
E2  = 240e9; % N/m^2 % modulus of elasticity of rod

g = 9.81; % m/s^2

I1  = pi*0.25*(D2/2)^4; % m^4 % moment of inertia of tube
I2  = pi*0.25*((D1e/2)^4 - (D1i/2)^4); % m^4 % moment of inertia of
tube

ro_1 = 7850 ; % kg/m^2
ro_2 = 7850 ; % kg/m^2

sigma_e = 448e6;

targetLoad = 15000;
safteyFactor = linspace(1,20,1000);
force_result = nan(size(safetyFactor));
for idx = 1:numel(safetyFactor)
    k = safetyFactor(idx);
    force_result(idx)                                       =
pin_mounted(D1e,D1i,D2,e_off_axis,E1,E2,g,I1,I2,k,L1,L2,L3,ro_1,ro_2,
sigma_e);
end
% figure(1)
% clf
% plot(safetyFactor,force_result-targetLoad)
```

```
% grid on

% k = safetyFactor(find(force_result-targetLoad<=0,1))
k = 1;
force_result                                                    =
pin_mounted(D1e,D1i,D2,e_off_axis,E1,E2,g,I1,I2,k,L1,L2,L3,ro_1,ro_2,
sigma_e);
end
```

C.2 force_result

```
function force_result =
pin_mounted(D1e,D1i,D2,e_off_axis,E1,E2,g,I1,I2,k,L1,L2,L3,ro_1,ro_2,
sigma_e)
% ea = e_off_axis;
% ed = e_off_axis;

coef_force_1 = 0.005;
coef_force_2 = 0.005;
counter_max = 500;

if (E1*I1)<(E2*I2)
    f_euler = pi*2*E2*I2 / ((L1+L2)^2);
else
    f_euler = pi*2*E1*I1 / ((L1+L2)^2);
end
epsilon = f_euler*coef_force_1;

force_det = critical_buckling_load(E1,I1,L1,E2,I2,L2,L3,k,epsilon);
force_a = force_det * coef_force_2;
force_b = force_det * (1-coef_force_2);

force = force_a;
sigma_a =
piston_rod_stress(D1e,D1i,D2,I1,I2,L1,L2,L3,e_off_axis,g,k,force,ro_1
,ro_2,E1,E2);
f_a = sigma_a - sigma_e;

force = force_b;
sigma_b =
piston_rod_stress(D1e,D1i,D2,I1,I2,L1,L2,L3,e_off_axis,g,k,force,ro_1
,ro_2,E1,E2);
f_b = sigma_b - sigma_e;

if f_a>=0
    force_result = 0;
elseif f_b <= 0
    force_result = force_det;
else
    counter = 0;
    force_c = force_a;
    convergence = false;
    while ~convergence
        counter = counter + 1;
        force_d = force_c;
        force_c = force_a - (force_b - force_a)*f_a/(f_b-f_a);
        force = force_c;
        sigma_c =
piston_rod_stress(D1e,D1i,D2,I1,I2,L1,L2,L3,e_off_axis,g,k,force,ro_1
,ro_2,E1,E2);
```

```matlab
        f_c = sigma_c - sigma_e;
        if (f_c*f_a)>=0
            force_a = force_c;
            f_a = f_c;
        else
            force_b = force_c;
            f_b = f_c;
        end
        if abs(force_d-force_c) <= epsilon
            convergence = true;
            break
        end
        if counter >= counter_max
            break
        end
    end

    if convergence
        force_result = force_c;
    else
        force_result = -inf;
    end
end
end
```

C.3 force_det

```matlab
function force_det =
critical_buckling_load(E1,I1,L1,E2,I2,L2,L3,k,epsilon)

epsilon_1 = 0.0001;

%%
if (E1*I1)<(E2*I2)
    f_euler = pi*2*E2*I2 / ((L1+L2)^2);
else
    f_euler = pi*2*E1*I1 / ((L1+L2)^2);
end
x_0 = f_euler * epsilon_1;
x_n = f_euler * (1-epsilon_1);

%%
nb_step = 100;
[change_sign,x_d,x_f] =
interval_change_sign(k,E1,I1,L1,E2,I2,L2,L3,x_0,x_n,nb_step);
if ~change_sign
    disp('unable to find critical buckling load')
end
%%
[x_zero,convergence] =
zero_cord(k,E1,I1,L1,E2,I2,L2,L3,x_d,x_f,epsilon);
if ~convergence
    disp('unable to find critical buckling load')
end
force_det = x_zero;
end
```

C.4 interval_change_sign

```
function [change_sign,x_d,x_f] =
interval_change_sign(k,E1,I1,L1,E2,I2,L2,L3,x_0,x_n,nb_step)
step = (x_n-x_0)/nb_step;
change_sign = false;
x_d = x_0;

equation_d = equation(x_d,k,E1,I1,L1,E2,I2,L2,L3);

for isx = 1:nb_step;
    x_f = x_d + step;
    equation_f = equation(x_f,k,E1,I1,L1,E2,I2,L2,L3);
    if (equation_d*equation_f) <= 0
        change_sign = true;
        break
    else
        x_d = x_f;
        equation_d = equation_f;
    end
end
end
```

C.5 equation

```
function eqn = equation(f,k,E1,I1,L1,E2,I2,L2,L3)
q1 = sqrt((k*f)/(E1*I1));
q2 = sqrt((k*f)/(E2*I2));
s1 = sin(q1*L1);
s2 = sin(q2*L2);
c1 = cos(q1*L1);
c2 = cos(q2*L2);

eqn = k*f*L3*s1*s2;
eqn = eqn - 3*E2*I2*q1*c1*s2;
eqn = eqn - 3*E2*I2*q2*s1*c2;
end
```

C.6 zero_cord

```
function [x_zero,convergence] =
zero_cord(k,E1,I1,L1,E2,I2,L2,L3,x_d,x_f,epsilon)

counter_max = 500;

if abs(x_f-x_d)<epsilon
    x_zero = x_d;
else
    equation_d = equation(x_d,k,E1,I1,L1,E2,I2,L2,L3);
    equation_f = equation(x_f,k,E1,I1,L1,E2,I2,L2,L3);

    convergence = false;
    counter = 0;
    x_c = x_d;

    while ~convergence
        counter = counter+1;
```

```
        x_0 = x_c;
        x_c = x_d - (x_f-x_d)*equation_d/(equation_f-equation_d);
        equation_c = equation(x_c,k,E1,I1,L1,E2,I2,L2,L3);
        if (equation_c*equation_d)>=0
            x_d = x_c;
            equation_d = equation_c;
        else
            x_f = x_c;
            equation_f = equation_c;
        end
        if abs(x_0-x_c)<=epsilon
            convergence = true;
            break
        end
        if counter>counter_max
            break
        end
    end

    x_zero = x_c;
end
```

C.7 piston_rod_stress

```
function sigma =
piston_rod_stress(D1e,D1i,D2,I1,I2,L1,L2,L3,e_off_axis,g,k,f,ro_1,ro_2,E1,E2)
[matrix,vector_data] =
linear_system(k,D1i,D1e,D2,E1,E2,e_off_axis,f,g,I1,I2,L1,L2,L3,ro_1,ro_2);
vector_solution = matrix\vector_data';
ra = vector_solution(1);
rb = vector_solution(2);
rbc = vector_solution(3);
mbc = vector_solution(4);
teta = vector_solution(5);
psi_a = vector_solution(6);
psi_d = vector_solution(7);
phi_b = vector_solution(8);
phi_c = vector_solution(9);

q2 = k*f/(E2*I2);
q2 = sqrt(q2);

c2 = -mbc+ro_2*pi*D2*g/(4*q2^2);
c2 = -c2/(k*f);
c1 = -rbc*L2;
c1 = c1 + (-mbc+ro_2*pi*D2^2*g/(4*q2^2))*(cos(q2*L2)-1);
c1 = c1 +k*f*L2*psi_d;
c1 = c1 + ro_2*pi*D2^2*g*L2^2/8;
c1 = c1/(k*f*sin(q2*L2));

terme_arctg = atan(c1/c2);

x = 0;
moment =
piston_rod_bending_moment(k,D2,E2,f,g,I2,L2,mbc,psi_d,rbc,ro_2,x);
moment_beginning = abs(moment);

x = L2;
```

```
moment =
piston_rod_bending_moment(k,D2,E2,f,g,I2,L2,mbc,psi_d,rbc,ro_2,x);
moment_end = abs(moment);


moment_int = 0;
for input = -2:0.01:2
    x = (terme_arctg + input*pi)/q2;
    if (x>0) && (x<L2)
        moment =
piston_rod_bending_moment(k,D2,E2,f,g,I2,L2,mbc,psi_d,rbc,ro_2,x);
        if abs(moment)>moment_int
            moment_int = abs(moment_int);
        end
    end
end

moment_max = abs(moment_beginning);
if abs(moment_int)>moment_max
    moment_max = moment_int;
end
if abs(moment_end>moment_max)
    moment_max  = moment_end;
end

sigma = 4*k*f/(pi*D2^2);
sigma = sigma+3200*moment_max/(pi*D2^3);
end
```

C.8 linear_system

```
function [matrix,vector_data] =
linear_system(k,D1i,D1e,D2,E1,E2,e_off_axis,f,g,I1,I2,L1,L2,L3,ro_1,ro_2)
q1 = k*f/(E1*I1);
q1 = sqrt(q1);
q2 = k*f/(E2*I2);
q2 = sqrt(q2);

matrix(1,1) = 0;
matrix(1,2) = 0;
matrix(1,3) = 0;
matrix(1,4) = 0;
matrix(1,5) = 0;
matrix(1,6) = L1;
matrix(1,7) = -L2;
matrix(1,8) = 0;
matrix(1,9) = 0;


matrix(2,1) = 0;
matrix(2,2) = 0;
matrix(2,3) = 0;
matrix(2,4) = 0;
matrix(2,5) = 1;
matrix(2,6) = -1;
matrix(2,7) = -1;
matrix(2,8) = 1;
matrix(2,9) = -1;


matrix(3,1) = 0;
```

```
matrix(3,2) = 0;
matrix(3,3) = L1 / (3*E2*I2);
matrix(3,4) = 1;
matrix(3,5) = 0;
matrix(3,6) = 0;
matrix(3,7) = 0;
matrix(3,8) = 0;
matrix(3,9) = 0;

matrix(4,1) = 1;
matrix(4,2) = 0;
matrix(4,3) = 1;
matrix(4,4) = 0;
matrix(4,5) = 0;
matrix(4,6) = 0;
matrix(4,7) = 0;
matrix(4,8) = 0;
matrix(4,9) = 0;

matrix(5,1) = 0;
matrix(5,2) = L1;
matrix(5,3) = 1;
matrix(5,4) = 0;
matrix(5,5) = k*f*L1;
matrix(5,6) = 0;
matrix(5,7) = 0;
matrix(5,8) = 0;
matrix(5,9) = 0;

matrix(6,1) = 0;
matrix(6,2) = 0;
matrix(6,3) = q1*L1 - sin(q1*L1);
matrix(6,4) = q1*(1-cos(q1*L1));
matrix(6,5) = 0;
matrix(6,6) = k*f*(q1*L1 - sin(q1*L1));
matrix(6,7) = 0;
matrix(6,8) = k*f*sin(q1*L1);
matrix(6,9) = 0;

matrix(7,1) = 0;
matrix(7,2) = 1;
matrix(7,3) = 1;
matrix(7,4) = 0;
matrix(7,5) = 0;
matrix(7,6) = 0;
matrix(7,7) = 0;
matrix(7,8) = 0;
matrix(7,9) = 0;

matrix(8,1) = 0;
matrix(8,2) = 0;
matrix(8,3) = -L2;
matrix(8,4) = 1;
matrix(8,5) = 0;
matrix(8,6) = 0;
matrix(8,7) = k*f*L2;
matrix(8,8) = 0;
matrix(8,9) = 0;

matrix(9,1) = 0;
matrix(9,2) = 0;
matrix(9,3) = q2*L2 - sin(q2*L2);
```

```
matrix(9,4) = -q2*(1-cos(q2*L2));
matrix(9,5) = 0;
matrix(9,6) = 0;
matrix(9,7) = -k*f*(q2*L2 - sin(q2-L2));
matrix(9,8) = 0;
matrix(9,9) = k*f*sin(q2*L2);

vector_data(1) = 0;
vector_data(2) = 0;
vector_data(3) = 0;
vector_data(4) = -ro_1*L1*pi*(D1e^2-D1i^2)*g/4;
vector_data(5) = -ro_1*L1*L1*pi*(D1e^2-D1i^2)*g/8 - f*e_off_axis;
vector_data(6) = ro_1*pi*(D1e^2-D1i^2)*g*q1*(-L1^2/2+(1-
cos(q1*L1))/(q1^2))/4;
vector_data(7) = ro_2*L2*pi*D2^2*g/4;
vector_data(8) = -ro_2*L2^2*pi*D2^2*g/8-f*e_off_axis;
vector_data(9) = ro_2*pi*D2^2*g*q2*(L2^2/2-(1-cos(q2*L2))/(q2^2))/4;
end
```

C.9 piston_rod_bending_moment

```
function moment =
piston_rod_bending_moment(k,D2,E2,f,g,I2,L2,mbc,psi_d,rbc,ro_2,x)

q2 = k*f/(E2*I2);
q2 = sqrt(q2);

c1 = -rbc*L2;
c1 = c1 + (-mbc+ro_2*pi*D2^2*g/(4*q2^2))*(cos(q2*L2)-1);
c1 = c1 + k*f*L2*psi_d;
c1 = c1 + ro_2*pi*D2^2*g*L2^2/8;
c1 = c1/(k*f*sin(q2*L2));
c2 = -mbc+ro_2*pi*D2^2*g/(4*q2^2);
c2 = -c2/(k*f);
c3 = -ro_2*pi*D2^2*g/(8*k*f);
c4 = rbc-k*f*psi_d;
c4 = c4 / (k*f);
c5 = -mbc+ro_2*pi*D2^2*g/(4*q2^2);
c5 = c5/(k*f);

y = c1*sin(q2*x)+c2*cos(q2*x)+c3*x^2+c4*x+c5;

moment = -ro_2*pi*D2^2*g*x^2/8;
moment = moment + (rbc-k*f*psi_d)*x;
moment = moment - mbc;
moment = moment - k*f*y;
end
```

Appendix D

Customer Needs in the Exoskeleton Project

(modified for thesis)

No.	Need	Unique Identifier
	The device shall be an upper-body exoskeleton.	N-1
	The kinematic design of the frame shall allow the device to perform activities specified in Appendix E.	N-2
	The frame shall be adjustable for different user size.	N-3
	The frame shall be modular.	N-4
	The joint and the actuator for each DOF shall be a separable module.	N-5
	The primary product shall be untethered, i.e. energetically independent.	N-6
	The load-carrying capacity shall be the maximum achievable amount (90kg), considering safety.	N-7
	The system shall be able to sense human motion (kinematics and dynamics).	N-8
	The device shall be easy to use.	N-9
	The device shall be easily adaptable to a new user.	N-10
	The device shall be safe.	N-11
	The device shall be reliable.	N-12
	The device shall be weight-efficient.	N-13
	The power consumption of the device shall be efficient.	N-14
	The operation (as explained in Appendix E) duration time shall be long.	N-15
	The system shall be cost-effective.	N-16
	The appearance of the device shall be acceptable.	N-17

	The user shall not be burdened with any extra effort to carry the exoskeleton (while not carrying any payload).	N-18
	The device shall comply with BS EN ISO 13482:2014.	N-20
	There shall be a feasible maintenance scheme in place.	N-21
	The device should decrease the metabolic cost of the load-carrying task.	N-23
	The actuators of the device should be dynamically strong enough to perform activities specified in Appendix E except for running.	N-24
	The device should not impede movements.	N-25
	The device may be clean.	N-26
	The device may be easily put on and off by the user without any assistance.	N-27
	The Type 1 variation of the device may be possible to achieve via modular changes (low cost, assistive, with the minimum possible actuators).	N-29
	The Type 3 variation of the device may be possible to achieve via modular changes (lower limb with a backpack frame, enhancive).	N-30
	The Type 5 variation of the device may be possible to achieve via modular changes (lower limb exoskeleton, hung from a frame or the ceiling, used for rehabilitation).	N-31
	The design should allow for subsystems of the product to be used as orthotic devices.	N-32

Activities to be performable by the device

(modified for this thesis)

No.	Activity	Unique Identifier
	Walk on level ground forwards	NA-1
	Pick up a load from the ground (deadlift)	NA-40
	Pick up a load from the ground (stiff legs)	NA-41
	Opening doors	NA-42
	Turning valves horizontally	NA-43
	Turning valves vertically	NA-44
	Walk on level ground with load[13] forwards	NA-11
	Walk on level ground with load backwards	NA-45
	Walk on level ground whilst crouching with a load	NA-53
	Turning 90 deg with load whilst walking	NA-46
	Walk on rough terrain with a load	NA-12
	Run with load	NA-13
	Walk up the stairs with a load	NA-16
	Walk up the slopes with a load	NA-17
	Walk down the stairs with a load	NA-18
	Walk down the slopes with a load	NA-19
	Lift load above shoulder height and hold	NA-22
	Walking forwards whilst holding load above the head	NA-52
	Lift load to shoulder height from hip level	NA-54
	Horizontal push on a flat surface walking forwards	NA-25

[13] 3 different shapes of load: 1) large – 120 cm x 80 cm x 80 cm empty cardboard box, 2) medium – 61 cm x 46 cm x 46 cm empty cardboard box, 3) cylindrical – 30 cm in diameter x 1 m long empty cardboard box

	Horizontal pull on a flat surface walking backwards	NA-26
	Horizontal push on an inclined surface walking forwards	NA-48
	Horizontal pull on an inclined surface walking backwards	NA-49
	Upper extremities ranges of motion (moving arms freely)	NA-50
	Swing arms from above the head downwards holding a cylindrical object ending at hip level.	NA-55
	Pull up	NA-51

Types of devices

TBD

Deviations from the needs in the prototype

Object Identifier	Need	Comment
N-20	The device *may* comply with BS EN ISO 13482:2014.	Taking into consideration requirements imposed by the norm, achieving full compliance with it is beyond timeframe for building a prototype. Safety-related sensory system and algorithms seem still to be viable fields of innovation.

Appendix E

Product Requirements in the Exoskeleton Project

Need (N-*X*)	Metric	Unit	Priority[14]	Marginally acceptable Value	Ideal Value	Unique Identifier
7	Mechanical Strength (weight of the user and load)	kg	1	45 (50% over average human)	90 (200%)	M-1
2	Possible manoeuvres	-	1	Appendix D to Customer Needs	Appendix D to Customer Needs	M-2
4, 29, 31, 32, 30, 5	List of separate modules	list	1 (TBD)	lower body with spine, upper body exoskeleton	each motor, each link, each joint	M-4
3	Adjusting features	list	1	limbs length, trunk length	limbs length, trunk length	M-5
26	Cleanliness	subj.	3	no fume	no by-products of energy production	M-7
6	Untethered	-	1	tethered	untethered	M-8
13	Weight	kg	1	68	21	M-13

---

[14] Where '1' is the highest priority and higher natural numbers represent lower priorities

14	Power consumption	W	1	lowest possible considering the other requirements	lowest possible considering the other requirements	M-14
15	Operation duration	minute	1	1 h	2h 40 min	M-15
16	Price	£, $, €	1	$30k	$10k	M-16
17	Appearance	subj.	1	not a concern	socially acceptable	M-17
10	Ease of control system adaptation	-	1	1 - 2 Week	wear-and-use	M-19
18	Endurance augmentation (decrease of metabolic cost) without load.	%	1	no excessive burden	5-12% without load, 15 with 36.7 kg (at 2MPH)	M-20
21	Maintenance scheme feasibility	subj.	1	once/week (periodic check and operation hours)	once/year	M-21
23	Endurance augmentation (decrease of metabolic cost) with maximum load.	%	2	actuation system rated not to decrease the metabolic cost	0% no decrease in measured metabolic cost	M-24

8	Human motions sensed	list	1			M-25
9	Ease of use	subj.	1	trained users can use the exoskeleton	any user can naturally move within the exoskeleton	M-26
12	Reliability	subj.	1	reliable	reliable	M-27
11, 25, 2	Ranges of motion of joints	rad	1 (TBD)	as required by the manoeuvres listed in Appendix D	full human range	M-28
20	Standard BS EN ISO 13482:2014 compliance	subj.	1	not-compliant	compliant	M-30
21	Maintainability	subj.	1	maintainable by technician	maintainable by a technician	M-31
27	Ease of putting on and off	min. , subj.	3	additional 1 person to aid the user	no help required from another person	M-33
9, 10	Time to learn to operate the device	h	1	one week training	immediate	M-37
2	Size of the longest dimension	m	1	100% of the average human	25% of the average human	M-38

	increase of the system					

Appendix F

Motion Data

Shoulder FlexionData
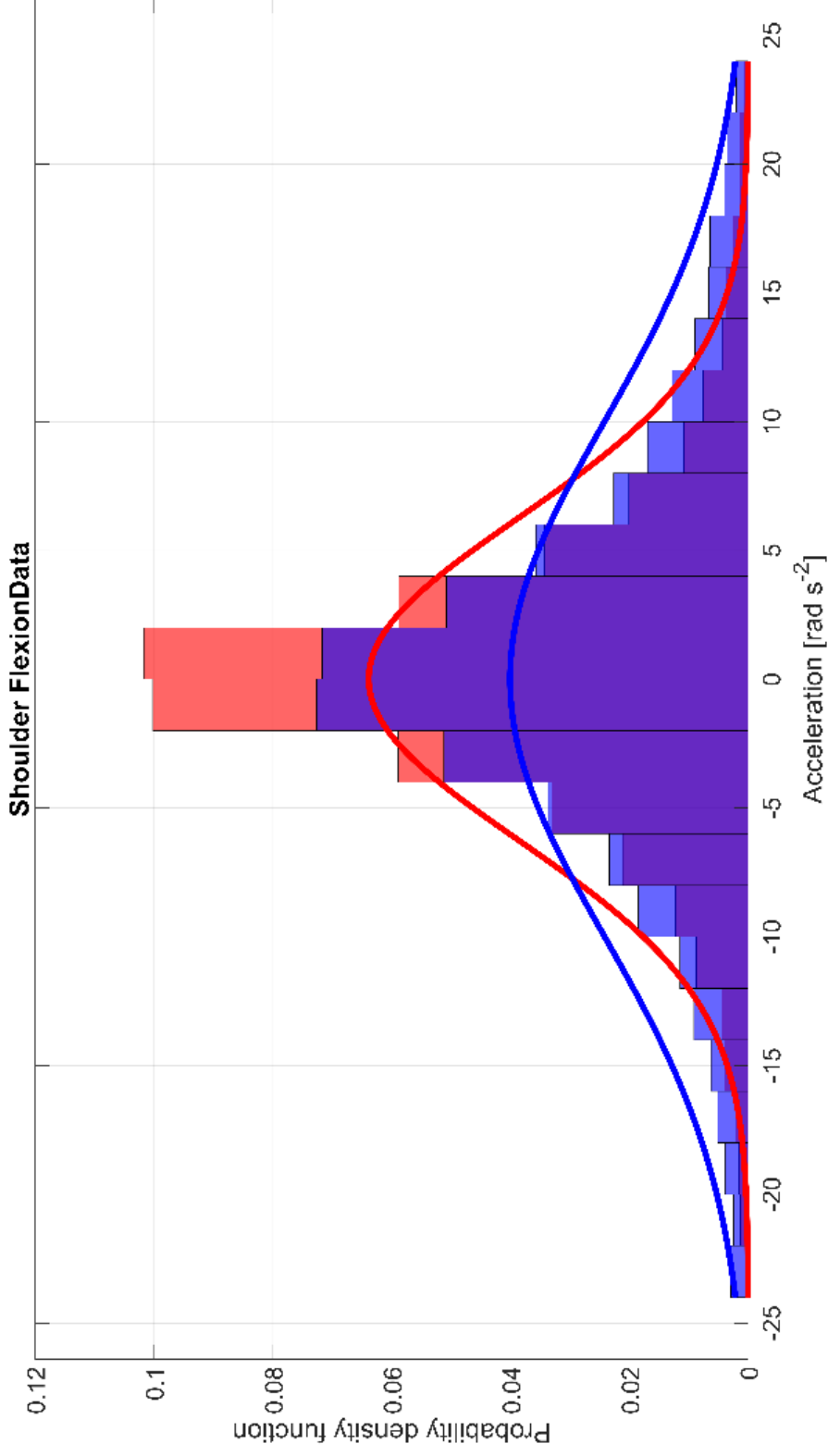
Figure F.1: Probability density function of the acceleration for the shoulder flexion for a range of motions
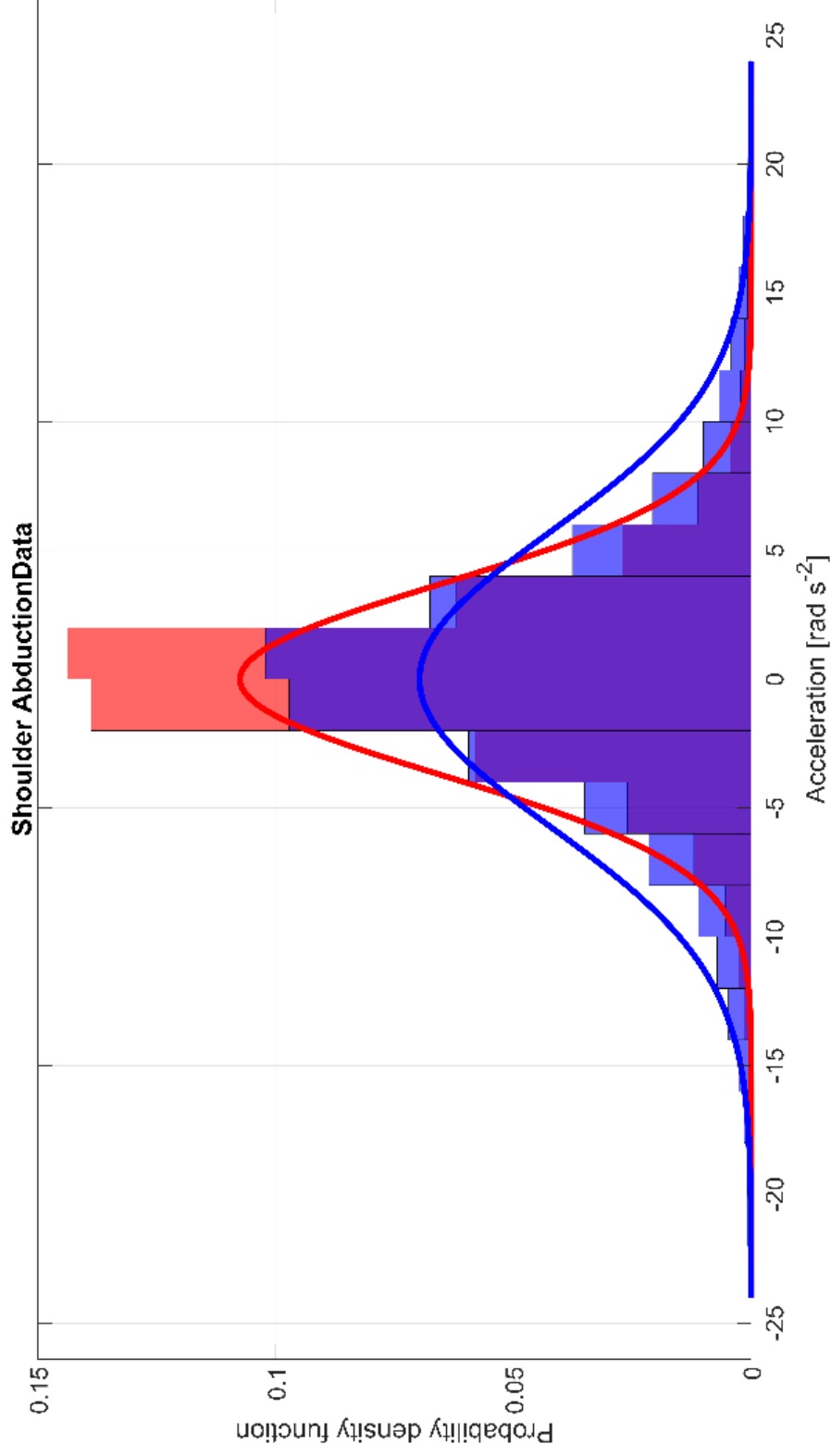
Figure F.2: Probability density function of the acceleration for the shoulder abduction for a range of motions
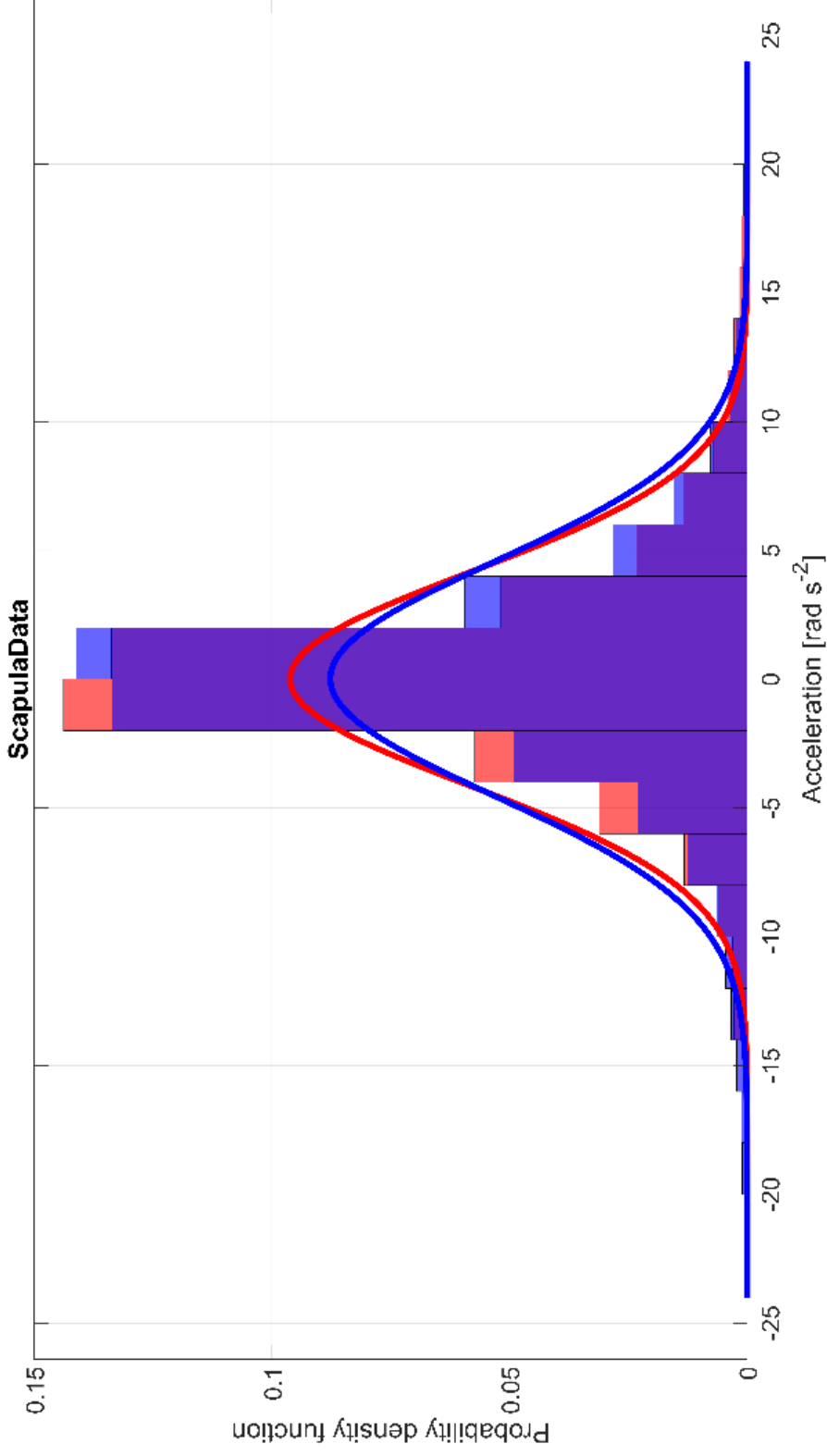
Figure F.3: Probability density function of the acceleration for the scapula joint for a range of motions

Appendix G
Single joint initial development

G.1 Introduction

As part of the team project work, an initial prototype was required to allow the development of other students PhDs. A single joint setup was therefore decided upon to allow a collaborative development platform.

This work was completed at the start of the PhD and thus the system did not include any of the optimisation techniques within the rest of this thesis.

G.2 Initial Single Joint

The initial simulation and design work is focused on a single joint with one degree of freedom. The knee was selected for this, as it is a major joint and the focus of many exoskeleton systems.

G.3 Initial designs

Linear actuators power the majority of hydraulically powered exoskeletons. BLEEX uses a single hydraulic actuator under the thigh for the motion of the knee, whilst SARCOS uses opposed cylinders around a pulley system. Both have demonstrated the ability to walk, though squat motion data is limited. BLEEX has documented intentions for a powered squat, though no video evidence exists for this. A single image from a thesis on BLEEX [G.1], Figure G.1, shows the intention, though this is from initial design work rather than a powered unit.

Figure G.1: Mock-up design for the BLEEX system showing squat motion [G.1]

For a squat, avoiding singularities becomes an issue due to the range of motion of the knee. With a varying angle of force, there are points within the cycle where the available torque reduces. Examining the BLEEX system, it can be seen that there are areas where the max torque reduces [G.1], especially towards the limits for the actuator. For a squat with lift motion, this could be a critical issue as the initial force will be high to start motion. Determining the torque output is also dependant on the extension of the actuator, due to the changing moment arm. SARCOS does not have issues with displacement dependent torque, as the moment is put directly into the joint rather than via lever arms.

G.3.1 Initial calculations

Using BLEEX as an initial starting point for the design, allowing full movement of the joint to allow squatting is critical. According to BLEEX documentation, it can allow 121° of motion [G.1] whilst according to human anatomy the knee can rotate up to 150° [G.2]. This will be an issue with squatting if the person is limited in the downward motion. To allow the full range of motion, the actuator has to have a larger travel, as well as be located such that singularities cannot exist.

Using standard human anthropomorphic data [G.3, G.4], outlined in Table G.1 [G.3], and initial sizing can be generated. The tibial height is defined as the *"vertical distance from the floor to the tibiale"* and the iliac spine height as the *"vertical distance from the floor to the anterosuperior iliac spine (the most downward-directed point of the iliac crest)"* [G.3]. These have been used to give the location of the knee and hip joints with the difference being the length of the thigh.

Table G.1: Anthropomorphic data from BSI standards [G.3]

	4.1.6 Iliac Spine Height			4.1.8 Tibal Height			Estimated Thigh Length		
	5%	50%	95%	5%	50%	95%	5%	50%	95%
Japan	842	912	982	387	421	457	455	491	525
Kenya	833	920	1027	406	457	500	427	463	527
Korea	832	914	990	397	438	480	435	476	510
Thailand	849	915	995	410	452	498	439	463	497
Average	839	915	999	400	442	484	439	473	515

As the exoskeleton is modular for all users within the 5th-95th percentile, the exoskeleton limbs lengths have been set to the 95th percentile to give an anthropomorphic design, with the system becoming less so as the percentile reduces. Figure G.2 shows the shin and thigh, blue and red respectively, of the 50th percentile male user with the exoskeleton shin and thigh, green and black, the 95th percentile male user. The system was simulated to give the full 150°

of knee motion with the corresponding motion of the exoskeleton plotted. The shin of the human is fixed, showing the range of motion of the exoskeleton joint in relation to this.
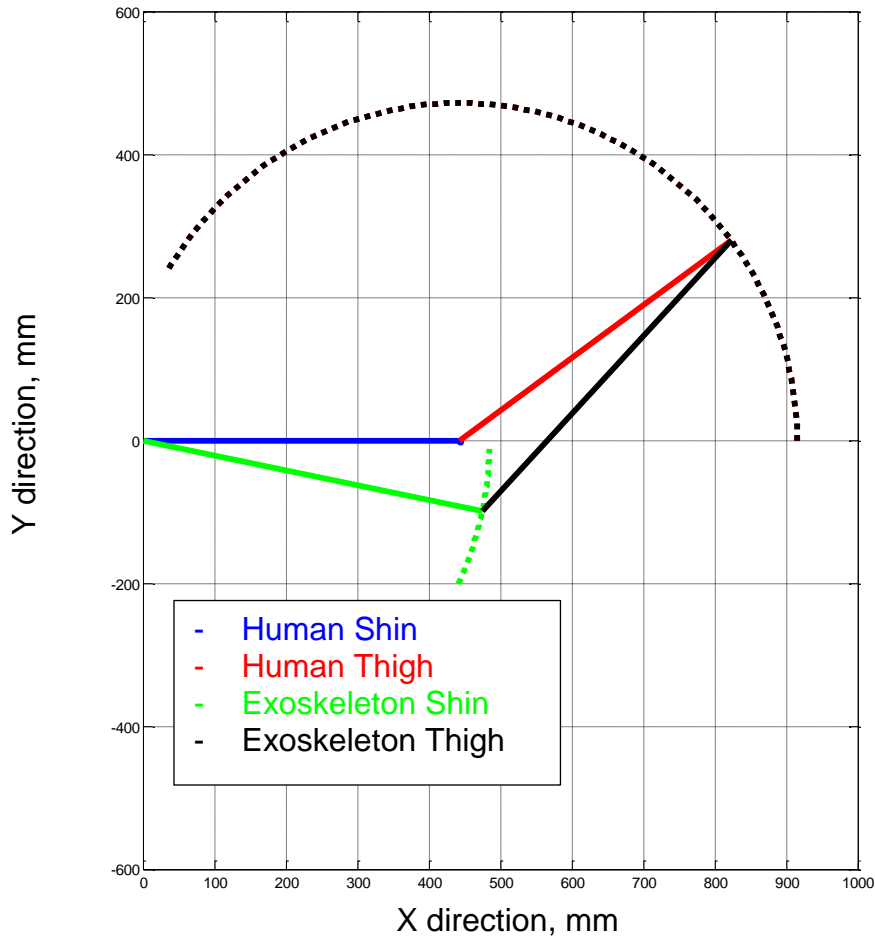
Figure G.2: Motion range of leg (blue and red) with attached Exoskeleton leg (green and black)

Putting together a simple simulation of the BLEEX design with the current dimensions and giving the actuator fixing offsets of 100mm from ankle and hip, and 50mm from the exoskeleton itself to allow mounting clearance, the initial results are shown in Figure G.3. The top left figure is the motion of the unit as per Figure G.2, with the user leg shown in blue and the exoskeleton in red. The green lines are for the ends of the connectors with black being the actuator. The knee angle versus actuator length shows that there needs to be a range of around 150mm of travel for the actuator to allow squat motion, which is fifty per cent larger than that of BLEEX value of 101mm. For the moment arm, lower left plot, it can be seen that there is a large range with a singularity near 145°

meaning that the system could not completely squat. This is an initial model, and optimisation could be used to improve the results.
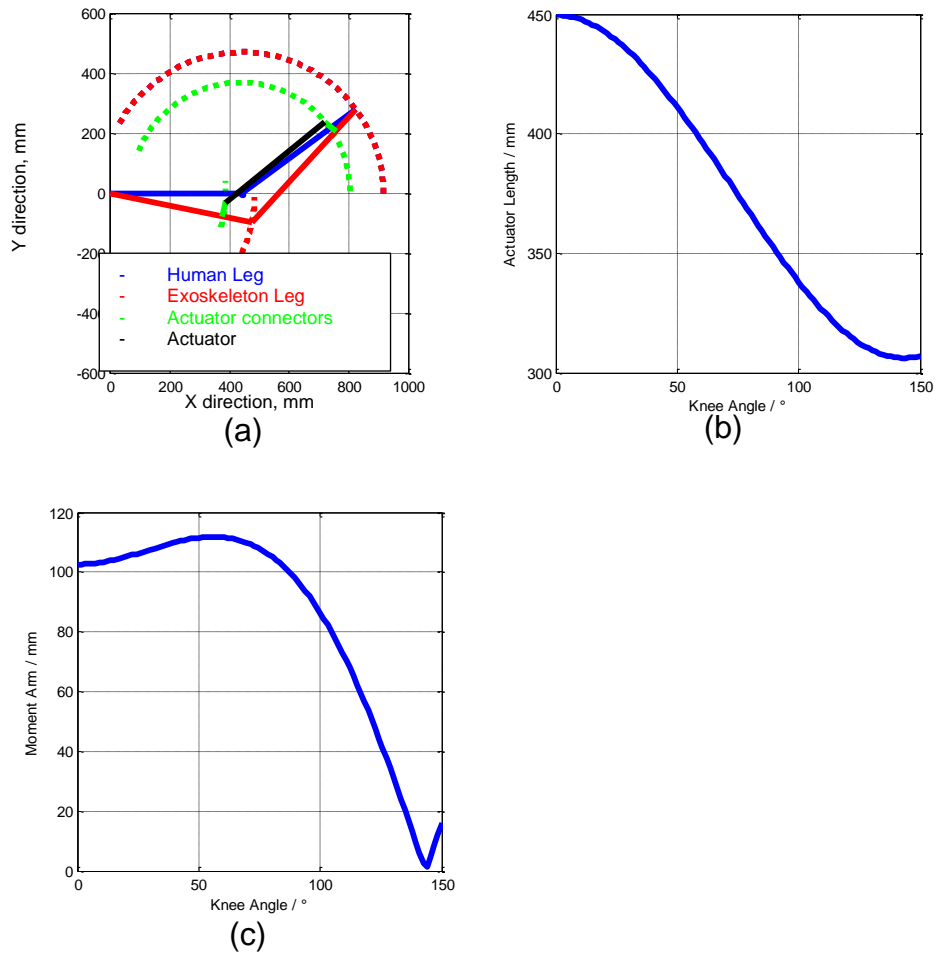
Figure G.3: Simple BLEEX setup
a) outline of joint and actuator, b) knee angle versus actuator
length, c) knee angle versus actuator moment arm

One location of the joint that could be utilised is the top of the thigh and shin with a patella to transfer the motion. This is based on human anatomy, though has additional benefits. With two cylinders, the speed of the system could be half of that of the single joint unit. It also means that the moment arms will vary less, as the cylinders will lie close to parallel to the limbs. It also allows additional protection of the knee joint, similar to a human patella.

Doing a similar simulation on an initial design, where the actuator is set 300mm from the knee joint, and offset 50mm as per the BLEEX, there are several improvements to the displacement and moment arm, Figure G.4. The top left figure shows the motion range, with the bottom right showing a close up of the

patella setup. The knee angle versus actuator length shows only 40mm of travel, greatly reducing the overall length of the actuator, as well as giving the option for greater speeds. The moment arm also reduces with increasing angle, though there is no singularity and only reduces by 18mm, which means that calculating torque is easier. The moment arm is lower than the BLEEX design thus requiring larger actuators to give the same torque, but as force is related to a square law of diameter of the piston, this should be within reasonable limits.
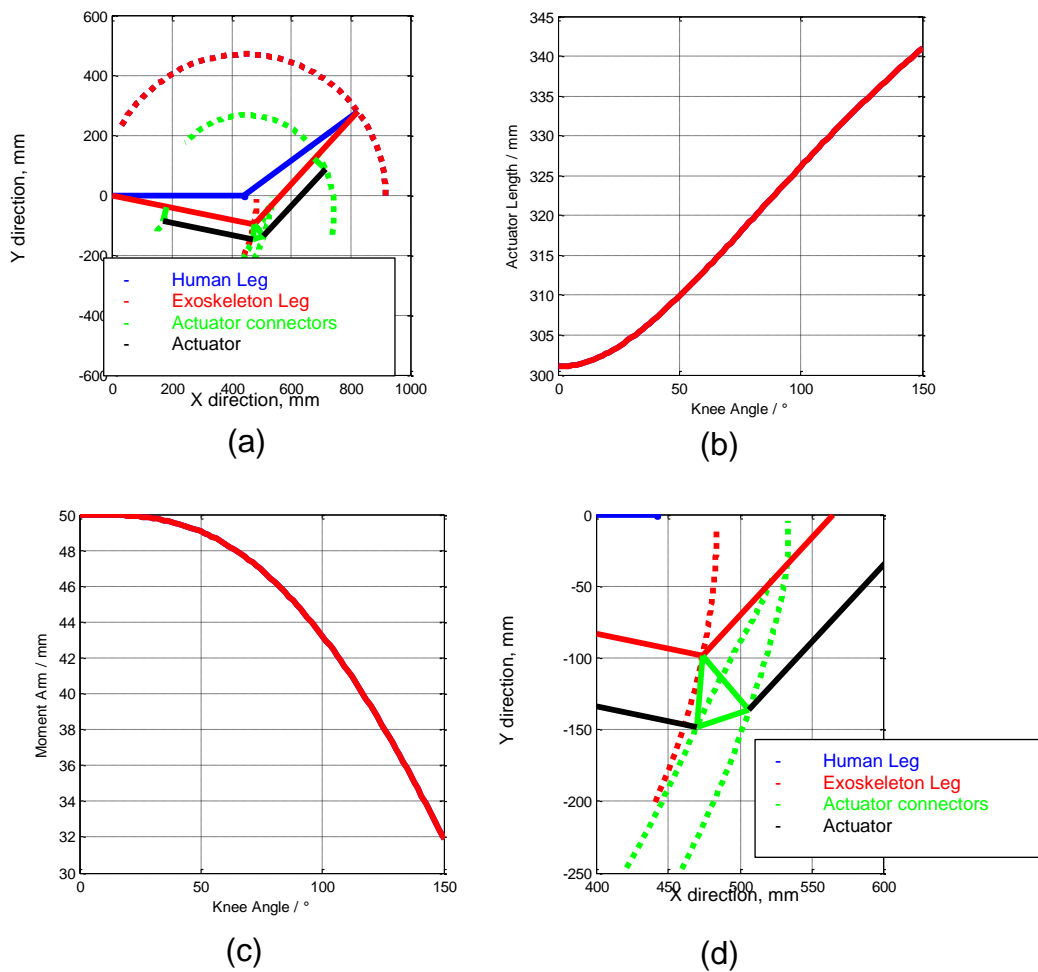
Figure G.4: Simple patella setup
a) outline of joint and actuator, b) knee angle versus actuator
length, c) knee angle versus actuator moment arm, d) close up of
knee joint

SARCOS uses four opposed cylinders, which are single-acting though the sizes of each do not need to be equal to allow different torque and flow requirements dependant on the actuator [G.5]. BLEEX has a single-cylinder with motion such that the largest area of the cylinder is in the direction of extension. With the

patella design, the units are extending the leg with the smaller area, thus requiring larger cylinders or higher pressure.

G.3.2 Initial Sizing

Using a hydraulic system requires a balance of pressure versus flow rate. With a smaller piston, the flow rate is reduced, though it requires higher pressures to give the same force. This is also balanced against the buckling force that the actuator can resist. With the worst-case scenario of having the user starting to stand from a seating position, as this gives the largest moment arm for the downward load, an initial sizing of the actuator can be determined. Figure G.5 shows this graphically.

(a)

(b)
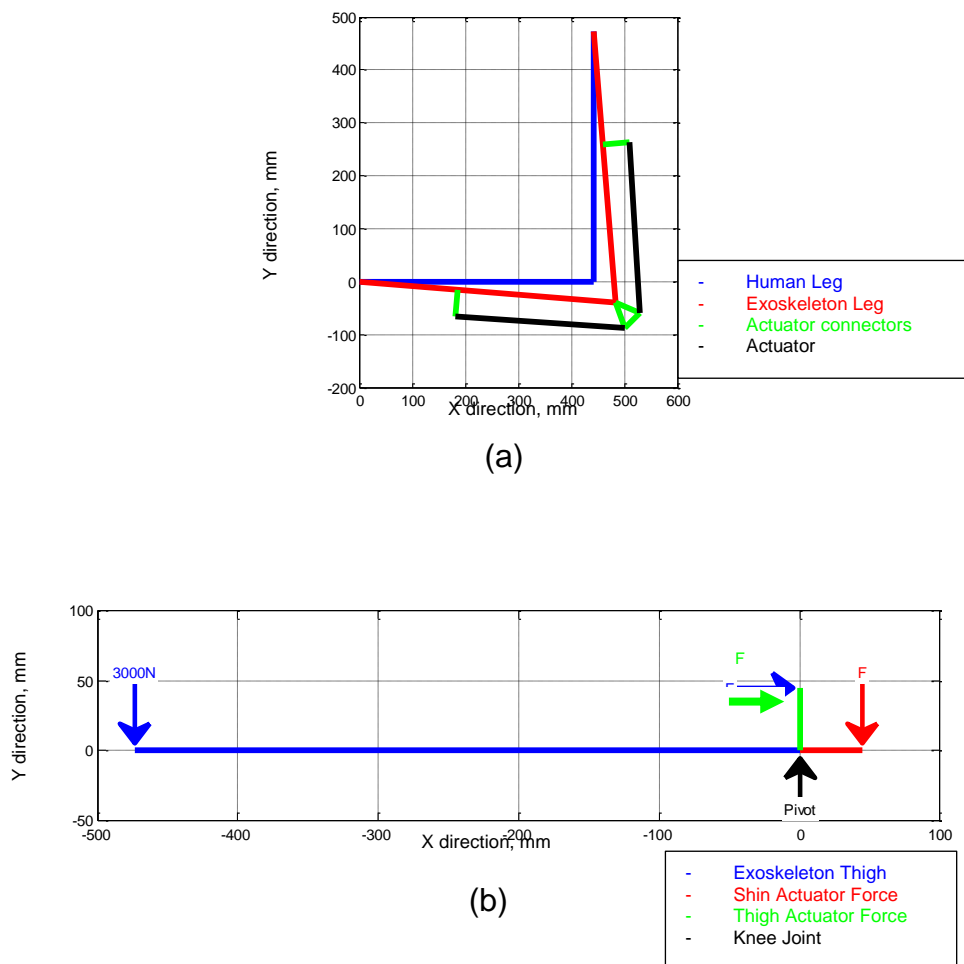
Figure G.5: Simple outline of force required
a) diagram of the patella knee joint, b) force balance of the patella

With a downward force of the exoskeleton, user and load, L is 3000N acting at the distance T of 473mm. This is based on the user carrying 120kg of mass

and the exoskeleton weighing 180kg. The compensating force from the actuator can be simplified to a downward and horizontal force F, H acting at distance d of 44.9mm. This can be written down in the following equations

$$L \times T = 2 \times F \times d \qquad \qquad \text{(G.19)}$$

$$\frac{L \times T}{2 \times d} = H \qquad \qquad \text{(G.20)}$$

$$\frac{3000 \times 0.473}{2 \times 0.0449} = 15802N \qquad \qquad \text{(G.21)}$$

With the force determined, this can then be looked up with different manufacturers' tables to determine the required size of the actuator. For example, using Miller Fluid Power HV2 series documentation [G.6], the stroke factor is 2, Appendix I. This is then multiplied by the actual stroke to give the basic length. As Miller is an American company, the units are imperial, so the basic length is 8 inches, and 16kN is converted to 3597lbf. This is then looked up on Figure G.6 to give the required rod diameter
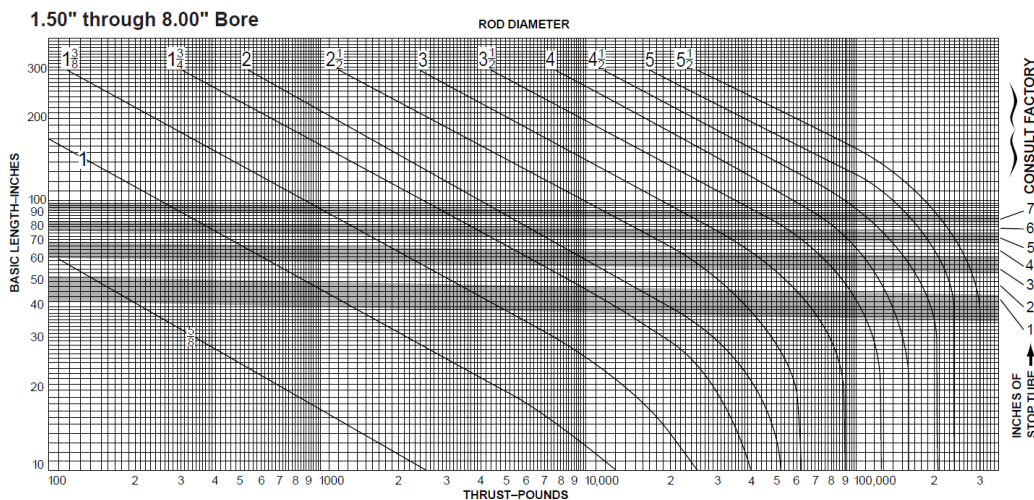
Figure G.6: Force versus extension to give the required rod diameter [G.6]

This gives the initial rod diameter to be one inch, which can then be looked up regarding cylinder bore diameters. The sizes available are 1.5", 2" and 2.5" for a rod of 1" according to Miller available units for HV2 series [G.6]. Determining which size is viable depends on the flow rate and force required for the system, though compared to BLEEX with around 20mm for the cylinder size; the initial

calculations show that this design will be larger than that. This would be due to the focus on having a larger carrying load than BLEEX.

G.4 Simmechanics™ simulation

The initial exoskeleton was been transferred to Simmechanics, a simulation package developed by MathWorks®, with a human skeleton attached to the inside to the proposed fixed locations. This skeleton has human motion data applied to it, and the motion of the exoskeleton to match this input is recorded. This is fed back into the simulation to move the exoskeleton itself to give force requirements of the system. This does require two simulation cycles, with human data being used to generate exoskeleton motion and then this being used to determine force requirements.

With the motion and force requirements, the actuator and pump can be further refined. With a larger cylinder to resist buckling of max force input, this requires a larger flow supply. The simulation also gives the simulated force output, though determining whether these cover all eventualities is important. The buckling calculations will already include a safety factor so increasing the estimated force with another would end up with the cylinder being significantly larger than required.

G.4.1 Simulation construction

Simmechanics has an optional small program that can be attached to a CAD package like Solidworks. This allows the user to directly extract the design and insert it into the simulation environment. This converts the CAD files into STL formats[15] so that they can be visualised as well as determining the joint and mass properties.

This is not a perfect transfer with additional joints and limitations being transferred to the simulation environment. For example, the skeleton within the CAD model was joined together with balls as per the export from the motion capture software. This was converted into Simulink as a sphere joint where the input is a single data stream. The data from the motion capture is based on the planes of the human body; sagittal, coronal and transverse and thus the joint

---

[15] Latest versions of MATLAB include direct Solidworks part importing

needed to be converted into a gimbal joint. This also allows the locking of an axis such that motion is limited in that one plane.

Each component within the exoskeleton CAD model is transferred to Simmechanics, and thus each has a mass associated with it. This is modelled with a solid component of Simmechanics with links to fixture points, as in Figure G.7.
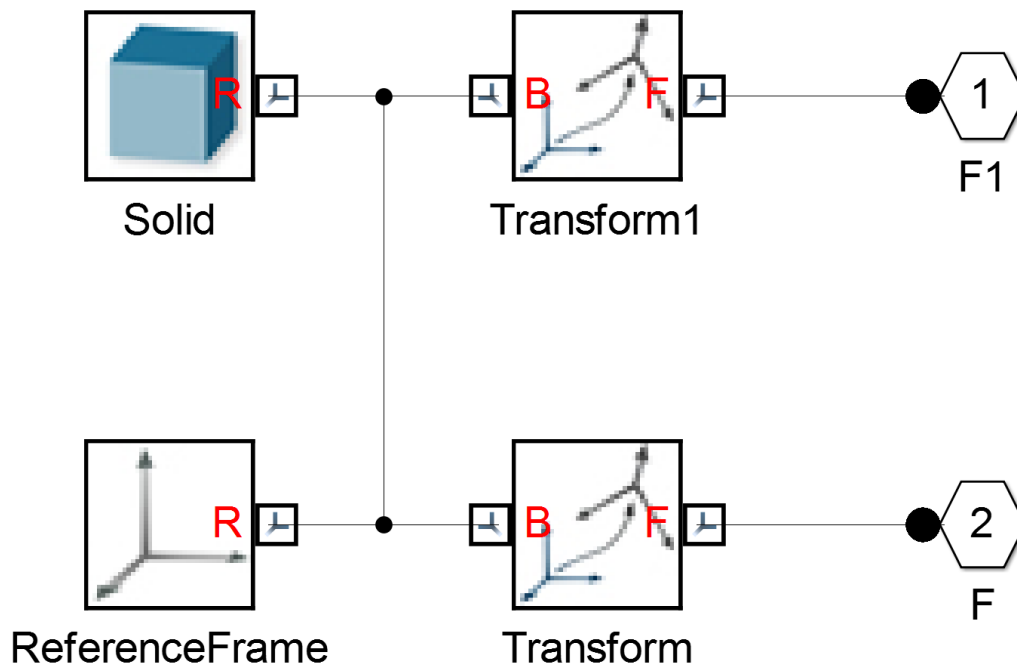
Figure G.7: Simple object block from SimMechanics

There are several joint types within Simmechanics, with the majority of the joints of the exoskeleton being revolute joints. The hydraulics are modelled with prismatic joints and currently, do not have any data associated with the actual hydraulics components. This will be analysed outside of the simulation, and eventually with a hydraulics model within the simulation itself.

With Simscape™ models, MathWorks recommends using either ode15s or ode23t [G.7]. Ode15s is a stiff solver and has low to medium order of accuracy though damps oscillations. Ode2t is moderately stiff and has a low order of accuracy, though does not damp oscillations. For the initial simulation, ode15s was selected to give a quick response though with the introduction of hydraulics, the frequency response will become more important and possible oscillations will be critical.

G.4.2 Simulation outputs

The simulation once built calculates all of the joints and motions, though only the knee joint data is extracted at the current time for the single joint focus. The force and motion are the two variables of focus, though need to be converted into pressure and flow to allow actuator and pump selection.

The pressure is simple to calculate based on the actuator dimensions, though is the differential pressure rather than the true pressure on either side of the piston head. This also means that the actual pressure will be higher from the system. This will require additional simulation determination with a hydraulics package to determine pressure losses from components. Whether the force is extending or retracting also effects the required pressure due to the difference in areas either side of the piston. Similar to the pressure, the flow requirements is also a simple calculation with the actuator dimensions and can be plotted. With the pressure and flow known, these can be plotted against each other to determine the required pump characteristics.

For certain events of the system, the pressure required and direction of travel might not be in opposition to each other. This could, therefore, be seen as a braking motion rather than a driving motion. For example, the squat motion, the lowering of the body needs to be controlled, but no force is required as gravity is pulling the exoskeleton down. This controlled flow can, therefore, be used to generate power back into the system. The distribution of driving to breaking events and the efficiency of the system can be calculated to determine the motion power usage. This is dependent on the circuit design.

G.4.3 Gait without floor contact

The initial simulation was modelled with gait motion, but without ground contact forces, including 90kg of carrying load. The basic results are outlined in Figure G.8. It can be seen (a) that for this gait motion, there is a requirement
for nearly 10kN of force for the gait motion. This also corresponds to about 20mm of travel of the cylinder. BLEEX, according to [G.1] has 100mm of travel for full motion. To give full angle motion, only 80mm of travel is required for the patella design per actuator, so is technically longer travel than BLEEX with two actuators.

Putting the data onto the actual actuator size, the pressure requirements, (b), can be determined as well as the flow requirements, (c). The pressure does

reach up to 150bar, though this does not take into account the pressure on the retracting side of the actuator. The velocity is converted into the flow requirements of the cylinder with around 8L/min required for parts of the cycle. This can be plotted against each other to assist with pump selection, (d), as has been compared to several pumps available.

For the power recovering options, e and f, this would give energy recovery for 38% of the cycle. This means that power recovery is an option for the gait cycle.
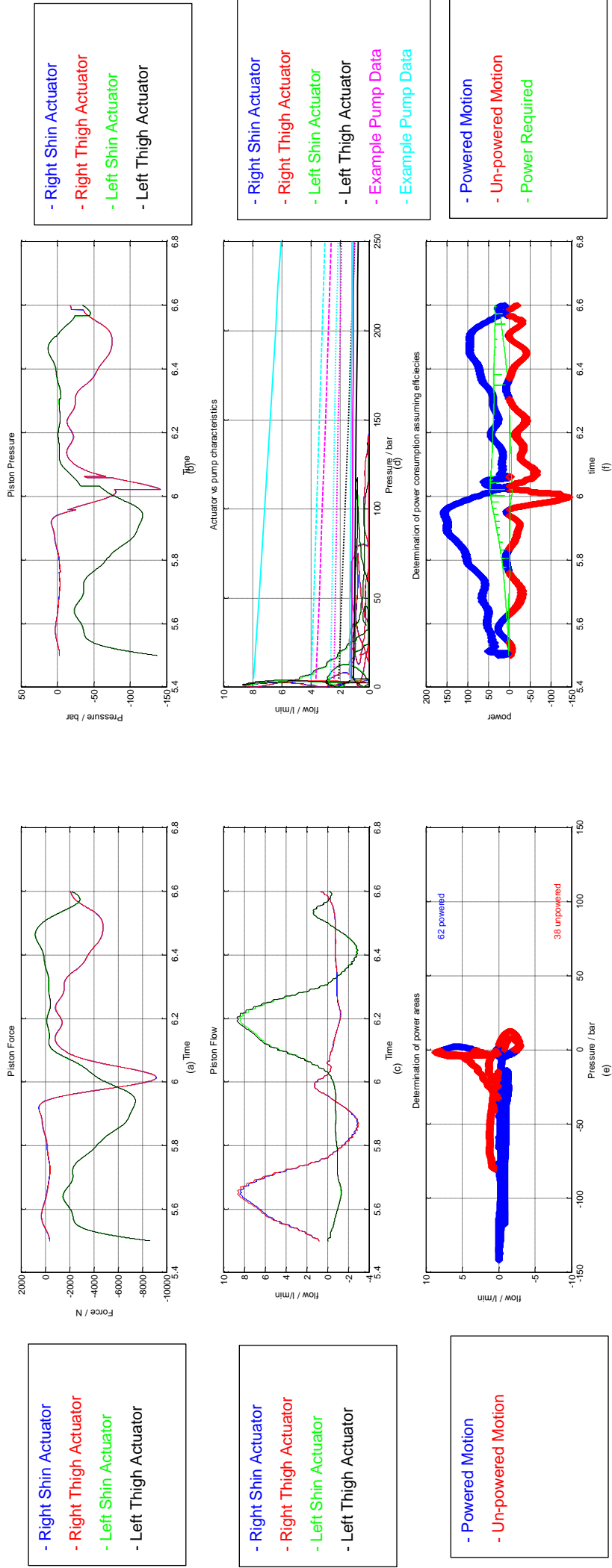
Figure G.8: Outline of simulation results for gait without floor contact

a) Actuator force required, b) pressure of cylinder, c) flow requirements, d) pressure versus flow, e) pressure versus force to determine power requirements, f) power determination

G.4.4 Gait with floor contact

The analysis applied to the gait without floor contact can also be applied to a system that attempts to mimic the floor contact. This allows shock loads to be simulated and understood.

Figure G.9 shows that while the motion is the same, the force required has large peaks and wave within it, (a). This is due to limited damping in the model generating shockwaves up the leg and transferring to the cylinder. This needs to be corrected within future simulations. As the peaks are of magnitude larger than the base signal, these have been suppressed.

The flow requirements, (c), is the same as without floor contact as this does not change with the forces, as it is motion-based.

The power requirements, (e), show that 57% is unpowered, which is significant for power recovery. If the system is assumed to be 90% efficient for power into and power out of the system, the cycle residual power can be calculated. This is around zero overall power requirements which means that the power usage could be very little, (f).

G.4.5 Squat with floor contact

With the squat motion, the force and velocity requirements are reduced as both legs are used in the motion at a slower speed. The only critical requirement is for the displacement allowance of nearly 50mm of travel. This means that the motion required for the squat is similar to the total allowed motion for the BLEEX system, but with two cylinders, the flow requirements per unit is halved. This is important for an EHA based design, though limited for a valve-based design.

The results, Figure G.10, show that the cylinder pairs give different force requirements, (a), though the piston flow is the same, (c). This means that the piston pressure is different depending on the orientation of the cylinder. This needs to be understood so that the control system can work correctly.

The flow and pressure requirements are lower than that of the gait motion, and thus dynamic modelling will need to focus more on that motion. The gait has a larger motion range requirements and thus is the design issue for the cylinder length.

Similar to the gait motion with contact, the power requirements dependant on motion means that 58% is unpowered as it is a controlled descent, (e). The overall power requirements are nearly balanced (f).
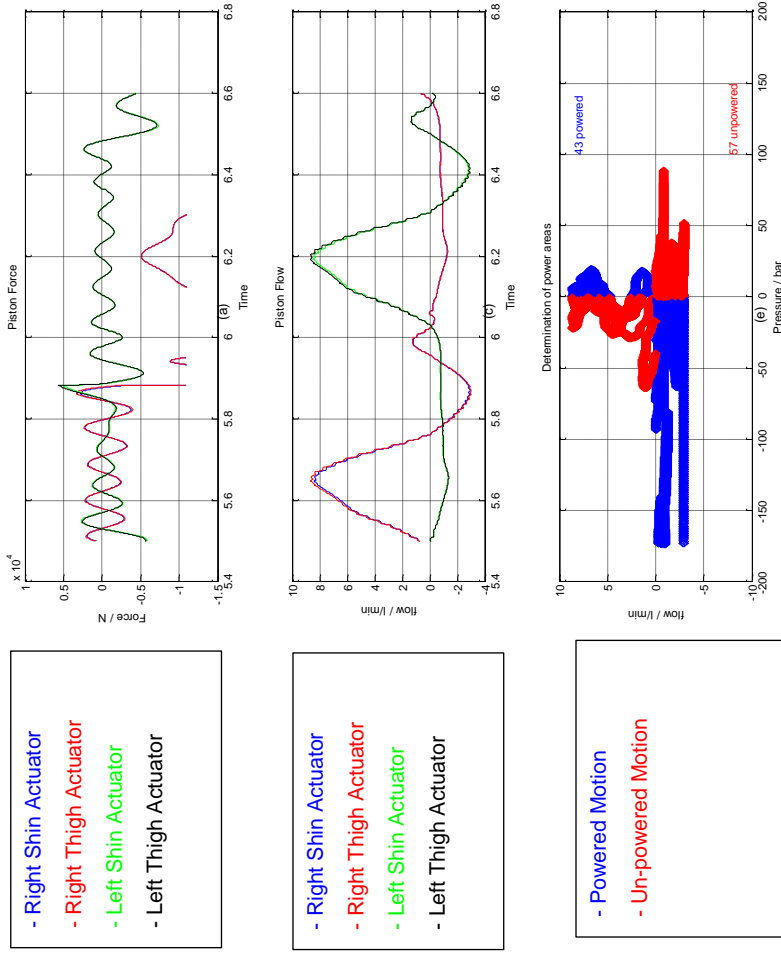
Figure G.9: Outline of simulation results for gait with floor contact

a) Actuator force required, b) pressure of cylinder, c) flow requirements, d) pressure versus flow, e) pressure versus force to determine power requirements, f) power determination
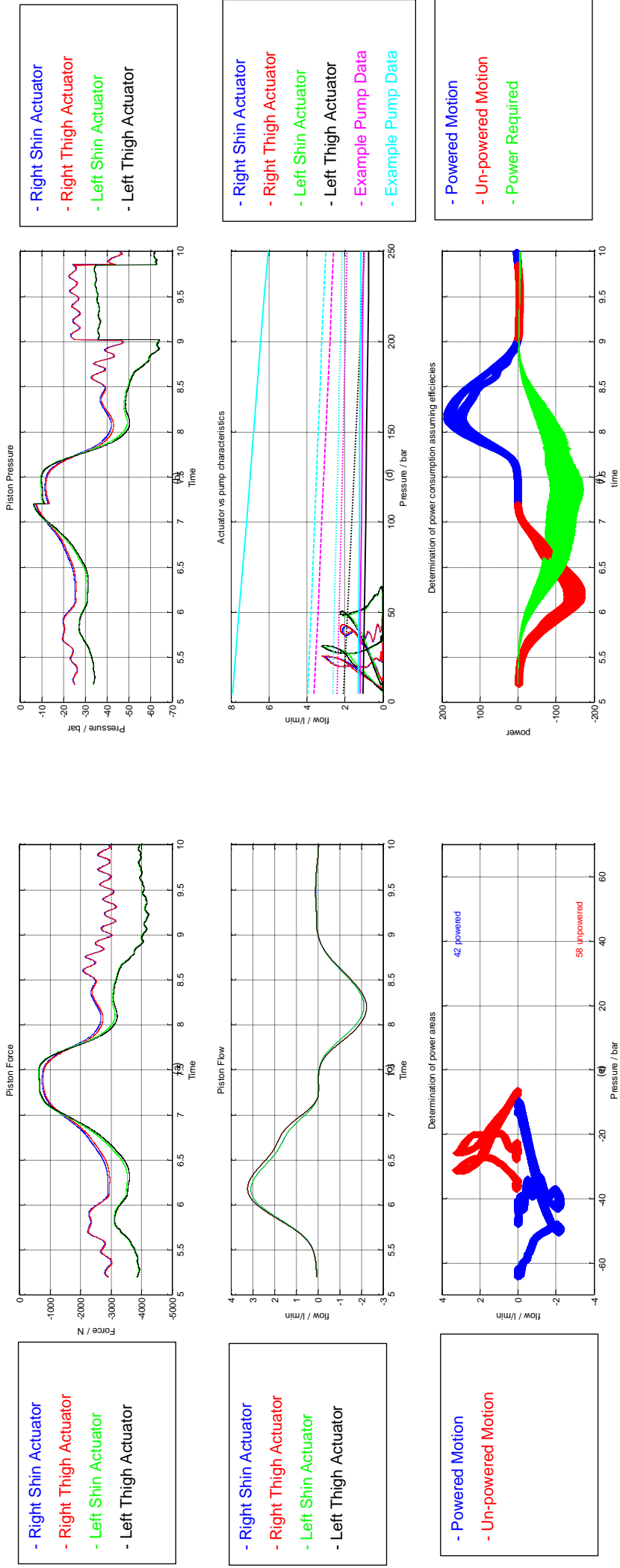
Figure G.10: Outline of simulation results for squat

a) Actuator force required, b) pressure of cylinder, c) flow requirements, d) pressure versus flow, e) pressure versus force to determine power requirements, f) power determination

G.4.6 Simulation analysis and conclusions

With the initial motions simulated, the actuator and pump can, therefore, be sized. Based on the data, the requirements show that the system has a power law for the pressure and flow requirements whereas the pump data is linear. This is likely due to the pump attempting to give constant flow and increasing current draw to give the higher pressure. This means that a lower power motor, with a higher capacity pump, could be a solution for a pump-based circuit. The required power for this system is 200-400W, which is a reasonable size for a motor and can be powered with a DC supply.

The calculations also show that the sizing of the actuator is larger than that of the BLEEX system. This could be that the estimates of the force are higher than they will be in reality, though this could also be due to the target of higher carrying capacity.   The only issue with the increased actuator size is the requirement for a large pump capacity, which could become a limiting factor. Strength and buckling are less of an issue with the larger actuators which being safety-critical to protecting the user.

Putting in the largest force, around 10kN for the gait, the actuator size can be recalculated. This still gives a 1-inch bore requirement, which would increase the safety factor of the actuator.

G.5 Automation Studio™ simulation

Automation Studio is a hydraulic and electrical circuit simulator, which can be used to determine initial circuit layout and design. It can take inputs from Excel to help determine transient behaviour, though this is limited in the available number of data points.

One option that it does have is using manufacturer's libraries allowing the direct insertion of current products. This does mean that any estimations of critical flow values or discharge rates will be based on the manufacturer's estimates and determinations.

Automation Studio does allow user interaction during simulation, which helps in determining ideal circuit design for the system. For example, the location of pressure relief valves in relation to check valves makes sure that areas of high pressure cannot build and cause system failure. It also allows the estimation of

possible cavitation events, which can be investigated in other simulation packages.

G.6 Valve Circuit

The power requirements of the system can be calculated as pressure multiplied by the flow rate, which is done, as a time-based system is only 400watts. A Valve based system needs to be able to supply peak pressure all the time and thus also needs to be able to supply the max flow at this point. This increases the size of the pump to several kilowatts of power, increasing the price and requiring AC power supply.

The circuit supplied is a 4.5 kW with two 4WRPEH 6 C3 B12L-2X/G24K0/A1M proportional directional valves to control the motion of the actuators. A local hydraulics company has supplied this. This also includes a pressure regulator and accumulator to smooth the flow. This is a single-phase AC motor, which would not be suitable for being carried by a user. There is also a bypass valve so that the system cannot build pressure if turned on without authorisation.

G.7 Alternative designs

With two actuators, there is a concern that the cylinders can become out of sync, and cause the floating patella to contact the limbs causing damage. Feedback loops based upon the flow rate into and out of the limbs or absolute measurements of the extension would reduce this possibility. If one cylinder becomes damaged, or inoperable, this system would need to be robust enough to compensate. A locked cylinder would not have any motion or flow rate, but a split cylinder would have motion and flow, which would need to be determined.

A mechanical linkage such that movement of one limb causes motion of the other can be developed. Figure G.11 shows a simple set up for this. A sprocket is rigidly connected to the left plain limb and connected to a sprocket on the patella. This second sprocket is connected to a third socket on a keyed shaft. A second chain connects sprocket three and four. Sprocket four is connected to a pinion and rack.
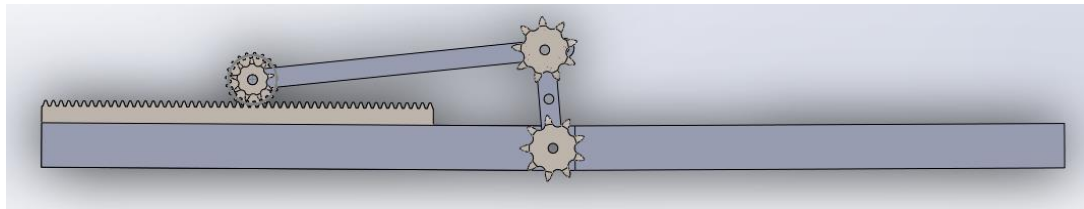
(a)
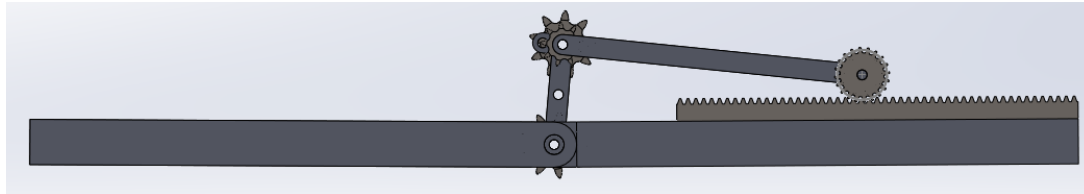
(b)

Figure G.11: Example of mechanical linkage to keep patella at a bisecting angle to the limbs, front and rear
a) front side of the system, b) rear side of the system

Sprockets one and two work similar to sun and planetary gears, though with both rotating the same direction. These translate rotary motion to the pinion, which pushes or pulls on the rack. The ratio of gears is such that the patella bisects the angle between the two limbs.

The issue with this design is strength and weight. The rack being a near-solid piece of metal will weigh the most for this system. Atlanta Drives is an example company that manufacture rack and pinion systems [G.8] and with a safety factor of 1.5 and load factor of 2.25, initial loading of 50.6kN will be required. An Ultra High precision Rack, Atlanta quality 3, a module of 5 will take a max feed force of 78.5kN. This weighs 12.15kg per meter so will be 3.6kg for the system. This is about the same as the actuator system and does not include the pinion, chain and sprockets, which could add another 2-3kg to the weight.

G.8 Summary

The initial sizing of the actuator for a joint needs to start with determining the motion limits. The actuator needs to be able to allow the full range of motion required for the joint, and thus the positioning of the joint is critical. Some joints could require two actuators working in tandem to allow the range of motion. BLEEX has issues with the squat motion due to the location of the actuator generating singularities, whilst SARCOS has a patented design that utilises

multiple actuators. A patella-based design has been developed to overcome the singularities issues.

Once the location has been determined, then the velocities and forces for the different motions need to be calculated. This then gives an initial maximum force that the unit will experience and the rod size can be looked up. This does have a safety factor on the tables, and thus increasing the force with a safety factor is not required. For the patella design, one-inch units have been selected to prevent buckling which is larger than the BLEEX design.

Once the actuator has been selected, the flow rates can then be calculated to give the required motion. This can then either be used to calculate the requirements for a valve-based system or for a pump-based system. The actual selection of which system is the focus of the PhD and thus will be covered further as the project develops.

References

G.1.   Chu, A. *Design of the Berkeley Lower Extremity Exoskeleton (BLEEX).* Doctor of Philosophy thesis, University of California, Berkeley, 2005.

G.2.   Soucie, J.M. et al. Range of motion measurements: reference values and a database for comparison studies. *Haemophilia.* 2011, **17**(3), pp.500-507.

G.3.   BSI. *Basic human body measurements for technological design.* https://0-bsol.bsigroup.com.wam.leeds.ac.uk/Bibliographic/BibliographicInfoData /000000000030128122: BSI, 2010.

G.4.   BSI. CEN ISO/TR 7250-2:2011+A1:2013. *Basic human body measurements for technological design. Statistical summaries of body measurements from national populations.* 2013.

G.5.   Jacobsen, S.C. et al. *Biomimetic mechanical joint.* US 8,516,918 B2. 2013.

G.6.   Power, M.F. *Miller HV2 Series, Corporation, P.H., January 2011.* January, 2011 ed. [Exhibition catalogue]. 2011.

G.7.   MathWorks. *Making Optimal Solver Choices for Physical Simulation.* [Online]. 2016. [Accessed 17/02/2016]. Available from: http://uk.mathworks.com/help/physmod/simscape/ug/making-optimal-solver-choices-for-physical-simulation.html

G.8.   Systems, A.D. *Atlanta Servo-Drive Systems, 2015.* 1st Edition ed. [Exhibition catalogue]. ATLANTA Drive Systems Inc.: ATLANTA Drive Systems Inc., 2015.

Appendix H
Single Joint Design

H.1 Introduction

With the initial simulation design completed, there is a requirement for validating the results with empirical data. Using the joint design from the structural engineer, a member of the project team, a system can be designed based on the requirements from the simulation results.

This will initially focus on a single joint of the exoskeleton rather than the full exoskeleton. The setup will help to validate the joint, hydraulics and control system for the exoskeleton.

H.2 Hydraulic circuit

The initial design and development was for a pump-based circuit, similar to an EHA unit, though this requires circuit design and control over the pump. Due to time constraints, it was suggested that the initial design use a tethered hydraulic power pack that can supply several joints using proportional valves.

This was calculated from the simulation data, such that a 4.5 kW pump and 50L tank were required. 12L proportional servo valves were selected for the control of the actuators.

H.3 Design

There are several hydraulic actuators designs varying from welded construction to tie rods. With tie rod actuators being easier to construct and modify for the requirements, their reduced manufacture time was ideal for getting the system in quickly. Based on the results from the simulations from G.4, a 1-inch rod with a 1.5-inch cylinder was selected, with imperial sizes due to the American specification of the manufacturer. A max displacement of 100mm was also selected as it is recommended that the actual displacement should only be 80% of the total travel [H.1]. This is to give enough support for any side loading that might occur.

There are several methods of attaching the cylinder, and pinion joints at both ends of the actuator were selected. A force gauge can be put in line with the actuator between the rod and the eye. This also means that the connection to the frame is simplified as the rear of the unit connects to a simple plate whilst the active end connects directly to the patella with a rod.

H.3.1 Patella

The patella needs to be able to transfer the force between the two actuators, and thus resist up to 15kN, though the initial simulations gave less than 10kN without impact forces. This is to give the worst-case scenario, though whether the frame would take this or not will need to be determined with higher fidelity simulation results. The patella will spend the majority of time also having to transfer the load into the knee joint in the radial direction. There should be no axial loading of the patella from the actuators, though whether there is any gravitation force due to the weight could be an issue if the axis is not parallel to the floor.

H.3.1.1 Patella Bearings

The patella needs to be able to rotate independently of the knee joint and thus bearings are needed to allow this. The radial loading could be up to 30kN with the actuators either pushing or pulling in the squat motion. The axial loading should just be resisting the weight of the system, which for initial estimates will be 5kg. It is not expected to be this final weight but will give allowance for this. This gives around 50N of axial loading. As the axial load is relatively small compared to the radial loading, there are options for ball bearing system rather than taper bearings.   Taking SKF® as an example manufacture, they recommended deep groove ball bearings and spherical roller bearings where the axial load is relatively small compared to the radial load [H.2]. There are self-aligning ball bearing units as well and cylindrical roller bearings designs that could be utilised. These loads could become moment loading and thus double row bearings or paired units are suitable.

One issue that the bearing also needs to overcome is the possibility of working in dirty environments, and sealing of the bearings will be important. The roller bearings do not have this option, and the spherical units are self-aligning limiting

their sealing options. This means that the deep groove units will be the selected solution.

As the unit is not running at high rpm values, it can start to appear to be a static load-bearing. From [H.2], the equation is

$$S_0 = \frac{C_0}{P_0} \tag{H.1}$$

Where S_0 is the static safety factor, C_0 is the basic static load rating, and P_0 is the equivalent static bearing load. The equivalent static bearing load is calculated from the actual system. For deep ball groove bearings, P_0 is equal to

$$P_0 = 0.6F_r + 0.5F_a \tag{H.2}$$

$$P_0 < F_r \rightarrow P_0 = F_r \tag{H.3}$$

This means that P_0 will be equal to the radial loading, thus 15kN. For non-rotating bearings, the safety factor is ≥ 2 for pronounced shock loads and high-performance requirements, thus giving a C_0 value of ≥ 30kN.

For the dynamic side of the system, in accordance with ISO 281 and modification for SKF bearings, the equation is

$$L_{onm} = \frac{180}{2\gamma} a_1 a_{skf} \left(\frac{C}{P}\right)^p \tag{H.4}$$

Where L_{onm} is the SKF rating life for million oscillation cycles, γ is half the angle of complete oscillation, a_1 is the modification factor to give a target reliability, a_{skf} is the SKF life modification factor, C is the basic dynamic load rating, P is the equivalent dynamic bearing load (kN), and p is the exponent for the life equation which is 3 for ball bearings. For 95% reliability, a_1 is 0.64, which for the ISO 281 has a value of 1 for 90% reliability.

a_{skf} is calculated from plots in [H.2] where cleanliness, fatigue strength, and viscosity of the grease is compared. As the units will be sealed in normal cleanliness, the factor is 0.5. To determine the viscosity, the rpm needs to be calculated, but as the joint is not directly rotating, this is difficult to determine. If the knee were rotating at 35° in one gait cycle, this would be 1,900 rpm, which limits the size of the bearing. As the actual value is actual over working

viscosity, this does mean at lower temperatures, the viscosity ratio increases. When K is less than one, this then requires additives to the grease to compensate. A value of 4 is ideal to keep full film conditions.

As the bearing will also be locating, there are some slight variations for the dynamic value based upon the axial and radial loads. If the axial load divided by the radial load is less than 0.19, which is it is, then the P value is equal to the radial loading. To alter the equation for P, the axial load needs to be 3000N, or 300kg, which is outside of a realistic weight for the patella.

If the bearing is to last 5 years, at 8hrs per working day with each gait cycle taking 1.1 seconds, that gives 34,036,363 revolutions. The angle for walking is around 35° [H.3].

This can then be used to calculate a value for C.

$$L_{nm} = \frac{180}{2\gamma} a_1 a_{skf} \left(\frac{C}{P}\right)^p \qquad \text{(H.5)}$$

$$\frac{2\gamma L_{nm}}{180 a_1 a_{skf}} = \left(\frac{C}{P}\right)^p \qquad \text{(H.6)}$$

$$\sqrt[p]{\frac{2\gamma L_{nm}}{180 a_1 a_{skf}}} = \frac{C}{P} \qquad \text{(H.7)}$$

$$C = P \times \sqrt[p]{\frac{2\gamma L_{nm}}{180 a_1 a_{skf}}} = 15 \times \sqrt[\frac{10}{3}]{\frac{35 \times 34}{180 \times 0.64 \times 1}} \qquad \text{(H.8)}$$
$$= 32.7 kN$$

These values will change as actual data is inputted, but a value of C of 32.7kN and C_0 of 30kN is a starting point.

The sealing of the units is critical, and the selection guidelines give that the RSH style gives the best dust and water exclusion. It does have poor low friction properties, as well as high-speed issues though, but the requirements that the unit might be working in contaminated areas and protecting the joints is important. The second best would be RS1, as there is a limit on the size that RSH size units will work up to.

The first unit that gives C greater than 32.7kN and C0 greater than 30kN is 45mm internal diameter and 100mm external diameter. This has a value for C

of 55.3 and a C0 value of 31.5. The Pu value is 1.34, which can be used in the a_{skf} equation. The code for this bearing is 6309-2RS1.

Putting this through the online calculator gives an a_{skf} value of 5.93, which decreases the value for C to 18.0484. It also gives the life of the bearing to be 2610 hours. This is for 90% reliability at continuous revolution at 1900 rpm. When this is converted to oscillation events, this is 489million oscillation cycles. This is five times the initial life duration.

H.3.1.2 Patella Design

The patella needs to transfer force between the actuators in linear opposition to each other as well as when the actuators are in parallel motion. When the limb is extended, the force applied by the actuators is directed directly through the patella, while when retracted, the force is through the joint. For when the limb is straight, the force can simply be put through a direct connection, for example, a plate. For when it is bent, it creates a cantilever set up around the limb, which is the worst-case scenario.

One major issue with the patella is likely to be the weight of the component. Using stainless steel is stronger than aluminium by weights significantly more. According to the British Stainless Steel Association (BSSA) [H.4], the two most common grades are 304/304L and 316/316L. 304 is the most commonly used grade of stainless steel, though 316 has higher corrosion resistance. The examples given by the BSSA for 316 are for laboratory and marine equipment and as the exoskeleton could be used in areas with high seawater content, for example, flood reconstruction; it would be an ideal material.

Aalco® is the supplier of metals to the University of Leeds, and have data sheets that can be used to compare 6061 aluminium and 316 stainless steel. 316 stainless steel has a tensile strength of between 500 MPa and 700 MPa whilst the 6061 aluminium has a tensile strength of 260 Mpa. Their densities are 8.0 g/cm³ and 2.7 g/cm³ respectively. A 100 mm cube of stainless steel can withstand 5-7 MN of force, whilst the aluminium only 2.6 MN. To withstand the same force, the aluminium needs to be 139.7mm square top face. The weight of these components would be 8kg and 5.19kg respectively. This is an increase of volume by 92% for a reduction of 65% of the weight.

As the patella is an assembly, the test loading of it for structural purposes should ideally be done as a complete assembly. This means that loading will include cantilever effects of the off-centre loading for certain parts. The simulation will also require loading both vertically and horizontally as well as for the retraction and extension of the cylinders. The load applied will be for the worst-case scenario of 15kN.

Horizontal force transfer plate

Horizontal force can be transfer via a simple stainless steel plate. The example in Figure H.1 shows the actuator connectors at each end, as well as holes for four bolts.

Figure H.1: Horizontal transfer plate

Force testing of the horizontal transfer plate can be seen in Appendix JK. The results show that the lowest safety factor is 2.6 for the vertical extension loading.

Vertical force transfer component

The vertical transfer component needs to resist up to 30kN on a cantilever design. This is the largest component of the patella component, and thus could be the heaviest. With stainless steel being nearly five times stronger by only three times as dense as aluminium, it is an ideal choice for this component.

The bearing needs to be connected to the vertical section, which defines the initial volume of the component. This also needs to connect to the horizontal

transfer plate with bolts.   Having symmetrical bolting, so that the threaded section is on the top right and the bottom left allows the component to only have one design.

Figure H.2: Vertical transfer component

Force testing of the vertical transfer component can be seen in Appendix J. The results show that the lowest safety factor is 3.5 for the vertical extension loading within the horizontal extension loading, having a safety factor of 8.7.

Separation component

The eyes of the hydraulic actuator need space to work, and thus a separator for the horizontal transfer plates is needed. This should not be a load-bearing component or directly transfer the force, though it will be loaded in the axial direction with bolts. This means that it can be made from lighter material than steel, for example, aluminium.

Figure H.3: Separation component

There are stress issues that can occur for the separation unit, and as it is part of the complete assembly, has been stress tested. The results are shown in Appendix JK. The worst case is when the force is applied in horizontal retraction and has a value of 2.4.

Pinion

The pinions need to transfer the force from the eyelets of the actuator to the patella and thus need to be one of the strongest parts of the system. Solid stainless steel rods are thus the ideal solution to the design and are easy to acquire. As the hydraulics are American based, it will be 0.75 inches in diameter.
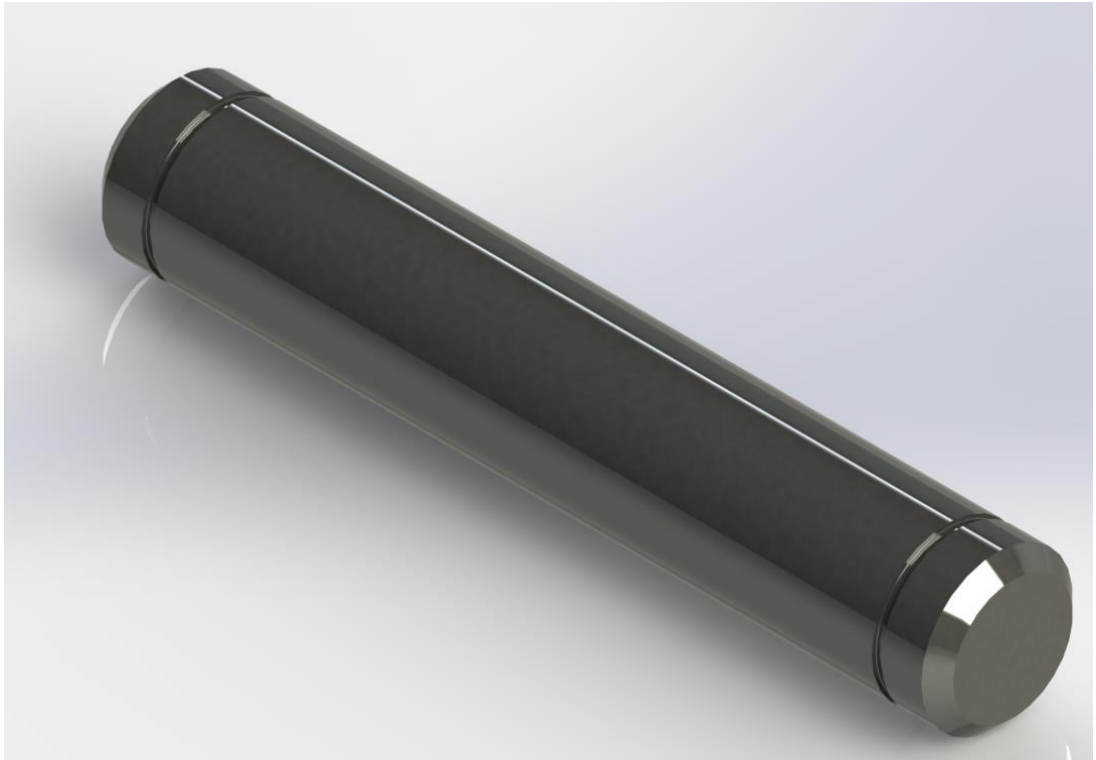
Figure H.4: Pinion component

This is a major load-bearing component so has been stress tested. The results are shown in K and have the lowest safety factor of 3.3.

Pinon bearings

To give the pinion and actuator the ability to rotate, there needs to be a bearing to prevent wear and heat being generated. This can be either a similar bearing to that of the main patella or a plain bearing. With a ball bearing, this will increase the weight the size of the patella unit, which needs to be as light as possible.

A plain bearing does allow motion though has issues with wear possibilities. They can either be sintered metals with oil impregnation or plastic. Using Igus® GmnH as an example manufacturer of plastic plain bearings, and utilising their selection software, part number ZFI-1214-12 is an initial starting point. This plain bearing has a flange that allows it to be pushed into the housing without the issue of it passing through it, as well as having the correct shaft diameter of the pinion.

The life of the bearing can be calculated with Igus® online calculator [H.5] which is based upon their products and does not reveal the calculations behind it. Putting in a dynamic load maximum of 7500N, based upon the 15kN being split

between the bearings, and shock loading. The calculator can also take into account chemical environments, though this should not occur for the exoskeleton. The calculator allows the input of a pivoting motion with an angle range of 45° with a pivoting frequency of 55 per minute, which is based on the gait motion of 1.1 seconds. Input the materials of the shaft and housing, both stainless steel, and max wear of 0.25mm gives a service life of 44 hours. This is not a large service life though this is for continuously walking with a max load. Putting in the lower forces associated with the gait simulation, the service life increases to 149 hours. This would equate to 18.6 workdays before needing to be replaced for 8 hours shifts. For the single joint, this is a reasonable starting point. The service life can be extended with using CF53 hardened and ground steel to 303 hours, though this means that the chemical resistance of the metal is reduced. An image of the bearing is shown in Figure H.5.
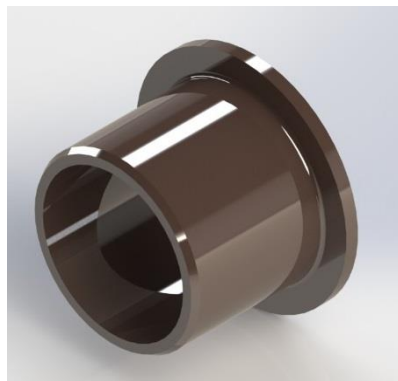
Figure H.5: Plain Bearing

Force sensor

The output of the actuators needs to be measured for the control system, and with the 15kN estimated peak value, a force sensor that will give this range is required. The force sensor will also need to have a high accuracy so that the control system can work safely. An accuracy of 1% would give 150N as the resolution of the system, which is large enough to cause damage to the user.

Novatech Measurements Ltd were found to be able to supply a 20kN force sensor that would be in the line with the actuators. It has a repeatability of

0.02%RL, so for a tension/compression force sensor of 20kN is 8N. It also has that same thread as the actuators allowing easy install of the sensor[16].

Joint connector

With the joint design complete by Pourshid Fani, the patella needs to connect to it. With the vertical section on the outside of the bearing, the joint connector houses the inner bearing. The connections to the joint are predefined, and thus just needs to be strong enough to resist the loading from the patella. As the force is put through two bearings, this will be 15kN. Figure H.6 shows this design.

Figure H.6: Joint to patella connector

The bearing is contained against a shoulder and a locking nut. This allows easy removal of the bearing, as well as the allowance of tolerances. This also allows the setting of the preload of the bearing. The bearing will also require some interference fitting on to the shaft. For a static inner ring with a rotating outer ring and load, an interference fit on the inner ring with a loose fit on the outer is recommended. According to [H.2], for a fit to a hollow shaft where there is an

---

[16] It was found that the force sensor and the piston had a different thread pitch so adaptors were required. This increased the length of the structure, and thus reduced the motion range of the system.

interference fit, there needs to be an increase of the interference fit to give the same pressure as that of a solid shaft. The equations are $C_i = \frac{d_i}{d}$ and $C_e = \frac{d}{d_e}$, where C_i is the diameter ratio of the hollow shaft, C_e is the diameter ratio of the inner ring, d is the outside diameter of the hollow shaft / inner diameter of the bearing, d_i is the inside diameter of the hollow shaft and d_e is the average outside diameter of the inner ring. C_i is 45mm divided by 60mm or 2/3. From [I.2], the value for d_e is 62.1 and thus the value for Ce is 0.72. Looking this up on the associated plot, Figure H.7 [H.2], this gives a value of around 1.37.
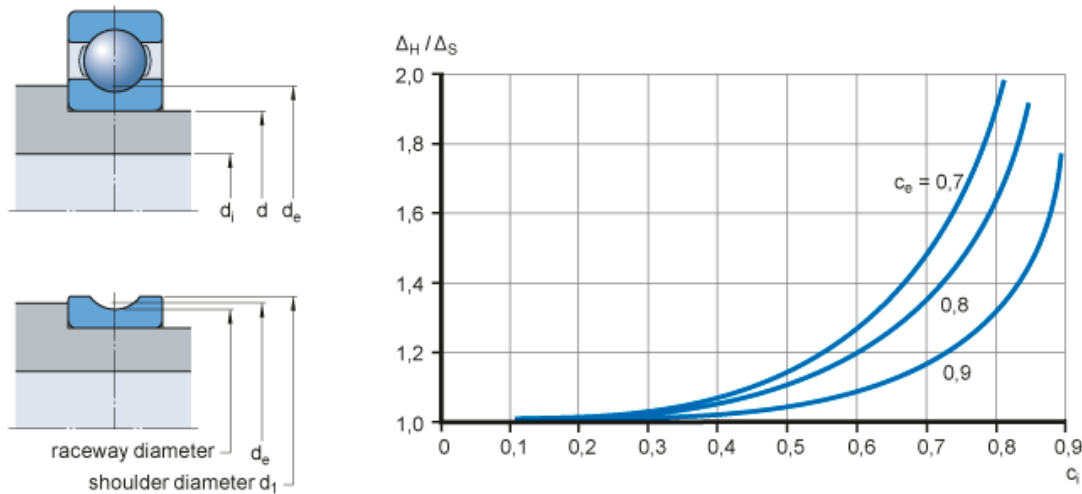
Figure H.7: Relationship of interference Δ_H, needed for a hollow steel shaft, to the known interference Δ_S for a solid steel shaft

For a 45mm shaft with a normal to heavy load, a k5 interference fit is recommended [H.2]. The mean probably interference is $\Delta_V = \frac{(22+5)}{2} = 13.5 \mu m$, which multiplied by the Δ_H/Δ_S is 18.5µm. This gives a fit of m5Ⓔ

Putting this loading into simulation gives peak stress of less than 115MPa and thus a safety factor of 1.8. This is shown in Figure H.8. This is enough to make sure that the connection between the exoskeleton joint and the patella is strong enough.
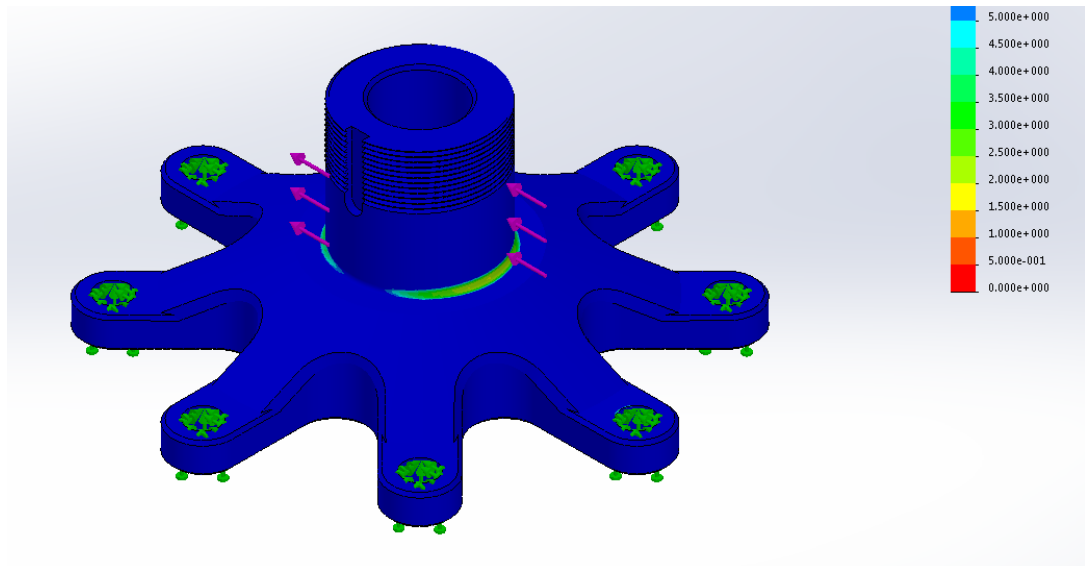
Figure H.8: FEA analysis of the connector between the exoskeleton joint and the patella

Assembly components

The patella is held together with 120mm M10 bolts, which are holding the unit together but will have some radial loading. This is minimised by having additional cross rods through the system to take this loading.

The bearings are held in with locking nuts onto the joint connector and are acquired from the bearing manufacturer. Locking nuts with lock washers do not have issues with losing torque that a lock nut with integral locking device will have. It does have the requirement that the shaft has a key way to prevent rotation. KM 9 locknut with MB9 lock washer is the correct size for the bearing and has an axial load carrying capacity in a static system of 78kN which exceeds the expected load significantly.

The bearings are held into the patella with circlips, though the loading limit is not specified within the British Standard 3673 [H.6]. There does appear to be some loading values for DIN 472 circlips, though these appear to be defined by the manufacturer, for example, Springmaster Ltd [H.7] has an internal bore circlip of 100mm stated that the circlip will withstand 188kN and the groove 93.1kN. The circlip value will be based on the manufacturer's data; thought the groove strength will be based on the material of the retaining structure. There are stainless steel circlips available, but they are limited in size. Alternative designs with stronger retention are available, but this should not be required.

The pinions should not be taking the axial load, though still need to have some retention. This can be done either with circlips or grip rings. Using a grip ring means that grooves will not be required on the part, which can cause a stress riser. Baker & Finnemore Limited manufacture are an example of a grip ring manufacturer. Their datasheet for a 19mm shaft states that the push on force is 157N with a pull-off force of 3776N [H.8]. This is more than enough to retain the pinions. These are spring steel components with coatings of either Bronze and Varnish or Mechanical zinc plated. This is shown in Figure H.9 [H.8].
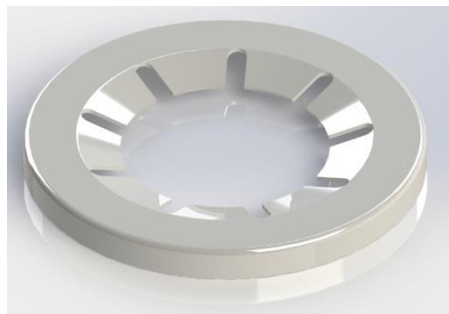
Figure H.9: Grip ring by Baker and Finnemore

With the requirement that the pinons might need to be extracted, circlips have been selected, though star washers will also be used on the cross rod to determine their suitability in future component retention.

H.3.1.3 Connections to limb

The end of the actuator needs to be connected to the limb, though there will be a plate and pivot already attached to the actuator base. This is perpendicular to the actuator and limb and thus requires a connection component. This needs to be able to resist the 15kN extension and retraction loading both within the connection component itself and stop motion along the limb. This is simply an angle bracket, which is a common material to get.

The supplier of metals for the University of Leeds is Aalco, and they have several angle bar options of 304 and 316 grade. The initial dimensions for the bracket are for 120mmx120mm, which comes in 6mm and 10mm thicknesses. An initial outline of the design is in Figure H.10.
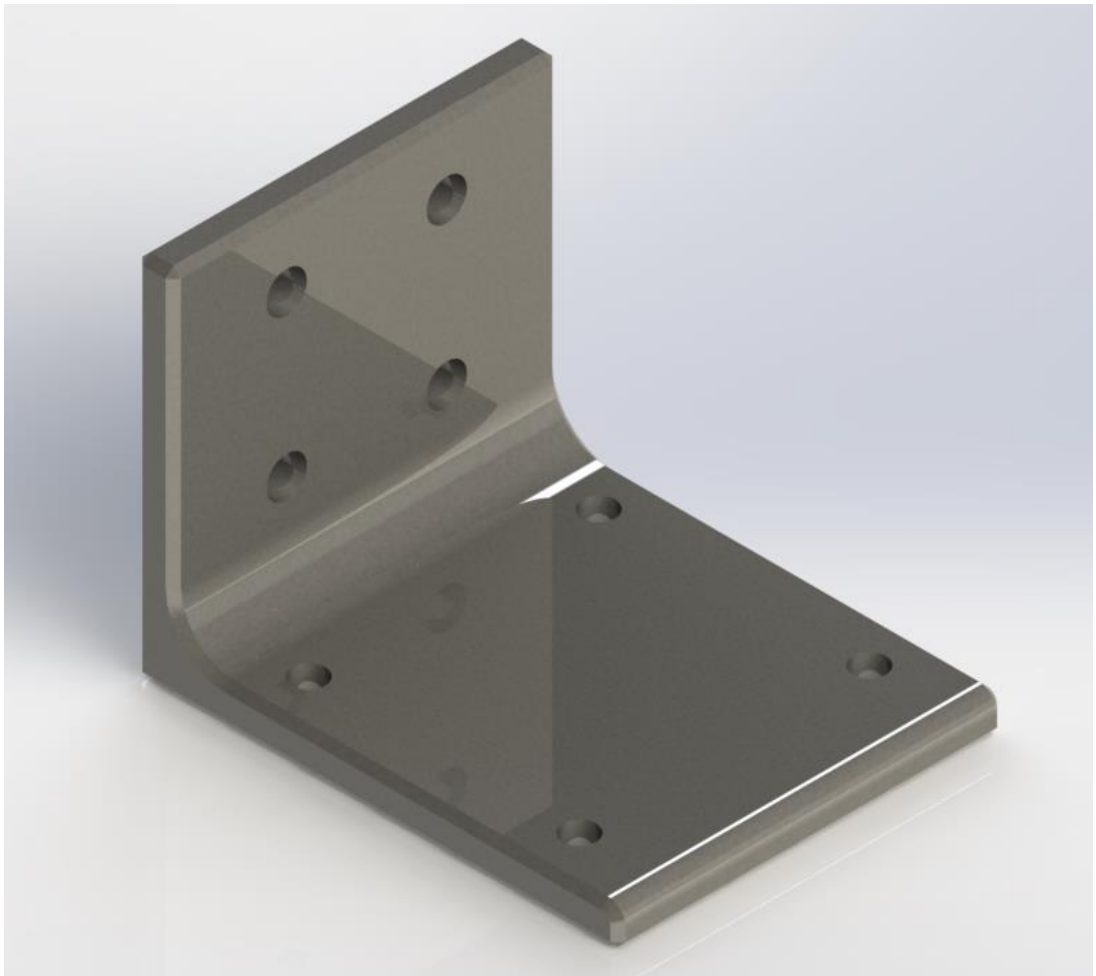
Figure H.10: Connector Block

Putting the loading on to the block gives initial safety factors of 0.92 and 0.94 for extension and retraction respectively. This is unacceptable, and thus additional structural elements are needed.

Stainless steel is wieldable, and thus an angle section can be added to help transfer the force between the angle sections, Figure H.11
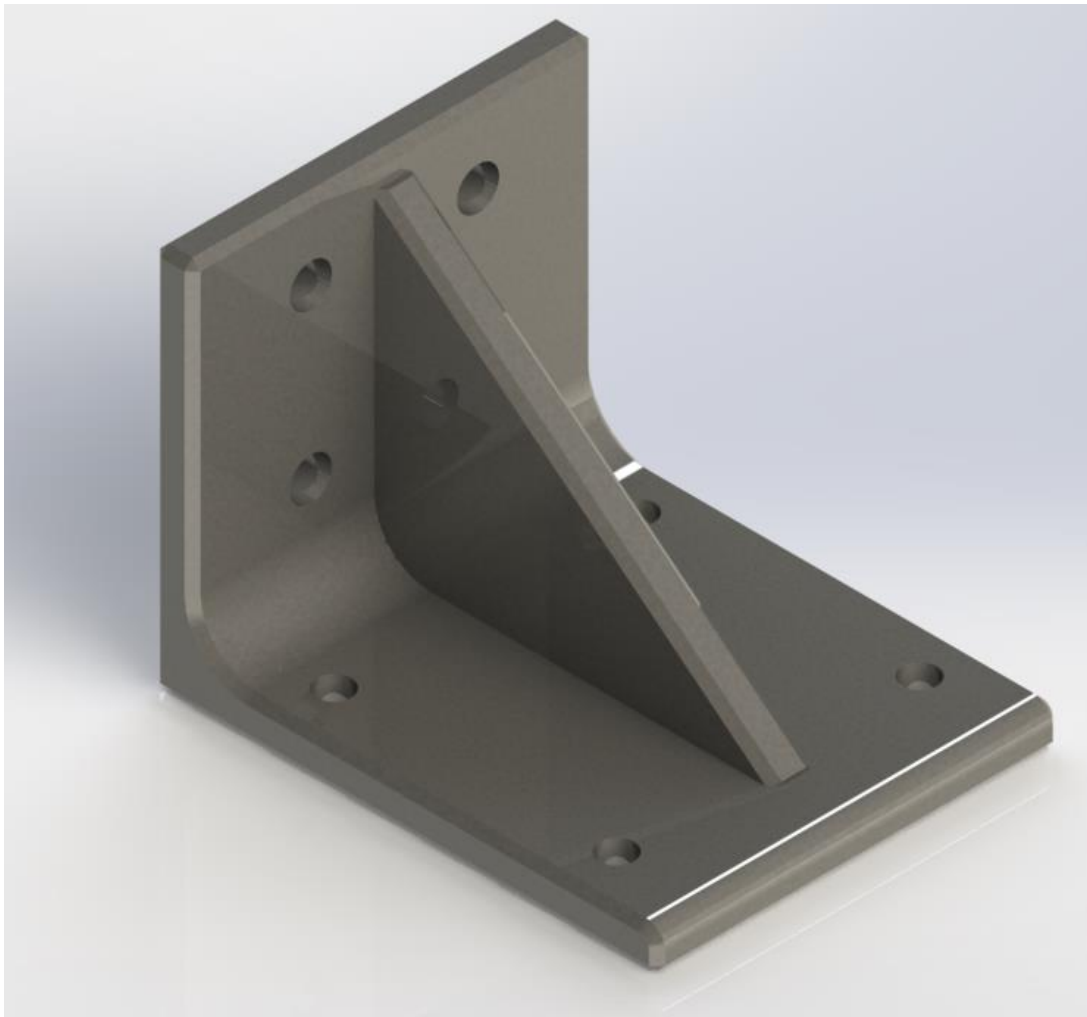
Figure H.11: Connector Block with angle support welded to the angle bracket

When this is stress-tested, it comes out to have a safety factor of 6.1 and 3.5 respectively, Figure H.12, which are reasonable values.

(a)   **(b)**
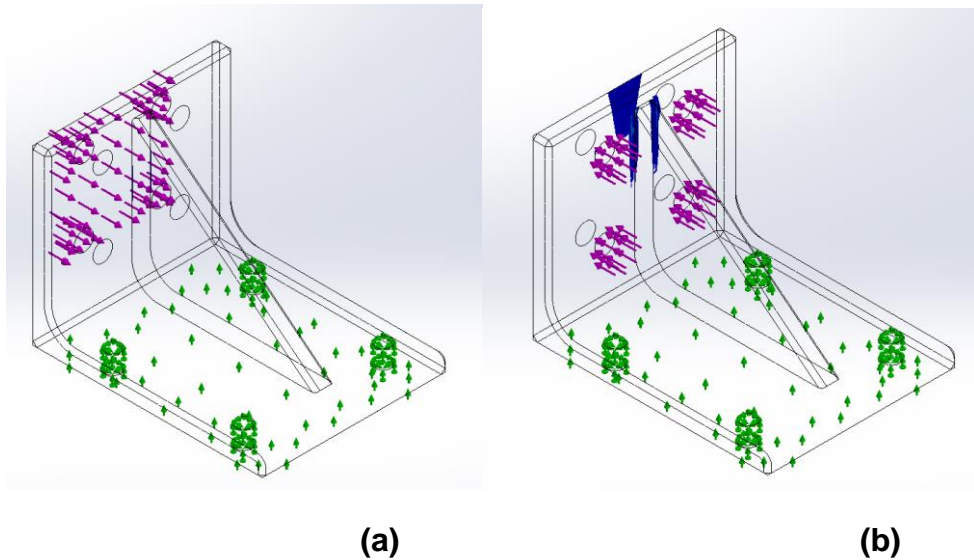
**Figure H.12: Connector Block with angle support welded to angle
bracket stress results
a) with extension force applied, b) with retraction force applied**

The connector block is attached to the limb using a 'u' shaped block, which surrounds the limb to distribute the locking nuts.

H.4 Final single joint design

With the component parts designed and simulated, these can be put together to give an initial idea of what the design will look like. This is shown in Figure H.13

Figure H.13: Completed single joint design

H.5 Summary

The single joint design has several components within the system that have large loads placed upon them that could cause failure. Determining the material and dimensions of the components to give a reasonable safety factor is critical to making sure that the user is safe within the exoskeleton suit.

The system was simulated as a complete system, which though takes longer to compute, gives the interactions of the components and the loading transfer.

With the different loading orientations, this creates different failure routes for the components. Table H.1 shows the range of safety factors of the system, showing that the lowest is 1.8.

Table H.1: Safety factors for the single joint design

	Vertical Extension	Vertical Retraction	Horizontal Extension	Horizontal Retraction
Horizontal force transfer plate	2.4	2.8	2.6	3.5
Vertical force transfer component	3.5	3.7	8.7	7.9
Separation component	2.5	2.4	2.7	3.7
Pinion	3.9	3.8	3.3	3.3
Joint connector	1.8			
Limb Connector	6.1	3.5	6.1	3.5

With the design completed, it needs to be tested to determine what force range is actually seen as well as the motion range and speeds that can be reached. This will be conducted within the exoskeleton test gantry where the system is kept separate from the user behind polycarbonate screens.

The joint is dependent on the cylinders working in tandem, which is reliant on the control algorithm. Another member of the enhancive exoskeleton team is developing this.

The single joint is heavier than expected at 29 kg, whereas the initial loading was expecting 15 kg. This is due to the increased strength required from both the actuation system and the framework. With safety being critical, making sure that the frame and actuation system withstands shock loading is important.

References

H.1. Enerpac. *Safety seminar handbook.* [Leaflet]. http://www.enerpac.com/sites/default/files/safetyhandbook_eng_3.pdf: Enerpac, 2016.

H.2. SKF. *Rolling Bearings, SKF, August 2013.* 2 ed. [Exhibition catalogue]. http://www.skf.com/binary/56-121486/SKF-rolling-bearings-catalogue.pdf, 2013.

H.3. Zoss, A.B. et al. Biomechanical design of the Berkeley lower extremity exoskeleton (BLEEX). *Ieee-ASME Transactions on Mechatronics.* 2006, **11**(2), pp.128-138.

H.4. Association, B.S.S. *50 Grades of Stainless Steel.* [Online]. 2016. [Accessed 18th January 2016]. Available from: http://www.bssa.org.uk/50-grades-of-stainless-steel.php

H.5. GmbH, I. *iglidur Expert System 3.0.* [Online]. 2016. [Accessed 01/002/2016]. Available from: http://www.igus.co.uk/iglidurConf/Iglidur/Step1

H.6. STANDARD, B. 3673-4. *Specification for Spring retaining rings.* https://0-bsol.bsigroup.com.wam.leeds.ac.uk/Bibliographic/BibliographicInfoData/000000000000067707: British Standards, 1977.

H.7. Ltd, S. *Standard Internal Circlips: To DIN 472 Metric.* [Online]. 2012. [Accessed 01/02/2016]. Available from: https://www.springmasters.com/sp/standard-internal-circlips.html

H.8. Limited, B.F. *Starlock® Push On Fasteners for Metric Round Shafts.* [Online]. 2011. [Accessed 01/02/2016]. Available from: http://www.bakfin.com/starlock/metric-roundshaft.html

Appendix I
Miller Cylinders Data Sheets [I.1]

Piston Rod Selection Data

Heavy-Duty Hydraulic Cylinders
HV2 Series

How to Use the Chart

The selection of a piston rod for thrust (push) conditions requires the following steps:

1. Determine the type of cylinder mounting style and rod end connection to be used. Then consult the chart below and find the "stroke factor" that corresponds to the conditions used.

2. Using this stroke factor, determine the "basic length" from the equation:

$$\frac{Basic}{Length} = \frac{Actual}{Stroke} \times \frac{Stroke}{Factor}$$

The graph is prepared for standard rod extensions beyond the face of the rod gland retainers. For rod extensions greater than standard, add the increase to the stroke in arriving at the "basic length."

3. Find the load imposed for the thrust application by multiplying the full bore area of the cylinder by the system pressure.

4. Enter the graph along the values of "basic length" and "thrust" as found above and note the point of intersection:

   A) The correct piston rod size is read from the diagonally curved line labeled "Rod Diameter" nad above the point of intersection.
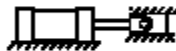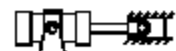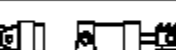
   B) The required length of stop tube is read from the right of the graph by following the shaded band in which the point of intersection lies.

C) If required length of stop tube is in the region labeled "consult factory," submit the following information for an individual analysis:

   1) Cylinder mounting style.

   2) Rod end connection and method of guiding load.

   3) Bore, required stroke, length of rod extension (Dim. "A" & "WP") if greater than standard, and series of cylinder used.

   4) Mounting position of cylinder. (Note: If at an angle or vertical, specify direction of piston rod.)

   5) Operating pressure of cylinder if limited to less than standard pressure for cylinder selected.

Warning ⚠

Piston rods are not normally designed to absorb bending moments or loads which are perpendicular to the axis of piston rod motion. These additional loads can cause the piston rod end to fail. If these types of additional loads are expected to be imposed on the piston rods, their magnitude should be made known to our Engineering Department so they may be properly addressed. Additionally, cylinder users should always make sure that the piston rod is securely attached to the machine member.

Recommended Mounting Styles for Maximum Stroke and Thrust Loads	Rod End Connection		Case	Stroke Factor
Groups 1 or 3 Long stroke cylinders for thrust loads should be mounted using a heavy-duty mounting style at one end, firmly fixed and aligned to take the principal force. Additional mounting should be specified at the opposite end, which should be used for alignment and support. An intermediate support may also be desirable for long stroke cylinders mounted horizontally. See "Tie Rod Supports — Rigidity of Envelope" for a guide. Machine mounting pads can be adjustable for support mountings to achieve proper alignment.	Fixed and Rigidly Guided	I		.50
	Pivoted and Rigidly Guided	II		.70
	Supported but not Rigidly Guided	III		2.00
Group 2 Model 61 — Trunnion on Head	Pivoted and Rigidly Guided	IV		1.00
Models 57 & 58 — Intermediate Trunnion	Pivoted and Rigidly Guided	V		1.50
Model 62 — Trunnion on Cap or Clevis on Cap	Pivoted and Rigidly Guided	VI		2.00

- 303 -

Catalog HY08-M1140-4/NA
Piston Rod Selection Data

Heavy-Duty Hydraulic Cylinders
HV2 Series

Piston Rod — Stroke Selection Chart

1.50" through 8.00" Bore

Piston Rod — Stroke Selection Chart

10.00" through 20.00" Bore
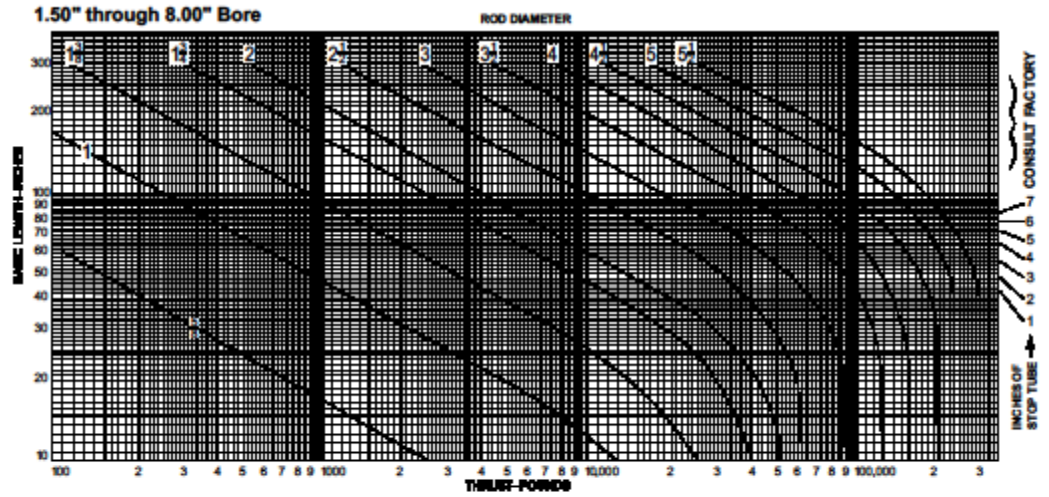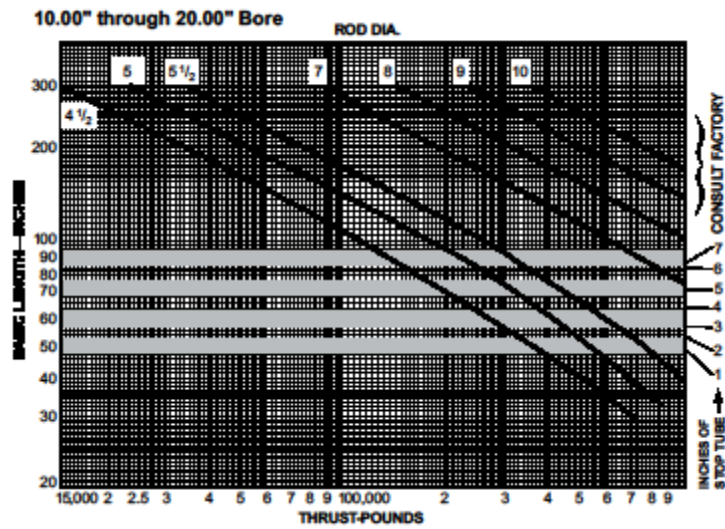
References

I.1.   Power, M.F. *Miller HV2 Series, Corporation, P.H., January 2011.* January, 2011 ed. [Exhibition catalogue]. 2011.

Appendix J

Structural Results
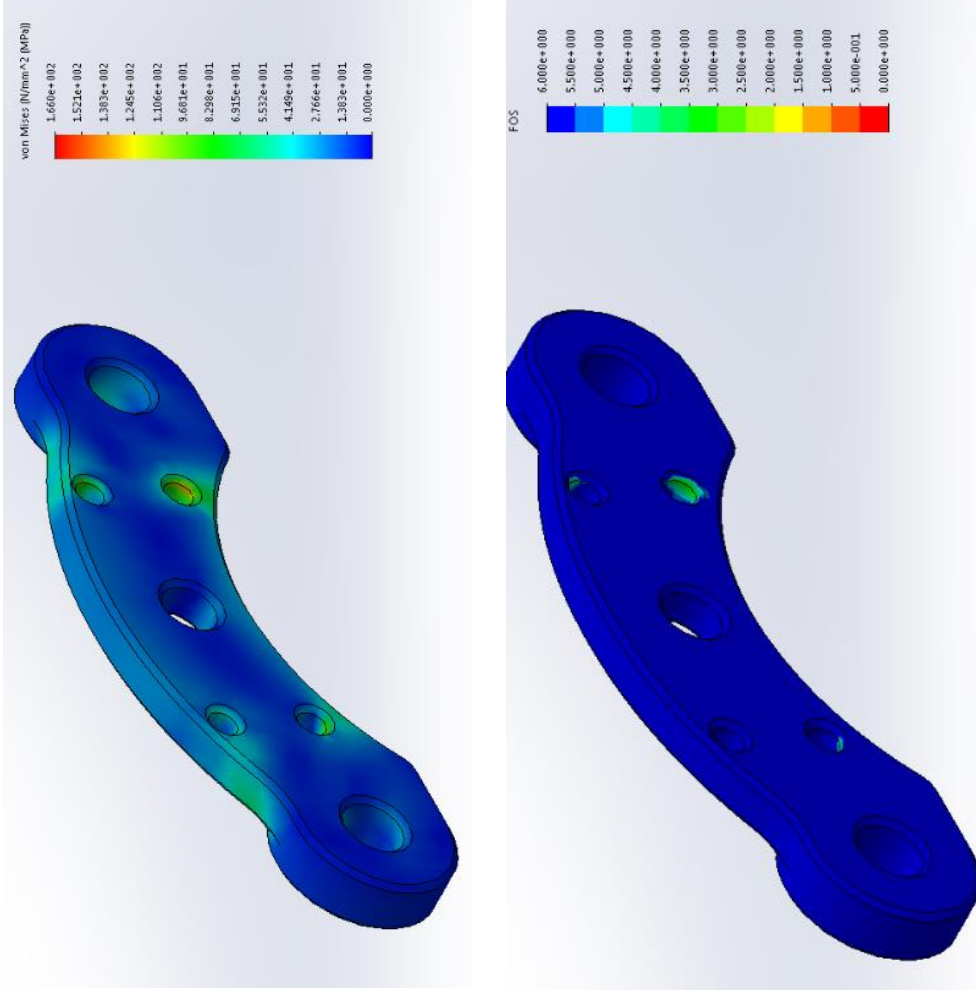
Figure J.1: Horizontal component with vertical extension force applied from actuators. Stress and factor of safety shown. The minimum factor of safety is 2.4
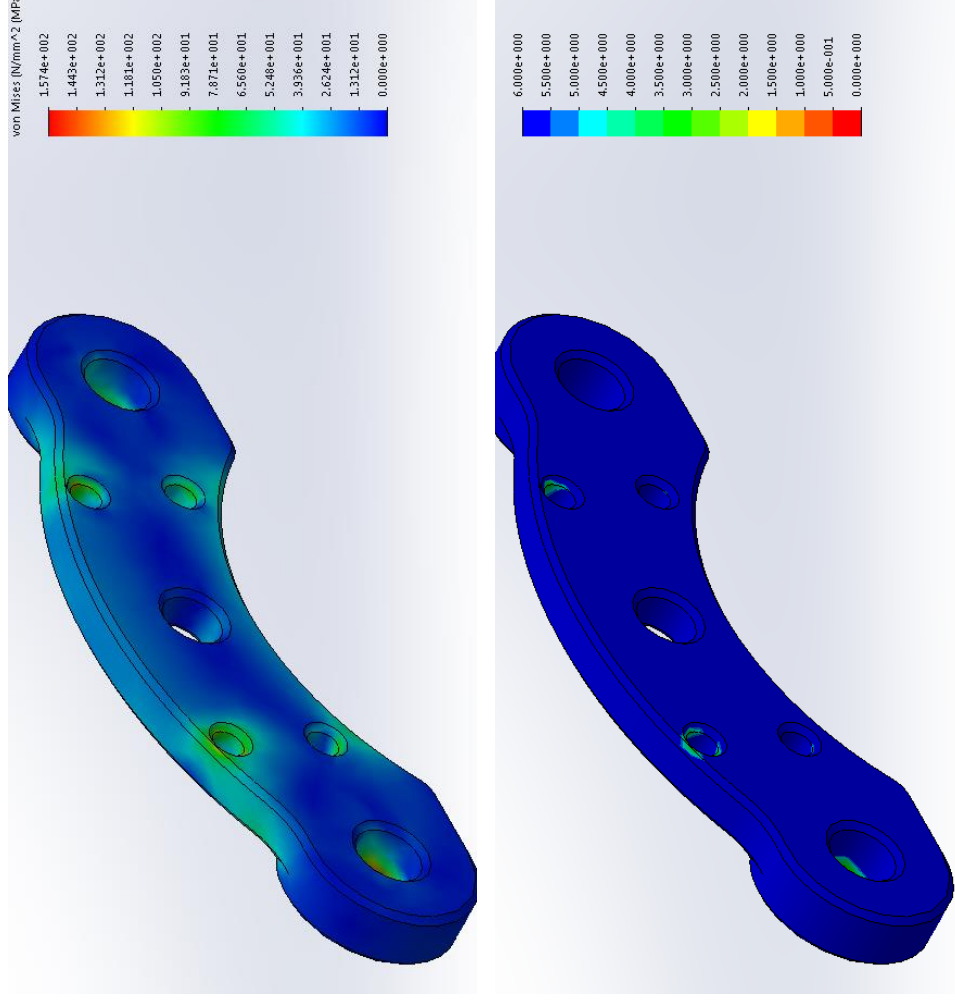
Figure J.2: Horizontal component with horizontal retraction force applied from actuators. Stress and factor of safety shown. The minimum factor of safety is 2.8
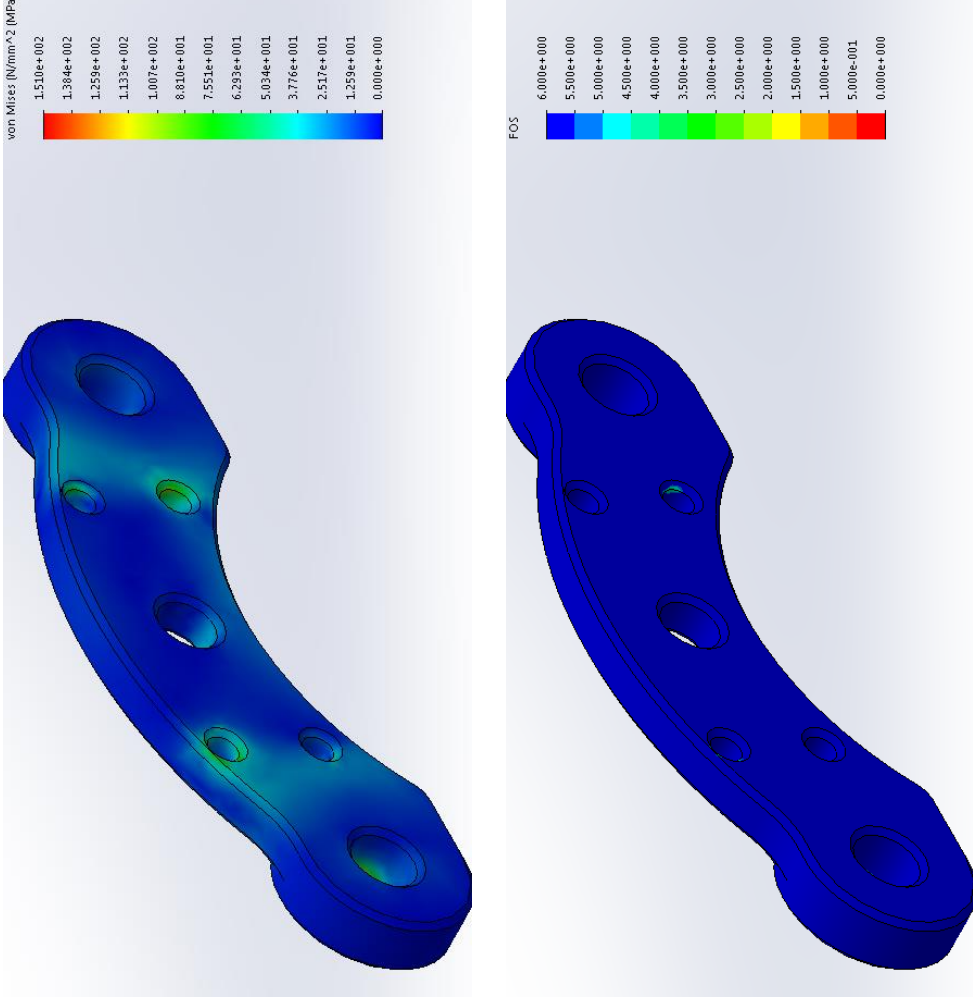
Figure J.3: Horizontal component with horizontal extension force applied from actuators. Stress and factor of safety shown. The minimum factor of safety is 2.6
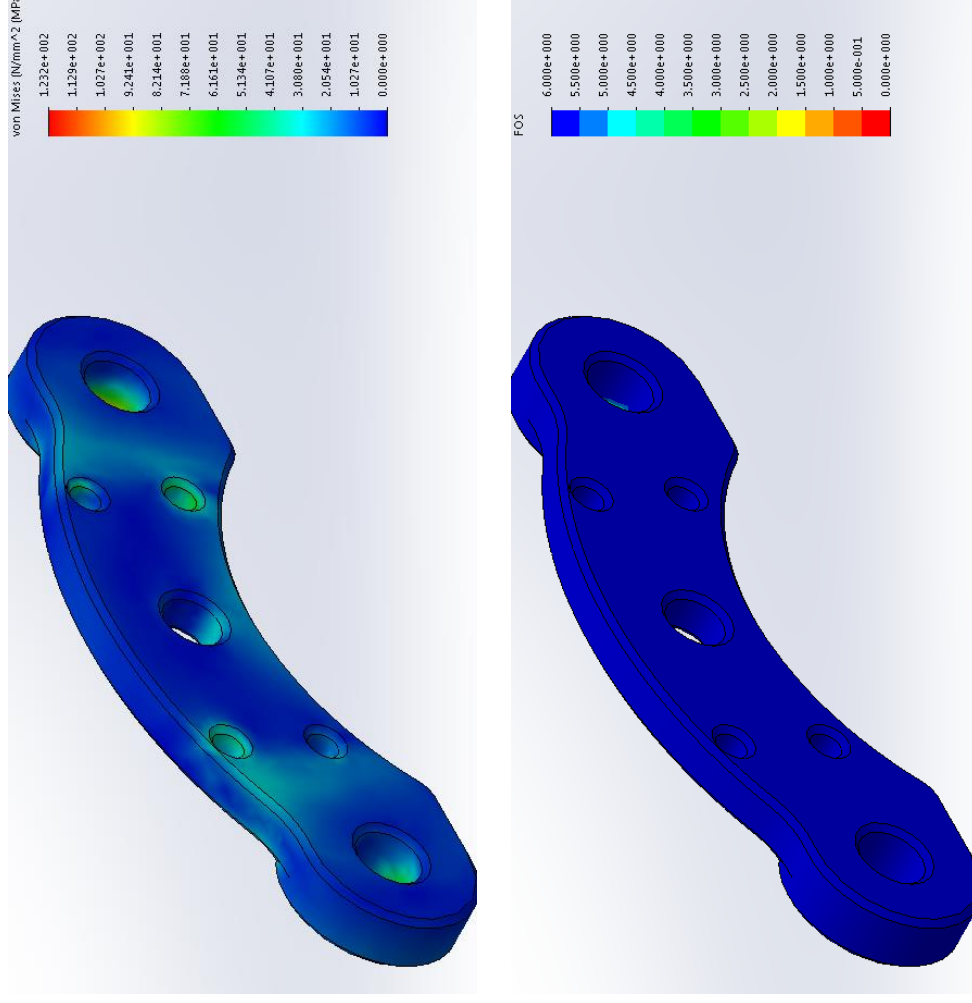
Figure J.4: Horizontal component with horizontal retraction force applied from actuators. Stress and factor of safety shown. The minimum factor of safety is 3.5
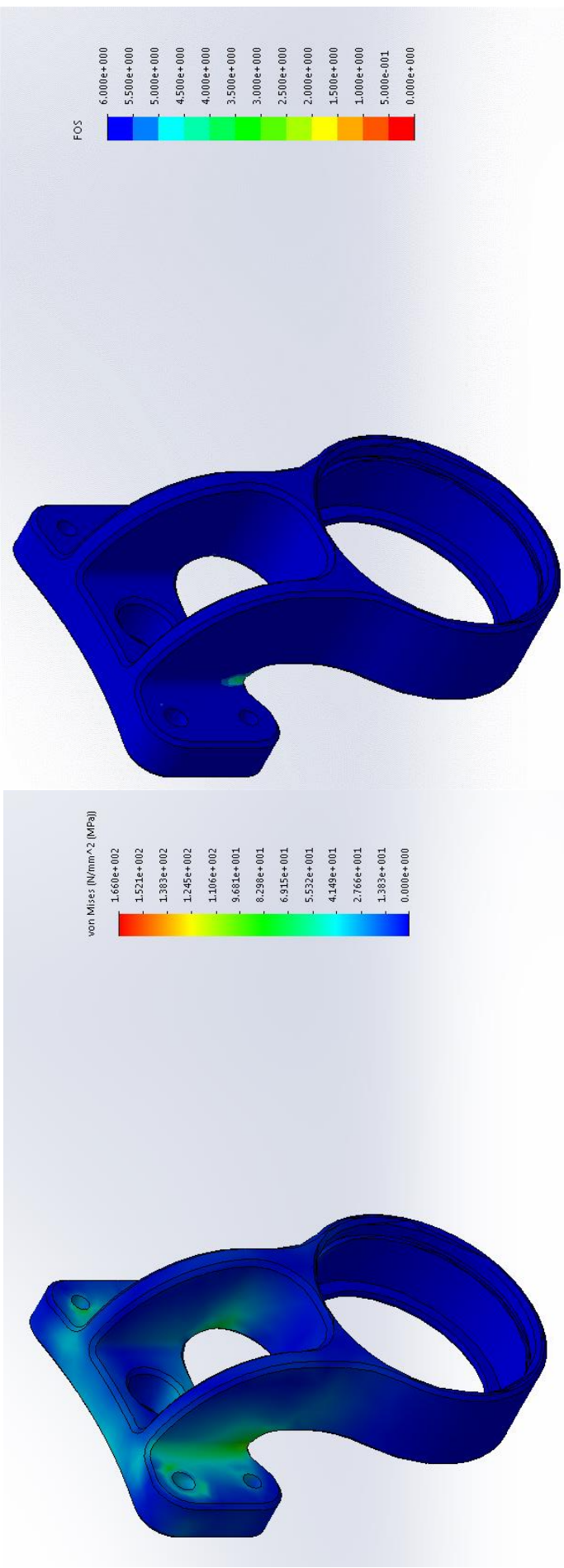
Figure J.5: Vertical component with vertical extension force applied from actuators. Stress and factor of safety shown. The minimum factor of safety is 3.5
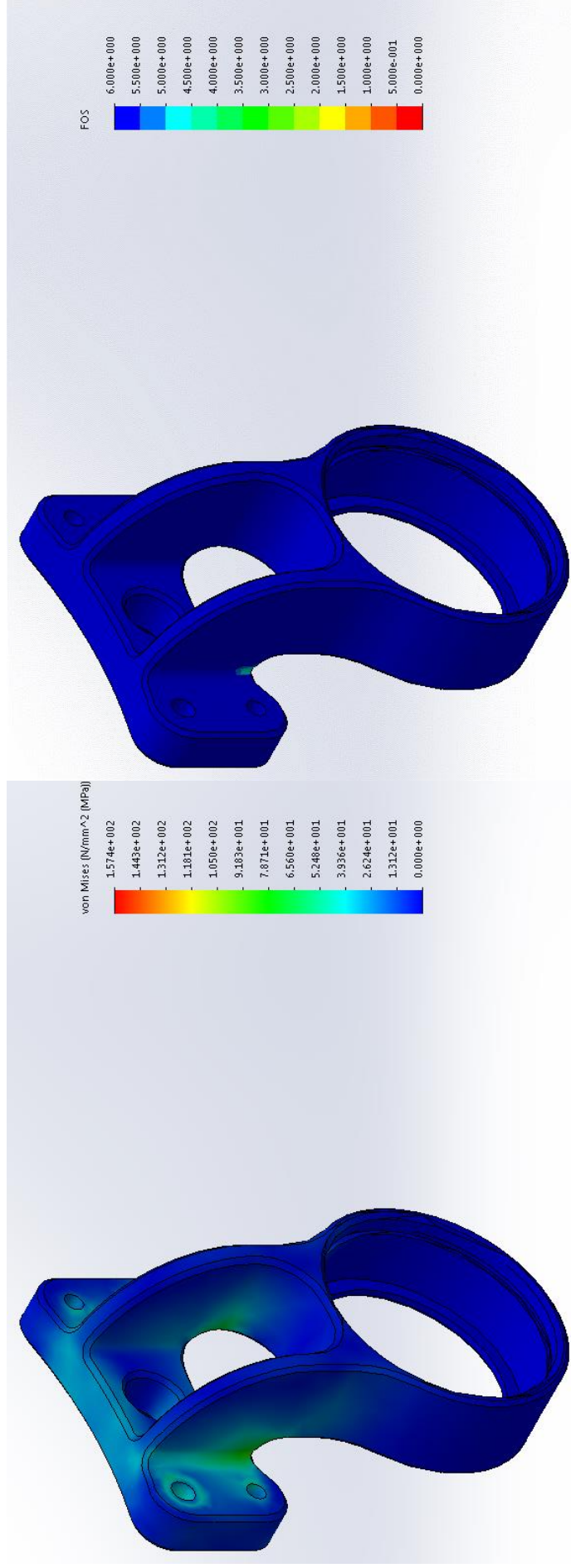
Figure J.6: Vertical component with vertical retraction force applied from actuators. Stress and factor of safety shown. The minimum factor of safety is 3.7
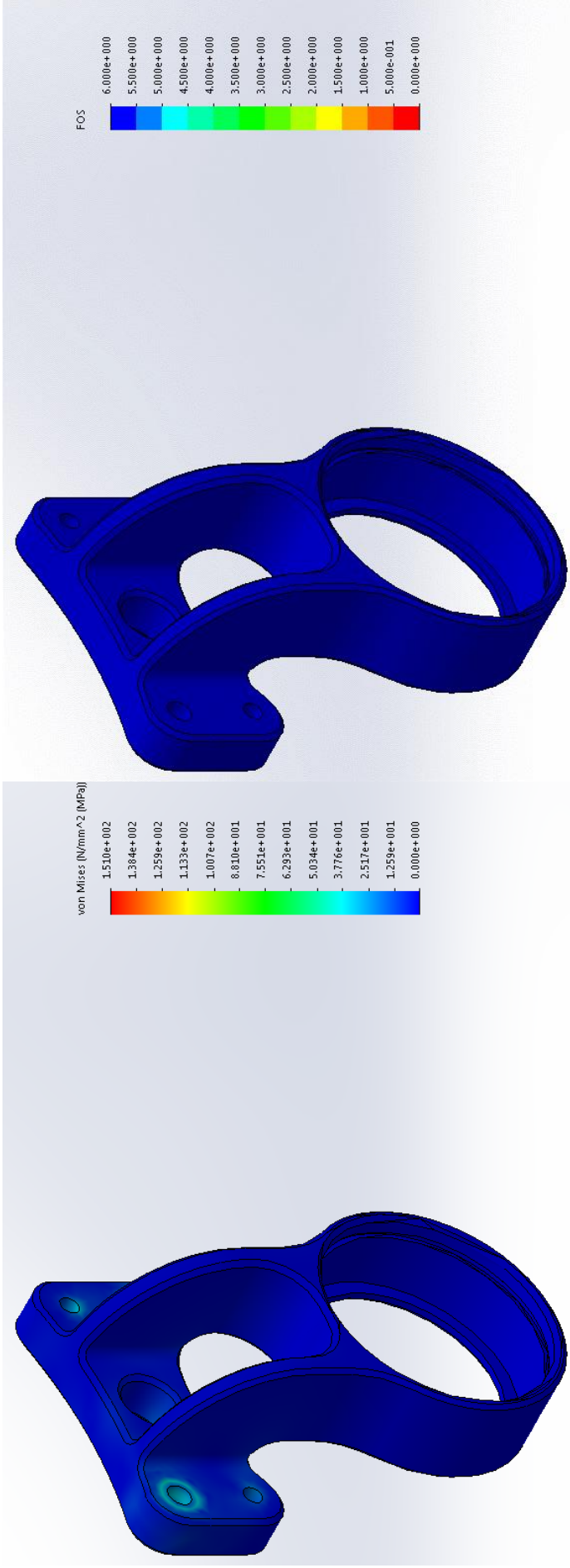
Figure J.7: Vertical component with horizontal extension force applied from actuators. Stress and factor of safety shown. The minimum factor of safety is 8.7
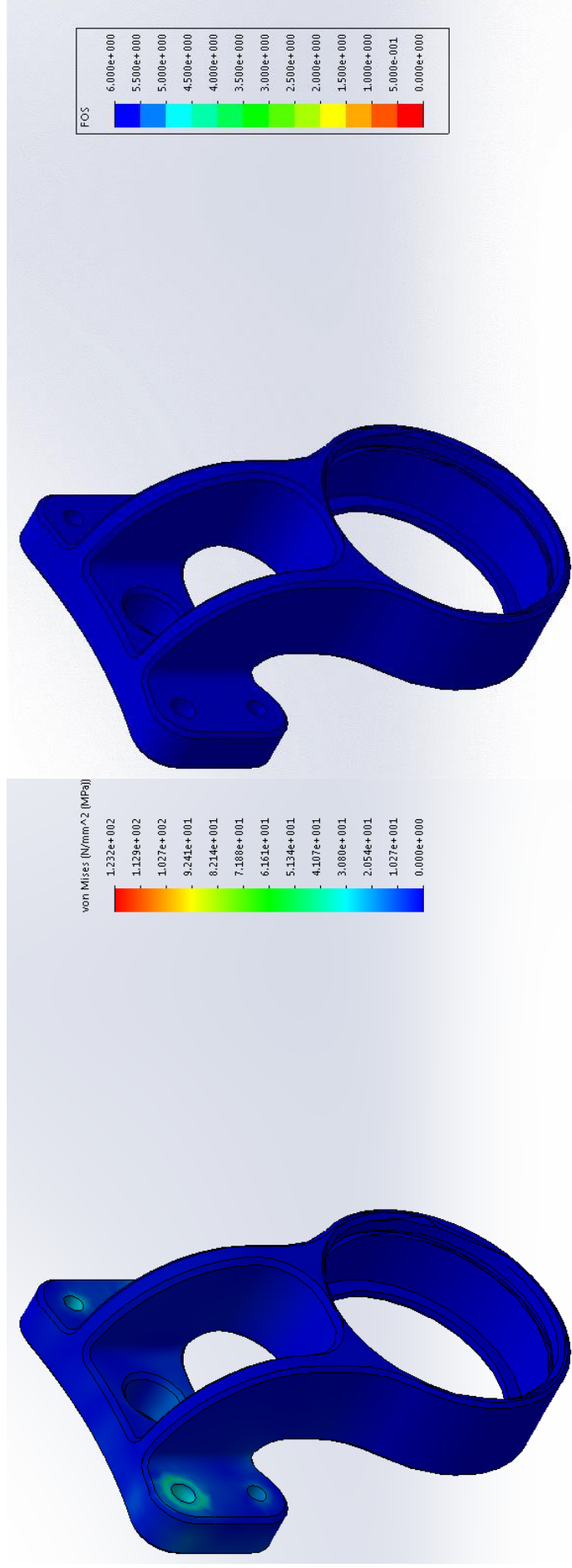
Figure J.8: Vertical component with horizontal retraction force applied from actuators. Stress and factor of safety shown. The minimum factor of safety is 7.9
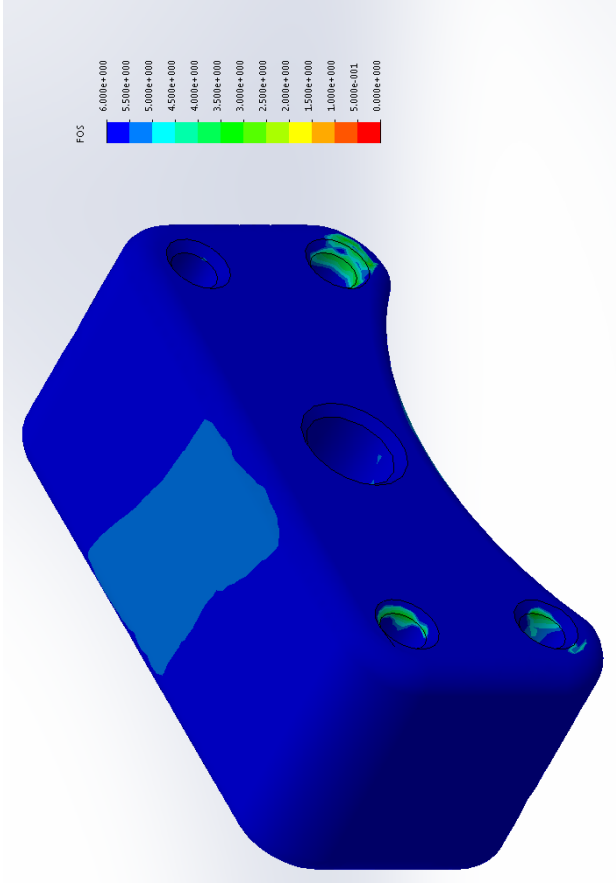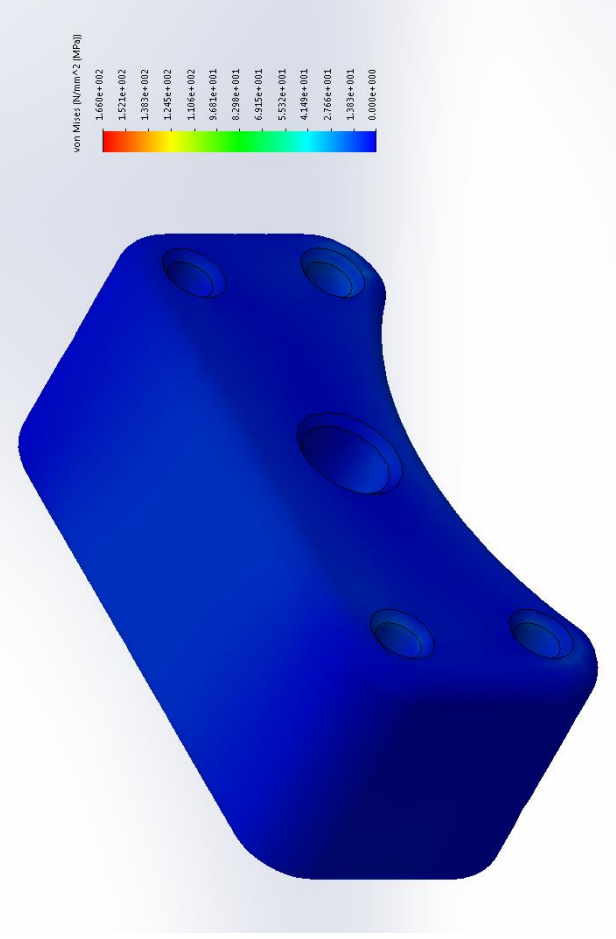
Figure J.9: Spacer component with vertical extension force applied from actuators. Stress and factor of safety shown. The minimum factor of safety is 2.5
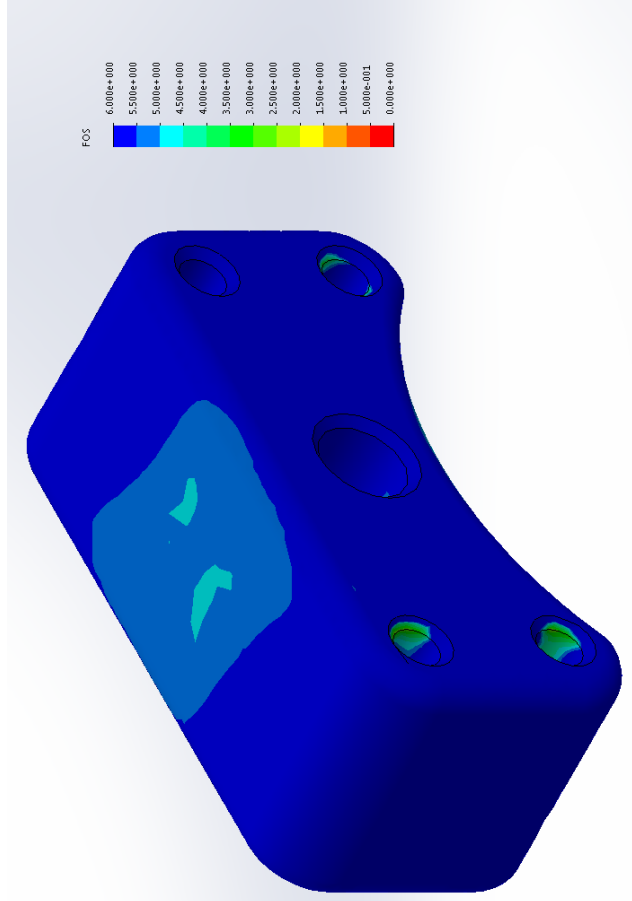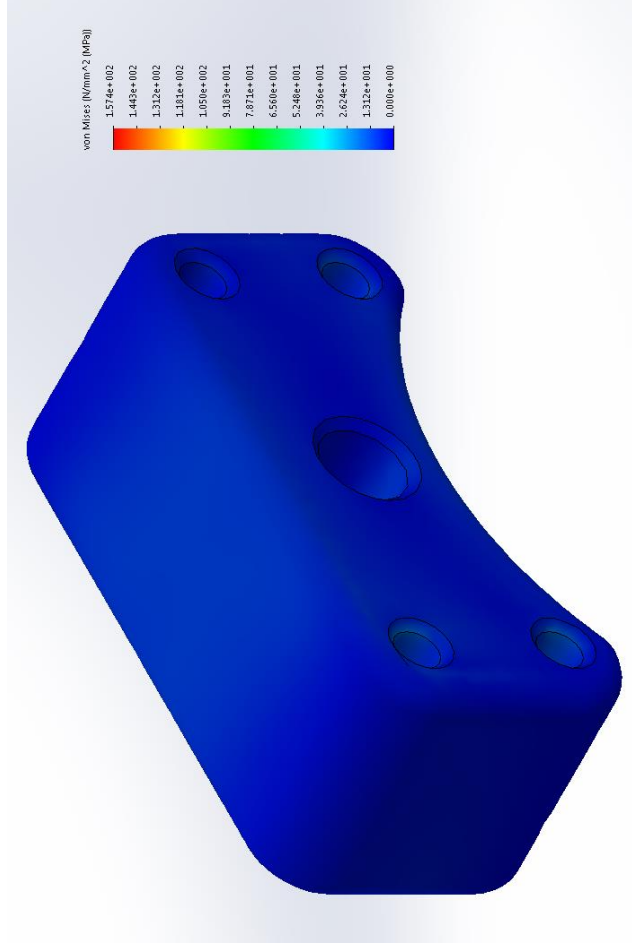
Figure J.10: Spacer component with vertical retraction force applied from actuators. Stress and factor of safety shown. The minimum factor of safety is 2.4
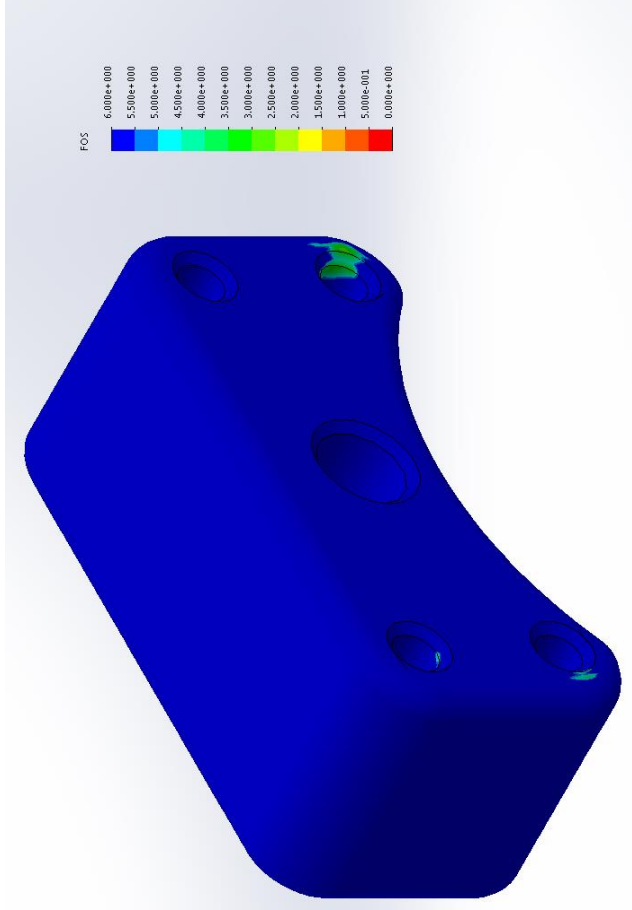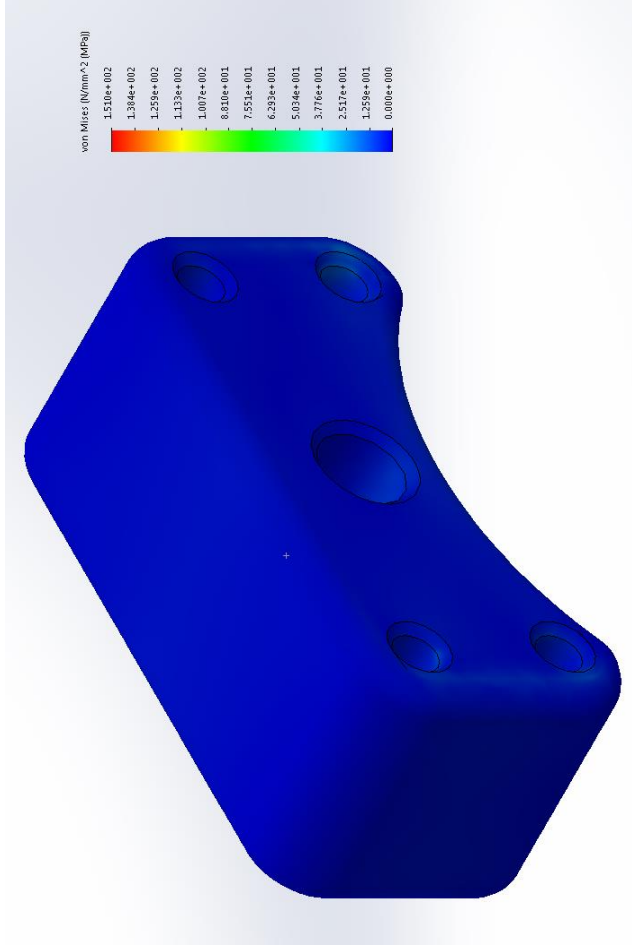
Figure J.11: Spacer component with horizontal extension force applied from actuators. Stress and factor of safety shown. The minimum factor of safety is 2.7
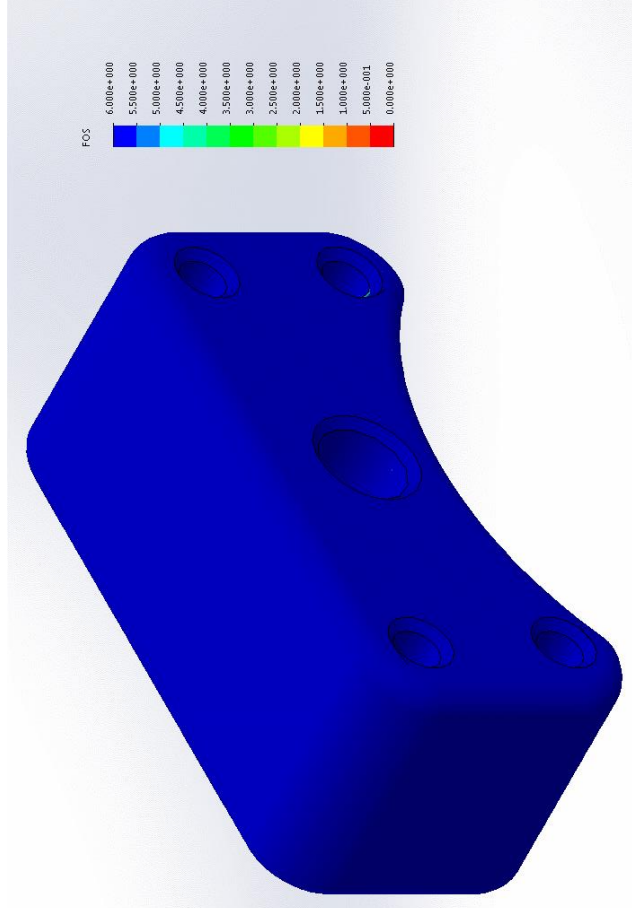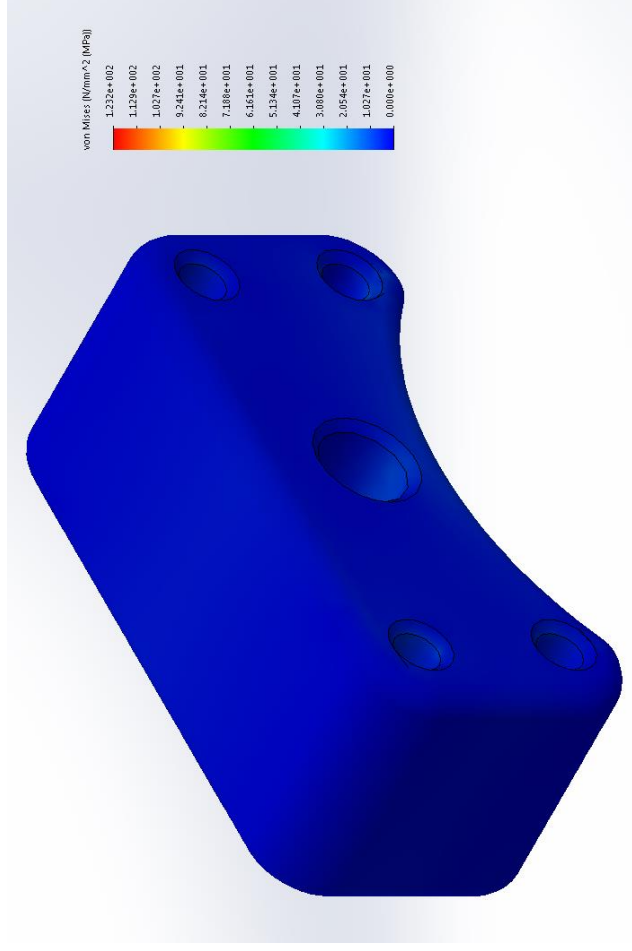
Figure J.12: Spacer component with horizontal retraction force applied from actuators. Stress and factor of safety shown. The minimum factor of safety is 3.7
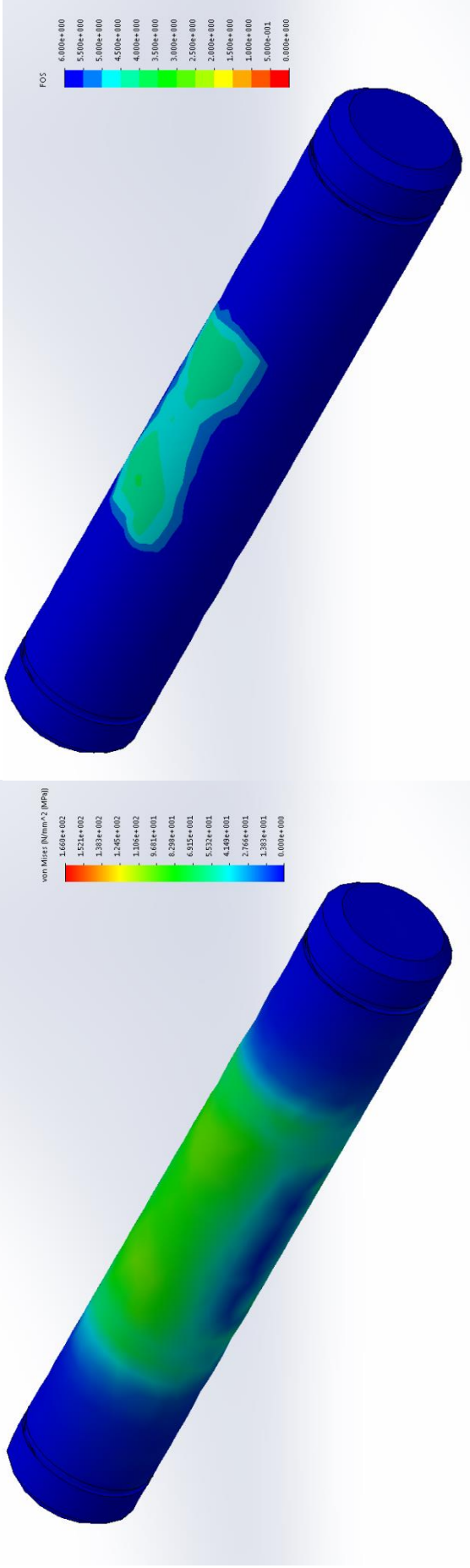
Figure J.13: Connection pin with vertical extension force applied from actuators. Stress and factor of safety shown. The minimum factor of safety is 3.9
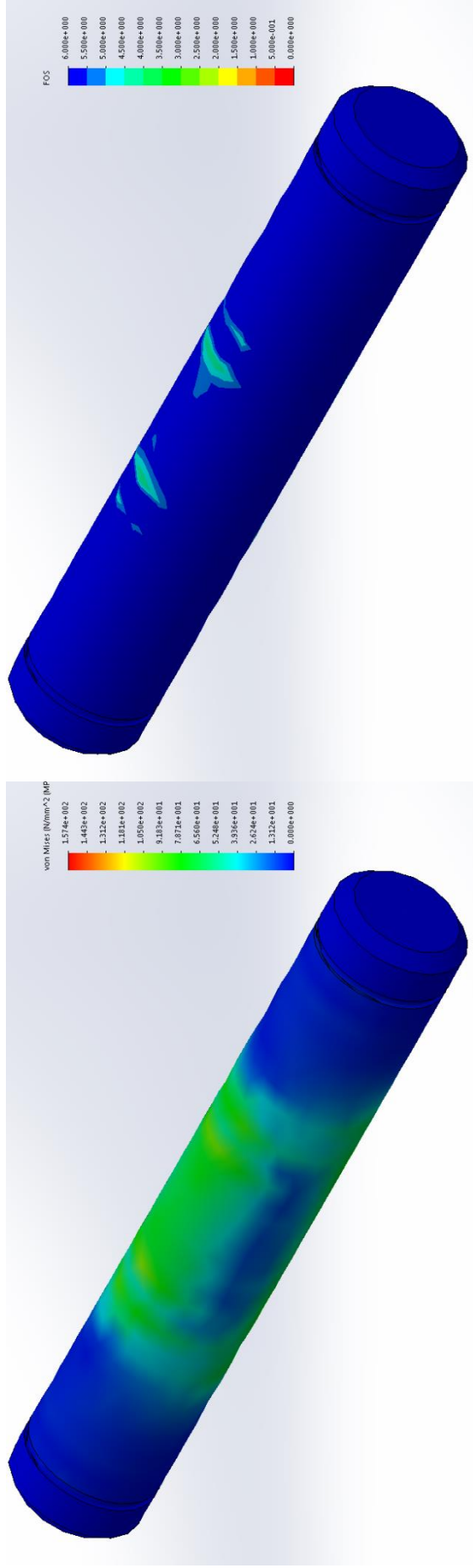
Figure J.14: Connection pin with vertical retraction force applied from actuators. Stress and factor of safety shown. The minimum factor of safety is 3.8
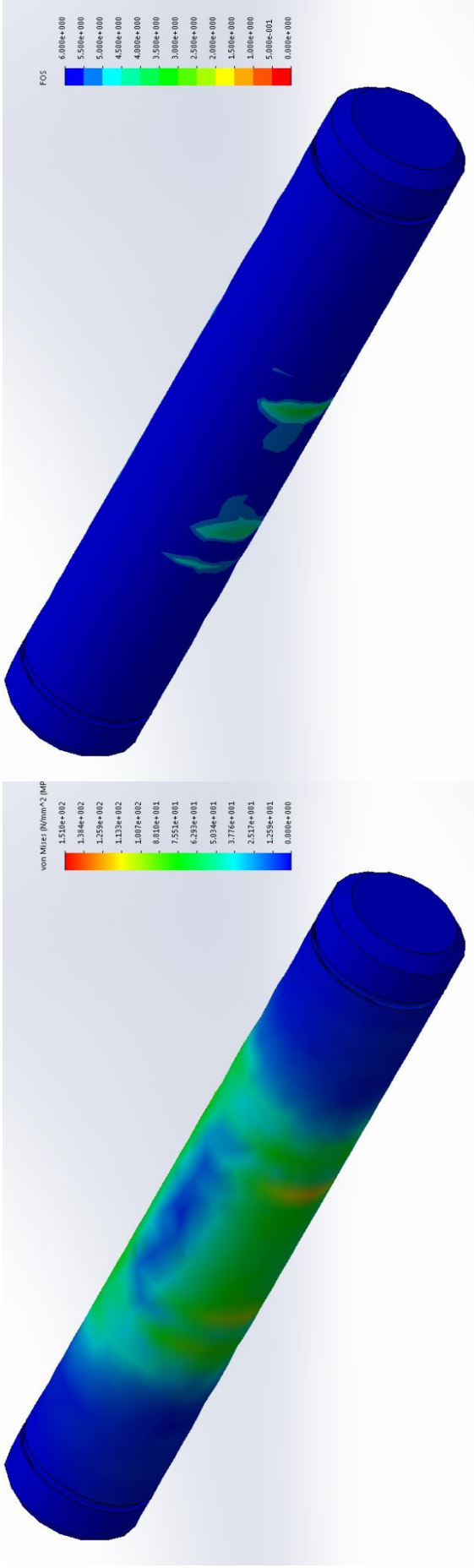
Figure J.15: Connection pin with horizontal extraction force applied from actuators. Stress and factor of safety shown. The minimum factor of safety is 3.3
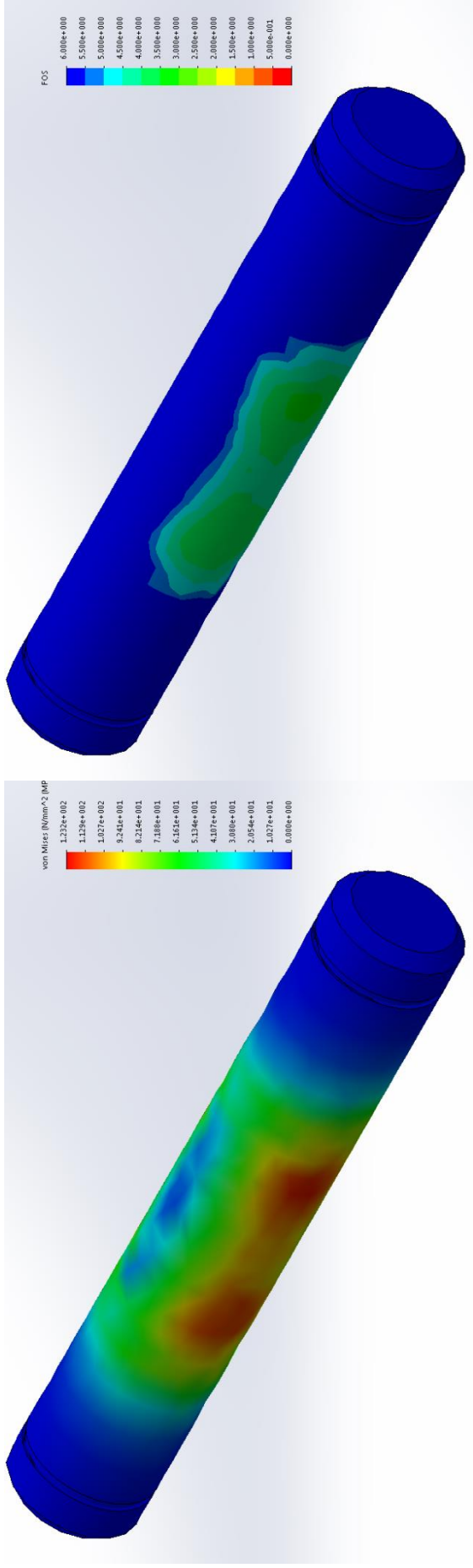
Figure J.16: Connection pin with horizontal retraction force applied from actuators. Stress and factor of safety shown. The minimum factor of safety is 3.3

Appendix K
Testing Results

K.1 Introduction

As the initial single joint design was developed for another PhD student, they led the testing of the system [K.1]. The plan was for the system to mimic gait, but the input device for the system to follow was unable to do this.

K.2 System images

The system as described in Appendices G to J was manufactured in the University of Leeds workshops and is shown in Figure K.

The patella structure can be seen on the right of the image between the two blue actuators. Between the actuators and the patella are the force sensors and adaptors. The hydraulic pump is contained within its own enclosed area to protect people working in the area.

The vertical bar separated from the main leg by the white and yellow supports is for the test input joint, currently not shown. This would connect to a multi-axis force sensor, which in the image is currently connected to a red handle. The weight on the leg is 60kg.

The electronics developed by Maciej can be seen in the top left and utilised the force sensors, an LVDT and the multi-axis force sensor to control the motion of the actuators via a simple servo valve system. The multi-axis force sensor would be used to detect the user motion and activate the hydraulics to reduce the force load on the user.

Figure K.1: Complete single joint test rig for the University of Leeds enhancive exoskeleton [K.1]

The testing was conducted in an enclosed environment to protect the tester and others in the environment. The system was also set up with 'Lockout, Tag-Out' as a requirement to prevent tampering and unintended use.

K.3 Positional testing

Due to issues with the initial development, the motion range was limited to only 73.3°. This still gives a range of motion that can be tested and is within the range for gait, which Maciej was using the joint for.

The initial testing covered the motion range of the system, as well as testing the algorithms to make sure that the rod extensions were coordinated. The results

of a zero load position cycle, including actuator displacement, are shown in Figure K.2. The difference between the two actuator displacements is due to the actuators entering the cushioned area.
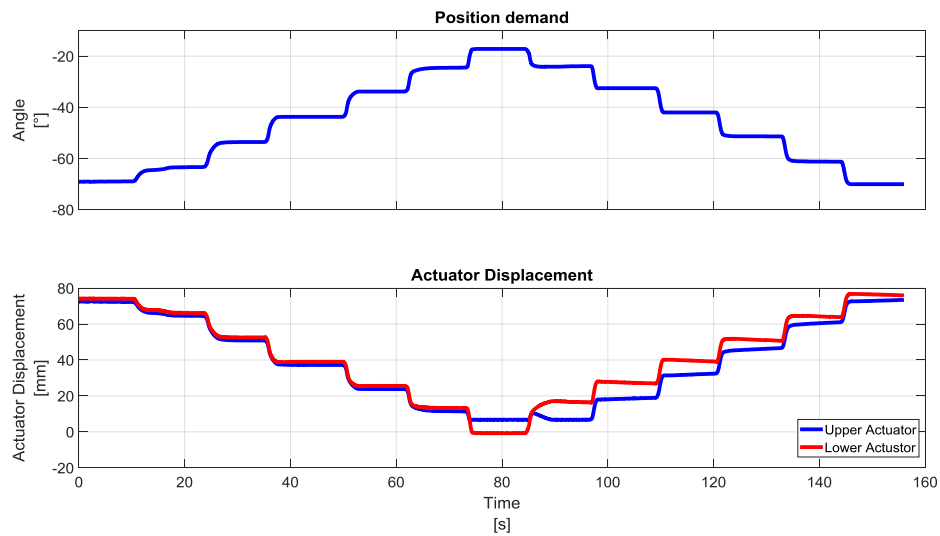
Figure K.2: Angle at the knee joint and actuator displacement

K.4 Load testing

The system, as shown in Figure K., was dynamically tested with zero and 60 kg of load, and was reported to have the response as shown in

Table K.1: Dynamic response of the single joint system with different loads [K.1]

Weight	Bandwidth	Actuator displacement error	Max User Load
kg	Hz	mm	N
0	0.6	10	40
60	0.5	5	20

It can be seen that the system is close to being weight indifferent, in that the bandwidth and the user load input is similar. The maximum user load is what the human would feel as the load to their motion, and is low compared to the actual value. With the 60 kg load at 80° from the vertical, the true torque required to resist this 579.7·D Nm, where D is the moment arm. The torque the user is actually feeling is 20·D Nm, and thus is a 1:29.0 reduction in the force experienced. This shows that the initial single joint design is capable of giving a load reduction, though additional work is required to increase the bandwidth.

References

K.1. Napora, M.G. *Control Aspects of a Full-body Enhancive Robotic Exoskeleton.* PhD thesis, University of Leeds, 2018.

Appendix L

Material Selection

L.1 Material Selection

There are several materials that could be used for the structure of the exoskeleton, ranging from aluminium to steel. There are several common ones for each category and need to be compared against each other to determine the correct material to use.

With the selected material's specification, a rough decision matrix can be generated. Assuming that the shoulder is likely to have the largest torque, the dimensions and loading for this will be used for the analysis. If each part of the arm is 400mm, with a load of 65kg at the end and 20kg for the elbow, a rough point load can be determined for the elbow.

L.2 Beam selection method

Using the equations from (mechanical engineering design} the calculations for the materials can be defined.

$$R_1 = F \tag{L.1}$$
$$M = F(x - L_2) \tag{L.2}$$

Where R_1 is the reaction force at the end of the beam, and M is the moment at the end of the beam. L_2 is the length of the beam. These can then give the stress, strain and deflection for the system.

$$\sigma = \frac{Mb}{I} \tag{L.3}$$

$$\tau = \frac{3R_1}{2A} \tag{L.4}$$

$$y_{max} = \left| \frac{-F \times L_2^3}{3EI} \right| \tag{L.5}$$

Where

$$A = b^2 \tag{L.6}$$

$$I = \frac{b^4}{12} \tag{L.7}$$

Assuming that the beams are square in section, with the length of b and where E is the modulus of elasticity.

If σ and τ are limited by the material yield strength and the deflection is limited to 1mm, the follow equation for the beam size is

$$b = max\left(\left(\frac{12M \times SF}{\sigma}\right)^{\frac{1}{3}}, \frac{\sqrt{6}\sqrt{R_1}\sqrt{SF}}{2\sqrt{\tau}}, \left(\frac{4F \times L_2^3}{E \times d_{min}}\right)^{\frac{1}{4}}\right) \quad \textbf{(L.8)}$$

Where SF is the safety factor and d_{min} is the minimum deflection Figure L. shows the resulting values
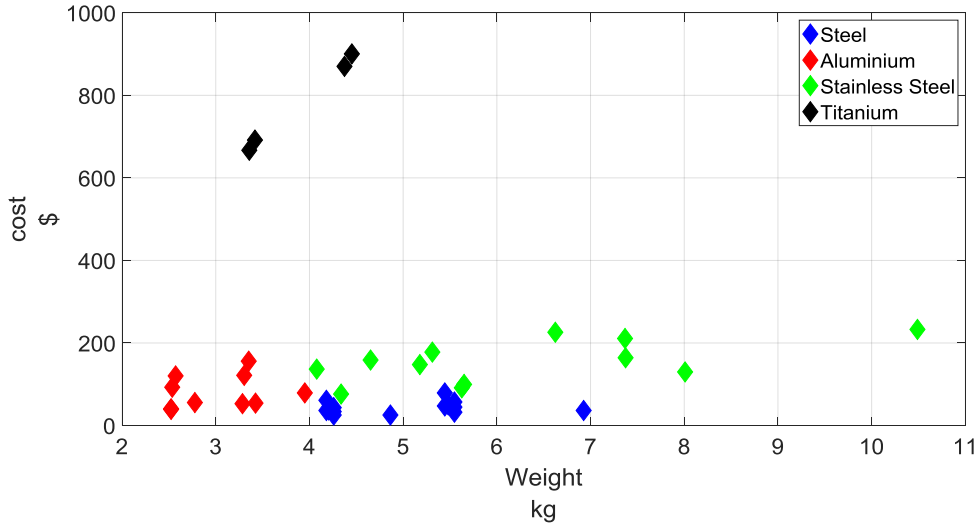
Figure L.1: Weight versus Cost for the bar design selection

It would appear that the aluminium are the ideal materials, but this is confused by the titanium skew of the cost. If the distance of cost and weight to the origin are calculated then the following polar plot is generated in Figure L.2. The distance from the centre is the distance of the results from the origin with the materials equally spaced in angle around the origin.
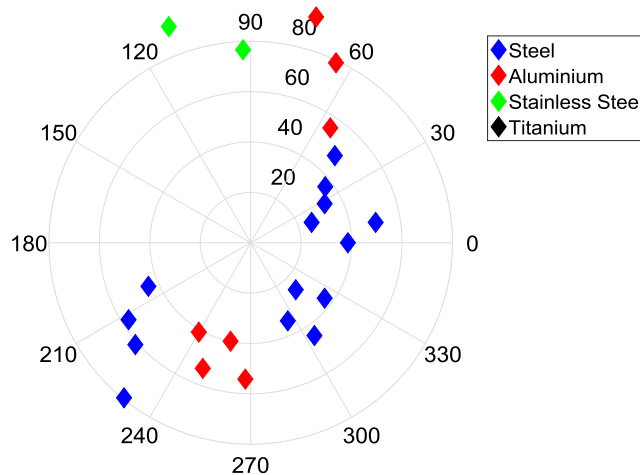
Figure L.2: Norm of Minimum Cost and Weight of materials based on bar design selection

From this, it can be seen that the steels are actually the ideal material for the system. The closest material to the origin is 1045 steel.

L.2.1 Hub Selection Method

If the system requires attaching to shafts, then the use of keyless bushings is an option. An example of these are made by SKF. There is an equation to relate the outside diameter of the bushing to the hub diameter. This is dependent on the strength of the material and the installation setup. These are looked up with the hub surface pressure, which is bushing dependant.

This then gives a volume for a hollow cylinder that has a weight and a cost, as shown in Figure L.3.
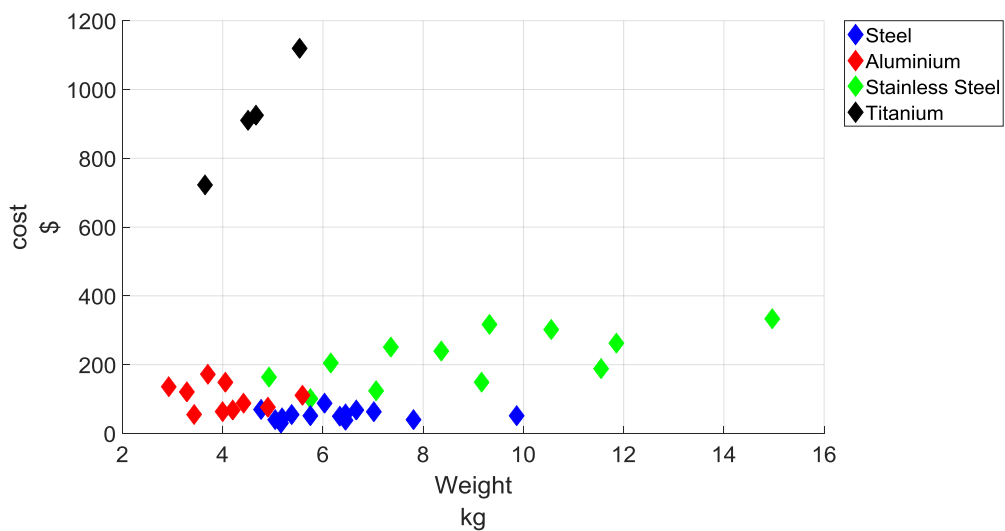
Figure L.3: Weight versus Cost for the bar design with hub included

As the hub could result in a large diameter, this also needs to be taken into account. This is shown in Figure L.4.
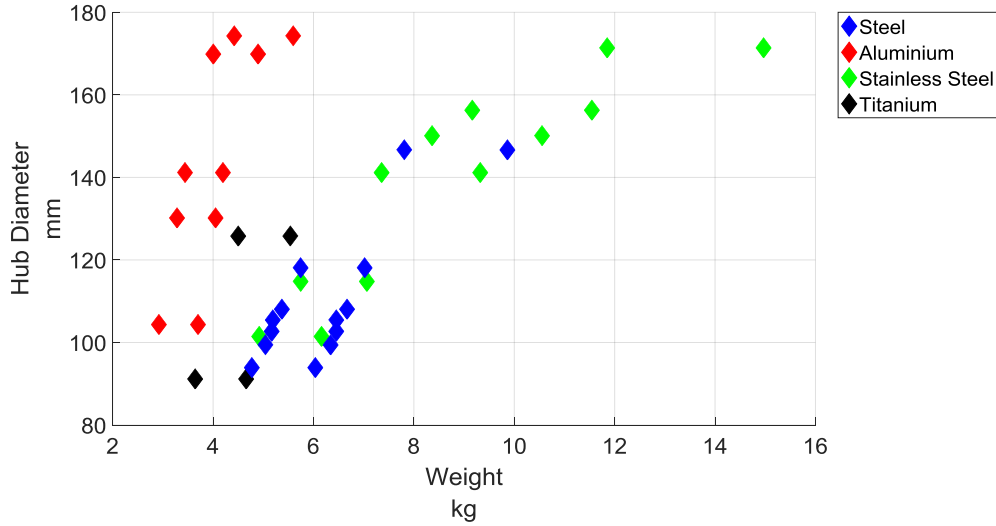
Figure L.4: Weight versus hub diameter for the bar design with hub included

Similarly to the pure bar results, the distance from, the origin to the point based on cost, weight and hub diameter is shown in Figure L.5
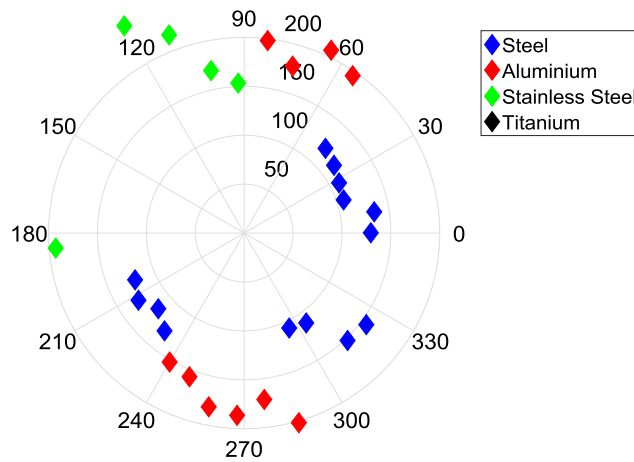
Figure L.5: Minimum Cost, Weight of materials and Hub Diameter based on bar design selection

Though the steels are the closest materials to the origin, this is due to the low cost of several of them. If there is a limit to the weight, for example, 5 kg, and a limit on the price of $200 and a limit of the hub diameter to 120mm, then the results are shown in Figure L.6
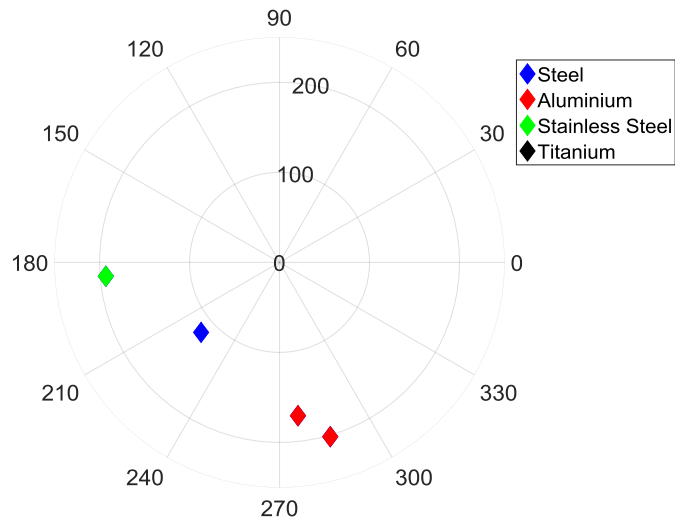
Figure L.6: Minimum Cost, Weight of materials and Hub Diameter based on bar design selection based on limits

There are four materials that are within the limitations as shown in Figure L.6. 4140 is a Society of Automotive Engineers (SAE) grade steel, primarily used for structural tubing including bicycles and roll bars. 4140 has issues with welding and requires pre and post heat treatment. 7075-T6 is a high strength aluminium often used in transport applications like aircraft. 410 is a stainless steel.

Table L.1: Final Material selection

	Weight	Cost	Hub Diameter
4140 SQUARE	4.77	$ 69.45	93.94
7075-T6 SQUARE	2.92	$ 136.03	104.41
410 SQUARE	4.92	$ 164.53	101.46
7075-T6 ROUND	3.70	$ 172.31	104.41

With the strength, weight and cost examined, one other requirement that will be important for a hazardous use is corrosion resistance. 4140 does not have significant corrosion resistance, and thus would need to be protected with a coating. 7075 being an aluminium has better corrosion resistance than the steel, though will still have some reaction in use. 410 being a stainless steel will have improved resistance to corrosion.

7075 will be selected for the exoskeleton design for extremities to reduce the weight requirements for the actuators. Localised structures like the rear of the unit could be steel to reduce the cost

Appendix M

Torque requirement calculation

The selection of the actuator is based upon the torque requirements for the motion [M.1]. This can be determined by adding together the different torque requirements for the system. This is outlined in (M.1).

$$M_D = \left(M_L + M_f + M_\alpha\right) \times design\ safety\ factor \qquad \textbf{(M.1)}$$

Where M_D is the demand torque, M_L is the load torque, M_f is the friction torque and M_α is the acceleration torque. The load torque is the value to support the weight of the load in a static position. The friction torque is the value required to overcome any friction in the system particularly any bearing surfaces. The acceleration torque is the value to overcome any inertia of the load to accelerate or decelerate the load. This is the rotational mass moment of inertia multiplied by the angular acceleration.

This is expanded with the cushion torque, M_C, which is the value used to slow down the load, based on the deceleration α*. This is shown in (M.2).

$$M_C = \left(M_D + M_{\alpha^*} - M_f\right) \times design\ safety\ factor \qquad \textbf{(M.2)}$$

For an over centre load, these equations become
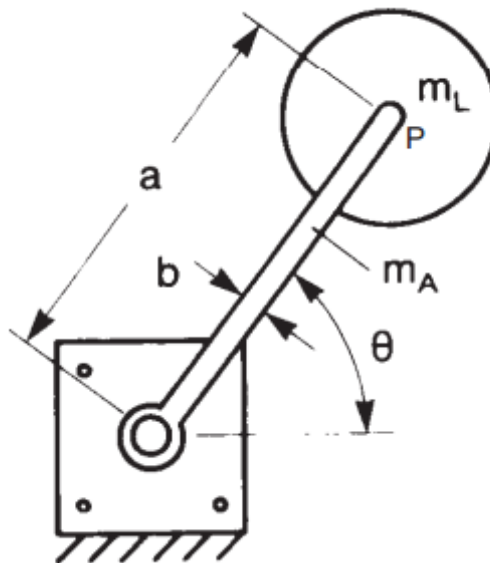
Figure M.1: Over centre load system [N.1]

$$M_D = (M_L + M_f + M_\alpha) \times design\ safety\ factor \qquad \textbf{(M.3)}$$

$$\pm M_L = \left(m_L g + \frac{1}{2} m_A g\right) \mathbf{a} \cos \theta \qquad \textbf{(M.4)}$$

$$M_f = 0, assuming\ no\ external\ bearings \qquad \textbf{(M.5)}$$

$$M_\alpha = \left[\frac{1}{12} m_A(a^2 + b^2) + \frac{m_A a^2}{4} + J_L + m_L a^2\right]\alpha \qquad \textbf{(M.6)}$$

$$M_{Dmax} = \left(\left(m_L g + \frac{1}{2} m_A g\right)\right.$$
$$+ \left[\frac{1}{12} m_A(a^2 + b^2) + \frac{m_A a^2}{4} + J_L \qquad \textbf{(M.7)}\right.$$
$$\left.\left. + m_L a^2\right]\alpha\right) \times design\ safety\ factor$$

Where J_L is the moment of inertia of the mass itself.

Though the frictional moment can be assumed to be zero, SKF has a bearing friction estimator [M.2] as the joint will need out of rotation moment support. The equation is

$$M_f = 0.5\mu Pd \qquad \textbf{(M.8)}$$

Where µ is the constant coefficient of friction for the bearing, P is the equivalent dynamic bearing load and d is the bore diameter. The constant-coefficient is 0.0015 for deep groove ball bearings and 0.0018 for tapered roller bearings.

References

M.1.   Hydraulics, P. Rotary Actuator Applications Guide. [Online]. **Bulletin 1230/2-GB**, p.20. [Accessed 16th November 2016].
M.2.   SKF. *Estimating the frictional moment* [Online]. [Accessed 16th November 2016]. Available from: http://www.skf.com/uk/products/bearings-units-housings/ball-bearings/principles/friction/estimating-frictional-moment/index.html

Appendix N

Actuators used in the optimisation

Record Number	Manufacturer	Model	Diameter			Stroke	Pressure Bar
			External	Internal	Shaft		
1	APH	Pencyl 6	20.0	10.0	6.0	50.0	350
2	APH	Pencyl 6	20.0	10.0	6.0	75.0	350
3	APH	Pencyl 6	20.0	10.0	6.0	100.0	350
4	APH	Pencyl 6	20.0	10.0	6.0	125.0	350
5	APH	Pencyl 6	20.0	10.0	6.0	150.0	350
6	APH	Pencyl 6	20.0	10.0	6.0	50.0	350
7	APH	Pencyl 6	20.0	10.0	6.0	75.0	350
8	APH	Pencyl 6	20.0	10.0	6.0	100.0	350
9	APH	Pencyl 6	20.0	10.0	6.0	125.0	350
10	APH	Pencyl 6	20.0	10.0	6.0	150.0	350
11	APH	Pencyl 10	25.0	16.0	10.0	50.0	350
12	APH	Pencyl 10	25.0	16.0	10.0	75.0	350
13	APH	Pencyl 10	25.0	16.0	10.0	100.0	350
14	APH	Pencyl 10	25.0	16.0	10.0	125.0	350
15	APH	Pencyl 10	25.0	16.0	10.0	150.0	350
16	APH	Pencyl 10	25.0	16.0	10.0	50.0	350
17	APH	Pencyl 10	25.0	16.0	10.0	75.0	350
18	APH	Pencyl 10	25.0	16.0	10.0	100.0	350
19	APH	Pencyl 10	25.0	16.0	10.0	125.0	350
20	APH	Pencyl 10	25.0	16.0	10.0	150.0	350
21	KYB Fluid Power	MMP		34.0	20.0	150.0	
22	KYB Fluid Power	MMP		34.0	20.0	200.0	
23	KYB Fluid Power	MMP		34.0	20.0	250.0	
24	KYB Fluid Power	MMP		34.0	20.0	300.0	
25	KYB Fluid Power	MMP		34.0	20.0	350.0	
26	CC cylinders	ccHyd 71220	28.0	20.0	12.0	25.0	250
27	CC cylinders	ccHyd 71220	28.0	20.0	12.0	50.0	250
28	CC cylinders	ccHyd 71220	28.0	20.0	12.0	80.0	250
29	CC cylinders	ccHyd 71220	28.0	20.0	12.0	100.0	250
30	BOSCH	CDL2	32.0	25.0	14.0	50.0	160
31	BOSCH	CDL2	32.0	25.0	14.0	75.0	160
32	BOSCH	CDL2	32.0	25.0	14.0	100.0	160
33	BOSCH	CDL2	32.0	25.0	14.0	125.0	160
34	BOSCH	CDL2	32.0	25.0	14.0	150.0	160
35	BOSCH	CDL2	32.0	25.0	14.0	50.0	160
36	BOSCH	CDL2	32.0	25.0	14.0	75.0	160
37	BOSCH	CDL2	32.0	25.0	14.0	100.0	160
38	BOSCH	CDL2	32.0	25.0	14.0	125.0	160
39	BOSCH	CDL2	32.0	25.0	14.0	150.0	160
40	APH	Pencyl 14	31.8	20.0	14.0	50.0	350
41	APH	Pencyl 14	31.8	20.0	14.0	75.0	350
42	APH	Pencyl 14	31.8	20.0	14.0	100.0	350
43	APH	Pencyl 14	31.8	20.0	14.0	125.0	350
44	APH	Pencyl 14	31.8	20.0	14.0	150.0	350
45	APH	Pencyl 14	31.8	20.0	14.0	50.0	350

46	APH	Pencyl 14	31.8	20.0	14.0	75.0	350
47	APH	Pencyl 14	31.8	20.0	14.0	100.0	350
48	APH	Pencyl 14	31.8	20.0	14.0	125.0	350
49	APH	Pencyl 14	31.8	20.0	14.0	150.0	350
50	BOSCH	CDM1	35.0	25.0	18.0	50.0	160
51	BOSCH	CDM1	35.0	25.0	18.0	75.0	160
52	BOSCH	CDM1	35.0	25.0	18.0	100.0	160
53	BOSCH	CDM1	35.0	25.0	18.0	125.0	160
54	BOSCH	CDM1	35.0	25.0	18.0	150.0	160
55	BOSCH	CDM1	35.0	25.0	18.0	50.0	160
56	BOSCH	CDM1	35.0	25.0	18.0	75.0	160
57	BOSCH	CDM1	35.0	25.0	18.0	100.0	160
58	BOSCH	CDM1	35.0	25.0	18.0	125.0	160
59	BOSCH	CDM1	35.0	25.0	18.0	150.0	160
60	Interfluid	interfluid	35.0	25.0	16.0	50.0	210
61	Interfluid	interfluid	35.0	25.0	16.0	100.0	210
62	Interfluid	interfluid	35.0	25.0	16.0	150.0	210
63	Interfluid	interfluid	35.0	25.0	16.0	200.0	210
64	KYB Fluid Power	MMP		40.0	20.0	150.0	
65	KYB Fluid Power	MMP		40.0	20.0	200.0	
66	KYB Fluid Power	MMP		40.0	20.0	250.0	
67	KYB Fluid Power	MMP		40.0	20.0	300.0	
68	KYB Fluid Power	MMP		40.0	20.0	350.0	
69	CC cylinders	ccHyd 71625	35.0	25.0	16.0	50.0	250
70	CC cylinders	ccHyd 71625	35.0	25.0	16.0	100.0	250
71	CC cylinders	ccHyd 71625	35.0	25.0	16.0	150.0	250
72	CC cylinders	ccHyd 71625	35.0	25.0	16.0	200.0	250
73	APH	Pencyl 17	38.0	25.0	18.0	50.0	350
74	APH	Pencyl 17	38.0	25.0	18.0	75.0	350
75	APH	Pencyl 17	38.0	25.0	18.0	100.0	350
76	APH	Pencyl 17	38.0	25.0	18.0	125.0	350
77	APH	Pencyl 17	38.0	25.0	18.0	150.0	350
78	APH	Pencyl 17	38.0	25.0	18.0	50.0	350
79	APH	Pencyl 17	38.0	25.0	18.0	75.0	350
80	APH	Pencyl 17	38.0	25.0	18.0	100.0	350
81	APH	Pencyl 17	38.0	25.0	18.0	125.0	350
82	APH	Pencyl 17	38.0	25.0	18.0	150.0	350
83	BOSCH	CDM1	35.0	25.0	14.0	50.0	160
84	BOSCH	CDM1	35.0	25.0	14.0	75.0	160
85	BOSCH	CDM1	35.0	25.0	14.0	100.0	160
86	BOSCH	CDM1	35.0	25.0	14.0	125.0	160
87	BOSCH	CDM1	35.0	25.0	14.0	150.0	160
88	BOSCH	CDL2	40.0	32.0	18.0	50.0	160
89	BOSCH	CDL2	40.0	32.0	18.0	75.0	160
90	BOSCH	CDL2	40.0	32.0	18.0	100.0	160
91	BOSCH	CDL2	40.0	32.0	18.0	125.0	160
92	BOSCH	CDL2	40.0	32.0	18.0	150.0	160
93	BOSCH	CDL2	40.0	32.0	18.0	50.0	160
94	BOSCH	CDL2	40.0	32.0	18.0	75.0	160
95	BOSCH	CDL2	40.0	32.0	18.0	100.0	160
96	BOSCH	CDL2	40.0	32.0	18.0	125.0	160
97	BOSCH	CDL2	40.0	32.0	18.0	150.0	160

98	KYB Fluid Power	MMP		46.0	20.0	150.0	
99	KYB Fluid Power	MMP		46.0	20.0	200.0	
100	KYB Fluid Power	MMP		46.0	20.0	250.0	
101	KYB Fluid Power	MMP		46.0	20.0	300.0	
102	KYB Fluid Power	MMP		46.0	20.0	350.0	
103	BOSCH	CDM1	42.0	32.0	22.0	50.0	160
104	BOSCH	CDM1	42.0	32.0	22.0	75.0	160
105	BOSCH	CDM1	42.0	32.0	22.0	100.0	160
106	BOSCH	CDM1	42.0	32.0	22.0	125.0	160
107	BOSCH	CDM1	42.0	32.0	22.0	150.0	160
108	BOSCH	CDM1	42.0	32.0	22.0	50.0	160
109	BOSCH	CDM1	42.0	32.0	22.0	75.0	160
110	BOSCH	CDM1	42.0	32.0	22.0	100.0	160
111	BOSCH	CDM1	42.0	32.0	22.0	125.0	160
112	BOSCH	CDM1	42.0	32.0	22.0	150.0	160
113	BOSCH	CDM1	42.0	32.0	18.0	50.0	160
114	BOSCH	CDM1	42.0	32.0	18.0	75.0	160
115	BOSCH	CDM1	42.0	32.0	18.0	100.0	160
116	BOSCH	CDM1	42.0	32.0	18.0	125.0	160
117	BOSCH	CDM1	42.0	32.0	18.0	150.0	160
118	BOSCH	CDM1	42.0	32.0	18.0	50.0	160
119	BOSCH	CDM1	42.0	32.0	18.0	75.0	160
120	BOSCH	CDM1	42.0	32.0	18.0	100.0	160
121	BOSCH	CDM1	42.0	32.0	18.0	125.0	160
122	BOSCH	CDM1	42.0	32.0	18.0	150.0	160
123	BOSCH	CDL2	50.0	40.0	22.0	50.0	160
124	BOSCH	CDL2	50.0	40.0	22.0	75.0	160
125	BOSCH	CDL2	50.0	40.0	22.0	100.0	160
126	BOSCH	CDL2	50.0	40.0	22.0	125.0	160
127	BOSCH	CDL2	50.0	40.0	22.0	150.0	160
128	BOSCH	CDL2	50.0	40.0	22.0	50.0	160
129	BOSCH	CDL2	50.0	40.0	22.0	75.0	160
130	BOSCH	CDL2	50.0	40.0	22.0	100.0	160
131	BOSCH	CDL2	50.0	40.0	22.0	125.0	160
132	BOSCH	CDL2	50.0	40.0	22.0	150.0	160
133	Enerpac	Enerpac	50.0	25.4	19.0	28.0	700
134	Enerpac	Enerpac	50.0	25.4	19.0	79.0	700
135	Enerpac	Enerpac	50.0	25.4	19.0	155.0	700
136	BOSCH	CDH1 MP3	52.0	40.0	28.0	50.0	250
137	BOSCH	CDH1 MP3	52.0	40.0	28.0	75.0	250
138	BOSCH	CDH1 MP3	52.0	40.0	28.0	100.0	250
139	BOSCH	CDH1 MP3	52.0	40.0	28.0	125.0	250
140	BOSCH	CDH1 MP3	52.0	40.0	28.0	150.0	250
141	BOSCH	CDM1	50.0	40.0	28.0	50.0	160
142	BOSCH	CDM1	50.0	40.0	28.0	75.0	160
143	BOSCH	CDM1	50.0	40.0	28.0	100.0	160
144	BOSCH	CDM1	50.0	40.0	28.0	125.0	160
145	BOSCH	CDM1	50.0	40.0	28.0	150.0	160
146	BOSCH	CDM1	50.0	40.0	28.0	50.0	160
147	BOSCH	CDM1	50.0	40.0	28.0	75.0	160
148	BOSCH	CDM1	50.0	40.0	28.0	100.0	160
149	BOSCH	CDM1	50.0	40.0	28.0	125.0	160
150	BOSCH	CDM1	50.0	40.0	28.0	150.0	160
151	BOSCH	CDH1 MP3	52.0	40.0	28.0	50.0	250

152	BOSCH	CDH1 MP3	52.0	40.0	28.0	75.0	250
153	BOSCH	CDH1 MP3	52.0	40.0	28.0	100.0	250
154	BOSCH	CDH1 MP3	52.0	40.0	28.0	125.0	250
155	BOSCH	CDH1 MP3	52.0	40.0	28.0	150.0	250
156	BOSCH	CDL2	52.0	40.0	25.0	60.0	250
157	BOSCH	CDL2	52.0	40.0	25.0	75.0	250
158	BOSCH	CDL2	52.0	40.0	25.0	100.0	250
159	BOSCH	CDL2	52.0	40.0	25.0	125.0	250
160	BOSCH	CDL2	52.0	40.0	25.0	150.0	250
161	BOSCH	CDL2	52.0	40.0	25.0	50.0	250
162	BOSCH	CDL2	52.0	40.0	25.0	75.0	250
163	BOSCH	CDL2	52.0	40.0	25.0	100.0	250
164	BOSCH	CDL2	52.0	40.0	25.0	125.0	250
165	BOSCH	CDL2	52.0	40.0	25.0	150.0	250
166	BOSCH	CDH1 MP3	52.0	40.0	22.0	50.0	250
167	BOSCH	CDH1 MP3	52.0	40.0	22.0	75.0	250
168	BOSCH	CDH1 MP3	52.0	40.0	22.0	100.0	250
169	BOSCH	CDH1 MP3	52.0	40.0	22.0	125.0	250
170	BOSCH	CDH1 MP3	52.0	40.0	22.0	150.0	250
171	BOSCH	CDM1	50.0	40.0	22.0	50.0	160
172	BOSCH	CDM1	50.0	40.0	22.0	75.0	160
173	BOSCH	CDM1	50.0	40.0	22.0	100.0	160
174	BOSCH	CDM1	50.0	40.0	22.0	125.0	160
175	BOSCH	CDM1	50.0	40.0	22.0	150.0	160
176	BOSCH	CDM1	50.0	40.0	22.0	50.0	160
177	BOSCH	CDM1	50.0	40.0	22.0	75.0	160
178	BOSCH	CDM1	50.0	40.0	22.0	100.0	160
179	BOSCH	CDM1	50.0	40.0	22.0	125.0	160
180	BOSCH	CDM1	50.0	40.0	22.0	150.0	160
181	BOSCH	CDH1 MP3	52.0	40.0	22.0	50.0	250
182	BOSCH	CDH1 MP3	52.0	40.0	22.0	75.0	250
183	BOSCH	CDH1 MP3	52.0	40.0	22.0	100.0	250
184	BOSCH	CDH1 MP3	52.0	40.0	22.0	125.0	250
185	BOSCH	CDH1 MP3	52.0	40.0	22.0	150.0	250

Appendix O

Rotary Actuators

Type	Manufacture	Model	Angle	Pressure	Max Force	Weight	Specific Torque
			°	bar	Nm	kg	Nm/kg
Helical	Helac	L10 1.7	180	207	192	6.4	30.0
Helical	Helac	L10 3	180	207	339	10.0	33.9
Helical	Helac	L10 3	360	207	339	12.7	26.7
Helical	Helac	L10 5.5	180	207	622	14.1	44.1
Helical	Helac	L10 5.5	360	207	622	19.1	32.6
Helical	Helac	L10 9.5	180	207	1074	25.9	41.5
Helical	Helac	L10 9.5	360	207	1074	34.9	30.8
Helical	Helac	L10 15	180	207	1696	43.1	39.4
Helical	Helac	L10 15	360	207	1696	54.4	31.2
Helical	Helac	L10 25	180	207	2825	56.7	49.8
Helical	Helac	L10 25	360	207	2825	83.0	34.0
Helical	HKS	SA-H 30	90	210	63	5.6	11.3
Helical	HKS	DA-H 40	90	210	201.6	4.3	46.9
Helical	HKS	DA-H 40	180	210	201.6	4.8	42.0
Helical	HKS	DA-H 40	270	210	201.6	5.8	34.8
Helical	HKS	DA-H 40	360	210	201.6	6.2	32.5
Helical	HKS	SA-H 42	90	210	199.5	6.9	28.9
Helical	HKS	DA-H 50	90	210	340.2	6.0	56.7
Helical	HKS	DA-H 50	180	210	340.2	6.8	50.0
Helical	HKS	DA-H 50	270	210	340.2	7.8	43.6
Helical	HKS	DA-H 50	360	210	340.2	8.7	39.1
Helical	HKS	M-DA-H 50	180	210	190	7.4	25.7
Helical	HKS	SA-H 55	90	210	441	8.2	53.8
Helical	HKS	M-DA-H 60	180	210	340	10.6	32.1
Helical	HKS	M-DA-H 60	360	210	340	13.5	25.2
Helical	HKS	DA-H 63	90	210	651	8.5	76.6
Helical	HKS	DA-H 63	180	210	651	9.8	66.4
Helical	HKS	SA-H 63	90	210	630	12.0	52.5
Helical	HKS	DA-H 63	270	210	651	12.9	50.5
Helical	HKS	M-DA-H 63	180	210	720	14.4	50.0
Helical	HKS	DA-H 63	360	210	651	14.0	46.5
Helical	HKS	M-DA-H 63	180	210	1073	26.5	40.5
Helical	HKS	M-DA-H 63	360	210	720	18.8	38.3
Helical	HKS	M-DA-H 63	360	210	1073	36.0	29.8
Helical	HKS	M-DA-H-F1 70	180	210	500	12.1	41.3
Helical	HKS	M-DA-H 70	180	210	500	12.8	39.1
Helical	HKS	DA-H 80	90	210	1302	16.7	78.0
Helical	HKS	SA-H 80	90	210	1512	20.6	73.4
Helical	HKS	DA-H 80	180	210	1302	19.1	68.2
Helical	HKS	DA-H 80	270	210	1302	21.5	60.6
Helical	HKS	DA-H 80	360	210	1302	24.0	54.3
Helical	HKS	DA-H 100	90	210	2499	24.1	103.7
Helical	HKS	DA-H 100	180	210	2499	29.2	85.6

Helical	HKS	DA-H 100	270	210	2499	34.0	73.5
Helical	HKS	DA-H 100	360	210	2499	38.5	64.9
Helical	HKS	M-DA-H-F5 115	180	210	1920	35.0	54.9
Helical	HKS	M-DA-H-F5 115	360	210	1920	47.0	40.9
Helical	HKS	M-DA-H-F5 125	180	210	2820	48.0	58.8
Helical	HKS	DA-H 125	90	210	5107.2	47.0	108.7
Helical	HKS	DA-H 125	180	210	5107.2	55.0	92.9
Helical	HKS	DA-H 125	270	210	5107.2	63.5	80.4
Helical	HKS	DA-H 125	360	210	5107.2	72.5	70.4
Helical	HKS	DA-H 140	90	210	7098	74.0	95.9
Helical	HKS	DA-H 140	180	210	7098	87.0	81.6
Helical	HKS	DA-H 140	270	210	7098	101.0	70.3
Helical	HKS	DA-H 140	360	210	7098	115.0	61.7
Helical	HKS	DA-H 160	90	210	11298	114.0	99.1
Helical	HKS	DA-H 160	180	210	11298	136.0	83.1
Helical	HKS	DA-H 160	270	210	11298	154.0	73.4
Helical	HKS	DA-H 160	360	210	11298	170.0	66.5
Helical	HKS	DA-H 180	90	210	16199.4	150.0	108.0
Helical	HKS	DA-H 180	180	210	16199.4	187.0	86.6
Helical	HKS	DA-H 180	270	210	16199.4	213.0	76.1
Helical	HKS	DA-H 180	360	210	16199.4	245.0	66.1
Helical	HKS	DA-H 200	90	210	22302	194.0	115.0
Helical	HKS	DA-H 200	180	210	22302	238.0	93.7
Helical	HKS	DA-H 200	270	210	22302	264.0	84.5
Helical	HKS	DA-H 200	360	210	22302	306.0	72.9
Helical	HKS	DA-H 225	90	210	31999.8	404.0	79.2
Helical	HKS	DA-H 225	180	210	31999.8	488.0	65.6
Helical	HKS	DA-H 225	270	210	31999.8	565.0	56.6
Helical	HKS	DA-H 225	360	210	31999.8	630.0	50.8
Helical	HKS	DA-H 225 S	90	210	38919.3	487.0	79.9
Helical	HKS	DA-H 225 S	180	210	38919.3	543.0	71.7
Helical	HKS	DA-H 225 S	270	210	38919.3	637.0	61.1
Helical	HKS	DA-H 225 S	360	210	38919.3	684.0	56.9
Vane	Micromatic	SS 12	280	206.9	2533	55.0	46.1
Vane	Micromatic	26R 10	280	206.9	2056.6	52.0	39.6

Vane	Micromatic	SS 130	280	206.9	26442	442.0	59.8
Vane	Micromatic	SS 65	280	206.9	13221	254.0	52.1
Vane	Micromatic	SS 25	280	206.9	5065	100.0	50.7
Vane	Micromatic	SS 40	280	206.9	8136	161.0	50.5
Vane	Micromatic	26R 124	280	206.9	24860	554.0	44.9
Vane	Micromatic	26R 62	280	206.9	12656	308.0	41.1
Vane	Micromatic	26R 31	280	206.9	6215	152.0	40.9
Vane	Micromatic	26R 17	280	206.9	3435.2	94.0	36.5
Vane	Micromatic	MPJ 116	280	69	8113	250.4	32.4
Vane	Micromatic	MPJ 105	280	69	4972	157.9	31.5
Vane	Micromatic	MPJ 128	280	69	11565	378.8	30.5
Vane	Micromatic	SS 1	100	206.9	515	10.0	51.5
Vane	Micromatic	MPJ 32	100	69	381.94	9.1	42.0
Vane	Micromatic	SS 1	280	206.9	244	9.8	25.0
Vane	Micromatic	SS 130	100	206.9	55822	469.0	119.0
Vane	Micromatic	SS 65	100	206.9	27911	254.0	109.9
Vane	Micromatic	SS 25	100	206.9	10692	104.0	102.8
Vane	Micromatic	SS 40	100	206.9	17176	168.0	102.2
Vane	Micromatic	SS 8	100	206.9	3435	36.3	94.7
Vane	Micromatic	SS 12	100	206.9	5347	57.0	93.8
Vane	Micromatic	26R 124	100	206.9	52432	598.0	87.7
Vane	Micromatic	SS 0.5A	100	137.9	183	1.5	126.2
Vane	Micromatic	26R 62	100	206.9	26787	331.0	80.9
Vane	Micromatic	26R 31	100	206.9	13175.8	165.0	79.9
Vane	Micromatic	26R 10	100	206.9	4361.8	56.0	77.9
Vane	Micromatic	MPJ 22	90	69	168.03	1.5	115.9
Vane	Micromatic	26R 17	100	206.9	7277.2	102.0	71.3
Vane	Micromatic	SS 4	100	206.9	1634	23.0	71.0
Vane	Micromatic	MPJ 11	90	69	36.39	0.4	95.8
Vane	Micromatic	26R 5	100	206.9	1858.9	32.0	58.1
Vane	Micromatic	26R 2	100	206.9	824.9	15.0	55.0
Vane	Micromatic	SS 0.2A	280	206.9	38	0.7	52.1
Vane	Micromatic	SS 8	280	206.9	1627	35.0	46.5
Vane	Micromatic	MRP 1x1	90	51.7107	6.1	0.1	43.6
Vane	Micromatic	MPJ 116	100	69	17187	263.5	65.2
Vane	Micromatic	MPJ 105	100	69	10542.9	165.1	63.9
Vane	Micromatic	SS 0.5A	280	137.9	86	1.4	63.2
Vane	Micromatic	MPJ 34	100	69	762.75	12.2	62.5

						396.9	61.7
Vane	Micromatic	MPJ 128	100	69	24490	396.9	61.7
Vane	Micromatic	MPJ 22	270	69	76.73	1.4	56.4
Vane	Micromatic	MPJ 84	100	69	5277	96.2	54.9
Vane	Micromatic	SS 4	280	206.9	775	23.0	33.7
Vane	Micromatic	26R 5	280	206.9	881.4	30.0	29.4
Vane	Micromatic	MPJ 11	270	69	13.22	0.3	38.9
Vane	Micromatic	26R 2	280	206.9	388.7	15.0	25.9
Vane	Micromatic	MPJ 63	100	69	2214.8	57.2	38.7
Vane	Micromatic	MRP 1x4	90	51.7107	2.26	0.1	22.6
Vane	Micromatic	MPJ 34	280	69	360.47	11.8	30.5
Vane	Micromatic	MPJ 84	280	69	2497.3	92.1	27.1
Vane	Micromatic	MPJ 32	280	69	180.24	8.6	21.0
Vane	Micromatic	MPJ 63	280	69	1048.64	55.2	19.0
Vane - Hollow Shaft	Micromatic	HS 15	280	206.9	3051	37.6	81.1
Vane - Hollow Shaft	Micromatic	HS 10	280	206.9	1943.6	30.4	64.0
Vane - Hollow Shaft	Micromatic	HS 6	280	206.9	1292.72	26.3	49.2
Vane - Hollow Shaft	Micromatic	HS 4	280	206.9	813.6	18.6	43.8
Vane - Hollow Shaft	Micromatic	HS 2.5	280	206.9	508.5	15.4	33.0
Vane - Hollow Shaft	Micromatic	HS 1.5	280	206.9	305.1	13.5	22.6
	Parker	LTR 201	90	103.4214	479.0556792	6.6	72.6
	Parker	LTR 152	90	103.4214	410.1349329	5.7	72.0
	Parker	LTR 201	180	103.4214	479.0556792	7.2	66.5
	Parker	LTR 152	180	103.4214	398.8364499	6.4	62.3
	Parker	LTR 201	270	103.4214	479.0556792	7.9	60.6
	Parker	LTR 152	270	103.4214	398.8364499	7.1	56.2
	Parker	LTR 201	360	103.4214	479.0556792	8.6	55.7
	Parker	LTR 152	360	103.4214	398.8364499	8.8	45.3
	Parker	HTR1.8	90	206.8428	203.372694	9.0	22.6
	Parker	LTR 202	90	103.4214	1069.96634	9.9	108.1
	Parker	LTR 202	180	103.4214	1069.96634	11.1	96.4
	Parker	LTR 252	90	103.4214	1455.809535	15.2	95.8
	Parker	LTR 252	180	103.4214	1455.809535	16.8	86.7

	Parker	LTR 202	270	103.42 14	1069.966 34	12.5	85.6
	Parker	LTR 322	90	68.947 6	2577.522 927	30.2	85.3
	Parker	LTR 202	360	103.42 14	1069.966 34	13.8	77.5
	Parker	LTR 322	180	68.947 6	2577.522 927	33.4	77.2
	Parker	LTR 252	270	103.42 14	1455.809 535	19.4	75.0
	Parker	LTR 322	270	68.947 6	2577.522 927	35.5	72.6
	Parker	LTR 251	90	103.42 14	727.9612 597	10.3	70.7
	Parker	LTR 252	360	103.42 14	1455.809 535	21.4	68.0
	Parker	LTR 101	90	103.42 14	66.88701 936	1.0	66.9
	Parker	LTR 322	360	68.947 6	2577.522 927	39.5	65.3
	Parker	LTR 251	180	103.42 14	727.9612 597	11.2	65.0
	Parker	HTR15	90	206.84 28	1694.772 45	27.0	62.8
	Parker	LTR 321	90	68.947 6	1288.817 956	21.1	61.1
	Parker	LTR 101	180	103.42 14	66.88701 936	1.1	60.8
	Parker	LTR 251	270	103.42 14	727.9612 597	12.4	58.7
	Parker	LTR 321	180	68.947 6	1288.817 956	22.7	56.8
	Parker	HTR15	180	206.84 28	1694.772 45	30.0	56.5
	Parker	LTR 101	270	103.42 14	66.88701 936	1.2	55.7
	Parker	LTR 251	360	103.42 14	727.9612 597	13.3	54.7
	Parker	LTR 321	270	68.947 6	1288.817 956	24.3	53.0
	Parker	LTR 101	360	103.42 14	66.88701 936	1.3	51.5
	Parker	LTR 151	90	103.42 14	199.9831 491	4.0	50.0
	Parker	LTR 321	360	68.947 6	1288.817 956	25.8	50.0
	Parker	HTR7.5	90	206.84 28	847.3862 25	17.0	49.8
	Parker	HTR7.5	180	206.84 28	847.3862 25	18.0	47.1
	Parker	LTR 151	180	103.42 14	199.9831 491	4.4	45.9
	Parker	HRN 700D	90	68.947 6	1960	43.0	45.6
	Parker	LTR 151	270	103.42 14	199.9831 491	4.7	42.5
	Parker	HTR7.5	360	206.84 28	847.3862 25	20.0	42.4
	Parker	LTR 102	90	51.710 7	66.88701 936	1.6	41.8

	Parker	LTR 151	360	103.42 14	199.9831 491	5.0	40.0
	Parker	LTR 102	270	51.710 7	66.88701 936	1.7	39.3
	Parker	HTR7.5	270	206.84 28	847.3862 25	22.0	38.5
	Parker	LTR 102	180	51.710 7	66.88701 936	1.8	37.2
	Parker	HTR10	90	206.84 28	1129.848 3	32.0	35.3
	Parker	HRN 400D	90	68.947 6	1078	33.0	32.7
	Parker	LTR 102	360	51.710 7	66.88701 936	2.1	31.9
	Parker	HRN 200D	90	68.947 6	627	20.5	30.6
	Parker	HTR10	180	206.84 28	1129.848 3	40.0	28.2
	Parker	HTR3.7	180	206.84 28	418.0438 71	16.0	26.1
	Parker	HRN 30D	90	68.947 6	117	4.5	26.0
	Parker	HTR10	270	206.84 28	1129.848 3	44.0	25.7
	Parker	HTR3.7	90	206.84 28	418.0438 71	17.0	24.6
	Parker	HRN 700S-C	90	68.947 6	1078	44.0	24.5
	Parker	HRN 700S	270	68.947 6	980	41.0	23.9
	Parker	HRN 100D	90	68.947 6	245	10.4	23.6
	Parker	HTR5	270	206.84 28	564.9241 5	25.0	22.6
	Parker	HTR5	90	206.84 28	564.9241 5	25.0	22.6
	Parker	HTR3.7	270	206.84 28	418.0438 71	19.0	22.0
	Parker	HTR10	360	206.84 28	1129.848 3	53.0	21.3
	Parker	HTR5	360	206.84 28	564.9241 5	27.0	20.9
	Parker	HTR0.9	90	206.84 28	101.6863 47	5.0	20.3
	Parker	HRN 10D	90	68.947 6	20	1.0	20.0
	Parker	HRN 15D	90	68.947 6	40	2.0	20.0
	Parker	HRN 20D	90	68.947 6	60	3.0	20.0
	Parker	HTR5	180	206.84 28	564.9241 5	30.0	18.8
	Parker	HTR1.8	180	206.84 28	203.3726 94	11.0	18.5
	Parker	HTR3.7	360	206.84 28	418.0438 71	24.0	17.4
	Parker	HTR0.9	180	206.84 28	101.6863 47	6.0	16.9
	Parker	HRN 400S	270	68.947 6	539	32.0	16.8

	Parker	HRN 400S-C	90	68.9476	539	34.0	15.9
	Parker	HRN 200S	270	68.9476	314	20.0	15.7
	Parker	HTR1.8	270	206.8428	203.372694	13.0	15.6
	Parker	HTR0.9	360	206.8428	101.686347	7.0	14.5
	Parker	HTR1.8	360	206.8428	203.372694	14.0	14.5
	Parker	HRN 30S	270	68.9476	60	4.3	14.0
	Parker	HRN 30S-C	90	68.9476	58	4.7	12.3
	Parker	HRN 200S-C	90	68.9476	314	25.7	12.2
	Parker	HRN 100S	270	68.9476	123	10.2	12.1
	Parker	HTR0.9	270	206.8428	101.686347	9.0	11.3
	Parker	HRN 10S	270	68.9476	10	1.0	10.0
	Parker	HRN 15S	270	68.9476	20	2.0	10.0
	Parker	HRN 20S	270	68.9476	30	3.0	10.0
	Parker	HRN 100S-C	90	68.9476	123	13.5	9.1
	Parker	HRN 20S-C	90	68.9476	29	3.3	8.8
	Parker	HRN 10S-C	90	68.9476	10	1.2	8.3
	Parker	HRN 15S-C	90	68.9476	20	2.4	8.3
	Torko	28D	270	210	5376	52.0	103.4
	Torko	28D	360	210	5376	58.0	92.7
	Torko	28D	180	210	5376	46.0	116.9
	Torko	18S	90	210	546	6.0	91.0
	Torko	18S	180	210	546	6.8	80.9
	Torko	18S	270	210	546	7.5	72.8
	Torko	18S	360	210	546	8.3	66.2
	Torko	18D	90	210	1092	9.5	114.9
	Torko	28D	90	210	5376	40.0	134.4
	Torko	18D	180	210	1092	11.0	99.3
	Torko	28S	90	210	2688	28.0	96.0
	Torko	24S	90	210	1050	12.0	87.5
	Torko	18D	270	210	1092	12.5	87.4
	Torko	28S	180	210	2688	31.0	86.7
	Torko	24S	180	210	1050	13.0	80.8
	Torko	28S	270	210	2688	34.0	79.1
	Torko	18D	360	210	1092	14.0	78.0
	Torko	24S	270	210	1050	14.0	75.0
	Torko	28S	360	210	2688	37.0	72.6
	Torko	24S	360	210	1050	15.0	70.0
Helical	DS Dynatec	HRSA 30	90	210	63	5.6	11.3
Helical	DS Dynatec	HRSA 42	90	210	199.5	6.9	28.9
Helical	DS Dynatec	HRSA 55	90	210	441	8.2	53.8
Helical	DS Dynatec	HRSA 63	90	210	630	12.0	52.5

Helical	DS Dynatec	HRSA 80	90	210	1512	20.6	73.4
Helical	DS Dynatec	HRSA 100	90	210	3087	27.7	111.4
Helical	DS Dynatec	HRSA 125	90	210	4620	47.0	98.3
Helical	DS Dynatec	HRSA 140	90	210	6300	74.0	85.1
Helical	DS Dynatec	HRSA 160	90	210	10500	114.0	92.1
Helical	DS Dynatec	HRSA 180	90	210	14910	150.0	99.4
Helical	DS Dynatec	HRSA 200	90	210	21000	194.0	108.2
Helical	DS Dynatec	HRSA 225	90	210	29820	354.0	84.2
Helical	DS Dynatec	HRSA 225S	90	210	36750	462.0	79.5
Helical	DS Dynatec	HRSA 250	90	210	42000	551.0	76.2
Helical	DS Dynatec	HRSA 280	90	210	57750	764.0	75.6
Helical	DS Dynatec	HRSA 300	90	210	73500	1100.0	66.8
Helical	DS Dynatec	HRDA 40	90	210	200	4.0	50.0
Helical	DS Dynatec	HRDA 50	90	210	340	5.0	68.0
Helical	DS Dynatec	HRDA 63	90	210	650	8.5	76.5
Helical	DS Dynatec	HRDA 80	90	210	1300	16.7	77.8
Helical	DS Dynatec	HRDA 100	90	210	2500	24.1	103.7
Helical	DS Dynatec	HRDA 125	90	210	5107	47.0	108.7
Helical	DS Dynatec	HRDA 140	90	210	7100	74.0	95.9
Helical	DS Dynatec	HRDA 160	90	210	11300	114.0	99.1
Helical	DS Dynatec	HRDA 180	90	210	16200	150.0	108.0
Helical	DS Dynatec	HRDA 200	90	210	22300	194.0	114.9
Helical	DS Dynatec	HRDA 225	90	210	32000	404.0	79.2
Helical	DS Dynatec	HRDA 225S	90	210	37920	487.0	77.9
Helical	DS Dynatec	HRDA 250	90	210	44000	630.0	69.8
Helical	DS Dynatec	HRDA 280	90	210	60800	874.0	69.6
Helical	DS Dynatec	HRDA 300	90	210	76000	1126.0	67.5
Helical	DS Dynatec	HRDA 40	180	210	200	4.5	44.4
Helical	DS Dynatec	HRDA 50	180	210	340	5.8	58.6
Helical	DS Dynatec	HRDA 63	180	210	650	9.8	66.3
Helical	DS Dynatec	HRDA 80	180	210	1300	19.1	68.1
Helical	DS Dynatec	HRDA 100	180	210	2500	29.2	85.6
Helical	DS Dynatec	HRDA 125	180	210	5107	55.0	92.9
Helical	DS Dynatec	HRDA 140	180	210	7100	87.0	81.6
Helical	DS Dynatec	HRDA 160	180	210	11300	136.0	83.1
Helical	DS Dynatec	HRDA 180	180	210	16200	187.0	86.6
Helical	DS Dynatec	HRDA 200	180	210	22300	238.0	93.7
Helical	DS Dynatec	HRDA 225	180	210	32000	488.0	65.6

Helical	DS Dynatec	HRDA 225S	180	210	37920	543.0	69.8
Helical	DS Dynatec	HRDA 250	180	210	44000	726.0	60.6
Helical	DS Dynatec	HRDA 280	180	210	60800	1011.0	60.1
Helical	DS Dynatec	HRDA 300	180	210	76000	1308.0	58.1
Helical	DS Dynatec	HRDA 40	270	210	200	5.0	40.0
Helical	DS Dynatec	HRDA 50	270	210	340	6.9	49.3
Helical	DS Dynatec	HRDA 63	270	210	650	11.0	59.1
Helical	DS Dynatec	HRDA 80	270	210	1300	21.5	60.5
Helical	DS Dynatec	HRDA 100	270	210	2500	34.0	73.5
Helical	DS Dynatec	HRDA 125	270	210	5107	63.5	80.4
Helical	DS Dynatec	HRDA 140	270	210	7100	101.0	70.3
Helical	DS Dynatec	HRDA 160	270	210	11300	154.0	73.4
Helical	DS Dynatec	HRDA 180	270	210	16200	213.0	76.1
Helical	DS Dynatec	HRDA 200	270	210	22300	264.0	84.5
Helical	DS Dynatec	HRDA 225	270	210	32000	565.0	56.6
Helical	DS Dynatec	HRDA 225S	270	210	37920	637.0	59.5
Helical	DS Dynatec	HRDA 250	270	210	44000	815.0	54.0
Helical	DS Dynatec	HRDA 280	270	210	60800	1164.0	52.2
Helical	DS Dynatec	HRDA 300	270	210	76000	1484.0	51.2
Helical	DS Dynatec	HRDA 40	360	210	200	5.5	36.4
Helical	DS Dynatec	HRDA 50	360	210	340	7.4	45.9
Helical	DS Dynatec	HRDA 63	360	210	650	12.2	53.3
Helical	DS Dynatec	HRDA 80	360	210	1300	24.0	54.2
Helical	DS Dynatec	HRDA 100	360	210	2500	38.5	64.9
Helical	DS Dynatec	HRDA 125	360	210	5107	72.5	70.4
Helical	DS Dynatec	HRDA 140	360	210	7100	115.0	61.7
Helical	DS Dynatec	HRDA 160	360	210	11300	170.0	66.5
Helical	DS Dynatec	HRDA 180	360	210	16200	245.0	66.1
Helical	DS Dynatec	HRDA 200	360	210	22300	306.0	72.9
Helical	DS Dynatec	HRDA 225	360	210	32000	630.0	50.8
Helical	DS Dynatec	HRDA 225S	360	210	37920	684.0	55.4
Helical	DS Dynatec	HRDA 250	360	210	44000	912.0	48.2
Helical	DS Dynatec	HRDA 280	360	210	60800	1292.0	47.1
Helical	DS Dynatec	HRDA 300	360	210	76000	1677.0	45.3
Helical	DS Dynatec	HRMD 50	180	210	190	7.4	25.7
Helical	DS Dynatec	HRMD 60	180	210	340	10.6	32.1
Helical	DS Dynatec	HRMD 63	180	210	720	14.4	50.0

Helical	DS Dynatec	HRMD 70-FU	180	210	500	12.8	39.1
Helical	DS Dynatec	HRMD 80	180	210	1073	26.5	40.5
Helical	DS Dynatec	HRMD 85-FU	180	210	930	16.6	56.0
Helical	DS Dynatec	HRMD 90	180	210	1700	43.0	39.5
Helical	DS Dynatec	HRMD 100	180	210	2900	56.7	51.1
Helical	DS Dynatec	HRMD 120-FU	180	210	1690	30.0	56.3
Helical	DS Dynatec	HRMD 125-FU	180	210	2940	52.0	56.5
Helical	DS Dynatec	HRMD 145-FU	180	210	4400	77.0	57.1
Helical	DS Dynatec	HRMD 60	360	210	340	13.6	25.0
Helical	DS Dynatec	HRMD 63	360	210	720	18.8	38.3
Helical	DS Dynatec	HRMD 80	360	210	1073	36.0	29.8
Helical	DS Dynatec	HRMD 90	360	210	1700	54.4	31.3
Helical	DS Dynatec	HRMD 100	360	210	2900	81.6	35.5
vane	DS Dynatec	HPHP 1015	270	200	25	0.9	28.1
vane	DS Dynatec	HPHP 2015	90	200	50	0.9	55.6
vane	DS Dynatec	HPHP 1025	270	200	60	1.0	61.9
vane	DS Dynatec	HPHP 2025	90	200	120	1.0	120.0
vane	DS Dynatec	HPHP 1035	270	200	126	1.9	66.3
vane	DS Dynatec	HPHP 2035	90	200	260	2.0	132.0
vane	DS Dynatec	HPHP 1045	270	200	244	2.7	92.1
vane	DS Dynatec	HPHP 2045	90	200	504	2.8	180.6
vane	DS Dynatec	HPSD 102	270	100	30	0.6	50.0
vane	DS Dynatec	HPSD 103	270	100	63	1.3	48.5
vane	DS Dynatec	HPSD 106	270	100	112	1.7	65.9
vane	DS Dynatec	HPSD 110	270	140	420	6.0	70.0
vane	DS Dynatec	HPSD 119	270	140	840	8.5	98.8
vane	DS Dynatec	HPSD 132	270	140	2300	14.0	164.3
vane	DS Dynatec	HPSD 184	270	140	8400	100.0	84.0
vane	DS Dynatec	HPSD 202	90	100	60	0.7	85.7
vane	DS Dynatec	HPSD 203	90	100	130	1.4	92.9
vane	DS Dynatec	HPSD 206	90	100	252	1.9	132.6
vane	DS Dynatec	HPSD 210	100	140	900	7.5	120.0
vane	DS Dynatec	HPSD 219	100	140	1750	9.5	184.2
vane	DS Dynatec	HPSD 232	100	140	4800	15.0	320.0
vane	DS Dynatec	HPSD 284	100	140	16800	105.0	160.0
vane	DS Dynatec	HPSD 1015	90	50	6	0.7	8.5
vane	DS Dynatec	HPSD 1018	180	50	6	0.7	8.7
vane	DS Dynatec	HPSD 1025	270	70	30	0.6	50.0
vane	DS Dynatec	HPSD 2025	90	70	60	0.7	85.7
vane	DS Dynatec	HPSD 1035	270	70	63	1.3	48.5
vane	DS Dynatec	HPSD 2035	90	70	130	1.4	92.9
vane	DS Dynatec	HPSD 1045	270	70	122	1.7	71.8
vane	DS Dynatec	HPSD 2045	90	70	252	1.9	132.6
vane	DS Dynatec	HPSD 1055	280	100	420	6.0	70.0
vane	DS Dynatec	HPSD 2055	90	100	900	7.5	120.0
vane	DS Dynatec	HPSD 1065	280	100	840	8.5	98.8
vane	DS Dynatec	HPSD 2065	100	100	1750	9.5	184.2
vane	DS Dynatec	HPSD 1075	280	100	2300	23.0	100.0
vane	DS Dynatec	HPSD 2075	100	100	4800	24.0	200.0

vane	DS Dynatec	HPSD 1085	280	100	8400	100.0	84.0
vane	DS Dynatec	HPSD 2085	100	100	16800	105.0	160.0
vane	DS Dynatec	HPSD 160	270	35	1400	107.0	13.1
vane	DS Dynatec	HPSD 9011	180	35	3.5	0.1	32.2
vane	DS Dynatec	HPSD 9020	150	35	3.5	0.1	27.6
vane	DS Dynatec	HPSD 9022	100	250	500	2.8	178.6
vane	DS Dynatec	HPSD 9025	90	70	260	3.2	81.8
vane	DS Dynatec	HPSD 9030	270	250	130	3.3	39.4
vane	DS Dynatec	HPSD 9041	90	250	260	3.4	77.4
vane	DS Dynatec	HPSD 9063	115	200	120	2.5	48.8
vane	DS Dynatec	HPSD 9071	180	200	185	3.1	60.6
vane	DS Dynatec	HPSD 9076	100	200	120	1.0	121.6
vane	DS Dynatec	HPSD 9076	280	160	60	0.8	77.1
vane	DS Dynatec	HPSD 9079	180	200	126	1.9	65.9
vane	DS Dynatec	HPSD 9081	270	200	244	2.6	94.2
vane	DS Dynatec	HPSD 9082	280	140	1150	9.8	117.9
vane	DS Dynatec	HPSD 9084	270	200	126	1.8	68.9

Appendix P

Heavy actuators used in the optimisation

Record Number	Manufacturer	Model	Diameter			Stroke	Pressure Bar
			External	Internal	Shaft		
H_1	BOSCH	CDL2 MT4	52.0	40.0	25.0	50.0	250
H_2	BOSCH	CDL2 MT4	52.0	40.0	25.0	75.0	250
H_3	BOSCH	CDL2 MT4	52.0	40.0	25.0	100.0	250
H_4	BOSCH	CDL2 MT4	52.0	40.0	25.0	125.0	250
H_5	BOSCH	CDL2 MT4	52.0	40.0	25.0	150.0	250
H_6	BOSCH	CDL2 MT4	52.0	40.0	25.0	175.0	250
H_7	BOSCH	CDL2 MT4	52.0	40.0	25.0	200.0	250
H_8	BOSCH	CDL2 MT4	62.0	50.0	32.0	50.0	250
H_9	BOSCH	CDL2 MT4	62.0	50.0	32.0	75.0	250
H_10	BOSCH	CDL2 MT4	62.0	50.0	32.0	100.0	250
H_11	BOSCH	CDL2 MT4	62.0	50.0	32.0	125.0	250
H_12	BOSCH	CDL2 MT4	62.0	50.0	32.0	150.0	250
H_13	BOSCH	CDL2 MT4	62.0	50.0	32.0	175.0	250
H_14	BOSCH	CDL2 MT4	62.0	50.0	32.0	200.0	250
H_15	BOSCH	CDL2 MT4	78.0	63.0	40.0	50.0	250
H_16	BOSCH	CDL2 MT4	78.0	63.0	40.0	75.0	250
H_17	BOSCH	CDL2 MT4	78.0	63.0	40.0	100.0	250
H_18	BOSCH	CDL2 MT4	78.0	63.0	40.0	125.0	250
H_19	BOSCH	CDL2 MT4	78.0	63.0	40.0	150.0	250
H_20	BOSCH	CDL2 MT4	78.0	63.0	40.0	175.0	250
H_21	BOSCH	CDL2 MT4	78.0	63.0	40.0	200.0	250
H_22	BOSCH	CDL2 MT4	100.0	80.0	50.0	50.0	250
H_23	BOSCH	CDL2 MT4	100.0	80.0	50.0	75.0	250
H_24	BOSCH	CDL2 MT4	100.0	80.0	50.0	100.0	250
H_25	BOSCH	CDL2 MT4	100.0	80.0	50.0	125.0	250
H_26	BOSCH	CDL2 MT4	100.0	80.0	50.0	150.0	250
H_27	BOSCH	CDL2 MT4	100.0	80.0	50.0	175.0	250
H_28	BOSCH	CDL2 MT4	100.0	80.0	50.0	200.0	250
H_29	BOSCH	CDL2 MT4	125.0	100.0	63.0	50.0	250
H_30	BOSCH	CDL2 MT4	125.0	100.0	63.0	75.0	250
H_31	BOSCH	CDL2 MT4	125.0	100.0	63.0	100.0	250
H_32	BOSCH	CDL2 MT4	125.0	100.0	63.0	125.0	250
H_33	BOSCH	CDL2 MT4	125.0	100.0	63.0	150.0	250
H_34	BOSCH	CDL2 MT4	125.0	100.0	63.0	175.0	250
H_35	BOSCH	CDL2 MT4	125.0	100.0	63.0	200.0	250
H_36	BOSCH	CDL2 MT4	160.0	125.0	80.0	50.0	250
H_37	BOSCH	CDL2 MT4	160.0	125.0	80.0	75.0	250
H_38	BOSCH	CDL2 MT4	160.0	125.0	80.0	100.0	250
H_39	BOSCH	CDL2 MT4	160.0	125.0	80.0	125.0	250
H_40	BOSCH	CDL2 MT4	160.0	125.0	80.0	150.0	250
H_41	BOSCH	CDL2 MT4	160.0	125.0	80.0	175.0	250
H_42	BOSCH	CDL2 MT4	160.0	125.0	80.0	200.0	250
H_43	Interfluid	HFR0160050	35	25	16	50	200
H_44	Interfluid	HFR0160100	35	25	16	100	200
H_45	Interfluid	HFR0160150	35	25	16	150	200
H_46	Interfluid	HFR0160200	35	25	16	200	200
H_47	Interfluid	HFR0200050	42	32	20	50	200

H_48	Interfluid	HFR0200100	42	32	20	100	200
H_49	Interfluid	HFR0200150	42	32	20	150	200
H_50	Interfluid	HFR0200200	42	32	20	200	200
H_51	Interfluid	HFR0200250	42	32	20	250	200
H_52	Interfluid	HFR0200300	42	32	20	300	200
H_53	Interfluid	HFR0200400	42	32	20	400	200
H_54	Interfluid	HFR0200500	42	32	20	500	200
H_55	Interfluid	NFR1250100	50	40	25	100	200
H_56	Interfluid	NFR1250150	50	40	25	150	200
H_57	Interfluid	NFR1250200	50	40	25	200	200
H_58	Interfluid	NFR1250250	50	40	25	250	200
H_59	Interfluid	NFR1250300	50	40	25	300	200
H_60	Interfluid	NFR1250400	50	40	25	400	200
H_61	Interfluid	NFR1250500	50	40	25	500	200
H_62	Interfluid	NFR1250600	50	40	25	600	200
H_63	Interfluid	NFR1250700	50	40	25	700	200
H_64	Interfluid	NFR1250800	50	40	25	800	200
H_65	Interfluid	NFR2300100	60	50	30	100	200
H_66	Interfluid	NFR2300150	60	50	30	150	200
H_67	Interfluid	NFR2300200	60	50	30	200	200
H_68	Interfluid	NFR2300250	60	50	30	250	200
H_69	Interfluid	NFR2300300	60	50	30	300	200
H_70	Interfluid	NFR2300400	60	50	30	400	200
H_71	Interfluid	NFR2300500	60	50	30	500	200
H_72	Interfluid	NFR2300600	60	50	30	600	200
H_73	Interfluid	NFR2300700	60	50	30	700	200
H_74	Interfluid	NFR2300800	60	50	30	800	200
H_75	Interfluid	NFR2300900	60	50	30	900	200
H_76	Interfluid	NFR2301000	60	50	30	1000	200
H_77	Interfluid	NFR3300100	70	60	30	100	200
H_78	Interfluid	NFR3300150	70	60	30	150	200
H_79	Interfluid	NFR3300200	70	60	30	200	200
H_80	Interfluid	NFR3300250	70	60	30	250	200
H_81	Interfluid	NFR3300300	70	60	30	300	200
H_82	Interfluid	NFR3300350	70	60	30	350	200
H_83	Interfluid	NFR3300400	70	60	30	400	200
H_84	Interfluid	NFR3300450	70	60	30	450	200
H_85	Interfluid	NFR3300500	70	60	30	500	200
H_86	Interfluid	NFR3300600	70	60	30	600	200
H_87	Interfluid	NFR3300700	70	60	30	700	200
H_88	Interfluid	NFR3350200	70	60	35	200	200
H_89	Interfluid	NFR3350300	70	60	35	300	200
H_90	Interfluid	NFR3350400	70	60	35	400	200
H_91	Interfluid	NFR3350500	70	60	35	500	200
H_92	Interfluid	NFR3350600	70	60	35	600	200
H_93	Interfluid	NFR3350700	70	60	35	700	200
H_94	Interfluid	NFR3350800	70	60	35	800	200
H_95	Interfluid	NFR3350900	70	60	35	900	200
H_96	Interfluid	NFR3351000	70	60	35	1000	200
H_97	Interfluid	NFR4400200	80	70	40	200	200
H_98	Interfluid	NFR4400250	80	70	40	250	200
H_99	Interfluid	NFR4400300	80	70	40	300	200
H_100	Interfluid	NFR4400350	80	70	40	350	200
H_101	Interfluid	NFR4400400	80	70	40	400	200

H_102	Interfluid	NFR4400450	80	70	40	450	200
H_103	Interfluid	NFR4400500	80	70	40	500	200
H_104	Interfluid	NFR4400600	80	70	40	600	200
H_105	Interfluid	NFR4400700	80	70	40	700	200
H_106	Interfluid	NFR4400800	80	70	40	800	200
H_107	Interfluid	NFR4400900	80	70	40	900	200
H_108	Interfluid	NFR5400200	92	80	40	200	200
H_109	Interfluid	NFR5400250	92	80	40	250	200
H_110	Interfluid	NFR5400300	92	80	40	300	200
H_111	Interfluid	NFR5400350	92	80	40	350	200
H_112	Interfluid	NFR5400400	92	80	40	400	200
H_113	Interfluid	NFR5400500	92	80	40	500	200
H_114	Interfluid	NFR5400600	92	80	40	600	200
H_115	Interfluid	NFR5400700	92	80	40	700	200
H_116	Interfluid	NFR5400800	92	80	40	800	200
H_117	Interfluid	NFR5400900	92	80	40	900	200
H_118	Interfluid	NFR5401000	92	80	40	1000	200
H_119	Interfluid	NFR6500200	115	100	50	200	200
H_120	Interfluid	NFR6500300	115	100	50	300	200
H_121	Interfluid	NFR6500400	115	100	50	400	200
H_122	Interfluid	NFR6500500	115	100	50	500	200
H_123	Interfluid	NFR6500700	115	100	50	700	200
H_124	Interfluid	NFR6500900	115	100	50	900	200
H_125	Interfluid	NFR6501000	115	100	50	1000	200
H_126	Prince	F150040	47.625	38.1	19.05	101.6	206.8428
H_127	Prince	F150060	47.625	38.1	19.05	152.4	206.8428
H_128	Prince	F150080	47.625	38.1	19.05	203.2	206.8428
H_129	Prince	F150100	47.625	38.1	19.05	254	206.8428
H_130	Prince	F150120	47.625	38.1	19.05	304.8	206.8428
H_131	Prince	F150160	47.625	38.1	19.05	406.4	206.8428
H_132	Prince	F150200	47.625	38.1	19.05	508	206.8428
H_133	Prince	F150240	47.625	38.1	19.05	609.6	206.8428
H_134	Prince	F175040	53.975	44.45	25.4	101.6	206.8428
H_135	Prince	F175060	53.975	44.45	25.4	152.4	206.8428
H_136	Prince	F175080	53.975	44.45	25.4	203.2	206.8428
H_137	Prince	F175100	53.975	44.45	25.4	254	206.8428
H_138	Prince	F175120	53.975	44.45	25.4	304.8	206.8428
H_139	Prince	F175160	53.975	44.45	25.4	406.4	206.8428
H_140	Prince	F175200	53.975	44.45	25.4	508	206.8428
H_141	Prince	F175240	53.975	44.45	25.4	609.6	206.8428
H_142	Prince	F200040	60.325	50.8	28.575	101.6	206.8428
H_143	Prince	F200060	60.325	50.8	28.575	152.4	206.8428
H_144	Prince	F200080	60.325	50.8	28.575	203.2	206.8428
H_145	Prince	F200100	60.325	50.8	28.575	254	206.8428
H_146	Prince	F200120	60.325	50.8	28.575	304.8	206.8428
H_147	Prince	F200160	60.325	50.8	28.575	406.4	206.8428
H_148	Prince	F200200	60.325	50.8	28.575	508	206.8428
H_149	Prince	F200240	60.325	50.8	28.575	609.6	206.8428
H_150	Prince	F200300	60.325	50.8	28.575	762	206.8428
H_151	Prince	F225040	66.675	57.15	31.75	101.6	206.8428
H_152	Prince	F225060	66.675	57.15	31.75	152.4	206.8428
H_153	Prince	F225080	66.675	57.15	31.75	203.2	206.8428
H_154	Prince	F225100	66.675	57.15	31.75	254	206.8428
H_155	Prince	F225120	66.675	57.15	31.75	304.8	206.8428

H_156	Prince	F225160	66.675	57.15	31.75	406.4	206.8428
H_157	Prince	F225200	66.675	57.15	31.75	508	206.8428
H_158	Prince	F225240	66.675	57.15	31.75	609.6	206.8428
H_159	Prince	F225300	66.675	57.15	31.75	762	206.8428
H_160	Prince	F250040	73.025	63.5	34.925	101.6	206.8428
H_161	Prince	F250060	73.025	63.5	34.925	152.4	206.8428
H_162	Prince	F250080	73.025	63.5	34.925	203.2	206.8428
H_163	Prince	F250100	73.025	63.5	34.925	254	206.8428
H_164	Prince	F250120	73.025	63.5	34.925	304.8	206.8428
H_165	Prince	F250160	73.025	63.5	34.925	406.4	206.8428
H_166	Prince	F250200	73.025	63.5	34.925	508	206.8428
H_167	Prince	F250240	73.025	63.5	34.925	609.6	206.8428
H_168	Prince	F250300	73.025	63.5	34.925	762	206.8428
H_169	Prince	F250360	73.025	63.5	34.925	914.4	206.8428
H_170	Prince	F275040	79.375	69.85	38.1	101.6	206.8428
H_171	Prince	F275060	79.375	69.85	38.1	152.4	206.8428
H_172	Prince	F275080	79.375	69.85	38.1	203.2	206.8428
H_173	Prince	F275100	79.375	69.85	38.1	254	206.8428
H_174	Prince	F275120	79.375	69.85	38.1	304.8	206.8428
H_175	Prince	F275160	79.375	69.85	38.1	406.4	206.8428
H_176	Prince	F275200	79.375	69.85	38.1	508	206.8428
H_177	Prince	F275240	79.375	69.85	38.1	609.6	206.8428
H_178	Prince	F275300	79.375	69.85	38.1	762	206.8428
H_179	Prince	F275360	79.375	69.85	38.1	914.4	206.8428
H_180	BOSCH	CD210B	63	40	16	50	210
H_181	BOSCH	CD210B	63	40	16	75	210
H_182	BOSCH	CD210B	63	40	16	100	210
H_183	BOSCH	CD210B	63	40	16	125	210
H_184	BOSCH	CD210B	63	40	16	150	210
H_185	BOSCH	CD210B	63	40	16	175	210
H_186	BOSCH	CD210B	63	40	16	200	210
H_187	BOSCH	CD210B	63	40	18	50	210
H_188	BOSCH	CD210B	63	40	18	75	210
H_189	BOSCH	CD210B	63	40	18	100	210
H_190	BOSCH	CD210B	63	40	18	125	210
H_191	BOSCH	CD210B	63	40	18	150	210
H_192	BOSCH	CD210B	63	40	18	175	210
H_193	BOSCH	CD210B	63	40	18	200	210
H_194	BOSCH	CD210B	63	40	25	50	210
H_195	BOSCH	CD210B	63	40	25	75	210
H_196	BOSCH	CD210B	63	40	25	100	210
H_197	BOSCH	CD210B	63	40	25	125	210
H_198	BOSCH	CD210B	63	40	25	150	210
H_199	BOSCH	CD210B	63	40	25	175	210
H_200	BOSCH	CD210B	63	40	25	200	210
H_201	BOSCH	CD210B	76	50	22	50	210
H_202	BOSCH	CD210B	76	50	22	75	210
H_203	BOSCH	CD210B	76	50	22	100	210
H_204	BOSCH	CD210B	76	50	22	125	210
H_205	BOSCH	CD210B	76	50	22	150	210
H_206	BOSCH	CD210B	76	50	22	175	210
H_207	BOSCH	CD210B	76	50	22	200	210
H_208	BOSCH	CD210B	76	50	25	50	210
H_209	BOSCH	CD210B	76	50	25	75	210

H_210	BOSCH	CD210B	76	50	25	100	210
H_211	BOSCH	CD210B	76	50	25	125	210
H_212	BOSCH	CD210B	76	50	25	150	210
H_213	BOSCH	CD210B	76	50	25	175	210
H_214	BOSCH	CD210B	76	50	25	200	210
H_215	BOSCH	CD210B	76	50	36	50	210
H_216	BOSCH	CD210B	76	50	36	75	210
H_217	BOSCH	CD210B	76	50	36	100	210
H_218	BOSCH	CD210B	76	50	36	125	210
H_219	BOSCH	CD210B	76	50	36	150	210
H_220	BOSCH	CD210B	76	50	36	175	210
H_221	BOSCH	CD210B	76	50	36	200	210
H_222	BOSCH	CD210B	89	63	25	50	210
H_223	BOSCH	CD210B	89	63	25	75	210
H_224	BOSCH	CD210B	89	63	25	100	210
H_225	BOSCH	CD210B	89	63	25	125	210
H_226	BOSCH	CD210B	89	63	25	150	210
H_227	BOSCH	CD210B	89	63	25	175	210
H_228	BOSCH	CD210B	89	63	25	200	210
H_229	BOSCH	CD210B	89	63	28	50	210
H_230	BOSCH	CD210B	89	63	28	75	210
H_231	BOSCH	CD210B	89	63	28	100	210
H_232	BOSCH	CD210B	89	63	28	125	210
H_233	BOSCH	CD210B	89	63	28	150	210
H_234	BOSCH	CD210B	89	63	28	175	210
H_235	BOSCH	CD210B	89	63	28	200	210
H_236	BOSCH	CD210B	89	63	36	50	210
H_237	BOSCH	CD210B	89	63	36	75	210
H_238	BOSCH	CD210B	89	63	36	100	210
H_239	BOSCH	CD210B	89	63	36	125	210
H_240	BOSCH	CD210B	89	63	36	150	210
H_241	BOSCH	CD210B	89	63	36	175	210
H_242	BOSCH	CD210B	89	63	36	200	210
H_243	BOSCH	CD210B	89	63	45	50	210
H_244	BOSCH	CD210B	89	63	45	75	210
H_245	BOSCH	CD210B	89	63	45	100	210
H_246	BOSCH	CD210B	89	63	45	125	210
H_247	BOSCH	CD210B	89	63	45	150	210
H_248	BOSCH	CD210B	89	63	45	175	210
H_249	BOSCH	CD210B	89	63	45	200	210
H_250	BOSCH	CD210B	114	80	36	50	210
H_251	BOSCH	CD210B	114	80	36	75	210
H_252	BOSCH	CD210B	114	80	36	100	210
H_253	BOSCH	CD210B	114	80	36	125	210
H_254	BOSCH	CD210B	114	80	36	150	210
H_255	BOSCH	CD210B	114	80	36	175	210
H_256	BOSCH	CD210B	114	80	36	200	210
H_257	BOSCH	CD210B	114	80	45	50	210
H_258	BOSCH	CD210B	114	80	45	75	210
H_259	BOSCH	CD210B	114	80	45	100	210
H_260	BOSCH	CD210B	114	80	45	125	210
H_261	BOSCH	CD210B	114	80	45	150	210
H_262	BOSCH	CD210B	114	80	45	175	210
H_263	BOSCH	CD210B	114	80	45	200	210

H_264	BOSCH	CD210B	114	80	56	50	210
H_265	BOSCH	CD210B	114	80	56	75	210
H_266	BOSCH	CD210B	114	80	56	100	210
H_267	BOSCH	CD210B	114	80	56	125	210
H_268	BOSCH	CD210B	114	80	56	150	210
H_269	BOSCH	CD210B	114	80	56	175	210
H_270	BOSCH	CD210B	114	80	56	200	210
H_271	BOSCH	CD210B	114	80	36	50	210
H_272	BOSCH	CD210B	114	80	36	75	210
H_273	BOSCH	CD210B	114	80	36	100	210
H_274	BOSCH	CD210B	114	80	36	125	210
H_275	BOSCH	CD210B	114	80	36	150	210
H_276	BOSCH	CD210B	114	80	36	175	210
H_277	BOSCH	CD210B	114	80	36	200	210
H_278	BOSCH	CD210B	114	80	45	50	210
H_279	BOSCH	CD210B	114	80	45	75	210
H_280	BOSCH	CD210B	114	80	45	100	210
H_281	BOSCH	CD210B	114	80	45	125	210
H_282	BOSCH	CD210B	114	80	45	150	210
H_283	BOSCH	CD210B	114	80	45	175	210
H_284	BOSCH	CD210B	114	80	45	200	210
H_285	BOSCH	CD210B	114	80	56	50	210
H_286	BOSCH	CD210B	114	80	56	75	210
H_287	BOSCH	CD210B	114	80	56	100	210
H_288	BOSCH	CD210B	114	80	56	125	210
H_289	BOSCH	CD210B	114	80	56	150	210
H_290	BOSCH	CD210B	114	80	56	175	210
H_291	BOSCH	CD210B	114	80	56	200	210
H_292	BOSCH	CD210B	114	80	36	50	210
H_293	BOSCH	CD210B	114	80	36	75	210
H_294	BOSCH	CD210B	114	80	36	100	210
H_295	BOSCH	CD210B	114	80	36	125	210
H_296	BOSCH	CD210B	114	80	36	150	210
H_297	BOSCH	CD210B	114	80	36	175	210
H_298	BOSCH	CD210B	114	80	36	200	210
H_299	BOSCH	CD210B	114	80	45	50	210
H_300	BOSCH	CD210B	114	80	45	75	210
H_301	BOSCH	CD210B	114	80	45	100	210
H_302	BOSCH	CD210B	114	80	45	125	210
H_303	BOSCH	CD210B	114	80	45	150	210
H_304	BOSCH	CD210B	114	80	45	175	210
H_305	BOSCH	CD210B	114	80	45	200	210
H_306	BOSCH	CD210B	114	80	56	50	210
H_307	BOSCH	CD210B	114	80	56	75	210
H_308	BOSCH	CD210B	114	80	56	100	210
H_309	BOSCH	CD210B	114	80	56	125	210
H_310	BOSCH	CD210B	114	80	56	150	210
H_311	BOSCH	CD210B	114	80	56	175	210
H_312	BOSCH	CD210B	114	80	56	200	210
H_313	BOSCH	CD210B	127	100	45	75	210
H_314	BOSCH	CD210B	127	100	45	100	210
H_315	BOSCH	CD210B	127	100	45	125	210
H_316	BOSCH	CD210B	127	100	45	150	210
H_317	BOSCH	CD210B	127	100	45	175	210

H_318	BOSCH	CD210B	127	100	45	200	210
H_319	BOSCH	CD210B	127	100	50	75	210
H_320	BOSCH	CD210B	127	100	50	100	210
H_321	BOSCH	CD210B	127	100	50	125	210
H_322	BOSCH	CD210B	127	100	50	150	210
H_323	BOSCH	CD210B	127	100	50	175	210
H_324	BOSCH	CD210B	127	100	50	200	210
H_325	BOSCH	CD210B	127	100	70	75	210
H_326	BOSCH	CD210B	127	100	70	100	210
H_327	BOSCH	CD210B	127	100	70	125	210
H_328	BOSCH	CD210B	127	100	70	150	210
H_329	BOSCH	CD210B	127	100	70	175	210
H_330	BOSCH	CD210B	127	100	70	200	210
H_331	BOSCH	CD210B	127	100	45	75	210
H_332	BOSCH	CD210B	127	100	45	100	210
H_333	BOSCH	CD210B	127	100	45	125	210
H_334	BOSCH	CD210B	127	100	45	150	210
H_335	BOSCH	CD210B	127	100	45	175	210
H_336	BOSCH	CD210B	127	100	45	200	210
H_337	BOSCH	CD210B	127	100	50	75	210
H_338	BOSCH	CD210B	127	100	50	100	210
H_339	BOSCH	CD210B	127	100	50	125	210
H_340	BOSCH	CD210B	127	100	50	150	210
H_341	BOSCH	CD210B	127	100	50	175	210
H_342	BOSCH	CD210B	127	100	50	200	210
H_343	BOSCH	CD210B	127	100	70	75	210
H_344	BOSCH	CD210B	127	100	70	100	210
H_345	BOSCH	CD210B	127	100	70	125	210
H_346	BOSCH	CD210B	127	100	70	150	210
H_347	BOSCH	CD210B	127	100	70	175	210
H_348	BOSCH	CD210B	127	100	70	200	210
H_349	BOSCH	CD210B	165	125	50	100	210
H_350	BOSCH	CD210B	165	125	50	125	210
H_351	BOSCH	CD210B	165	125	50	150	210
H_352	BOSCH	CD210B	165	125	50	175	210
H_353	BOSCH	CD210B	165	125	50	200	210
H_354	BOSCH	CD210B	165	125	56	100	210
H_355	BOSCH	CD210B	165	125	56	125	210
H_356	BOSCH	CD210B	165	125	56	150	210
H_357	BOSCH	CD210B	165	125	56	175	210
H_358	BOSCH	CD210B	165	125	56	200	210
H_359	BOSCH	CD210B	165	125	63	100	210
H_360	BOSCH	CD210B	165	125	63	125	210
H_361	BOSCH	CD210B	165	125	63	150	210
H_362	BOSCH	CD210B	165	125	63	175	210
H_363	BOSCH	CD210B	165	125	63	200	210
H_364	BOSCH	CD210B	165	125	90	100	210
H_365	BOSCH	CD210B	165	125	90	125	210
H_366	BOSCH	CD210B	165	125	90	150	210
H_367	BOSCH	CD210B	165	125	90	175	210
H_368	BOSCH	CD210B	165	125	90	200	210
H_369	BOSCH	CD210B	165	125	50	100	210
H_370	BOSCH	CD210B	165	125	50	125	210
H_371	BOSCH	CD210B	165	125	50	150	210

H_372	BOSCH	CD210B	165	125	50	175	210
H_373	BOSCH	CD210B	165	125	50	200	210
H_374	BOSCH	CD210B	165	125	56	100	210
H_375	BOSCH	CD210B	165	125	56	125	210
H_376	BOSCH	CD210B	165	125	56	150	210
H_377	BOSCH	CD210B	165	125	56	175	210
H_378	BOSCH	CD210B	165	125	56	200	210
H_379	BOSCH	CD210B	165	125	63	100	210
H_380	BOSCH	CD210B	165	125	63	125	210
H_381	BOSCH	CD210B	165	125	63	150	210
H_382	BOSCH	CD210B	165	125	63	175	210
H_383	BOSCH	CD210B	165	125	63	200	210
H_384	BOSCH	CD210B	165	125	90	100	210
H_385	BOSCH	CD210B	165	125	90	125	210
H_386	BOSCH	CD210B	165	125	90	150	210
H_387	BOSCH	CD210B	165	125	90	175	210
H_388	BOSCH	CD210B	165	125	90	200	210
H_389	BOSCH	CD210G	63	40	16	50	210
H_390	BOSCH	CD210G	63	40	16	75	210
H_391	BOSCH	CD210G	63	40	16	100	210
H_392	BOSCH	CD210G	63	40	16	125	210
H_393	BOSCH	CD210G	63	40	16	150	210
H_394	BOSCH	CD210G	63	40	16	175	210
H_395	BOSCH	CD210G	63	40	16	200	210
H_396	BOSCH	CD210G	63	40	18	50	210
H_397	BOSCH	CD210G	63	40	18	75	210
H_398	BOSCH	CD210G	63	40	18	100	210
H_399	BOSCH	CD210G	63	40	18	125	210
H_400	BOSCH	CD210G	63	40	18	150	210
H_401	BOSCH	CD210G	63	40	18	175	210
H_402	BOSCH	CD210G	63	40	18	200	210
H_403	BOSCH	CD210G	63	40	25	50	210
H_404	BOSCH	CD210G	63	40	25	75	210
H_405	BOSCH	CD210G	63	40	25	100	210
H_406	BOSCH	CD210G	63	40	25	125	210
H_407	BOSCH	CD210G	63	40	25	150	210
H_408	BOSCH	CD210G	63	40	25	175	210
H_409	BOSCH	CD210G	63	40	25	200	210
H_410	BOSCH	CD210G	76	50	22	50	210
H_411	BOSCH	CD210G	76	50	22	75	210
H_412	BOSCH	CD210G	76	50	22	100	210
H_413	BOSCH	CD210G	76	50	22	125	210
H_414	BOSCH	CD210G	76	50	22	150	210
H_415	BOSCH	CD210G	76	50	22	175	210
H_416	BOSCH	CD210G	76	50	22	200	210
H_417	BOSCH	CD210G	76	50	25	50	210
H_418	BOSCH	CD210G	76	50	25	75	210
H_419	BOSCH	CD210G	76	50	25	100	210
H_420	BOSCH	CD210G	76	50	25	125	210
H_421	BOSCH	CD210G	76	50	25	150	210
H_422	BOSCH	CD210G	76	50	25	175	210
H_423	BOSCH	CD210G	76	50	25	200	210
H_424	BOSCH	CD210G	76	50	36	50	210
H_425	BOSCH	CD210G	76	50	36	75	210

H_426	BOSCH	CD210G	76	50	36	100	210
H_427	BOSCH	CD210G	76	50	36	125	210
H_428	BOSCH	CD210G	76	50	36	150	210
H_429	BOSCH	CD210G	76	50	36	175	210
H_430	BOSCH	CD210G	76	50	36	200	210
H_431	BOSCH	CD210G	89	63	25	50	210
H_432	BOSCH	CD210G	89	63	25	75	210
H_433	BOSCH	CD210G	89	63	25	100	210
H_434	BOSCH	CD210G	89	63	25	125	210
H_435	BOSCH	CD210G	89	63	25	150	210
H_436	BOSCH	CD210G	89	63	25	175	210
H_437	BOSCH	CD210G	89	63	25	200	210
H_438	BOSCH	CD210G	89	63	28	50	210
H_439	BOSCH	CD210G	89	63	28	75	210
H_440	BOSCH	CD210G	89	63	28	100	210
H_441	BOSCH	CD210G	89	63	28	125	210
H_442	BOSCH	CD210G	89	63	28	150	210
H_443	BOSCH	CD210G	89	63	28	175	210
H_444	BOSCH	CD210G	89	63	28	200	210
H_445	BOSCH	CD210G	89	63	36	50	210
H_446	BOSCH	CD210G	89	63	36	75	210
H_447	BOSCH	CD210G	89	63	36	100	210
H_448	BOSCH	CD210G	89	63	36	125	210
H_449	BOSCH	CD210G	89	63	36	150	210
H_450	BOSCH	CD210G	89	63	36	175	210
H_451	BOSCH	CD210G	89	63	36	200	210
H_452	BOSCH	CD210G	89	63	45	50	210
H_453	BOSCH	CD210G	89	63	45	75	210
H_454	BOSCH	CD210G	89	63	45	100	210
H_455	BOSCH	CD210G	89	63	45	125	210
H_456	BOSCH	CD210G	89	63	45	150	210
H_457	BOSCH	CD210G	89	63	45	175	210
H_458	BOSCH	CD210G	89	63	45	200	210
H_459	BOSCH	CD210G	114	80	36	50	210
H_460	BOSCH	CD210G	114	80	36	75	210
H_461	BOSCH	CD210G	114	80	36	100	210
H_462	BOSCH	CD210G	114	80	36	125	210
H_463	BOSCH	CD210G	114	80	36	150	210
H_464	BOSCH	CD210G	114	80	36	175	210
H_465	BOSCH	CD210G	114	80	36	200	210
H_466	BOSCH	CD210G	114	80	45	50	210
H_467	BOSCH	CD210G	114	80	45	75	210
H_468	BOSCH	CD210G	114	80	45	100	210
H_469	BOSCH	CD210G	114	80	45	125	210
H_470	BOSCH	CD210G	114	80	45	150	210
H_471	BOSCH	CD210G	114	80	45	175	210
H_472	BOSCH	CD210G	114	80	45	200	210
H_473	BOSCH	CD210G	114	80	56	50	210
H_474	BOSCH	CD210G	114	80	56	75	210
H_475	BOSCH	CD210G	114	80	56	100	210
H_476	BOSCH	CD210G	114	80	56	125	210
H_477	BOSCH	CD210G	114	80	56	150	210
H_478	BOSCH	CD210G	114	80	56	175	210
H_479	BOSCH	CD210G	114	80	56	200	210

H_480	BOSCH	CD210G	114	80	36	50	210
H_481	BOSCH	CD210G	114	80	36	75	210
H_482	BOSCH	CD210G	114	80	36	100	210
H_483	BOSCH	CD210G	114	80	36	125	210
H_484	BOSCH	CD210G	114	80	36	150	210
H_485	BOSCH	CD210G	114	80	36	175	210
H_486	BOSCH	CD210G	114	80	36	200	210
H_487	BOSCH	CD210G	114	80	45	50	210
H_488	BOSCH	CD210G	114	80	45	75	210
H_489	BOSCH	CD210G	114	80	45	100	210
H_490	BOSCH	CD210G	114	80	45	125	210
H_491	BOSCH	CD210G	114	80	45	150	210
H_492	BOSCH	CD210G	114	80	45	175	210
H_493	BOSCH	CD210G	114	80	45	200	210
H_494	BOSCH	CD210G	114	80	56	50	210
H_495	BOSCH	CD210G	114	80	56	75	210
H_496	BOSCH	CD210G	114	80	56	100	210
H_497	BOSCH	CD210G	114	80	56	125	210
H_498	BOSCH	CD210G	114	80	56	150	210
H_499	BOSCH	CD210G	114	80	56	175	210
H_500	BOSCH	CD210G	114	80	56	200	210
H_501	BOSCH	CD210G	114	80	36	50	210
H_502	BOSCH	CD210G	114	80	36	75	210
H_503	BOSCH	CD210G	114	80	36	100	210
H_504	BOSCH	CD210G	114	80	36	125	210
H_505	BOSCH	CD210G	114	80	36	150	210
H_506	BOSCH	CD210G	114	80	36	175	210
H_507	BOSCH	CD210G	114	80	36	200	210
H_508	BOSCH	CD210G	114	80	45	50	210
H_509	BOSCH	CD210G	114	80	45	75	210
H_510	BOSCH	CD210G	114	80	45	100	210
H_511	BOSCH	CD210G	114	80	45	125	210
H_512	BOSCH	CD210G	114	80	45	150	210
H_513	BOSCH	CD210G	114	80	45	175	210
H_514	BOSCH	CD210G	114	80	45	200	210
H_515	BOSCH	CD210G	114	80	56	50	210
H_516	BOSCH	CD210G	114	80	56	75	210
H_517	BOSCH	CD210G	114	80	56	100	210
H_518	BOSCH	CD210G	114	80	56	125	210
H_519	BOSCH	CD210G	114	80	56	150	210
H_520	BOSCH	CD210G	114	80	56	175	210
H_521	BOSCH	CD210G	114	80	56	200	210
H_522	BOSCH	CD210G	127	100	45	75	210
H_523	BOSCH	CD210G	127	100	45	100	210
H_524	BOSCH	CD210G	127	100	45	125	210
H_525	BOSCH	CD210G	127	100	45	150	210
H_526	BOSCH	CD210G	127	100	45	175	210
H_527	BOSCH	CD210G	127	100	45	200	210
H_528	BOSCH	CD210G	127	100	50	75	210
H_529	BOSCH	CD210G	127	100	50	100	210
H_530	BOSCH	CD210G	127	100	50	125	210
H_531	BOSCH	CD210G	127	100	50	150	210
H_532	BOSCH	CD210G	127	100	50	175	210
H_533	BOSCH	CD210G	127	100	50	200	210

H_534	BOSCH	CD210G	127	100	70	75	210
H_535	BOSCH	CD210G	127	100	70	100	210
H_536	BOSCH	CD210G	127	100	70	125	210
H_537	BOSCH	CD210G	127	100	70	150	210
H_538	BOSCH	CD210G	127	100	70	175	210
H_539	BOSCH	CD210G	127	100	70	200	210
H_540	BOSCH	CD210G	127	100	45	75	210
H_541	BOSCH	CD210G	127	100	45	100	210
H_542	BOSCH	CD210G	127	100	45	125	210
H_543	BOSCH	CD210G	127	100	45	150	210
H_544	BOSCH	CD210G	127	100	45	175	210
H_545	BOSCH	CD210G	127	100	45	200	210
H_546	BOSCH	CD210G	127	100	50	75	210
H_547	BOSCH	CD210G	127	100	50	100	210
H_548	BOSCH	CD210G	127	100	50	125	210
H_549	BOSCH	CD210G	127	100	50	150	210
H_550	BOSCH	CD210G	127	100	50	175	210
H_551	BOSCH	CD210G	127	100	50	200	210
H_552	BOSCH	CD210G	127	100	70	75	210
H_553	BOSCH	CD210G	127	100	70	100	210
H_554	BOSCH	CD210G	127	100	70	125	210
H_555	BOSCH	CD210G	127	100	70	150	210
H_556	BOSCH	CD210G	127	100	70	175	210
H_557	BOSCH	CD210G	127	100	70	200	210
H_558	BOSCH	CD210G	165	125	50	100	210
H_559	BOSCH	CD210G	165	125	50	125	210
H_560	BOSCH	CD210G	165	125	50	150	210
H_561	BOSCH	CD210G	165	125	50	175	210
H_562	BOSCH	CD210G	165	125	50	200	210
H_563	BOSCH	CD210G	165	125	56	100	210
H_564	BOSCH	CD210G	165	125	56	125	210
H_565	BOSCH	CD210G	165	125	56	150	210
H_566	BOSCH	CD210G	165	125	56	175	210
H_567	BOSCH	CD210G	165	125	56	200	210
H_568	BOSCH	CD210G	165	125	63	100	210
H_569	BOSCH	CD210G	165	125	63	125	210
H_570	BOSCH	CD210G	165	125	63	150	210
H_571	BOSCH	CD210G	165	125	63	175	210
H_572	BOSCH	CD210G	165	125	63	200	210
H_573	BOSCH	CD210G	165	125	90	100	210
H_574	BOSCH	CD210G	165	125	90	125	210
H_575	BOSCH	CD210G	165	125	90	150	210
H_576	BOSCH	CD210G	165	125	90	175	210
H_577	BOSCH	CD210G	165	125	90	200	210
H_578	BOSCH	CD210G	165	125	50	100	210
H_579	BOSCH	CD210G	165	125	50	125	210
H_580	BOSCH	CD210G	165	125	50	150	210
H_581	BOSCH	CD210G	165	125	50	175	210
H_582	BOSCH	CD210G	165	125	50	200	210
H_583	BOSCH	CD210G	165	125	56	100	210
H_584	BOSCH	CD210G	165	125	56	125	210
H_585	BOSCH	CD210G	165	125	56	150	210
H_586	BOSCH	CD210G	165	125	56	175	210
H_587	BOSCH	CD210G	165	125	56	200	210

H_588	BOSCH	CD210G	165	125	63	100	210
H_589	BOSCH	CD210G	165	125	63	125	210
H_590	BOSCH	CD210G	165	125	63	150	210
H_591	BOSCH	CD210G	165	125	63	175	210
H_592	BOSCH	CD210G	165	125	63	200	210
H_593	BOSCH	CD210G	165	125	90	100	210
H_594	BOSCH	CD210G	165	125	90	125	210
H_595	BOSCH	CD210G	165	125	90	150	210
H_596	BOSCH	CD210G	165	125	90	175	210
H_597	BOSCH	CD210G	165	125	90	200	210
H_598	BOSCH	CD210R	63	40	16	50	210
H_599	BOSCH	CD210R	63	40	16	75	210
H_600	BOSCH	CD210R	63	40	16	100	210
H_601	BOSCH	CD210R	63	40	16	125	210
H_602	BOSCH	CD210R	63	40	16	150	210
H_603	BOSCH	CD210R	63	40	16	175	210
H_604	BOSCH	CD210R	63	40	16	200	210
H_605	BOSCH	CD210R	63	40	18	50	210
H_606	BOSCH	CD210R	63	40	18	75	210
H_607	BOSCH	CD210R	63	40	18	100	210
H_608	BOSCH	CD210R	63	40	18	125	210
H_609	BOSCH	CD210R	63	40	18	150	210
H_610	BOSCH	CD210R	63	40	18	175	210
H_611	BOSCH	CD210R	63	40	18	200	210
H_612	BOSCH	CD210R	63	40	25	50	210
H_613	BOSCH	CD210R	63	40	25	75	210
H_614	BOSCH	CD210R	63	40	25	100	210
H_615	BOSCH	CD210R	63	40	25	125	210
H_616	BOSCH	CD210R	63	40	25	150	210
H_617	BOSCH	CD210R	63	40	25	175	210
H_618	BOSCH	CD210R	63	40	25	200	210
H_619	BOSCH	CD210R	76	50	22	50	210
H_620	BOSCH	CD210R	76	50	22	75	210
H_621	BOSCH	CD210R	76	50	22	100	210
H_622	BOSCH	CD210R	76	50	22	125	210
H_623	BOSCH	CD210R	76	50	22	150	210
H_624	BOSCH	CD210R	76	50	22	175	210
H_625	BOSCH	CD210R	76	50	22	200	210
H_626	BOSCH	CD210R	76	50	25	50	210
H_627	BOSCH	CD210R	76	50	25	75	210
H_628	BOSCH	CD210R	76	50	25	100	210
H_629	BOSCH	CD210R	76	50	25	125	210
H_630	BOSCH	CD210R	76	50	25	150	210
H_631	BOSCH	CD210R	76	50	25	175	210
H_632	BOSCH	CD210R	76	50	25	200	210
H_633	BOSCH	CD210R	76	50	36	50	210
H_634	BOSCH	CD210R	76	50	36	75	210
H_635	BOSCH	CD210R	76	50	36	100	210
H_636	BOSCH	CD210R	76	50	36	125	210
H_637	BOSCH	CD210R	76	50	36	150	210
H_638	BOSCH	CD210R	76	50	36	175	210
H_639	BOSCH	CD210R	76	50	36	200	210
H_640	BOSCH	CD210R	89	63	25	50	210
H_641	BOSCH	CD210R	89	63	25	75	210

H_642	BOSCH	CD210R	89	63	25	100	210
H_643	BOSCH	CD210R	89	63	25	125	210
H_644	BOSCH	CD210R	89	63	25	150	210
H_645	BOSCH	CD210R	89	63	25	175	210
H_646	BOSCH	CD210R	89	63	25	200	210
H_647	BOSCH	CD210R	89	63	28	50	210
H_648	BOSCH	CD210R	89	63	28	75	210
H_649	BOSCH	CD210R	89	63	28	100	210
H_650	BOSCH	CD210R	89	63	28	125	210
H_651	BOSCH	CD210R	89	63	28	150	210
H_652	BOSCH	CD210R	89	63	28	175	210
H_653	BOSCH	CD210R	89	63	28	200	210
H_654	BOSCH	CD210R	89	63	36	50	210
H_655	BOSCH	CD210R	89	63	36	75	210
H_656	BOSCH	CD210R	89	63	36	100	210
H_657	BOSCH	CD210R	89	63	36	125	210
H_658	BOSCH	CD210R	89	63	36	150	210
H_659	BOSCH	CD210R	89	63	36	175	210
H_660	BOSCH	CD210R	89	63	36	200	210
H_661	BOSCH	CD210R	89	63	45	50	210
H_662	BOSCH	CD210R	89	63	45	75	210
H_663	BOSCH	CD210R	89	63	45	100	210
H_664	BOSCH	CD210R	89	63	45	125	210
H_665	BOSCH	CD210R	89	63	45	150	210
H_666	BOSCH	CD210R	89	63	45	175	210
H_667	BOSCH	CD210R	89	63	45	200	210
H_668	BOSCH	CD210R	114	80	36	50	210
H_669	BOSCH	CD210R	114	80	36	75	210
H_670	BOSCH	CD210R	114	80	36	100	210
H_671	BOSCH	CD210R	114	80	36	125	210
H_672	BOSCH	CD210R	114	80	36	150	210
H_673	BOSCH	CD210R	114	80	36	175	210
H_674	BOSCH	CD210R	114	80	36	200	210
H_675	BOSCH	CD210R	114	80	45	50	210
H_676	BOSCH	CD210R	114	80	45	75	210
H_677	BOSCH	CD210R	114	80	45	100	210
H_678	BOSCH	CD210R	114	80	45	125	210
H_679	BOSCH	CD210R	114	80	45	150	210
H_680	BOSCH	CD210R	114	80	45	175	210
H_681	BOSCH	CD210R	114	80	45	200	210
H_682	BOSCH	CD210R	114	80	56	50	210
H_683	BOSCH	CD210R	114	80	56	75	210
H_684	BOSCH	CD210R	114	80	56	100	210
H_685	BOSCH	CD210R	114	80	56	125	210
H_686	BOSCH	CD210R	114	80	56	150	210
H_687	BOSCH	CD210R	114	80	56	175	210
H_688	BOSCH	CD210R	114	80	56	200	210
H_689	BOSCH	CD210R	114	80	36	50	210
H_690	BOSCH	CD210R	114	80	36	75	210
H_691	BOSCH	CD210R	114	80	36	100	210
H_692	BOSCH	CD210R	114	80	36	125	210
H_693	BOSCH	CD210R	114	80	36	150	210
H_694	BOSCH	CD210R	114	80	36	175	210
H_695	BOSCH	CD210R	114	80	36	200	210

H_696	BOSCH	CD210R	114	80	45	50	210
H_697	BOSCH	CD210R	114	80	45	75	210
H_698	BOSCH	CD210R	114	80	45	100	210
H_699	BOSCH	CD210R	114	80	45	125	210
H_700	BOSCH	CD210R	114	80	45	150	210
H_701	BOSCH	CD210R	114	80	45	175	210
H_702	BOSCH	CD210R	114	80	45	200	210
H_703	BOSCH	CD210R	114	80	56	50	210
H_704	BOSCH	CD210R	114	80	56	75	210
H_705	BOSCH	CD210R	114	80	56	100	210
H_706	BOSCH	CD210R	114	80	56	125	210
H_707	BOSCH	CD210R	114	80	56	150	210
H_708	BOSCH	CD210R	114	80	56	175	210
H_709	BOSCH	CD210R	114	80	56	200	210
H_710	BOSCH	CD210R	114	80	36	50	210
H_711	BOSCH	CD210R	114	80	36	75	210
H_712	BOSCH	CD210R	114	80	36	100	210
H_713	BOSCH	CD210R	114	80	36	125	210
H_714	BOSCH	CD210R	114	80	36	150	210
H_715	BOSCH	CD210R	114	80	36	175	210
H_716	BOSCH	CD210R	114	80	36	200	210
H_717	BOSCH	CD210R	114	80	45	50	210
H_718	BOSCH	CD210R	114	80	45	75	210
H_719	BOSCH	CD210R	114	80	45	100	210
H_720	BOSCH	CD210R	114	80	45	125	210
H_721	BOSCH	CD210R	114	80	45	150	210
H_722	BOSCH	CD210R	114	80	45	175	210
H_723	BOSCH	CD210R	114	80	45	200	210
H_724	BOSCH	CD210R	114	80	56	50	210
H_725	BOSCH	CD210R	114	80	56	75	210
H_726	BOSCH	CD210R	114	80	56	100	210
H_727	BOSCH	CD210R	114	80	56	125	210
H_728	BOSCH	CD210R	114	80	56	150	210
H_729	BOSCH	CD210R	114	80	56	175	210
H_730	BOSCH	CD210R	114	80	56	200	210
H_731	BOSCH	CD210R	127	100	45	75	210
H_732	BOSCH	CD210R	127	100	45	100	210
H_733	BOSCH	CD210R	127	100	45	125	210
H_734	BOSCH	CD210R	127	100	45	150	210
H_735	BOSCH	CD210R	127	100	45	175	210
H_736	BOSCH	CD210R	127	100	45	200	210
H_737	BOSCH	CD210R	127	100	50	75	210
H_738	BOSCH	CD210R	127	100	50	100	210
H_739	BOSCH	CD210R	127	100	50	125	210
H_740	BOSCH	CD210R	127	100	50	150	210
H_741	BOSCH	CD210R	127	100	50	175	210
H_742	BOSCH	CD210R	127	100	50	200	210
H_743	BOSCH	CD210R	127	100	70	75	210
H_744	BOSCH	CD210R	127	100	70	100	210
H_745	BOSCH	CD210R	127	100	70	125	210
H_746	BOSCH	CD210R	127	100	70	150	210
H_747	BOSCH	CD210R	127	100	70	175	210
H_748	BOSCH	CD210R	127	100	70	200	210
H_749	BOSCH	CD210R	127	100	45	75	210

H_750	BOSCH	CD210R	127	100	45	100	210
H_751	BOSCH	CD210R	127	100	45	125	210
H_752	BOSCH	CD210R	127	100	45	150	210
H_753	BOSCH	CD210R	127	100	45	175	210
H_754	BOSCH	CD210R	127	100	45	200	210
H_755	BOSCH	CD210R	127	100	50	75	210
H_756	BOSCH	CD210R	127	100	50	100	210
H_757	BOSCH	CD210R	127	100	50	125	210
H_758	BOSCH	CD210R	127	100	50	150	210
H_759	BOSCH	CD210R	127	100	50	175	210
H_760	BOSCH	CD210R	127	100	50	200	210
H_761	BOSCH	CD210R	127	100	70	75	210
H_762	BOSCH	CD210R	127	100	70	100	210
H_763	BOSCH	CD210R	127	100	70	125	210
H_764	BOSCH	CD210R	127	100	70	150	210
H_765	BOSCH	CD210R	127	100	70	175	210
H_766	BOSCH	CD210R	127	100	70	200	210
H_767	BOSCH	CD210R	165	125	50	100	210
H_768	BOSCH	CD210R	165	125	50	125	210
H_769	BOSCH	CD210R	165	125	50	150	210
H_770	BOSCH	CD210R	165	125	50	175	210
H_771	BOSCH	CD210R	165	125	50	200	210
H_772	BOSCH	CD210R	165	125	56	100	210
H_773	BOSCH	CD210R	165	125	56	125	210
H_774	BOSCH	CD210R	165	125	56	150	210
H_775	BOSCH	CD210R	165	125	56	175	210
H_776	BOSCH	CD210R	165	125	56	200	210
H_777	BOSCH	CD210R	165	125	63	100	210
H_778	BOSCH	CD210R	165	125	63	125	210
H_779	BOSCH	CD210R	165	125	63	150	210
H_780	BOSCH	CD210R	165	125	63	175	210
H_781	BOSCH	CD210R	165	125	63	200	210
H_782	BOSCH	CD210R	165	125	90	100	210
H_783	BOSCH	CD210R	165	125	90	125	210
H_784	BOSCH	CD210R	165	125	90	150	210
H_785	BOSCH	CD210R	165	125	90	175	210
H_786	BOSCH	CD210R	165	125	90	200	210
H_787	BOSCH	CD210R	165	125	50	100	210
H_788	BOSCH	CD210R	165	125	50	125	210
H_789	BOSCH	CD210R	165	125	50	150	210
H_790	BOSCH	CD210R	165	125	50	175	210
H_791	BOSCH	CD210R	165	125	50	200	210
H_792	BOSCH	CD210R	165	125	56	100	210
H_793	BOSCH	CD210R	165	125	56	125	210
H_794	BOSCH	CD210R	165	125	56	150	210
H_795	BOSCH	CD210R	165	125	56	175	210
H_796	BOSCH	CD210R	165	125	56	200	210
H_797	BOSCH	CD210R	165	125	63	100	210
H_798	BOSCH	CD210R	165	125	63	125	210
H_799	BOSCH	CD210R	165	125	63	150	210
H_800	BOSCH	CD210R	165	125	63	175	210
H_801	BOSCH	CD210R	165	125	63	200	210
H_802	BOSCH	CD210R	165	125	90	100	210
H_803	BOSCH	CD210R	165	125	90	125	210

H_804	BOSCH	CD210R	165	125	90	150	210
H_805	BOSCH	CD210R	165	125	90	175	210
H_806	BOSCH	CD210R	165	125	90	200	210
H_807	BOSCH	CD210E	63	40	16	50	210
H_808	BOSCH	CD210E	63	40	16	75	210
H_809	BOSCH	CD210E	63	40	16	100	210
H_810	BOSCH	CD210E	63	40	16	125	210
H_811	BOSCH	CD210E	63	40	16	150	210
H_812	BOSCH	CD210E	63	40	16	175	210
H_813	BOSCH	CD210E	63	40	16	200	210
H_814	BOSCH	CD210E	63	40	18	50	210
H_815	BOSCH	CD210E	63	40	18	75	210
H_816	BOSCH	CD210E	63	40	18	100	210
H_817	BOSCH	CD210E	63	40	18	125	210
H_818	BOSCH	CD210E	63	40	18	150	210
H_819	BOSCH	CD210E	63	40	18	175	210
H_820	BOSCH	CD210E	63	40	18	200	210
H_821	BOSCH	CD210E	63	40	25	50	210
H_822	BOSCH	CD210E	63	40	25	75	210
H_823	BOSCH	CD210E	63	40	25	100	210
H_824	BOSCH	CD210E	63	40	25	125	210
H_825	BOSCH	CD210E	63	40	25	150	210
H_826	BOSCH	CD210E	63	40	25	175	210
H_827	BOSCH	CD210E	63	40	25	200	210
H_828	BOSCH	CD210E	76	50	22	50	210
H_829	BOSCH	CD210E	76	50	22	75	210
H_830	BOSCH	CD210E	76	50	22	100	210
H_831	BOSCH	CD210E	76	50	22	125	210
H_832	BOSCH	CD210E	76	50	22	150	210
H_833	BOSCH	CD210E	76	50	22	175	210
H_834	BOSCH	CD210E	76	50	22	200	210
H_835	BOSCH	CD210E	76	50	25	50	210
H_836	BOSCH	CD210E	76	50	25	75	210
H_837	BOSCH	CD210E	76	50	25	100	210
H_838	BOSCH	CD210E	76	50	25	125	210
H_839	BOSCH	CD210E	76	50	25	150	210
H_840	BOSCH	CD210E	76	50	25	175	210
H_841	BOSCH	CD210E	76	50	25	200	210
H_842	BOSCH	CD210E	76	50	36	50	210
H_843	BOSCH	CD210E	76	50	36	75	210
H_844	BOSCH	CD210E	76	50	36	100	210
H_845	BOSCH	CD210E	76	50	36	125	210
H_846	BOSCH	CD210E	76	50	36	150	210
H_847	BOSCH	CD210E	76	50	36	175	210
H_848	BOSCH	CD210E	76	50	36	200	210
H_849	BOSCH	CD210E	89	63	25	50	210
H_850	BOSCH	CD210E	89	63	25	75	210
H_851	BOSCH	CD210E	89	63	25	100	210
H_852	BOSCH	CD210E	89	63	25	125	210
H_853	BOSCH	CD210E	89	63	25	150	210
H_854	BOSCH	CD210E	89	63	25	175	210
H_855	BOSCH	CD210E	89	63	25	200	210
H_856	BOSCH	CD210E	89	63	28	50	210
H_857	BOSCH	CD210E	89	63	28	75	210

H_858	BOSCH	CD210E	89	63	28	100	210
H_859	BOSCH	CD210E	89	63	28	125	210
H_860	BOSCH	CD210E	89	63	28	150	210
H_861	BOSCH	CD210E	89	63	28	175	210
H_862	BOSCH	CD210E	89	63	28	200	210
H_863	BOSCH	CD210E	89	63	36	50	210
H_864	BOSCH	CD210E	89	63	36	75	210
H_865	BOSCH	CD210E	89	63	36	100	210
H_866	BOSCH	CD210E	89	63	36	125	210
H_867	BOSCH	CD210E	89	63	36	150	210
H_868	BOSCH	CD210E	89	63	36	175	210
H_869	BOSCH	CD210E	89	63	36	200	210
H_870	BOSCH	CD210E	89	63	45	50	210
H_871	BOSCH	CD210E	89	63	45	75	210
H_872	BOSCH	CD210E	89	63	45	100	210
H_873	BOSCH	CD210E	89	63	45	125	210
H_874	BOSCH	CD210E	89	63	45	150	210
H_875	BOSCH	CD210E	89	63	45	175	210
H_876	BOSCH	CD210E	89	63	45	200	210
H_877	BOSCH	CD210E	114	80	36	50	210
H_878	BOSCH	CD210E	114	80	36	75	210
H_879	BOSCH	CD210E	114	80	36	100	210
H_880	BOSCH	CD210E	114	80	36	125	210
H_881	BOSCH	CD210E	114	80	36	150	210
H_882	BOSCH	CD210E	114	80	36	175	210
H_883	BOSCH	CD210E	114	80	36	200	210
H_884	BOSCH	CD210E	114	80	45	50	210
H_885	BOSCH	CD210E	114	80	45	75	210
H_886	BOSCH	CD210E	114	80	45	100	210
H_887	BOSCH	CD210E	114	80	45	125	210
H_888	BOSCH	CD210E	114	80	45	150	210
H_889	BOSCH	CD210E	114	80	45	175	210
H_890	BOSCH	CD210E	114	80	45	200	210
H_891	BOSCH	CD210E	114	80	56	50	210
H_892	BOSCH	CD210E	114	80	56	75	210
H_893	BOSCH	CD210E	114	80	56	100	210
H_894	BOSCH	CD210E	114	80	56	125	210
H_895	BOSCH	CD210E	114	80	56	150	210
H_896	BOSCH	CD210E	114	80	56	175	210
H_897	BOSCH	CD210E	114	80	56	200	210
H_898	BOSCH	CD210E	114	80	36	50	210
H_899	BOSCH	CD210E	114	80	36	75	210
H_900	BOSCH	CD210E	114	80	36	100	210
H_901	BOSCH	CD210E	114	80	36	125	210
H_902	BOSCH	CD210E	114	80	36	150	210
H_903	BOSCH	CD210E	114	80	36	175	210
H_904	BOSCH	CD210E	114	80	36	200	210
H_905	BOSCH	CD210E	114	80	45	50	210
H_906	BOSCH	CD210E	114	80	45	75	210
H_907	BOSCH	CD210E	114	80	45	100	210
H_908	BOSCH	CD210E	114	80	45	125	210
H_909	BOSCH	CD210E	114	80	45	150	210
H_910	BOSCH	CD210E	114	80	45	175	210
H_911	BOSCH	CD210E	114	80	45	200	210

H_912	BOSCH	CD210E	114	80	56	50	210
H_913	BOSCH	CD210E	114	80	56	75	210
H_914	BOSCH	CD210E	114	80	56	100	210
H_915	BOSCH	CD210E	114	80	56	125	210
H_916	BOSCH	CD210E	114	80	56	150	210
H_917	BOSCH	CD210E	114	80	56	175	210
H_918	BOSCH	CD210E	114	80	56	200	210
H_919	BOSCH	CD210E	114	80	36	50	210
H_920	BOSCH	CD210E	114	80	36	75	210
H_921	BOSCH	CD210E	114	80	36	100	210
H_922	BOSCH	CD210E	114	80	36	125	210
H_923	BOSCH	CD210E	114	80	36	150	210
H_924	BOSCH	CD210E	114	80	36	175	210
H_925	BOSCH	CD210E	114	80	36	200	210
H_926	BOSCH	CD210E	114	80	45	50	210
H_927	BOSCH	CD210E	114	80	45	75	210
H_928	BOSCH	CD210E	114	80	45	100	210
H_929	BOSCH	CD210E	114	80	45	125	210
H_930	BOSCH	CD210E	114	80	45	150	210
H_931	BOSCH	CD210E	114	80	45	175	210
H_932	BOSCH	CD210E	114	80	45	200	210
H_933	BOSCH	CD210E	114	80	56	50	210
H_934	BOSCH	CD210E	114	80	56	75	210
H_935	BOSCH	CD210E	114	80	56	100	210
H_936	BOSCH	CD210E	114	80	56	125	210
H_937	BOSCH	CD210E	114	80	56	150	210
H_938	BOSCH	CD210E	114	80	56	175	210
H_939	BOSCH	CD210E	114	80	56	200	210
H_940	BOSCH	CD210E	127	100	45	75	210
H_941	BOSCH	CD210E	127	100	45	100	210
H_942	BOSCH	CD210E	127	100	45	125	210
H_943	BOSCH	CD210E	127	100	45	150	210
H_944	BOSCH	CD210E	127	100	45	175	210
H_945	BOSCH	CD210E	127	100	45	200	210
H_946	BOSCH	CD210E	127	100	50	75	210
H_947	BOSCH	CD210E	127	100	50	100	210
H_948	BOSCH	CD210E	127	100	50	125	210
H_949	BOSCH	CD210E	127	100	50	150	210
H_950	BOSCH	CD210E	127	100	50	175	210
H_951	BOSCH	CD210E	127	100	50	200	210
H_952	BOSCH	CD210E	127	100	70	75	210
H_953	BOSCH	CD210E	127	100	70	100	210
H_954	BOSCH	CD210E	127	100	70	125	210
H_955	BOSCH	CD210E	127	100	70	150	210
H_956	BOSCH	CD210E	127	100	70	175	210
H_957	BOSCH	CD210E	127	100	70	200	210
H_958	BOSCH	CD210E	127	100	45	75	210
H_959	BOSCH	CD210E	127	100	45	100	210
H_960	BOSCH	CD210E	127	100	45	125	210
H_961	BOSCH	CD210E	127	100	45	150	210
H_962	BOSCH	CD210E	127	100	45	175	210
H_963	BOSCH	CD210E	127	100	45	200	210
H_964	BOSCH	CD210E	127	100	50	75	210
H_965	BOSCH	CD210E	127	100	50	100	210

H_966	BOSCH	CD210E	127	100	50	125	210
H_967	BOSCH	CD210E	127	100	50	150	210
H_968	BOSCH	CD210E	127	100	50	175	210
H_969	BOSCH	CD210E	127	100	50	200	210
H_970	BOSCH	CD210E	127	100	70	75	210
H_971	BOSCH	CD210E	127	100	70	100	210
H_972	BOSCH	CD210E	127	100	70	125	210
H_973	BOSCH	CD210E	127	100	70	150	210
H_974	BOSCH	CD210E	127	100	70	175	210
H_975	BOSCH	CD210E	127	100	70	200	210
H_976	BOSCH	CD210E	165	125	50	100	210
H_977	BOSCH	CD210E	165	125	50	125	210
H_978	BOSCH	CD210E	165	125	50	150	210
H_979	BOSCH	CD210E	165	125	50	175	210
H_980	BOSCH	CD210E	165	125	50	200	210
H_981	BOSCH	CD210E	165	125	56	100	210
H_982	BOSCH	CD210E	165	125	56	125	210
H_983	BOSCH	CD210E	165	125	56	150	210
H_984	BOSCH	CD210E	165	125	56	175	210
H_985	BOSCH	CD210E	165	125	56	200	210
H_986	BOSCH	CD210E	165	125	63	100	210
H_987	BOSCH	CD210E	165	125	63	125	210
H_988	BOSCH	CD210E	165	125	63	150	210
H_989	BOSCH	CD210E	165	125	63	175	210
H_990	BOSCH	CD210E	165	125	63	200	210
H_991	BOSCH	CD210E	165	125	90	100	210
H_992	BOSCH	CD210E	165	125	90	125	210
H_993	BOSCH	CD210E	165	125	90	150	210
H_994	BOSCH	CD210E	165	125	90	175	210
H_995	BOSCH	CD210E	165	125	90	200	210
H_996	BOSCH	CD210E	165	125	50	100	210
H_997	BOSCH	CD210E	165	125	50	125	210
H_998	BOSCH	CD210E	165	125	50	150	210
H_999	BOSCH	CD210E	165	125	50	175	210
H_1000	BOSCH	CD210E	165	125	50	200	210
H_1001	BOSCH	CD210E	165	125	56	100	210
H_1002	BOSCH	CD210E	165	125	56	125	210
H_1003	BOSCH	CD210E	165	125	56	150	210
H_1004	BOSCH	CD210E	165	125	56	175	210
H_1005	BOSCH	CD210E	165	125	56	200	210
H_1006	BOSCH	CD210E	165	125	63	100	210
H_1007	BOSCH	CD210E	165	125	63	125	210
H_1008	BOSCH	CD210E	165	125	63	150	210
H_1009	BOSCH	CD210E	165	125	63	175	210
H_1010	BOSCH	CD210E	165	125	63	200	210
H_1011	BOSCH	CD210E	165	125	90	100	210
H_1012	BOSCH	CD210E	165	125	90	125	210
H_1013	BOSCH	CD210E	165	125	90	150	210
H_1014	BOSCH	CD210E	165	125	90	175	210
H_1015	BOSCH	CD210E	165	125	90	200	210
H_1016	BOSCH	CD210S	63	40	16	50	210
H_1017	BOSCH	CD210S	63	40	16	75	210
H_1018	BOSCH	CD210S	63	40	16	100	210
H_1019	BOSCH	CD210S	63	40	16	125	210

H_1020	BOSCH	CD210S	63	40	16	150	210
H_1021	BOSCH	CD210S	63	40	16	175	210
H_1022	BOSCH	CD210S	63	40	16	200	210
H_1023	BOSCH	CD210S	63	40	18	50	210
H_1024	BOSCH	CD210S	63	40	18	75	210
H_1025	BOSCH	CD210S	63	40	18	100	210
H_1026	BOSCH	CD210S	63	40	18	125	210
H_1027	BOSCH	CD210S	63	40	18	150	210
H_1028	BOSCH	CD210S	63	40	18	175	210
H_1029	BOSCH	CD210S	63	40	18	200	210
H_1030	BOSCH	CD210S	63	40	25	50	210
H_1031	BOSCH	CD210S	63	40	25	75	210
H_1032	BOSCH	CD210S	63	40	25	100	210
H_1033	BOSCH	CD210S	63	40	25	125	210
H_1034	BOSCH	CD210S	63	40	25	150	210
H_1035	BOSCH	CD210S	63	40	25	175	210
H_1036	BOSCH	CD210S	63	40	25	200	210
H_1037	BOSCH	CD210S	76	50	22	50	210
H_1038	BOSCH	CD210S	76	50	22	75	210
H_1039	BOSCH	CD210S	76	50	22	100	210
H_1040	BOSCH	CD210S	76	50	22	125	210
H_1041	BOSCH	CD210S	76	50	22	150	210
H_1042	BOSCH	CD210S	76	50	22	175	210
H_1043	BOSCH	CD210S	76	50	22	200	210
H_1044	BOSCH	CD210S	76	50	25	50	210
H_1045	BOSCH	CD210S	76	50	25	75	210
H_1046	BOSCH	CD210S	76	50	25	100	210
H_1047	BOSCH	CD210S	76	50	25	125	210
H_1048	BOSCH	CD210S	76	50	25	150	210
H_1049	BOSCH	CD210S	76	50	25	175	210
H_1050	BOSCH	CD210S	76	50	25	200	210
H_1051	BOSCH	CD210S	76	50	36	50	210
H_1052	BOSCH	CD210S	76	50	36	75	210
H_1053	BOSCH	CD210S	76	50	36	100	210
H_1054	BOSCH	CD210S	76	50	36	125	210
H_1055	BOSCH	CD210S	76	50	36	150	210
H_1056	BOSCH	CD210S	76	50	36	175	210
H_1057	BOSCH	CD210S	76	50	36	200	210
H_1058	BOSCH	CD210S	89	63	25	50	210
H_1059	BOSCH	CD210S	89	63	25	75	210
H_1060	BOSCH	CD210S	89	63	25	100	210
H_1061	BOSCH	CD210S	89	63	25	125	210
H_1062	BOSCH	CD210S	89	63	25	150	210
H_1063	BOSCH	CD210S	89	63	25	175	210
H_1064	BOSCH	CD210S	89	63	25	200	210
H_1065	BOSCH	CD210S	89	63	28	50	210
H_1066	BOSCH	CD210S	89	63	28	75	210
H_1067	BOSCH	CD210S	89	63	28	100	210
H_1068	BOSCH	CD210S	89	63	28	125	210
H_1069	BOSCH	CD210S	89	63	28	150	210
H_1070	BOSCH	CD210S	89	63	28	175	210
H_1071	BOSCH	CD210S	89	63	28	200	210
H_1072	BOSCH	CD210S	89	63	36	50	210
H_1073	BOSCH	CD210S	89	63	36	75	210

H_1074	BOSCH	CD210S	89	63	36	100	210
H_1075	BOSCH	CD210S	89	63	36	125	210
H_1076	BOSCH	CD210S	89	63	36	150	210
H_1077	BOSCH	CD210S	89	63	36	175	210
H_1078	BOSCH	CD210S	89	63	36	200	210
H_1079	BOSCH	CD210S	89	63	45	50	210
H_1080	BOSCH	CD210S	89	63	45	75	210
H_1081	BOSCH	CD210S	89	63	45	100	210
H_1082	BOSCH	CD210S	89	63	45	125	210
H_1083	BOSCH	CD210S	89	63	45	150	210
H_1084	BOSCH	CD210S	89	63	45	175	210
H_1085	BOSCH	CD210S	89	63	45	200	210
H_1086	BOSCH	CD210S	114	80	36	50	210
H_1087	BOSCH	CD210S	114	80	36	75	210
H_1088	BOSCH	CD210S	114	80	36	100	210
H_1089	BOSCH	CD210S	114	80	36	125	210
H_1090	BOSCH	CD210S	114	80	36	150	210
H_1091	BOSCH	CD210S	114	80	36	175	210
H_1092	BOSCH	CD210S	114	80	36	200	210
H_1093	BOSCH	CD210S	114	80	45	50	210
H_1094	BOSCH	CD210S	114	80	45	75	210
H_1095	BOSCH	CD210S	114	80	45	100	210
H_1096	BOSCH	CD210S	114	80	45	125	210
H_1097	BOSCH	CD210S	114	80	45	150	210
H_1098	BOSCH	CD210S	114	80	45	175	210
H_1099	BOSCH	CD210S	114	80	45	200	210
H_1100	BOSCH	CD210S	114	80	56	50	210
H_1101	BOSCH	CD210S	114	80	56	75	210
H_1102	BOSCH	CD210S	114	80	56	100	210
H_1103	BOSCH	CD210S	114	80	56	125	210
H_1104	BOSCH	CD210S	114	80	56	150	210
H_1105	BOSCH	CD210S	114	80	56	175	210
H_1106	BOSCH	CD210S	114	80	56	200	210
H_1107	BOSCH	CD210S	114	80	36	50	210
H_1108	BOSCH	CD210S	114	80	36	75	210
H_1109	BOSCH	CD210S	114	80	36	100	210
H_1110	BOSCH	CD210S	114	80	36	125	210
H_1111	BOSCH	CD210S	114	80	36	150	210
H_1112	BOSCH	CD210S	114	80	36	175	210
H_1113	BOSCH	CD210S	114	80	36	200	210
H_1114	BOSCH	CD210S	114	80	45	50	210
H_1115	BOSCH	CD210S	114	80	45	75	210
H_1116	BOSCH	CD210S	114	80	45	100	210
H_1117	BOSCH	CD210S	114	80	45	125	210
H_1118	BOSCH	CD210S	114	80	45	150	210
H_1119	BOSCH	CD210S	114	80	45	175	210
H_1120	BOSCH	CD210S	114	80	45	200	210
H_1121	BOSCH	CD210S	114	80	56	50	210
H_1122	BOSCH	CD210S	114	80	56	75	210
H_1123	BOSCH	CD210S	114	80	56	100	210
H_1124	BOSCH	CD210S	114	80	56	125	210
H_1125	BOSCH	CD210S	114	80	56	150	210
H_1126	BOSCH	CD210S	114	80	56	175	210
H_1127	BOSCH	CD210S	114	80	56	200	210

H_1128	BOSCH	CD210S	114	80	36	50	210
H_1129	BOSCH	CD210S	114	80	36	75	210
H_1130	BOSCH	CD210S	114	80	36	100	210
H_1131	BOSCH	CD210S	114	80	36	125	210
H_1132	BOSCH	CD210S	114	80	36	150	210
H_1133	BOSCH	CD210S	114	80	36	175	210
H_1134	BOSCH	CD210S	114	80	36	200	210
H_1135	BOSCH	CD210S	114	80	45	50	210
H_1136	BOSCH	CD210S	114	80	45	75	210
H_1137	BOSCH	CD210S	114	80	45	100	210
H_1138	BOSCH	CD210S	114	80	45	125	210
H_1139	BOSCH	CD210S	114	80	45	150	210
H_1140	BOSCH	CD210S	114	80	45	175	210
H_1141	BOSCH	CD210S	114	80	45	200	210
H_1142	BOSCH	CD210S	114	80	56	50	210
H_1143	BOSCH	CD210S	114	80	56	75	210
H_1144	BOSCH	CD210S	114	80	56	100	210
H_1145	BOSCH	CD210S	114	80	56	125	210
H_1146	BOSCH	CD210S	114	80	56	150	210
H_1147	BOSCH	CD210S	114	80	56	175	210
H_1148	BOSCH	CD210S	114	80	56	200	210
H_1149	BOSCH	CD210S	127	100	45	75	210
H_1150	BOSCH	CD210S	127	100	45	100	210
H_1151	BOSCH	CD210S	127	100	45	125	210
H_1152	BOSCH	CD210S	127	100	45	150	210
H_1153	BOSCH	CD210S	127	100	45	175	210
H_1154	BOSCH	CD210S	127	100	45	200	210
H_1155	BOSCH	CD210S	127	100	50	75	210
H_1156	BOSCH	CD210S	127	100	50	100	210
H_1157	BOSCH	CD210S	127	100	50	125	210
H_1158	BOSCH	CD210S	127	100	50	150	210
H_1159	BOSCH	CD210S	127	100	50	175	210
H_1160	BOSCH	CD210S	127	100	50	200	210
H_1161	BOSCH	CD210S	127	100	70	75	210
H_1162	BOSCH	CD210S	127	100	70	100	210
H_1163	BOSCH	CD210S	127	100	70	125	210
H_1164	BOSCH	CD210S	127	100	70	150	210
H_1165	BOSCH	CD210S	127	100	70	175	210
H_1166	BOSCH	CD210S	127	100	70	200	210
H_1167	BOSCH	CD210S	127	100	45	75	210
H_1168	BOSCH	CD210S	127	100	45	100	210
H_1169	BOSCH	CD210S	127	100	45	125	210
H_1170	BOSCH	CD210S	127	100	45	150	210
H_1171	BOSCH	CD210S	127	100	45	175	210
H_1172	BOSCH	CD210S	127	100	45	200	210
H_1173	BOSCH	CD210S	127	100	50	75	210
H_1174	BOSCH	CD210S	127	100	50	100	210
H_1175	BOSCH	CD210S	127	100	50	125	210
H_1176	BOSCH	CD210S	127	100	50	150	210
H_1177	BOSCH	CD210S	127	100	50	175	210
H_1178	BOSCH	CD210S	127	100	50	200	210
H_1179	BOSCH	CD210S	127	100	70	75	210
H_1180	BOSCH	CD210S	127	100	70	100	210
H_1181	BOSCH	CD210S	127	100	70	125	210

H_1182	BOSCH	CD210S	127	100	70	150	210
H_1183	BOSCH	CD210S	127	100	70	175	210
H_1184	BOSCH	CD210S	127	100	70	200	210
H_1185	BOSCH	CD210S	165	125	50	100	210
H_1186	BOSCH	CD210S	165	125	50	125	210
H_1187	BOSCH	CD210S	165	125	50	150	210
H_1188	BOSCH	CD210S	165	125	50	175	210
H_1189	BOSCH	CD210S	165	125	50	200	210
H_1190	BOSCH	CD210S	165	125	56	100	210
H_1191	BOSCH	CD210S	165	125	56	125	210
H_1192	BOSCH	CD210S	165	125	56	150	210
H_1193	BOSCH	CD210S	165	125	56	175	210
H_1194	BOSCH	CD210S	165	125	56	200	210
H_1195	BOSCH	CD210S	165	125	63	100	210
H_1196	BOSCH	CD210S	165	125	63	125	210
H_1197	BOSCH	CD210S	165	125	63	150	210
H_1198	BOSCH	CD210S	165	125	63	175	210
H_1199	BOSCH	CD210S	165	125	63	200	210
H_1200	BOSCH	CD210S	165	125	90	100	210
H_1201	BOSCH	CD210S	165	125	90	125	210
H_1202	BOSCH	CD210S	165	125	90	150	210
H_1203	BOSCH	CD210S	165	125	90	175	210
H_1204	BOSCH	CD210S	165	125	90	200	210
H_1205	BOSCH	CD210S	165	125	50	100	210
H_1206	BOSCH	CD210S	165	125	50	125	210
H_1207	BOSCH	CD210S	165	125	50	150	210
H_1208	BOSCH	CD210S	165	125	50	175	210
H_1209	BOSCH	CD210S	165	125	50	200	210
H_1210	BOSCH	CD210S	165	125	56	100	210
H_1211	BOSCH	CD210S	165	125	56	125	210
H_1212	BOSCH	CD210S	165	125	56	150	210
H_1213	BOSCH	CD210S	165	125	56	175	210
H_1214	BOSCH	CD210S	165	125	56	200	210
H_1215	BOSCH	CD210S	165	125	63	100	210
H_1216	BOSCH	CD210S	165	125	63	125	210
H_1217	BOSCH	CD210S	165	125	63	150	210
H_1218	BOSCH	CD210S	165	125	63	175	210
H_1219	BOSCH	CD210S	165	125	63	200	210
H_1220	BOSCH	CD210S	165	125	90	100	210
H_1221	BOSCH	CD210S	165	125	90	125	210
H_1222	BOSCH	CD210S	165	125	90	150	210
H_1223	BOSCH	CD210S	165	125	90	175	210
H_1224	BOSCH	CD210S	165	125	90	200	210

Appendix Q

Drawings
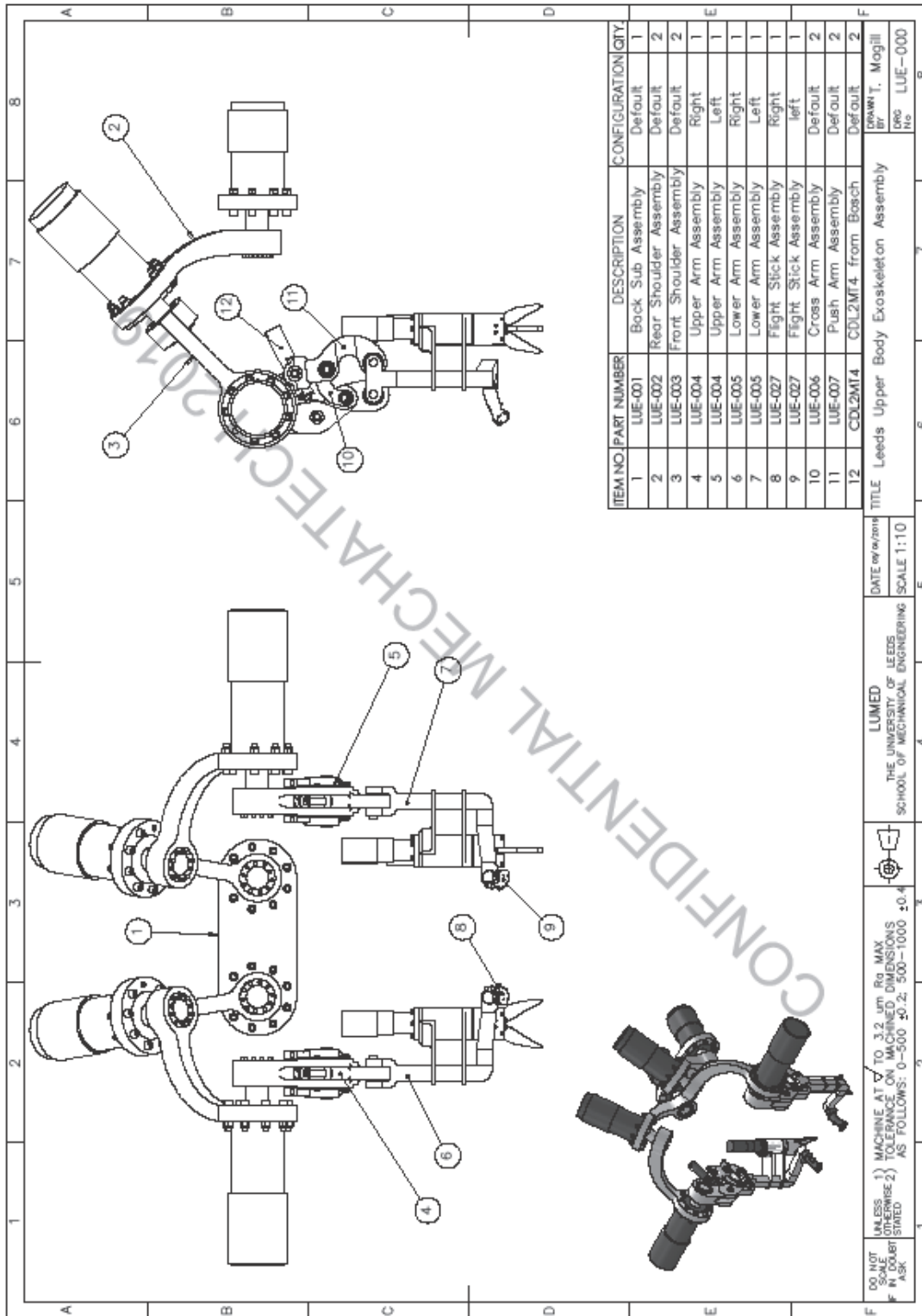
ITEM NO.	PART NUMBER	DESCRIPTION	CONFIGURATION	QTY.
1	LUE-001	Back Sub Assembly	Default	1
2	LUE-002	Rear Shoulder Assembly	Default	2
3	LUE-003	Front Shoulder Assembly	Default	2
4	LUE-004	Upper Arm Assembly	Right	1
5	LUE-004	Upper Arm Assembly	Left	1
6	LUE-005	Lower Arm Assembly	Right	1
7	LUE-005	Lower Arm Assembly	Left	1
8	LUE-027	Fight Stick Assembly	Right	1
9	LUE-027	Fight Stick Assembly	left	1
10	LUE-006	Cross Arm Assembly	Default	2
11	LUE-007	Push Arm Assembly	Default	2
12	CDL2MT4	CDL2MT4 from Bosch	Default	2

TITLE: Leeds Upper Body Exoskeleton Assembly

DRAWN BY: T. Magill
DRG No: LUE-000

DATE: 09/06/2019
SCALE 1:10

LUMED
THE UNIVERSITY OF LEEDS
SCHOOL OF MECHANICAL ENGINEERING

1 of 1

CONFIDENTIAL MECHATECH 2019
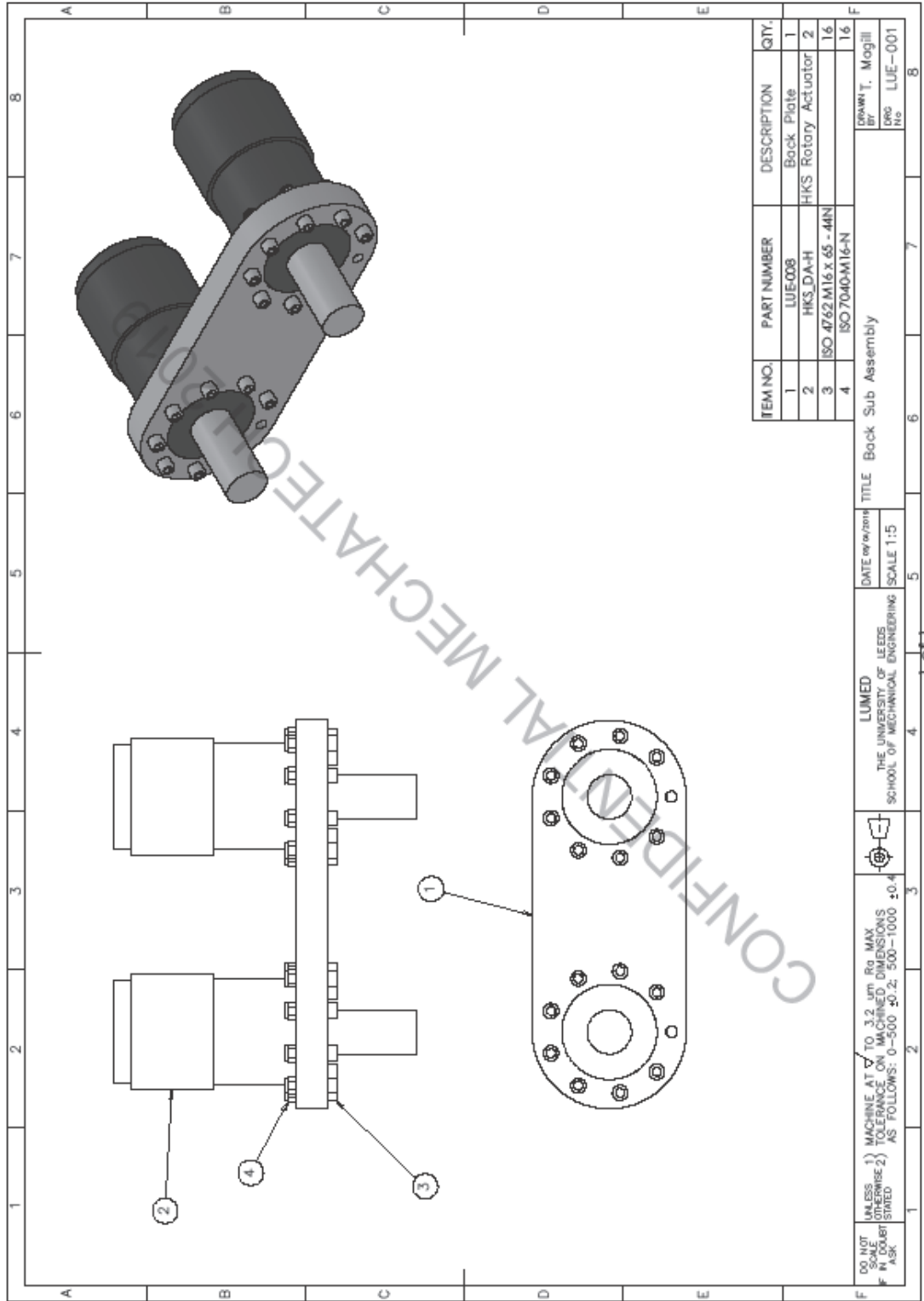
ITEM NO.	PART NUMBER	DESCRIPTION	QTY.
1	LUE-008	Back Plate	1
2	HKS_DA-H	HKS Rotary Actuator	2
3	ISO 4762 M16 x 65 - 44N		16
4	ISO 7040-M16-N		16

DRAWN BY T. Magill
DRG No LUE-001

DATE 09/09/2016

TITLE Back Sub Assembly

SCALE 1:5

LUMED
THE UNIVERSITY OF LEEDS
SCHOOL OF MECHANICAL ENGINEERING

1 of 1

UNLESS OTHERWISE STATED
1) MACHINE AT ∇ TO 3.2 um Ra MAX
2) TOLERANCE ON MACHINED DIMENSIONS AS FOLLOWS: 0-500 ±0.2; 500-1000 ±0.4

DO NOT SCALE
IF IN DOUBT ASK

ITEM NO.	PART NUMBER	DESCRIPTION	QTY.
1	LUE-031	Rear Shoulder Arm	1
2	HKS_DA-H	HKS Rotary Actuator	1
3	PHF FX400-70X110	SKF keyless bearing	1
4	ISO 4762 M16 x 80 - 44N		8
5	ISO 7040-M16-N		8

TITLE Rear Shoulder Assembly

DATE 01/06/2019

SCALE 1:5

DRAWN BY T. Magill

DRG No LUE-002

LUMED

THE UNIVERSITY OF LEEDS
SCHOOL OF MECHANICAL ENGINEERING

1 of 1

UNLESS OTHERWISE STATED 1) MACHINE AT ∇ TO 3.2 um Ra MAX
2) TOLERANCE ON MACHINED DIMENSIONS
AS FOLLOWS: 0-500 ±0.2; 500-1000 ±0.4

DO NOT SCALE IF IN DOUBT ASK

ITEM NO.	PART NUMBER	DESCRIPTION	QTY.
1	LUE-032	Front Shoulder Arm	1
2	HKS_DA-H	HKS Rotary Actuator	1
3	PHF FX400-70X110	SKF keyless bearing	1
4	ISO 4762 M16 x 80 - 44N		8
5	ISO 7040-M16-N		8

TITLE Front Shoulder Assembly

DRAWN BY T. Magill
DRG No LUE-003

DATE 09/09/2019 SCALE 1:5

LUMED
THE UNIVERSITY OF LEEDS
SCHOOL OF MECHANICAL ENGINEERING

1 of 1

RIGHT

LEFT

DETAIL A
SCALE 1 : 1

DETAIL B
SCALE 1 : 1

NOTE:
Difference between LEFT and RIGHT is
orientation of part number 5:
PHF FX400-70X110

ITEM NO.	PART NUMBER	DESCRIPTION	RIGHT/QTY.
1	LUE-009	Upper Arm	1
2	LUE-010	Cylinder Pin	1
3	H-E32304J	Nachi Bearing	2
4	25KBE13	Nachi Bearing	1
5	PHF FX400-70X110	SKF keyless bearing	1
6	BS 3673-4 - S020M		2
7	BS 3673-4 - B062M		2

TITLE Upper Arm Assembly

DATE 09/06/2016

SCALE 1:5

LUMED
THE UNIVERSITY OF LEEDS
SCHOOL OF MECHANICAL ENGINEERING

DRAWN T. Magill
BY

DRG LUE-004
No

UNLESS 1) MACHINE AT ∇ TO 3.2 um Ra MAX
OTHERWISE 2) TOLERANCE ON MACHINED DIMENSIONS
STATED   AS FOLLOWS: 0-500 ±0.2; 500-1000 ±0.4

DO NOT
SCALE
IF IN DOUBT
ASK

1 of 1

LEFT

RIGHT

ITEM NO.	PART NUMBER	DESCRIPTION	Left/QTY.
1	LUE-011	Lower Arm	1
2	LUE-012	Gripper Assembly	1
3	LUE-023	Elbow Pin	2
4	LUE-024	Elbow Lock Plate	1
5	LUE-025	Spacer	4
6	LUE-026	Control Arm	1
7	ISO 4762 M8 x 25 — 25N		2

TITLE Lower Arm Assembly

DRAWN BY T. Magill
DRG No LUE-005

LUMED
THE UNIVERSITY OF LEEDS
SCHOOL OF MECHANICAL ENGINEERING

SCALE 1:5

DATE 09/06/2019

1 of 1

- 382 -

ITEM NO.	PART NUMBER	DESCRIPTION	QTY.
1	LUE-028	Cross Linkage	2
2	LUE-029	Cross Linkage Short Pin	1
3	LUE-030	Cross Linkage Long Pin	1
4	H-E32304J	Nachi Bearing	2
5	AN 04 locknut	Nachi Bearings	4
6	AW 04X lockwasher	Nachi Bearings	4

TITLE Cross Arm Assembly

LUMED
THE UNIVERSITY OF LEEDS
SCHOOL OF MECHANICAL ENGINEERING

DRAWN BY T. Magill
DRG No LUE-006

DATE 09/06/2016
SCALE 1:2

UNLESS OTHERWISE STATED
1) MACHINE AT ▽ TO 3.2 um Ra MAX
2) TOLERANCE ON MACHINED DIMENSIONS AS FOLLOWS: 0-500 ±0.2; 500-1000 ±0.4

DO NOT SCALE IF IN DOUBT ASK

CONFIDENTIAL MECHATECH 2019

1 of 1

ITEM NO.	PART NUMBER	DESCRIPTION	QTY.
1	LUE-033	Push Arm	1
2	LUE-034	Bearing Cap	2
3	25KBE13	Nachi Bearing	1
4	H-E32304J	Nachi Bearing	2
5	BS 3673-4 - B062M		2
6	BS 3673-4 - B062M		2
7	ISO 4762 M10 x 30 — 30N		4

DRAWN BY: T. Magill
DRG No: LUE-007

TITLE: Push Arm Assembly
DATE 09/06/2018
SCALE 1:2

LUMED
THE UNIVERSITY OF LEEDS
SCHOOL OF MECHANICAL ENGINEERING

1 of 1

MACHINE AT √ TO 3.2 um Ra MAX
UNLESS 1) TOLERANCE ON MACHINED DIMENSIONS
OTHERWISE 2) AS FOLLOWS: 0-500 ±0.2; 500-1000 ±0.4
STATED

DO NOT
SCALE
IF IN DOUBT
ASK

ISO 13715:2000

ISO 1101:2004, 8015:1985, 1302:2002

Material 7075-T6 (SN)

Mass [g] 6985.67

DRAWN BY T. Magill

DRG No LUE-008

SECTION A-A

2 × ⌀150 H8 $^{+0.06}_{0}$

⌀195

9 × ⌀18.27/18.00

RT121

⌀195

9 × ⌀18.27/18.00

RT121

DATE 01/09/2019

TITLE Back Plate

SCALE 1:5

LUMED

THE UNIVERSITY OF LEEDS
SCHOOL OF MECHANICAL ENGINEERING

1 of 1

UNLESS OTHERWISE STATED
1) MACHINE AT ▽ TO 3.2 um Ra MAX
2) TOLERANCE ON MACHINED DIMENSIONS
AS FOLLOWS: 0-500 ±0.2; 500-1000 ±0.4

DO NOT SCALE
IF IN DOUBT ASK

Upper Arm — Engineering Drawing

91.60
70
42.80
78
100
363

ø62
H7 +0.03
0

ø110
H7 +0.04
0

R40
R39.50
R50
R50.50
R50.00
R75.50
R75.00

A
B
Z
Y

0.2 | A | B
0.1

0.2 | A
0.1

0.2 | A | B
0.1

0.1

Material 7075-T6 (SN)
Mass [g] 6086.17

DRAWN BY T. Magill
DRG No LUE-009

DATE 09/04/2019
TITLE Upper Arm
SCALE 1:2

LUMED
THE UNIVERSITY OF LEEDS
SCHOOL OF MECHANICAL ENGINEERING
1 of 1

UNLESS OTHERWISE STATED
DO NOT SCALE IF IN DOUBT ASK

1) MACHINE AT TO 3.2 um Ra MAX
2) TOLERANCE ON MACHINED DIMENSIONS
AS FOLLOWS: 0-500 ±0.2; 500-1000 ±0.4

ISO 13715:2000

ISO 1101:2004, 8015:1985, 1302:2002

| Material | 7075-T6 (SN) |
| Mass [g] | 6086.17 |

DRAWN BY: T. Magill
DRG No: LUE-009

MACHINE AT ∇ TO 3.2 um Ra MAX
UNLESS 1)
OTHERWISE 2) TOLERANCE ON MACHINED DIMENSIONS
STATED   AS FOLLOWS: 0-500 ±0.2; 500-1000 ±0.4

DO NOT SCALE
IF IN DOUBT ASK

DATE 09/06/2019 TITLE Upper Arm

LUMED
THE UNIVERSITY OF LEEDS
SCHOOL OF MECHANICAL ENGINEERING

SCALE 1:2

2 of 1

φ52.00
φ51.00

⌖ 0.2 A
⟋ 0.2

H7 +0.03
       0

2 x φ47
⌖ 0.05 A
⟂ 0.1

R50

272.40

180.60

H7 +0.02
       0

2 x φ20
⌖ 0.05 A
⟂ 0.1

φ40
⌖ 0.05 A

±1/1/0

CIRCLIP GROOVE TO
BS 3673-4-1977

DETAIL A
SCALE 5 : 1

⌀19.00
⌀18.79

1.70
1.50

1.44
1.30

⌀20 h6 0 / -0.01

100.10
100.00

ISO 13715:2000

ISO 1101:2004, 8015:1985, 1302:2002

Material	7075-T6 (SN)
Mass [g]	92.96

DRAWN BY	T. Magill
DRG No	LUE-010

DATE	01/09/2019	TITLE	Cylinder Pin

LUMED
THE UNIVERSITY OF LEEDS
SCHOOL OF MECHANICAL ENGINEERING

SCALE 2:1

1 of 1

UNLESS OTHERWISE STATED
1) MACHINE AT TO 3.2 um Ra MAX
2) TOLERANCE ON MACHINED DIMENSIONS
AS FOLLOWS: 0-500 ±0.2; 500-1000 ±0.4

DO NOT SCALE
IF IN DOUBT ASK

ISO 13715:2000
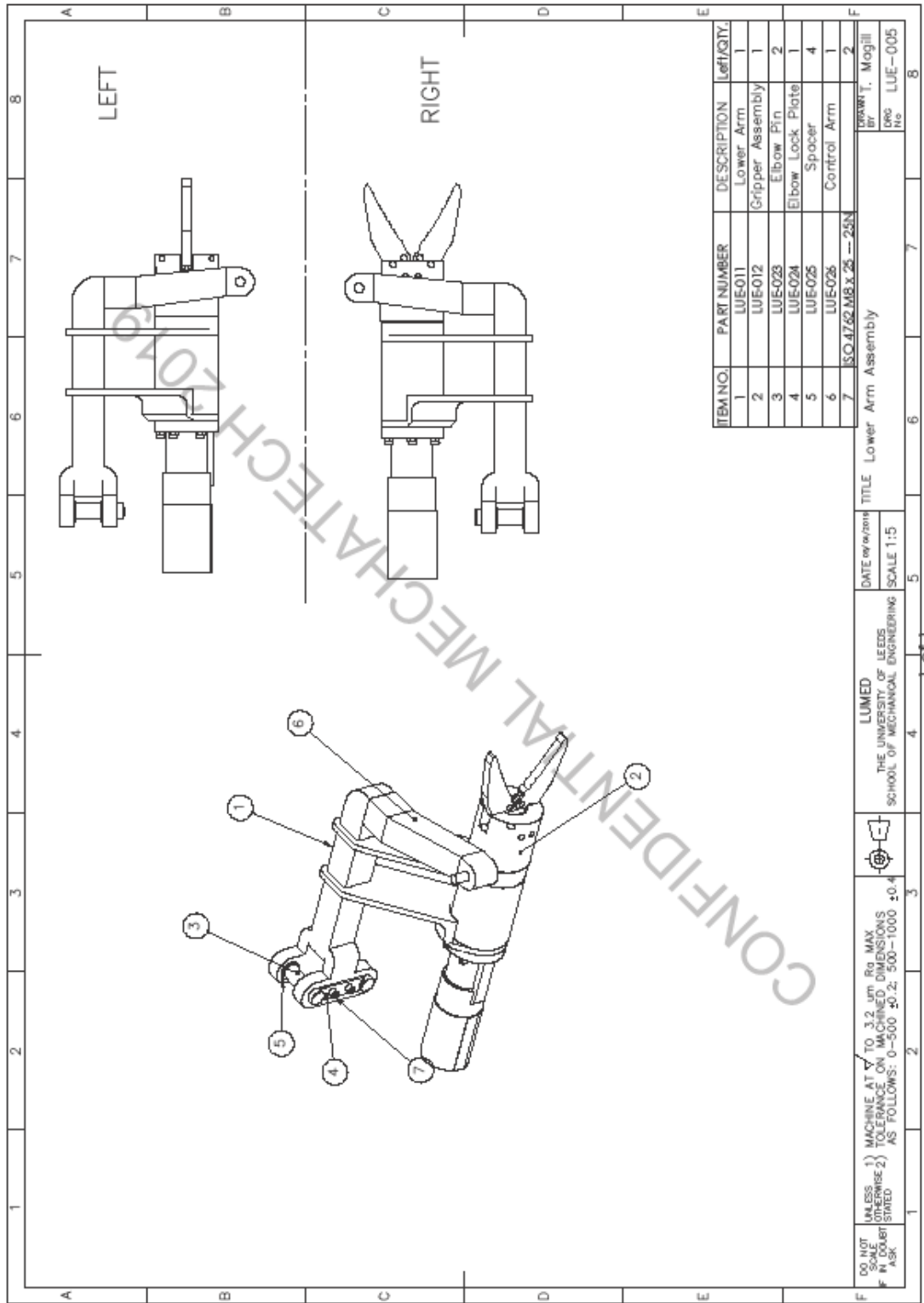
ISO 1101:2004, 8015:1985, 1302:2002

// 0.1 A — B

H7 +0.02 0

2 x ⌀25

2 x ⌀ 6.80 ▽ 30 M8 — 6H ▽ 16

⊕ 0.1 A — B

R25

⊕ 0.1 B

370.50

R24.50

⊕ 0.1 A

25

25

66

99

A

B

⊕ 0.1 A

2 x R50

3 x R9

2 x R16

SECTION B–B

75

25

R40

B

// 0.1 C

20

// 0.1 C

R22.50

// 0.1 C

⊕ 0.1 A B

C

22.50

57.50

90

B

B

DO NOT SCALE IF IN DOUBT ASK	UNLESS 1) OTHERWISE 2) STATED	MACHINE AT ▽ TO 3.2 um Ra MAX TOLERANCE ON MACHINED DIMENSIONS AS FOLLOWS: 0–500 ±0.2; 500–1000 ±0.4			
		LUMED THE UNIVERSITY OF LEEDS SCHOOL OF MECHANICAL ENGINEERING	DATE 09/09/2019	TITLE Lower Arm	
			SCALE 1:2		Material 7075–T6 (SN)
				DRAWN BY T. Magill	Mass [g] 3300.74
				DRG No LUE–011	

1 of 1

ITEM NO.	PART NUMBER	DESCRIPTION	Default/QTY.
1	LUE-013	Rear Support Arm	1
2	LUE-014	Front Support Arm	1
3	LUE-015	Manipulator Weight Offset Cylinder	1
4	LUE-016	Transfer Shaft	1
5	LUE-017	Manipulator Head	1
6	LUE-018	Manipulator Jaw	2
7	LUE-019	Manipulator Linkage	2
8	LUE-020	Manipulator Long Pin	4
9	LUE-021	Manipulator Short Pin	2
10	LUE-022	Manipulator Tie Rod	5
11	DHK-HZH-40	HKS Rotary Lift Actuator	1
12	40KB02	Nachi Bearing	5
13	ISO 7040-M8-N		5
14	ISO 4762 M6 x 16 — 16N		1
15	BS 3673-4 - S040M		1
16	BS 3673-4 - B080M		1

TITLE: Gripper Assembly

LUMED — THE UNIVERSITY OF LEEDS, SCHOOL OF MECHANICAL ENGINEERING

DRAWN BY: T. Magill DRG No: LUE-012 SCALE 1:5

SECTION A—A SECTION B—B

ALL EDGES

ISO 13715:2000

ISO 1101:2004, 8015:1985, 1302:2002

| Material | 7075-T6 (SN) |
| Mass [g] | 136.87 |

SECTION A-A

20

0.1 | A

B

5

A

A

100

10

⌀25 k6 +0
+0.02

A

DATE 01/09/2019 TITLE Elbow Pin

LUMED
THE UNIVERSITY OF LEEDS
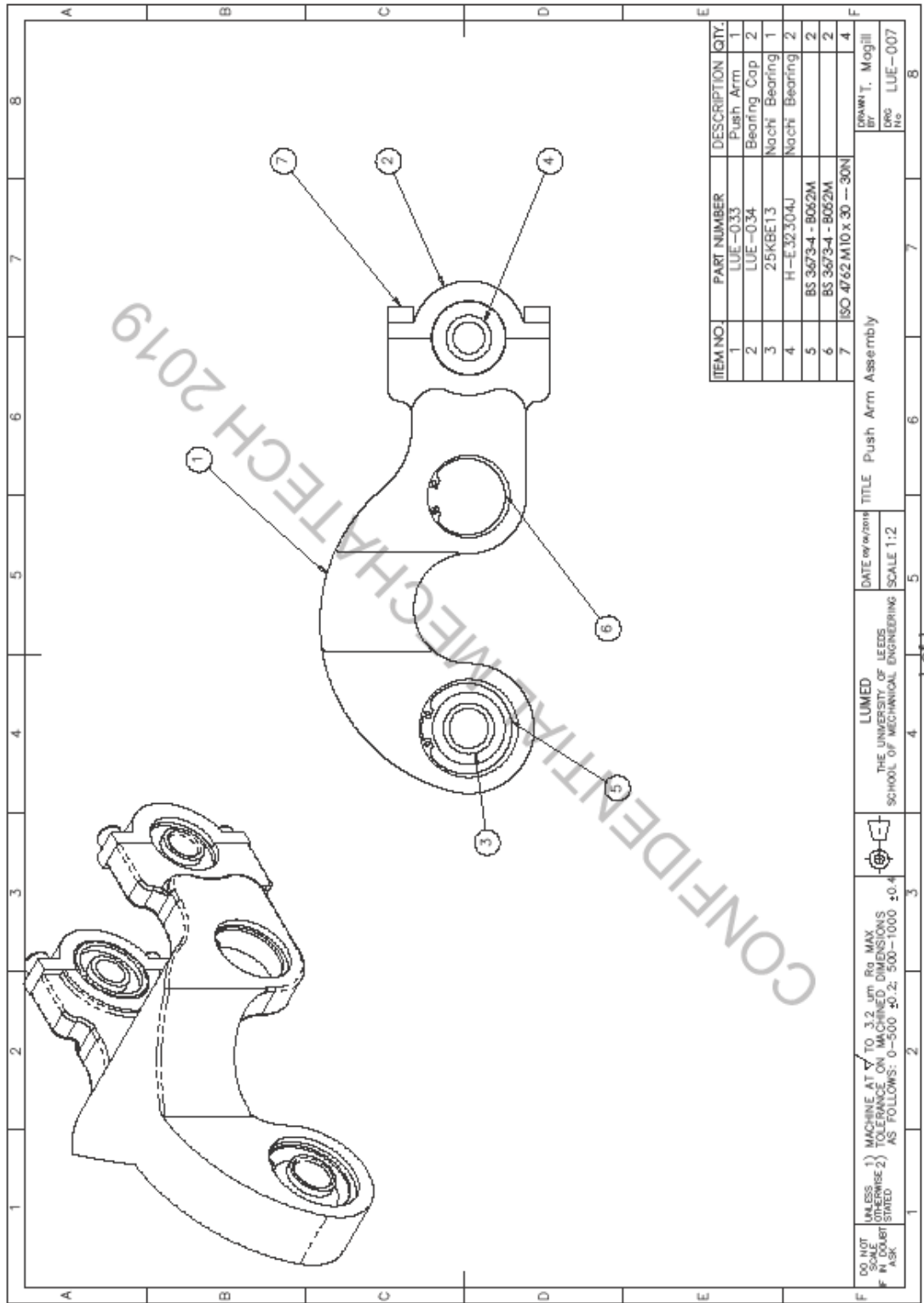SCHOOL OF MECHANICAL ENGINEERING

SCALE 1:1

1 of 1

DRAWN
BY T. Magill

DRG
No LUE-023

UNLESS 1) MACHINE AT ⌀ TO 3.2 um Ra MAX
OTHERWISE 2) TOLERANCE ON MACHINED DIMENSIONS
STATED   AS FOLLOWS: 0-500 ±0.2; 500-1000 ±0.4

DO NOT
SCALE
IF IN DOUBT
ASK

CONFIDENTIAL MECHATECH 2019

2 x ⌀8.40 H8 +0.02 / 0

83

33

25

⌖ 0.1 A

A

B

Material 7075-T6 (SN)

Mass [g] 22.08

DRAWN BY T. Magill

DRG No LUE-024

DATE 09/04/2019
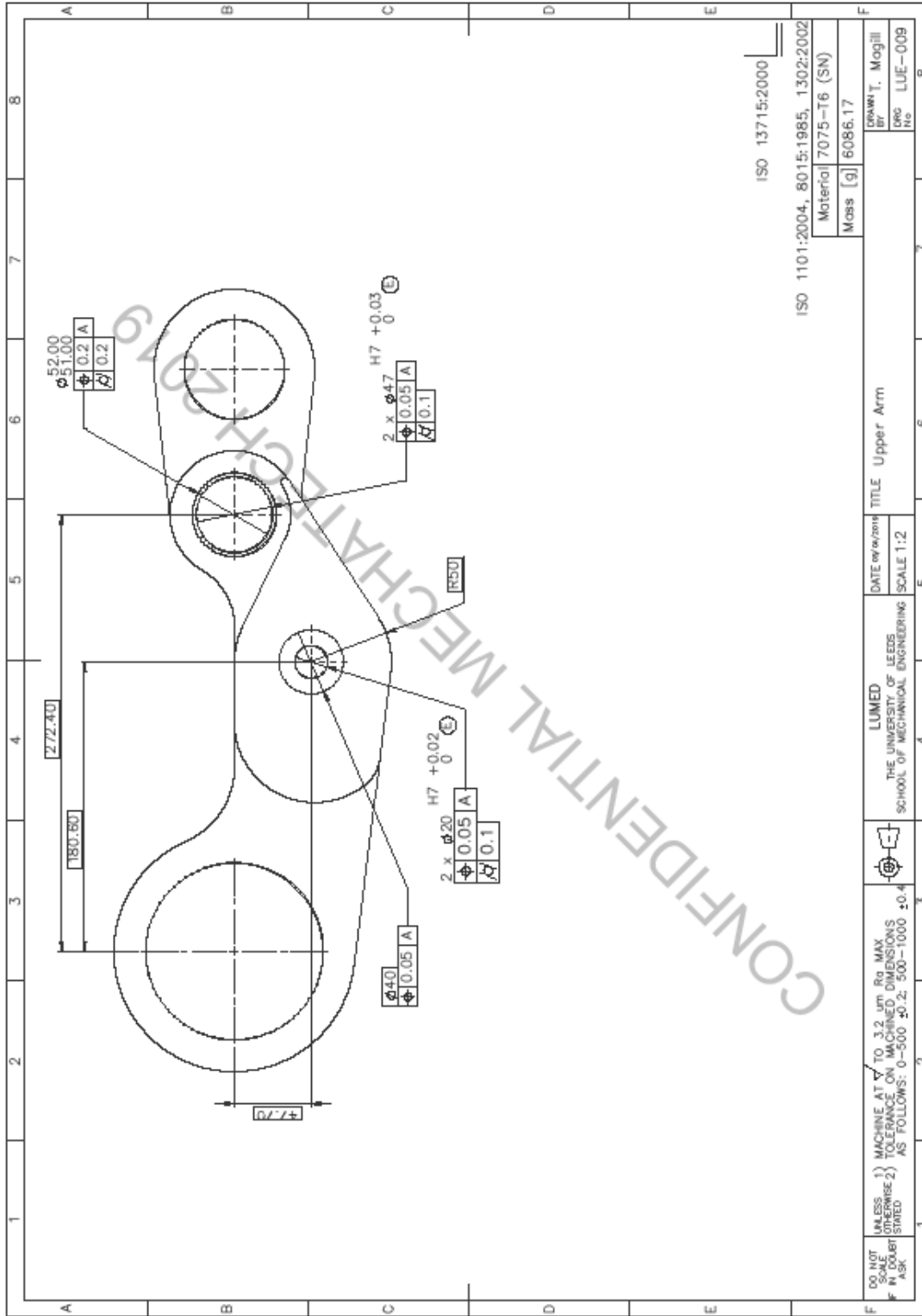
TITLE Elbow Lock Plate

SCALE 2:1
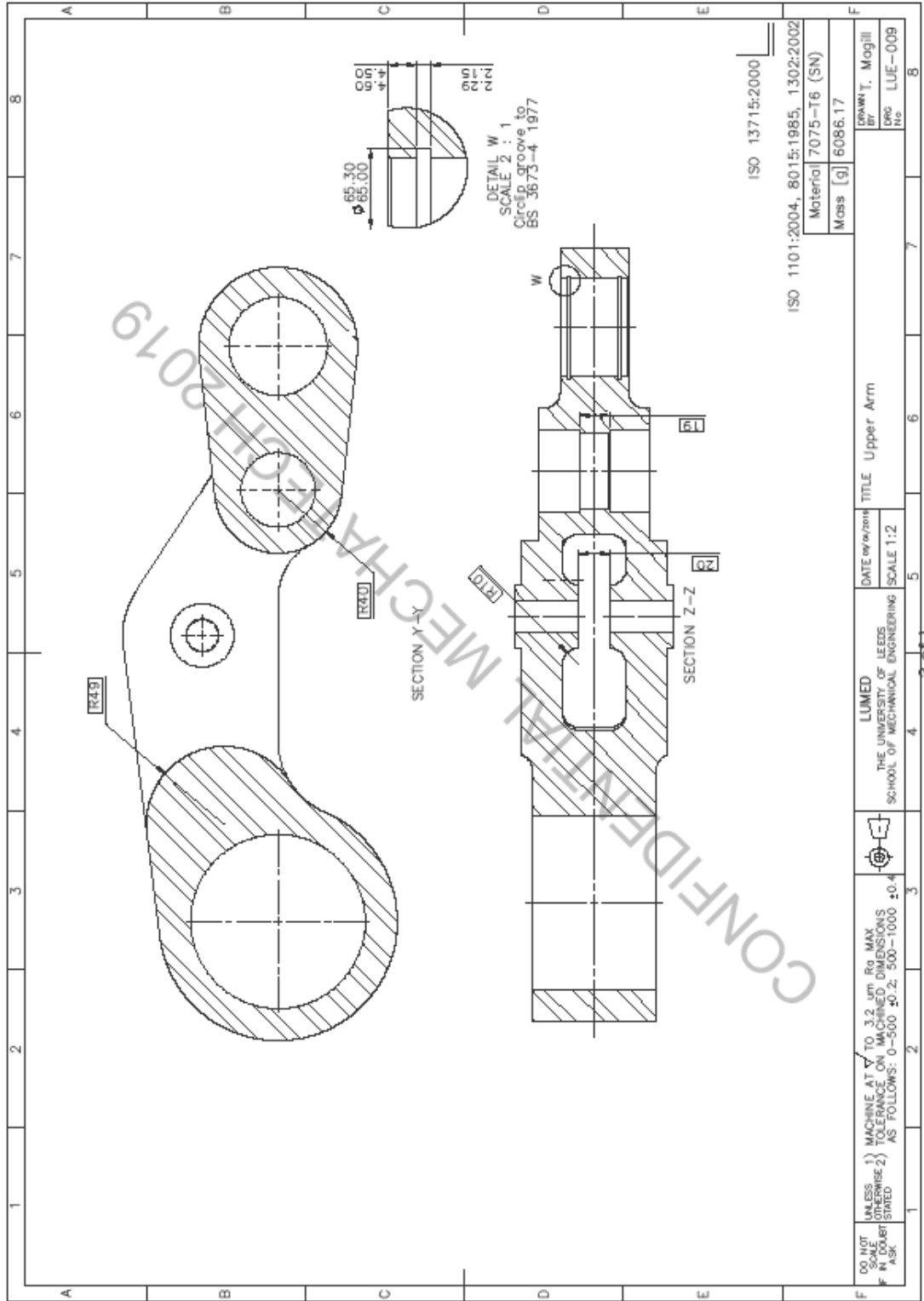
LUMED
THE UNIVERSITY OF LEEDS
SCHOOL OF MECHANICAL ENGINEERING

1 of 1

UNLESS OTHERWISE STATED
1) MACHINE AT TO 3.2 um Ra MAX
2) TOLERANCE ON MACHINED DIMENSIONS
AS FOLLOWS: 0-500 ±0.2; 500-1000 ±0.4

DO NOT SCALE
IF IN DOUBT ASK

ISO 13715:2000

ISO 1101:2004, 8015:1985, 1302:2002

| Material | Brass |
| Mass [g] | 6.66 |

DRAWN BY: T. Magill
DRG No: LUE-025

TITLE Spacer

DATE 01/09/2019

SCALE 2:1

LUMED
THE UNIVERSITY OF LEEDS
SCHOOL OF MECHANICAL ENGINEERING

1 of 1

UNLESS OTHERWISE STATED
1) MACHINE AT ∇ TO 3.2 μm Ra MAX
2) TOLERANCE ON MACHINED DIMENSIONS AS FOLLOWS: 0-500 ±0.2; 500-1000 ±0.4
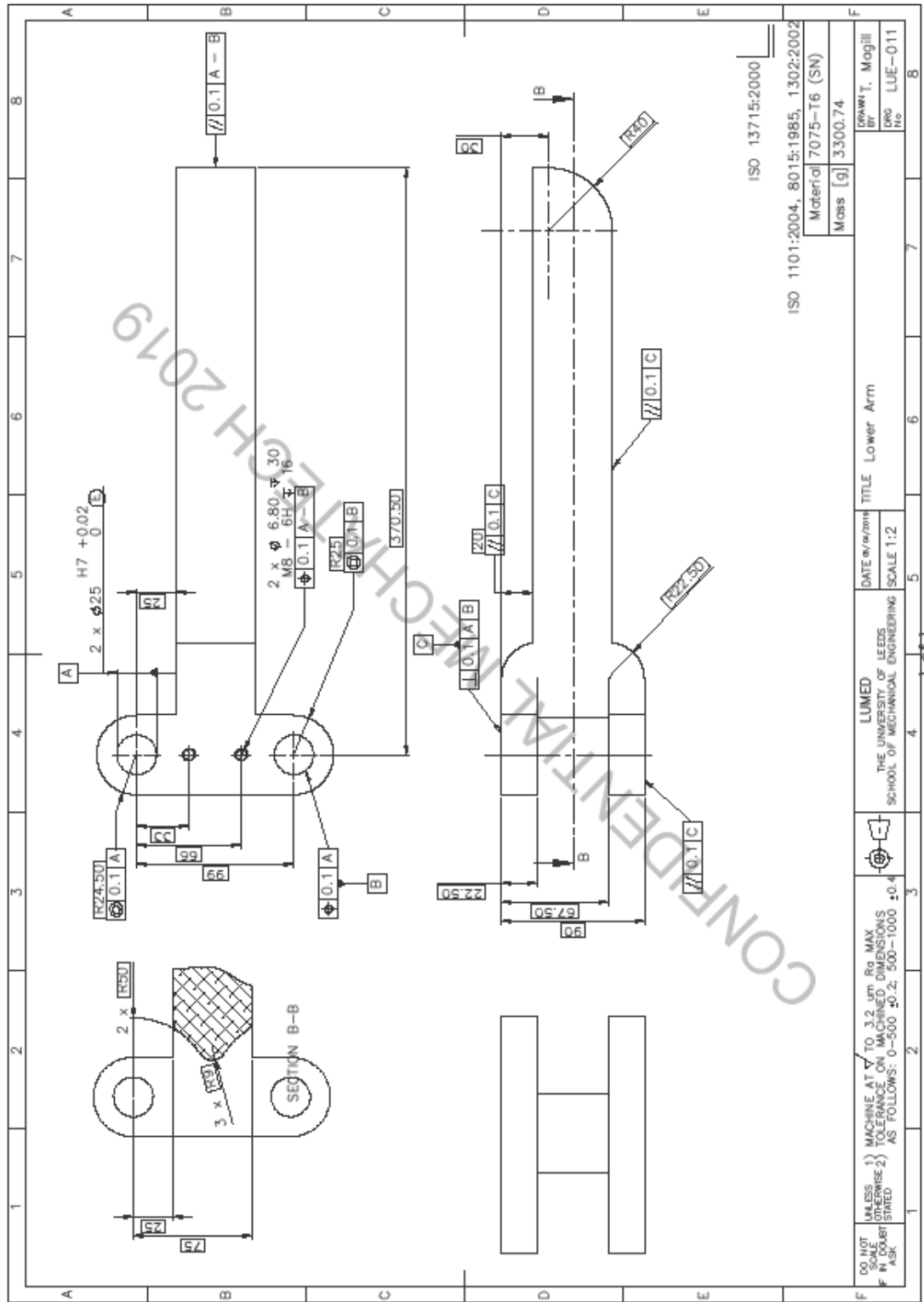
DO NOT SCALE
IF IN DOUBT ASK

2.50 ±0.20

⌖ 0.02 A

B

A

φ25 H7 +0.02 / 0

A

φ32 ±0.20

⌖ φ0.1 B A

ISO 13715:2000

ISO 1101:2004, 8015:1985, 1302:2002

Material	7075-T6 (SN)
Mass [g]	198.23

DRAWN BY: T. Magill

DRG No: LUE-028

TITLE Cross Linkage

DATE 06/06/2019

SCALE 1:1

LUMED
THE UNIVERSITY OF LEEDS
SCHOOL OF MECHANICAL ENGINEERING

1 of 1

UNLESS OTHERWISE STATED
1) MACHINE AT TO 3.2 um Ra MAX
2) TOLERANCE ON MACHINED DIMENSIONS AS FOLLOWS: 0-500 ±0.2; 500-1000 ±0.4

DO NOT SCALE IF IN DOUBT ASK

⌀27.20 / ⌀27.00

R22.50

⌀20 H7 +0.02 / 0

R80.00

R37.00 / 35.00

18.50

∅20 H7 +0.02 / 0

ALL EDGES

2 x 18.50

⟂ 0.1 A
B

2 x ⊕

120.50

2 x M20 ⊕

A

$\phi20\ h6\ ^{0}_{-0.013}$ Ⓔ

Material	7075-T6 (SN)
Mass [g]	106.05

DRAWN BY T. Magill
DRG No LUE-029

DATE 09/04/2019
TITLE Cross Linkage Short Pin
SCALE 1:1

LUMED
THE UNIVERSITY OF LEEDS
SCHOOL OF MECHANICAL ENGINEERING

1 of 1

UNLESS OTHERWISE STATED
1) MACHINE AT ▽ TO 3.2 um Ra MAX
2) TOLERANCE ON MACHINED DIMENSIONS AS FOLLOWS: 0-500 ±0.2; 500-1000 ±0.4

DO NOT SCALE
IF IN DOUBT ASK

ALL EDGES

ISO 13715:2000

ISO 1101:2004, 8015:1985, 1302:2002

| Material | 7075-T6 (SN) |
| Mass [g] | 143.13 |

DRAWN BY: T. Magill

DRG No: LUE-030

18.50

2 ×

0.1 A

B

2 × ∅

2 × M20

162.50

A

∅20 h6 −0.01

0

TITLE: Cross Linkage Long Pin

DATE: 09/09/2019

SCALE 1:1

LUMED
THE UNIVERSITY OF LEEDS
SCHOOL OF MECHANICAL ENGINEERING

1 of 1

UNLESS OTHERWISE STATED
1) MACHINE AT TO 3.2 um Ra MAX
2) TOLERANCE ON MACHINED DIMENSIONS
AS FOLLOWS: 0-500 ±0.2; 500-1000 ±0.4

DO NOT SCALE
IF IN DOUBT ASK

CONFIDENTIAL MECHATECH 2019

VIEW F

VIEW G

9 x ⌀17.50

⌀1.95

⌀150

R50

R121

R50

R75

⌀110

50

78

+80

45.60

G

+80

12

49

DRAWN BY	T. Magill
DRG No	LUE-008
Material	7075-T6 (SN)
Mass [g]	5559.22

DATE 09/04/2019 TITLE Back Plate

SCALE 1:5

LUMED
THE UNIVERSITY OF LEEDS
SCHOOL OF MECHANICAL ENGINEERING

1 of 1

MACHINE AT ∇ TO 3.2 um Ra MAX
TOLERANCE ON MACHINED DIMENSIONS
AS FOLLOWS: 0-500 ±0.2; 500-1000 ±0.4

UNLESS
OTHERWISE
STATED

DO NOT
SCALE
IF IN DOUBT
ASK

SECTION Z-Z

SPLINE

ELLIPSE

105.00
104.00

75.50
74.50

410.00
409.00

ISO 13715:2000

ISO 1101:2004, 8015:1985, 1302:2002

Material	7075-T6 (SN)
Mass [g]	5559.22

DATE 09/06/2019	TITLE Rear Arm

DRAWN BY	T. Magill
DRG No	LUE-008

LUMED
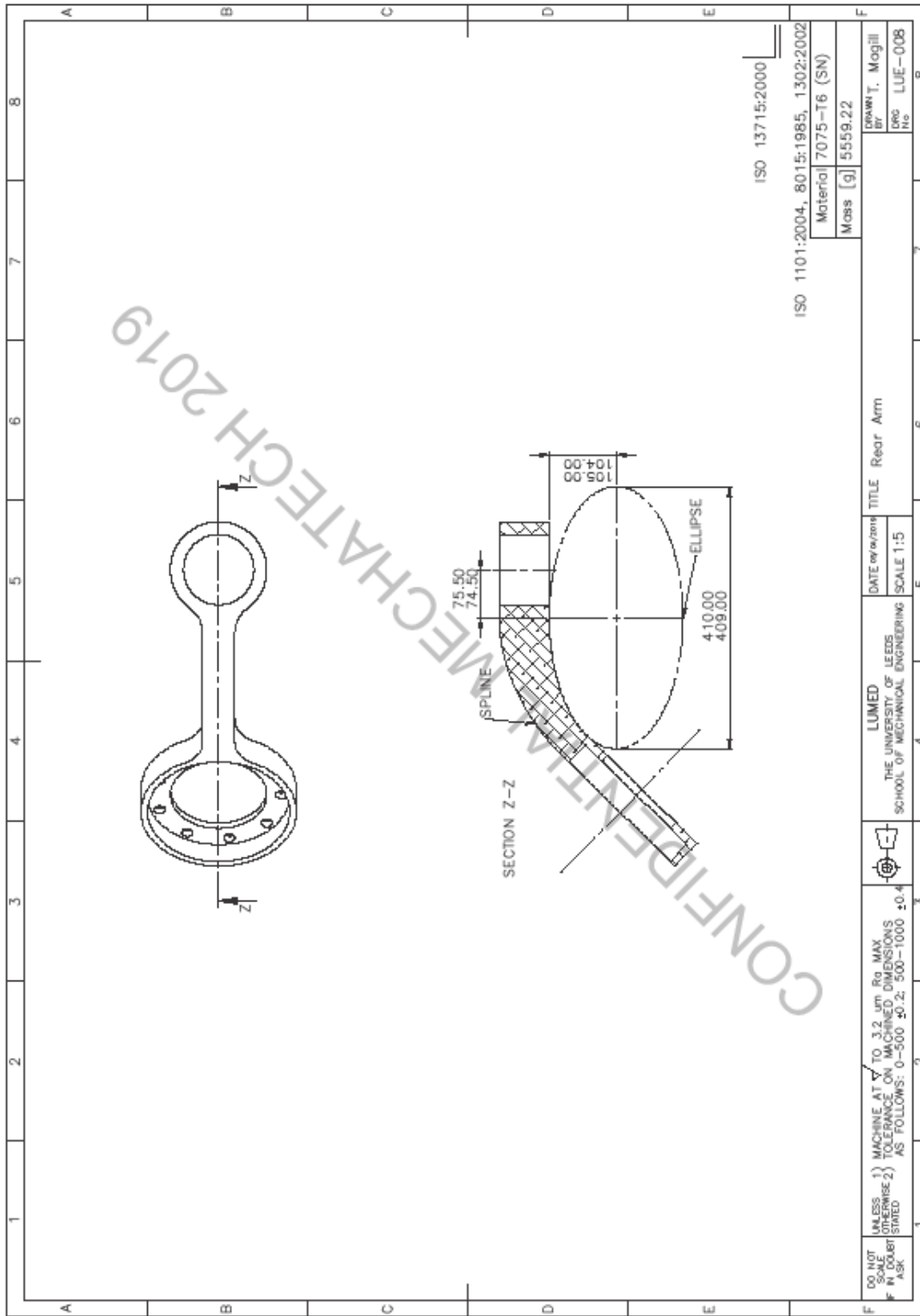THE UNIVERSITY OF LEEDS
SCHOOL OF MECHANICAL ENGINEERING

SCALE 1:5

2 of 1

UNLESS OTHERWISE STATED
1) MACHINE AT ∇ TO 3.2 um Ra MAX
2) TOLERANCE ON MACHINED DIMENSIONS AS FOLLOWS: 0-500 ±0.2; 500-1000 ±0.4

DO NOT SCALE IF IN DOUBT ASK

CONFIDENTIAL MECHATECH 2019

- 400 -

SECTION Z–Z

ELLIPSE
ELLIPSE

566.00
567.00
595.00
596.00

205.00
206.00

197.00
198.00

75.50
74.50

498.50
497.50

597.50
596.50

CONFIDENTIAL MECHATECH 2019

ISO 13715:2000

ISO 1101:2004, 8015:1985, 1302:2002

| Material | 7075–T6 (SN) |
| Mass [g] | 6985.67 |

DRAWN BY: T. Magill
DRG No: LUE–008

DATE 09/04/2019
TITLE Back Plate

LUMED
THE UNIVERSITY OF LEEDS
SCHOOL OF MECHANICAL ENGINEERING

SCALE 1:5

2 of 1

UNLESS OTHERWISE STATED
1) MACHINE AT ∇ TO 3.2 um Ra MAX.
2) TOLERANCE ON MACHINED DIMENSIONS
AS FOLLOWS: 0–500 ±0.2; 500–1000 ±0.4

DO NOT SCALE
IF IN DOUBT ASK

- 401 -

SECTION Z-Z

R10

R40

R15

29.50

2 × 2.29 / 2.15

2 × Ø65.30 / Ø65.00

2 × 4.70 / 4.50

SECTION Y-Y
SCALE 1:1
CIRCLIP GROOVE TO
BS 3673-4 1977

ISO 13715:2000

ISO 1101:2004, 8015:1985, 1302:2002

| Material | 7075-T6 (SN) |
| Mass [g] | 3231.19 |

| DRAWN BY | T. Magill |
| DRG No | LUE-033 |

| DATE 09/06/2019 | TITLE | Push Arm |

LUMED
THE UNIVERSITY OF LEEDS
SCHOOL OF MECHANICAL ENGINEERING

SCALE 1:2

2 of 1

UNLESS OTHERWISE STATED
1) MACHINE AT ▽ TO 3.2 um Ra MAX
2) TOLERANCE ON MACHINED DIMENSIONS
AS FOLLOWS: 0-500 ±0.2; 500-1000 ±0.4

DO NOT SCALE
IF IN DOUBT ASK

SECTION A–A

R26

H7 +0.02 / 0

10 ±0.50

R36

R24.50

A

B

C

// 0.1 C

⟂ 0.1 B

0.1 A

0.1 A

⌀7

102

4.50

22.50

UNLESS OTHERWISE STATED
1) MACHINE AT ▽ TO 3.2 um Ra MAX
2) TOLERANCE ON MACHINED DIMENSIONS AS FOLLOWS: 0–500 ±0.2; 500–1000 ±0.4

DO NOT SCALE IF IN DOUBT ASK

LUMED
THE UNIVERSITY OF LEEDS
SCHOOL OF MECHANICAL ENGINEERING

DATE 05/04/2019

SCALE 1:1

TITLE Bearing Cap

DRAWN BY T. Magill

DRG No LUE-034

Material 7075-T6 (SN)

Mass [g] 78.73

Appendix R

Hydraulics setup

In order to determine whether a valve or pump based system gives increased benefits to the exoskeleton system. Using Simscape as a simulation basis, individual components can be set up.

R.1 Control valve

The basics of the valve basis system are the valves themselves. These have a flow rate response as well as the frequency response. Setting this up requires the use of the manufacturer's data sheets as well as the use of the Optimization Toolbox™ by MathWorks. This is outlined in the files from the MathWorks file ID 27260 [R.1].

Using Bosch Rexroth valves as the basis of the units as the units bought for the power pack are 4WRPEH 6 C3 B12L-2X/G24K0/A1M. These are four-port units, with integrated electronics. They have linear flow characteristics so do not have any inflexion responses.

R.1.1 Valve parameter optimisation

Using the setup from the supplied m-files, and the valve data from the catalogues, the parameters are inputted and the tuning run. The pressure drop across the valve is

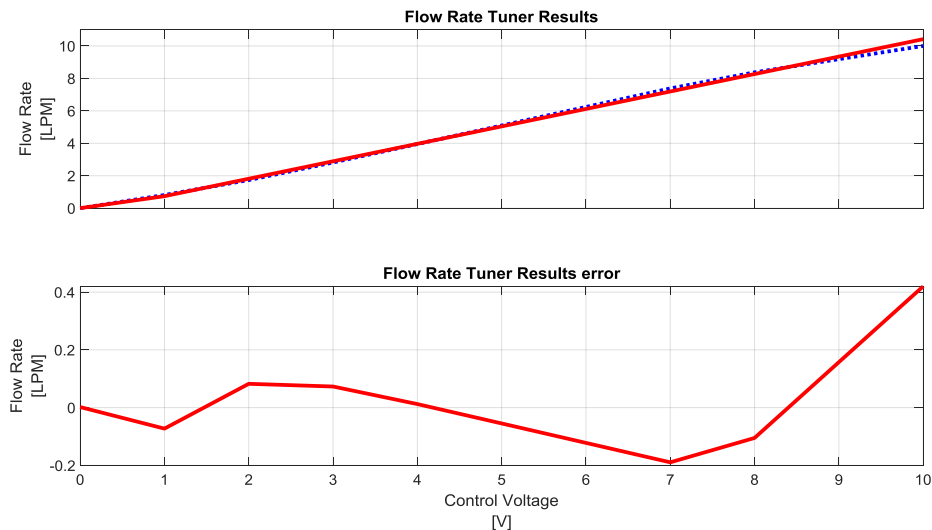This runs for 43 steps and gives the following results.

Figure R.1: Valve response from tuning where the blue dotted line is the empirical data, and the red lines are the tuned results

The error ranges from 0.3% to 9% over the range of control voltage.

R.2 Relief Valve

The relief valve for the hydraulic circuit also needs to be set up for the system, though as there are different valves for different uses throughout the system. Using the Direct-Acting Pressure Relief Valve Test Rig in the Simscape fluids examples as a base circuit, different valves can be set up. This does depend on the pressure load required as well as the flow rate needed to be bled off.

Swagelok is a manufacturer of pressure relief valves that are compact as well as allowing customisation of pressure control. The peak flow for these units is only 7.5L/min, though, for the higher pressures, less than 1L/min flow is given. These could be useful for smaller systems, but for high motion units, these will not be viable for safety reasons.

Sunhydraulics do manufacture higher flow units, which will work for the system. The CE marked units start at 90L/min, which is too high, though as the system will lie in the sound engineering practise area, the direct requirement of a CE marked unit could be a smaller requirement. Without CE marking, then there are units that work for 2.7L/min though for a max flow of 20L/min, the next flow size up is 54.6L/min

Hydac is another hydraulic manufacturer that has pressure relief valves. Unit DB4E-CE is a 28L/min unit that is also CE marked to conform to the pressure

equipment directive, with a max pressure of 360bar. This does mean that the tank pressure port must be at zero bar.

R.2.1 Valve Setup

Using the Hydac valve, and the example code, the valve can be set up. The valve requires the maximum passage area, valve pressure setting, valve regulation range, and leakage area values to be set.

The valve pressure setting is 200bar, as this is the value that the valve is supplied at, though the company is likely to be able to set it to 210bar if required.

The maximum passage area can be set using the orifice equation with the flow rate set to 30L/min and pressure to 200bar. The density is for ISO VG 32 (ESSO UNIVIS N 32) at 40°C.

$$Q = A * cd * \sqrt{\frac{2 * \Delta P}{\rho}} \qquad \text{(R.1)}$$

$$A = \frac{Q}{cd * \sqrt{\frac{2 * \Delta P}{\rho}}} = \frac{\frac{30}{60 * 1000}}{0.7 * \sqrt{\frac{2 * 200e5}{857.2}}} = 3.56e - 6 \qquad \text{(R.2)}$$

This can be repeated for the leakage area though this is only 0.25 cm³/min at 350bar. This gives an area of 1.25e-9 m².

R.3 Check Valve

The check valve for the simulation is set up like the relief valve and follow the same process. In several instances, check and relief valves are referenced in similar situations, though the actual action for each is different. A check valve is for continuous use, holding pressure within a section of the circuit. A relief valve is for intermittent use and is for safety rather than process.

R.4 Cylinder

The use of the double-acting hydraulic cylinder from the Simscape Fluids toolbox is used as the initial base for the actuator. This assumes that there is no leakage and no friction, though the latter has been added in with an additional block.

The input parameters are:

- Piston areas
- Piston stroke
- Dead volumes
- Specific heat ratio
- Hard stop contact stiffness
- Hard stop contact damping
- Initial conditions

The dimensional values are determined by the actuator size, whilst the initial conditions are from the initial setup simulations. The specific heat ratio is left at the default 1.4. The contact stiffness and damping are set from the values for steel from Solidworks.

R.5 Rotatory actuator

The rotary actuator is similar to the cylinder in setup and requires the following information.

- Actuator displacement
- Shaft stroke
- Dead volumes
- Leak coefficient
- Specific heat ratio
- Hard stop contact stiffness
- Hard stop contact damping
- Initial conditions

R.6 Pump

There are several options for the pump, ranging from diaphragm to servo-controlled variable displacement piston pumps. The unit would need to be a positive-displacement pump to make sure that there is a known displacement per pump cycle. A non-positive-displacement pump like a centrifugal pump has delivery dependant on the pressure and would be difficult to control. Each pump mechanism type has different characteristics and abilities. Gear pumps rely on the meshing of gears to create a volume imbalance so that more flow travels

around the outside of the gear than the area where they mesh. These have on driver gear and one driven gear that rotates around with it. They tend to be 93% volumetrically efficient. An alternative is a piston pump that turns rotary into linear motion to compress a volume with a plunger.

Rotary units have larger leakage values than piston units as fluid can bypass the faces of the gears as well as the outside edges of the teeth, whilst a piston pump as leakage down the sides of the piston.

Variable displacement units that can alter the delivered volume either with automatic feedback or user control is also an option. Gear pumps do not have the option for variable delivery, but vane and piston units do. This is done by altering the eccentricity of the swept volume for the vane units or the swashplate angle for a piston pump. These add the option to reduce the amount of volume being displaced so that there is increased control over the delivered amount for small motions. They do require additional hardware in order to allow this control.

There are several small pumps on the market, though several of these are designed for lower pressures, around 10bar, so are not suitable for an exoskeleton system. For the delivery required, around 20Lmin-1 at 3000rpm would require a unit that delivers 1.06cm³ per rev. Parker makes small pumps under the Oildyne brand, though these only go up to 0.865cc/rev. Their larger pumps are around 4cc/rev, but also have the issue of only being able to rotate in one direction. Takako supply small axial piston pumps and claim to be

"The world's smallest class Small Axial Piston Pump"

Takako have pumps up to 6.3cm³/rev with the next size larger than the required delivery of 1.6cm³/rev. They are able to rotate in both directions as well as being able to be used as a motor for energy recovery opportunities. Takako pumps currently used in another exoskeleton project.

The unit would set up similar to the Takako pump unit, though with this is limited in the angle of use. The reservoir would be replaced with an accumulator so that there would be constant pressure feeing the system. From the Takako documentation, this would be set to a maximum of two bar. The documentation also states that the drainpipe should not be connected to other return pipes to stop the pump draining completely. This could be done with a check valve

within the return line so that a pressure of two bar is kept within the pump before entering the accumulator set to a lower pressure. The accumulator pressure would only have to be above atmosphere to make sure that there is no air contained within the system. Cavitation could become an issue with the local valves.
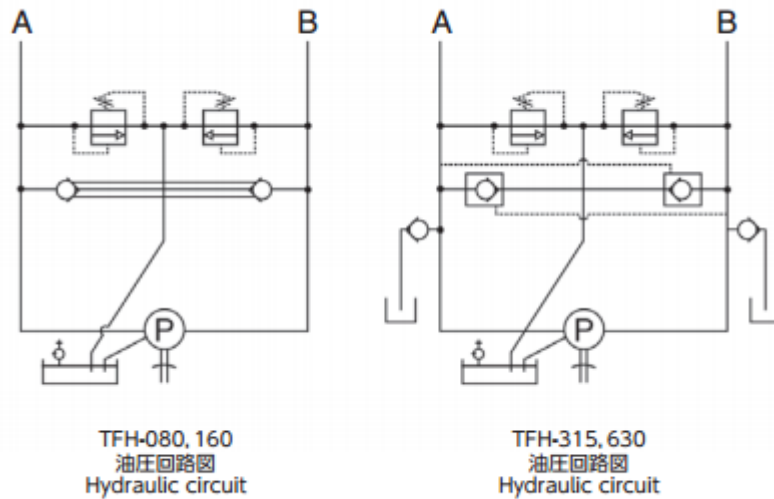

Figure R.2: Takako piston pump unit layout [R.2]

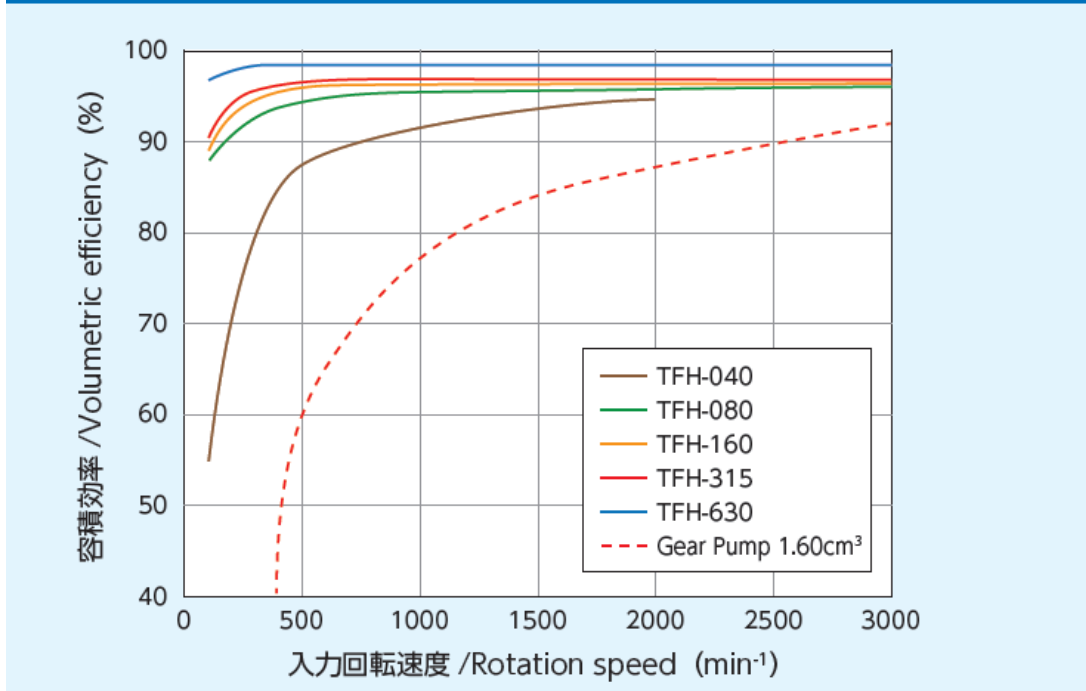TAKAKO outline their pump efficiency as shown in Figure R.3

Figure R.3: TAKAKO volumetric efficiency curves [R.2]

This has been tuned in the simulation as shown in Figure R.4
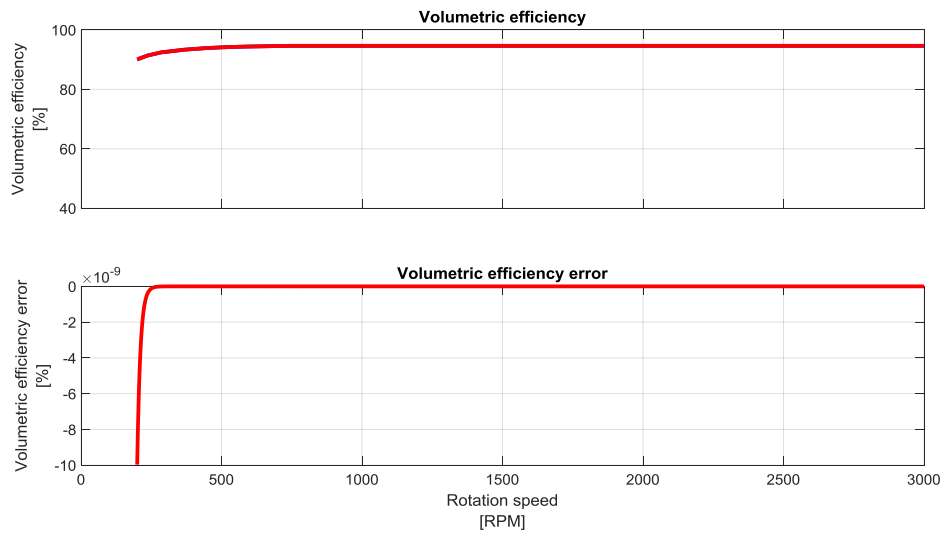

Figure R.4: tuned pump results

References

R.1.   Valery Tchkalov, S.M., MathWorks. Parameterization of Directional and Proportional Valves in SimHydraulics. 2016a ed. http://uk.mathworks.com/matlabcentral/fileexchange/27260-hydraulic-valve-parameters-from-data-sheets-and-experimental-data: MathWorks, 2016.

R.2.   Takako Industries INC. Small Axial Piston Pump, [Exhibition catalogue]. https://www.takako-inc.com/english/products/pdf/pump.pdf: Takako Industries, INC., 2019.